15 January 2010 $10

Science

Innate Immunity

AAAS

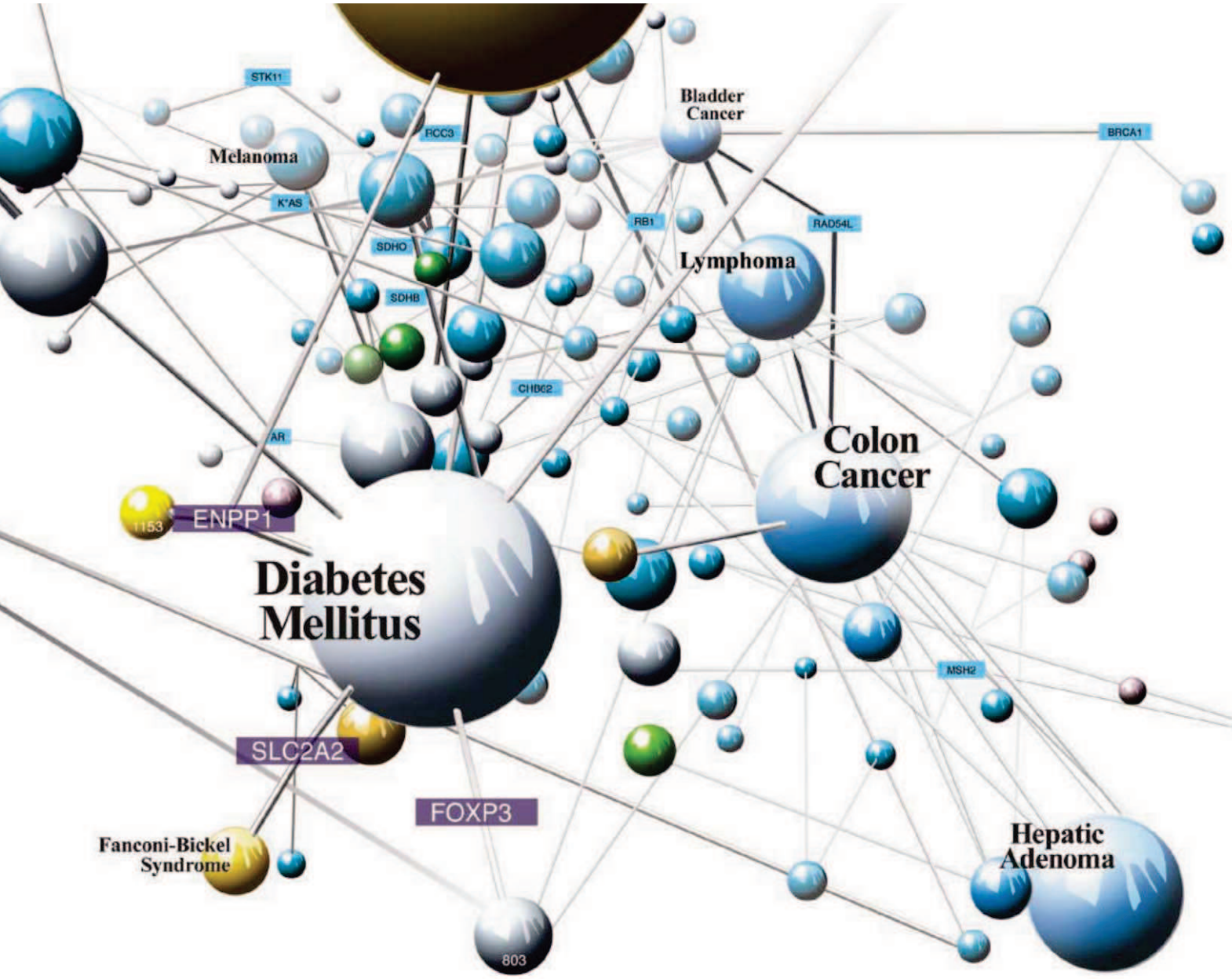

FIND THE CONNECTIONS AND YOU'LL FIND SOLUTIONS

Mapping the genetic linkages among diseases can advance whole categories of medical research—just one example of how Northeastern University's world-leading Center for Complex Network Research connects the dots on the global challenges of our time.

Interdisciplinary research at Northeastern University: Developing practical solutions to the global challenges of health, security, and sustainability.

northeastern.edu/research

Northeastern University

Call for Papers

Science Signaling

Science Signaling, from the publisher of ***Science***, AAAS, features top-notch, peer-reviewed, original research weekly. Submit your manuscripts in the following areas of cellular regulation:

- Biochemistry
- Bioinformatics
- Cell Biology
- Development
- Immunology
- Microbiology
- Molecular Biology
- Neuroscience
- Pharmacology
- Physiology and Medicine
- Systems Biology

Science Signaling is indexed in CrossRef and MEDLINE.

Submit your research at:
www.sciencesignaling.org/about/help/research.dtl

Subscribing to the weekly ***Science Signaling*** ensures that you and your lab have the latest cell signaling resources. For more information visit **www.ScienceSignaling.org**

Science Signaling
AAAS

Choose QIAGEN for detection

Detection platforms, assays, and analysis software by QIAGEN

AUTODetec0110S1WWDPS

Use QIAGEN® solutions from sample to result, and benefit from sensitive and reliable detection:

- **Quantitative, real-time PCR detection**
- **Automated analysis of DNA fragments and RNA**
- **Pyrosequencing® sequence-based DNA detection and quantification**
- **Optimized, ready-to-use assays and reagents**

Making improvements in life possible — www.qiagen.com

QIAGEN®

Sample & Assay Technologies

GE Healthcare
Life Sciences

See more
See beyond

For years, scientists have relied on ImageQuant™ and Typhoon™. Now we can offer a new standard of performance with the Typhoon FLA 9000, Typhoon FLA 7000, ImageQuant 4000, and ImageQuant 4000 mini. Covering the full spectrum of imaging methods including quantitative Westerns, UV, IR, visible fluorescence, phosphorimaging, and 2-D DIGE, the new imagers provide exceptional sensitivity, speed, and versatility.

At GE Healthcare, our focus is on helping scientists achieve more, faster. However simple or complex your imaging needs, you can depend on us for quantitative imaging that's quantifiably better.

To find out more about our new range of imagers, contact us today.
Visit **www.gelifesciences.com/imaging**

I ÄKTA I Amersham I Biacore I IN Cell Analyzer I Whatman I GE Service I

imagination at work

GE Healthcare Bio-Sciences AB, Björkgatan 30, 751 84 Uppsala, Sweden
GE01-10. First published January 2010.

SPECIAL SECTION

Innate Immunity

pages 260 & 343

CONTENTS continued >>

COVER

Dendritic cells of the immune system recognize and bind bacteria and other microbes by means of receptors expressed on the dendritic cell membrane and within the cell, thus triggering an immune response. Microbial sensing is associated with the innate arm of the immune system, and recent developments in this area are described in the special section starting on page 283.

Image: Chris Bickel

DEPARTMENTS

CONTENTS

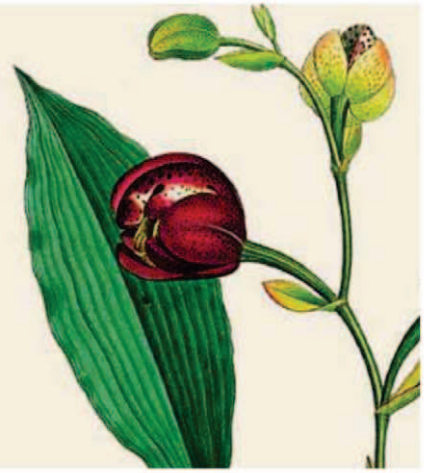

page 271

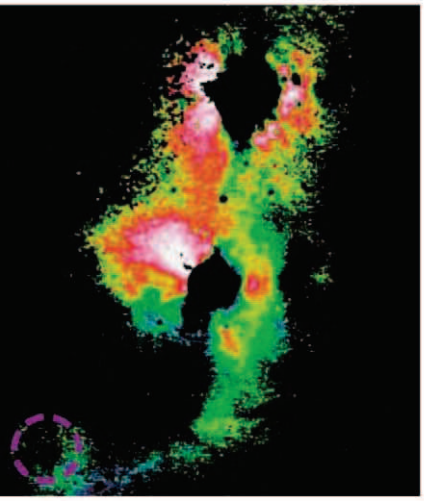

page 306

page 338

SCIENCEONLINE

SCIENCEXPRESS
www.sciencexpress.org

A Genetic Variant BDNF Polymorphism Alters Extinction Learning in Both Mouse and Human
F. Soliman et al.
Commonly genetic variation in fear learning operates through the same pathways in mice and men.
10.1126/science.1181886

Evolutionary Dynamics of Complex Networks of HIV Drug-Resistant Strains: The Case of San Francisco
R. J. Smith? et al.
Modeling of data from the U.S. indicates the potential for an epidemic wave of antiretroviral-resistant HIV.
10.1126/science.1180556

Ferroelectric Control of Spin Polarization
V. Garcia et al.
Ferroelectric tunnel junctions control the spin polarization of electrons emitted from iron electrodes.
10.1126/science.1184028

Effect of Ocean Acidification on Iron Availability to Marine Phytoplankton
D. Shi et al.
Ocean acidification caused by anthropogenic carbon dioxide is changing the chemistry and bioavailability of iron in seawater.
10.1126/science.1183517

Deglacial Meltwater Pulse 1B and Younger Dryas Sea Levels Revisited with Boreholes at Tahiti
E. Bard et al.
A coral-based record of sea level from Tahiti defines changes in the rate of sea-level rise between 14,000 and 9000 years ago.
10.1126/science.1180557

SCIENCENOW
www.sciencenow.org
Highlights From Our Daily News Coverage

Egyptian Eyeliner May Have Warded Off Disease
Lead-based cosmetics could have killed bacteria on the skin.

Bering Strait's Ups and Downs Alter Climate
Rise and fall of the land bridge affect the extent of ice sheets.

Why Light Makes Migraines Worse
Researchers trace effect to a particular receptor in the eye.

SCIENCESIGNALING
www.sciencesignaling.org
The Signal Transduction Knowledge Environment

RESEARCH ARTICLE: Extensive Crosstalk Between O-GlcNAcylation and Phosphorylation Regulates Cytokinesis
Z. Wang et al.
Protein O-GlcNAcylation regulates cell division.

RESEARCH ARTICLE: Quantitative Phosphoproteomics Reveals Widespread Full Phosphorylation Site Occupancy During Mitosis
J. V. Olsen et al.
Protein phosphorylation during the cell cycle may be an all-or-none process in many instances.

PERSPECTIVE: Cyclic Nucleotides Converge on Brown Adipose Tissue Differentiation
P. S. Amieux and G. S. McKnight
cGMP-mediated signaling pathways are required for the differentiation and function of brown adipocytes.

REVIEW: Basal Release of ATP—An Autocrine-Paracrine Mechanism for Cell Regulation
R. Corriden and P. A. Insel
Responses to ATP play an important role in regulating the signaling and function of a diverse array of cells and tissues.

GLOSSARY
Discover what RANKL and RANK mean in the world of signaling.

SCIENCECAREERS
www.sciencecareers.org/career_magazine
Free Career Resources for Scientists

Tenure-Track Jobs Remain Scarce
S. Carpenter
Although most universities have cut faculty hiring, a few are taking advantage of a rich applicant pool.

Tooling Up: What's Your Mission?
D. Jensen
Your unique life philosophy is the cornerstone of your success and job satisfaction.

Science Careers Blog
Science *Careers Staff*
Get frequent advice, opinion, news, funding opportunities, and links to other career resources.

SCIENCETRANSLATIONAL MEDICINE
www.sciencetranslationalmedicine.org
Integrating Medicine and Science

PERSPECTIVE: Why Most Gene Expression Signatures of Tumors Have Not Been Useful in the Clinic
S. Koscielny
Gene microarray literature polluted with invalidated gene expression signatures needs revamping.

COMMENTARY: Translational Medicine Policy Issues in Infectious Disease
R. Fears et al.
European policy strategies can guide the scientific community to improve the translational medicine environment.

SCIENCESIGNALING
Global view of the cell cycle phosphoproteome.

RESEARCH ARTICLE: Uncovering Residual Effects of Chronic Sleep Loss on Human Performance
D. A. Cohen et al.
Sleep loss may be lost forever.

RESEARCH ARTICLE: Intermittent Prophylaxis with Oral Truvada Protects Macaques from Rectal SHIV Infection
J. G. Garcia-Lerma et al.
Treating monkeys with an antiretroviral drug before and after exposure to SHIV provides protection against infection.

SCIENCEPODCAST
www.sciencemag.org/multimedia/podcast
Free Weekly Show
Download the 15 January *Science* Podcast to hear about a carbon capture catalyst, parasitoid wasp diversity, innate immunity, and more.

SCIENCEINSIDER
blogs.sciencemag.org/scienceinsider
Science Policy News and Analysis

SCIENCE (ISSN 0036-8075) is published weekly on Friday, except the last week in December, by the American Association for the Advancement of Science, 1200 New York Avenue, NW, Washington, DC 20005. Periodicals Mail postage (publication No. 484460) paid at Washington, DC, and additional mailing offices. Domestic individual membership and subscription (51 issues): $146 ($74 allocated to subscription). Domestic institutional subscription (51 issues): $910; Foreign postage extra: Mexico, Caribbean (surface mail) $55; other countries (air assist delivery) $85. First class, airmail, student, and emeritus rates on request. Canadian rates with GST available upon request, GST #1254 88122. Publications Mail Agreement Number 1069624. **Printed in the U.S.A.**

Change of address: Allow 4 weeks, giving old and new addresses and 8-digit account number. **Postmaster:** Send change of address to AAAS, P.O. Box 96178, Washington, DC 20090–6178. **Single-copy sales:** $10.00 current issue, $15.00 back issue prepaid includes surface postage; bulk rates on request. **Authorization to photocopy** material for internal or personal use under circumstances not falling within the fair use provisions of the Copyright Act is granted by AAAS to libraries and other users registered with the Copyright Clearance Center (CCC) Transactional Reporting Service, provided that $20.00 per article is paid directly to CCC, 222 Rosewood Drive, Danvers, MA 01923. The identification code for *Science* is 0036-8075. *Science* is indexed in the *Reader's Guide to Periodical Literature* and in several specialized indexes.

AAAS
ADVANCING SCIENCE, SERVING SOCIETY

CREDIT: M. L. MILLER, C. KUMAR, AND J. V. OLSEN/MAX PLANCK INST. FOR BIOCHEM. (J. V. O., C. K.); UNIV. OF COPENHAGEN (J. V. O., M. L. M.); LILLY SINGAPORE CENTRE FOR DRUG DISCOVERY (C. K.); MEMORIAL SLOAN-KETTERING CANCER CENTER (M. L. M.)

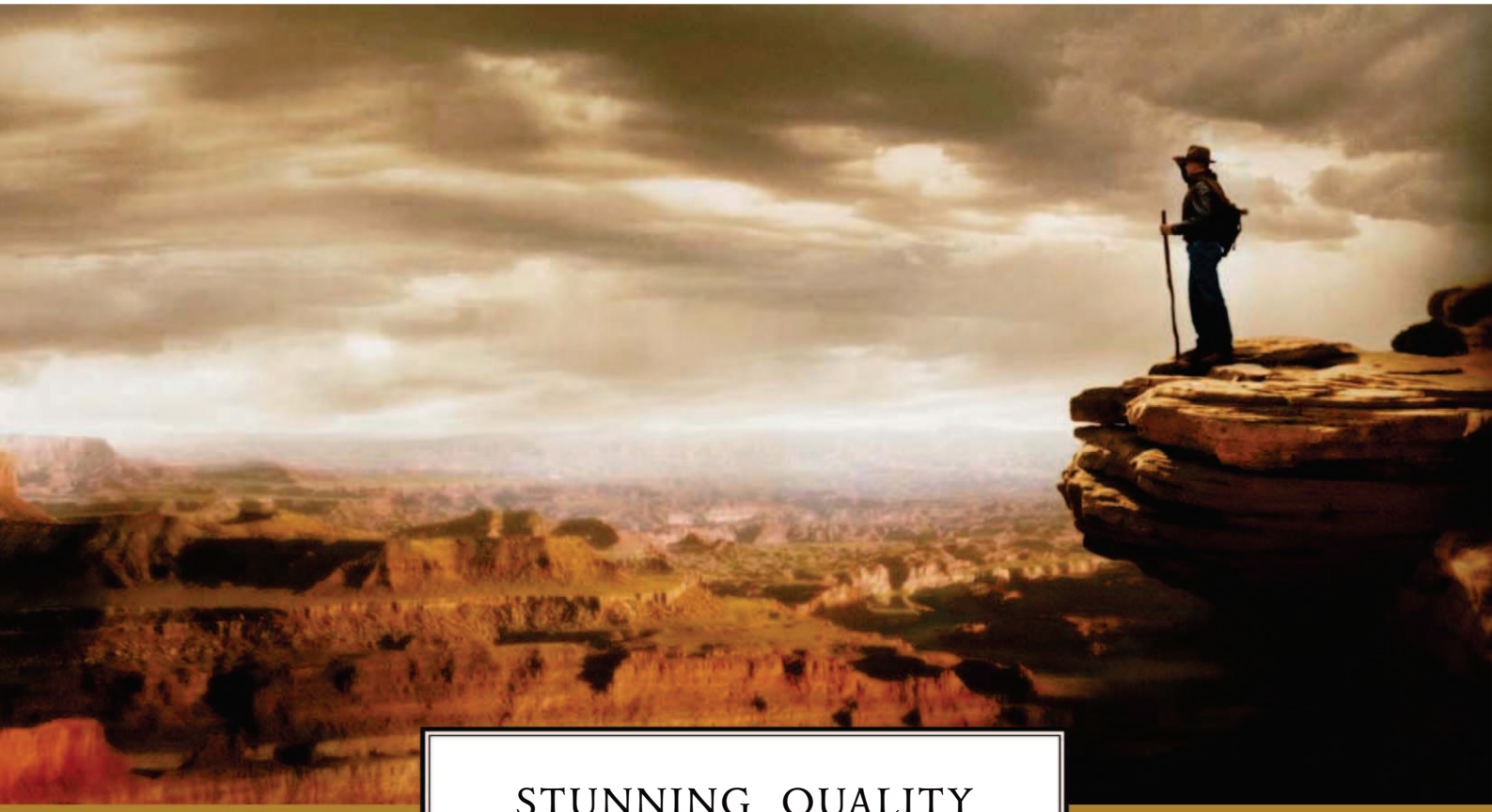

STUNNING QUALITY

Reagents for Sample Preparation from New England Biolabs

Introducing NEBNext™, a series of highly pure reagents that facilitate sample preparation for downstream applications such as next generation sequencing and expression library construction. Available in sets, master mixes and modules, these robust reagents undergo stringent quality controls and functional validation, ensuring maximum yield, convenience and value.

Sequencing coverage map of the *E. coli* genome after using NEBNext™ DNA Sample Prep Reagent Set 1 for Sample Preparation

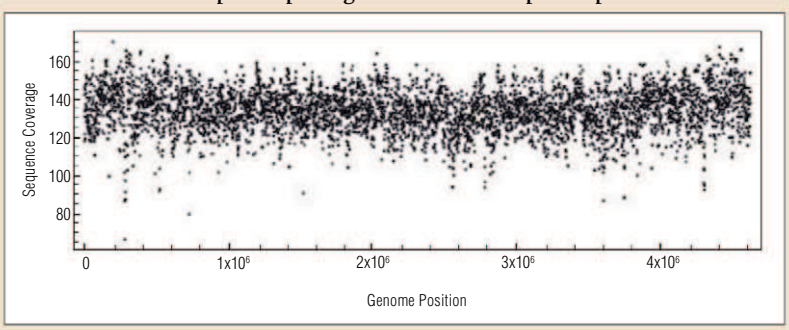

E. coli strain MG1655 gDNA was prepared with NEBNext DNA Sample Prep Reagent Set I and sequenced on an Illumina Genome Analyzer II.

For more information about NEBNext, including customized solutions, please contact NEBNext@neb.com.

Now available:
NEBNext™ dsDNA Fragmentase™
an enzyme-based solution for the fragmentation of DNA

CELEBRATING 35 YEARS
NEW ENGLAND BioLabs® Inc.
enabling technologies in the life sciences

CLONING & MAPPING	**DNA AMPLIFICATION & PCR**	RNA ANALYSIS	PROTEIN EXPRESSION & ANALYSIS	GENE EXPRESSION & CELLULAR ANALYSIS

www.neb.com

EDITED BY STELLA HURTLEY

Parasitoid Wasp Genomes

Parasitoid wasps, which prey on and reproduce in host insect species, play important roles in plant herbivore interactions, and may provide valuable tools in the biological control of pest species. **The *Nasonia* Genome Working Group** (p. 343; see the news story by **Pennisi**) presents the genome of three very closely related species: *Nasonia vitripennis, N. girault,* and *N. longicornis*. The findings document rapid evolution between a host and endosymbiont that can cause nuclear-cytoplasmic incompatibilities that may affect speciation.

Adaptive Girdle Loss in Sticklebacks

How do molecular changes give rise to phenotypic adaptation exemplified by the repeated reduction in the pelvic girdle observed in separate populations of sticklebacks? Now **Chan *et al.*** (p. 302, published online 10 December) have identified the specific DNA changes that control this major skeletal adaptation. The key locus controlling pelvic phenotypes mapped to a noncoding regulatory region upstream of the *Pituitary homeobox transcription factor 1* gene, which drives a tissue-specific pelvic enhancer. Multiple populations showed independent deletions in this region and enhancer function was inactivated. Reintroduction of the enhancer restored pelvic development in a pelvic-reduced stickleback.

Planetary Midwifery

Planets form from the materials left behind after a star is formed. Unlike the Sun, most stars are members of binary systems. **Mayama *et al.*** (p. 306, published online 19 November) present an infrared image of the protoplanetary disks around a young binary star system taken with the coronagraph mounted on the Subaru Telescope in Hawaii. Each individual disk is clearly visible around its star, and comparison with numerical simulations suggests that there could be gas flow from one disk to the other. The nature of this potential gas flow is important in determining where planets could form in binary systems.

It's the Network

Numerous reactions of small molecules and ions in the atmosphere take place in the confines of watery aerosols. **Relph *et al.*** (p. 308; see the Perspective by **Siefermann and Abel**) explored the specific influence of a water cluster's geometry on the transformation of solvated nitrosonium (NO^+) to nitrous acid (HONO). The reaction involves (O)N–O(H) bond formation with one water molecule, concomitant with proton transfer to additional, surrounding water molecules. Vibrational spectroscopy and theoretical simulations suggest that certain arrangements of the surrounding water network are much more effective than others in accommodating this charge transfer, and thus facilitating the reaction.

Heck of an Alternative

The Mizoroki-Heck reaction is widely used in organic synthesis to link together unsaturated carbon fragments such as olefins and arenes. However, one of its drawbacks is the need to append a reactive group such as a halogen to one of the reagents beforehand. **Wang *et al.*** (p. 315, published online 26 November) present an alternative palladium-catalyzed reaction that links olefins directly to aryl acids. Oxygen added to the reaction medium concurrently oxidizes the aryl C-H bond at the linkage site, eliminating the need for prior halogenation. Introducing amino acid–derived ligands tunes the aryl site at which the reaction takes place, and efficient reactivity can be achieved across a diverse range of substrates.

Measuring Methanogenesis

After carbon dioxide, methane is the second most important greenhouse gas, and an important species in terms of its role in atmospheric chemistry. The sources and sinks of methane, particularly the natural ones, are too poorly quantified, however, even to explain why the decades-long, steady increase of its concentration in the atmosphere was interrupted between 1999 and 2006. **Bloom *et al.*** (p. 322) use a combination of satellite data, which indicate water table depth and surface temperature, and atmospheric methane concentrations to determine the location and strength of methane emissions from wetlands, the largest natural global source. The constraints placed on these sources should help to improve predictions of how climate change will affect wetland emissions of methane.

Methanol Coupling Catalyzed with Gold

Gold surfaces can be effective catalysts for partial oxidation reactions, in part because lower interaction strengths of molecules absorbed on gold allow products to desorb before further unwanted oxidations occur. One challenge in these reactions is the low rate of formation of reactive atomic surface oxygen. **Wittstock *et al.*** (p. 319; see the Perspective by **Christensen and Nørskov**) created high–surface area gold catalysts by leaching silver from gold-silver alloys. This material proved to be an effective catalyst for partial oxidative coupling of methanol, yielding methyl formate. Residual silver appears to play a key role in activating the dissociation of molecular oxygen.

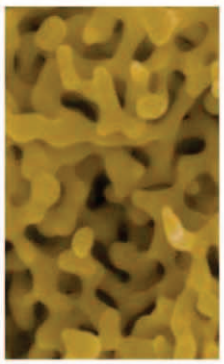

Predator Avoidance Strategy

Selective pressures influencing bird migration can include availability of food, pressure from parasites and pathogens, and predation risk. The importance of the last of these is revealed by **McKinnon *et al.*** (p. 326; see the Perspective by **Gilg and Yoccoz**), who present an experimental analysis of the benefits of long-distance migration for reproduction in arctic-nesting birds. Measurements of a controlled effect of predation risk along a 3350-kilometer north-south gradient across arctic Canada provides evidence that the risk of nest predation decreases with latitude. Thus, birds migrating further north may acquire reproductive benefits in the form of reduced predation risk.

Continued on page 248

This Week in *Science*

Continued from page 247

Targeting Copper Clusters

Tetrathiomolybdate (TM) is a copper-depleting agent that has potential in treating copper-dependent diseases. **Alvarez *et al.*** (p. 331, published online 26 November) used spectroscopic and structural studies to show that TM inhibits the yeast copper chaperone Atx1 by forming a TM-Cu-ATx1 complex that is stabilized by a sulfur-bridged copper-molybdenum cluster. Cluster formation prevents transfer of copper from the chaperone to target enzymes. The results provide a basis for developing drugs that target metallation pathways.

To Stall or Not to Stall

Recent studies in mammals and *Drosophila* have shown that RNA polymerase II frequently stalls shortly after initiating messenger RNA synthesis and that this stalling is important for proper expression of genes. Although several protein factors that affect polymerase stalling are known, the role of DNA sequence in this process has remained unclear. Now **Nechaev *et al.*** (p. 335, published online 10 December) report that the initially transcribed sequences of many genes contain a signal that works like a stop sign for the elongating polymerase. Expression of genes may thus be regulated by a combination of a DNA signal that induces promoter-proximal stalling and protein factors that alter its duration.

Alligator Breath

Birds have a unidirectional system of airflow within their lungs that has been attributed to the peculiarities of flight. However, **Farmer and Sanders** (p. 338) provide evidence that this unidirectional and more or less continuous flow of air also occurs through parts of the alligator lung; in contrast to the tidal, biphasic system in mammals. By analyzing lung and tracheal structures, the similarities of the alligator lungs were compared with those of birds. The data suggest that the unusual properties of bird lungs originated before the divergence of the alligator line from the dinosaur or avian line.

The Art of *Artemisia*

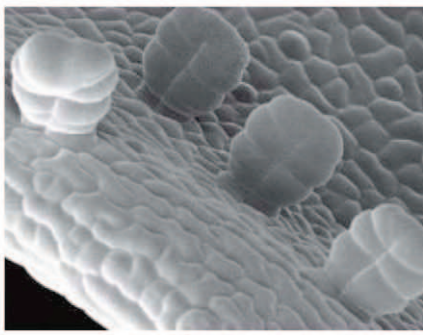

As the malaria parasite, which is transmitted through mosquito vectors, develops resistance, previously useful control mechanisms are beginning to fail. Combination therapies based on the plant product artemisinin are a promising alternative. **Graham *et al.*** (p. 328; see the Perspective by **Milhous and Weina**) have now developed a genetic map of the plant *Artemisia annua* from which artemisinin is derived. The results lay the foundation for improving agricultural productivity of this natural product, which is becoming increasingly important in the fight against malaria.

Integrin G Protein

Adhesion molecules, known as integrins, are found on the surface of cells. When integrins adhere to components of the extracellular matrix, they act as receptors and initiate signaling events within the cell. **Gong *et al.*** (p. 340) show that they do so in part by partnering with a signal-transducing protein called $G\alpha_{13}$. Such α subunits of heterotrimeric guanine nucleotide-binding proteins are well known for transducing signals from the large class of G protein–coupled receptors, but were not known to work with integrins. $G\alpha_{13}$ appears to interact directly with the integrin $\alpha_{IIb}\beta_3$ and to transmit signals that regulate cell spreading.

Behavioral Profiling

The complexity of the brain makes it difficult to predict how a drug will affect behavior without direct testing in live animals. **Rihel *et al.*** (p. 348) developed a high-throughput assay to assess the effects of thousands of drugs on sleep/wake behaviors of zebrafish larvae. The data set reveals a broad conservation of zebrafish and mammalian sleep/wake pharmacology and identifies pathways that regulate sleep. Moreover, the biological targets of poorly characterized small molecules can be predicted by matching their behavioral profiles to those of well-known drugs. Thus, behavioral profiling in zebrafish offers a cost-effective way to characterize neuroactive drugs and to predict biological targets of novel compounds.

CREDIT: THE CNAP ARTEMISIA RESEARCH PROJECT

Paul G. Thomas is an Assistant Member in the Department of Immunology at St. Jude Children's Research Hospital in Memphis, TN. E-mail: Paul.Thomas@STJUDE.ORG.

Peter C. Doherty is the Michael F. Tamer Chair of Biomedical Research in the Department of Immunology at St. Jude Children's Research Hospital in Memphis, TN, and a Laureate Professor in the Department of Microbiology and Immunology, University of Melbourne, Australia. He received the Nobel Prize in Physiology and Medicine in 1996. E-mail: Peter.Doherty@STJUDE.ORG.

New Approaches in Immunotherapy

THE PAST DECADE OF RESEARCH ON THE IMMUNE SYSTEM HAS SEEN AN INCREDIBLE EXPANSION OF knowledge in the area of innate immunity. Analysis over the preceding years had focused largely on how T and B cells orchestrate immune responses to specific pathogens, and how their memory of these encounters confers long-lasting protection. In contrast to these specific "adaptive" mechanisms, innate immunity is driven by a plethora of proteins produced by a wide range of cells throughout the body, and it provides immediate broad-spectrum responses to foreign invaders. This new understanding of innate immunity is providing insights into host reactions to noninfectious diseases such as cancer, to antigen-independent inflammatory conditions such as periodic fever syndromes, and to the inflammatory modulation of basic cellular metabolic processes. As this special issue on innate immunity points out (p. 283), ongoing research to further characterize this complex response system has great potential for identifying new therapies to treat human disease.

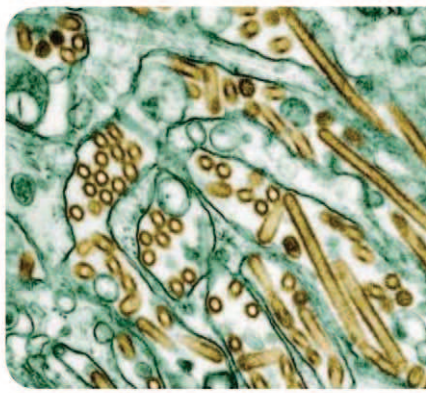

Three major families of molecules function in innate recognition and are a focus of the special issue: the Toll-like receptors, the RIG-I–like receptors, and the Nod-like receptors. Most is known about the first two types, which have important roles in recognizing viral and bacterial components. The Nod-like receptor family—the largest and most diverse of the three—has many unresolved features. Much of the focus has been on this family's functional association with the inflammasome, a scaffold of proteins that triggers specific inflammation pathways and cell death. But there is growing evidence that this represents only one aspect of Nod-like receptor activity, and analyses of their actions in other inflammatory pathways will probably lead to important new insights.

A feature of all three molecular families is that, despite wide upstream divergences, multiple signals tend to converge on shared, downstream effector signaling pathways. To date, relatively little is known about how responses are nevertheless adjusted to appropriately match the diversity of upstream pathogen recognition events. Research on the regulation of pathways controlled by the RIG-I–like receptors has been promising in this respect. But an important goal, essential for the design of next-generation adjuvants, is to develop a thorough understanding of how all these innate immune signaling pathways are modulated to produce qualitatively different outputs in response to different types of threats. This knowledge is also likely to advance our understanding of immune dysregulation and hyperactivation, such as that producing the "cytokine storm" implicated in the deaths of individuals infected with the H5N1 influenza virus.

We now know that the first responders to pathogens are often the infected (or bystander) host epithelial and endothelial cells, rather than the arsenal of "professional" innate immune cells (macrophages and dendritic cells). These "nonimmune" host cells can potentially express members of all three innate recognition receptor families, and activation of the signaling pathways that they control results in the secretion of chemokines that recruit and activate the antimicrobial programs of adaptive responders. In parallel, nonimmune host cells alter key components of their own biology and metabolism to subvert and contain intracellular pathogens.

Detailing the relationship between innate immune recognition and host cell metabolism remains an important priority, as these physiological perturbations are likely to affect organ-level function. Thus, for example, although influenza infection may be cleared by the adaptive immune response or controlled by drugs, an individual may still succumb to severe lung damage, either as a direct consequence of viral insult or from the associated inflammatory response. Similarly, as we look more closely at the interplay between injured coronary tissue and the monocytes and macrophages that contribute to arterial plaque formation in cardiovascular disease, it becomes clear that expanding the scope of innate immunity research to include the entire diversity of cells in an organism is a major priority for molecular medicine. **– Paul G. Thomas and Peter C. Doherty**

10.1126/science.1186704

EDITED BY GILBERT CHIN AND JAKE YESTON

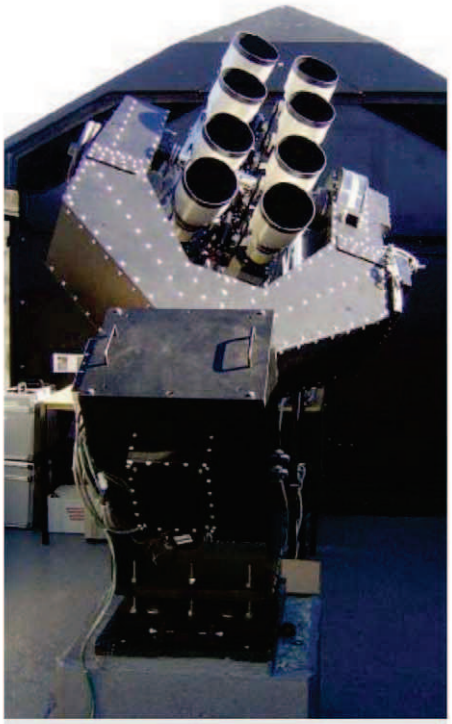

ASTRONOMY

Too Close for Comfort

More than 400 planets have been detected orbiting stars other than the Sun, often with properties radically different from those of the planets in our solar system. Many, termed 'hot Jupiters,' have a mass similar to or exceeding that of Jupiter but orbit much closer to their host stars. Researchers believe that these planets could not have formed so close to the stars, and so must have formed at larger distances and then migrated to their present positions. Some are dangerously close to their host stars and may ultimately spiral into them. Such is the case with WASP-19b, the planet with the shortest period yet detected. Its period is only 0.79 days and its mass and radius are 1.15 and 1.31 those of Jupiter. The data collected by Hebb *et al.* using the WASP-South telescope suggest that WASP-19b has been spiraling into its host star throughout its lifetime and has spun up the star in the process. The processes that end the inward migration of planets are not well understood. WASP-19b may contribute to our understanding of the evolution of close-in planets and may provide information about the properties of its host star. — MJC

Astrophys. J. **708**, 224 (2010).

PHYSICS

Clocking Single Photons

Quantum information processing requires a protocol for transferring data between memories comprising atomic energy states. Light, in the form of single photons, is the natural candidate for such applications: Photons can couple to the atomic memories, move fast, and remain relatively robust against noise. Though generating single photons is not a big problem, generating them on demand is. Melholt Nielsen *et al.* demonstrate a technique based on a modification of spontaneous parametric down-conversion, wherein two entangled photons are generated in a nonlinear optical crystal, and one of the photons is heralded by the detection of the other. Although such a process is usually stochastic, the authors show that by pumping an optical parametric oscillator under certain conditions, they can control the generation of single photons deterministically. The quality and properties of the heralded single photons, as well as the inherent tunability of the process, should make it simpler to implement quantum information protocols. — ISO

Opt. Lett. **34**, 3872 (2009).

GENETICS

Individual Differences

RNA splicing serves to stitch together the protein-coding regions of genes while snipping out the intervening noncoding sequences. As a consequence, RNAs may differ if the splicing machinery chooses one set of regions over an alternative set, and the resulting protein isoforms may vary in a genetically determined way. In a study of the amount of alternative splicing in humans, Coulombe-Huntington *et al.* have found that over 70% of genes show genetically controlled splice site usage that varied across individuals, and in some cases, they were able to identify the single-nucleotide polymorphism responsible. Understanding the underlying causes of variation in protein levels and isoforms may help to explain the genetic determination of phenotypic diversity. — LMZ

PLoS Genet. **5**, e1000766 (2009).

IMMUNOLOGY

Taking a Peek

Our bodies are covered by epithelial layers inside and out, which keeps the outside out and the inside in. How then can the immune system, which sits inside the wall of epithelial cells, sense potentially pathogenic antigens without making holes in this protective barrier? Kubo *et al*. show that during inflammation, epidermal Langerhans cells acquire external antigens by extending cellular protrusions, known as dendrites, through the tight seals between keratinocytes in the skin. Receptors on the tips of the dendrites bind to external antigens, which are then internalized and

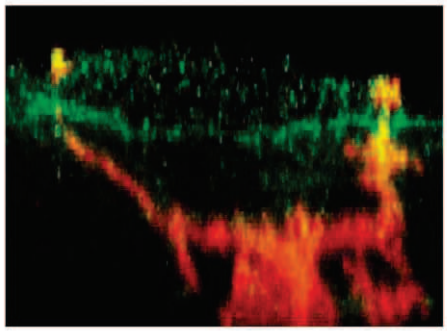

Langerhans cell (red) punctures tight junction (green).

brought inward to the cell body for further processing. In order to maintain the seal despite breaching the tight junctions, the Langerhans cells form secondary junctions with the surrounding keratinocytes. This ability to screen incoming antigens provides an important first defense against attack. — SMH

J. Exp. Med. **206**, 2937 (2009).

MOLECULAR BIOLOGY

Activation from Within

The protein complexes that wrap DNA come in two flavors: core histones and variant histones. Although the H2A histone variant MacroH2A1 is known for its role in repressing transcription in the context of X chromosome inactivation, Gamble *et al.* describe an activating effect of this factor on autosomal gene expression. They have used chromatin immunoprecipitation and genomic tiling arrays (ChIP-chip) to map the distribution of MacroH2A1 in human primary fibroblasts and a breast cancer cell. MacroH2A1 associates with large chromatin domains (greater than 500 kb) with boundaries near transcription start sites; when MacroH2A1 sits within a transcribed region, repression is often the result, but some genes, such as those involved in responding to serum starvation, are instead protected from silencing. — BAP

Genes Dev. **24**, 21 (2010).

CREDITS: (LEFT) DAVID R. ANDERSON, SUPERWASP; (RIGHT) KUBO *ET AL., J. EXP. MED.* **206**, 2937 (2009)

www.sciencemag.org

Science

1200 New York Avenue, NW
Washington, DC 20005
Editorial: 202-326-6550, FAX 202-289-7562
News: 202-326-6581, FAX 202-371-9227
Bateman House, 82-88 Hills Road
Cambridge, UK CB2 1LQ
+44 (0) 1223 326500, FAX +44 (0) 1223 326501

Subscription Services For change of address, missing issues, new orders and renewals, and payment questions: 866-434-AAAS (2227) or 202-326-6417, FAX 202-842-1065. Mailing addresses: AAAS, P.O. Box 96178, Washington, DC 20090-6178 or AAAS Member Services, 1200 New York Avenue, NW, Washington, DC 20005

Institutional Site Licenses please call 202-326-6755 for any questions or information

Reprints: Author Inquiries 800-635-7181
Commercial Inquiries 803-359-4578

Permissions 202-326-7074, FAX 202-682-0816

Member Benefits AAAS/Barnes&Noble.com bookstore www.aaas.org/bn; AAAS Online Store www.apisource.com/aaas/ code MKB6; AAAS Travels: Betchart Expeditions 800-252-4910; Apple Store www.apple.com/eppstore/aaas; Bank of America MasterCard 1-800-833-6262 priority code FAA3YU; Cold Spring Harbor Laboratory Press Publications www.cshlpress.com/affiliates/aaas.htm; GEICO Auto Insurance www.geico.com/landingpage/go51.htm?logo=17624; Hertz 800-654-2200 CDP#343457; Office Depot https://bsd.officedepot.com/portalLogin.do; Seabury & Smith Life Insurance 800-424-9883; Subaru VIP Program 202-326-6417; VIP Moving Services www.vipmayflower.com/domestic/index.html; Other Benefits: AAAS Member Services 202-326-6417 or www.aaasmember.org.

science_editors@aaas.org	(for general editorial queries)
science_letters@aaas.org	(for queries about letters)
science_reviews@aaas.org	(for returning manuscript reviews)
science_bookrevs@aaas.org	(for book review queries)

Published by the American Association for the Advancement of Science (AAAS), *Science* serves its readers as a forum for the presentation and discussion of important issues related to the advancement of science, including the presentation of minority or conflicting points of view, rather than by publishing only material on which a consensus has been reached. Accordingly, all articles published in *Science*—including editorials, news and comment, and book reviews—are signed and reflect the individual views of the authors and not official points of view adopted by AAAS or the institutions with which the authors are affiliated.

AAAS was founded in 1848 and incorporated in 1874. Its mission is to advance science, engineering, and innovation throughout the world for the benefit of all people. The goals of the association are to: enhance communication among scientists, engineers, and the public; promote and defend the integrity of science and its use; strengthen support for the science and technology enterprise; provide a voice for science on societal issues; promote the responsible use of science in public policy; strengthen and diversify the science and technology workforce; foster education in science and technology for everyone; increase public engagement with science and technology; and advance international cooperation in science.

Information for Authors
See pages 352 and 353 of the 15 January 2010 issue or access www.sciencemag.org/about/authors

EDITOR-IN-CHIEF **Bruce Alberts**
EXECUTIVE EDITOR **Monica M. Bradford**
NEWS EDITOR **Colin Norman**
MANAGING EDITOR, RESEARCH JOURNALS **Katrina L. Kelner**
DEPUTY EDITORS **R. Brooks Hanson, Barbara R. Jasny, Andrew M. Sugden**

Editorial senior editors/commentary Lisa D. Chong, Brad Wible; **senior editors** Gilbert J. Chin, Pamela J. Hines, Paula A. Kiberstis (Boston), Marc S. Lavine (Toronto), Beverly A. Purnell, L. Bryan Ray, Guy Riddihough, H. Jesse Smith, Phillip D. Szuromi (Tennessee), Valda Vinson, Jake S. Yeston; **associate editors** Kristen L. Mueller, Jelena Stajic, Nicholas S. Wigginton, Laura M. Zahn; **research associate** Alexis Wynne Mogul; **online editor** Stewart Wills; **associate online editors** Robert Frederick, Tara S. Marathe; **web content developers** Martyn Green, Andrew Whitesell; **book review editor** Sherman J. Suter; **associate letters editor** Jennifer Sills; **editorial manager** Cara Tate; **senior copy editors** Jeffrey E. Cook, Cynthia Howe, Harry Jach, Barbara P. Ordway, Trista Wagoner; **copy editors** Chris Filiatreau, Lauren Kmec; **editorial coordinators** Carolyn Kyle, Beverly Shields; **publications assistants** Ramatoulaye Diop, Joi S. Granger, Jeffrey Hearn, Lisa Johnson, Scott Miller, Jerry Richardson, Jennifer A. Seibert, Brian White, Anita Wynn; **editorial assistants** Emily Guise, Michael Hicks, Patricia M. Moore, Miriam Weinberg; **executive assistant** Sylvia S. Kihara; **administrative support** Maryrose Madrid; **editorial fellow** Melissa R. McCartney

News deputy news editors Robert Coontz, Eliot Marshall, Jeffrey Mervis, Leslie Roberts; **contributing editors** Elizabeth Culotta, Polly Shulman; **news writers** Yudhijit Bhattacharjee, Adrian Cho, Jennifer Couzin, David Grimm, Constance Holden, Jocelyn Kaiser, Sam Kean, Richard A. Kerr, Eli Kintisch, Greg Miller, Elizabeth Pennisi, Robert F. Service (Pacific NW), Erik Stokstad, Jue Wang; **intern** Lauren Schenkman; **contributing correspondents** Jon Cohen (San Diego, CA), Daniel Ferber, Ann Gibbons, Robert Koenig, Andrew Lawler, Mitch Leslie, Charles C. Mann, Virginia Morell, Gary Taubes; **copy editors** Linda B. Felaco, Melvin Gatling, Melissa Raimondi; **administrative support** Scherraine Mack; **bureaus** San Diego, CA: 760-942-3252, FAX 760-942-4979; Pacific Northwest: 503-963-1940

Production director James Landry; **senior manager** Wendy K. Shank; **assistant manager** Rebecca Doshi; **senior specialists** Steve Forrester, Chris Redwood; **specialist** Anthony Rosen; **Preflight director** David M. Tompkins; **manager** Marcus Spiegler; **specialist** Jason Hillman

Art director Yael Kats; **associate art director** Laura Creveling; **senior illustrators** Chris Bickel, Katharine Sutliff; **illustrator** Yana Greenman; **senior art associates** Holly Bishop, Preston Huey, Nayomi Kevitiyagala; **art associates** Jessica Newfield, Matthew Twombly; **photo editor** Leslie Blizard

***Science* International**

Europe (science@science-int.co.uk) **editorial: international managing editor** Andrew M. Sugden; **senior editor/commentary** Julia Fahrenkamp-Uppenbrink; **senior editors** Caroline Ash, Stella M. Hurtley, Ian S. Osborne, Peter Stern; **associate editor** Maria Cruz; **locum editor** Helen Pickersgill; **editorial support** Deborah Dennison, Rachel Roberts, Alice Whaley; **administrative support** John Cannell, Janet Clements, Louise Moore; **news: europe news editor** John Travis; **deputy news editor** Daniel Clery; **contributing correspondents** Michael Balter (Paris), John Bohannon (Vienna), Martin Enserink (Amsterdam and Paris), Gretchen Vogel (Berlin)

Latin America contributing correspondent Antonio Regalado

Asia Japan Office: Asca Corporation, Tomoko Furusawa, Rustic Bldg. 7F, 77 Tenjin-cho, Shinjuku-ku, Tokyo 162-0808, Japan; +81 3 6802 4616, FAX +81 3 6802 4615, inquiry@sciencemag.jp; **asia news editor** Richard Stone (Beijing: rstone@aaas.org); **contributing correspondents** Dennis Normile [Japan: +81 (0) 3 3391 0630, FAX +81 (0) 3 5936 3531; dnormile@gol.com]; Hao Xin [China: +86 (0) 10 6307 4439 or 6307 3676, FAX +86 (0) 10 6307 4358; cindyhao@gmail.com]; Pallava Bagla [South Asia: +91 (0) 11 2271 2896; pbagla@vsnl.com]

EXECUTIVE PUBLISHER **Alan I. Leshner**
PUBLISHER **Beth Rosner**

Fulfillment Systems and Operations (membership@aaas.org); **director** Waylon Butler; **senior systems analyst** Nomuna Nyamaa; **customer service supervisor** Pat Butler; **specialists** Latoya Casteel, LaVonda Crawford, Vicki Linton, April Marshall; **data entry supervisor** Cynthia Johnson; **specialists** Shirlene Hall, Tarrika Hill, William Jones

Business Operations and Administration director Deborah Rivera-Wienhold; **assistant director, business operations** Randy Yi; **manager, business analysis** Eric Knott; **manager, business operations** Jessica Tierney; **financial analysts** Priti Pamnani, Celeste Troxler; **rights and permissions: administrator** Emilie David; **associate** Elizabeth Sandler;

marketing director Ian King; **marketing managers** Allison Pritchard, Alison Chandler, Julianne Wielga; **marketing associates** AimeeAponte, MaryEllen Crowley, Wendy Wise; **marketing executive** Jennifer Reeves;

director, site licensing Tom Ryan; **director, corporate relations** Eileen Bernadette Moran; **publisher relations, eresources specialist** Kiki Forsythe; **senior publisher relations specialist** Catherine Holland;

publisher relations, east coast Phillip Smith; **publisher relations, west coast** Philip Tsolakidis; **fulfillment supervisor** Iquo Edim; **fulfillment coordinator** Carrie MacDonald; **marketing manager** Christina Schlecht;

marketing associate Mary Lagnaoui; **electronic media: manager** Lizabeth Harman; **project manager** Trista Snyder; **assistant manager** Lisa Stanford; **senior production specialists** Ryan Atkins, Christopher Coleman, Walter Jones; **production specialists** Nichele Johnston, Kimberly Oster;

director, web and new media Will Collins

advertising director, worldwide ad sales Bill Moran
commercial editor Sean Sanders: 202-326-6430
project director, outreach Brianna Blaser

Product (science_advertising@aaas.org); **midwest/w. canada** Rick Bongiovanni: 330-405-7080, FAX 330-405-7081; **east coast/e. canada** Laurie Faraday: 508-747-9395, FAX 617-507-8189;
west coast Lynne Stickrod: 415-931-9782, FAX 415-520-6940;
uk/europe/asia japan Roger Goncalves: TEL/FAX +41 43 243 1358; ASCA Corporation, Nanako Ide +81 (0) 3 6802 4616, FAX +81 (0) 3 6802 4615; ads@sciencemag.jp; **senior traffic associate** Deiandra Simms

worldwide associate director of *Science* Careers Tracy Holmes: +44 (0) 1223 326525, FAX +44 (0) 1223 326532

AAAS
ADVANCING SCIENCE, SERVING SOCIETY

Easy as Pi

A French computer programmer has announced a new record for approximating π—this time on a desktop computer. Fabrice Bellard of Télécom Paris Tech took 103 days to compute 2.7 trillion digits and another 28 days to check the result. Bellard has thus toppled the previous record of 2.577 trillion digits, set last August by Daisuke Takahashi at the University of Tsukuba in Japan. That feat only took 29 hours. But, Bellard points out in a press release, previous modern π champs used multimillion-euro computers; his PC cost less than €2000.

Reefs of the Future

Giant barrel sponges, sometimes called "redwoods of the deep" because of their great size and age, are burgeoning on the reefs of the Florida Keys, scientists report. Sponges compete with corals, which have been dying from disease and environmental changes, says marine biologist Joseph Pawlik of the University of North Carolina, Wilmington, a co-author of a paper on sponge demographics appearing in next month's issue of *Ecology*. Unlike corals, sponges produce no calcium carbonate and are not affected by ocean acidification, he says: "That means [Caribbean] coral reefs are actually going to be sponge reefs in the future."

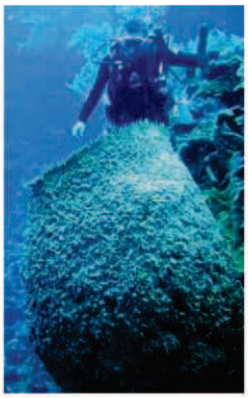

Bruegel's Statistical Signature

Beauty may be in the eye of the beholder, but a painting's authenticity may be encoded in patterns a computer can detect. To show that, mathematician Daniel Rockmore and colleagues at Dartmouth College applied a technique from neuroscience called sparse coding to analyze digitized gray-scale images of 16th century paintings by Pieter Bruegel the Elder and imitations of his work.

They fed tiny square patches of the images through an algorithm to modify and "train" a different set of squares that started out randomly shaded. The trained squares could then be superimposed on each other to reconstruct any patch from a painting. Crucially, the algorithm patterned the squares so that a few would suffice to reproduce a patch from a real Bruegel. If the team trained the patterns using any seven of eight real Bruegels, then, on average, the number needed to recreate a random patch from the eighth was smaller than the number needed to fit a patch from any of five fakes (with one exception). So the scheme distinguishes real Bruegels from fakes, the team reported last week online in the *Proceedings of the National Academy of Sciences*.

The technique would be "just one tool" to help determine a painting's authenticity, Rockmore cautions. James Coddington, chief conservator at the Museum of Modern Art in New York City, says its real utility may lie in comparing the works of one or several artists. "Ask the art historians—is it telling us something that we already knew, or is it giving us new food for thought?"

CREDITS (TOP TO BOTTOM): AP PHOTO; JOSEPH PAWLIK, UNC WILMINGTON; MET

ENGINEERS AND MUJAHIDEEN

The fact that Christmas Day would-be bomber Umar Farouk Abdulmutallab (whose "operation" is celebrated in the above poster) has a degree in mechanical engineering has drawn fresh attention to a controversial study linking engineers with terrorism.

In October 2007, sociologist Diego Gambetta of the University of Oxford and political scientist Steffen Hertog of Sciences Po in Paris caused a stir with "Engineers of Jihad," a paper that analyzed the known membership of extremist organizations since World War II. They concluded that right-wing groups and violent Islamist groups had attracted almost four times as many engineers as would be expected by chance. (Leftist groups, by contrast, were almost engineer-free.) The terrorists weren't recruiting engineers for their technical skills, Gambetta and Hertog concluded. Instead, they speculated, engineers' personal traits—such as preferences for clear-cut solutions to problems and tendencies toward political and religious conservatism—and poor employment prospects in much of the Middle East make them riper-than-average candidates for radicalization. The pair fleshed out their thesis in a paper in the August 2009 *European Journal of Sociology*.

Now the blogosphere is abuzz again, and Gambetta and Hertog say they are working on a book—amplified with new data that coalition forces have captured in Iraq. William Wulf, former president of the U.S. National Academy of Engineering, doesn't buy any of it. "The sample size is so small that … I just don't believe" their conclusion, he says. "This is really bad science." Terrorism expert Thomas Hegghammer of the Institute for Advanced Study in Princeton, New Jersey, disagrees. He says the authors "convincingly demonstrate" the disproportionate presence of engineers in jihad groups and commends them for breaking the "taboo" on studying "the role of innate cognitive features on political behavior."

The earliest galaxies
258

The amazing parasitic wasp menagerie
260

VIROLOGY

An Indefatigable Debate Over Chronic Fatigue Syndrome

Here we go again. The search for the cause of chronic fatigue syndrome, which just months ago seemed to be gaining traction, now seems likely to descend into the same confusion and acrimony that characterized it for years, as a supposed viral link to CFS published just last autumn might be unraveling.

Many patients with CFS—long-term fatigue and other ailments that have no known biological cause—report that their symptoms began after an acute viral infection, and scientists have tried many times, but never successfully, to pin CFS to viruses such as Epstein-Barr. Patients have faced skepticism for years over whether CFS is a "real" disease; a viral trigger could vindicate them and explain their nebulous symptoms.

Null results. A team led by Myra McClure (*left*, with a student) found no evidence of a retrovirus, XMRV, in chronic fatigue syndrome patients, which contradicts the research of Vincent Lombardi and Judy Mikovits (*right*).

That's why a paper published online 8 October 2009 in *Science* (http://www.sciencemag.org/cgi/content/abstract/1179052) caused such a stir. A U.S. team reported finding DNA traces of a virus, XMRV, in the blood cells of two-thirds of 101 patients with CFS, compared with 4% of 218 healthy controls. Strangely, XMRV, a rodent retrovirus, had previously been implicated in an aggressive prostate cancer. No one knows how XMRV might contribute to either or both diseases, but the authors argued that the link made some sense: XMRV ravishes natural killer blood cells, which attack both tumors and cells infected by viruses.

Other scientists thought the link dubious, criticizing the team, led by Vincent Lombardi and Judy Mikovits at the Whittemore Peterson Institute for Neuro-Immune Disease in Reno, Nevada, for not explaining enough about the demographics of their patients or the procedures to prevent contamination (*Science*, 9 October 2009, p. 215). Several virologists around the world practically sprinted to their labs to redo the experiments, and the discovery that a clinic associated with some people at Whittemore was selling, among other CFS services, a $650 diagnostic test for XMRV made the issue more pressing. A U.K. team already exploring the XMRV–prostate cancer link won the race, submitting a paper to *PLoS ONE* challenging the claim on 1 December 2009. It was accepted for publication after 3 days of review.

The British team, led by retrovirologist Myra McClure of Imperial College London, examined DNA from the blood of 186 CFS patients ranging in age from 19 to 70, with an average age of 40. Most were markedly unwell. McClure's team used a PCR machine—which copies and amplifies scraps of DNA—to search for two viral sequences, one from XMRV and the other from a closely related virus. They discovered nothing. At a press conference discussing the results, published online 6 January in *PLoS ONE*, McClure was blunt and confident: "If there was one copy of the virus in those samples, we would have detected it."

This null result prompts the question of what—if anything—was wrong with the original paper. The *PLoS ONE* authors seem to suggest that contamination was at fault, stating that they were careful to work in labs that had never handled XMRV and use PCR machines that analyze no mouse tissues. But McClure says her group merely wanted to make that explicit, not accuse anyone.

The U.S. team followed the same procedures, retorts Lombardi, a biochemist. He also expressed bewilderment that the McClure group didn't search its CFS samples for the same DNA sequence as his team had, raising the possibility that they had different results because they searched for different things. The McClure team, however, looked for not only an XMRV sequence but also a sequence in a closely related virus, MLV. That MLV sequence, highly conserved among viruses of its class, would presumably have been found if XMRV was present, they said.

One distinct possibility, says John Coffin, a microbiologist at Tufts University in Boston who studies retroviruses and wrote a separate analysis for *Science* when the original paper was published (http://www.sciencemag.org/cgi/content/short/1181349), is that both papers are right. He called the *PLoS ONE* paper too "preliminary" to settle the debate and said XMRV could show more genetic variety, and thus be harder to detect, than anyone assumed. It's also possible that distinct strains of XMRV appear in different parts of the world, as do the retroviruses HIV and HTLV (a leukemia virus). Intriguingly, although research teams in the United States have linked XMRV to prostate cancer, multiple teams in Germany and Ireland have failed to find a connection.

Coffin says one more possibility, raised by many scientists, is that CFS is actually a suite of diseases that present the same symptoms and so might have many causes. Lombardi agrees. "It's naïve to think that everyone with chronic fatigue has the same etiology. There's probably going to be a subset of people with CFS that have XMRV, and it will probably end up being classified as XMRV-related CFS."

All of this leaves doctors and patients in a

CREDITS (LEFT TO RIGHT): © IMPERIAL COLLEGE LONDON/DAVE GUTTRIDGE; DAVID B. PARKER/*RENO GAZETTE-JOURNAL*

Alaskan gold mine sparks a dispute
263

Q's but few A's in Q-fever outbreak
266

muddle. There's no doubt they're hungry for information. Out of curiosity, Lombardi did a Google search on "XMRV" the day before the *Science* paper hit and found about 22,500 hits. Three months later, there are 400,000.

But some scientists, including Coffin and McClure, fear that the Viral Immune Pathology Diagnostics clinic (VIP Dx) took advantage of that hunger by offering the $650 diagnostic test for XMRV, 300 of which have been administered so far and which already has a 4 to 6 week backlog. "Leaving aside the issue of who's right and who's wrong," says Coffin, "the original paper did not establish the virus [caused CFS] and didn't establish it as a viable marker." So it's not clear what a patient or physician could do with a positive result.

Steve Kaye, a colleague of McClure's at Imperial College London and a co-author of the *PLoS ONE* paper, noted with some alarm that the authors of the *Science* paper had speculated about treating XMRV with antiretroviral drugs, which can have harsh side effects.

However, VIP Dx developed its XMRV test only after a different company began offering one; VIP Dx officials saw their test as a more expert alternative. What's more, Lombardi—an unpaid consultant for VIP Dx who helped set up and manage the testing program—argues that the test is useful. Patients could in theory avoid infecting other people with XMRV and can have their diagnoses validated, if nothing else. His test results also bolster the science in the original paper; he says 36% of tests have detected XMRV, including a few from the United Kingdom. (Test proceeds roll back into research and development at Whittemore, which licenses the test to VIP Dx. VIP Dx has also received financial support from the Whittemore family in the past.)

To resolve the dispute, both sides say they are willing to work with the other and possibly test each other's samples. In the meantime, more papers exploring the link are slated to appear in the next few months, and each side says it knows of work supporting its results. All that suggests that the field will continue to churn. As McClure told *Science*, "we take no pleasure in finding colleagues wrong or dashing the hopes of patients, but it's imperative the truth gets out." **–SAM KEAN**

ARCHAEOLOGY

Neandertal Jewelry Shows Their Symbolic Smarts

Neandertals had big brains and were skilled hunters, but their sites reveal few objets d'art. So some researchers have suggested that Neandertals weren't cognitively up to the job of producing art and symbols, although a growing number disagree. Now a handful of marine mollusk shells, possibly used as necklaces and paint cups, shows that Neandertals did express themselves symbolically, say the authors of a paper published online this week in the *Proceedings of the National Academy of Sciences*. They argue that the findings suggest that social and demographic factors, rather than cognitive differences, best explain why so-called modern behavior was relatively rare among Neandertals. The paper suggests that "Neandertals too had such [symbolic] capacities," says archaeologist John Speth of the University of Michigan, Ann Arbor.

The shells were found in the Aviones cave and the Antón rock shelter in southeast Spain, both identified as Neandertal sites from their ages and stone tools. Radiocarbon dating of shells at Aviones puts the Neandertal occupation there at between 45,000 and 50,000 years ago—before modern humans entered the area—and charcoal at Antón came out at between 37,000 and 43,000 years old.

An international team led by archaeologist João Zilhão of the University of Bristol in the United Kingdom examined three cockleshells from Aviones that were perforated near their hinges and were found alongside lumps of yellow and red pigments. A fourth, unperforated, thorny oyster shell contained residues of red and black pigments and was perhaps used as a paint container, the team says. At Antón, a perforated scallop shell was painted on its external side with a blend of orange pigments, perhaps to make the shell's outside resemble its naturally red inside surface. Zilhão's team concludes that although the perforations were not humanmade, Neandertals selected shells with holes of 4.5 to 6.5 millimeters, ideal for stringing as ornaments.

"The authors make a good case" that the shells and pigments were used in "an aesthetic and presumably symbolic" way, says archaeologist Erella Hovers of The Hebrew University of Jerusalem. Hovers cites similar finds from Israel's ▶

Signs of symbolism. Neandertal perforated shells, some painted (*right*), suggest artistic expression.

Qafzeh Cave, which was occupied by modern humans as early as 92,000 years ago and where perforated cockleshells and red ochre pigments have been widely accepted as evidence of modern human behavior.

Although signs of Neandertal symbolism are rare, ornaments become more common at Neandertal sites when modern humans arrive in Europe about 40,000 years ago, leading some to argue that the Neandertals copied modern human symbolic behavior rather than inventing it themselves.

But as the older perforated shells suggest, that does not mean Neandertals were not capable of creating symbols, Speth says. "The assumption [has been] that when you first see symbolic media such as ornaments, that's the first time humans had the mental wherewithal to make them. By that logic, humans lacked the cognitive capacities necessary to invent the atomic bomb until World War II. That is obviously nonsense."

So why are ornaments plentiful at modern human sites and rare at Neandertal ones? Social and demographic factors, Zilhão and others say. In this view the Neandertals, with relatively low population densities, may have lacked the widespread social networks that required symbolic communication within and among population groups. Early humans engaged in symbolic behavior only "when it was advantageous," says Hovers, and when "populations were stable enough over time to keep these canons and traditions alive."

–MICHAEL BALTER

ACADEMIC FACILITIES

NIST Grants Help Schools Build for Tomorrow's Research

Habib Dagher, a structural engineer at the University of Maine, Orono, wants to replace the heating oil that warms most Maine homes with a cheaper, renewable fuel—electricity generated by wind turbines 30 km offshore in the Gulf of Maine. To withstand the punishing ocean conditions, the 100-meter turbines would be made from a polymer composite, stiffened by cellulose fibers, created by researchers at the university's Advanced Structures and Composites Center he directs. But researchers need more lab space to design, prototype, and test the unique building material.

In the wind. Researchers at Maine's Advanced Structures and Composites Center are getting a new lab to test offshore wind-turbine blades.

CREDIT: UNIVERSITY OF MAINE

Fortunately for the center, Dagher not only thinks green but also knows where to find the green. Last week, the center learned it was one of 12 winners in the second and final round of a $180 million competitive construction grants program at the National Institute of Standards and Technology (NIST). The $12.4 million NIST grant, combined with $5 million from the state of Maine, will allow Dagher to build the Advanced Nanocomposites in Renewable Energy Laboratory at the center. The center has received a $5 million earmark inserted into the Department of Energy's 2010 budget by the state's congressional delegation, and it's part of a consortium that won a $7 million grant in October from DOE to test the offshore wind turbines. In addition, Dagher hopes that Maine voters will approve a $6 million bond issue this summer to equip the new lab.

The NIST program is a small component of the $787 billion stimulus package designed to revive the U.S. economy (*Science*, 27 November 2009, p. 1176). Aimed at funding "shovel-ready" projects such as the nanocomposites lab, the grants address a gap in the federal government's academic research portfolio, which traditionally has favored supporting scientists over bricks and mortar. "This is the hardest type of money to get," says Dagher. "And without the NIST grant, the whole project would have been slowed down considerably."

The NIST competition attracted 167 proposals from universities clamoring for help in funding new construction during tough economic times. (A smaller competition in 2008 chose three winners from 93 proposals, and in July, NIST gave $55 million in stimulus money to four institutions that had just missed the cut.) The new facilities are intended to enhance the mission of either NIST or the National Oceanic and Atmospheric Administration (NOAA), its sister agency within the Commerce Department. The federal dollars leverage money already on the table: The $123 million allocated last week will make possible more than $250 million in new laboratory construction.

The University of Pittsburgh in Pennsylvania, for example, had already committed $12.7 million toward 13 new physics laboratories, part of a 12-year strategic plan, and the $15 million NIST grant gives it a green light to proceed. "Without this grant, I don't know how many years it would have taken us" to complete the project, says N. John Cooper, dean of arts and sciences. Despite an overall 5% spending cut this year that has slowed hiring, Cooper says the NIST grant "positions us to be more competitive when the upturn comes."

For the Woods Hole Oceanographic Institution (WHOI) in Massachusetts, an $8.1 million award for a laboratory for ocean sensors and observing systems will help it do a better job as a major contractor for a project supported by the National Science Foundation (NSF). The Ocean Observatories Initiative (OOI) will deploy networks of sensors to collect long-term data from the sea floor (*Science*, 16 November 2007, p. 1056), and Laurence Madin, WHOI's executive vice president and director of research, explains that "once we got the NSF award, we realized that we needed a special facility to do everything that OOI would require." Although WHOI has received NOAA funding for many years, says Madin, "this is actually our first NIST award."

Some of the NIST construction funding will help improve construction practices themselves. An $11.8 million NIST grant to build the Center for High-Performance Buildings will allow Purdue University scientists to reconfigure office space to maximize comfort, safety, and energy efficiency, says James Braun, a professor of mechanical engineering. The new lab space, he adds, may even boost the team's application, now pending at NSF, for an Engineering Research Center on the topic.

–JEFFREY MERVIS

CHEMISTRY

Catalyst Offers New Hope for Capturing CO_2 on the Cheap

If international agreements can't slash carbon dioxide emissions fast enough to tame global warming, how about sucking it out of the air? Technology using chemicals that bind CO_2 already exists, but it's so expensive that using it on a large scale could increase energy demand—and the cost of energy—by at least one-third.

On page 313, however, researchers in the Netherlands report a new copper-based catalyst that can capture CO_2, convert it to a different form, and then release it with a small fraction of the energy other techniques require. "This is an important fundamental advance," says William Tolman, an inorganic chemist at the University of Minnesota, Twin Cities. "But there's a long way to go before you could turn it into a catalytic process" for reducing atmospheric CO_2, he adds.

The new method targets the step that so far has proved to be the Achilles' heel of air capture: prying the trapped CO_2 loose so the capture compound can be used again. Various processes do that through heat, electricity, or changes in air pressure, all of which require a lot of energy.

Researchers led by Elisabeth Bouwman, a chemist at Leiden University in the Netherlands, hit on a possible way to lower the penalty while working on a very different problem: designing small metal-containing organic compounds to mimic the behavior of an enzyme called superoxide dismutase. In living organisms, the enzyme neutralizes superoxide, a reactive form of oxygen that is generated inside cells and that can damage DNA.

One copper-containing candidate compound surprised them. Instead of oxygen, it bound carbon dioxide by stitching two CO_2 molecules together into a compound known as oxalate. X-ray crystallography showed that two pairs of the carbon complexes join together in a single unit to knit four CO_2 molecules into two oxalates (see figure). Kenneth Karlin, an inorganic chemist at Johns Hopkins University in Baltimore, Maryland, who has worked on related compounds, says the new catalyst's ability to selectively bind CO_2 and cause it to react is impressive. "This is amazing," he says.

Bouwman's group also worked out a way to regenerate the starting copper complex so that it could be used again. They simply added a lithium salt to their solution. The lithium swipes the oxalate from the copper complex, creating lithium oxalate. Then applying a very small voltage of –0.03 volts to the copper complex restores it to its original form. Adding an electron directly to CO_2—the first step in converting CO_2 into more complex, and useful, molecules—would require –2 volts, Bouwman says.

Bouwman acknowledges that the new CO_2 catalyst isn't yet ready to become a bona fide air-capture technology. It works too slowly, and the lithium salt is too expensive. Bouwman says transferring the oxalate to a cheaper chemical shouldn't be difficult, and her group is already working to improve the catalyst's reaction rate.

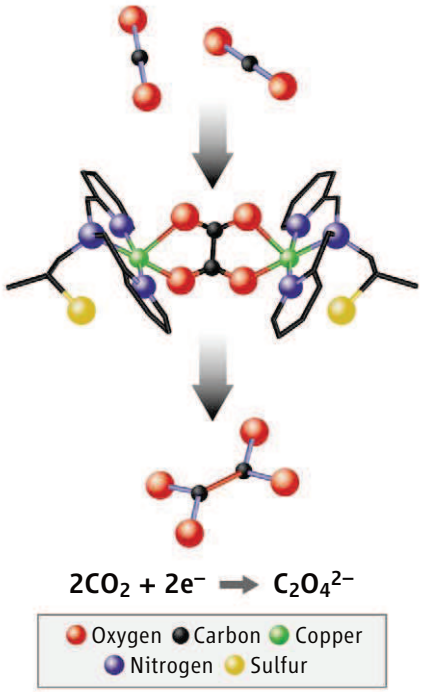

Gotcha. Probing the inner workings of an enzyme, chemists discovered a catalyst that binds to pairs of CO_2 molecules (*top*), knitting them together to form oxalate (*middle*), which is later released (*above*).

Ultimately, if a CO_2 air-capture technology is to be realistic on a large scale, the cost and energy requirements must come down, says Andrew Dessler, a climate scientist at Texas A&M University in College Station. "Air capture could be viable, but not unless research like this gets the energy requirement way down from where we are now," Dessler says. "So this kind of research is very exciting."

–ROBERT F. SERVICE

CREDITS (TOP TO BOTTOM): D. VIGEARS/C2RMF; ADAPTED FROM E. BOUWMAN, UNIVERSITY OF LEIDEN

ScienceNOW.org

From *Science*'s Online Daily News Site

Egyptian Eyeliner May Have Warded Off Disease
Clearly, ancient Egyptians didn't get the memo about lead poisoning. Their eye makeup was full of the stuff. Although today we know that lead can cause brain damage and miscarriages, the Egyptians believed that lead-based cosmetics protected against eye diseases. Now, new research suggests that they may have been on to something. http://bit.ly/egypteyes

Why Light Makes Migraines Worse
Migraine sufferers often retreat to a dark room or pull the shades down. Any light just makes the searing pain worse. Now, scientists think they know why—thanks to some help from blind volunteers. http://bit.ly/lightmigraines

Bering Strait's Ups and Downs Alter Climate
The Bering Strait, the 80-kilometer-wide stretch of ocean between Russia and Alaska, can strongly influence the climate of the entire Northern Hemisphere, researchers have calculated. The findings answer a question that has dogged scientists for the past decade, and they demonstrate how seemingly slight changes in certain factors can impact global climate. http://bit.ly/bearingstrait

The Spiky Penis Gets the Girl
When it came to insect penises, Charles Darwin had it right. The famed naturalist suspected that insect genitalia, which are frequently festooned with bizarre combinations of hooks, spines, and knobs, essentially functioned like peacock tails. That is, they helped males beat out their rivals for females. Now, researchers have confirmed this hypothesis by zapping fly penises with a laser. http://bit.ly/penislaser

Read the full postings, comments, and more on **sciencenow.sciencemag.org**.

ASTRONOMY

Oldest Galaxies Show Stars Came Together in a Hurry

Sifting through images taken by the newly refurbished Hubble Space Telescope, astronomers have spotted five galaxies that date back to a mere 600 million years after the big bang—the earliest galaxies found so far by 200 million years. The discoveries take researchers close to the primordial stage of cosmic evolution, when the first galaxies were taking shape.

Astronomers have already learned a few things about the newly discovered galaxies. For one, they are tiny compared with contemporary galaxies—barely 5% the size of the Milky Way and less than 1% its mass. "These are the seeds of the great galaxies of today," says Garth Illingworth of the University of California, Santa Cruz, who presented the findings at the American Astronomical Society meeting in Washington, D.C., last week.* Illingworth led the survey team that took the new images using Wide Field Camera 3, one of two new instruments mounted on Hubble in a servicing mission last year.

Another striking fact about the galaxies is that they are populated by stars that had already been burning for 300 million years. That pushes back the birth of the earliest stars of the universe to within a few hundred million years of the big bang—a blink of an eye in astronomical time.

Volker Bromm, an astrophysicist at the University of Texas, Austin, says the new galaxies "clearly demonstrate the hierarchical nature of structure formation—small objects formed first—and provide interesting constraints for early star formation."

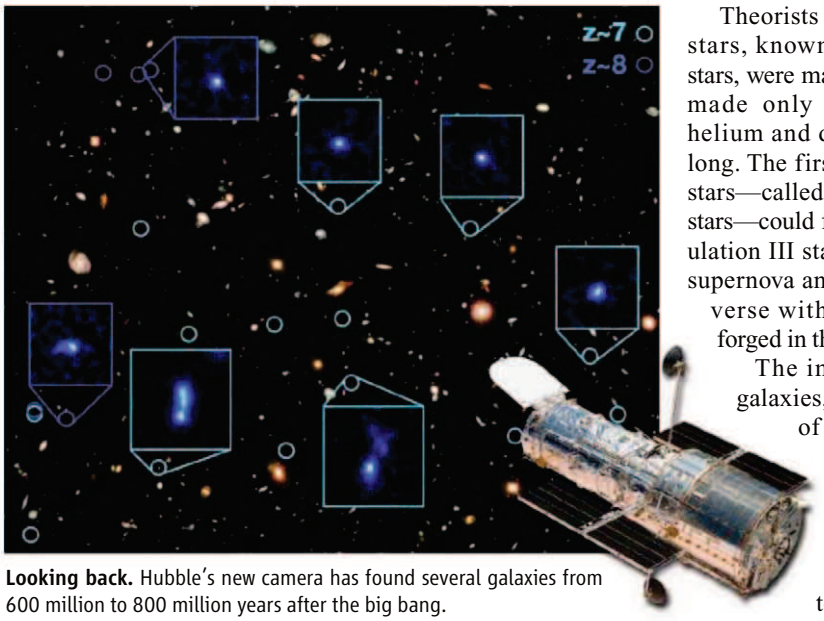

Looking back. Hubble's new camera has found several galaxies from 600 million to 800 million years after the big bang.

Theorists think the very first stars, known as Population III stars, were massive stellar objects made only of hydrogen and helium and didn't live for very long. The first normal low-mass stars—called Population II and I stars—could form only after Population III stars had exploded as supernova and enriched the universe with heavier elements forged in the process.

The imaging of the new galaxies, with the discovery of Population I and II stars within them, implies that "the transition in cosmic star formation mode, from Pop III to Pop I and II, took place quickly, in dark-matter systems that were even smaller" than the refurbished Hubble can see, Bromm says. He adds that the "true moment of first light remains elusive, and its discovery has to await the James Webb Space Telescope"—planned for launch in 2014.

In addition to Illingworth's team, four research groups have reported similar findings from their analyses of the new Hubble data. **–YUDHIJIT BHATTACHARJEE**

*215th AAS Meeting, Washington, D.C., 3–7 January.

CREDITS: NASA, ESA, G. ILLINGWORTH, R. BOUWENS (UNIVERSITY OF CALIFORNIA, SANTA CRUZ), AND THE HUDF09 TEAM; (INSET) COURTESY NASA

ASTRONOMY

Inventory Asks: Where Is All the *Non*-Dark Matter Hiding?

Astrophysicists know that 83% of the matter in the universe is dark matter—invisible stuff as yet undetected. The other 17% is detectable "baryonic matter," the atoms and ions that make up stars, planets, dust, and gas. To astronomers' surprise, the ratio of baryonic matter to dark matter seems to vary from galaxy to galaxy like the ratio of chocolate chips to dough in different batches of home-baked cookies. Now, a team led by Stacy McGaugh at the University of Maryland, College Park, has determined that the proportion varies by scale: The largest galaxies have the highest percentage of baryonic matter, although not quite 17%; whereas the smallest galaxies have less than 1%.

McGaugh and colleagues compiled the ratios for more than 100 galaxies ranging from supermassive ones to dwarfs. Researchers infer the amount of dark matter in a galaxy from the motion of its stars. They estimate its baryonic mass from the amount of light the galaxy emits, which can be converted to the total mass of its stars, and a measure of atomic hydrogen in the galaxy, which provides an estimate of the interstellar gas.

"What we find is that there is a very systematic variation in the ratio with scale," says McGaugh, who presented the findings at the American Astronomical Society meeting in Washington, D.C., last week.* "When you go to the very large galaxies, the baryonic matter can be as much as 14%. As you go down in size, you see that galaxies fall short of the cosmic fraction [17:83] by an ever-increasing amount." In galaxies the size of the Milky Way, "all the stars and gas add up to only a third of the baryonic matter you would expect," which is about 5%. And in the smallest dwarfs, baryonic matter is a hundredth of what's expected—as minuscule as 0.2%. "These are very interesting results" that quantify the "missing baryonic matter problem," says Joel Bregman, an astronomer at the University of Michigan, Ann Arbor.

Where is all the missing baryonic matter lurking? One hypothesis is that its particles are interspersed within the galaxy's dark matter halo in the form of undetectable hot gas. Another is that supernova explosions have blown it into intergalactic space. This second idea would square with McGaugh's findings: Large galaxies, with stronger gravitational pulls, would be able to retain more of their baryonic matter, whereas smaller galaxies would let more escape. But so far, McGaugh says, that explanation is just one of several lines of speculation. **–YUDHIJIT BHATTACHARJEE**

*215th AAS Meeting, Washington, D.C., 3–7 January.

PUBLISHING

White House Mulls Plan to Broaden Access to Published Papers

Should all papers that result from U.S. taxpayer–funded research be made freely available? The White House science office likes the idea and has asked for input on whether many federal agencies should formally adopt it. So-called open access advocates are enthusiastic in comments submitted to a White House forum, but some scientific societies remain wary, fearing that a too-broad public-access policy could kill journal subscriptions.

Both sides agree that the White House appears to be moving toward a plan. "They're focusing not on should we do this but how would we do this," says Heather Joseph, executive director of the Scholarly Publishing and Academic Resources Coalition, a librarian group and open-access proponent.

The push for mandatory release of research papers started 2 years ago at the National Institutes of Health, which required that grantees send copies of their peer-reviewed, accepted papers to the agency. NIH posts the final manuscripts or published papers in its free PubMedCentral archive; release can be delayed on request up to 12 months after publication. The objective has been to give patients and the public broader access to research results. Despite grumbling from publishers, NIH says the policy is working smoothly.

Last month, as part of President Barack Obama's "open government" activities, the Office of Science and Technology Policy (OSTP) launched an online discussion about whether the NIH model should be expanded to other agencies. The OSTP forum asks nine questions, including how to ensure that authors comply.

About 400 comments have been submitted so far from scores of individual scientists, librarians, publishers, and others. The majority support broadening public access, says OSTP Assistant Director of Life Sciences Diane DiEuliis, a neuroscientist on detail from NIH. "There was a fair consensus on the general issue," she told *Science* by e-mail, as well as on other questions, such as "embargo times": how long an author and journal can keep a paper under private control. Many suggested using the current NIH embargo—12 months—and preferred central repositories like PubMedCentral rather than university archives.

But even a 12-month delay worries some nonprofit scientific publishers. For example, mineralogists and anthropologists argued that their papers—unlike those in biomedical research—may have a very long "half life" and that releasing the full text on the Internet could cause journals to lose subscribers. Katherine McCarter of the Ecological Society of America, which has not yet submitted comments, says that for ecology journals, "even a 1-year delay could be a real disincentive to buy a subscription."

The cost of producing a single paper can run significantly higher in social sciences because papers need more space and require a "more robust peer-review process," argues William E. Davis III, executive director of the American Anthropological Association. His letter warns that mandatory release of such papers "could well result in the demise of the very journals that … advocates seek to make more freely available."

> ***Mandatory release of social science papers "could well result in the demise of the very journals that … advocates seek to make more freely available."***
>
> **—WILLIAM E. DAVIS III, THE AMERICAN ANTHROPOLOGICAL ASSOCIATION**

Despite such concerns, OSTP seems to be moving inexorably toward a general open-access policy. DiEuliis says OSTP will sort through all comments (the deadline has been extended until 21 January) and send suggestions to an interagency working group. This panel will also consider a report due this week from a group of publishers and other stakeholders that OSTP and the House Science Committee convened last June. One possibility, DiEuliis says, is that OSTP could draft an executive order or memo that would set out "minimum standards" but "give agencies flexibility to create custom plans."

–JOCELYN KAISER

ScienceInsider

From the *Science* Policy Blog

The director of the **Royal Institution of Great Britain**, the London-based science institution, has been dismissed and her position eliminated in what appears to be a cost-saving move. But neuroscientist Susan Greenfield, who has held the job for more than 10 years, says she is considering a legal challenge, possibly including discrimination charges, to her dismissal. http://bit.ly/4Hk4wS

The White House has released a much-awaited report on strengthening **U.S. biosecurity rules**. Instead of applying the same security standards to all so-called select agents, the report recommends a stratified system that would toughen security for the most hazardous agents and ease rules for less dangerous ones. That's the approach, favored by many scientists, that lawmakers envisioned in a bill introduced in the U.S. Senate last fall. http://bit.ly/4JYlM7

The U.K. House of Lords Science and Technology Committee says there's no evidence that **foods containing nanometer-scale particles**—dubbed nanofoods—constitute a danger to consumers. In the new report, the committee said that nanofoods nonetheless deserve scrutiny, citing "huge gaps" in current knowledge. In addition, "we urge the European Commission to clarify the definition of a nanoparticle in the context of food," said committee chair John Krebs. http://bit.ly/7SQeQ7

Senior Democratic lawmaker Byron Dorgan (D–SD) has decided not to seek reelection this year. Insider analyzed his record as "Cardinal" of the Senate subcommittee that controls **Department of Energy funding**. Some lobbyists have claimed that Dorgan has emphasized nuclear waste cleanup or water projects at the expense of basic physical science research, but under his 3-year tenure, research and development spending at DOE has risen. The subcommittee's staff clerk, who wields considerable influence, is appointed by the Appropriations Committee chair and is likely to be staying on. http://bit.ly/5I0Wn4

For the full postings and more, go to **blogs.sciencemag.org/scienceinsider**.

The Little Wasp That Could

The sequencing of the genome of a parasitoid wasp promises to bring wider recognition to these tiny, underappreciated insects

Lab rat. *Nasonia vitripennis* lays eggs in a fly pupa through an ovipositor emerging from her abdomen. Sequences of *N. vitripennis* and two related species are being published this week.

THE BRITISH GENETICIST J. B. S. HALDANE once famously quipped that God seems to have had an inordinate fondness for beetles, given their numbers and diversity. If so, then he must have been besotted by parasitoid wasps. Tinkerbells of the animal kingdom, many of these insects are no bigger than fleas, yet they may well outnumber beetles.

Unlike beetles, however, parasitoid wasps aren't exactly charismatic. "You get one in your eye and pull it out with your finger and think it's a piece of dust," says Daniel Janzen, an ecologist at the University of Pennsylvania. "There's millions of individuals out there, and you don't even know they exist." Yet these inconspicuous insects play a crucial role in natural ecosystems and in agriculture. They destroy the eggs, larvae, or cocoons of countless species of insects and arthropods, sometimes with hugely beneficial effects: The U.S. Department of Agriculture (USDA) estimates that parasitic wasps save the United States at least $20 billion annually by controlling invasive species. "I think very few people realize what a force they are in the biology of our planet," says Michael Strand, an entomologist at the University of Georgia, Athens.

Scientists, on the other hand, have long appreciated their attributes. The wasps' unusual genetic makeup has made one a lab favorite—"yeast with wings," says John Werren, an evolutionary geneticist at the University of Rochester in New York state. Entomologists are fascinated by the wasps' sometimes bizarre life histories, and ecologists have recently come to recognize their astonishing diversity. Now, their scientific value is about to increase: On page 343 of this issue, a 157-person consortium presents the genome sequence of three parasitoid wasps, members of the genus *Nasonia*, which attack flies. The genome "not only solidifies *Nasonia*'s standing as the lead model organism for the vast insect order Hymenoptera but [also] brings it on par with traditional heavyweights such as *C. elegans* and *Drosophila*," says William Sullivan of the University of California (UC), Santa Cruz.

Online
sciencemag.org
Podcast interview with author Elizabeth Pennisi.

Beetles, stand aside!

Janzen first started noticing parasitoid wasps when they played havoc with his studies of Lepidoptera in Costa Rica. Since the early 1980s, he has been collecting caterpillars and raising them to adulthood to see which butterfly or moth they belonged to. All too often the caterpillar would turn to mush, and out of it would emerge parasitoid wasp larvae. But, fanatic collector that he was, Janzen saved these tiny insects and documented their food source. Each year, he would take them to a wasp expert for identification. Two decades later, his inventory totals about 20,000 wasps, and his awareness of how common they are has grown exponentially.

They don't just prey on moth and butterfly caterpillars. Adult females lay eggs in or on the eggs, larvae, or pupae of many insects and arthropods, on which the wasp larvae feed. Some can lay 200 eggs in one caterpillar; others inject a single egg that divides many times to give rise to separate, cloned larvae. Sometimes, the larval wasps can sit quietly in the caterpillar, evading the immune system, until their host has fattened up, then they eat it from the inside out in a matter of days.

Several species treat their insect host as a nest and set up a social hierarchy to defend it. All nestmates are clones, but only some developing embryos inherit germ cells. The sterile clones become soldiers and help protect larvae destined to become reproductive adults from other parasites, says Strand.

Parasitoid wasps have intimate connections with microbial partners as well. Many wasps are infected with the bacterium *Wolbachia*, which can skew the sex ratio of offspring. Others carry a "male-killing" microbe that eliminates males in a developing brood. Some have even co-evolved with a virus that a female injects into a caterpillar along

CREDIT: PETER KOOMEN AND COMPOSED BY MATHIJS ZWIER/EVOLUTIONARY GENETICS, UNIVERSITY OF GRONINGEN, THE NETHERLANDS

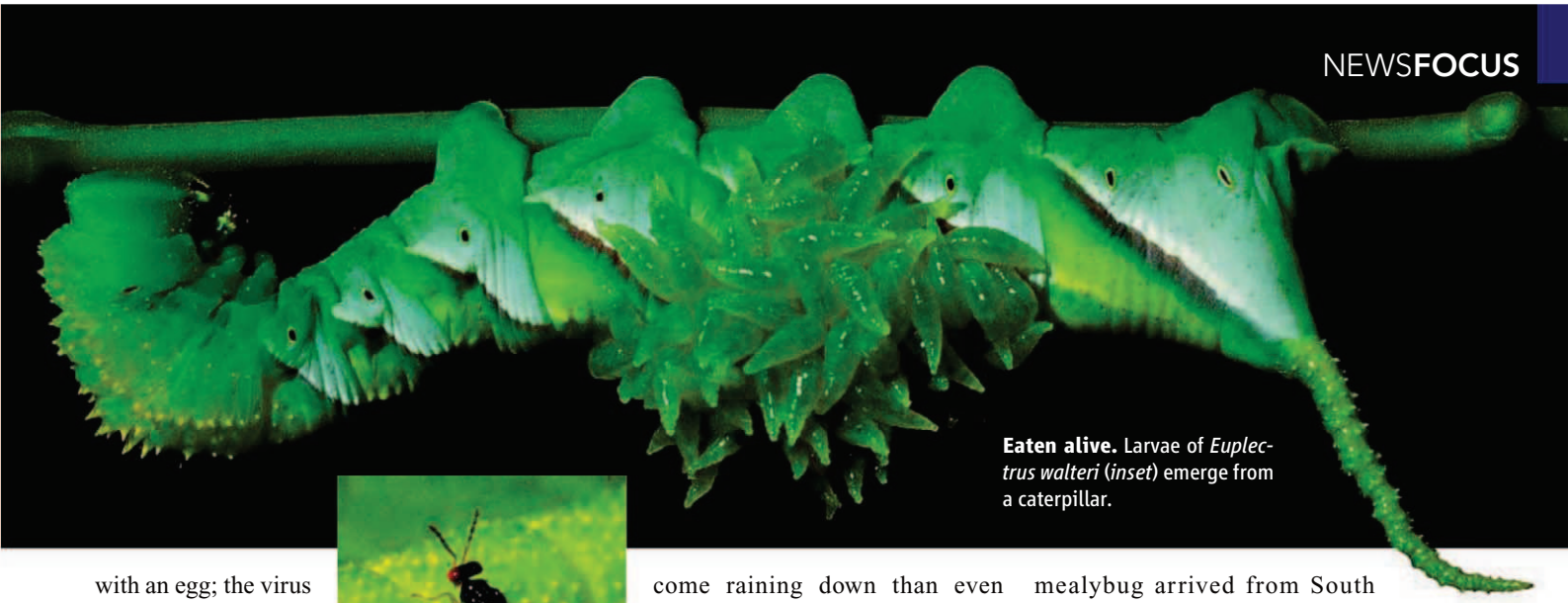

Eaten alive. Larvae of *Euplectrus walteri* (*inset*) emerge from a caterpillar.

with an egg; the virus disarms the caterpillar's immune system. These viruses are now part of the wasps' DNA. "The diversity of life histories of [these insects] is hair-raising," says Strand.

These tiny wasps may have diverse lifestyles, but many tend to look alike. Even experts have trouble identifying which species individuals belong to. So when DNA bar-coding was just getting started and its proponents were looking for groups of animals on which to try this short-hand species-identification tool, Janzen volunteered his collections. There turned out to be "a lot more species out there than we realized," says Janzen.

A 2008 DNA bar-coding analysis of 2597 parasitoid wasps from his collection turned up 313 species, not the 171 researchers had previously thought. M. Alex Smith of the University of Guelph in Canada and Josephine Rodriguez of UC Santa Barbara discovered that what was believed to be a single species—a 2-millimeter-long wasp called *Apanteles leucostigmus* with a black body and a white rhomboid patch on its wing—proved to be 36. And there were many more examples of previously unrecognized species, Janzen, Rodriguez, Smith, and their colleagues reported in the 26 August 2008 issue of the *Proceedings of the National Academy of Sciences*.

Between 50,000 and 60,000 different species of parasitoid wasps have now been described. But systematists think that's just the tip of the iceberg. "It's one of the groups that has been understudied historically," says James Whitfield, a parasitic wasp systematist at the University of Illinois, Urbana-Champaign (UIUC), who works with Janzen. When researchers sampling tropical insects use foggers to down all the insects in a tree canopy, sometimes more parasitoid wasps come raining down than even beetles, and "the percentage that are new is just really high," says Whitfield. The group he studies contains many species that can't be told apart except through molecular studies. "There's a really compelling argument that these parasitoid wasps may be more diverse than beetles," says Strand. "Virtually every arthropod on Earth is attacked by one or more of these parasitoid wasps."

Biocontrol agents

Some researchers think this diversity has arisen in part because these wasps are such picky eaters. A few are generalists, laying eggs in a variety of pupae or caterpillars. But many attack only one particular prey; Janzen's records show, for example, that more than 90% of the wasps parasitize only one or two species of caterpillar. "These parasitoids are vastly more host-specific than anyone thought they were," says Janzen.

This specificity not only underlies the diversity of wasp species—the wasps are as diverse as the species they invade—but also makes the insects appealing for biological pest control. "The goal is host-specific natural enemies," says Kevin Hackett, an entomologist with the USDA Agricultural Research Service in Beltsville, Maryland. Indeed, one of these little wasps saved the African cassava crop in the 1980s.

Cassava comes from South America, but in the past 400 years, it has become a crucial staple for millions of Africans, particularly those living on marginal land where few other crops thrive. In the early 1970s, the cassava mealybug arrived from South America in some planting materials and quickly spread. Within a decade, the insect was causing crop losses of up to 80%.

Mealybugs are relatively rare on cassava in South America. The reason, scientists discovered, is the parasitoid wasp *Apoanagyrus lopezi*, which parasitizes the bug. After studying the wasp to assure themselves that it would not become a pest itself in Africa, researchers reared large numbers of the wasp in Benin, then introduced it into 30 African countries. The mealybug is no longer a problem in Africa.

Parasitic wasps have come to the rescue elsewhere, but finding the right wasp for the job hasn't always been easy. The wasp must come from a climate similar to the one in which it will be working, it

Pest and controller. The cabbage butterfly (*top*) is kept in check by a parasitic wasp, *Cotesia rubecula*, imported to the United States from China.

CREDITS (TOP TO BOTTOM): DANIEL JANZEN AND WINNIE HALLWACHS; TIBOR BUKOVINSZKY; WWW.BUGSINTHEPICTURE.COM; HANS SMID/WWW.BUGSINTHEPICTURE.COM

must be released at the right time of the year, and researchers must learn enough about the species to raise and feed a few thousand for release. But the potential need is high, says Hackett: One new invasive species arrives in the United States every 6 weeks, on average.

Take the case of the cabbage butterfly (*Pieris rapae*), which invaded North America in the late 1800s. More than a century ago, Charles Riley, the chief entomologist at USDA, turned his sights on this butterfly, whose caterpillar munched its way through kale and cabbage crops. He imported a parasitoid wasp from England in 1881, but "they got the wrong wasp," says Roy Van Driesche, an entomologist at the University of Massachusetts, Amherst. By 1884, a population had been established near Washington, D.C., but it was never very effective; neither was a wasp brought in from Yugoslavia in the 1970s.

Only now, with the spread of a wasp imported from Beijing in the 1980s, is the cabbage butterfly being thwarted, says Van Driesche, who orchestrated the new introduction. The Chinese wasp hails from a similar climate, and it kills the caterpillar early in its life, before it has a chance to do much damage.

Despite their promise as biological control agents, parasitoid wasps have some commercial drawbacks. Private companies are not much interested in them because once the wasps are established, nature takes over and sales dry up. And concerns about the possible risks of releasing introduced species into the wild have also dampened enthusiasm for the technique.

Six-legged lab rat

Within the lab, however, interest in parasitoid wasps has blossomed. "They provide excellent model organisms to explore a broad variety of questions in ecology and evolution," says Charles Godfray of the University of Oxford in the United Kingdom. Others are keen to use them to study complex traits such as longevity, host preference, or female mate choice and to investigate the mechanisms of speciation.

One wasp in particular is emerging as the lab rat among parasitoids, a fly hunter called *Nasonia vitripennis*. This wasp is easy to raise in the lab, has a short life cycle, and can interbreed with several closely related species if treated with antibiotics. (Otherwise, a *Wolbachia* infection makes the species incompatible.) And now *N. vitripennis* and its two closest relatives have joined the elite ranks of organisms whose genomes have been sequenced. "This wasp genome is very exciting," says Hackett. In addition to helping scientists take advantage of *Nasonia* as a model system, it "will serve as a genetic resource for understanding other parasitoids," he adds. Moreover, the publication of genomes of two closely related species, with a third on the way, "gives a real insight into how speciation occurred," says Godfray.

Werren and Stephen Richards of the Baylor College of Medicine in Houston, Texas, spearheaded the *Nasonia* genome project. Werren has long pushed to expand this insect's use in genetic and behavioral studies. Male wasps develop from unfertilized eggs and thus have a single copy of each chromosome, which simplifies certain genetic analyses: In experiments that generate mutants, any altered genes become readily apparent because there isn't a second copy to mask an effect. Moreover, it's easier to track a gene down and to detect interactions among genes in these so-called haploid organisms.

N. vitripennis parasitizes larvae of house flies and other filth flies and is not too picky about its hosts. But its sibling species attack only blow flies found in bird nests. Cross-breeding studies have led Werren and postdoc Christopher Desjardins to a region of the genome responsible for host preference, and with further work, they hope to pin down the gene and figure out what it does. Such progress will promote a better understanding of speciation and can help entomologists figure out how to manipulate the genomes of parasitoids to improve their ability as biological control agents, says Werren.

These wasps may prove useful in biomedicine as well. They produce venom that causes temporary paralysis and alters other physiological properties. When researchers recently combined a computer search of the newly sequenced *Nasonia* genome with a sophisticated mass-spectrometry analysis of the wasp's venom, they turned up 79 constituent proteins. Half the proteins were not previously associated with venom, including 23 that were unlike any seen before, Dirk de Graaf of Ghent University in Belgium and his colleagues will report in an upcoming issue of *Insect Molecular Biology*. "There is great potential that new drugs could emerge from the venom repertoire of parasitoids," says Werren.

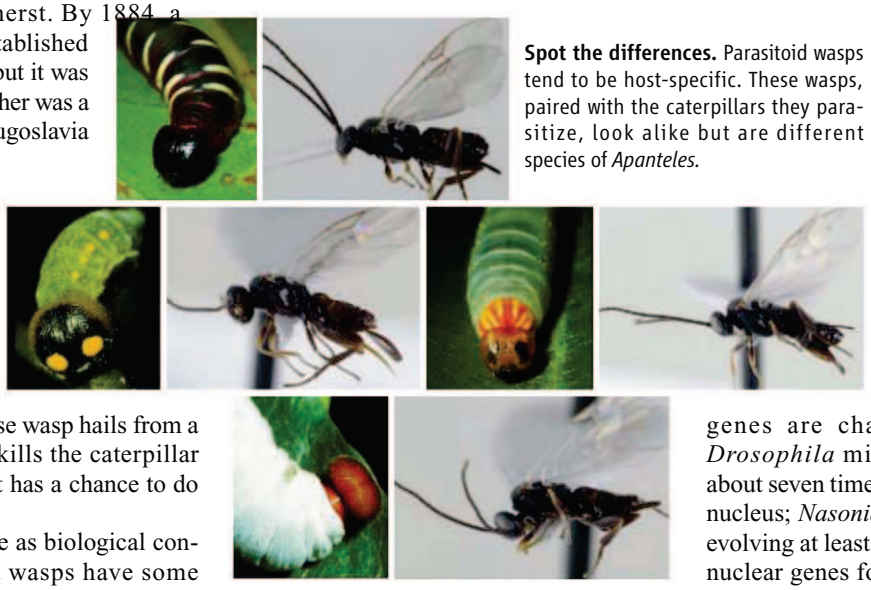

Spot the differences. Parasitoid wasps tend to be host-specific. These wasps, paired with the caterpillars they parasitize, look alike but are different species of *Apanteles*.

These first genome comparisons also hint at what may underlie parasitoid wasp diversity. Not only are the venoms evolving very quickly and enabling the wasps to adapt quickly to new hosts, but mitochondrial genes are changing in double time. *Drosophila* mitochondria genes evolve about seven times faster than do genes in the nucleus; *Nasonia*'s mitochondrial genes are evolving at least 35 times faster. That means nuclear genes for proteins that work in the mitochondria in one population of wasps very quickly become incompatible with another population's mitochondria, setting the stage for a species split.

In addition to teaching researchers more about parasitoid wasps, the *Nasonia* genome "can play a crucial role in sharpening our insights" into the molecular basis of social life, says Gene Robinson, an entomologist at UIUC. It can begin to reveal which genes are common to all ants, bees, and wasps and which are specific to social insects.

There is much more to be learned from this insect and its genome. It has 450 genes in common with humans that are not also found in fruit flies, including the full set of genes needed for methylation, a process involved in turning genes off semipermanently. "This species is no longer a 'weird' species with interesting features," says Claude Desplan, a developmental geneticist at New York University in New York City. "It has graduated to be of help to address questions that cannot be investigated that easily in flies."

–ELIZABETH PENNISI

CREDITS: JOSEPHINE RODRIGUEZ

Claim stake. A lone stake casts a shadow on the site of the proposed Pebble Mine.

FISHERIES

Fishing for Gold in The Last Frontier State

A gargantuan gold and copper deposit leaves some Alaskans fearful that they must choose between two great loves: salmon and mining

Tiffany's tastes are decidedly caviar, but the jewelry company has devoted itself lately to saving a less chichi seafood: sockeye salmon. Two years ago, Tiffany & Co. pledged never to buy gold from a gargantuan mine proposed for several dozen kilometers northeast of Bristol Bay, Alaska, a prolific salmon habitat. Since then, Tiffany has helped recruit a dozen other major jewelers to the preemptive boycott—some prestigious (Helzberg Diamonds), some less so (Sears, Walmart)—and continues to apply pressure. In October 2009, it took out a full-page, cyan-colored ad in the trade magazine *National Jeweler*, pleading that the "threat" to Bristol Bay "rises above all our immediate financial self-interests."

The jewelers' boycott is the most public skirmish in the touchy fight over the proposed Pebble Mine. In some ways, the fight feels familiar: Environmentalists see doomsday, whereas mining companies promise jobs and tax revenue. In other ways, this clash is atypical. Joining environmentalists are their sometime foes, fisheries, whose work buoys up much of Bristol Bay's economy. As a result, many people paint Pebble Mine as pitting two moneyed industries, mines and fisheries, against each other. And although people oppose the mine for other reasons, including a desire to shield other flora and fauna, salmon earn the most sympathy.

In another twist, it's not clear how much the mine would threaten the 40 million salmon in the bay. Foes and proponents agree that the mine, as planned, would disturb less productive salmon habitats there. But scientists are amassing evidence that the unproductive habitats of today may be vital for a robust salmon population tomorrow. By mucking around in ancient mud, they have charted salmon populations over hundreds, even thousands of years. They've discovered that somewhat barren streams and lakes were wildly productive once, and populations in each habitat wax and wane naturally with shifts in climate. So, as a precautionary measure and to ensure that Alaska has fish to fish in the future, scientists contend that the state must preserve its variety of habitats—by killing Pebble.

The Pebble Partnership—a joint venture of the mining companies Anglo American US LLC and Northern Dynasty Minerals—has said, many times, that it will proceed only if the project results in "zero loss" to fisheries, says Ken Taylor, head of the partnership's eight-person, $100 million (so far) environmental-assessment project. Taylor argues that giant mines and fisheries can co-exist.

Pebble officials also stress that they are merely exploring the site and have no firm plans. In fact, given the fickleness of Alaskan politics, it's not clear whether the mine will ever open. Pebble needs to secure state air and water permits, among others, and submit an environmental impact statement that the federal government will spend years scrutinizing. Tom Crafford, coordinator for large mines at the Alaska Department of Natural Resources, says Pebble would not crush its first rock until 2014, and that's if everything goes smoothly—if permits sail through, and court challenges end quickly. When Crafford mentions even that date, he chuckles, hard: "The likelihood of Pebble going smoothly is pretty minimal."

Mother lodes

The 3-km by 4-km Pebble deposit sits below marshy tan tundra, an expanse broken by mountains and veins of streams. Pebble West, 3.7 trillion kg of minerals, was discovered in 1988. Its ore was marginal, mostly low grade. Near the end of the survey, in 2005, engineers drilled a few last holes on the eastern edge. They hit the mother lode: Pebble East, an additional 3.1 trillion kg of higher-grade ore interred beneath a 1-km wedge of volcanic rock.

With that discovery, Pebble became a national environmental issue. The tiff with Tiffany focused attention on gold, but the Pebble deposit is largely copper—33 billion kg compared with 2.9 million kg (94 million oz.) of gold. (There's also 2.2 billion kg of molybdenum.) Metal markets can swing manically, but at today's healthy prices (gold at $1100 an oz.; copper at $7 per kg), the total deposit could be worth some $370 billion.

Most people surmise that Pebble East would be a subterranean "cave" dig that would require moving 4 trillion kg of rock. Pebble West, likely a strip mine, would remove 4 trillion kg more from an open pit. (Foes of the mine claim the pit would stretch 3 km across and 600 m deep. Taylor says it would be much smaller.) Pebble would have to build its own power supply, as well as a 160-km service road to a Pacific Ocean port in a region not conducive to ground transport—no road exists to Anchorage 330 km away. Pebble must also accommodate 1000 or so on-site employees for up to 80 years.

Some scientists fear that those mining jobs, coveted by some locals, would undermine jobs in fishing. To scrub its low-grade ore, Pebble would require massive amounts of water, and as Crafford recognizes, "For mining projects, water, and water quality, and the protection of water quality, are the name of the game." With the identity of the region

CREDIT: ERIN MCKITTRICK/WWW.GROUNDTRUTHTREKKING.ORG

The Secret Lives of Ocean Fish

It's easy to monitor the health of stocks of salmon because salmon spawn in small, discrete, and accessible freshwater bodies. Tracking fish in the ocean is a little tougher. But many scientists argue that ocean fish such as cod segregate themselves into distinct environments, as salmon do—and thrive or struggle for the same reasons.

For cod, population health depends on both human fishing and ecological factors. The 6 billion or so kilograms of cod living off Newfoundland and Labrador in Canada in the 1940s has dropped to hundreds of thousands of kilograms today, partly due to overfishing, says George Rose, a professor of fisheries conservation at Memorial University of Newfoundland in St. John's. "People thought little stocks [of cod] weren't important, and they got wiped out," he says. When large stocks faltered too, nothing could replace them.

But Rose's research reveals tremendous variation in the way cod stocks responded to the collapse. "Groups … very close geographically in fact are subject to very different ecological conditions," he says. As a result, "even in the worst possible times, in the 1990s, we had a couple of groups that were actually doing beautifully."

Work in biocomplexity—the physical diversity of fish habitats—explains why. To terrestrial animals (such as humans), oceans look homogenous—cold, deep, and empty—says Larry Crowder, a marine biologist at Duke University in Durham, North Carolina. However, oceans have currents, canyons, mountains, reefs, and forests of plants, which alter a habitat from top to bottom. Submerged vegetation supports prey at the expense of predators, given that prey can slip away in tangles of weeds. Fish rely on submarine currents to transport eggs and larvae from nests to feeding grounds. Climate change or fishing can alter habitats, and depending on how a stock's habitat responds, its population contracts or expands.

To thrive overall, species need to hedge themselves, by finding a balanced array of habitats to supply more or fewer fish as need be. "I guess it's like an orchestra," Rose says. "You have the horns playing for a bit, then the strings come in." **–S.K.**

tied up with salmon, he adds, "Pebble will be under an unprecedented microscope."

To outsiders, the names of local waterways blur together in a series of gutturals: Ugashik, Egegik, Naknek, Kvichak. To salmon, each "run" is a unique ecosystem, as distinct as a city. Salmon spend their adult lives at sea but spawn—mate and lay eggs in gravel beds—in fresh water, a biological quirk that requires them to thrash upstream for sometimes hundreds of kilometers. And salmon are homebodies; they spawn in the waterway where they were born, so depleting a run can doom a population.

Preliminary permit applications suggest that Pebble would draw at least 76 million liters of water (estimates by opposition groups range up to 265 million) per day from the Koktuli and Talarik rivers, which drain into other rivers and lakes and then Bristol Bay. Pebble would also likely discharge processed water into streams—a prospect that worries environmentalists, who fear that even clean discharge could alter a habitat's temperature or salinity or sediment composition, preventing adults from reaching spawning sites or retarding the growth of juveniles. And unfortunately, metal mines don't have a history of clean living. Again, Pebble has no firm plans, but many gold mines use cyanide for extraction; ground-up waste rock could also release sulfides, rendering water more acidic. Some evidence suggests that aqueous copper—at concentrations below Alaska's legal limit—interferes with the way salmon navigate and detect predators and disrupts their food chain, although ecologists also admit that the harm, if any, is impossible to predict because natural processes often mitigate the effects of copper.

Scientists also worry about pollutants leaking horizontally through the wet tundra, because Pebble would straddle two watersheds with complex hydrology, says Sarah O'Neal, a population biologist at State of the Salmon, a Portland, Oregon, environmental group. "It's really hard to tell where the water's going there, even the surface water. It can cross watershed boundaries, and you can find any potential contaminants across any watershed." It's therefore difficult to gauge which habitats are at risk, she says—and there are innumerable habitats: "Even the teeniest tiniest places, above disconnected channels, there are still fish in those little ponds."

Ups and downs. The productivity of different salmon streams varies greatly over decades, and some scientists worry that the Pebble Mine would harm tomorrow's prolific habitats.

CREDIT: © NATALIE FOBES/CORBIS

Biocomplexity

Teeny-tiny ponds and creeks obviously don't supply millions of salmon and other fish, like trout, for Bristol Bay, but they're not irrelevant in the long term, say fishery scientists Daniel Schindler and Ray Hilborn, part of a University of Washington, Seattle, team studying the issue in Alaska with support from federal agencies and the Moore and Pew foundations. (A small percentage of support also comes from fisheries groups.) Hilborn estimates that the mine could threaten four or five of 15 distinct stocks of sockeye salmon, the most economically important species. Those four stocks account for 20% of the sockeye population now, "but at some times [those stocks] would have accounted for 80% of the production," he says. In different eras, "there's an enormous variation in what's being productive."

A few years before Pebble East was discovered, Schindler began charting those variations by using nitrogen-14 and nitrogen-15 isotopes in lake sediment. Oceans contain more of the heavy isotope than fresh water contains, so salmon have a higher percentage in their bodies than freshwater fauna. By plotting the rising and falling nitrogen-15/-14 ratio in cores of lakebed mud (where salmon

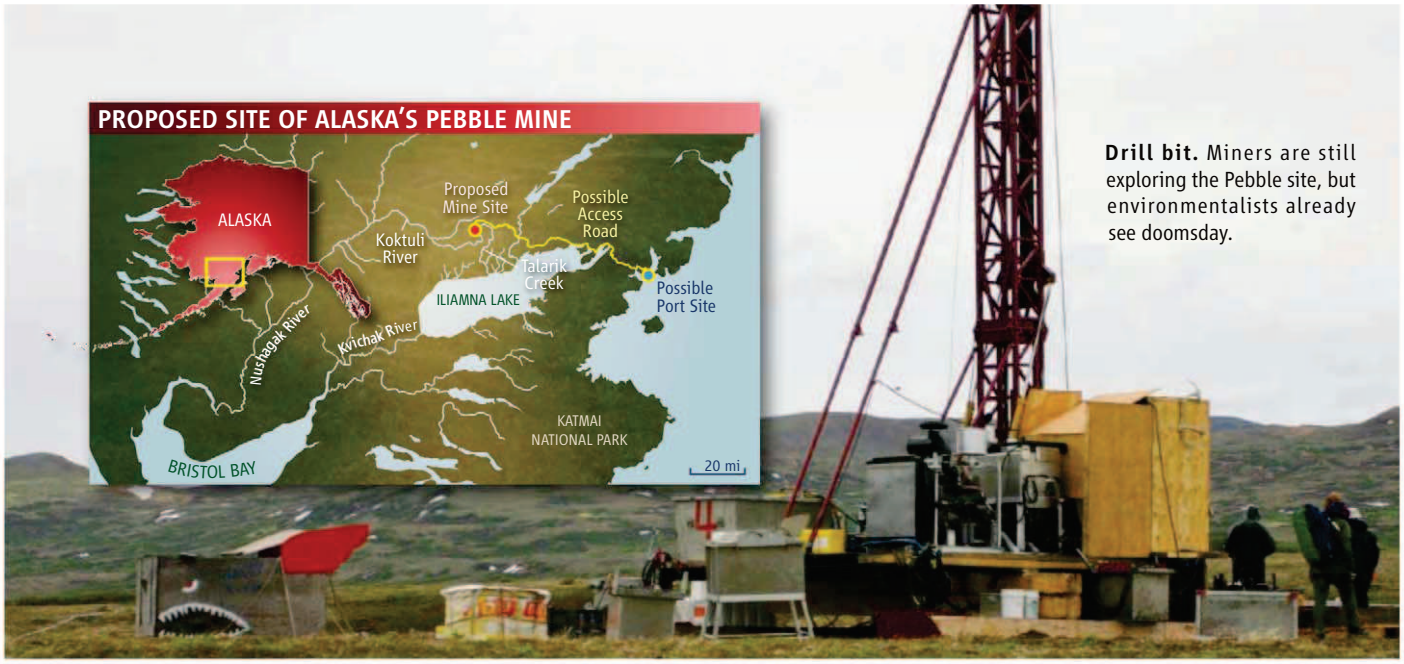

Drill bit. Miners are still exploring the Pebble site, but environmentalists already see doomsday.

CREDIT: ERIN MCKITTRICK, WWW.GROUNDTRUTHTREKKING.ORG; (MAP SOURCE) RENEWABLE RESOURCES COALITION/ALASKA DEPARTMENT OF NATURAL RESOURCES

sink when they expire, exhausted, after spawning), Schindler can trace demographic booms and busts back 10,000 years in some areas. He found that the population in each inland waterway—whether a mountain creek just centimeters deep, a meter-deep river from an underground spring, a lake beach, etc.—fluctuates erratically and independently of its neighbors. That's because its temperature, depth, and other qualities respond to different environmental factors—heavy rains, ice, tree cover, floods—in unique ways. Salmon also spawn or migrate back to sea as juveniles in different months, and El Niño and decades-long weather patterns fiddle with ocean habitats. Salmon thrive where conditions are favorable each decade, and given the diversity of Bristol Bay, odds are they will be favorable somewhere.

Schindler and Hilborn refer to this buffer of redundant habitats as "biocomplexity." "Regular biodiversity focused on the biotic component of the system, like genetic diversity, population diversity, species diversity," Schindler explains. "But that's not thinking about the coupled physical landscape. In the case of salmon, it's important to consider them together because the habitat is evolving." Other fish scientists argue that biocomplexity underlies the health of many fish populations worldwide. George Rose of Memorial University of Newfoundland in St. John's, Canada, finds only subtle genetic differences between some of the thriving and crashing stocks of Atlantic cod he studies. "There's nothing obviously different between these fish—except they have a different home." The reasons are murky, he says, "but one group does really well for a while, then the other does well for a while" (see sidebar, p. 264).

But that murkiness has been clearing up lately, and Schindler and Hilborn argue that the failure of some fisheries shows the folly of focusing only on productive watersheds. Dams in the U.S. Pacific Northwest—often built decades ago on nonproductive runs—have cut off spawning grounds that might have helped salmon recover when the population in other places flat-lined. In British Columbia, Canada, fishers long neglected all but the teeming Fraser River stock, which replenished itself each year. But extenuating circumstances caused the stock to collapse last summer to just 1.7 million salmon, well under the expected 11 million to 13 million, and left the industry gasping.

But the Fraser situation holds other lessons, too, claim Pebble officials. Large mines had been excavating copper within 10 km of Fraser River for decades before the salmon collapse, with seemingly no toxic effects. (Most scientists, including Schindler and Hilborn, blame the collapse on climate change or a lice infestation from fish farms.) Taylor, Pebble's environmental man, also points out that Alaska's Copper River, named after nearby and well-mined deposits, supports some of the premium salmon runs in Alaska. Moreover, the Bristol Bay salmon are hardly endangered or reeling: Schindler has never seen a higher population in his demographic studies.

Given Alaska's unreliable political climate—the state has a history of mavericks and ruthless moneyed interests (the *Anchorage Daily News* has a Web page to help sort through the endless federal inquiries into corruption there, http://www.adn.com/fbi)—most people declined to handicap whether Pebble Mine will actually open, much less when. Governor Sean Parnell has taken no public stand on Pebble. Neither has former Governor Sarah Palin, though her husband, Todd, works part-time fishing salmon. Nevertheless, those who read tea leaves interpret her comments and actions as pro-Pebble. Other former governors, as well as former U.S. Senator Ted Stevens, widely viewed as in favor of mining anything, have denounced Pebble.

Alaskan citizens send conflicting signals, too. Polls have shown that over half of Alaskans oppose the Pebble project, including about 70% of the people, largely Native Americans, near Bristol Bay. Then again, native groups recently opposed a strict clean-water initiative that many viewed as a referendum on Pebble, because it would have made mining there effectively impossible. (Some residents worried that the initiative would hamper all large mines in the state.) The initiative lost 57% to 43% during a statewide election in August 2008. So for now, Pebble lives, and, ultimately, Taylor feels, public pressure won't sway or disturb the regulatory agencies that will decide its fate. Pebble likely will not begin submitting permits until 2011.

Perhaps the one thing more uncertain than Alaskan politics is the potential effect of global warming on salmon runs. Alaska has grown rainier and warmer in the past few decades, and as glaciers melt and established ocean currents wobble, scientists do not pretend they can predict what will happen to spawning grounds. But really, that's the point of the biocomplexity work: Nobody can know. An empty river today could be boiling over with salmon in 20 years—if it remains habitable. "Life choices that work in one decade may not work in another," says Hilborn. "You want something out there that's going to be doing well in a warmer world."

–SAM KEAN

INFECTIOUS DISEASES

Questions Abound in Q-Fever Explosion in the Netherlands

A burgeoning goat-farm sector appears to be behind the worst outbreak ever recorded of a rare zoonosis

VINKEL, NETHERLANDS—Jan van Lokven has been a goat farmer for 23 years, but he's about to lose half his livelihood. Later this month, government officials will show up at his barn to kill all of his pregnant goats—more than 60% of his flock of almost 650 animals. Drinking coffee at his kitchen table, Van Lokven says he isn't sure what he'll do that day. His animals would be more at ease if he's around while the culling team does its grisly job, he says. "I just don't know if I can watch it."

Grisly job. A vet injects marked, pregnant goats with a sedative during a mass culling operation at a Dutch farm.

Just before Christmas, the Dutch government decided to cull about 40,000 pregnant goats at more than 60 farms in hopes of halting the worst outbreak ever of a little-known bacterial disease called Q fever. The problem isn't that the goats are suffering; it's that they are microbiological time bombs that threaten human health.

Q fever causes little disease in animals, and most farmers don't see it as a problem. But it can lead to abortions and stillbirths—and when it does, the animals' placentas and birth fluids contain many billions of microbes that spread easily into the environment. Such outbursts are assumed to have caused increasingly bigger waves of human Q-fever victims—most of whom come down with pneumonia—in the Netherlands the past 3 years. In 2009, there were more than 2300 human cases, including six deaths.

Until now, Q fever has been seen primarily as a rare occupational disease for farmers, veterinarians, and slaughterhouse workers and as a potential—if not very deadly—bioterror agent. Nobody is sure what triggered the explosive outbreak in the Netherlands, which has sickened mainly people who never had contact with animals, so the small cadre of Q-fever experts elsewhere in the world are following the Dutch struggle with fascination. "Nothing like this has ever been reported," says Jennifer McQuiston of the U.S. Centers for Disease Control and Prevention in Atlanta. She adds that between 100 and 170 human cases are reported annually in the United States. Faced with major gaps in scientific understanding and criticism that public health has taken a back seat to farmers' interests, the Dutch government has launched a flurry of studies of the disease and of *Coxiella burnetii*, the intracellular bacterium that causes it.

Q fever was first described in abattoir workers in Brisbane, Australia, in 1935. Its name—short for "query" because of its mysterious nature—was meant to be temporary, but it stuck even after *C. burnetii* was isolated in 1937. As it turned out, the microbe can be found almost anywhere in the world, and it has a bewildering range of hosts and ways to spread. It can infect mammals, birds, and arthropods, including ticks, which contribute to its spread by producing large amounts of it in their feces.

Scientists don't understand exactly why *C. burnetii* amasses in the wombs of pregnant animals, but past epidemiological studies have shown that the resulting abortions—especially in sheep and goats—are by far the biggest risk factor for human infections. However, human transmission from consuming contaminated milk and cheese, getting bitten by ticks, and having sex with an infected person have been reported as well.

In the United States, Q fever is classified as a "Category B" bioterrorism agent because it would be relatively easy to use and because, although not as deadly as anthrax or plague, attacks could still create widespread disease and panic. The U.S. Army exposed human volunteers to it as part of its biowarfare program in the 1950s; the Soviet Union experimented with it as well, as did the Japanese cult Aum Shinrikyo, known for its 1995 sarin attack. Bioterror worries brought more attention to it in the '90s and prompted the United States to make it reportable in 1999.

Humans, Animals—It's One Health. Or Is It?

A "holistic approach" and "synergism" working for the health of all species. Those are the buzzwords of the One Health movement, which aims to bring veterinary and human health closer together. Because people and animals form such a close-knit ecosystem—and most new or re-emerging diseases come from animals—the classic divide between veterinarians and doctors is hampering disease control, three scientists argued when they began promoting the concept 3 years ago (*Science*, 15 June 2007, p. 1553).

But the Dutch Q-fever outbreak provides a vivid example of how those two worlds often don't get along, especially when the stakes are different for each. Public health officials have complained that the veterinary community didn't properly inform them and that the outbreak spiraled out of control in part because economic interests trumped human health. "Sure, One Health, it's a nice concept, but we clearly have a long way to go," says Roel Coutinho, head of the Centre for Infectious Disease Control.

What makes Q fever tricky is that the vast majority of animals are healthy and asymptomatic, says French epidemiologist Didier Raoult of the Université de la Méditeranée in Marseille, France. The disease does trigger some abortion and premature birth, but the economic damage is limited, so there's little incentive to do anything about an outbreak. "The vets don't care about it," says Raoult—and human health suffers as a result.

Animal health authorities were slow to investigate suspected farms even as human cases started pouring into hospitals in 2008, says Jos van de Sande, a doctor at a regional health service in Noord-Brabant, the hardest-hit province.

CREDIT: MICHAEL KOOREN/REUTERS/LANDOV

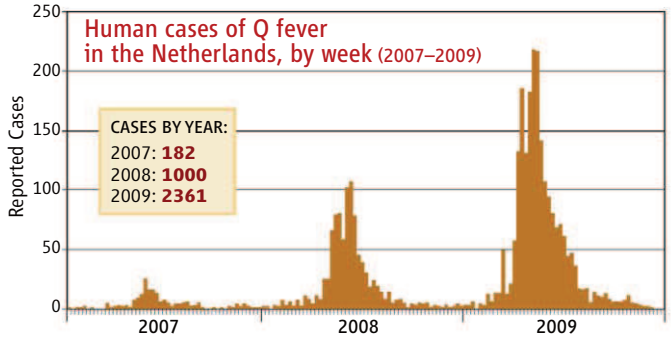

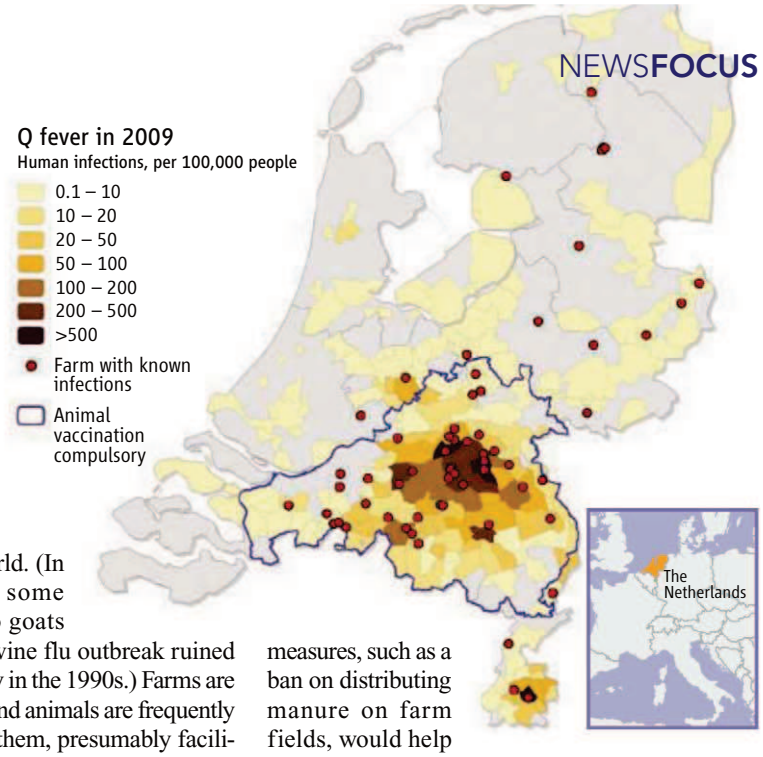

Rising tide. The number of human Q-fever cases exploded in the past 3 years, and the disease, originally concentrated in the south, spread north and east.

This increased awareness—along with better diagnostic tests—may explain the rising number of reported outbreaks of Q fever over the past 10 years worldwide, says epidemiologist Didier Raoult of the Université de la Méditeranée in Marseille, France, the foremost expert in human Q fever. "Once you start looking for Q fever, you'll find more and more of it," he says.

But what's going on in the Netherlands now is not just better detection but something new and different, says epidemiologist Roel Coutinho, head of the Centre for Infectious Disease Control in Bilthoven. When 182 human cases were detected in and around a town called Herpen in the summer of 2007, it seemed like a one-off outbreak. But in 2008, a new wave erupted, quickly filling up intensive-care units in the province of Noord-Brabant. A thousand cases were reported that year. In 2009, the number of new cases jumped to almost 2200, and the disease was found across the country.

It's still unclear what's behind the massive spread. Part of the reason has to be the recent expansion of high-intensity goat farming in the densely populated country, says Coutinho. The number of goats has quadrupled in Holland to more then 350,000 since 1995, and the number of them per farm has tripled; the country is now home to some of the biggest goat farms in the world. (In a sad twist of fate, some farmers switched to goats after a devastating swine flu outbreak ruined the Dutch pig industry in the 1990s.) Farms are often close together, and animals are frequently transported between them, presumably facilitating spread, says Coutinho. Bacteria released during abortions end up in manure, which is often spread onto farm fields; the wind may have carried them to the many surrounding towns and cities.

But Hendrik-Jan Roest, a scientist at the Central Veterinary Institute of Wageningen UR in Lelystad, says the sudden increase could be linked to a more virulent subtype of the microbe that started spreading in about 2005. Genetic typing by Corné Klaassen at Canisius Wilhelmina Hospital in Nijmegen has shown that all Dutch farms and patients are infected by a single subtype of *C. burnetii*. That suggests that the strain is somehow better at propagating itself than others, Roest says. He plans to compare strains in a collaborative study with Annie Rodolakis of the French National Institute for Agricultural Research in Tours, who has developed a mouse model of Q fever.

A more urgent question is how to bring the outbreak under control. In 2008, veterinary and public health authorities hoped that hygienic measures, such as a ban on distributing manure on farm fields, would help reduce human exposure. Now, the hope is that an animal vaccine produced by CEVA, a French company, can help bring the microbe under control. In short supply in 2008 and '09, the vaccine will be plentiful this year, says Christianne Bruschke, chief veterinary officer at the agriculture ministry. The vaccine does not prevent all infections, but it does prevent most abortions, which should help curtail the spread of the disease.

The vaccine does not work in infected animals, however, which is why an expert panel recommended in early December the emergency slaughter of all pregnant goats at affected farms. (There is no reliable way to quickly distinguish infected goats from healthy goats.) Bruschke says the cull is a one-time measure to prevent another massive release of microbes in the spring of 2010, when the goats would normally give birth. Then from 2011 on, the effects of the vaccine should start kicking in.

The impact on some farmers could be devastating, says Van Lokven. The Dutch government reimburses farmers for the current value of the goats but doesn't do so for the loss of income while they rebuild their flocks.

How well the measure will work is unclear as well. The huge numbers of *C. burnetii* already in the environment may persist for months or years; there's no good way to measure their numbers or to assess the threat they pose, says Roest. And there are many other questions. Although there is little doubt that goat farms are key amplifiers in the current outbreak, the role of cattle farms is unclear. For now, most experts say another surge of human cases this spring is inevitable—they just hope it will be smaller than that of 2009.

–MARTIN ENSERINK

To protect farmers from stigmatization, Van de Sande and his colleagues weren't told the exact location of contaminated holdings, only the general area. "You can't fight an epidemic like that," he says. Coutinho adds: "We just weren't able to get across how serious the human problem was getting."

Christianne Bruschke, the country's chief veterinary officer, dismisses those claims. From the onset, policy was set by a working group with members from both the agriculture and the health ministries—and it included Coutinho and other scientists. "They should have spoken up before if they disagreed," says Bruschke. She says the government had to strike a balance between farmers' interests and public health in the face of insufficient data about how Q fever spread: "You can't impose draconian measures on farmers if you have no idea whether they will have an effect."

The Dutch government plans to investigate how the epidemic was handled. Coutinho says one lesson is already clear: Veterinarians should notify their colleagues in public health anytime a zoonotic disease starts spreading in animals—as Q fever did in 2005, 2 years before the human explosion began.

–M.E.

SOURCES (LEFT TO RIGHT): RIVM/CIB/EPI; RIVM/CBS/VWA

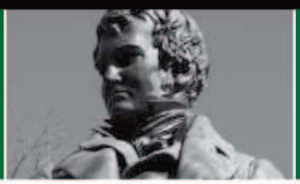

LETTERS

edited by Jennifer Sills

The Potential of Nutritional Therapy

WE THANK J. BOHANNON ("THE THEORY? DIET CAUSES VIOLENCE. The lab? Prison." News Focus, 25 September 2009, p. 1614) for drawing attention to Gesch's research on the use of complex micronutrient therapy to reduce violence by prison inmates. Many studies of nutritional therapies of mental disorders were done in the past century and showed limited benefit (*1*), probably because each study investigated a single nutrient at a time. Nutritional therapies do not draw the financial support of pharmaceutical companies, which cannot patent them. Clinicians resist using supplements as treatments, mostly because they lack knowledge about them. In the realm of mental health, recent research highlights the importance of investigating complex micronutrient supplementation for the treatment of mental illness (*2*–*4*). This emerging research stems from multiple conceptual frameworks, including the "orthomolecular" tradition mentioned by Bohannon as well as the observation that psychiatric symptoms and neuropathic pain can accompany mitochondrial disorders that may be ameliorated by complex nutritional therapies (*5*–*8*).

Patients who do not respond to prescription drugs are more common than previously thought (*9*), and this, along with the frequent side effects of medications, should compel researchers to study those alternatives gaining both empirical and theoretical support.

Medical journalism may be one important agent for spreading information about legitimate research on nutrition and mental health, especially in the face of the lack of profit-generated funding. This also implies a special responsibility for medical journalists, since the danger of "pseudoscience" is close at hand.

ANN GARDNER,[1]* BONNIE J. KAPLAN,[2] JULIA J. RUCKLIDGE,[3] BO H. JONSSON,[1] MATS B. HUMBLE[1]

[1]Department of Clinical Neuroscience, Division of Psychiatry, Karolinska Institutet, Stockholm, Sweden. [2]Departments of Paediatrics, and Community Health Sciences, University of Calgary, AB, Canada. [3]Department of Psychology, University of Canterbury, Christchurch, New Zealand.

*To whom correspondence should be addressed. E-mail: agtorndal@odenhall.se

References

1. B. J. Kaplan, S. G. Crawford, C. J. Field, J. S. Simpson, *Psychol. Bull*. **133**, 747 (2007).
2. D. Gately, B. J. Kaplan, *Clin. Med. Psychiat*. **4**, 3 (2009).
3. J. J. Rucklidge, *J. Anxiety Disord*. **23**, 836 (2009).
4. E. A. Frazier, M. A. Fristad, L. E. Arnold, *J. Child. Adolesc. Psychopharmacol*. **19**, 453 (2009).
5. A. Gardner, R. G. Boles, *Curr. Psychiat. Rev*. **1**, 255 (2005).
6. O. Fattal, J. Link, K. Quinn, B. H. Cohen, K. Franco, *CNS Spectr*. **12**, 429 (2007).
7. T. Higashimoto, E. E. Baldwin, J. I. Gold, R. G. Boles, *Arch. Dis. Child*. **93**, 390 (2008).
8. M. A. Tarnopolsky, *Adv. Drug Deliv. Rev*. **60**, 1561 (2008).
9. T. R. Insel, P. S. Wang, *Psychiatr. Serv*. **60**, 1466 (2009).

Emissions Omissions

S. C. JACKSON ("PARALLEL PURSUIT OF NEAR-term and long-term climate mitigation," Policy Forum, 23 October 2009, p. 526) ranks the roles that long-lived versus medium- and short-lived pollutants will play 20 years in the future. However, in constructing the ranking, Jackson assumed either that emissions of CO_2, volatile organic compounds (VOCs), NO_x, SO_x, CO, and black and organic aerosols in 2030 would be the same as those in 2000 [taken from EDGAR database and Bond *et al*. (*1*)], or that CO_2 and ozone precursors both grew at a nonzero rate from 2000 to 2030. We believe that this is a critical error in the analysis; in many key sectors (e.g., power generation and road transport) the emission trends for short- and long-lived pollutants are opposite, and the ratio of the emissions of short- and long-lived pollutants in 2030 will be very different from that in 2000.

A closer consideration of road transport supports this argument. The International Energy Agency (IEA) collaborated with the World Business Council for Sustainable Development in 2002 to 2004 as part of the Sustainable Mobility Project (SMP) to develop the IEA/SMP global transport spreadsheet model (*2*), which provides estimates for global emissions of CO_2, particulate matter (PM), NO_x, CO, and VOCs from road transport for 2000 to 2050. Over the past few decades, technologies (such as catalytic converters, particulate filters, oxidation catalysts, and NO_x traps) have been developed that have led to large reductions in the emissions of criteria pollutants (NO_x, VOCs, PM, and CO) from new vehicles. As the on-road fleet is replaced by vehicles with new emission control systems and as the technology diffuses to less-developed nations in the coming decades, the emissions of criteria pollutants from road vehicles will decline substantially.

The global emissions in the IEA/SMP reference case for road transport (light-duty vehicles, freight trucks, buses, two- and three-wheelers) in 2000 for CO_2, NO_x, VOC, and CO are consistent with those in the EDGAR (*3*) database used by Jackson. Road transport CO_2 emissions in the IEA/SMP reference scenario (*2*) increase by approximately 57% from 2000 to 2030, reflecting increased demand for road transport services. In contrast, road transport PM, NO_x, VOC, and CO emissions in the


Predators and prey in the Arctic
276

Plants to combat malaria
279

IEA/SMP reference scenario decrease by approximately 63, 70, 90, and 86%, respectively, from 2000 to 2030, reflecting improved emission control mandated in most regions of the world. The use of constant emission values for PM, NO_x, VOC, and CO leads to an overestimation of the relative impact of these short-lived pollutants compared with that of CO_2 by approximately an order of magnitude. Similarly, the emissions of SO_x from power plants in 2030 are likely to be greatly overestimated by assuming that the emission levels were the same as in 2000 [full implementation of the U.S. Clean Air Interstate Rule is estimated (*4*) to lead to an approximately 70% reduction in SO_x emissions from power plants in the United States].

In assessing the likely future contribution of PM, NO_x, VOC, SO_x, and CO to radiative forcing of climate change, the substantial ongoing reductions that are occurring in the emissions of these criteria air pollutants must be included. Analyses that do not include this factor are likely to greatly overestimate the importance of such short-lived air pollutants to climate change.

T. J. WALLINGTON,* J. E. ANDERSON, S. A. MUELLER, S. WINKLER, J. M. GINDER

Systems Analytics and Environmental Sciences Department, Ford Motor Company, Mail Drop RIC-2122, Dearborn, MI 48121–2053, USA.

*To whom correspondence should be addressed. E-mail: twalling@ford.com

References

1. T. C. Bond *et al*., *Glob. Biogeochem. Cycles* **21**, GB2018 (2007).
2. World Business Council for Sustainable Development, *Mobility 2030: Meeting the Challenges to Sustainability* (World Business Council for Sustainable Development, Geneva, 2004); www.wbcsd.org.
3. EDGAR 3.2 (www.mnp.nl/edgar/model/).
4. U.S. EPA Clean Air Interstate Rule (www.epa.gov/cair/).

Response

THE ESSENCE OF WALLINGTON *ET AL.*'S COMMENT is that emissions of short-lived pollutants in the global road transport and U.S. power sectors are forecasted to decline and that this forecast should have been included in the steady-growth scenario in my Policy Forum. In the steady-growth scenario, emissions of some short-lived pollutants were held constant and others increased.

The auto industry does indeed have a goal and a forecast (*1*) to reduce short-lived road transport emissions more quickly than the multisector growth rates I applied. However, this forecast represents only one possible future path, and achievement of the forecast is not a foregone conclusion; the report (*1*) cited by Wallington *et al*. explicitly articulates assumptions about future policies, economics, and behavioral change that require active mitigation effort.

Regardless of the trends in global road transport and U.S. power plant emissions, these sectors represent a fraction of short-lived pollutants. Specifically, of total global emissions in year 2000, global road transport and U.S. power plants represented 15% of total black carbon (*2*), 40% of fossil fuel–generated black carbon (*2*), less than 20% of two ozone precursors (CO and nonmethane volatile organic compounds) (*3*), about 40% of another ozone precursor (NO_x) (*3*), and about 10% of sulfur dioxide (SO_2) (*3*). Thus, declining emission forecasts in these sectors do not necessarily represent the overall trend for short-lived emissions.

In fact, from 1990 to 2000, the global trends for short-lived pollutants were flat to increasing (*2*, *4*), except for SO_2, which had a cumulative global decline of 3 to 10% (*3*–*5*). From 2000 to 2030, the global projections for all short-lived pollutants, including SO_2 (*6*), continue a trajectory that is flat to increasing in the majority of Intergovernmental Panel on Climate Change scenarios (*4*, *7*, *8*), with negative trends for a minority of pollutants in a minority of scenarios.

My conclusions are robust across a wide range of scenarios. As shown in the Policy Forum, short- and medium-lived pollutants represent a majority (57 to 60%) of the positive radiative forcing (RF) generated in years 1 to 20 in both the constant-emissions and steady-growth scenarios, which approximately bound the IPCC marker scenarios (*4*). Applying this methodology to the sectors and pollutants under discussion, holding all else equal, neither complete elimination of auto industry black carbon nor complete elimination of global ozone precursor emissions would reduce the short- and medium-lived contribution to positive RF to less than 50%. This highlights the fragmentation and diversity of global sources of short- and medium-lived pollutants, and the consequent difficulty of reducing their contribution. Reductions of each pollutant in each sector are essential, but do little individually to change the mathematics of global contribution ratios.

Forecasted reductions of short-lived warming pollutants by the auto industry represent a beneficial and critically important step toward climate mitigation, but do not indicate that the climate contribution of this category of pollutants is already resolved. Indeed, active mitigation of short- and medium-lived pollutants across many sectors is essential to near-term climate mitigation and must be pursued aggressively in parallel with reduction of long-lived pollutants.

STACY C. JACKSON

Energy and Resources Group, University of California, Berkeley, Berkeley, CA 94720, USA. E-mail: stacyjackson@berkeley.edu

References and Notes

1. World Business Council for Sustainable Development, *Mobility 2030: Meeting the Challenges to Sustainability* (World Business Council for Sustainable Development, Geneva, 2004); www.wbcsd.org.
2. T. C. Bond *et al*., *Glob. Biogeochem. Cycles* **21**, GB2018 (2007).
3. EDGAR 3.2 (www.mnp.nl/edgar/model/).
4. N. Nakicenovic, R. Swart, Eds., *Special Report on Emissions Scenarios* (IPCC, Cambridge Univ. Press, Cambridge, 2000).
5. S. J. Smith, E. Conception, R. Andres, J. Lurz, *Historical Sulfur Dioxide Emissions 1850–2000: Methods and Results* (Pacific NW National Laboratory, College Park, MD, 2004).
6. Developing world SO_2 emissions outpace developed world reductions in the near-term in the majority of scenarios (*8*).
7. S. Rao, K. Riahi, K. Kupiainen, Z. Klimont, *Environ. Sci.* **2-3**, 205 (2005).
8. S. J. Smith, H. Pitcher, T. M. L. Wigley, *Clim. Change* **73**, 267 (2005).

CORRECTIONS AND CLARIFICATIONS

Reports: "Impact of genome reduction on bacterial metabolism and its regulation" by E. Yus *et al*. (27 November 2009, p. 1263). In the author list, Luis Serrano should have been designated as corresponding author along with Peer Bork. Their respective e-mail addresses are: luis.serrano@crg.es (L.S.); bork@embl.de (P.B.).

Essay: "GE prize essay" (4 December 2009, p. 1361). In the biography of Masahiro Kitano, the regional winner from Japan, the title of his winning essay was incorrect. The correct title is "Elucidating the mechanisms of corpse engulfment by live-cell protein activity monitoring."

Letters to the Editor

Letters (~300 words) discuss material published in *Science* in the previous 3 months or issues of general interest. They can be submitted through the Web (www.submit2science.org) or by regular mail (1200 New York Ave., NW, Washington, DC 20005, USA). Letters are not acknowledged upon receipt, nor are authors generally consulted before publication. Whether published in full or in part, letters are subject to editing for clarity and space.

HISTORY OF SCIENCE

Recovering a Humboldtian Legacy

Nicolaas A. Rupke

On the way back from his historic journey of exploration of the equatorial Americas (1799–1804), Alexander von Humboldt briefly set foot on the soil of the still-young American republic. He spent seven weeks in the United States visiting Philadelphia and Washington, where he met Thomas Jefferson, James Madison, and other prominent figures. Humboldt's classic narrative of travel, translated from the original French into English by the remarkable Helen Maria Williams under the title *Personal Narrative of Travels to the Equinoctial Regions of the New Continent* (*1*), never got as far as the tail end of his journey. Yet during the decades that followed his East Coast visit, Humboldt became a major force in "the shaping of America." In his multivolume *Reisewerk* (travel oeuvre) (*2*) and, toward the end of his life, in *Cosmos* (*3*), he taught how to observe and treasure nature's monuments. His large-scale view and vision of the physical world led the way in what we have come to call an ecological understanding of nature. On both sides of the Atlantic, many were inspired to follow in Humboldt's footsteps or go beyond him, to explore the North American interior and west, for example. Among them were such eminent Humboldtians as Prince Maximilian of Wied and Balduin Möllhausen, who in their travel narratives included grand illustrations of wilderness. Painters of North America's late Romantic period also went west and beheld the landscape with what recent geographers term the "Humboldtian physiognomic gaze."

Honored in St. Louis. Ferdinand von Miller's statue (1878) of Humboldt in Tower Grove Park, St. Louis, Missouri.

Perhaps the most famous Humboldtian of all was Charles Darwin, who devoured the *Narrative of Travels* on his journey around the world aboard *HMS Beagle*. The body of secondary literature on the two men is enormous, and new books and articles—scholarly as well as popular—on them keep rolling off the presses year after year. From this literature, it appears that each generation of biographers has produced its own Darwin as well as its own Humboldt. Admittedly, in North America, interest in Humboldt waned after the 1869 centenary of his birth, only to show a reversal in recent decades. Humboldt is being rediscovered and, what's more, honored by historians as a founding father of North American environmentalism.

Substantially boosting this reversal, Laura Dassow Walls, an expert on American Romanticism and Transcendentalism and a connoisseur of environmental literature (at the University of South Carolina) gives us a Humboldt fit for our times. Walls's *The Passage to Cosmos* is more than a scholarly study of Humboldt. It also is a subjective account of Walls's own "passage to Cosmos." The author briefly but movingly recounts what she calls her "kinglet moment": As a young student assistant at a natural history museum she was given, for the purpose of preparing a study skin, a ruby-crowned kinglet, "freshly dead, tiny, a mere tuft of down. And beautiful, so beautiful I was shocked to tears—softly shaded olive browns, elegant to the last detail, topped with that brilliant jewel-bright ruby crown. Every feather was an astonishment. I held that kinglet in my hand, bewildered, and something inside me broke." It was this experience that brought Walls to the naturalist, writer, and early environmentalist Henry David Thoreau and thence to Humboldt, both of whom unified scientific knowledge and aesthetic-emotional sensibilities. "Humboldt's science had heart," Walls states.

In her magisterial sweep across "the cult of Humboldt that peaked in the United States in the 1850s," Walls shows that Humboldt's envisioning of nature stamped its mark on a distinctive American fine arts tradition that remains alive today. She is at her most inspired where she treats of Thoreau, the painter Frederic Edwin Church, and the poet Walt Whitman. Church is a particular favorite of hers, someone who went where Humboldt had gone before, quite literally, when producing in situ the sketches for his great painting Heart of the Andes (1859).

From the start of Humboldtianism in the United States, antebellum Americans constructed various Humboldts, the great explorer-naturalist being appropriated by different political camps. Northern Whigs stressed Humboldt's view that "all [races] are alike designed for freedom." In contrast, Southern Jacksonian Democrats interpreted Humboldt's "global and egalitarian cosmopolitanism through a nationalistic and racist lens." Moreover, in both North and South, Humboldt—who never mentioned "God" in his *Cosmos*—required reframing for Christian, Puritan purposes. His sublimely heroic landscapes needed to be translated into "religious assertions of the presence of God in wild nature." Furthermore, Humboldtian scenery had to be nationalized to represent "an idyll of colonial civilization" that showed none of the

The Passage to Cosmos
Alexander von Humboldt and the Shaping of America
by Laura Dassow Walls
University of Chicago Press, Chicago, 2009. 420 pp. $35, £24. ISBN 9780226871820.

The reviewer, author of *Alexander von Humboldt: A Metabiography*, is at the Faculty of Humanities, University of Goettingen, Papendiek 16, D-37073 Goettingen, Germany. E-mail: nrupke@gwdg.de

inhumanity of the wilderness nor the rampant deforestation that shook Thoreau. But, as Walls notes in discussing the writer and naturalist Susan Fenimore Cooper, "[t]he true passage to Cosmos is not found, but forged." This forging was carried out by "Humboldt's American children," prominently among them the environmentalists John Muir and George Perkins Marsh. And Walls does her own forging, too.

By recovering the excitement of Humboldtian explorations and travel experiences, Walls wins back Humboldt for the 21st century. Through her account, he joins forces with present-day heroes such as Edward O. Wilson and his *Cosmos* of a sort, *Consilience* (*4*), all of them reorienting and transforming disciplines and divisions that threaten "to leach the poetry out of our technologically driven lives." Walls reclaims for the present a man whose personality and work had a formative influence on the cultural landscape of antebellum America and whose legacy may to good effect be used in addressing current affairs. I recommend *The Passage to Cosmos* as a fine piece of Humboldt scholarship, a heartfelt plea for environmental holism, and an enjoyable read.

References and Notes

1. A. von Humboldt, *Voyage de Humboldt et Bonpland. Première partie. Relation historique* (Schoell, Paris, 1814–1825).
2. *Voyage aux régions équinoxiales du Nouveau Continent fait en 1799, 1800, 1801, 1802, 1803 et 1804, par Al. de Humboldt et A. Bonpland* [for its complex publication history, see (*5*)].
3. A. von Humboldt, *Kosmos: Entwurf einer physischen Weltbeschreibung* (Cotta, Stuttgart and Tübingen, 1845–1862).
4. E. O. Wilson, *Consilience: The Unity of Knowledge* (Knopf, New York, 1998); reviewed in (*6*).
5. H. Fiedler, U. Leitner, *Alexander von Humboldt Schriften: Bibliographie der selbständig erschienenen Werke* (Akademie, Berlin, 2000).
6. J. Dupré, *Science* **280**, 1395 (1998).

10.1126/science.1183462

BROWSINGS

Alexander von Humboldt and the Botanical Exploration of the Americas.
H. Walter Lack. Prestel, Munich, 2009. 280 pp. $185, £125. ISBN 9783791341422.
Although "botany was never the real focus of Humboldt's interests," his 1799–1804 travels with Aimé Bonpland made an enormous contribution to the recording of plant diversity. Humboldt and his collaborators described and named hundreds of plant species from the northern Andes, Mexico, and Cuba. (Although several 18th-century Spanish expeditions had also collected many of these, their findings long remained unpublished.) Lack offers a short account of this research, highlighting links between the 19 volumes of "Partie 6: Botanique" of *Voyage aux régions équinoxiales du Nouveau Continent* and the underlying letters, field notes, herbarium specimens, drawings, and botanical prints. The author notes that Bonpland carried out most of the actual botanical work in the field but once back in Paris failed to complete the two major texts he started. Humboldt then recruited Carl Sigismund Kunth and a small team of researchers, artists, engravers, and printers who saw the work through to publication. Lack stresses Humboldt's organizational talents and the modern aspects of his methodology: careful numbering of specimens, preservation of notebooks, production of illustrations, and deposition of specimens in prominent public institutions. The richly illustrated volume includes a selection of 82 full-color plates from "Partie 6" (such as *Acineta superba*, an epiphytic orchid Humboldt and Bonpland collected from cloudforest in Ecuador).

CREDIT: COURTESY PRESTEL

HISTORY OF SCIENCE

Icons of Early Conservation Biology

Jared Farmer

The U.S. Fish and Wildlife Service's May 2008 listing of the polar bear (*1*) in Alaska as a threatened species was a politically and emotionally charged moment. Environmentalists had worked hard to turn the already-iconic bear into a symbol of global warming. As part of the species recovery plan, the government will continue to census bear populations. As historian Mark Barrow shows, politically motivated inventories of wildlife long predate the Endangered Species Act and the discipline of conservation biology. *Nature's Ghosts* is essentially a chronicle of proto-professional scientists making lists of threatened totemic species.

Nature's Ghosts
Confronting Extinction from the Age of Jefferson to the Age of Ecology
by Mark V. Barrow Jr.
University of Chicago Press, Chicago, 2009. 509 pp. $35, £24. ISBN 9780226038148.

By using in the subtitle *from the Age of Jefferson* instead of "the Age of Cuvier" or "the Age of Geology," Barrow (a professor at Virginia Tech) unapologetically announces his American bias. His nationalist perspective allows him to draw a simple narrative arc: At the time of the founding of the U.S. republic, American naturalists, including Thomas Jefferson, did not believe in the possibility of extinction, for it seemed to violate the economy of nature. Two centuries later, the United States passed the world's gold-standard law for protecting species from extinction. What happened between? No single book could explain it all, and Barrow doesn't try. *Nature's Ghosts* skimps on cultural, economic, and political analysis. Instead, the book means to restore the stature of the U.S. naturalists who created the concept of endangered species.

Barrow's narrative begins with a quick summary of the geologists, paleontologists, and comparative anatomists in Europe who established the reality of extinction. The original icon of prehistoric extinction was the American mastodon. Thinking forward in time, Cuvier and Lyell posited that human-caused extinction was possible,

The reviewer is at the Department of History, State University of New York, Stony Brook, NY 11794, USA. E-mail: jared.farmer@stonybrook.edu

even inevitable, and potentially regrettable, but not unnatural. Finally, in the 1830s and 1840s, investigations into the histories of three kinds of flightless birds—the dodo, the moa family, and the great auk—proved that humans could in fact eliminate whole species. Of these, the auk is most important to Barrow's story because it was the first species to die in front of naturalists' eyes—or their gunsights. Various collectors and museums vied for the final specimens.

It was, however, the dramatic, continental declines of the American bison and the passenger pigeon in the late 19th century that turned U.S. naturalists into conservationists. For example, the American Bison Society began a captive breeding program at the Bronx Zoo to save the shaggy national symbol. Propagation of passenger pigeons proved much harder, and the final two birds—a childless pair named George and Martha Washington—died in the Cincinnati Zoo.

In the first half of the 20th century, U.S. naturalists enlarged their scope of concern. They looked beyond the nation's borders—first to the big-game country of Africa, then to the Galápagos Islands. Naturalists promoted the passage of the Western Hemisphere Convention in 1940 and the creation of the International Union for the Protection of Nature in 1948. In the same era, they added predators and scavengers to the list of mammals and birds worthy of attention and preservation. Under the influence of the new discipline of ecology, naturalists began to inventory endangered habitats instead of just hunting and mounting, capturing and breeding.

In the pre–World War II era, naturalists and ecologists could not apply for government grants to conduct their baseline studies. Institutional support then largely came from privately endowed natural history museums and conservation groups. The Audubon Society, for example, sponsored graduate fellowships, including one that produced the first documentation of the last days of a doomed population (the heath hen). On a larger scale, the American Committee for International Wildlife Protection bankrolled three seminal inventories of the world's endangered and extinct animals.

Barrow heroizes the work of these politically engaged inventory makers. He gives numerous capsule biographies of naturalists such as Carl Koford, who conducted the first life history of the California condor, and James T. Tanner, who did the same for the ivory-billed woodpecker. He celebrates an era when biologists—almost all of them men—camped in the field. These scientists performed no lab work, no applied mathematics, no computer modeling. In Barrow's telling, their greatest tool was their "powerful emotional response" to wildlife, their "deep sense of connection" to nature. After World War II, naturalists found a home in new nongovernmental organizations like the World Wildlife Fund and enlarged agencies like the U.S. Fish and Wildlife Service. Not until Michael Soulé's generation did "indoor biologists" within academia try to recover the American naturalist tradition—a move applauded by Barrow, who locates the roots of conservation biology in natural history.

Icon of extinction. When Martha, the last known passenger pigeon, died on 1 September 1914, her body was rushed to the Smithsonian Institution, where it was long displayed as a warning that even a species whose population numbered in the billions could fall victim to humans.

The author's admiration for his biographical subjects creates problems. In passing, he provides evidence that many of his players were racists, but he fails to discuss the deep connections between Progressive-era wildlife conservation and nativism and eugenics (*2*). This is a significant omission because eugenicists worked against another kind of "extinction"—the threatened status of the "Nordic race" in America.

Barrow misses other opportunities to contextualize the concept of extinction. He says nothing about the enthusiasm for dinosaurs that has marked America culture since the 1890s—a phenomenon that has changed the way people think about mass extinction events. He grants just one throwaway paragraph to Paul Martin's hugely influential Pleistocene overkill hypothesis (*3*). Lastly, the author's decision to exclude plants from his book means that the reader doesn't learn about the sustained efforts to save the giant sequoia—an American symbol linked to the mastodon in 19th-century popular culture, a species long thought to be an evolutionary relict doomed to natural extinction and in danger of human-caused extinction.

Nonetheless, Barrow has produced something noteworthy—the definitive prehistory of conservation biology in America. The book is especially strong in its treatment of the underappreciated cohort of field biologists between William T. Hornaday and Aldo Leopold.

Overall, *Nature's Ghosts* is rousing and depressing. Despite great changes in U.S. attitudes about nature, Americans still care more about charismatic megafauna than lowly, ugly creatures. Although the original wording of the Endangered Species Act was surprisingly sweeping, in application it has been something else. As famously shown by the snail darter court case, not all threatened beings are created equal. Ironically, the narrative of *Nature's Ghosts* replicates the popular disregard for certain classes of life. Pigeons were not, after all, the only species that darkened the American sky with awesome flocks. There was also the Rocky Mountain locust—a once-prodigious species that went extinct about the same time without any fuss or expression of human regret (*4*). How many people feel a deep sense of connection to grasshoppers? Barrow's naturalists made no comment about this extinction event, and neither does he.

References and Notes

1. Scientific names of taxa mentioned in the text: polar bear, *Ursus maritimus*; American mastodon, *Mammut americanum*; dodo, *Raphus cucullatus*; moa family, Dinornithidae; great auk, *Pinguinus impennis*; American bison, *Bison bison*; passenger pigeon, *Ectopistes migratorius*; heath hen, *Tympanuchus cupido cupido*; California condor, *Gymnogyps californianus*; ivory-billed woodpecker, *Campephilus principalis*; giant sequoia, *Sequoiadendron giganteum*; snail darter, *Percina tanasi*; Rocky Mountain locust, *Melanoplus spretus*.
2. J. P. Spiro, *Defending the Master Race: Conservation, Eugenics, and the Legacy of Madison Grant* (Univ. Vermont Press, Burlington, 2009).
3. P. S. Martin, in *Quaternary Extinctions: A Prehistoric Revolution*, P. S. Martin, R. G. Klein, Eds. (Univ. Arizona Press, Tucson, 1984), pp. 354–403.
4. J. A. Lockwood, *Locust: The Devastating Rise and Mysterious Disappearance of the Insect That Shaped the American Frontier* (Basic, New York, 2004).

10.1126/science.1185483

HEALTH CARE POLICY

Reforming Off-Label Promotion to Enhance Orphan Disease Treatment

Allowing off-label promotion by drug companies may improve access to key treatments for orphan disease patients.

Bryan A. Liang[1,2]* and Tim Mackey[1]

Once the U.S. Food and Drug Administration (FDA) approves uses for new drugs, physicians are free to prescribe them for any clinical condition they see fit (*1*). Promotion (by manufacturers) and patient use (guided by clinicians) for any indication, population, dosage, administration, or treatment duration other than that approved by a country's regulatory authority is deemed "off-label" (*2*). Such use is highly prevalent; 21% of all prescription drug use, and up to 83% for certain diseases and drugs, are off-label (*3*).

Off-label prescribing allows physicians to innovate with treatments based on emerging clinical data (*4*). They can monitor individual patients to assess what newer, unapproved treatments are beneficial (*5*). But many physicians lack knowledge about rare diseases, leaving patients without a definitive diagnosis or treatment (*6*). This occurs despite efforts to disseminate rare disease information, including accurate diagnosis and treatments (*7*, *8*). In addition, the ad hoc nature of off-label regulation, knowledge, and drug use may constitute human experimentation without informed consent. Off-label promotion can present clear patient safety risks, such as efforts to market Zyprexa (olanzapine) for dementia treatment in the elderly (*9*). But carboplatin, FDA-approved for adult cancer treatment, is appropriately used (under evidence-based medical assessments) off-label for children (*10*).

Drug manufacturers have little incentive to seek FDA approval for orphan diseases (defined in the United States as affecting <200,000 patients) because of the generally low return on investment, despite some well-known treatments such as epoetin. So off-label drug use may be the only means to provide effective treatment. Indeed, up to 90% of drug use for rare conditions is off-label (*11*). Yet off-label access to drugs by orphan disease patients is inconsistent (*12*–*14*). Although FDA may provide exceptions regarding access, stakeholders have indicated a need for reform (*12*–*15*). A systemic approach is essential to better serve these patients. Permitting appropriate off-label drug promotion for orphan disease treatment can accomplish this goal.

[1]Institute of Health Law Studies, California Western School of Law, San Diego, CA 92101, USA. [2]Department of Anesthesiology, San Diego Center for Patient Safety, University of California, San Diego School of Medicine, San Diego, CA 92103, USA.

*Author for correspondence. E-mail: baliang@alum.mit.edu

CREDIT: ISTOCKPHOTO.COM

Orphan Drug Act

Under the 1983 Orphan Drug Act (ODA) (Public Law 97-414), FDA reviews and approves manufacturer applications for orphan designations (*16*). Other countries have similar laws (*17*). If approved, companies are eligible for incentives, including 7-year market exclusivity (i.e., no drug sales by a competitor); tax credits for clinical trial costs; federal grants to support clinical testing of rare disease treatments; exemption from FDA user fees; and expedited review of orphan drugs treating life-threatening diseases (*16*).

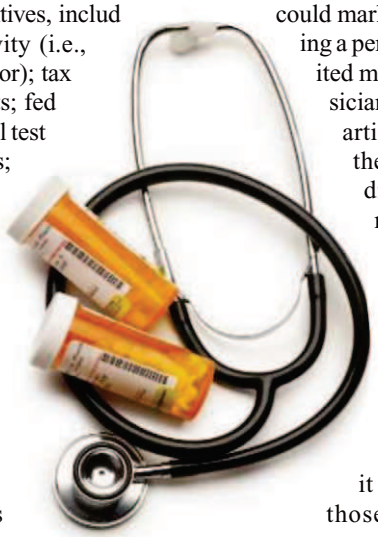

Although ODA has arguably provided treatment for some rare disease patients, concerns remain. Market exclusivity and high prices limit access to orphan drugs (*18*). ODA's effectiveness in encouraging orphan disease drug development has also been questioned (*18*). Only 300 approvals for orphan disease indications have been made since ODA enactment, out of an identified 6800 rare diseases (*14*) (table S1). Up to 20 million U.S. orphan disease patients do not have access to treatments because of limited physician knowledge and/or drug manufacturer investment (*14*).

Regulatory Confusion and Evolution

The Food, Drug, and Cosmetic Act [21 U.S. Code (U.S.C.) Ch. 9] (which authorizes FDA to oversee drug safety) prohibits drug manufacturers from promoting, marketing, or labeling for off-label uses. However, these prohibitions do not extend to medical practice (*19*), which results in confusion about off-label regulation. In the 1990s, drug companies attempted indirect means to promote off-label use by distributing scientific literature and funding continuing medical education (*19*). FDA issued guidance documents attempting to regulate these activities (*20*, *21*), but a court ruled these violated commercial free speech protections (*19*).

Shortly thereafter, the 1997 FDA Modernization Act (Public Law 105-115) permitted, for the first time, some off-label activities (*5*). It required manufacturers to apply for approval of off-label uses through a supplemental new drug application (sNDA); they could market off-label while indicating a pending sNDA review. It limited materials to be given to physicians (i.e., only peer-reviewed articles submitted to support the sNDA application) and disclosure that they were not FDA "approved or cleared" (*5*).

Recent FDA guidance is more permissive (*22*). The policy no longer limits manufacturers to disseminating only those materials filed with the sNDA, nor does it require that FDA review those materials (*23*). However, concerns regarding selective publication, data manipulation and omission, and ghostwriting have raised concerns regarding whether this new policy will protect public health (*22*).

Physicians must be able to extend use of approved drugs to orphan conditions and patients, particularly where no other alternative is approved. This requires greater education of providers and patients, improved patient access and consent, and, critically, a policy infrastructure that yields information on drug effects and provides for risk management and pharmacovigilance for patient safety. To reach these goals, we suggest the following.

Manufacturer application. Manufacturers would apply for authorization to promote off-label uses directly to physicians through an application similar to an ODA request for orphan designation. This application would

include rare disease treated, disease prevalence, biological rationale for the drug's use, drug regulatory and marketing status and history, drug safety or efficacy data for the orphan disease, promotional materials for FDA review and approval, risk-management and pharmacovigilance plan for monitoring and reporting off-label use effects, and attestation that promotion would not be false or misleading and that all materials would be peer-reviewed and FDA-approved before use. An application could be rejected or additional information required if FDA determined the risk versus benefit unacceptable or supporting evidence insufficient. This application would be updated when additional clinical information became available. Fraudulent materials would subject the applicant to federal fraud claims and patient tort suits if they are injured.

Patient base. Authorized off-label promotion would be limited to a fraction of the rare disease population, such as 4000 patients often required for standard FDA drug approval. If off-label prescribing exceeded this threshold, the manufacturer would be required to file a sNDA to continue any off-label promotion. Patients could still gain access through other, albeit cumbersome, FDA programs such as compassionate use, or existing low-cost or no-cost drug programs (*24*).

Drug monitoring. Similar to FDA-restricted distribution programs for high-risk drugs such as Tysabri (natalizumab) in Crohn's disease, FDA would establish efficacy parameters, and all patients and physicians participating in the off-label program would enroll in risk-assessment programs and would agree to extensive education and monitoring guidelines (*25*). A mandated efficacy assessment (after a defined time, based on the specific drug) would be established to collect data on clinical effectiveness and adverse events using enhanced data detection techniques as employed in the European Union (EU) for biosimilars (*24*). Updated off-label program data would be listed on a public Web site similar to clinicaltrials.gov (e.g., offlabeldrugs.gov).

The manufacturer would be responsible for an approved risk-management and pharmacovigilance plan to detect and report adverse events associated with off-label use. This approach is consistent with extensive monitoring guidelines that have been successful in other, similar contexts (*24*).

Funding. Given the financial benefits they would likely realize from off-label promotion, manufacturers would support this program by paying user fees for FDA review (but discounted compared with fees required for full New Drug Application review).

Program Benefits

The enrollment, risk-management, and pharmacovigilance mandates will ensure proper drug study and monitoring. Provider knowledge and patient informed consent are better addressed than in the current haphazard system, which may rely on limited physician knowledge and disparate sources of information (*14*). Indeed, under the program, physicians, professional societies, patients, and advocacy groups would have access to organized data and drug information. Generated data could be a basis for FDA assessment of warnings and use limits of these drugs, as well as more efficient identification of drugs that need further testing. Grant funding for clinical research would promote development of a knowledge base of off-label uses in orphan disease populations, again to the benefit of provider knowledge and patient informed consent. This program will also provide an expanded opportunity to study these drugs and orphan diseases, a particularly challenging area for physician-scientists (*14*). Organized manufacturer monitoring and adverse-event reporting would allow FDA to more proactively to enact drug-safety measures if needed.

Appropriate off-label promotion and information-sharing for orphan diseases, by promoting and expanding the systematic collection of and access to data, could also increase the potential that reimbursement for off-label use would be approved by public programs. This could lead to lower patient costs and increased access, as has occurred in the Medicare program for cancer drugs (*26*).

Drug manufacturers would also benefit, including small companies that have developed many of these drugs but face substantial financial issues. They would be able, legally, to increase awareness of and access to these drugs. This would remove large barriers to investing in orphan drugs, both by reducing costs of entry due to discounted fees and increasing manufacturer revenues from drug sales. It could also lead to competition and to lower patient costs by facilitating market entry of additional manufacturers, since exclusivity incentives (as in the ODA) would not apply. Manufacturers whose unapproved, off-label drug use in the program that proved successful could subsequently also access ODA incentives and full market approval to maximize returns for these drugs, or clinical trials–oriented accelerated approval (*15*).

The themes of this proposal can serve as an approach for developed countries to address the problem of uneven access and regulation of off-label drug use in orphan disease populations while improving efforts to monitor drug safety. For example, EU regulators can adapt the Committee for Orphan Medicinal Products (COMP) to serve as the prime off-label program authority. COMP would then coordinate drug review, monitoring, and oversight, by using established drug surveillance systems (*24*).

Manufacturers' obligations and marketing content must be monitored to ensure program integrity. The policy and included drugs must be revisited so that stakeholders have up-to-date information. Through this system, better access, knowledge, and benefits of off-label drug use can inure to orphan disease populations.

References and Notes

1. 21 U.S.C. § 396 (2000).
2. B. M. Psaty, W. Ray, *JAMA* **299**, 1949 (2008).
3. D. C. Radley, S. N. Finkelstein, R. S. Stafford, *Arch. Intern. Med.* **166**, 1021 (2006).
4. R. S. Stafford, *N. Engl. J. Med.* **358**, 1427 (2008).
5. S. Salbu, *Fla. Law Rev.* **51**, 181 (1999).
6. M. G. Krammer, *National Organization for Rare Disorders and the Experiences of the Rare Disorders Community* (National Organization for Rare Disorders, Washington, DC, 2003).
7. National Institutes of Health (NIH), NIH launches undiagnosed diseases program, *NIH News* (NIH, Bethesda, MD, 2008); www.nih.gov/news/health/may2008/nhgri-19.htm.
8. In Need of Diagnostics, Inc., http://inod.org/default.aspx.
9. A. Berenson, *New York Times*, 18 December 2006, p. A1.
10. J. Boos, *Ann. Oncol.* **14**, 1 (2003).
11. T. Hampton, *JAMA* **297**, 683 (2007).
12. Rarer Cancers Forum, *Off Limits: An Investigation into How NHS Organisations Determine Requests for the Use of Off-Label Treatments for Cancer Patients* (Rarer Cancers Forum, Canterbury, UK, 2009); www.rarercancers.org.uk/news/current/off_limits__new_rarer_cances_forum_report/.
13. M. Schlander, M. Beck, *Curr. Med. Res. Opin.* **25**, 1285 (2009).
14. G. J. Brewer, *Transl. Res.* **154**, 314 (2009).
15. E. A. Richey *et al.*, *J. Clin. Oncol.* **27**, 4398 (2009).
16. Department of Human and Health Services (DHHS), *The Orphan Drug Act: Implementation and Impact* (OEI-09-00-00380, DHHS, Washington, DC, 2001).
17. Canadian Organization for Rare Disorders, *Canada's Orphan Drug Policy: Learning from the Best* (Canadian Organization for Rare Disorders, Toronto, 2005).
18. A. Pollack, *New York Times*, 30 April 1990, p. D1.
19. *Wash. Legal Found*. v. *Friedman*, 13 F. Supp. 2d 51, 55 (D.D.C. 1998).
20. FDA, *Fed. Regist.* **61**, 52800 (1996).
21. FDA, *Fed. Regist.* **62**, 64073 (1997).
22. M. M. Mello, D. M. Studdert, T. A. Brennan, *N. Engl. J. Med.* **360**, 1557 (2009).
23. FDA, *Good Reprint Practices for the Distribution of Medical Journal Articles and Medical or Scientific Reference Publications on Unapproved New Uses of Approved Drugs and Approved or Cleared Medical Devices* (FDA, Silver Spring, MD, 2009).
24. B. A. Liang, *Harvard J. Legis.* **44**, 363 (2007).
25. FDA, *FDA Approves Tysabri to Treat Moderate-to-Severe Crohn's Disease* (FDA news release, FDA, Silver Spring, MD, 2008); www.fda.gov/NewsEvents/Newsroom/PressAnnouncements/2008/ucm116835.htm.
26. R. Abelson, A. Pollack, *New York Times*, 27 January 2009, p. A22.

Supporting Online Material www.sciencemag.org/cgi/content/full/327/5963/273/DC1

10.1126/science.1181567

BIOCHEMISTRY

CO_2mmon Sense

Animals and plants use the same enzyme to detect carbon dioxide.

Wolf B. Frommer

Plants and animals sense and respond to carbon dioxide (CO_2), but the means by which they do so have not been well defined. Plants detect and respond to an increase in environmental CO_2 concentration by closing the gas valves in their leaves (thus conserving water), but the CO_2 sensing mechanism has been debated. Fruit flies, mosquitoes, and moths sense CO_2 to find food resources such as decaying fruits, human prey, and flowers, respectively, but as well, the sensing mechanisms are not yet fully characterized. Pressurized CO_2 is used in many food products, such as carbonated beverages, but it is not clear how humans sense the gas, nor what advantage this might serve. It is particularly interesting that two recent studies have unraveled, independently, how organisms as diverse as plants and mammals sense CO_2, and come up with a similar mechanism whose output triggers responses not previously linked to CO_2 detection (*1*, *2*).

Chandrashekar *et al*. (*1*) examined how we experience CO_2 on our tongues—a combined physical and chemical sensation. It turns out that the feel of fizz relies in part on the detection of CO_2 bubbles that stimulate somatosensory receptors on the tongue. CO_2 appears to provoke a taste response for acidity that we associate with carbonation. The authors first determined that CO_2–induced action potentials occur in nerves that connect to taste receptor cells in the mouse tongue. When they analyzed the electrical activity of these nerves in mice lacking specific taste receptors, they made the surprising observation that the response to CO_2 disappeared only if the sour sensor cells were missing. A survey of genes in the sour sensor cells revealed that a gene encoding a carbonic anhydrase was specifically expressed in these cells. Then they showed that the enzyme is essential for mice to detect CO_2.

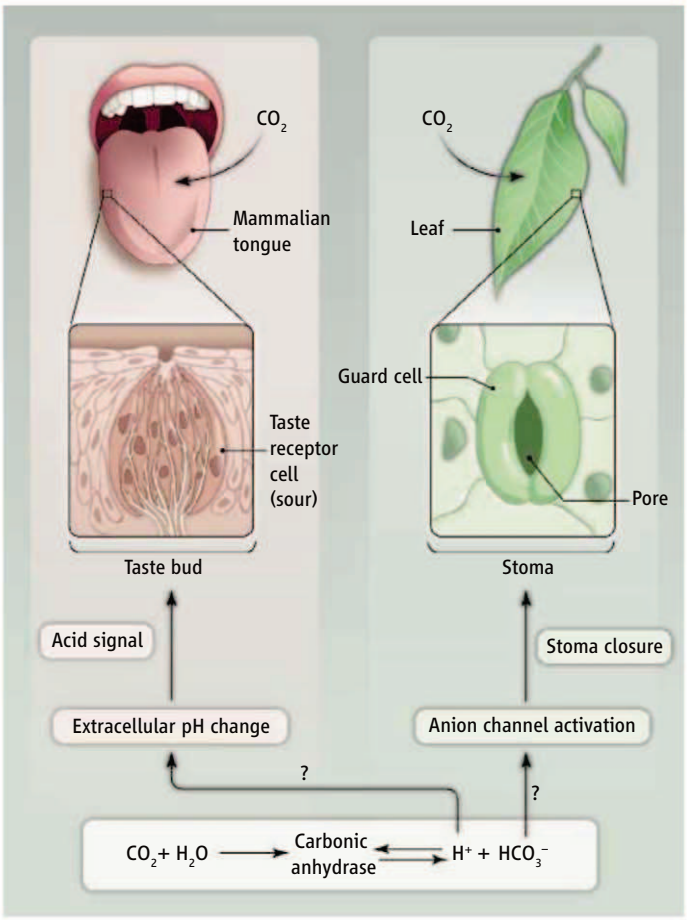

Transponder or senzyme? Carbonic anhydrase operates in CO_2 sensing in mammals (α-carbonic anhydrase at the cell surface) and plants (β-carbonic anhydrases in the cytoplasm and chloroplast). In both cases, it is possible that an increase in protons and/or bicarbonate, and/or a decrease CO_2, are detected (two possible mechanisms are shown). As a transponder, the enzyme promotes the conversion of CO_2 and water into bicarbonate and protons, and the ultimate signal that is sensed is either bicarbonate or acidification by protons. Alternatively, as a senzyme, the binding of CO_2 to the enzyme may cause a conformational change that is detected by a protein that connects to a signaling cascade.

Carbonic anhydrase is one of the most efficient enzymes known. It facilitates the interconversion of CO_2 and water to bicarbonate and protons, with a turnover rate of up to 1 million CO_2 molecules per second. Chandrashekar *et al*. suggest that carbonic anhydrase—specifically, α-carbonic anhydrase isoform 4 (CA4)—produces a local increase in protons in response to CO_2. CA4 is anchored at the surface of gustatory cells in the mammalian tongue, where it produces protons that may acidify the immediate extracellular environment. The link between sour and CO_2 sensing implicates pH change as a key component of the CO_2 response (see the figure). If this is the case, then carbonic anhydrase is not a sensor in the strict sense, but a transponder that promotes the conversion of CO_2 and water into molecules that indirectly report CO_2. One could argue that the two processes together create the CO_2 sensor, although any other mechanism that leads to a local proton concentration increase (acidification by compounds such as vinegar, for example) should lead to the same response. How the proton increase is detected remains a puzzle.

Alternatively, carbonic anhydrase may have a dual function as both enzyme and sensor (a "senzyme"), as has previously been suggested for hexokinase (*3*). Hexokinase phosphorylates glucose in the cytosol, but also senses and responds to glucose by entering the nucleus and binding to DNA (promoters) to regulate gene expression. Dual functionality has been found for many transporters, such as the plant transporter Chl1, which senses and transports nitrate (*4*). In the case of carbonic anhydrase, a conformational change of the enzyme upon binding of CO_2, as described for β-carbonic anhydrases (*5*), might be detected by a protein that couples to a signaling pathway. Analysis of mutants that lack enzymatic function but retain the allosteric site may indicate whether carbonic anhydrases work as senzymes.

The ability to sense CO_2 gas concentrations is also crucial for plants. Plants use atmospheric CO_2 and the Sun's energy to build their biomass. They are covered with a cuticle that prevents water loss through their surface. Stomata—microscopic pores in the epidermis of leaves—act as controlled valves to take up CO_2 while limiting water loss. Thus, CO_2 is sensed by the plants to adjust the opening of these pores in response

Plant Biology, Carnegie Institution for Science, 260 Panama Street, Stanford, CA 94305, USA. E-mail: wfrommer@stanford.edu

to demand. CO_2 even controls the density of stomata; as a compensatory mechanism, their numbers increase if the concentration of CO_2 drops. Similar to animals, a major puzzle has been how plants sense CO_2. Hu *et al*. (*2*) found that the carbonic anhydrases βCA1 and βCA4 in the model plant *Arabidopsis thaliana* function in CO_2 sensing. Plants lacking the two enzymes were greatly impaired in their response to increases in atmospheric CO_2, showing much less stomatal pore closure. In contrast to the extracellular location of the mouse carbonic anhydrase, the plant enzymes are inside the cell, both adjacent to the cell membrane and inside chloroplasts. Thus, although the enzymatic function of the enzymes—as either transponder or senzyme—is conserved, the site of action is very different, implying that the sensing mechanism also may be different. Astonishingly, Hu *et al*. (*2*) found that expressing a structurally unrelated mammalian α-carbonic anhydrase in *Arabidopsis* plants lacking carbonic anhydrases restored CO_2 responsiveness. This supports the transponder hypothesis, as it is less probable that the downstream signaling machinery in the plant can function with this very different enzyme.

A key element of stomatal closure is the efflux of ions. Hu *et al*. (*2*) further showed that intracellular bicarbonate released by carbonic anhydrase activates anion channels in guard cells, allowing ions to efflux, thus triggering the closure of stomatal pores (see the figure). Plants overexpressing the β-carbonic anhydrases in guard cells also improved conservation of water, which suggests a possible means to engineer plants that use less water.

Although plants and humans diverged about 1 billion years ago, they use similar mechanisms to detect CO_2 sensing. Two main observations suggest that their common sensing mechanism must have evolved independently. There is a striking difference in the cellular location of the enzymes. Moreover, there are five classes of carbonic anhydrase enzymes that are unrelated in protein sequence and structure; plants and animals express different family members (*6*).

Why plants evolved this mechanism is obvious—they need to adjust the valves to optimize CO_2 uptake from the atmosphere while minimizing water loss. In humans, one may speculate that this mechanism was retained to help identify rotting food, and now serves mainly to identify carbonated drinks. The observation that carbonic anhydrase is also present in insect gustatory and olfactory cells and may cooperate with ionotropic receptors (ion channels that, when activated by a ligand, open and permit ion flow) may help to identify how insects and mammals use CO_2 sensors to discern food sources (*7*).

References

1. J. Chandrashekar *et al*., *Science* **326**, 443 (2009).
2. H. Hu *et al*., *Nat. Cell Biol.* **12**, 87 (2009).
3. Y. H. Cho, S. D. Yoo, J. Sheen, *Cell* **127**, 579 (2006).
4. C. H. Ho, S. H. Lin, H. C. Hu, Y. F. Tsay, *Cell* **138**, 1184 (2009).
5. R. S. Rowlett, *Biochim. Biophys. Acta* 10.1016/j.bbapap.2009.08.002 (2009).
6. S. Elleuche, S. Pöggler, *Curr. Genet.* **55**, 211 (2009).
7. M. Luo *et al*., *Curr. Opin. Neurobiol.* **19**, 354 (2009).

10.1126/science.1186022

ECOLOGY

Explaining Bird Migration

Predation pressure falls with increasing latitude, helping to explain why many birds migrate as far north as the high Arctic.

Olivier Gilg[1,2] and Nigel G. Yoccoz[3]

Arctic shorebirds can travel tens of thousands of kilometers every year as they fly along intercontinental flyways from their southern wintering grounds to their remote, harsh breeding sites. How these birds solve the navigational and physiological constraints has been largely answered, but why they migrate is still a question with many possible answers (*1*). On page 326 of this issue, McKinnon *et al*. (*2*) present a continent-wide study that points to predation as a driving mechanism for migration. The study also elucidates the role of predation in shaping Arctic terrestrial biodiversity.

For migration to be sustained in evolutionary terms, the associated costs and benefits must balance. The costs—higher energetic requirements and mortality risk—increase with flyway length and, hence, with latitude. The benefits of Arctic breeding grounds include open landscapes, permanent daylight, time-limited but abundant resources, limited competition, lower pathogen loads, and lower predation pressure, but not all these benefits increase with latitude. For example, if Arctic migrants were just looking for rich and open habitats to be exploited under permanent daylight, they would stop in the low-Arctic zone, never reaching the northernmost regions in Greenland and Canada. Although other hypotheses still need to be properly tested (*3*), McKinnon *et al*. provide convincing evidence of lowered predation pressure the further north one gets. The authors focus on shorebirds, but their results might be relevant for other ground-nesting birds, because all their sites share a key predator in these ecosystems: the Arctic fox.

The results also shed light on the dominant role played by predation in the functioning and structuring of Arctic terrestrial vertebrate communities. In this region more than anywhere else, populations are strongly impacted, and sometimes driven, by predator-prey interactions. The key pieces of this puzzle are several species of Arctic lemmings, whose dynamics are typically cyclic. Lemming densities depend on, but also determine, the functional and numerical responses of predator species (mainly Arctic fox, snowy owl, jaegers, and small mustelids) (*4*). In turn, the 3- to 4-year lemming cycles strongly affect the dynamics of alternate prey, such as shorebirds and wildfowl, through indirect predator-prey interactions (*5*–*7*): In the low phase of the lemming cycle, the fraction of these alternate prey increases in the predators' diets; in the peak phase, predators specialize on lemmings and release their predation pressure on alternate prey. Surprisingly, the mechanisms behind latitudinal trends in predation pressure and the impact of lemming cyclic phases are not discussed by McKinnon *et al*.

In this cat-and-mouse game, shorebirds are both impacting (by contributing to increase predators' survival rates) and impacted by lemming-predator interactions. For the shorebird species that are most sensitive to predation, high predation pressure by the Arctic fox cannot be compensated by reproduction or survival. Viable populations of these species may hence occur only within the lemming distribution range, where the pressure imposed by the Arctic fox is regu-

[1]Department of Biological and Environmental Sciences, 00014 University of Helsinki, Finland. [2]Lab Biogéosciences, University of Burgundy, 21000 Dijon, France. [3]Department of Arctic and Marine Biology, University of Tromsø, 9037 Tromsø, Norway. E-mail: olivier.gilg@gmail.com

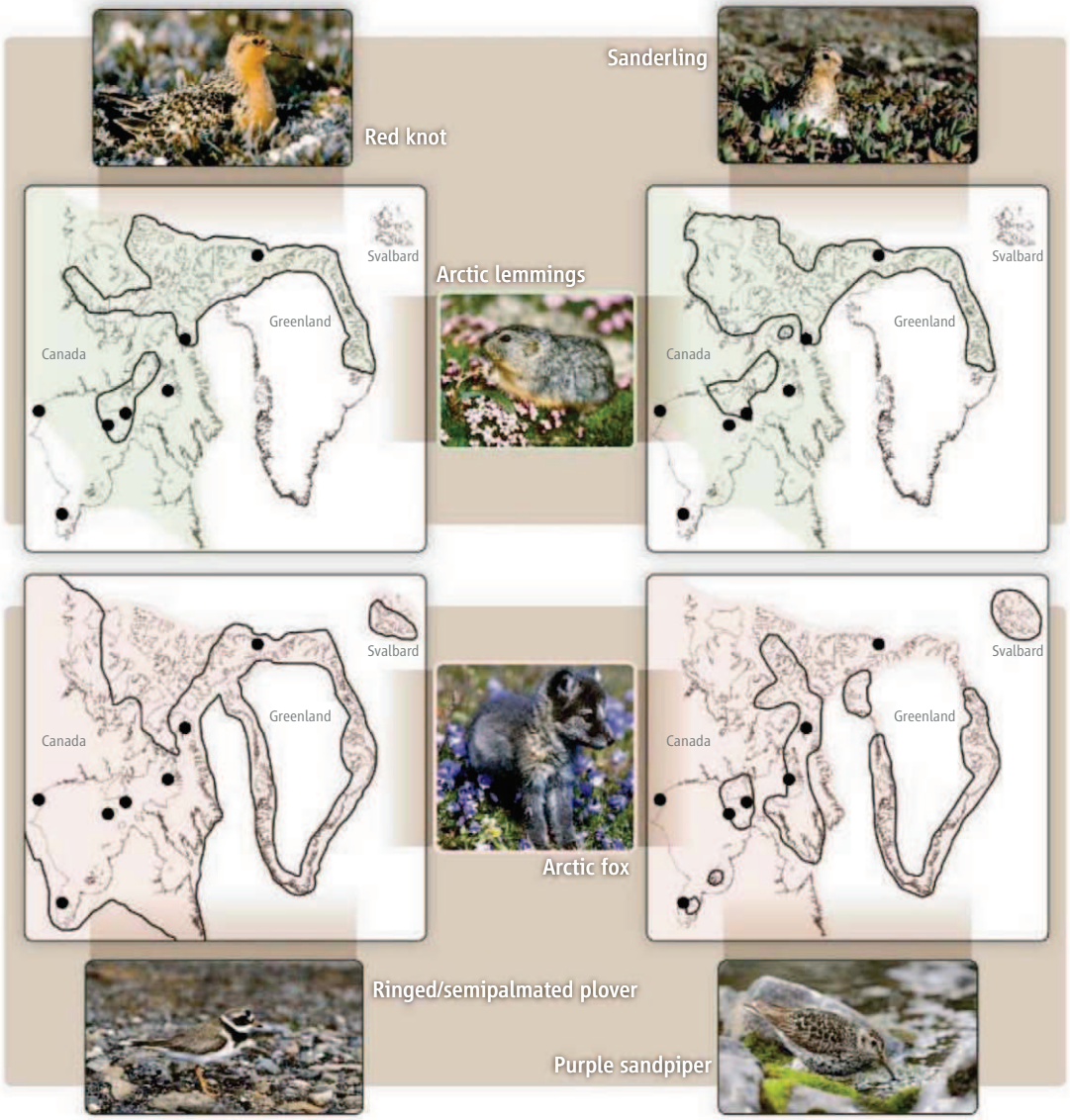

Follow the lemmings. Using artificial nests at several field sites in the Canadian Arctic (black dots), McKinnon *et al*. show that Arctic shorebirds face declining predation pressure toward the north (*2*), an important benefit for long-distance migrants whose biogeography should hence partly be driven by predator-prey interactions. The distribution ranges of several species support the latter hypothesis. In Svalbard and South and West Greenland, lemmings (light green) are absent and terrestrial predators like the Arctic fox (light pink) impose a higher predation pressure on birds. The perfect mismatch between these lemming-free areas and the ranges of some high-Arctic shorebirds (**upper panels**) supports such a predation-driven pattern and suggests that these species are more sensitive to predation than are species that can breed further south or within the entire distribution range of the Arctic fox (**lower panels**). Data are from (*14*–*16*) and additional regional sources (*17*–*23*).

PHOTO CREDITS: OLIVIER GILG

larly released when lemmings are plentiful (*8*). Empirical data support this assumption: The highest diversity of *Calidris* species is found within the lemming distribution range (*9*), and some species (such as Sanderling and Knot) are absent outside of this range (see the figure). Using molecular tools to test for spatial and temporal synchrony in the postglacial expansion of lemmings, fox, and shorebirds, and measuring predation pressures on natural nests from different species and in different communities, should provide additional evidence for the hypothesis, overlooked in previous research [such as (*10*)], that shorebird biogeography can be explained by predator-prey interactions.

During the 2007–2008 International Polar Year, many large-scale initiatives (*11*) studied the importance of top-down processes such as changes in predation pressure versus bottom-up processes such as greening of vegetation. The growing evidence that predation is a driving force in structuring Arctic ecosystems, and the quality of these programs' results, call for the continuation and extension of such circumpolar networks.

Climate change already affects many Arctic species (*12*). Because these ecosystems are structured by only a handful of species, these changes immediately diffuse to lower and upper trophic levels through strong direct or indirect predator-prey interactions. Scientists in the Arctic must therefore increase their efforts in documenting and modeling changes in predator behavior and dynamics, including the species currently invading from the south (*13*).

References and Notes

1. T. Alerstam, A. Hedenström, S. Åkesson, *Oikos* **103**, 247 (2003).
2. L. McKinnon *et al*., *Science* **327**, 326 (2010).
3. T. Piersma, *Oikos* **80**, 623 (1997).
4. O. Gilg *et al*., *Oikos* **113**, 193 (2006).
5. R. W. Summers, L. G. Underhill, E. E. Syroechkovski, *Ecography* **21**, 573 (1998).
6. J. Bêty, G. Gauthier, J. F. Giroux, E. Korpimäki, *Oikos* **93**, 388 (2001).
7. B. Sittler, O. Gilg, T. B. Berg, *Arctic* **53**, 53 (2000).
8. S. Larson, *Oikos* **11**, 276 (1960).
9. C. Zöckler, *WCMC Biodivers. Bull.* **3**, 1 (1998).
10. S. S. Henningsson, T. Alerstam, *J. Biogeogr.* **32**, 383 (2005).
11. Examples are www.cen.ulaval.ca/arcticwolves/, which includes the work in (*1*), and www.arctic-predators.uit.no.
12. E. Post *et al*., *Science* **325**, 1355 (2009).
13. R. A. Ims, E. Fuglei, *Bioscience* **55**, 311 (2005).
14. Caff, *Arctic Flora and Fauna: Status and Conservation* (Edita, Helsinki, 2001).
15. P. Hayman, J. Marchant, T. Prater, *Shorebirds* (Croom Helm, London, 1986).
16. C. Zöckler, The Arctic Bird Library, www.unep-wcmc.org/arctic/birds/ArcticBirdLibrary.htm.
17. D. Boertmann, *Medd. Gronl. Biosci.* **38**, 1 (1994).
18. K. M. Kovacs, C. Lydersen, *Birds and Mammals of Svalbard* (Norwegian Polar Institute, Tromso, 2006).
19. A. W. F. Banfield, *The Mammals of Canada* (Univ. of Toronto Press, Toronto, 1974).
20. W. E. Godfrey, *Les Oiseaux du Canada* (Broquet-Musée nationaux Canada, Ottawa, 1986).
21. B. Génsbøl, *A Nature and Wildlife Guide to Greenland* (Gyldendal, Copenhagen, 2004).
22. D. Lepage, D. N. Nettleship, A. Reed, *Arctic* **51**, 125 (1998).
23. O. Gilg *et al., Ecopolaris—Tara 5 expedition to NE Greenland 2004* (GREA, Francheville, 2005).

10.1126/science.1184964

CHEMISTRY

Green Gold Catalysis

High–surface area gold catalysts exhibit promising properties suitable for industrial application.

Claus Hviid Christensen[1] and Jens K. Nørskov[2]

In the efforts to develop a more sustainable chemical industry, there is an urgent need to discover and implement cleaner chemical transformations that should preferably use only renewable resources as starting materials, and produce no hazardous waste at all. Thus, catalytic oxidations that use atmospheric air as the oxidant and form pure water as the only by-product are of utmost importance. It is clear that catalysts featuring nanometer-sized gold particles can play an important role in advancing such green oxidations (*1*). On page 319 of this issue, Wittstock *et al.* (*2*) take green gold catalysis one step closer toward industrial application.

Methylformate, an important industrial chemical, is produced efficiently by low-temperature, aerobic oxidation of methanol through the use of an unsupported nanoporous gold catalyst prepared by controlled leaching of silver from a bulk gold-silver alloy. Wittstock *et al.* show how the catalytic performance is improved by the presence of residual silver, but moreover, that such silver-promoted gold catalysts exhibit sufficient lifetime to be interesting industrially.

Since the first reports of the spectacular performance of gold nanoparticles in the aerobic oxidation of carbon monoxide (*3*), efforts have been devoted to understanding the fundamentals of this surprising reactivity. Many possible explanations have been proposed (*4*), but one issue has continuously attracted most attention—the role of the support. Gold nanoparticles are usually supported on a high–surface area oxide, and it has been suggested that this oxide support plays an important role in the special properties of nanoparticle gold catalysts. Some suggest that the support activates some of the reactants (*5*)—for example, O_2—while others point to special chemical properties of the interface between the gold and the support (*6*), or to charge transfer to or from the support to the gold (*7*). Wittstock *et al.* show that completely unsupported gold nanoparticles can carry out partial oxidation, thus supporting the view that a hierarchy of effects is at play, where the size (or number of low-coordinated gold atoms) is the most important (*8*). Wittstock *et al.* suggest that most of the reaction takes place on the nanoporous gold while the silver promotes the O_2 dissociation (*2*), in agreement with calculations showing that O_2 dissociation is considerably more facile at low-coordinated silver atoms than at gold atoms (*9*). The reason for this difference is that the 4d shell of silver is considerably less extended in space than the gold 5d valence states, which leads to a weaker Pauli repulsion between the surface and the adsorbing oxygen. This means that even a single silver atom can enhance the reactivity of gold atoms by providing reduced repulsion in proportion to the ratio of silver to gold atoms involved in the bonding. This is an example of interpolation of surface chemical properties between different elements in the periodic table (*10*).

Most studies on heterogeneous gold catalysts so far have concerned the aerobic oxidation of carbon monoxide. This particular

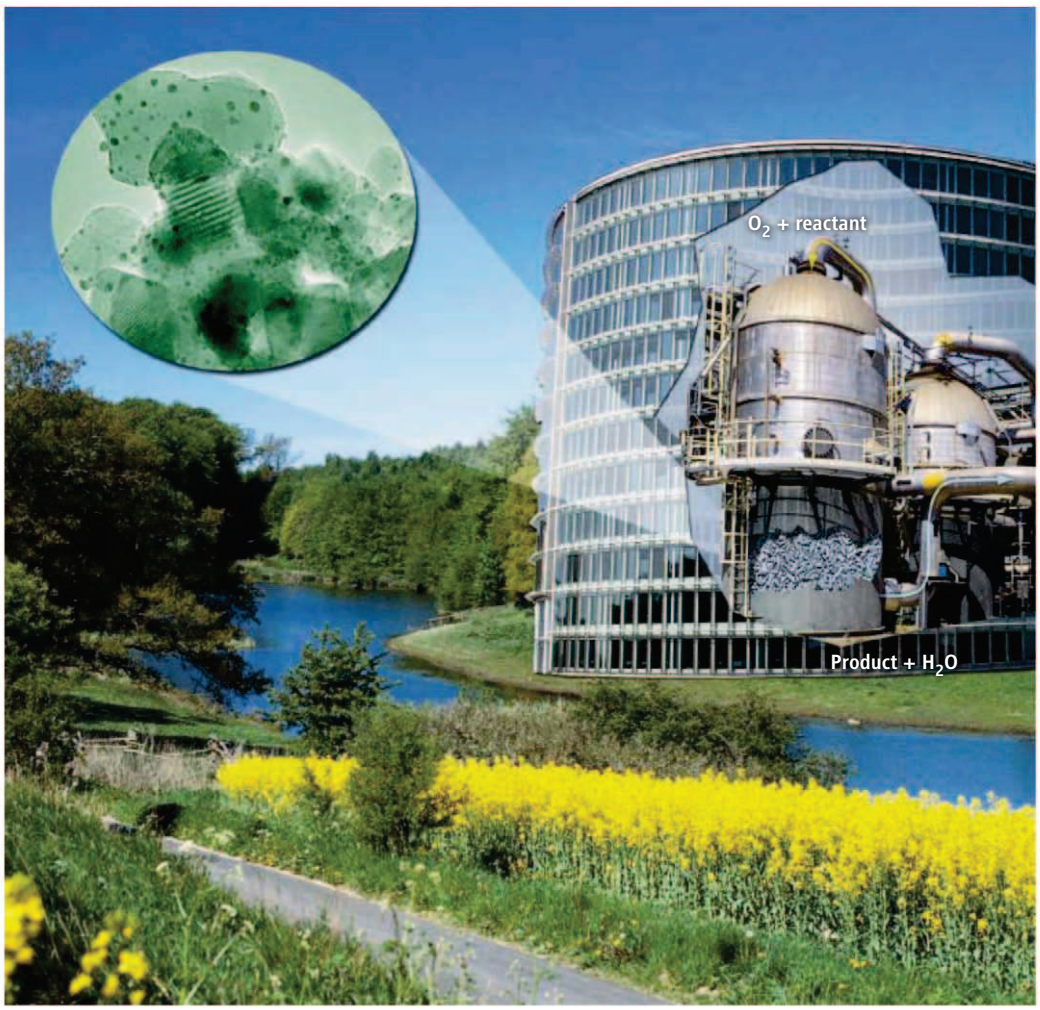

Green chemistry. The ultimate green catalytic oxidation process uses atmospheric air as the oxidant and forms water as the only by-product. This chemical transformation is achieved by use of an active and selective catalyst featuring suitably designed gold nanoparticles as the active ingredient.

CREDIT: CLAUS CHRISTENSEN AND POUL MØLLER

[1]Haldor Topsøe A/S, Nymøllevej 55, DK-2800 Lyngby, Denmark. [2]Center for Atomic-Scale Materials Design, Department of Physics, Technical University of Denmark, DK-2800 Lyngby, Denmark. E-mail: chc@topsoe.dk

reaction is primarily important as a model reaction, although it might eventually prove technically relevant in the purification of various gas streams containing minor carbon monoxide impurities. However, during the last decade, more examples of aerobic oxidations of other substrates have been reported over gold nanoparticle catalysts (*11*). Several of these reports have targeted potentially interesting large-scale industrial chemicals, such as gluconic acid (*12*), acetic acid (*13*), and propylene oxide (*14*). For such reactions, it is highly desirable to use air as the oxidant and have pure water as the only side product. With proper catalysts available that feature both high activity and selectivity, this can be considered the ultimate way to conduct oxidations (see the figure). Even though the gold catalysts have shown promising performance in these reactions, they have apparently not been competitive with existing technologies. Accordingly, some studies have attempted to improve the catalytic activity and selectivity—for example, by proper alloying (*11*) or by strategies to prolong the catalyst lifetime (*15*). Wittstock *et al*. specifically show how silver alloying promotes oxygen activation, and how the unsupported, nanoporous gold catalysts are stable for prolonged test runs (*2*). It is tempting to assume that this type of catalyst could also prove beneficial in some of the aerobic oxidation reactions in which only supported pure gold catalysts have been tested until now. Possibly, this will take green gold catalysis closer toward industrial applications.

References

1. G. J. Hutchings, *Gold Bull.* **37**, 3 (2004).
2. A. Wittstock, V. Zielasek, J. Biener, C. M. Friend, M. Bäumer, *Science* **327**, 319 (2010).
3. M. Haruta, T. Kobayashi, H. Sano, N. Yamada, *Chem. Lett.* **16**, 405 (1987).
4. R. Meyer, C. Lemire, S. Shaikhutdinov, H. J. Freund, *Gold Bull.* **37**, 72 (2004).
5. G. C. Bond, D. T. Thomson, *Catal. Rev., Sci. Eng.* **41**, 319 (1999).
6. H. Sakurai, T. Akita, S. Tsubota, M. Kiuchi, M. Haruta, *Appl. Catal. A* **291**, 179 (2005).
7. A. Sanchez *et al*., *J. Phys. Chem. A* **103**, 9573 (1999).
8. N. Lopez *et al*., *J. Catal.* **223**, 232 (2004).
9. H. Falsig *et al*., *Angew. Chem. Int. Ed.* **47**, 4835 (2008).
10. C. J. H. Jacobsen *et al*., *J. Am. Chem. Soc.* **123**, 8404 (2001).
11. A. Corma, H. Garcia, *Chem. Soc. Rev.* **37**, 2096 (2008).
12. S. Biella, L. Prati, M. Rossi, *J. Catal.* **206**, 242 (2002).
13. C. H. Christensen *et al*., *Angew. Chem. Int. Ed.* **45**, 4648 (2006).
14. A. K. Sinha, S. Seelan, S. Tsubota, M. Haruta, *Top. Catal.* **29**, 95 (2004).
15. B. K. Min, W. T. Wallace, D. W. Goodman, *J. Phys. Chem. B* **108**, 14609 (2004).

10.1126/science.1184203

PLANT SCIENCE

The Botanical Solution for Malaria

Improved breeding of a plant that produces a major antimalarial compound is now possible based on knowledge of its genetic map.

Wilbur K. Milhous[1] and Peter J. Weina [2]

For thousands of years, Chinese herbalists used leaves from the plant *Artemisia annua* to treat numerous illnesses, including malaria. Today, the plant's natural antimalarial compound—a sesquiterpene lactone (and endoperoxide) called artemisinin—is the most effective drug for combating malarial infections (see the figure). A major hurdle in using this compound to treat malaria—estimated to cause 300 to 500 million cases and over 1 million deaths each year, worldwide—has been producing enough artemisinin to meet world demand. Attempts to efficiently extract sufficient quantities have been slowly improving. Now Graham *et al*. (*1*) have paved the way to fast-track breeding varieties of the *A. annua* plant with highly desirable genetic traits. On page 328 of this issue, the authors report a genetic map of the plant and identify key loci that could improve agricultural yields, decrease production costs, ensure a steady global supply of the drug, and improve grower confidence in the crop.

Graham *et al*. recognized that the yield of artemisinin varied by geographic origin and was inheritable when the super leafy strains possessing bountiful glandular trichomes—outgrowth structures where artemisinin is produced and stored by the plant—were crossed. They used a pedigree plant (Artemis) to establish the first genetic linkage and quantitative trait loci (QTL) maps for the plant species, and then validated positive QTL for artemisinin yield. The authors used deep sequencing of the plant transcriptome (all mRNA molecules present in the organism) to successfully identify genes and markers, which will

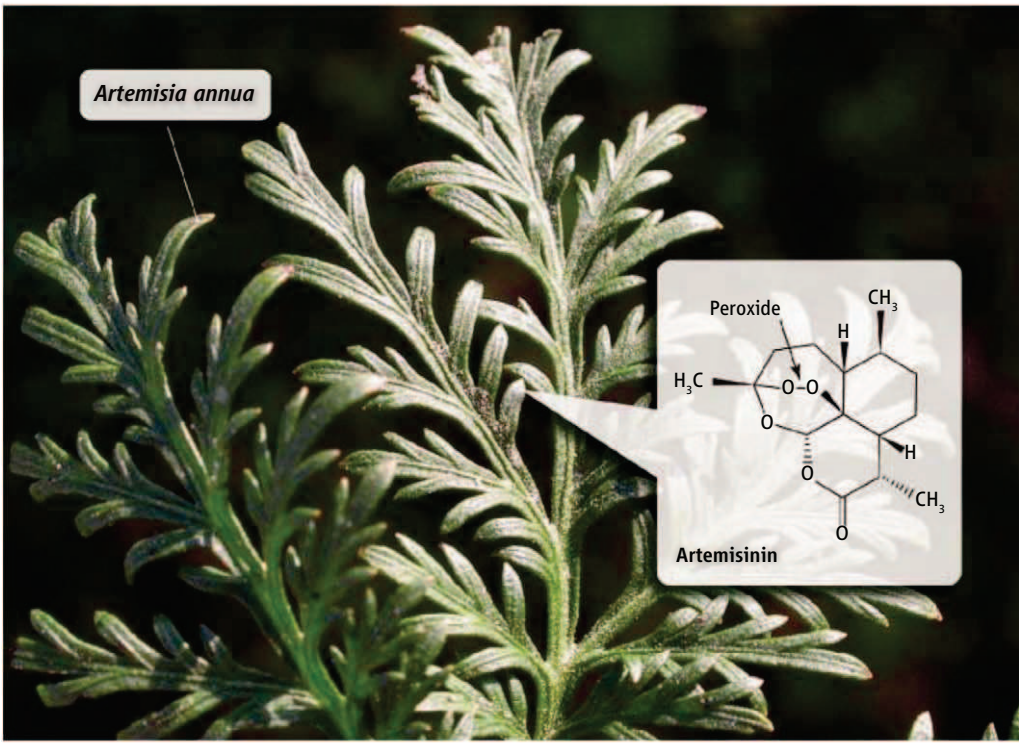

Natural drug resource. The antimalarial compound artemisinin is purified from the plant *Artemisia annua*. Information about the plant's genetic map should allow for breeding and selection of agronomic traits that will enable rapid development of improved varieties.

[1]College of Public Health, University of South Florida, Tampa, FL 33612, USA. [2]Walter Reed Army Institute of Research, Silver Spring, MD 20910–7500, USA. E-mail: wmilhous@health.usf.edu

facilitate crossing of highly productive varieties. Their results are innovative in terms of the scale of research and sophistication of the technologies involved.

This seminal result comes almost 25 years after artemisinin crystals were first reported in 1985 by Klayman (*2*). This achievement was pivotal because it also broke a code, but a medicinal chemistry process code rather than a genetic one. Prior to this report, only Chinese scientists could crystallize the purified compound from the plant source. Unfortunately, they would not share their technology with the Western world at that time.

Klayman assembled botanists from the Smithsonian Institute, and located a small naturally growing *A. annua* "crop" on the banks of the Potomac River. However, this discovery came at a low point for drug development at the Walter Reed Army Institute of Research, where scientists, including Klayman, were struggling with a slimmed down research budget—reduced from over $70 million (adjusted for inflation) per year during the Vietnam War era, to $4 million in the 1980s. Ironically, during the same period, the Vietnam government asked China for the Qinghaosu (Chinese word for artemisinin) miracle to combat malaria that had become resistant to other drugs. Another shocking blow to the Walter Reed effort was the discovery of brainstem lesions in animal models during advanced preclinical toxicology testing of drug candidates (*3*). It would take years to unravel the mystery of this neurotoxicity. Millions of dollars were spent to prove an acceptable safety profile of the water-soluble forms of the compound, such as artesunate and artelinate, over the lipid-soluble forms such as artemether or arteether (*4*). Finally, in 2004, a regulatory dossier was filed with the U.S. Food and Drug Adminstration (FDA) and artesunate was made available to treat severe and complicated malaria in the United States (*5*). Just last year, the FDA approved an oral artemisinin combined therapy for less severe cases.

The artemisinin yield from Klayman's 1985 Potomac River variety of *A. annua* was only 0.06% of dry weight of plant material, whereas the Chinese had described varieties in Sichuan province with yields of 0.01 to 0.5% (*2*). Even the best of basic crop science, though, would not keep pace with the growing global health demands and emerging resistance to the antimalarial mainstay, chloroquine. Solid financial backing and entrepreneurship by the Bill and Melinda Gates Foundation and the Medicines for Malaria Venture (an international public-private partnership) would prevail with a three-pronged strategy extending into 2015: Develop synthetic artemisinin-like peroxides that are easy and inexpensive to make and lack potential cross resistance to other drugs, exploit microbial-based systems that promote synthesis of the artemisinin precursor for chemical conversion to the mature form, and use innovative horticulture technologies to boost plant robustness and production. However, these strategies have had variable success. While thousands of synthetic artemisinin compounds have been made and tested, only a select few have been stable, orally available, and efficacious in animal models (*6*). The Medicines for Malaria Venture prioritized the development of next-generation compounds (ozonides), however, initial clinical efficacy trials were disappointing, and efforts refocused on molecules with improved druglike properties (*7*). Production of recombinant artemisinin in bacterial and yeast systems have experienced success, but still require at least three synthetics steps to achieve the final product (*8*, *9*).

So far, the strategy that has produced the most promise for the near term, and will likely provide the most cost-effective final product of this life-saving drug, rests with innovative horticultural technologies. The result of Graham *et al*. has placed us on that track. The next big hurdle for this molecule will be emerging resistance to the drug.

References

1. I. A. Graham *et al*., *Science* **327**, 328 (2010).
2. D. L. Klayman, *Science* **228**, 1049 (1985).
3. T. G. Brewer *et al*., *Trans. R. Soc. Trop. Med. Hyg.* **88**, (suppl. 1), 33 (1994).
4. R. F. Genovese, D. B. Newman, T. G. Brewer, *Pharmacol. Biochem. Behav.* **67**, 37 (2000).
5. 3 August 2007/56(30); 769-770 MMWR Notice to Readers: New Medication for Severe Malaria Available Under an Investigational New Drug Protocol (www.cdc.gov/malaria/features/artesunate_now_available.htm).
6. J. L. Vennerstrom *et al*., *Nature* **430**, 900 (2004).
7. T. N. Wells, *Nat. Rev. Drug Discov.* **8**, 879 (2009).
8. D. K. Ro *et al*., *Nature* **440**, 940 (2006).
9. J. M. Carothers, J. A. Goler, J. D. Keasling, *Curr. Opin. Biotechnol.* **20**, 498 (2009).

10.1126/science.1184780

CHEMISTRY

Ion Chemistry Mediated by Water Networks

The reaction of ions such as NO^+ with networks of only a few water molecules has implications for understanding chemistry in the ionosphere.

Katrin R. Siefermann[1] and Bernd Abel[1,2]

The remarkable properties of liquid water derive largely from its ability to form fluctuating networks of hydrogen bonds. However, even in the gas phase, where clusters of only a few water molecules may form, their sparse hydrogen-bonded networks may still absorb energy and stabilize reactants and products (*1*–*3*), stabilize intermediates as catalysts (*1*), or act as reaction partners. In the D region of the ionosphere (70 to 85 km above Earth), the positively charged ions that form there, such as NO^+, can formally transfer charge to one water molecule and add an OH^- group to form a neutral species (such as HONO). The resulting protonated water networks (*4*–*7*) are regarded as the major positive-charge carrier in the D region, which is the lowest ionospheric layer that affects radio communications. On page 308 of this issue, Relph *et al*. (*8*) report on a combined experimental and theoretical study that tries to unravel the relation between the hydrogen-bonding arrangement of a set of water molecules around an NO^+ ion and the chemical activity of this ensemble. Their results bear on a key open question: Are there particular water clusters that account for most of the reactivity?

The key processes in this reaction

$$NO^+(H_2O)_n + H_2O \rightarrow \{(HONO)\,H^+(H_2O)_n\} \rightarrow H^+(H_2O)_n + HONO \quad (1)$$

involve water clustering around the NO^+, charge separation, and finally the elimination of nitrous acid (HONO) and production of the $H^+(H_2O)_n$ "cations" (reaction 1). NO^+

[1]Institut für Physikalische Chemie, Universität Göttingen, Tammannstrasse 6, 37077 Göttingen, Germany. [2]Ostwald-Institut für Physikalische und Theoretische Chemie, Universität Leipzig, Linné-Strasse 2, 04103 Leipzig, Germany. E-mail: bernd.abel@uni-leipzig.de

is efficiently formed when NO is ionized by strong solar Lyman-α emission in the ultraviolet (wavelength of 121.7 nm).

The rate of reaction 1 in the ionosphere depends crucially on the number of water molecules (see the figure). For the reaction of NO^+ with just one water molecule, a substantial amount of energy (35 kcal/mol) must be added (*6*). This barrier is reduced for every added water molecule; the reaction is almost thermoneutral in the tetrahydrate, and even exothermic for larger clusters. Large clusters can react quickly, but the probability of their formation under atmospheric conditions is negligibly small. The trade-off of reaction rates and cluster abundance suggests that the tri- and tetrahydrates may be the key species for HONO production.

To explore this question, Relph *et al*. synthesized clusters of NO^+ with one to four water molecules in a supersonic expansion process that cooled the clusters to less than 5 K. This cooling allows infrared spectroscopy to be used to identify particular clusters, as it minimizes thermal broadening and blurring of spectral lines. High-level theoretical studies allow the spectra to be assigned to particular structures as well as changes caused by reactions.

Relph *et al*. found that in the smallest clusters (1 and 2 in the figure), NO^+ did not even transfer charge to the water network. Of the three different isomers formed by the trihydrate complex, only isomer 3-α (see the figure) transfers charge to the water network, whereas the charge stays on NO^+ in isomers 3-β and 3-γ, which were unreactive. This result shows that reactivity is sensitive to the geometrical arrangement of the water molecules. Adding another water molecule to 3-α leads to structure 4-α and formation of HONO, whereas adding water to the other two isomers still does not transfer charge. Thus, Relph *et al*. observed cluster-specific reactivity under the conditions of their experiment.

The keys to understanding the potential relevance of the species 3-α to ionospheric chemistry are the degree of its interconversion to form the other isomers, and the mechanism of the transformation step from 3-α to 4-α at the higher temperatures of the ionosphere, around 200 K (versus the low temperatures in the experiments and simulations). Energetic barriers may cause the interconversion of trihydrate isomers (*5*), or of the "reactive" complex 4-α and the "unreactive" complex 4-β, to be slow. In the latter case, the rate will depend on whether the excess energy in 4-α created by its collision or a recombination of 3-α with water can drive it over the barrier leading to the lower-energy isomer 4-β (*5*).

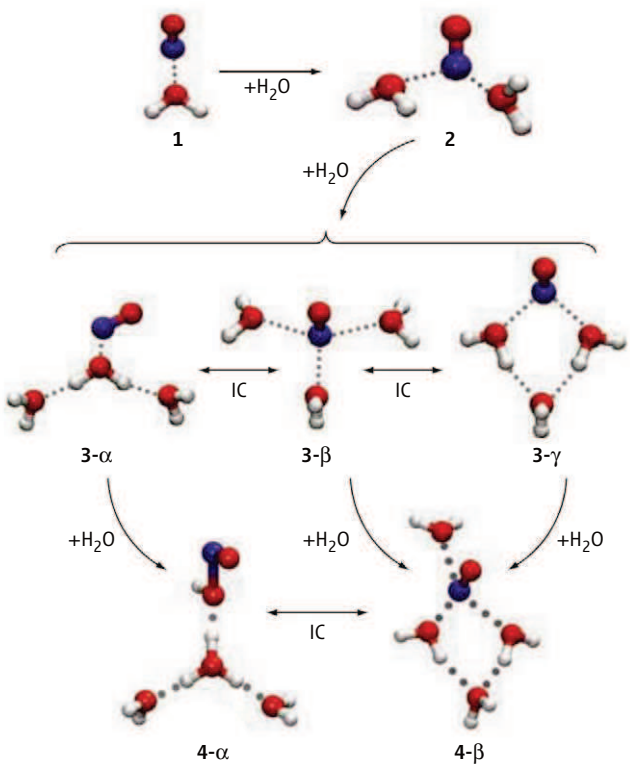

Just add a little water. The stepwise formation of clusters observed by Relph *et al*. when NO^+ binds up to four water molecules on its way to forming HONO. The interconversion (IC) of isomers likely is inhibited by energy barriers. Reactions such as these may bear on the chemistry of Earth's ionosphere.

Reaction 1 for the trihydrate in the atmosphere is surprisingly slow, occurring at about 5% of the collision frequency (*4*, *9*). The long-standing hypothesis explaining the bottleneck of reaction 1 is that the reactive species involves an "appropriate" (*6*) high-energy cluster configuration to facilitate release of a proton from a key, activated water molecule (*4*). It is tempting at first glance to simply assign the low-abundance isomer 3-α as the critical high-energy species in reaction 1. At a temperature of 200 K in the D region of the ionosphere (*10*), the calculated energy differences among the isomers in fact predict a low abundance of isomer 3-α relative to 3-β and 3-γ.

However, the addition of water to 3-α to form 4-α is by no means a simple water molecule addition to a linear "polarized" NO^+–water molecule chain (*4*, *6*), nor a trivial one-step barrierless process, but rather an insertion reaction or adduct formation followed by an isomerization and subsequent reaction. If we exclude isomerization routes for the same reasons we excluded interconversions between 4-α and 4-β or between the trihydrates, then the reaction would proceed by an insertion reaction. That is, the water molecule inserts into a hydrogen bond, adding its OH^- group to NO^+ and donating its proton to the adjacent water molecule in the network. Only a concerted, one-step reaction may take advantage of the charge separation and geometry in the reactant cluster 3-α. Such a step may be accompanied with a barrier or at least a substantial "anisotropy factor"—despite being energetically favorable, the reaction proceeds only for a small fraction of orientations of the incoming water molecule with the cluster (*3*), and the overall rate constant drops.

The work of Relph *et al*. may be relevant for the understanding of a key reaction in the ionosphere, but despite the beauty of the new results, it is premature to conclude that these isomer-specific reactions account for the observed ionospheric reactions. First, the species investigated experimentally and theoretically have their conformations virtually frozen both by very low temperatures and by the absence of collisions. We cannot be sure that interconversion processes are negligible at the higher temperatures and pressures of the ionosphere. The ionospheric reaction rate may still reflect the low formation or reaction rates of even larger clusters. These questions will likely only be resolved by further studies at more realistic conditions that might be achieved, for example, in Laval nozzle expansions (*1*). The interpretation of data from techniques such as double-resonance mass spectrometry would certainly be guided by the results of these model studies.

References

1. E. Vöhringer-Martinez *et al*., *Science* **315**, 497 (2007).
2. E. J. Hamilton, *J. Chem. Phys.* **63**, 3682 (1975).
3. J. Troe, *J. Chem. Soc. Faraday Trans.* **90**, 2303 (1994).
4. F. C. Fehsenfeld, M. Mosesman, E. E. Ferguson, *J. Chem. Phys.* **55**, 2120 (1971).
5. E. Hammam, E. P. F. Lee, J. M. Dyke, *J. Phys. Chem. A* **104**, 4571 (2000).
6. E. Hammam, E. P. F. Lee, J. M. Dyke, *J. Phys. Chem. A* **105**, 5528 (2001).
7. F. C. Fehsenfeld, E. E. Ferguson, *J. Geophys. Res.* **74**, 2217 (1969).
8. R. A. Relph *et al*., *Science* **327**, 308 (2010).
9. L. J. Puckett, M. W. Teague, *J. Chem. Phys.* **54**, 2564 (1971).
10. R. S. Narcisi, A. D. Bailey, *J. Geophys. Res.* **70**, 3687 (1965).

10.1126/science.1184555

RETROSPECTIVE

Paul A. Samuelson (1915–2009)

Robert M. Solow

A major figure in international economics laid the foundation for modern economics and transformed the atmosphere of economic study.

The death of Paul A. Samuelson last month signals the end of an era in economics in two separate but related ways. First, as a precocious undergraduate at the University of Chicago and then as a graduate student and Junior Fellow at Harvard University, he found economics to be a discursive, almost ruminative, discipline, even though its basic observables—prices and amounts of goods and services—were obviously ripe for systematic quantification. To his delight, he found that reformulation in standard mathematical terms led not only to great gains in clarity and transparency, but also to new analytical results, a broader scope for the discipline, and the uncovering of unifying principles that both simplified and deepened it. His work transformed the method, content, and whole atmosphere of economic research.

Second, Samuelson sometimes described himself as "the last generalist" in economics, and he was right. The unity that he discerned enabled him to make fundamental contributions to theory—he was never a systematic empiricist, although he was a constant observer of the current scene—across the whole spectrum of economics. The (eventual) seven volumes of his *Collected Scientific Papers* include pathbreaking papers on consumer demand, capital and interest, business cycles, international trade, general equilibrium pricing, taxation, the logic of public expenditure, welfare economics, the fruitful "overlapping generations model," duality, stability, and finance, to mention only the easily classifiable part of his output. The very fertility of these papers in enabling and stimulating research by others has made it impossible for anyone again to duplicate Samuelson's staggering range.

Paul Samuelson was born in Gary, Indiana, in 1915. His academic path led to joining the faculty of the Massachusetts Institute of Technology (MIT) in 1940, where he helped to forge a powerful economics department, and where he stayed until retirement in 1985. His earliest methodological and substantive discoveries were summed up in the *Foundations of Economic Analysis* (1947) that had served as his 1944 Ph.D. thesis. Some of the material had appeared in articles as early as 1937. But it was this book that carried the message to succeeding generations of economists, and it was the main work cited by the Swedish Academy of Science in awarding him the second Nobel Prize in economics in 1970 (the first was shared by Ragnar Frisch and Jan Tinbergen, also pioneers of the mathematical approach). For my cohort of economists, it was the *Foundations of Economic Analysis* that taught us what serious economics really was.

In Samuelson's revolutionary view, economic theory had three parts, beginning with the natural presumption that decision-makers (so-called actors), whether families, firms, or other, could maximize or minimize something—cost, income, wealth, profit, subjective well-being—if they were limited by legal, technological, budgetary, or other specified constraints. He was not preoccupied with what any given actor was trying to optimize, nor was he concerned with the specific constraints on behavior. According to his method of analysis—which did accommodate those concerns—the outcome of individual attempts to optimize a situation would define behavior rules for actors.

The second step in the Samuelson model was to define and impose the relevant conditions of equilibrium, the prototype being that supply should equal demand in each market. For some important sorts of markets, the equilibrium conditions might have to be different. The important thing was to define a rest point, and calculate in principle the prices and quantities at that rest point.

The third step was to ask and, in the abstract, answer questions like the following: Suppose something in the environment—normally, a parameter of one of the constraints, like a tax rate or a resource limit, or a characteristic of the technology—were to change. How would the equilibrium configuration change and how would the equilibrium prices and quantities change? Above all, are there general qualitative answers to those questions?

Foundations of Economic Analysis also directed attention to questions of dynamics for the first time. If an equilibrium is disturbed, in the sense that actors are moved away from their optima, and prices and quantities are moved away from their equilibrium values, would the natural behavioral rules of adjustment drive them back toward, or away from, the equilibrium configuration? An unstable equilibrium in this sense is likely to be ephemeral. Ever since he drew attention to dynamics, a large part of economics has followed this general pattern.

Samuelson's famous elementary textbook, *Economics: An Introductory Analysis* (1948), was for many years the best seller in the field, went through several editions, and was much imitated. It transformed undergraduate teaching in ways consistent with *Foundations*. The textbooks I read in 1940 were dense with imprecise prose. If they stimulated anything, it was along the uninspiring lines of "on the one hand/on the other hand." After Samuelson, the elementary student was taught to deal with data (real and hypothetical), analyze them by diagrammatic methods or with simple equations, and use economic principles to answer concrete questions: What would you expect to happen if…? Problem sets replaced essay questions. And all of this was presented in lively prose and with up-to-date references.

The young Samuelson was famous as an *enfant terrible*, likely to examine his examiners, and not give passing grades. He matured into a much loved *enfant terrible emeritus*, a public figure and adviser to several U.S. presidents, a gold mine for first-class graduate students, and the standard-bearer whose extraordinary talents enabled the economics department at MIT to develop from a nondescript service department to the world's best. He was producing new ideas into his 94th and last year.

Department of Economics, Massachusetts Institute of Technology, Cambridge, MA 02139, USA.

10.1126/science.1186205

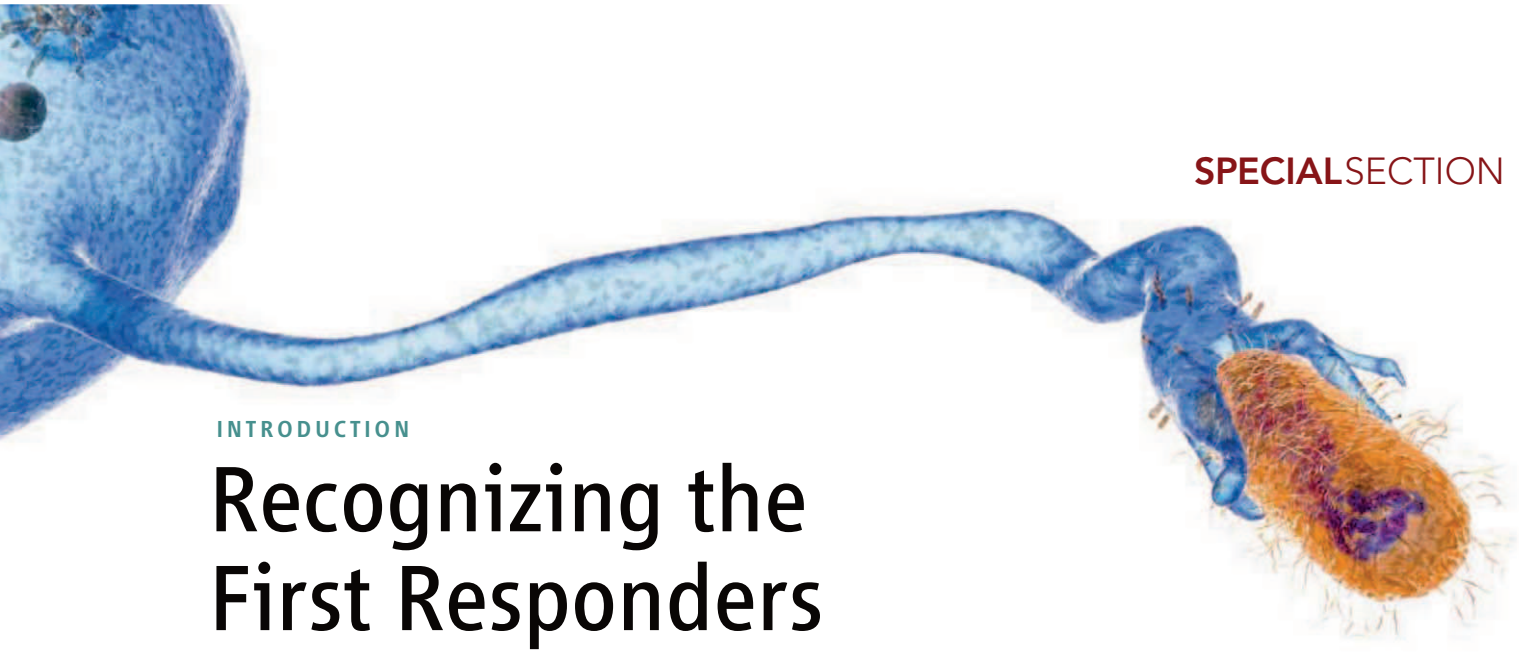

INTRODUCTION

Recognizing the First Responders

2009 MARKED THE 20TH ANNIVERSARY OF CHARLES JANEWAY'S SEMINAL HYPOTHESIS that the body's response to infection is mediated by receptors on immune cells that recognize microbial patterns. Before this, immunologists primarily studied T and B lymphocytes, which express highly specific antigen receptors, but Janeway's prediction that direct microbial detection by immune cells other than lymphocytes precedes and is required for subsequent lymphocyte activation helped open the door to a new field of immunology: the study of the innate immune system. Much work over the past 20 years has borne out Janeway's predictions, and the fundamental importance of the innate immune system is now well established.

The collection of articles in this issue encompasses both the primary focus of the field over the past two decades—the molecular dissection of microbial recognition—and also more recent areas of interest, including the interaction between the innate and adaptive immune systems and the identification of noninfectious diseases associated with innate immune system function. A Perspective by Rehwinkel and Reis e Sousa (p. 284) discusses recent advances in the elucidation of how members of the RIG-I–like receptor family distinguish viral nucleic acids from the abundance of host nucleic acids present in an infected cell. The ability to specifically recognize viral nucleic acids is critical for proper immune responses to viral infection. Another family of microbial receptors, the NLRs, is discussed in a Review by Ting and colleagues (p. 286). These receptors have received a great deal of recent attention because of their role in the inflammatory protein complex termed the inflammasome; however, as Ting *et al*. present, mounting evidence indicates that their inflammasome-independent functions may play an equally important role in the responses to pathogens by the innate immune system.

How microbial recognition by the innate immune system couples to the activation of T and B lymphocytes of the adaptive immune system is discussed in a Review by Iwasaki and Medzhitov (p. 291). This Review highlights the fact that we still have much to learn about this cooperation, particularly in cases when the microbes are being sensed within the cell. Although it is well recognized that the innate immune system is critical for responses to microbial insults, research has also emerged demonstrating that the innate immune system may play an unexpected role in diseases not classically associated with the immune system. A Review by Schroder and colleagues (p. 296) explores one example: the role of the innate immune receptor NLRP3 in the metabolic diseases type 2 diabetes and gout.

A collection of articles at *Science Signaling* (www.sciencemag.org/special/immunity) highlights immune responses to pathogens, the mechanism of interleukin-1 signaling, and aspects of the control of the adaptive immune response by dendritic cells.

Together, these articles highlight how far our understanding of the innate immune system has come in the past 20 years and suggest areas where the important discoveries of the next decades are likely to come.

– KRISTEN L. MUELLER

Innate Immunity

CONTENTS

Perspective

Reviews

See also related editorial on p. 249

CREDIT: C. BICKEL/*SCIENCE*

PERSPECTIVE

RIGorous Detection: Exposing Virus Through RNA Sensing

Jan Rehwinkel and Caetano Reis e Sousa*

Virus infection in mammals elicits a variety of defense responses that are initiated by signals from virus-sensing receptors expressed by the host. These receptors include the ubiquitously expressed RIG-I–like receptor (RLR) family of RNA helicases. RLRs are cytoplasmic proteins that act in cell-intrinsic antiviral defense by recognizing RNAs indicative of virus presence. Here, we highlight recent progress in understanding how RLRs discriminate between the RNA content of healthy versus virus-infected cells, functioning as accurate sensors of virus invasion.

Viruses are obligate intracellular parasites that infect all organisms, from bacteria to humans. Their evolution represents a constant arms race with the host: Viruses need to reprogram host cells in order to produce progeny virus, but this is often successfully limited by the host antiviral defense, which in turn is frequently targeted by the virus, and so forth. Mammals possess the most multifaceted antiviral defense program. Their reaction to viral infection includes the rapid induction of antiviral proteins, natural killer cells, neutralizing antibodies and cytotoxic T cells. These immune responses are coordinated by signaling molecules, including the type I interferons (IFN-α and IFN-β) and the related type III IFN (IFN-λ). All nucleated cells can synthesize IFNs in response to virus infection, which implies the existence of cell-intrinsic mechanisms for sensing viral presence. Some of these mechanisms have been identified recently and involve signaling for IFN gene transcription by members of the RIG-I–like receptor (RLR) family of pattern recognition receptors in response to specific RNA "patterns" that are generated during virus infection (*1*).

The RLR family has three members: retinoic acid inducible gene I (RIG-I), melanoma differentiation-associated gene 5 (MDA5), and laboratory of genetics and physiology 2 (LGP-2). These cytoplasmic proteins all share a central DExD/H-box RNA helicase domain. RIG-I and MDA5 also have two N-terminal caspase activation and recruitment domains (CARDs). CARDs allow for the interaction of activated RIG-I or MDA5 with the adaptor protein mitochondrial antiviral signaling (MAVS, also known as IPS-1, VISA, and Cardif), which localizes to the outer mitochondrial membrane. MAVS relays the signal to kinases such as TANK-binding kinase 1 (TBK1) and IκB kinase ε (IKKε), which in turn activate transcription factors, including interferon response factor 3 (IRF-3), IRF-7, and nuclear factor κB (NF-κB), which coordinate IFN gene induction (*1*). As well as this pathway, a MAVS-independent function of RIG-I was recently described: RIG-I directly activates the inflammasome, a protein complex that cleaves pro-interleukin-1β (IL-1β) into mature IL-1β, a pro-inflammatory cytokine (*2*).

RIG-I is indispensable for IFN responses to many single-stranded RNA viruses. These include negative-stranded viruses of the orthomyxovirus (such as influenza A virus) and paramyxovirus (such as measles, mumps, and Sendai virus) families and positive-stranded viruses like hepatitis C or Japanese encephalitis viruses. That RIG-I–deficient mice are highly susceptible to infection with these viruses underscores the importance of that RLR in antiviral defense. Similarly, MDA5 is essential for protection from a different set of viruses, including picornaviruses (such as poliovirus and encephalomyocarditis virus). The largely non-overlapping pattern of virus susceptibility in mice deficient for either RLR implies that the two receptors possess distinct virus specificities, although some viruses can be dually recognized by either RIG-I or MDA5. Little is known about virus sensing by LGP2, which may instead primarily play a regulatory role (*1*). The virulence of some viruses, including some strains of influenza A virus (*3*), is due at least in part to a dysregulation of the innate immune response. Therefore, understanding how RLRs become activated may allow the development of new strategies for the containment of viral spread and prevention of disease, as well as help to understand the basic principles underlying self/virus innate immune discrimination. Here, we summarize the rapid progress made in the last few years toward defining ligands for RLRs (Fig. 1).

Virus sensing is highly discriminative given that RLRs are localized in the cytoplasm, where host RNAs abound; yet, signaling occurs only in infected cells. Thus, for RLRs to be activated, they must detect RNA bearing a molecular pattern not found under normal conditions. Such patterns may be chemical modifications of RNA (or the absence of such modifications), specific secondary or tertiary RNA conformations, partic-

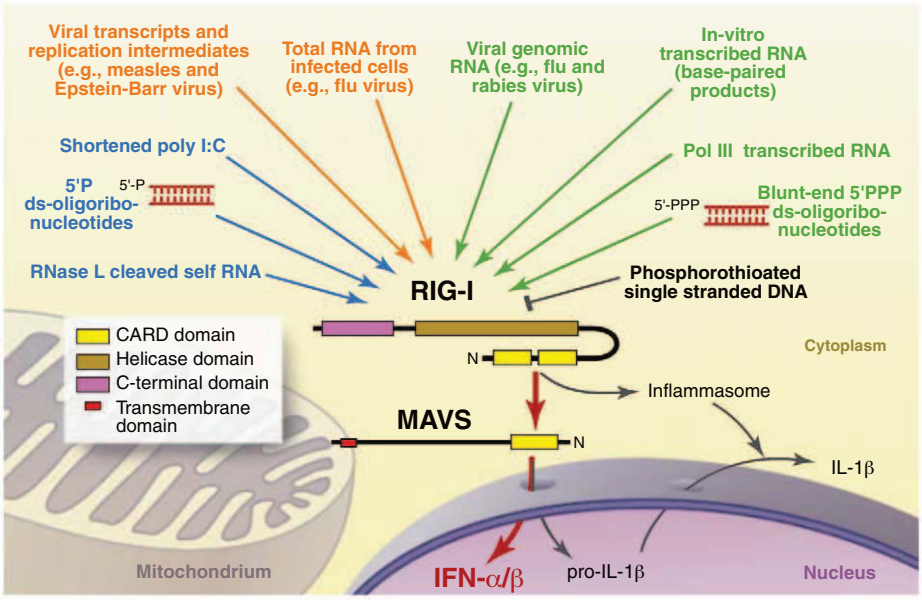

Fig. 1. Putative RIG-I ligands. RIG-I has been reported to be triggered experimentally by a variety of RNA agonists. 5′-PPP–bearing RNAs are shown in green, RNAs without 5′-PPPs in blue, and RNAs that may have different 5′-end characteristics in orange. An antagonist is shown in black. Activated RIG-I promotes the induction of interferons and other pro-inflammatory cytokines via the mitochondrial adaptor MAVS (bold red arrows). MAVS-dependent induction of pro-interleukin-1β allows it to be processed into mature interleukin-1β by the inflammasome, which can be directly activated by RIG-I in a MAVS-independent manner.

Immunobiology Laboratory, Cancer Research UK (CRUK) London Research Institute, 44 Lincoln's Inn Fields, London WC2A 3PX, UK.

*To whom correspondence should be addressed. E-mail: caetano@cancer.org.uk

ular sequences, or the annealing of two complementary RNA strands so as to form double-stranded RNA (dsRNA). Furthermore, the agonistic RNA may be of viral or cellular origin. Early studies demonstrated that RIG-I–dependent IFN production can be triggered by transfection of certain synthetic and natural RNAs into cells and provided the first insight into how RIG-I might discriminate virus from host RNA. These studies showed that RNA transcribed in vitro by phage polymerases (IVT-RNA) is a potent RIG-I agonist (*4*, *5*). IVT-RNAs have an uncapped 5′-triphosphate (5′-PPP) that is required for their IFN-inducing activity. 5′-PPPs promote the binding of RIG-I (*4*, *5*), activation of its adenosine triphosphatase (ATPase) activity, and conformational changes that allow RIG-I dimerization and exposure of CARDs for interaction with MAVS (*6*, *7*). Furthermore, structural analysis indicates that the C terminus of RIG-I folds into a domain that recognizes uncapped 5′-PPPs on RNA (*6*, *7*). This can explain why RIG-I does not respond to host cytoplasmic RNA because the latter lacks 5′-PPPs; for example, mRNAs are capped, and nuclear processing of ribosomal and tRNAs removes or modifies 5′-PPP groups before they reach the cytoplasm.

Surprisingly, two recent studies report that chemically synthesized RNAs bearing 5′-PPP do not trigger RIG-I, whereas the same RNAs can do so when made by means of in vitro transcription (*8*, *9*). This apparent contradiction can be explained by the fact that IVT-RNA preparations often contain small amounts of unexpected RNA species. These include RNAs made in error by phage polymerases that switch from transcribing the DNA template to copying their own RNA product. When this occurs, the polymerase effectively extends the 3′ end of the RNA into a self-complementary molecule that folds into a hairpin. Only these hairpins, and other base-paired RNAs present in IVT-RNA preparations, act as agonists for RIG-I (*8*, *9*). Furthermore, annealing of inert 5′-PPP RNA made through chemical synthesis to a complementary RNA oligonucleotide lacking 5′-PPP restores RIG-I activation, particularly if a blunt end is formed (*8*, *9*). These data indicate that base-pairing at the 5′-end of RNA, together with a 5′-PPP, is required for RIG-I activation. RIG-I can translocate on base-paired RNA, and this probably contributes to its signaling activity (*10*).

These findings are consistent with earlier observations that viral RNA genomes extracted from influenza A or rabies virus particles can trigger RIG-I (*4*, *5*). Those viruses have a 5′-PPP–bearing RNA genome, and enzymatic removal of the 5′-PPP abolishes stimulatory activity (*4*, *5*). Some viruses, such as Hantaan virus, Crimean-Congo hemorrhagic fever virus, and Borna disease virus, have genomes with 5′-monophosphate ends, and RNA extracted from these virus particles does not activate RIG-I (*11*). The RNA genomes of influenza A, rabies, and other viruses that are recognized by RIG-I have complementary 5′ and 3′ ends and adopt a "panhandle" conformation (*12*). Therefore, these RNAs provide the two features read by RIG-I: a 5′-PPP and base-pairing at the 5′-end. It is worth remembering that base-paired does not mean double-stranded; by definition, dsRNA requires two (complementary) RNA molecules. However, the IVT-RNA hairpins and viral genomic RNAs that trigger RIG-I are single-stranded, even if they form intra-molecular base pairs. This distinction is important: The RNA genome of RIG-I–dependent viruses provides all features required for RIG-I activation in a linear RNA molecule without the need for viral replication. We therefore suggest that the use of the term double-stranded be restricted to the situation in which two complementary RNA molecules anneal, such as after the replication of some viruses.

As well as a secondary structure at the 5′-PPP end, other properties of RNAs may also influence recognition by RIG-I. For example, incorporation of modified bases such as pseudouridine—which are often found in cellular RNAs—into IVT-RNA decreases its stimulatory potential (*5*). A sequence motif in the 3′ nontranslated region of the hepatitis C virus genome was suggested to be required for RIG-I activation, together with the 5′-PPP end of the genome (*13*). Surprisingly, some RNAs without 5′-PPPs have also been reported to trigger RIG-I. These include chemically synthesized dsRNA oligonucleotides as well as shortened forms of poly inosinic: polycytidylic acid (poly I:C), which is an analog of dsRNA (*7*, *14*). Furthermore, products of host RNA cleavage by ribonuclease (RNase) L, which bear 5′-hydroxyl- and 3′-monophosphate ends, were suggested to contribute to RIG-I activation (*15*). Finally, phosphorothioated single-stranded DNA oligonucleotides (containing a sulfur-substituted internucleotide bond) were recently identified as RIG-I antagonists (*16*).

Despite the wealth of information on the types of RNA that can activate RIG-I, the natural RIG-I agonist (or agonists) responsible for inducing IFN in virus-infected cells remains unclear. This is because all of the data identifying RIG-I stimulatory RNAs were obtained in non-physiological experimental settings, such as transfection of naked RNA into cells or in biochemical assays that measured RIG-I binding, ATPase activity, or conformational changes. Total RNA extracted from infected cells can trigger RIG-I (*14*, *17*); however, the specific agonist within such pools has not been identified. Candidates include viral genomes, viral transcripts, replication intermediates, or host RNA cleaved by RNase L. IFNs were originally discovered through the treatment of chicken cells with high doses of heat-inactivated influenza A virus (*18*). This treatment delivers viral RNA genomes to the cytosol in the absence of virus replication, suggesting that those genomes are sufficient to trigger RIG-I. Thus, RIG-I may act in infected cells primarily by sensing incoming viral genomes or ones generated during viral replication.

Much less is known about the nature of the RNAs that act as agonists for MDA5. Poly I:C is prepared by annealing inosine and cytosine homopolymers that have 5′-diphosphate and 5′-monophosphate ends. Transfection of poly I:C into cells triggers MDA5-dependent IFN induction, and a recent report shows that a minimum length of poly I:C is required for efficient MDA5 activation: Shortening poly I:C to around 1000 nucleotides or less is reported to convert it into a RIG-I agonist (*14*). These observations have been interpreted to indicate that MDA5 recognizes long dsRNA generated during infection. Indeed, dsRNA accumulates in cells infected with viruses that are recognized by MDA5 (*4*, *14*, *17*). When we size-fractionated total RNA from cells infected with encephalomyocarditis or vaccinia viruses, however, we found that only a high-molecular-weight RNA stimulated MDA5 upon transfection into reporter cells (*17*). This RNA was larger than most of the dsRNA generated during infection and was composed of both single- and double-stranded portions, suggesting a weblike conformation (*17*). Poly I:C may similarly adopt a branched structure given that the inosine and cytosine polymers have varying lengths. The definition of synthetic RNAs recognized by MDA5 and the characterization of MDA5 agonists purified from infected cells will help elucidate how that RLR can discriminate virus from self RNA.

An exciting recent development is the realization that the function of RLRs goes beyond the sensing of RNA viruses; they can also drive IFN responses to cytoplasmic DNA (*19*, *20*). Infection with DNA viruses or some bacteria can deliver DNA to the cytoplasm, and this can be mimicked experimentally by transfection of the DNA polymer poly dA:dT. Although poly dA:dT cannot be sensed directly by RLRs, it is transcribed by cytosolic RNA polymerase III into an uncapped RNA that triggers RIG-I (*19*, *20*). Consistent with observations using IVT-RNA or viral RNA genomes, 5′-PPPs and base-pairing are both required for RIG-I activation via the RNA polymerase III pathway (*19*, *20*). This pathway appears to contribute to IFN induction during infection with the bacterium *Legionella pneumophilia* (*20*) and with DNA viruses such as adenovirus, herpes simplex virus, and Epstein-Barr virus (*19*, *20*). Vaccinia virus is another DNA virus that triggers RLRs, in this case by generating an RNA agonist for MDA5 (*17*).

How do these findings illuminate the arms race between virus and host? In the case of negative-strand RNA virus-sensing (such as influenza A virus), RIG-I appears to recognize those features of the viral RNA genome that are indispensable for virus replication: The 5′-PPP end and the panhandle act as a promoter for the viral polymerase, and the virus cannot alter this pattern without sacrificing its own replication (*12*). Instead, viruses fight back by encoding proteins that inhibit RLRs or downstream signaling pathways. For example, influenza A virus can inhibit RIG-I by means of its NS1 protein, whereas hepatitis C virus cleaves MAVS off mitochondria (*1*). Much remains to be clarified as to how virus is sensed by the infected cell and how this is translated into an innate immune response. What beside IFN induction is regulated by RLR activation? What are the molecular patterns recognized by MDA5? What sensors detect cytoplasmic DNA (and how are they regulated at mitosis, when the nuclear envelope breaks down)? Do polymorphisms or mutations in RLRs and downstream adaptors affect human susceptibility to virus infection? Can aberrant activation of RLRs lead to detrimental autoreactive responses? Fifty years after the discovery of IFNs (*18*), the struggle between virus and host is only just beginning to reveal its molecular secrets.

References and Notes

1. A. Pichlmair, C. Reis e Sousa, *Immunity* **27**, 370 (2007).
2. H. Poeck *et al.*, *Nat. Immunol.* **11**, 63 (2010).
3. T. R. Maines *et al.*, *Immunol. Rev.* **225**, 68 (2008).
4. A. Pichlmair *et al.*, *Science* **314**, 997 (2006).
5. V. Hornung *et al.*, *Science* **314**, 994 (2006).
6. S. Cui *et al.*, *Mol. Cell* **29**, 169 (2008).
7. K. Takahasi *et al.*, *Mol. Cell* **29**, 428 (2008).
8. M. Schlee *et al.*, *Immunity* **31**, 25 (2009).
9. A. Schmidt *et al.*, *Proc. Natl. Acad. Sci. U.S.A.* **106**, 12067 (2009).
10. S. Myong *et al.*, *Science* **323**, 1070 (2009).
11. M. Habjan *et al.*, *PLoS ONE* **3**, e2032 (2008).
12. D. M. Knipe, P. M. Howley, *Fields' Virology* (Lippincott Williams & Wilkins, Philadelphia, ed. 5, 2007).
13. T. Saito, D. M. Owen, F. Jiang, J. Marcotrigiano, M. Gale Jr., *Nature* **454**, 523 (2008).
14. H. Kato *et al.*, *J. Exp. Med.* **205**, 1601 (2008).
15. K. Malathi, B. Dong, M. Gale Jr., R. H. Silverman, *Nature* **448**, 816 (2007).
16. C. T. Ranjith-Kumar *et al.*, *J. Biol. Chem.* **284**, 1155 (2009).
17. A. Pichlmair *et al.*, *J. Virol.* **83**, 10761 (2009).
18. A. Isaacs, J. Lindenmann, *Proc. R. Soc. London B Biol. Sci.* **147**, 258 (1957).
19. A. Ablasser *et al.*, *Nat. Immunol.* **10**, 1065 (2009).
20. Y. H. Chiu, J. B. Macmillan, Z. J. Chen, *Cell* **138**, 576 (2009).

21. J.R. is a recipient of a Human Frontier Science Program long-term fellowship. C.R.S. is funded by CRUK and a prize from the Fondation Bettencourt-Schueller.

10.1126/science.1185068

REVIEW

How the Noninflammasome NLRs Function in the Innate Immune System

Jenny P. Y. Ting,[1,2,3]* Joseph A. Duncan,[4,5] Yu Lei[2,3]

NLR (nucleotide-binding domain, leucine-rich repeat–containing) proteins have rapidly emerged as central regulators of immunity and inflammation with demonstrated relevance to human diseases. Much attention has focused on the ability of several NLRs to activate the inflammasome complex and drive proteolytic processing of inflammatory cytokines; however, NLRs also regulate important inflammasome-independent functions in the immune system. We discuss several of these functions, including the regulation of canonical and noncanonical NF-κB activation, mitogen-activated protein kinase activation, cytokine and chemokine production, antimicrobial reactive oxygen species production, type I interferon production, and ribonuclease L activity. We also explore the mechanistic basis of these functions and describe current challenges in the field.

The genomic mining of evolutionarily conserved gene families with structural similarity has led to the discovery of a large gene family (NLRs) encoding proteins with a characteristic arrangement of nucleotide-binding domain (NBD) and leucine-rich repeat (LRR) regions in both plants and animals. NLRs share structural similarity with a subgroup of plant disease resistance (R) genes, which confer resistance to infection caused by fungal, viral, parasitic, and insect pathogens by inducing cell death of infected cells (*1*). Among animals, NLR proteins are found in species as diverse as sea urchin and human (*2*).

The most prominent function of NLRs is the intracellular sensing of structures shared by classes of microbes and endogenous molecules associated with inflammation, known as pathogen-associated molecular patterns (PAMPs) and damage-associated molecular patterns (DAMPs), respectively. The precise mechanism by which this "sensing" occurs, however, remains a major challenge in the field (*2*). NLR proteins also have functions outside of the innate immune system, such as the regulation of cell death, or the regulation of the major histocompatibility complex (MHC) to affect adaptive immunity. Many PAMPs and DAMPs that are sensed through NLR-dependent pathways result in the activation of the inflammasome, a signaling complex composed of an NLR protein, the adaptor ASC (apoptotic speck–containing protein with a CARD), and procaspase-1, whose end result is the cleavage of the proinflammatory cytokines, interleukin (IL)–1β and IL-18. NLRs can also trigger inflammasome-independent pathways. We primarily focus on the role of noninflammasome NLRs in innate immunity because data are converging to indicate that these NLRs can be categorized into functional subgroups that regulate other crucial innate immune pathways, such as canonical and noncanonical nuclear factor κB (NF-κB), mitogen-activated protein kinase (MAPK), type I interferon (IFN), cytokines, chemokines, and reactive oxygen species (ROS) as well as ribonuclease L (RNase L) activation.

An underlying reason for the intense attention paid to NLRs is their association with genetic immunologic disorders in humans. For example, mutations in the class II MHC transactivator (CIITA), the master activator of MHC class II gene transcription, result in immunodeficiency. Mutations in nucleotide-binding oligomerization domain 2 gene (*NOD2*) are associated with susceptibility to Crohn's disease (a type of inflammatory bowel disease) and Blau syndrome (a granulomatous inflammatory disorder). Mutations in the gene encoding NLRP3 (NLR family, pyrin domain–containing 3) predispose patients to a variety of autoinflammatory disorders. Association of NLRs with asthma, vitiligo (a disease characterized by patchy depigmentation of skin), and urticaria skin rash has also been shown. Thus, NLRs are important determinants of human inflammatory disorders, and an in-depth understanding of their molecular mechanisms of action is crucial to the development of targeted therapies.

How Does Activation of NOD1 and NOD2 Regulate Immunity in the Host?

NOD1 and NOD2 were two of the first characterized members of the NLR family. Shortly after their identification, it was recognized that

[1]Department of Microbiology-Immunology, University of North Carolina, Chapel Hill, NC 27599, USA. [2]Curriculum of Oral Biology, University of North Carolina, Chapel Hill, NC 27599, USA. [3]Lineberger Comprehensive Cancer Center, University of North Carolina, Chapel Hill, NC 27599, USA. [4]Department of Medicine, University of North Carolina, Chapel Hill, NC 27599, USA. [5]Department of Pharmacology, University of North Carolina, Chapel Hill, NC 27599, USA.

*To whom correspondence should be addressed. E-mail: jpyting@med.unc.edu

several polymorphisms encoding nonconservative amino acids or frameshift mutations in the LRR of NOD2 were found in some familial cases of Crohn's disease. A different polymorphism in the nucleotide-binding domain of NOD2 was found to associate with Blau syndrome (*3*). Despite years of intensive research, however, the mechanism by which variant NOD2 proteins lead to the enhanced inflammation associated with Crohn's disease remains enigmatic. There are at least three working models. The first posits that NOD2 is a positive regulator of immune defense, and defective NOD2 cannot contain pathogen infection (*4*). Indeed, several Crohn's disease–associated NOD2 mutations confer impaired activation of the transcription factor NF-κB, whereas Blau syndrome–associated mutations lead to constitutive NF-κB activation (*5*). *Nod2*-deficient mice show a reduction in the level of antimicrobial α-defensins in Paneth cells of the intestine (*4*), consistent with samples from ileal Crohn's disease patients indicating an association between the *NOD2* variant genotype and reduced α-defensin (*6*). However, the association of NOD2 mutation with α-defensin was not found by all (*7*). The second model suggests that NOD2 is protective against Crohn's disease because it negatively regulates Toll-like receptor (TLR)–mediated responses to the intestinal bacterial flora. This model is supported by the analysis of a second *Nod2*-deficient mouse, which showed increased T helper 1–associated cytokine production and NF-κB activation in response to a TLR2 agonist (*8*). In support of this, TLR2 ligand administration in control but not *Nod2*-deficient mice greatly reduced TLR2-induced inflammatory responses. TLR2 ligand delivery also reduced chemically induced colitis in a NOD-dependent fashion. Remarkably, reintroduction of wild-type NOD2 into *Nod2*-deficient mice led to resistance to colitis (*9*). A third model hypothesizes that Crohn's disease–associated NOD2 variants cause increased inflammatory response, because the replacement of *Nod2* with a disease variant form resulted in elevated inflammatory responses, including enhanced IL-1β secretion and NF-κB activation in mice (*10*). Monocytes from Crohn's disease patients homozygous for this allele, however, actually demonstrate impaired IL-1β secretion (*11*), which suggests the possibility of context-dependent, species-specific differences. Finally, recent work suggests that a different Crohn's disease–associated mutation in *NOD2* leads to a novel interaction between the mutant NOD2 and heterogeneous nuclear ribonucleoprotein A1 (hnRNP A1). This interaction results in inhibition of hnRNP A1–mediated production of the anti-inflammatory cytokine IL-10 (*12*). Interestingly, the interaction between mutant NOD2 and hnRNP A1 was observed only with human NOD2 and the human IL-10 promoter but not the murine counterparts. The contribution of this novel inhibitory effect of disease-associated NOD2 mutant protein to Crohn's disease pathogenesis remains to be determined.

Early studies sought to identify the PAMPs responsible for activating NOD1 and NOD2. NOD1 and NOD2 respond to the bacterial peptidoglycan–derived molecules meso-diaminopimelic acid (DAP) and muramyl dipeptide (MDP), respectively (*3*, *13*). NOD1 can also be activated by meso-lanthionine, another peptidoglycan-associated diamino-amino acid. N-glycolylated MDP, which is made by mycobacteria and actinomycetes, is substantially more potent in its ability to elicit NOD2-dependent activation of NF-κB than N-acylated MDP, generated by typical Gram-positive and Gram-negative bacteria (*14*). Thus, NOD1 and NOD2 are activated in response to a number of peptidoglycan-derived moieties stemming from a broad range of bacterial sources. Although NLR proteins are now frequently referred to as receptors, it is important to note that neither NOD1 nor NOD2 has been shown to directly interact with their activating peptidoglycans in a manner consistent with a pattern recognition receptor. The LRR domains of these proteins are required to confer responsiveness to their respective stimuli, leading some to suggest that these domains either bind directly to the cognate peptidoglycan components or to other intracellular protein(s) that act as an intermediate between these bacterial products and NOD1 or NOD2.

Similar to other NLR molecules, NOD2 signals by acting as a scaffold for the assembly of large multicomponent signaling complexes (Fig. 1). NOD2 induces multiple effector pathways that are involved in the host response to microbial pathogens. The best-characterized effector signaling pathway of NOD2 leads to activation of NF-κB through interactions with receptor interacting protein–2 (RIP2, also known as RICK or CARDIAK), a serine/threonine kinase (*3*). After MDP is internalized by phagocytosis or bacterial invasion of the cytoplasm, intracellular NOD2 translocates to the plasma membrane (*15*). There, it associates with RIP2 through the homotypic interactions of caspase activation and recruitment domains (CARDs), thereby allowing membrane translocation of RIP2. Rather than inducing NF-κB activation through RIP2-mediated phosphorylation of IκB kinase, the NOD2-RIP2

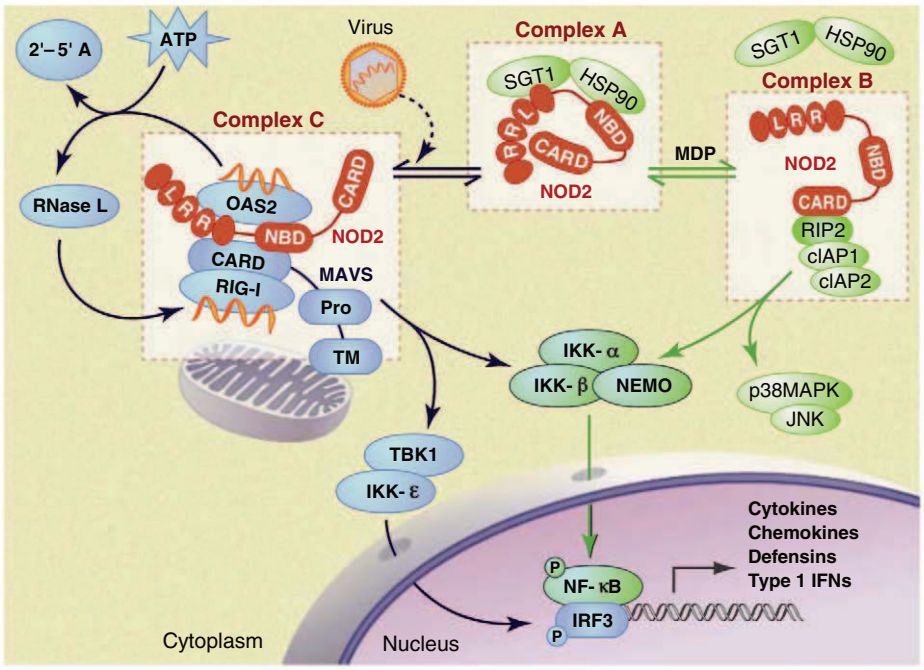

Fig. 1. NOD2 signaling bifurcates into antibacterial and antiviral effector arms. A model of NOD2 signaling is presented in which NOD2 is bound to the chaperonin–ubiquitin ligase pair, HSP90 (heat shock protein 90) and SGT1 (suppressor of G2 allele of skp1), in the basal state (complex A). This is thought to hold the inactive NOD2 in a signaling-competent form (*48*). Upon stimulation with MDP, NOD2 binds to RIP2 and activates NF-κB and MAPK (p38 and JNK) through recruitment of several intracellular proteins, including cIAP1 and cIAP2 (complex B). This leads to the induction of chemokines, cytokines, and defensins, which mediate the antimicrobial responses. Similarly, viral infection can activate NOD2, leading to its translocation to the mitochondria, association with mitochondrial antiviral signaling protein (MAVS), and induction of the antiviral cytokine type I IFN (complex C). NOD2 also interacts with the dsRNA-binding protein OAS2. Overexpression of NOD2 can activate the RNase L pathway, providing a positive feedback mechanism for the mito-signalosome in response to RNA viruses. (complex C). RIG-I is depicted because it is the PRR that binds to viral nucleic acids, whereas TANK-binding kinase 1 (TBK1) and IκB kinase–ε (IKK-ε) lie downstream of MAVS to activate IRF-3.

complex activates the IκB kinase complex through Lys^{63}-linked polyubiquitination of its γ subunit (also known as NEMO). This is achieved through the recruitment of the ubiquitin ligases cIAP1 and cIAP2 to the signaling complex (*16*). In parallel to the activation of NF-κB, the NOD2-RIP2 complex also stimulates MAPK (i.e., p38 and JNK). The molecular mechanisms that regulate the formation of a membrane-bound RIP2-NOD2 complex are not fully determined; however, numerous cellular proteins have been implicated in NOD2 signaling. The mechanism by which these multiple factors interact to regulate NOD2 signaling during physiologic responses to infection and under pathologic conditions such as Crohn's disease requires further investigation (*17*).

MDP-mediated activation of the NOD2-RIP2 complex is known to modulate both innate and adaptive immune responses by activating the expression of numerous cytokines and chemokines. NOD2 control of cytokine expression is mediated largely through its ability to activate NF-κB and p38 MAPK-dependent signaling. Several studies, however, suggest that NOD2 has a role in caspase-1 activation and subsequent IL-1β processing in response to MDP. One study carried out in cells isolated from NOD2-deficient mice suggests that MDP induces caspase-1 activation and IL-1β processing through the NOD2 and ASC/NLRP3 inflammasome (*18*), although another found that MDP activation of caspase-1 is independent of NOD2 (*19*). These discrepancies are likely due to the distinct inflammasome activation protocols used. There is also evidence indicating that NLRP1 activates caspase-1 in an MDP-responsive fashion (*20*, *21*). NOD2 has been reported to associate with NLRP1 and cooperate in caspase-1 activation in response to MDP (*21*). This heterotypic NLR-NLR interaction is interesting because in vitro cell-free reconstitution of MDP-stimulated NLRP1 inflammasome formation represents the only evidence that any NLR protein directly senses a PAMP. Verification of such a finding in the presence or absence of purified NOD2 would be crucial in assessing whether NLRP1 might be the cellular protein (or one of the cellular proteins) required to confer MDP responsiveness on NOD2, because direct binding of MDP by NOD2 has yet to be observed.

Besides regulating cytokine production, signaling through NOD2 also induces host antimicrobial responses in both immune and epithelial cells. Most of the NOD2-induced antimicrobial responses require NF-κB and MAPK activation, which regulates expression of antimicrobial peptides including α-defensins, β-defensins, and cryptidins (*4*). NOD2 also associates with the NADPH (reduced nicotinamide adenine dinucleotide phosphate) oxidase family member DUOX2 (*22*). Microbicidal reactive oxygen species (ROS) production by DUOX2 appears to be regulated through MDP-NOD2 signaling. These results indicate that recognition of MDP by NOD2 induces multiple effector responses to enhance intercellular communication through cytokine, chemokine, and defensin production, and to enhance antimicrobial function by ROS production. These new observations present the pressing challenge of defining whether these disparate actions of NOD2 are mediated by a single multifunctional complex or by distinct biochemical complexes.

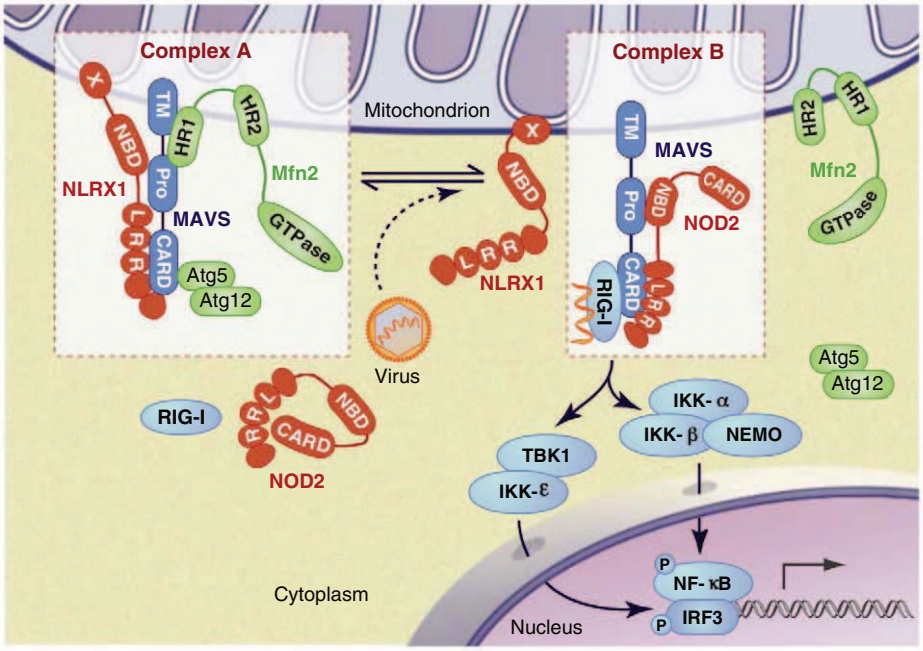

Fig. 2. NLR proteins and regulation of the mito-signalosome. In the quiescent state (complex A), the CARD-CARD homotypic interaction between MAVS and RIG-I is prevented by MAVS association with NLRX1 and/or Atg5-Atg12 conjugate, perhaps by steric hindrance. Mfn2 interacts with the C terminus and the transmembrane region of MAVS to abolish its immune-activating function. The three regulatory proteins target different regions of MAVS to execute the "molecular brake." In the presence of cytosolic 5′-triphosphate, ssRNA, or dsRNA, these brakes are released, which renders the assembly of the active form of mito-signalosome (complex B), in which MAVS interacts with NOD2 and RLRs, such as RIG-I, which directly interact with viral nucleic acid to trigger type I IFN production.

How Do NLRs Affect the Mito-Signalosome?

Besides the biochemical complexes defined above, recent reports have found a new linkage between NLRs and a newly defined multimeric complex that is located in the mitochondria, which together regulates the production of antiviral type I IFN and inflammatory cytokines. The mitochondria have been typically associated with pivotal roles in oxidative phosphorylation, adenosine triphosphate (ATP) generation, ROS production, cell survival, programmed cell death, and autophagy; however, recent evidence suggests that mitochondria can act as central platforms for innate antiviral responses. This function centers on the mitochondrial antiviral signaling protein (MAVS; also known as IPS-1, VISA, and Cardif), an immune-activating adaptor for type I IFN production that is located in the mitochondria (*23*–*26*). Functional and physical associations of MAVS with NLR proteins have been demonstrated and are proposed to regulate type I IFN and other inflammatory cytokines. We refer to this complex—which also includes helicases that directly bind to viral single-stranded RNA (ssRNA), viral double-stranded RNA (dsRNA) intermediates, RNase L–cleaved host RNA, and other regulatory proteins—as the mito-signalosome.

MAVS is ubiquitously expressed, and it mediates type I IFN production in response to specific signals (Fig. 2). Some cell types are heavily dependent on MAVS for the type I IFN response caused by RNA viruses, yet MAVS-independent, TLR-dependent machinery is important for type I IFN production in other cell types (*25*, *27*). MAVS activates the transcription factors IRF-3 (interferon response factor–3) and NF-κB. NF-κB, in turn, drives increased production of type I IFN and proinflammatory cytokines such as IL-6. MAVS can also induce apoptosis in response to some viral infections; however, certain viral proteins, such as those from SARS-coronavirus and hepatitis C virus, can antagonize this function (*28*).

A key pathway by which MAVS regulates inflammation is through its interaction with the retinoic acid–inducible protein I (RIG-I)–like family of pathogen recognition receptors (RLRs). Two of the RLR family members, RIG-I and melanoma differentiation–associated gene 5 (MDA-5), share

a conserved domain structure consisting of two N-terminal CARD domains and a DExD/H-box helicase domain; however, they exhibit distinct preferences for the molecular features of RNA ligands and RNA viruses (*29*). RIG-I binds to short dsRNA and 5′-triphosphate–bearing ssRNA, whereas MDA5 recognizes long dsRNA (*30*).

Given the substantial impact of type I IFN production, it is not surprising that MAVS is subjected to meticulous checks and balances by negative regulators. One such negative regulator is the NLR protein NLRX1 (*31*). NLRX1 is an unusual NLR member in that it is located at the mitochondria and contains a mitochondrial targeting sequence at its N terminus; however, its precise mitochondrial location is in dispute (*31*, *32*). Furthermore, it contains an N-terminal effector domain that bears similarity to both pyrin and CARD domains but cannot be categorized as either. Finally, the sequence encoding the central nucleotide-binding domain is split into two exons at the genomic level, and the encoded domain lacks a Walker A motif that is required for ATP binding found in other NLRs. Instead of direct microbial sensing, NLRX1 interacts with MAVS to prevent its binding to RIG-I, thus compromising the activation of NF-κB and IRF3 in response to cytosolic RNA and leading to the inhibition of type I IFN and proinflammatory cytokine production (*31*). Overexpression studies also suggest that NLRX1 might positively regulate the production of ROS from mitochondria in response to an intracellular bacterial pathogen, although verification with a nonoverexpression system is necessary (*33*). Further delineation of the physiologic function of NLRX1 would be aided by generation of *Nlrx1*-deficient mice.

Similar to NLRX1, five other proteins, including Atg5-Atg12 conjugate, gC1qR, Mfn2, PSMA7, and PCBP2, have recently been identified in the mito-signalosome negative regulatory module (*34*–*38*). Reduction of protein expression by RNA interference results in enhanced type I IFN production in response to certain RNA viruses. These proteins, however, are unlikely to be functionally redundant because they regulate mito-signalosome activation via distinct mechanisms, including molecular steric hindrance, autophagy, and posttranscriptional destabilization of MAVS. Interestingly, MAVS resides in a high–molecular weight complex in the quiescent state, and a substantial amount of MAVS migrates into lower–molecular weight fractions after stimulation, which suggests that it is released from a negative regulatory complex that precludes signal transduction at baseline (*37*).

NLRX1 and several negative regulators of MAVS are proposed to work by steric hindrance. For example, NLRX1 inhibits Sendai virus-induced homotypic CARD-CARD interactions between RIG-I and MAVS (*31*). Atg5-Atg12 conjugate-mediated inhibition of MAVS signaling acts by a similar mechanism (*35*). In contrast, Mfn2 interacts with the C-terminal and transmembrane region of MAVS rather than the N-terminal CARD domain (*37*), although it is unclear whether Mfn2 can sterically preclude upstream RLR engagement by MAVS. These findings are also compatible with the possibility that binding of inhibitory factors induces conformational changes in MAVS that reduce its affinity for RLRs. Furthermore, MAVS activity is also attenuated by its association with the proteasome subunit PSMA7 (*34*) and the ubiquitin ligase AIP4 via PCBP2 (*38*). Whether these are connected to the NLR pathway has not been investigated.

Besides NLRX1, a recent report demonstrated that interaction between MAVS and NOD2 regulates type I IFN (Fig. 2). Overexpression of NOD2, but not of other NLRs such as NOD1, NLRC4, NAIP, or NLRC3, provides human embryonic kidney 293 cells the capability to activate IRF3 in response to ssRNA or infection with respiratory syncytial virus (RSV), a ssRNA virus (*39*). Endogenous expression of NOD2 was also shown to be induced by ssRNA treatment or RSV infection. Depletion of NOD2 ablated type I IFN production in these cells. Furthermore, immunoprecipitation of NOD2 led to the recovery of RSV-specific RNA, which was substantiated in a cell-free system. Thus, this study suggests that NOD2 can positively regulate type I IFN by direct or indirect association with viral ssRNA. Patients with NOD2 polymorphisms that lead to altered NOD2 function, however, are not known to have difficulties with viral infection. This could be a species-specific difference, in that the antiviral role of NOD2 is specific to mice or that the disease-associated NOD2 variants are not affected in their antiviral function. As with MDP, however, it is still premature to define NOD2 as a bona fide pattern recognition receptor for ssRNA, because immunoprecipitation is likely to pull down NOD2-interacting proteins. MAVS associates with both NOD2 and RIG-I/MDA-5; thus, it is possible that the recovery of RSV-specific RNA is the result of coimmunoprecipitation of RIG-I.

NOD2 also has been found to interact with 2′-5′ oligoadenylate synthase type 2 (OAS2), a known RNA binding protein (*40*). Binding of dsRNA to OAS2 results in the generation of 2′-5′-adenosine oligomers, which activate intracellular RNase L. RNase L then destroys viral RNA and impairs further viral production in the infected cell by degrading cellular RNAs (*41*). RNase L–generated RNA species can also activate RLRs, thus endowing the mito-signalosome with a positive feedback mechanism. These data suggest that the association with OAS2 links NOD2-mediated type I IFN production to RNase L activation, which synergistically amplifies host antiviral responses (*40*).

It is intriguing to consider that the induction of type I IFN and RNase L activation by NOD2 in response to viral infection might parallel the bifurcated signaling and antimicrobial response seen during NOD2 activation by bacterially derived MDP (Fig. 1). It will be of great interest to assess whether NOD2 can bind RNA in the absence of accessory molecules such as RIG-I or OAS2, because evidence of direct binding would establish the structural basis for the classification of NOD2 as a pattern recognition receptor.

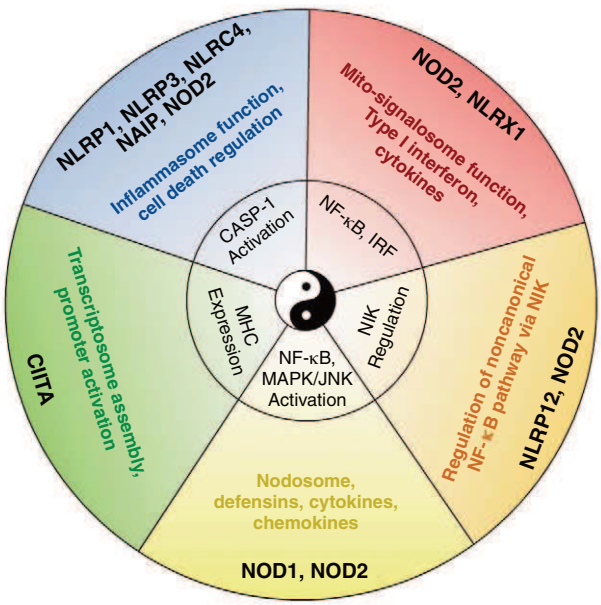

Fig. 3. NLR proteins signal through different multicomponent signalosomes. NLR signaling modules include the CIITA transcriptosome, the caspase-1–activating inflammasomes, the IFN/cytokine–inducing mito-signalosome, the NF-κB/MAPK–activating NOD1/2 complex (referred to as the nodosome), and the NIK pathway. This figure depicts the concept that one NLR can serve multiple functions, whereas multiple NLRs can also serve similar functions.

How Does NLR Affect the Noncanonical NF-κB Pathway?

One of the first pyrin-encoding NLR genes to be identified was *NLRP12* (also known as Monarch-1 or Pypaf7) (*42*–*44*). The expression of this gene is restricted to the myeloid-monocytic compartment, thus implicating a role in immunity. Early work using overexpression of NLRP12 demonstrated that it can activate NF-κB, and furthermore, the introduction of NLRP12, pro–IL-1β, pro–caspase-1, and the common inflammasome adaptor ASC/Pycard into 293T cells can activate caspase-1 with a corresponding increase in IL-1β produc-

tion (*43*). Thus, NLRP12 exhibits properties of an inflammasome NLR; however, gene silencing by short hairpin RNAs or gene deletion has not verified an effect of NLRP12 on IL-1β production. One possible explanation for these opposing results is that the specific activator of the NLRP12-dependent inflammasome was not used in these experiments.

In contrast to its proinflammatory role in inflammasome activation, NLRP12 has also been shown to impede activation of the noncanonical NF-κB pathway downstream of the tumor necrosis factor receptor (TNFR) (*42*). Activation of NF-κB can occur through two distinct mechanisms, referred to as the canonical and noncanonical pathways (*42*, *45*). Whereas the canonical pathway is triggered rapidly after cell stimulation, the noncanonical pathway exhibits much slower kinetics and is entirely dependent on the NF-κB–inducing kinase (NIK), which is not required for canonical NF-κB activation. NIK associates with the p100 subunit of NF-κB and induces its cleavage to its active form, p52, which causes the expression of a distinct subset of inflammatory genes. NLRP12 down-regulates the function of several important molecules involved in TNFR signaling, including NIK, RIP1, TNF receptor–associated factor 2 (TRAF2), and TRAF6 in human cell lines. Furthermore, both overexpression and small interfering RNA approaches show that NLRP12 reduces the level of NIK by a proteasome-dependent pathway, although the precise mechanism is unknown. Besides NLRP12, NOD2 may also regulate NIK function, an inference supported by several observations: When overexpressed, NIK can associate with NOD2; NOD2 and MDP can enhance p100 processing; and NIK is required for MDP-induced transcription of the chemokine CXCL13 (*46*, *47*). NIK function is only partially attenuated in macrophages lacking NOD2, which suggests that there might be redundant regulation of NIK by other proteins, including other NLRs.

What Are the Major Challenges in the NLR Field?

Studies of NLRs show that they interface with major regulatory pathways that affect the immune system, including caspase activation; cytokine, chemokine, and defensin production; canonical and noncanonical NF-κB pathways; MAPK, antimicrobial ROS, and IFN production; RNase L activity; MHC expression; and various forms of cell death (Fig. 3). A major challenge is to assess how NLRs function outside of the immune system, because many NLRs have broad tissue distribution and participate in signaling pathways that are broadly used throughout the organism. Such fields of research include developmental and reproductive biology, metabolism, and cancer, where connections with NLRs are less developed but are ripe for exploration.

Another challenge is to further understand the in vivo function of both well-studied and understudied NLRs in immune and nonimmune systems. This will require that we understand the cellular and tissue distribution of the endogenous NLRs, not just those that are overexpressed. It also requires that we understand dynamic changes in their subcellular localization upon activation with the appropriate agonists. This has not been addressed for most NLRs because of the lack of good antibodies specific for endogenous NLRs.

A third challenge is to determine which NLRs can undergo homo- and heterotypic association with other NLRs. Such interactions have long been proposed (*2*), but their importance might be unappreciated. The functional and physical interactions of NOD2 with NLRP1 or NLRP3 are prime examples where MDP stimulation of the inflammasome is achieved (*18*, *21*). Thus, the potential heterotypic association of multiple NLRs should exponentially expand the repertoire of biologic functions ascribed to NLRs not only in the immune system, but more broadly in all organs and tissues. A natural extension of such a model is that each NLR is not in a tidy functional group, but rather has multiple functions. Multiple functions could be executed by partnering with other NLRs and participating in large functional complexes, which (depending on the stimulatory signal) would be distinct in their composition and function (Fig. 3).

This leads to a fourth challenge, which is to decipher how a single NLR mediates distinct functions. For example, several NLRs participate in both caspase-1 activation and the induction of cell death. NOD2 affects not only RIP2, NF-κB, MAPK, and NIK, but also the mito-signalosome. Are these distinct functions achieved by its participation in the same or different signalosomes? Does NOD2 partner with different adaptors and NLR proteins?

A fifth challenge, which is fundamental to our understanding of NLRs, is to determine whether NLRs are simply components of large signaling complexes, are co-receptors for pattern recognition receptors, or are themselves pattern recognition receptors (or some combination of these possibilities). As presented above, there is abundant evidence that each NLR is a component of a large signaling complex. In the case of NLRP3, an inflammasome-activating NLR, it is difficult to envision how a single molecule might be the receptor for the multitude of PAMPs with divergent chemical compositions that can activate this inflammasome. In other cases where the function appears highly restricted, however, a receptor-ligand function seems to be a greater possibility.

This leads to a sixth challenge: What is the structure of NLR proteins? A resolution of the protein structure of each NLR protein will help to resolve the mechanism by which NLRs interact with other proteins within a signalosome and also whether NLRs directly bind to PAMPs. NLRs are notoriously difficult to purify, and thus resolving their full-length structure will be a major technical hurdle, whereas solving the structure of individual domains is more feasible. Although these are challenging issues to resolve, considering the rapid pace of NLR researches, much progress is likely in the near future.

References and Notes

1. F. M. Ausubel, *Nat. Immunol.* **6**, 973 (2005).
2. J. P. Ting, B. K. Davis, *Annu. Rev. Immunol.* **23**, 387 (2005).
3. T. D. Kanneganti, M. Lamkanfi, G. Núñez, *Immunity* **27**, 549 (2007).
4. K. S. Kobayashi *et al.*, *Science* **307**, 731 (2005).
5. M. Chamaillard *et al.*, *Proc. Natl. Acad. Sci. U.S.A.* **100**, 3455 (2003).
6. J. Wehkamp *et al.*, *Gut* **53**, 1658 (2004).
7. L. A. Simms *et al.*, *Gut* **57**, 903 (2008).
8. T. Watanabe, A. Kitani, P. J. Murray, W. Strober, *Nat. Immunol.* **5**, 800 (2004).
9. T. Watanabe *et al.*, *J. Clin. Invest.* **118**, 545 (2008).
10. S. Maeda *et al.*, *Science* **307**, 734 (2005).
11. J. Li *et al.*, *Hum. Mol. Genet.* **13**, 1715 (2004).
12. E. Noguchi, Y. Homma, X. Kang, M. G. Netea, X. Ma, *Nat. Immunol.* **10**, 471 (2009).
13. J. H. Fritz, L. Le Bourhis, J. G. Magalhaes, D. J. Philpott, *Trends Immunol.* **29**, 41 (2008).
14. F. Coulombe *et al.*, *J. Exp. Med.* **206**, 1709 (2009).
15. P. Lécine *et al.*, *J. Biol. Chem.* **282**, 15197 (2007).
16. M. J. Bertrand *et al.*, *Immunity* **30**, 789 (2009).
17. I. Tattoli, L. H. Travassos, L. A. Carneiro, J. G. Magalhaes, S. E. Girardin, *Semin. Immunopathol.* **29**, 289 (2007).
18. Q. Pan *et al.*, *J. Leukoc. Biol.* **82**, 177 (2007).
19. T. D. Kanneganti *et al.*, *Immunity* **26**, 433 (2007).
20. B. Faustin *et al.*, *Mol. Cell* **25**, 713 (2007).
21. L. C. Hsu *et al.*, *Proc. Natl. Acad. Sci. U.S.A.* **105**, 7803 (2008).
22. S. Lipinski *et al.*, *J. Cell Sci.* **122**, 3522 (2009).
23. T. Kawai *et al.*, *Nat. Immunol.* **6**, 981 (2005).
24. E. Meylan *et al.*, *Nature* **437**, 1167 (2005).
25. R. B. Seth, L. Sun, C. K. Ea, Z. J. Chen, *Cell* **122**, 669 (2005).
26. L. G. Xu *et al.*, *Mol. Cell* **19**, 727 (2005).
27. H. Kumar *et al.*, *J. Exp. Med.* **203**, 1795 (2006).
28. Y. Lei *et al.*, *PLoS ONE* **4**, e5466 (2009).
29. H. Kato *et al.*, *Nature* **441**, 101 (2006).
30. M. Yoneyama, T. Fujita, *Immunity* **29**, 178 (2008).
31. C. B. Moore *et al.*, *Nature* **451**, 573 (2008).
32. D. Arnoult *et al.*, *J. Cell Sci.* **122**, 3161 (2009).
33. I. Tattoli *et al.*, *EMBO Rep.* **9**, 293 (2008).
34. Y. Jia *et al.*, *J. Immunol.* **183**, 4241 (2009).
35. N. Jounai *et al.*, *Proc. Natl. Acad. Sci. U.S.A.* **104**, 14050 (2007).
36. L. Xu, N. Xiao, F. Liu, H. Ren, J. Gu, *Proc. Natl. Acad. Sci. U.S.A.* **106**, 1530 (2009).
37. K. Yasukawa *et al.*, *Sci. Signal.* **2**, ra47 (2009).
38. F. You *et al.*, *Nat. Immunol.* **10**, 1300 (2009).
39. A. Sabbah *et al.*, *Nat. Immunol.* **10**, 1073 (2009).
40. J. W. Dugan *et al.*, *Mol. Immunol.* **47**, 560 (2009).
41. K. Malathi *et al.*, *Proc. Natl. Acad. Sci. U.S.A.* **102**, 14533 (2005).
42. J. D. Lich *et al.*, *J. Immunol.* **178**, 1256 (2007).
43. L. Wang *et al.*, *J. Biol. Chem.* **277**, 29874 (2002).
44. K. L. Williams, D. J. Taxman, M. W. Linhoff, W. Reed, J. P. Ting, *J. Immunol.* **170**, 5354 (2003).
45. G. Bonizzi, M. Karin, *Trends Immunol.* **25**, 280 (2004).
46. Y. Ogura *et al.*, *J. Biol. Chem.* **276**, 4812 (2001).
47. Q. Pan *et al.*, *Infect. Immun.* **74**, 2121 (2006).
48. A. Mayor, F. Martinon, T. De Smedt, V. Pétrilli, J. Tschopp, *Nat. Immunol.* **8**, 497 (2007).

49. We acknowledge the very large number of researchers who have contributed to this field whose work was not cited or was cited through others' review articles because of space limitations. Supported by NIH grants CA131645, AI057157, and AI031496 and the Burroughs Wellcome Fund Career Award for Medical Scientists (J.A.D.) and by NIH grants AI063031, DE016326, U19AI077437, DK38108, and SERCEB (J.P.T.).

10.1126/science.1184004

REVIEW

Regulation of Adaptive Immunity by the Innate Immune System

Akiko Iwasaki[1]* and Ruslan Medzhitov[1,2]*

Twenty years after the proposal that pattern recognition receptors detect invasion by microbial pathogens, the field of immunology has witnessed several discoveries that have elucidated receptors and signaling pathways of microbial recognition systems and how they control the generation of T and B lymphocyte–mediated immune responses. However, there are still many fundamental questions that remain poorly understood, even though sometimes the answers are assumed to be known. Here, we discuss some of these questions, including the mechanisms by which pathogen-specific innate immune recognition activates antigen-specific adaptive immune responses and the roles of different types of innate immune recognition in host defense from infection and injury.

Metazoans are transiently or constitutively colonized by a variety of microorganisms that can engage in mutualistic or antagonistic interactions with their hosts. The nature of these interactions is still poorly understood, although recent studies have begun to elucidate the host receptors and signaling pathways involved in sensing both commensal and pathogenic microbes. These microbial sensing pathways are used by the immune system to maintain host-microbial homeostasis and to induce antimicrobial defense mechanisms. In vertebrates, two types of immunity are used to protect the host from infections: innate and adaptive. The innate immune system is genetically programmed to detect invariant features of invading microbes. Innate immune cells include dendritic cells (DCs), macrophages, and neutrophils, among others. In contrast, the adaptive immune system, which is composed of T and B lymphocytes, employs antigen receptors that are not encoded in the germ line but are generated de novo in each organism. Thus, adaptive immune responses are highly specific. The best-characterized microbial sensors are the so-called pattern recognition receptors (PRRs) of the innate immune system, which detect relatively invariant molecular patterns found in most microorganisms of a given class (*1*). These structures are referred to as pathogen-associated molecular patterns (PAMPs), though they are not unique to microbes that can cause a disease. Several families of PRRs have been characterized over the past decade, thus elucidating the basic mechanisms of sensing microbial infections; however, several questions remain unresolved, and new questions have arisen as a result of recent progress. Here we will discuss some of these emerging questions in the context of the current knowledge of innate immune recognition.

[1]Department of Immunobiology, School of Medicine, Yale University, New Haven, CT 06520, USA. [2]Howard Hughes Medical Institute, School of Medicine, Yale University, New Haven, CT 06520, USA.

*To whom correspondence should be addressed. E-mail: akiko.iwasaki@yale.edu (A.I.); ruslan.medzhitov@yale.edu (R.M.)

Are All PRRs Created Equal?

Microbial pathogens are recognized through multiple, distinct PRRs that can be broadly categorized into secreted, transmembrane, and cytosolic classes. Secreted PRRs (including collectins, ficolins, and pentraxins) bind to microbial cell surfaces, activate classical and lectin pathways of the complement system, and opsonize pathogens for phagocytosis by macrophages and neutrophils.

The transmembrane PRRs include the Toll-like receptor (TLR) family and the C-type lectins. TLRs in mammals are either expressed on the plasma membrane or in endosomal/lysosomal organelles (*2*). Cell-surface TLRs recognize conserved microbial patterns that are accessible on the cell surface, such as lipopolysaccharide (LPS) of Gram-negative bacteria (TLR4), lipoteichoic acids of Gram-positive bacteria and bacterial lipoproteins (TLR1/TLR2 and TLR2/TLR6), and flagellin (TLR5), whereas endosomal TLRs mainly detect microbial nucleic acids, such as double-stranded RNA (dsRNA) (TLR3), single-stranded RNA (ssRNA) (TLR7), and dsDNA (TLR9). Expression of TLRs is cell-type specific, allowing allocation of recognition responsibilities to various cell types (*3*). Dectin-1 and -2 are transmembrane receptors of the C-type lectin family that detect β-glucans and mannan, respectively, on fungal cell walls (*4*, *5*).

The cytosolic PRRs include the retinoic acid–inducible gene I (RIG-I)–like receptors (RLRs) and the nucleotide-binding domain and leucine-rich repeat–containing receptors (NLRs). RLRs detect viral pathogens (*6*). Unlike TLRs, most cell types express RLRs. RLR members RIG-I and melanoma differentiation factor 5 (MDA5) recognize viral RNA through their helicase domain and signal through their caspase recruitment domains (*7*, *8*). RLRs use a common adaptor molecule mitochondria antiviral signaling protein (MAVS) (*9*). Engagement of MAVS by RLRs leads to the activation of transcription factors nuclear factor κB (NF-κB) and interferon regulatory factor 3 (IRF3). RIG-I recognizes 5′ triphosphate–ssRNA with a dsRNA component: PAMPs associated with many ssRNA viruses (*8*). Similar RNA species are also generated by RNA polymerase III (Pol III) in the cytosol upon transcription of poly dA-dT–rich dsDNA (*10*, *11*). Thus, RIG-I is a sensor for both ssRNA viruses and some dsDNA viruses (via Pol III). MDA5 preferentially recognizes long dsRNA structures in the cytosol, a PAMP associated with positive ssRNA virus infections (*9*).

NLRs represent a large family of intracellular sensors that can detect pathogens and stress signals (*12*). NLRs are multidomain proteins that contain a C-terminal leucine-rich repeat domain, a central nucleotide-binding oligomerization domain (NOD), and an N-terminal effector domain (*13*). They can be divided into three subfamilies depending on their N-terminal domains. NLR family members detect (in most cases indirectly) degradation products of peptidoglycans, various forms of stress (for instance, ultraviolet irradiation), microbial products, and noninfectious crystal particles (*12*).

Most, if not all, PRRs that activate the transcription factors NF-κB, IRF, or nuclear factor of activated T cells (NFAT) are sufficient to induce both T and B cell responses, whereas secreted PRRs and some endocytic PRRs (scavenger receptors and mannose receptors) cannot induce adaptive immunity by themselves (*14*). TLRs are the best characterized receptors that can trigger activation of adaptive immune responses of several effector classes, including immunoglobulin M (IgM), IgG, and IgA antibody responses; T helper cell 1 (T_H1) and T_H17 $CD4^+$ T cell responses; and $CD8^+$ T cell responses (*3*). In a pathological setting, TLR4 can also induce T_H2 and IgE responses, although the functional importance of this pathway in protective immunity is currently unknown. Engagement of dectin-1 and -2 can drive T_H17 responses, which are required to clear fungal infections (*4*). Several recent studies have demonstrated that cytosolic PRRs, including RLRs and some NLRs, can also activate adaptive immunity (*15*–*19*). A cytosolic DNA sensor pathway is also sufficient for activation of T_H1, cytotoxic $CD8^+$ T cell, and antibody responses through TANK-binding kinase-1 (*20*).

The relative contribution of different PRRs to activation of specific arms of adaptive immune response during microbial infections is not fully understood. Somewhat surprisingly, inflammasomes, rather than signaling through the viral sensors RLRs, are required for adaptive immunity

against influenza infection (*21*, *22*). Similarly, infection with respiratory syncytial virus (RSV) activates MAVS-dependent antiviral innate host defenses, and yet, mice deficient in both MAVS and MyD88 (and adaptors used by most TLRs) can mount adaptive immune responses and clear RSV infection (*23*). Protective immunity to RSV was instead shown to depend on the NLR NOD2 (*24*). For many microbial infections, including the well-studied pathogens *Mycobacterium tuberculosis* and *Listeria monocytogenes*, the relevant innate immune recognition pathways are unknown, though some obvious candidates have been excluded. Activation of protective $CD8^+$ T cell responses to *L. monocytogenes* is MyD88-independent (*25*), and the intracellular stage of infection activates the transcription factor IRF3 (*26*), but the sensor responsible for the induction of the adaptive immune response is unknown. In the case of *Mycobacteria* infection, immune protection is MyD88-dependent, but this is probably due to the requirement for the interleukin-1 (IL-1) receptor signaling rather than TLR signaling (*27*). The sensors responsible for activation of adaptive immunity to *Mycobacteria* infection remain to be elucidated. Finally, the innate recognition events that trigger activation of adaptive immunity in response to retroviral and lentiviral infections, including HIV-1, are not fully understood. HIV-1 can activate TLR7 and TLR9 in plasmocytoid DCs (*28*), and the antibody response to Friend murine leukemia virus infection is MyD88-dependent, whereas $CD8^+$ T cell responses only partially depend on MyD88 (*29*). Thus, it is likely that retroviruses may also activate one of the intracellular nucleic acid sensing pathways, but the receptors and ligands involved still need to be determined.

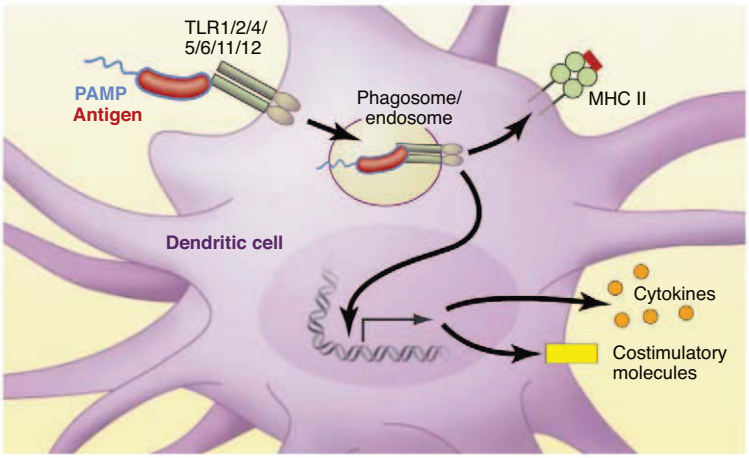

Fig. 1. Cell-extrinsic recognition of pathogens. Bacteria detected by DCs through TLRs are internalized into the phagosome where bacterial antigens are processed for presentation on MHC class II. Bacterial antigens (red) and PAMPs (blue) are present in the same phagosome, which indicates to the DC their common origin. TLR-mediated recognition of bacterial PAMPs promotes the selection of bacterial antigens for optimal presentation on MHC class II. TLR signaling also leads to the induction of costimulatory molecules and cytokines necessary for activation and differentiation of T lymphocytes.

Are Cell-Intrinsic and Cell-Extrinsic Innate Immune Recognition Equivalent?

Innate immune recognition can be cell-intrinsic or cell-extrinsic, depending on whether it is mediated by infected or noninfected cells (*30*). Cell-extrinsic innate immune recognition is mediated by transmembrane receptors (including TLRs and dectins); their activation does not require the cells expressing these receptors to be infected. In contrast, cell-intrinsic innate immune recognition is mediated by intracellular sensors, including NLRs and RLRs. Activation of these receptors generally requires that the cell is infected. Accordingly, these PRRs are broadly expressed because most cells can potentially be infected by pathogens, especially by viruses. In contrast, cell-extrinsic recognition is mainly mediated by specialized cells of the immune system, such as macrophages and DCs. Although both types of recognition can induce antimicrobial effectors upon activation, they may trigger adaptive immunity by different mechanisms, as discussed in more detail below.

The principal distinction is the way the origin of antigens is established by cell-extrinsic and -intrinsic innate immune recognition. In the former case, the detection of a microbial cell or a viral particle by, for example, a TLR expressed on DCs is followed by endocytosis or phagocytosis of the pathogen and subsequent processing and presentation of microbial antigens to T cells by major histocompatability complex (MHC) molecules. This presentation occurs in the context of several signals that are induced by the TLR and that are required for naive T cell activation, including costimulatory signals and cytokines (Fig. 1). The microbial origin of the antigens is established through the physical association between an antigen and a PAMP that triggered the TLR. The physical association is primarily due to the co-occurrence of the antigen and a PAMP within the same particle (bacterial, yeast, or protozoan cell or a viral particle). In cell biological terms, the association is interpreted, in part, through co-delivery of an antigen and a TLR ligand to the same phagosome or endosome, where the antigens are preferentially selected for presentation by MHC class II (*31*). During immunization, an antigen and a PAMP are generally mixed together and thus would not be perceived as having a common (microbial) origin unless both end up in the same endosome. This normally would require a large excess of PAMP over what is minimally required for activation of DCs. The co-recognition, however, is strongly facilitated by some adjuvants, such as mineral oil and alum, that promote antigen persistence and the co-recognition of the antigen and a PAMP. This effect of adjuvants can be substituted for by a physical association of an antigen and a PAMP, either by direct conjugation or by coabsorption on the same particles, because in both cases they will localize to the same endosomes, and the immune system will interpret this as an indication that the antigen is of microbial origin. Such associative recognition also explains why immunodominant antigens generally have both PAMP activity and antigenicity embedded within the same molecule. Examples include *Toxoplasma* profilin (*32*), several bacterial lipidated outer membrane proteins, and flagellin; in each case these antigens are also PAMPs that can activate various TLRs. Similarly, in the case of auto-antigens that trigger TLR7- and TLR9-mediated autoimmunity, ribonucleoproteins and chromatin complexes contain both self antigens and TLR agonists.

Associative recognition also plays an important role in cell-extrinsic recognition by B cells. The co-engagement of the B cell receptor (BCR) with one of several innate immune signaling pathways, such as the C3dg complement component, results in a profound enhancement of antibody responses (*33*). In this case, C3dg "flags" the antigen as foreign, thus instructing B cells about the origin of the antigen. Similarly, co-engagement of the BCR and TLRs enhances antibody responses, as exemplified by the strong immunogenicity of flagellin and other antigens that have TLR agonist activity (*14*).

The situation is less clear for cell-intrinsic immune recognition (Fig. 2). The intracellular (cytosolic) sensors, such as RIG-I and MDA-5, detect viral nucleic acids in infected cells, which in most cases are not professional antigen-presenting cells (APCs). In contrast to TLR-mediated recognition, where microbial antigens are "marked" by physical association with microbial PAMPs, cell-intrinsic sensing of viral nucleic acid is not known to be coupled to the viral antigens. It is possible that such an association does exist, and that RLR-mediated recognition of viral nucleic acids somehow promotes the selection of viral antigens for presentation to T cells. It is not obvious how this might work, especially if RLR-mediated recognition and

antigen presentation occur in different cells—for example, in virally infected cells and in DCs, respectively. Even when intracellular sensors are activated within an APC, it is unclear whether and how the microbial antigens are preferentially targeted for presentation to T cells. One possibility is that the innate recognition event somehow directs the microbial antigens for autophagic degradation followed by MHC presentation (Fig. 2). Autophagy has been linked to MHC class II antigen presentation (*34*). Alternatively, cell-intrinsic innate immune recognition may be coupled with induction of adaptive immunity by a mechanism that is independent of physical association but rather depends on another type of coincidence detection. Finally, a trivial but likely incomplete explanation of selective activation of pathogen-specific T cells following cell-intrinsic innate immune recognition is that all self antigen–specific T cells are deleted during negative selection, which would only allow for pathogen-specific T cells to become activated during an infection. This possibility, however, is inconsistent with the presence of mature self-reactive T cells in peripheral tissues that are activated when mechanisms of peripheral tolerance are compromised. Moreover, cell-intrinsic activation of a cytosolic DNA sensing pathway by endogenous DNA was recently shown to result in an autoimmune disease (*35*).

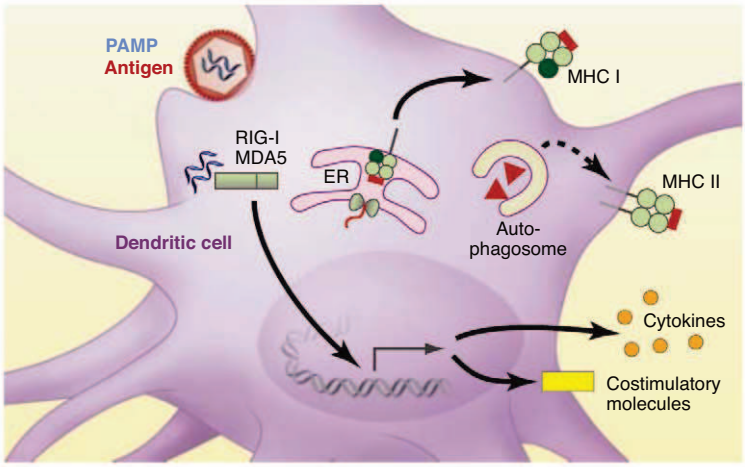

Fig. 2. Cell-intrinsic recognition. DCs directly infected by viruses recognize PAMPs (blue) within the cytosol via RIG-I like receptors (RLRs). Cytosolic viral proteins (red) are processed and presented on MHC class I (via the conventional endoplasmic reticulum pathway) or MHC class II (via autophagy). RLR signaling leads to the induction of costimulatory molecules and cytokines necessary for activation and differentiation of T lymphocytes. How the origin of antigen is established in this instance is unclear. In the case of the MHC class I pathway, this may depend on the abundance of viral antigens; for MHC class II, it may depend on targeting of viral antigens (red triangles) by the autophagy machinery.

Whether the pathogen detection occurs through cell-intrinsic or -extrinsic mechanisms, DCs presumably always have to be directly activated by a PRR to activate T cell responses (*36*). But can DCs use cell-extrinsic and -intrinsic innate immune recognition pathways equally? Activation of the cell-intrinsic pathway generally implies that the cell where recognition occurs is infected; however, infected DCs succumb to various pathogen-encoded strategies that can interfere with their function. Furthermore, most pathogens do not infect and replicate in DCs (*37*). When they do, such pathogens often use the biology of DCs to gain access to the target tissue within which they can replicate and disseminate. Examples of these include HIV-1 (*38*) and Venezuelan equine encephalitis virus (*39*). In many cases, noninfected DCs present antigen derived from infected cells. The most extreme case of this is the antigen-transfer model, in which DCs that have migrated from the infected tissue transfer antigen to the lymph node–resident DCs, thus amplifying T cell activation (*40*). How the origin of the antigen could be established in these models is not clear, although recent studies have suggested possible mechanisms. In one pathway, TLR3 in DC phagosomes detects viral nucleic acids (dsRNA) from infected cells and triggers DC activation and presentation of viral antigens on MHC class I (Fig. 3) (*41*). This finding is particularly interesting given the lack of evidence for the requirement of TLR3 in direct viral recognition by DCs in antiviral defense (*6*). Thus, TLR3 might recognize viral dsRNA from infected cells but not the viruses themselves. Infected apoptotic cells also induce the production of transforming growth factor–β and IL-6 by DCs, thus driving the differentiation of T_H17 cells (*42*). Thus, cell-extrinsic recognition of pathogens through the uptake of infected cells provides an additional layer of control of T cell responses generated by DCs.

What Is the Role of Pathogen Recognition by APCs Versus Infected Cells?

Besides being a source of microbial antigens, infected cells can engage DCs in other ways to provide critical signals for T cell activation. TLR-dependent signals in infected epithelial cells are required for DC-mediated induction of T_H1 responses in response to herpes simplex virus (HSV)–2 or *Toxoplasma gondii* (*43*, *44*). Moreover, epithelial cell–specific inactivation of NF-κB directs $CD4^+$ T cell differentiation toward unprotective T_H1/T_H17 responses against *Trichuris muris* infection in the gut (*45*). Furthermore, the TLR3 ligand polyinosinic:polycytidylic acid–induced T_H1 response to an HIV gag protein vaccine depends on MDA5-mediated recognition in both hematopoieitic and stromal cell compartments (*16*). These studies indicate that, at least in some cases, PRR signaling in DCs alone cannot generate robust protective immunity and that DCs must receive additional cues from the infected cells. Recognition of pathogens by the infected epithelial cells alone, however, cannot induce $CD4^+$ T cell responses (*43*, *44*). Rather, direct recognition of PAMPs by TLRs in DCs is required for $CD4^+$ T cell activation (*36*). Collectively, these studies indicate that, at least in some cases, DCs require two signals for $CD4^+$ T cell activation: (i) direct sensing of the PAMPs associated with the invading pathogen and (ii) detection of a PRR-induced signal from the infected cells. The observation that tissue-migrant DCs exposed to both of these signals are the primary APC for $CD4^+$ T cell activation (*46*) supports this idea. The nature of the second signal probably depends on the pathogen and the tissue microenvironment.

Whether similar requirements also apply to the generation of $CD8^+$ T cell responses is unclear. Infected cells present antigens on MHC class I, so that they can be killed by activated $CD8^+$ T cells. To become activated, however, $CD8^+$ T cells must recognize antigens presented by DCs, which in most cases are not infected by the same pathogen. Thus, to activate a $CD8^+$ T cell response, uninfected DCs must present microbial antigens on MHC class I, in a process known as cross-presentation. In the antigen-transfer model, migrant DCs from peripheral tissues, upon arrival in the draining lymph node, transfer antigens to blood-derived lymph node–resident DCs (*40*). Blood-derived $CD8\alpha^+$ DCs in the lymph node are the predominant APCs for $CD8^+$ T cells upon infection with influenza, HSV-1, or *Listeria* or encounter with apoptotic cells (*40*). How do these DCs receive the proper cues to become competent to prime $CD8^+$ T cells? PAMPs and antigens may be preserved within the migrant DCs, allowing $CD8\alpha^+$ DCs to acquire such information and drive $CD8^+$ T cell activation. Alternatively, cross-priming by DCs may not require signals from pathogens or infected cells, but instead may require a signal from antigen-specific $CD4^+$ T cells. For example, $CD4^+$ T cell help is necessary for DCs to activate the $CD8^+$ T cell response during HSV-1 infection

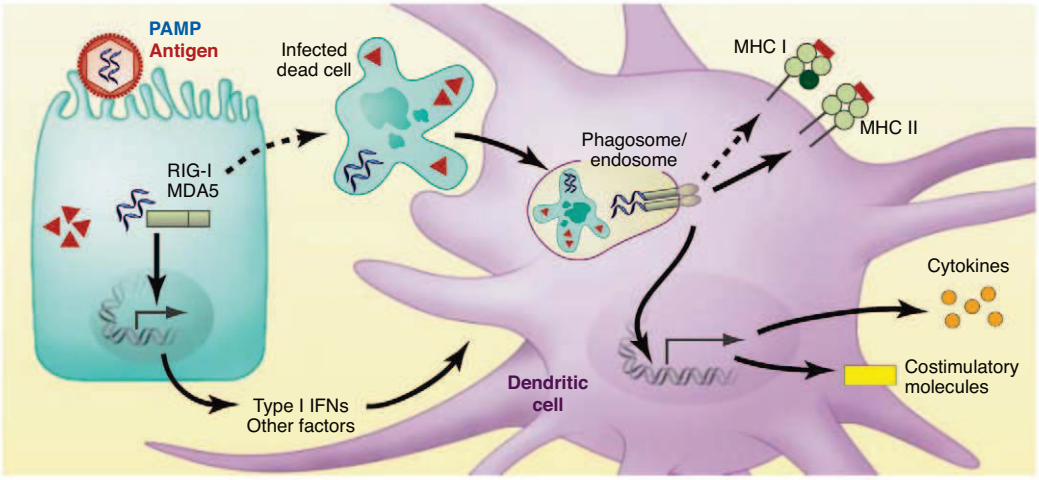

Fig. 3. Cell-extrinsic recognition of infected cells. A virally infected non-APC recognizes PAMPs (blue lines indicate viral nucleic acids) within the cytosol via the RLRs, leading to secretion of type I interferons (IFNs) and other factors that activate DCs. Infected dead cells are taken up by noninfected DCs, and viral PAMPs (blue) are recognized through endosomal TLRs. Viral antigens (red triangles) are processed and presented on MHC class II (via the conventional endosomal pathway) or MHC class I (via cross-presentation). TLR signaling leads to the induction of costimulatory molecules and cytokines necessary for activation and differentiation of T lymphocytes.

(*47*). Here, the information regarding the pathogen and the microenvironment might already have been processed by the $CD4^+$ T cells, thus alleviating the need for $CD8^+$ T cells to do the same. Future studies will help to resolve this issue.

Are Endogenous and Microbial TLR Ligands Equivalent?

In addition to recognition of microbial structures, several studies have demonstrated that some TLRs are also involved in sensing endogenous signals generated during tissue injury. Although some initial reports were probably artifacts caused by contamination of recombinant protein preparations, more recent analyses revealed a number of cases of *bona fide* endogenous TLR stimulators. One class of endogenous TLR ligands is chromatin fragments and ribonucleoprotein complexes released from dead cells. When clearance of apoptotic cells is insufficient, these complexes can activate TLR7 and TLR9 on DCs and B cells, which can result in the development of systemic autoimmune diseases (*48*). In these cases, TLR activation by self nucleic acids is clearly unintended. Self nucleic acids are simply mistaken for microbial pathogens.

Unlike the accidental TLR recognition of endogenous nucleic acids, detection of other endogenous ligands might serve a physiological purpose. The two common sources of endogenous TLR ligands are components of the extracellular matrix (ECM) and intracellular proteins. Inflammation and injury cause degradation and accumulation of several ECM components. Small molecular weight fragments of hyaluronic acid (HA) (*49*), biglycan (*50*), and versican produced by tumor cells (*51*) can trigger TLR2 and/or TLR4 activation. Fragments of heparan sulfate, an acidic polysaccharide found in cell membranes and ECMs, activates DCs through TLR4 (*52*). Furthermore, several intracellular proteins have been suggested to activate TLRs, including the high-mobility group box 1 (HMGB1) protein, which normally resides in the nucleus but is thought to be secreted or released from damaged or necrotic cells. Extracellular HMGB1 has proinflammatory effects, which are mediated by TLRs 2, 4, and 9 and the receptor for advanced glycation end products (RAGE) (*53*).

Both biglycan and HA fragments accumulate during tissue injury and activate macrophages to produce inflammatory chemokines and cytokines via TLR2 and TLR4 (*49*, *50*). Biglycan-deficient mice were less susceptible to death caused by TLR2- or TLR4-dependent sepsis due to lower amounts of circulating tumor necrosis factor–α and reduced leukocyte infiltration in the lung (*50*). Similarly, TLR4-mutant mice secrete less inflammatory cytokines after ischemic reperfusion, and this effect was mimicked by neutralization of HMGB1 in control mice but not TLR4-mutant animals (*54*). In contrast, in a noninfectious lung-injury model, mice deficient in both TLR2 and TLR4 show impaired leukocyte recruitment, increased tissue injury, and decreased survival (*49*). These studies indicate that several endogenous ligands provide signals through TLR2 and TLR4 to initiate inflammatory responses and promote tissue protection and repair.

These studies raise an important issue: Do microbial and endogenous agonists of TLR2 or TLR4 trigger identical responses? Microbial stimulators of TLRs activate inflammatory, tissue repair, and adaptive immune responses. Endogenous stimulators of TLR2 and TLR4 are only known to induce the inflammatory and tissue reparative responses. Activation of TLRs in the absence of infection can lead to autoimmune responses, as illustrated by the effects of accidental stimulation of TLR7 and TLR9 by self nucleic acids (*48*). Therefore, it is reasonable to assume that the endogenous TLR2 and TLR4 agonists, unlike their microbial counterparts, do not induce activation of adaptive immune responses (Fig. 4). Indeed, TLR2 activation by necrotic cells was shown to induce expression of inflammatory and tissue repair genes, but not genes associated with adaptive immunity (*55*). Likewise, HA triggers signals distinct from LPS, by engagement of TLR4, MD2, and CD44 (*56*).

Thus, the physiological, endogenous ligands of TLR2 and TLR4 probably trigger signals distinct from their microbial counterparts and specifically induce genes involved in tissue homeostasis and repair. The differential signaling by microbial versus endogenous TLR ligands may be due to the engagement of different co-receptors (Fig. 4). HA, but not LPS, signals through both CD44 and TLR4, whereas HMGB1 signals through TLRs and RAGE (*53*, *56*). Thus, the usage of differential co-receptors may potentially influence the signaling pathways induced by microbial and endogenous TLR ligands. Moreover, there are examples of differential TLR signaling from distinct subcellular compartments (*57*). It will be important to address these and other possibilities in future studies, because the prevailing view of the role of endogenous ligands as danger signals that activate the adaptive immune responses is probably incorrect. Physiological endogenous activators of TLRs, or any other PRRs, have not yet been shown to be sufficient to activate adaptive immune responses, whereas unintended stimulation of TLR7 and TLR9 results in autoimmune responses. This also applies to the endogenous activators of inflammasomes and is illustrated by the lack of autoimmunity in patients with gout, a condition caused by inflammasome activation by endogenous uric acid crystals (*12*). Furthermore, genetic mutations in the inflammasome components lead to autoinflammatory diseases that differ from autoimmune disorders in that they do not involve activation of autoreactive T and B cell responses (*58*).

Conclusions

As the basic functions of TLRs are becoming increasingly well defined, many new questions

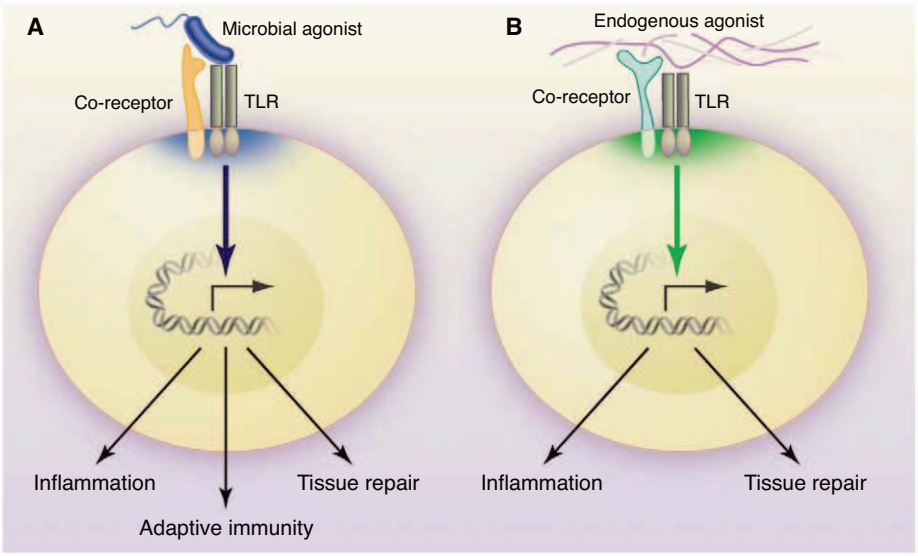

Fig. 4. Proposed consequences of TLR recognition of exogenous versus endogenous ligands. TLR engagement by exogenous (**A**) or endogenous (**B**) agonists leads to signaling from distinct subcellular compartments (indicated by blue and green, respectively) and/or engagement of co-receptors. Consequently, exogenous ligands induce transcription of genes leading to inflammation, tissue repair, and the initiation of adaptive immunity (A). In contrast, endogenous ligands induce TLR signaling for activation of inflammation and tissue repair but not the initiation of adaptive immunity (B).

emerge. One fundamental issue is that microbial TLR ligands are not unique to pathogens, but instead are common to all microbes of a given class. This creates a problem of discrimination between commensals and pathogens. One possibility is that pathogens are distinguished from commensals because of their unique virulence activities, such as production of pore-forming toxins. The notion of pathogen-commensal discrimination is complicated, however, because distinctions between them are often arbitrary and conditional upon the host immune status. A widespread assumption is that the immune system has to discriminate between commensals and pathogens, such that immune responses are generated exclusively toward the latter. It could be argued, however, that the immune system handles all microbes in the same way. In fact, immune responses are generated against commensals, and moreover, commensals maintain their "innocuous" status toward the host, in part because they are actively suppressed by the immune system. Of course, the immune response to microbes in highly colonized tissues, such as the intestine, is tightly regulated and has a distinct modality, so as to avoid immunopathology. Specific forms of immune responses to commensals do exist under normal conditions, however, as exemplified by commensal-specific IgA antibodies normally present in the intestinal lumen (*59*). This may be the reason that TLRs recognize structures present on all microbes, whether they are known to cause a disease under a particular condition or not.

Future studies will probably reveal additional mechanisms of immune recognition that may be superimposed on PRR-mediated recognition to ensure differential responses to commensals, pathogens, and endogenous TLR ligands. And perhaps the most interesting aspects of innate immune recognition are yet to be discovered. Though the field may be seen as approaching the beginning of the end, it is in fact just at the end of the beginning.

References and Notes

1. C. A. Janeway Jr., *Cold Spring Harb. Symp. Quant. Biol.* **54**, 1 (1989).
2. K. Takeda, S. Akira, *Int. Immunol.* **17**, 1 (2005).
3. A. Iwasaki, R. Medzhitov, *Nat. Immunol.* **5**, 987 (2004).
4. M. J. Robinson *et al.*, *J. Exp. Med.* **206**, 2037 (2009).
5. G. D. Brown, *Nat. Rev. Immunol.* **6**, 33 (2006).
6. A. Pichlmair, C. Reis e Sousa, *Immunity* **27**, 370 (2007).
7. T. Saito *et al.*, *Proc. Natl. Acad. Sci. U.S.A.* **104**, 582 (2007).
8. M. Yoneyama, T. Fujita, *Immunity* **29**, 178 (2008).
9. O. Takeuchi, S. Akira, *Immunol. Rev.* **227**, 75 (2009).
10. Y. H. Chiu, J. B. Macmillan, Z. J. Chen, *Cell* **138**, 576 (2009).
11. A. Ablasser *et al.*, *Nat. Immunol.* **10**, 1065 (2009).
12. F. Martinon, A. Mayor, J. Tschopp, *Annu. Rev. Immunol.* **27**, 229 (2009).
13. T. D. Kanneganti, M. Lamkanfi, G. Núñez, *Immunity* **27**, 549 (2007).
14. N. W. Palm, R. Medzhitov, *Immunol. Rev.* **227**, 221 (2009).
15. H. Kumar, S. Koyama, K. J. Ishii, T. Kawai, S. Akira, *J. Immunol.* **180**, 683 (2008).
16. M. P. Longhi *et al.*, *J. Exp. Med.* **206**, 1589 (2009).
17. S. M. Ngoi, M. G. Tovey, A. T. Vella, *J. Immunol.* **181**, 7670 (2008).
18. J. H. Fritz *et al.*, *Immunity* **26**, 445 (2007).
19. K. S. Kobayashi *et al.*, *Science* **307**, 731 (2005).
20. K. J. Ishii *et al.*, *Nature* **451**, 725 (2008).
21. S. Koyama *et al.*, *J. Immunol.* **179**, 4711 (2007).
22. T. Ichinohe, H. K. Lee, Y. Ogura, R. Flavell, A. Iwasaki, *J. Exp. Med.* **206**, 79 (2009).
23. V. G. Bhoj *et al.*, *Proc. Natl. Acad. Sci. U.S.A.* **105**, 14046 (2008).
24. A. Sabbah *et al.*, *Nat. Immunol.* **10**, 1073 (2009).
25. S. S. Way, T. R. Kollmann, A. M. Hajjar, C. B. Wilson, *J. Immunol.* **171**, 533 (2003).
26. M. O'Riordan, C. H. Yi, R. Gonzales, K. D. Lee, D. A. Portnoy, *Proc. Natl. Acad. Sci. U.S.A.* **99**, 13861 (2002).
27. N. Reiling, S. Ehlers, C. Hölscher, *Immunol. Lett.* **116**, 15 (2008).
28. A. S. Beignon *et al.*, *J. Clin. Invest.* **115**, 3265 (2005).
29. E. P. Browne, D. R. Littman, J. Luban, *PLoS Pathog.* **5**, e1000298 (2009).
30. D. B. Stetson, *Curr. Opin. Immunol.* **21**, 244 (2009).
31. J. M. Blander, R. Medzhitov, *Nature* **440**, 808 (2006).
32. F. Yarovinsky, H. Kanzler, S. Hieny, R. L. Coffman, A. Sher, *Immunity* **25**, 655 (2006).
33. P. W. Dempsey, M. E. D. Allison, S. Akkaraju, C. C. Goodnow, D. T. Fearon, *Science* **271**, 348 (1996).
34. D. Schmid, C. Münz, *Immunity* **27**, 11 (2007).
35. D. B. Stetson, J. S. Ko, T. Heidmann, R. Medzhitov, *Cell* **134**, 587 (2008).
36. R. Spörri, C. Reis e Sousa, *Nat. Immunol.* **6**, 163 (2005).
37. J. Banchereau, R. M. Steinman, *Nature* **392**, 245 (1998).
38. M. A. de Jong, T. B. Geijtenbeek, *J. Intern. Med.* **265**, 18 (2009).
39. G. H. MacDonald, R. E. Johnston, *J. Virol.* **74**, 914 (2000).
40. F. R. Carbone, G. T. Belz, W. R. Heath, *Trends Immunol.* **25**, 655 (2004).
41. O. Schulz *et al.*, *Nature* **433**, 887 (2005).
42. M. B. Torchinsky, J. Garaude, A. P. Martin, J. M. Blander, *Nature* **458**, 78 (2009).
43. A. Sato, A. Iwasaki, *Proc. Natl. Acad. Sci. U.S.A.* **101**, 16274 (2004).
44. L. A. Minns *et al.*, *J. Immunol.* **176**, 7589 (2006).
45. C. Zaph *et al.*, *Nature* **446**, 552 (2007).
46. R. N. Germain, M. K. Jenkins, *Curr. Opin. Immunol.* **16**, 120 (2004).
47. C. M. Smith *et al.*, *Nat. Immunol.* **5**, 1143 (2004).
48. A. Marshak-Rothstein, I. R. Rifkin, *Annu. Rev. Immunol.* **25**, 419 (2007).
49. D. Jiang *et al.*, *Nat. Med.* **11**, 1173 (2005).
50. L. Schaefer *et al.*, *J. Clin. Invest.* **115**, 2223 (2005).
51. S. Kim *et al.*, *Nature* **457**, 102 (2009).
52. G. B. Johnson, G. J. Brunn, Y. Kodaira, J. L. Platt, *J. Immunol.* **168**, 5233 (2002).
53. J. R. van Beijnum, W. A. Buurman, A. W. Griffioen, *Angiogenesis* **11**, 91 (2008).
54. A. Tsung *et al.*, *J. Exp. Med.* **201**, 1135 (2005).
55. M. Li *et al.*, *J. Immunol.* **166**, 7128 (2001).
56. K. R. Taylor *et al.*, *J. Biol. Chem.* **282**, 18265 (2007).
57. G. M. Barton, J. C. Kagan, *Nat. Rev. Immunol.* **9**, 535 (2009).
58. S. L. Masters, A. Simon, I. Aksentijevich, D. L. Kastner, *Annu. Rev. Immunol.* **27**, 621 (2009).
59. A. J. Macpherson, K. D. McCoy, F. E. Johansen, P. Brandtzaeg, *Mucosal Immunol.* **1**, 11 (2008).

60. The work in the authors' laboratories is supported by grants from the NIH [R01AI055502, R37AI046688, and R01DK071754 (R.M.) and R01AI064705, R21AI083242, and R01AI054359 (A.I.)], the Howard Hughes Medical Institute (R.M.), and the Investigators in Pathogenesis of Infectious Disease Award from the Burroughs Wellcome Fund (A.I.).

10.1126/science.1183021

REVIEW

The NLRP3 Inflammasome: A Sensor for Metabolic Danger?

Kate Schroder,[1,2] Rongbin Zhou,[1] Jurg Tschopp[1]*

Interleukin-1β (IL-1β), reactive oxygen species (ROS), and thioredoxin-interacting protein (TXNIP) are all implicated in the pathogenesis of type 2 diabetes mellitus (T2DM). Here we review mechanisms directing IL-1β production and its pathogenic role in islet dysfunction during chronic hyperglycemia. In doing so, we integrate previously disparate disease-driving mechanisms for IL-1β, ROS, and TXNIP in T2DM into one unifying model in which the NLRP3 inflammasome plays a central role. The NLRP3 inflammasome also drives IL-1β maturation and secretion in another disease of metabolic dysregulation, gout. Thus, we propose that the NLRP3 inflammasome contributes to the pathogenesis of T2DM and gout by functioning as a sensor for metabolic stress.

Type 2 diabetes mellitus (T2DM) manifests when pancreatic β cells fail to compensate for chronic elevated blood glucose (hyperglycemia) that occurs when glucose uptake in the periphery becomes dysregulated during insulin resistance. Insulin is secreted by pancreatic β cells upon hyperglycemia and regulates glucose utilization within the body. In healthy individuals, postfeeding hyperglycemia is transient, as insulin stimulates glucose uptake and restores normoglycemia. Insulin resistance, a state that precedes T2DM, prolongs hyperglycemia by inhibiting the action of insulin. It is becoming increasingly apparent that chronic, low-grade systemic inflammation accompanies obesity, insulin resistance, and T2DM and contributes to the progression from obesity to T2DM (*1*). Elevated proinflammatory cytokines can contribute to insulin resistance by antagonizing insulin signaling, thereby inhibiting insulin-dependent glucose uptake and contributing to failing glucose tolerance (*2*). Local inflammation in the insulin-secreting pancreatic islets is also implicated; immune cell infiltration and local cytokine production accompany the early stages of disease as β cells begin to fail to maintain normal blood glucose levels (*3*). These local inflammatory processes, coupled with the toxic effects of glucose, lead to the accelerated loss of β cell mass through cell death and severely impair the insulin-secreting capabilities of the remaining β cells in both T2DM patients and animal models (*4*–*6*). Expression of the potent proinflammatory cytokine, interleukin-1β (IL-1β), is elevated in the circulation and in pancreatic islets during the progression from obesity to T2DM, and IL-1β is implicated as an important driver of disease [reviewed in (*2*)]. Similarities to IL-1β–mediated pathology in islet destruction during type 1 autoimmune diabetes have led to the proposal that IL-1β presents a common final pathway for autoimmune diabetes and T2DM (*7*).

[1]Department of Biochemistry, University of Lausanne, CH-1066 Epalinges, Switzerland. [2]Monash Institute of Medical Research, Monash University, Melbourne, Victoria 3800, Australia.

*To whom correspondence should be addressed. E-mail: jurg.tschopp@unil.ch

Does IL-1β Contribute to Pancreatic Islet Dysfunction in T2DM?

Mechanisms of pancreatic islet failure in T2DM are beginning to be clarified, and, although somewhat controversial, an emerging literature suggests a pathogenic role for IL-1β. Pancreatic islets of T2DM patients contain a smaller β cell mass compared with nondiabetic controls, as a result of increased β cell death (*5*, *6*). This appears to be a direct consequence of prolonged hyperglycemia; although acute exposure of human pancreatic islets to glucose induced β cell proliferation and triggered insulin secretion (*4*), chronic exposure to elevated glucose inhibited β cell insulin secretion and induced cell death in an IL-1β–dependent manner (*8*, *9*). The potent proinflammatory properties of IL-1β are tightly regulated by expression, processing, secretion, and antagonism by a natural inhibitor (*10*). Initially, IL-1β expression was thought to be specific to cells of the immune system, and to macrophages in particular, but it is now clear that cells outside the immune system can express IL-1β (e.g., keratinocytes) (*11*). Pancreatic islets of T2DM patients and rodent models of T2DM exhibit immune cell infiltration, including macrophages (*3*), and these cells are likely to contribute to intra-islet IL-1β production; however, β cells can also secrete IL-1β in response to prolonged elevated glucose exposure (*8*, *12*). Furthermore, unlike normal controls, human and mouse pancreatic islets and purified human β cells under metabolic stress in T2DM express IL-1β (*8*, *12*). Although β cells secrete less IL-1β than macrophages (*13*), it is sufficient for a clear autocrine effect on β cell viability and insulin-secretion capacity that can be blocked by antagonism or ablation of IL-1β (*8*, *14*, *15*). The extreme sensitivity of β cells to IL-1β is likely to be conferred by high expression of the IL-1 type I receptor (IL1R1) chain in these cells (*16*). IL-1β induced within the islet impairs β cell insulin secretion (*17*, *18*) and induces Fas death receptor–dependent, apoptotic β cell death in a manner resembling glucose-dependent cell death (*8*), which suggests that the proapoptotic effects of glucose are at least partly mediated by IL-1β. Indeed, IL-1β deficiency (*14*) or IL-1R blockade by the IL-1 receptor antagonist (IL1RA) (*8*) improved β cell function and blocked the cytotoxic effects of chronic elevated glucose exposure to cultured mouse or human islets, respectively. Likewise, in vivo administration of IL1RA to mice fed a high-fat diet improved glucose tolerance and insulin secretion, as well as pancreatic islet survival and function (*15*). Collectively, these reports suggest that glucose-induced IL-1β is a key mediator of islet dysfunction and destruction.

Elevated circulating IL-1β is a risk factor for the development of T2DM in humans (*1*), and mouse models and human clinical trials suggest that IL-1β antagonism may be a promising treatment for T2DM. Despite inhibiting basal β cell proliferation, insulin secretory function, and glucose tolerance compared with control mice, IL-1β deficiency protected mouse islets from the toxic effects of prolonged hyperglycemia (*14*). This suggests that low IL-1β expression has a positive physiological function in healthy animals, consistent with the beneficial effects of low-dose IL-1β on β cell proliferation and insulin secretory function (*14*, *19*), whereas high concentrations of IL-1β negatively affect β cell function and mediate glucotoxicity. Indeed, IL1RA suppressed the toxic effects of both IL-1β and glucose in human and rat pancreatic islets (*8*, *20*), and injection of IL1RA (*15*) or a neutralizing antibody against IL-1β (*21*) protected against the diabetic effects of a high-fat diet in mice. IL-1β antagonism in this context inhibited β cell death, promoted β cell mass, potentiated β cell glucose-induced insulin secretion, and improved insulin sensitivity (*15*, *21*). Consistent with these results, a recent human clinical trial using IL1RA to treat T2DM ameliorated systemic inflammation and significantly improved glycemic control and β cell function (*22*, *23*).

How Is IL-1β Secretion Regulated?

Until recently, the mechanisms underlying glucose-regulated IL-1β secretion were unclear. The production of active IL-1β is tightly regulated, requiring at least two independent signals for induction and maturation. IL-1β is induced by proinflammatory signaling through Toll-like receptors (TLRs) or by cytokines, such as tumor necrosis factor or IL-1β itself; however, this proform of IL-1β is inactive and requires processing by the cysteine protease, caspase-1, for maturation and secretion (*24*). IL-1β maturation is controlled by multiprotein, caspase-1–activating

platforms called inflammasomes. The NLRP3 (also known as NALP3) inflammasome is the most fully characterized of the inflammasomes and contains the adaptor protein apoptosis-associated specklike protein (ASC); the proinflammatory caspase, caspase-1; and NLRP3. NLRP3 belongs to the nucleotide-binding oligomerization domain (NOD)–like receptor (NLR) family (also referred to as the nucleotide-binding domain and leucine-rich repeat–containing receptors by the Human Genome Organization and in the accompanying reviews) of pattern recognition receptors that include the NODs [NOD1 and 2, NLRC3 or NOD3, NLRC5 or NOD4, NLRX1 or NOD5, and the major histocompatibility complex II transactivator (CIITA)], the NLRPs (NLRP1 to 14), NAIP, and NLRC4 (or IPAF) (*25*). Of these, NLRP1, NLRC4, and NLRP3 can form caspase-1–activating inflammasomes. The HIN-200 family member, AIM2, can also drive assembly of a caspase-1–activating inflammasome (*26*). A variety of pathogen- and host-derived "danger" signals activate the NLRP3 inflammasome, including whole pathogens; pathogen-associated molecular patterns (PAMPs); other pathogen-associated molecules (e.g., bacterial pore–forming toxins and malarial hemozoin); host-derived indicators of cellular damage ("danger-associated molecular patterns" or DAMPs); and environmental irritants (Table 1). The potent immunomodulatory functions of the NLRP3 inflammasome are highlighted by several related autoinflammatory diseases, collectively called cryopyrin-associated periodic syndrome (CAPS), in which activating NLRP3 mutations result in dysregulated IL-1β production and inflammation [reviewed in (*25*)].

Upon activation, NLRP3 is thought to oligomerize via homotypic interactions between NACHT domains and thereby presents clustered pyrin (PYD) domains for interaction with the PYD domain of ASC (Fig. 1). ASC assembly, in turn, presents clustered caspase activation and recruitment domains (CARDs) for interaction with the CARD of procaspase-1. Procaspase-1 clustering enables autocleavage and activation, and activated caspase-1 can cleave other cytosolic targets, including the proinflammatory cytokines IL-1β and IL-18. An unconventional pathway that awaits clarification directs secretion of the cleaved, mature cytokines.

Pathways leading to inflammasome activation are a matter of debate, and several models have been suggested that may not be mutually exclusive (Fig. 1). Extracellular adenosine triphosphate (ATP) is an NLRP3-activating DAMP that is released at sites of cellular injury or necrosis. ATP stimulates rapid K^+ efflux from the purinergic P2X7 receptor, an ATP-gated ion channel (*27*), and triggers gradual recruitment and pore formation by the pannexin-1 hemichannel (*28*). It has been proposed that NLRP3 senses either low intracellular K^+ or a breakdown in membrane integrity or that hemichannel pore formation allows extracellular NLRP3 agonists to access the cytosol, to activate NLRP3 directly (*28*). Given that a direct interaction between NLRP3 and its activators has not been demonstrated and the structural diversity among agonists, it seems unlikely that NLRP3 directly senses its activating stimuli. Membrane disruption may also drive NLRP3 activation in response to particulate or crystalline activators. Under this model, inefficient clearance of phagocytosed material leads to phagosomal destabilization and release of the proteinase cathepsin B into the cytosol, which contributes to inflammasome activation through an undetermined mechanism (*29*). The proposed role for cathepsin B, however, may be based on off-target effects of the cathepsin B inhibitor (*30*). Moreover, cathepsin B–deficient macrophages respond normally to particulate NLRP3 agonists (*31*).

A crucial function of ROS in NLRP3 activation has also been proposed (*31*–*33*) and is strongly supported by recent mechanistic data (*13*). ROS is normally produced within resting cells (e.g., by cellular metabolism); however, ROS induced by cellular infection or stress can cause oxidative stress. Where examined, all known NLRP3 activators, including ATP and activators that require phagocytosis, induce ROS. Moreover, ROS inhibition by treatment with ROS scavengers blocks inflammasome activation by a range of NLRP3 agonists [reviewed in (*24*)], which suggests that ROS generation is a necessary upstream event for inflammasome activation. For these reasons, we favor a model in which, instead of sensing PAMPs or DAMPs per se, the NLRP3 inflammasome is activated by ROS generated as a cellular response to these ligands and is thereby a more general sensor of cellular stress. Future work is required to clarify the role of ROS in NLRP3 activation. For example, a recent report suggested that caspase-1 activity can be inhibited by oxidation and

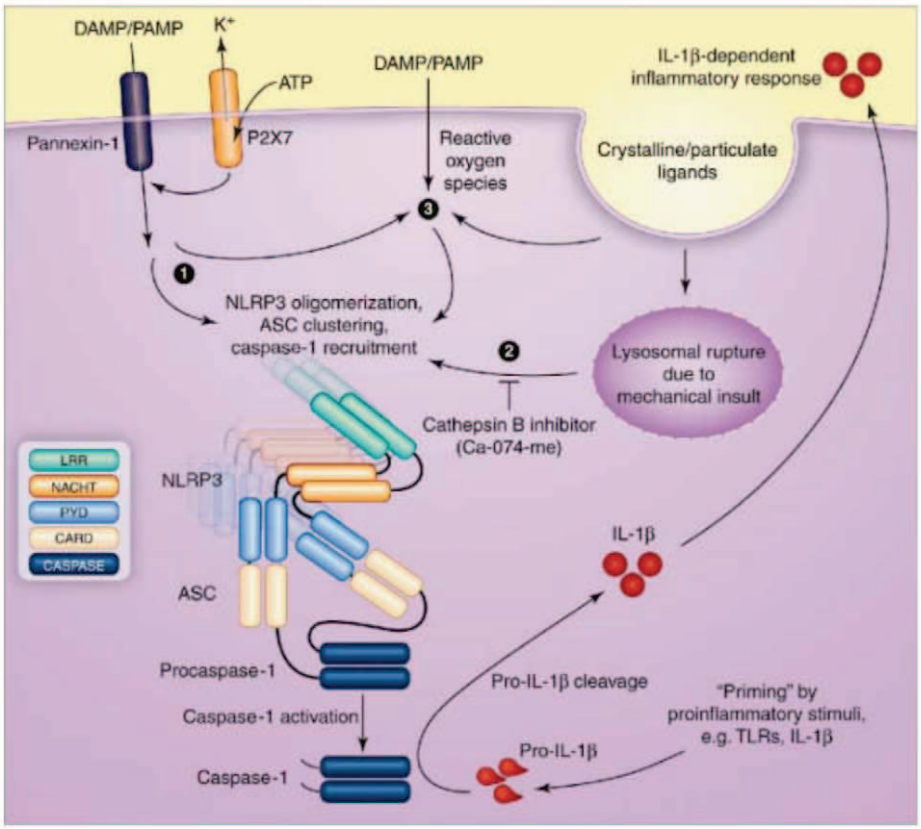

Fig. 1. Current models for activation of the NLRP3 inflammasome. NLRP3 oligomerization and recruitment of ASC and procaspase-1 trigger autoactivation of caspase-1 and the maturation and secretion of proinflammatory cytokines, such as IL-1β. Mechanisms leading to NLRP3 inflammasome activation are a matter of debate. Three models are widely favored in the literature and may not be mutually exclusive: (1) The NLRP3 inflammasome is activated by extracellular ATP by one of the following mechanisms: The purinergic P2X7 receptor–activated pannexin-1 pore allows cytoplasmic entry of extracellular factors that are direct NLRP3 ligands, or NLRP3 senses either K^+ efflux or a loss of membrane integrity. (2) Crystalline or particulate structures are phagocytosed, which leads to lysosomal rupture and cytoplasmic release of lysosomal content. This pathway is sensitive to the cathepsin B inhibitor, Ca-074-me, which suggests that cathepsin B potentiates this process. (3) All NLRP3 agonists trigger the production of ROS, which leads to the activation of the NLRP3 inflammasome via the ROS-sensitive TXNIP protein (see Fig. 3). LRR, leucine-rich repeat.

Table 1. NLRP3 inflammasome activators. Details of individual NLRP3 inflammasome activators are reviewed in (*24*, *25*).

Activator class	Activator	Disease associations
Whole pathogen	*Candida albicans*	Infection
	Saccharomyces cerevisiae[*]	Infection
	Staphylococcus aureus	Infection
	Listeria monocytogenes	Infection
	Influenza virus	Infection
	Sendai virus	Infection
	Adenovirus	Infection
Pathogen-associated molecules	Bacterial pore–forming toxins	Infection
	Hemozoin	Cerebral malaria
Environmental insults	Silica	Silicosis
	Asbestos	Asbestosis
	Skin irritants	Contact hypersensitivity reactions
	Ultraviolet light	Sunburn
Endogenous danger signals	ATP	Injury or necrotic cell death
	Glucose	Metabolic syndrome
	MSU	Gout
	Calcium pyrophosphate dihydrate (CPPD)	Pseudogout
	Amyloid β	Alzheimer's disease
	Hyaluronan	Injury
Adjuvant	Alum	

[*]Viable (*52*) but not heat-killed (*53*) *S. cerevisiae* activates the NLRP3 inflammasome.

glutathionation (*34*); whether this represents a negative feedback pathway to limit ROS-regulated caspase-1 function is presently unclear. Furthermore, although ROS appears to be necessary, it is not sufficient for NLRP3 activation, as some ROS-inducing agents (e.g., cytokines and nonimidazoquinoline TLR agonists) are not sufficient to trigger NLRP3 inflammasome activation. This implies either a specific requirement for the type or location of ROS or that ROS cooperates with a second, unidentified pathway for NLRP3-dependent caspase-1 activation. NLRP3 inflammasome activation can be suppressed by culturing cells in medium containing a high concentration of K^+ [reviewed in (*24*)], which implies a requirement for K^+ efflux for NLRP3 activation. The interplay between K^+ efflux and ROS generation is unclear, but it is possible that intracellular K^+ concentrations modulate ROS production or that low intracellular K^+ is required independently of ROS for NLRP3 activation.

Recent identification of a ROS-dependent NLRP3 ligand revealed several molecular events that may direct inflammasome activation (Fig. 2). NLRP3 agonists trigger the association of NLRP3 with thioredoxin-interacting protein (TXNIP), also known as vitamin D_3 up-regulated protein 1 (VDUP1), in human macrophages, and this association is suppressed by inhibiting ROS (*13*). In unstimulated cells, TXNIP is bound to the oxidoreductase thioredoxin; however, this complex dissociates when intracellular ROS increases. Free thioredoxin is then able to perform its function as a ROS scavenger. Dissociation of TXNIP from thioredoxin allows interaction with NLRP3 in a ROS-dependent manner (*13*). Furthermore, TXNIP knockdown or deletion suppresses caspase-1 activation and IL-1β secretion in response to NLRP3 agonists in human or mouse macrophages (*13*), and knockdown of the TXNIP inhibitor, thioredoxin, augments inflammasome activation in human macrophages (*31*). Taken together, these data suggest that TXNIP is an upstream activating ligand for NLRP3. Although unlikely, an indirect effect of TXNIP on NLRP3 activation via redox modulation, however, cannot be excluded at present. TXNIP-dependent inflammasome activation appears to be specific for NLRP3, as TXNIP deficiency did not affect the activity of other inflammasomes (e.g., NLRC4 and AIM2) (*13*).

How Do TXNIP and NLRP3 Collaborate to Sense Metabolic Stress?

A large body of literature implicates a pathogenic role for TXNIP in T2DM, which, until recently, was not known to be linked to IL-1β. TXNIP deficiency improves glucose tolerance and insulin sensitivity in mice fed a high-fat diet (*35*, *36*). These attributes may be due to TXNIP-induced activation of NLRP3, because NLRP3 ablation also improves these metrics (*13*). TXNIP expression is induced by glucose (*13*, *37*), repressed by insulin (*38*), and elevated in T2DM (*38*, *39*). Glucose is a potent inducer of TXNIP in pancreatic islets but not in macrophages (*13*), which suggests that tissue macrophages do not contribute to glucose-dependent TXNIP induction within the islet. Pancreatic islets express all NLRP3 inflammasome components (NLRP3, ASC, and caspase-1) (*13*), albeit at lower levels than macrophages, which may reflect their reduced capacity to secrete IL-1β. Glucose-dependent IL-1β secretion is ablated in both TXNIP- and NLRP3-deficient mouse pancreatic islets and is also antagonized by ROS inhibitors (*13*). Taken together, these findings suggest that the NLRP3 inflammasome, in collaboration with ROS-liberated TXNIP, drives IL-1β secretion from pancreatic islets in response to chronic elevated glucose. Furthermore, they suggest that the TXNIP-dependent NLRP3 inflammasome, activated under conditions of metabolic stress, mediates IL-1β–driven islet failure during the progression of T2DM.

The concept that the NLRP3 inflammasome is activated by pathways that culminate in metabolic stress is further supported by the crucial role of NLRP3-dependent IL-1β production in a very different disease of metabolic dysregulation, gout. Gout is linked to dysregulated purine metabolism, which leads to elevated blood uric acid levels and monosodium urate (MSU) crystal deposition in joints, resulting in severe joint inflammation. It is interesting that metabolic syndrome, which often precedes development of T2DM, is a predisposing factor for gout. In this context, gout is likely to manifest as a consequence of increased purine intake. In gout, MSU activates the NLRP3 inflammasome and drives IL-1β production, leading to local pain and inflammation (*40*). Similar to inflammasome activation by glucose, MSU-dependent IL-1β maturation depends on collaboration between TXNIP and NLRP3 (*13*). Like metabolic syndrome, this condition can be ameliorated by changes in diet. In the case of gout, this involves decreasing the intake of gout-inducing purine-rich foods (e.g., beer and seafood). Acute gout attacks can also be successfully treated with IL1R antagonists (*41*, *42*).

Does the NLRP3 Inflammasome Contribute to T2DM Progression?

In the majority of cases, T2DM is a complex disorder in which there is substantial interaction between environmental factors, such as food intake and exercise, and genetic predisposition. A number of genetic variants were shown to associate with β cell decline in T2DM in recent genome-wide association studies (*43*). Although components of the inflammasome pathway were not implicated, a number of potassium channel variants, presumed to mediate their diabetic effects through modulation of insulin secretion, may also modulate activation of the K^+-sensitive NLRP3 inflammasome. There is a clear link,

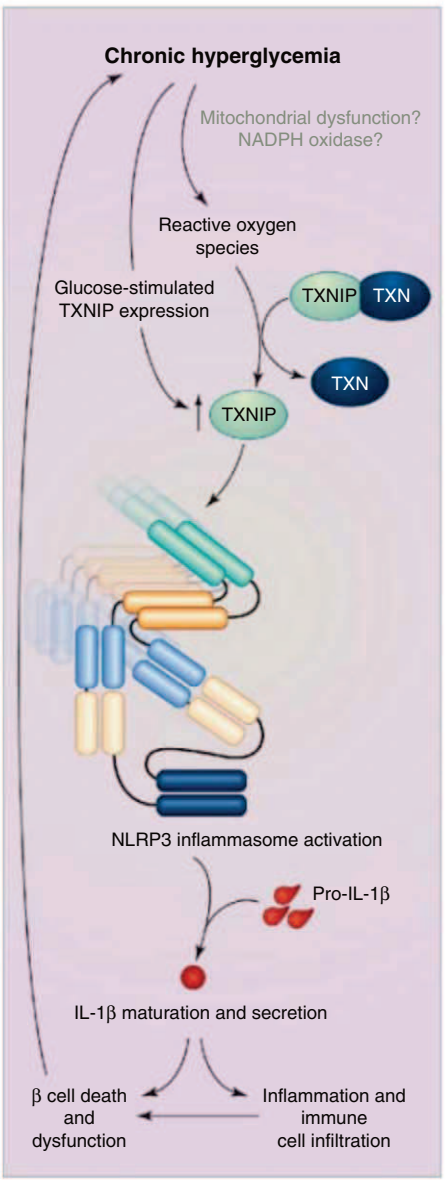

Fig. 2. Proposed model of NLRP3 inflammasome activation leading to pancreatic islet dysfunction in T2DM. Chronic hyperglycemia leads to ROS production, probably through overstimulation of the mitochondrial electron transport chain as a consequence of increased glycolysis. Glucose induces TXNIP expression, and ROS triggers the dissociation of TXNIP from thioredoxin (TXN), which results in increased TXNIP availability for activation of the NLRP3 inflammasome and caspase-1–dependent IL-1β maturation. The autocrine and/or paracrine action of secreted IL-1β mediates glucose-induced β cell death and dysfunction. β cell failure is further augmented by the local proinflammatory milieu created by infiltrating immune cells. β cell failure impairs glucose-stimulated insulin secretion and so contributes to decreased glucose uptake in the periphery and the maintenance of chronic hyperglycemia.

however, between prolonged hyperglycemia, whether driven by genetic or environmental factors, or both, and pancreatic islet failure. It is in this context that the data reviewed here suggest a pathogenic role for the NLRP3 inflammasome.

The evidence presented above suggests the following model for NLRP3 inflammasome activation in pancreatic islet failure during T2DM progression (Fig. 2). Chronic islet exposure to elevated glucose triggers ROS generation, through mechanisms that are currently unclear. Glucose was reported to induce ROS generation via the nicotinamide adenine dinucleotide phosphate (NADPH) oxidase system in rat pancreatic islets and a β cell line (*44*); however, it is more likely that increased glycolysis drives ROS production by increasing the activity of the mitochondrial electron transport chain (*45*). Indeed, mitochondrial dysfunction and oxidative stress in pancreatic islets are strongly implicated in T2DM progression (*45*). Elevated glucose also induces high expression of TXNIP, which together with its ROS-dependent dissociation from thioredoxin, switches TXNIP function from thioredoxin repressor to NLRP3 inflammasome activator. Once activated, caspase-1 cleaves pro-IL-1β to its mature form, and IL-1β is secreted and can signal in an autocrine and/or paracrine manner to promote β cell death and to impair β cell function.

Additional mechanisms may contribute to islet dysfunction and destruction. IL-1β signaling is likely to trigger secretion of other chemotactic factors to direct further immune cell infiltration. The combined effects of the proinflammatory milieu and activated immune cells would augment β cell death and would suppress β cell secretory functions. TXNIP was reported to contribute to β cell destruction (*39*); however, whether this is dependent on IL-1β is unclear. Inhibition of glucose uptake in the periphery by TXNIP (*38*) may also contribute to pancreatic islet failure by reducing blood glucose utilization and thereby sustaining hyperglycemia.

A number of questions remain unresolved, including the mechanism of pro-IL-1β induction in pancreatic islets. Potential mechanisms include induction by an autoamplification loop or by elevated circulating free fatty acids, which can signal through TLR4 (*46*, *47*). Alternatively, islet oxidative stress that is associated with T2DM (*45*) may activate the IL-1β promoter via the nuclear factor κB transcription factor (*48*). Any of these pathways would also promote secretion of other proinflammatory cytokines and chemokines, which would drive islet infiltration by immune cells and thereby amplify the local proinflammatory milieu. The specific contribution of intra-islet macrophages to IL-1β–mediated β cell dysfunction is currently uncertain.

Relative insulin resistance in the periphery, coupled with insufficient pancreatic insulin

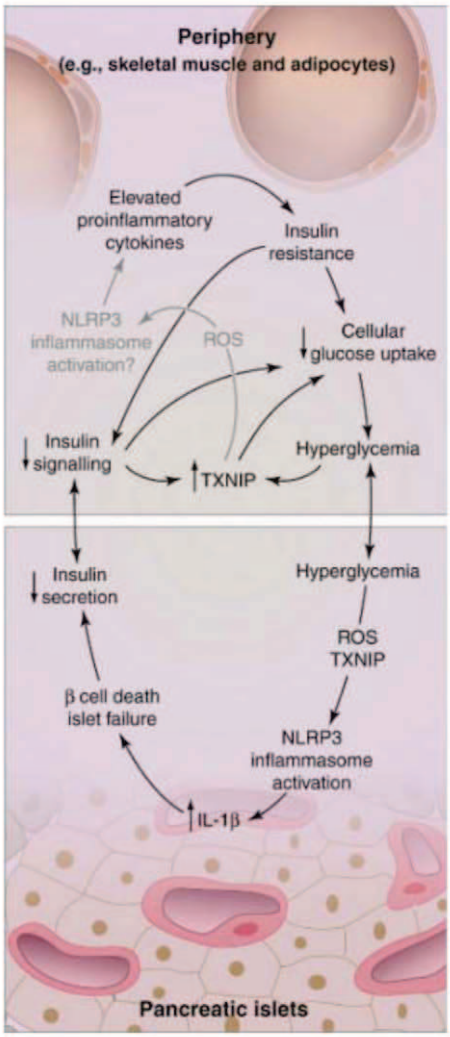

Fig. 3. Model for the role of ROS, TXNIP, and IL-1β in pancreatic β cell failure in T2DM. During the early stages of disease, pancreatic β cells can compensate for relative insulin resistance in the periphery by increasing the production of insulin and thereby ameliorate hyperglycemia. Increasing insulin resistance, however, overwhelms β cell compensatory mechanisms, leading to decreased insulin signaling and insulin-dependent glucose uptake, and contributing to sustained hyperglycemia. Prolonged hyperglycemia in pancreatic islets leads to the induction of ROS, which triggers TXNIP-dependent activation of the NLRP3 inflammasome, culminating in the secretion of mature IL-1β. Elevated IL-1β causes β cell death and dysfunction, leading to decreased glucose-stimulated insulin secretion and exacerbating chronic hyperglycemia. In the periphery, the combination of decreased insulin signaling and elevated glucose induces expression of TXNIP. High TXNIP expression, coupled with decreased insulin signaling, antagonizes glucose uptake and inhibits the return to normoglycemia. Glucose-induced NLRP3 inflammasome activation outside of the pancreatic islets may also contribute to elevated IL-1β, insulin resistance, and T2DM progression.

secretion during hyperglycemia, establishes a vicious cycle that drives the progression from insulin resistance to T2DM (Fig. 3). TXNIP is implicated as a disease-driver in both pancreatic islets and the periphery: TXNIP mediates glucose-induced cell death in islets and antagonizes glucose uptake in the periphery (*38*, *39*). The available data suggest a model in which hyperglycemia induces, whereas insulin signaling suppresses, TXNIP expression. Thus, the high-glucose and low-insulin signaling state in T2DM results in elevated TXNIP expression in both pancreatic islets and the periphery. High TXNIP expression within the islet sensitizes the cells to TXNIP-dependent cell death and NLRP3 inflammasome activation, whereas high TXNIP expression in the periphery further antagonizes glucose uptake and contributes to hyperglycemia. A major open question is whether extra-pancreatic tissues under metabolic stress (e.g., chronic hyperglycemia) drive NLRP3 inflammasome activation and IL-1β production in a manner similar to that of pancreatic islets, to contribute to IL-1β–dependent insulin resistance within tissues. The potential cooperation of TXNIP and NLRP3 in glucose-dependent inflammasome activation outside of the pancreatic islet awaits clarification and future research.

Concluding Remarks

T2DM manifests when blood glucose levels become so unbalanced, because of high nutrient consumption and poor peripheral glucose uptake, that the compensatory functions of pancreatic β cells become overwhelmed. Studies of IL-1β–deficient mice demonstrate that IL-1β has important homeostatic functions in glucose tolerance that may be linked to the ability of acute, low-dose IL-1β to stimulate pancreatic β cell proliferation and insulin secretory function. Furthermore, IL-1β suppresses appetite (*49*). Thus, glucose-dependent IL-1β secretion may be an important physiological compensatory mechanism for the maintenance of normoglycemia. Chronic elevation of IL-1β in T2DM, however, suggests a pathological role for IL-1β in disease progression. In gout, NLRP3-dependent IL-1β production in response to metabolic stress in the form of MSU is a well-established driver of disease. The evidence presented in this review suggests that NLRP3-dependent IL-1β production during metabolic stress, in this case chronic hyperglycemia, may also contribute to the progression of T2DM. This new hypothesis should be the focus of future investigations into the disease-driving mechanisms of T2DM. In support of a pathological role for the NLRP3 inflammasome in T2DM, the antidiabetic drug, glibenclamide, which is used to stimulate β cell insulin secretion, also suppresses glucose-induced inflammasome activation and downstream IL-1β release (*13*, *50*, *51*). Furthermore, antagonists of IL-1β or its receptor are proving highly effective for the treatment of T2DM in both mouse models and human clinical trials. The recent finding that the NLRP3 inflammasome forms a nexus linking TXNIP, oxidative stress, and IL-1β production during metabolic stress provides new avenues for research and therapy for T2DM, a disease often described as the next global pandemic.

References and Notes

1. J. Spranger *et al.*, *Diabetes* **52**, 812 (2003).
2. K. Maedler, G. Dharmadhikari, D. M. Schumann, J. Størling, *Expert Opin. Biol. Ther.* **9**, 1177 (2009).
3. J. A. Ehses *et al.*, *Diabetes* **56**, 2356 (2007).
4. M. Y. Donath, D. J. Gross, E. Cerasi, N. Kaiser, *Diabetes* **48**, 738 (1999).
5. A. E. Butler *et al.*, *Diabetes* **52**, 102 (2003).
6. H. Sakuraba *et al.*, *Diabetologia* **45**, 85 (2002).
7. M. Y. Donath, J. Størling, K. Maedler, T. Mandrup-Poulsen, *J. Mol. Med.* **81**, 455 (2003).
8. K. Maedler *et al.*, *J. Clin. Invest.* **110**, 851 (2002).
9. K. Maedler *et al.*, *Diabetes* **50**, 1683 (2001).
10. F. Martinon, A. Mayor, J. Tschopp, *Annu. Rev. Immunol.* **27**, 229 (2009).
11. L. Feldmeyer *et al.*, *Curr. Biol.* **17**, 1140 (2007).
12. M. Böni-Schnetzler *et al.*, *J. Clin. Endocrinol. Metab.* **93**, 4065 (2008).
13. R. Zhou, A. Tardivel, B. Thorens, I. Choi, J. Tschopp, *Nat. Immunol.*, published online 20 December 2009 (10.1038/ni.1831).
14. K. Maedler *et al.*, *Diabetes* **55**, 2713 (2006).
15. N. S. Sauter, F. T. Schulthess, R. Galasso, L. W. Castellani, K. Maedler, *Endocrinology* **149**, 2208 (2008).
16. M. Böni-Schnetzler *et al.*, *Endocrinology* **150**, 5218 (2009).
17. T. Mandrup-Poulsen *et al.*, *Diabetologia* **29**, 63 (1986).
18. D. L. Eizirik, D. E. Tracey, K. Bendtzen, S. Sandler, *Diabetologia* **34**, 445 (1991).
19. G. A. Spinas *et al.*, *Acta Endocrinol. (Copenhagen)* **113**, 551 (1986).
20. N. Téllez *et al.*, *Gene Ther.* **12**, 120 (2005).
21. O. Osborn *et al.*, *Cytokine* **44**, 141 (2008).
22. C. M. Larsen *et al.*, *Diabetes Care* **32**, 1663 (2009).
23. C. M. Larsen *et al.*, *N. Engl. J. Med.* **356**, 1517 (2007).
24. J. H. Pedra, S. L. Cassel, F. S. Sutterwala, *Curr. Opin. Immunol.* **21**, 10 (2009).
25. C. Bryant, K. A. Fitzgerald, *Trends Cell Biol.* **19**, 455 (2009).
26. K. Schroder, D. A. Muruve, J. Tschopp, *Curr. Biol.* **19**, R262 (2009).
27. J. M. Kahlenberg, G. R. Dubyak, *Am. J. Physiol. Cell Physiol.* **286**, C1100 (2004).
28. T. D. Kanneganti *et al.*, *Immunity* **26**, 433 (2007).
29. V. Hornung *et al.*, *Nat. Immunol.* **9**, 847 (2008).
30. Z. L. Newman, S. H. Leppla, M. Moayeri, *Infect. Immun.* **77**, 4327 (2009).
31. C. Dostert *et al.*, *Science* **320**, 674 (2008).
32. S. L. Cassel *et al.*, *Proc. Natl. Acad. Sci. U.S.A.* **105**, 9035 (2008).
33. C. M. Cruz *et al.*, *J. Biol. Chem.* **282**, 2871 (2007).
34. F. Meissner, K. Molawi, A. Zychlinsky, *Nat. Immunol.* **9**, 866 (2008).
35. S. T. Hui *et al.*, *Proc. Natl. Acad. Sci. U.S.A.* **105**, 3921 (2008).
36. S. Oka *et al.*, *Endocrinology* **150**, 1225 (2009).
37. A. H. Minn, C. Hafele, A. Shalev, *Endocrinology* **146**, 2397 (2005).
38. H. Parikh *et al.*, *PLoS Med.* **4**, e158 (2007).
39. J. Chen, G. Saxena, I. N. Mungrue, A. J. Lusis, A. Shalev, *Diabetes* **57**, 938 (2008).
40. F. Martinon, V. Pétrilli, A. Mayor, A. Tardivel, J. Tschopp, *Nature* **440**, 237 (2006).
41. A. So, T. De Smedt, S. Revaz, J. Tschopp, *Arthritis Res. Ther.* **9**, R28 (2007).
42. R. Terkeltaub *et al.*, *Ann. Rheum. Dis.* **68**, 1613 (2009).
43. M. G. Wolfs, M. H. Hofker, C. Wijmenga, T. W. van Haeften, *Curr. Genomics* **10**, 110 (2009).
44. D. Morgan *et al.*, *Diabetologia* **50**, 359 (2007).
45. T. Nishikawa, E. Araki, *Antioxid. Redox Signal.* **9**, 343 (2007).
46. H. Shi *et al.*, *J. Clin. Invest.* **116**, 3015 (2006).
47. M. Böni-Schnetzler *et al.*, *Endocrinology* **150**, 5218 (2009).
48. J. Hiscott *et al.*, *Mol. Cell. Biol.* **13**, 6231 (1993).
49. C. R. Plata-Salamán, J. M. Ffrench-Mullen, *Physiol. Behav.* **51**, 1277 (1992).
50. D. A. Muruve *et al.*, *Nature* **452**, 103 (2008).
51. M. Lamkanfi *et al.*, *J. Cell Biol.* **187**, 61 (2009).
52. O. Gross *et al.*, *Nature* **459**, 433 (2009).
53. M. Lamkanfi, R. K. Malireddi, T. D. Kanneganti, *J. Biol. Chem.* **284**, 20574 (2009).

54. K.S. is supported by a C. J. Martin Fellowship from the Australian National Health and Medical Research Council (ID 490993). J.T. is supported by grants of the Swiss National Science Foundation, European Union grants (Hermione, Apo-train, Apo-SYS, and Mugene), and the Institute of Arthritis Research. We thank K. Irvine, A. Yazdi, and M. Donath for critical reading of the manuscript.

10.1126/science.1184003

Hungry Codons Promote Frameshifting in Human Mitochondrial Ribosomes

Richard Temperley,* Ricarda Richter,* Sven Dennerlein, Robert N. Lightowlers, Zofia M. Chrzanowska-Lightowlers†

Ribosome frameshifting, although rare, must occur in mitochondrial (mt) translation systems with interrupted open reading frames (ORFs) (*1*), but all human mt-ORFs are unbroken. However, we show that human mitoribosomes do invoke –1 frameshift at the AGA and AGG codons predicted to terminate the two ORFs in *MTCO1* and *MTND6*, respectively. As a consequence, both ORFs terminate in the standard UAG codon, necessitating the use of only a single mitochondrial release factor (*2*).

Frameshifting could be promoted by (i) paused mitoribosomes on AGA or AGG triplets, because no mt-tRNAs exist that recognize these codons; (ii) upstream "slippery" sequences that are poorly defined in human mt-mRNA; or (iii) a downstream stable secondary structure predicted for both *MTCO1* and *MTND6* (fig. S1) (*3*). To demonstrate that –1 frameshifting occurs in human mitochondria, we targeted RelE, a bacterial endoribonuclease that specifically cleaves mRNA in the ribosomal A site, to the mitochondrion [mtRelE (*4, 5*), fig. S2]. This enzyme shows marked sequence preference for standard termination codons UAG and UAA with negligible predicted recognition of AGA and AGG (*4*). On induction, the majority of *MTCO1* (68 ± 1.73%, $n = 3$) and *MTCO2* (70 ± 1.4%, $n = 3$) were intact (Fig. 1A, lanes 1 and 3), ruling out nonspecific transcript degradation by mtRelE. However, mitochondrial translation was reduced for most mt-proteins, including COX1 and ND6 (Fig. 1B). Depletion of the mitochondrial release factor mtRF1a stabilizes transcripts through extended association with the mitoribosome, whereas RelE promotes release of cleaved mRNA from bacterial ribosomes (*4*). Therefore, mtRelE expression would be predicted to abrogate mitoribosome-mediated protection. mtRF1a depletion in tandem with mtRelE expression does reduce the amounts of full-length mt-transcripts and markedly so for *MTCO1* (Fig. 1A, lanes 2 and 4), indicating both recognition and cleavage by mtRelE.

Northern analysis could not resolve whether the short 3′ untranslated regions (3′UTRs) present in *MTCO1* [72 nucleotides (nt)] had been lost post–mtRelE cleavage. *MTND5*, however, possesses a longer 3′UTR (568 nt). On mtRelE induction, a species was detected that is consistent with cleavage at the stop codon and loss of this 3′UTR (Fig. 1A, lanes 3 and 4 indicated by asterisks). Human mtDNA encodes two transcripts with overlapping ORFs, one containing *MTATP8/6* (*RNA14*) and one *MTND4L/4* (*RNA7*). Cleavage at the stop codon of the upstream ORF would release an RNA with a 5′-truncated downstream ORF. As with *MTND5*, novel species were detected on mtRelE expression. This was particularly apparent for *RNA14*, where *MTATP8* terminates in UAG, a preferred stop codon for RelE (Fig. 1A).

Fine mapping was performed on *MTCO2* and the 5′ truncated site of *MTATP6* in the bicistronic *RNA14* (fig. S3). This revealed mtRelE cleavage in the UAG termination codon uniquely between nucleotides 2 and 3 before readenylation. This result therefore allowed us to determine unequivocally whether termination of *MTCO1* occurred at the AGA or UAG codon; AGA termination codon would result in –AAAAUCUAGA$_n$, whereas UAG would produce –AAAAUCUAA$_n$. On sequencing, 10 clones from control cells reflected full-length 3′UTR containing *MTCO1* transcripts; two were truncations in the antisense tRNA^{Ser}, a commonly identified expressed sequence tag. This species was also found in two of the mtRelE samples. However, all the remaining 33 mtRelE clones terminated in –AAAAUCUA followed by readenylation (Fig. 1C), signifying that *MTCO1* terminates at UAG rather than AGA. These data suggest that mtRF1a is sufficient to terminate all 13 human mt-ORFs.

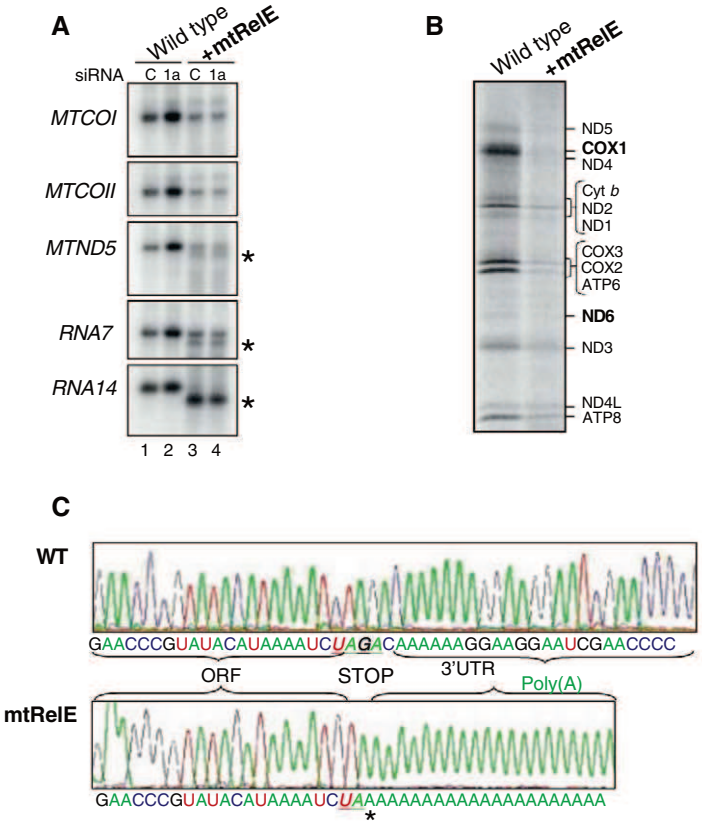

Fig. 1. Expression of mtRelE results in specific cleavage of mt-mRNA stop codons. Cells expressing mtRelE show (**A**) specific cleavage of mt-mRNA, generating novel products indicated by asterisks in both wild-type (WT) cells and those treated with siRNA to mtRF1a; (**B**) reduced metabolic labeling of mtDNA encoded gene products; and (**C**) cleavage of *MTCO1* transcripts specific at the UAG codon (33/35 clones, 2 were common truncated WT sequences) whereas WT cells retained the 3′UTR.

References and Notes

1. R. D. Russell, A. T. Beckenbach, *J. Mol. Evol.* **67**, 682 (2008).
2. H. R. Soleimanpour-Lichaei *et al.*, *Mol. Cell* **27**, 745 (2007).
3. R. F. Gesteland, R. B. Weiss, J. F. Atkins, *Science* **257**, 1640 (1992).
4. K. Pedersen *et al.*, *Cell* **112**, 131 (2003).
5. Materials and methods are available as supporting material on *Science* Online.
6. This work was supported by the Wellcome Trust (074454/Z/04/Z) and Biotechnology and Biological Sciences Research Council (BB/F011520/1). We thank K. Gerdes for kindly providing the clone and antibodies to bacterial RelE.

Supporting Online Material

www.sciencemag.org/cgi/content/full/327/5963/301/DC1
Materials and Methods
SOM Text
Figs. S1 to S4
Table S1
References and Notes

17 August 2009; accepted 30 November 2009
10.1126/science.1180674

The Mitochondrial Research Group, Institute for Ageing and Health, Newcastle University, Framlington Place, Newcastle upon Tyne NE2 4HH, UK.

*These authors contributed equally to this work.
†To whom correspondence should be addressed. E-mail: Z.Chrzanowska-Lightowlers@ncl.ac.uk

Adaptive Evolution of Pelvic Reduction in Sticklebacks by Recurrent Deletion of a *Pitx1* Enhancer

Yingguang Frank Chan,[1]* Melissa E. Marks,[1]† Felicity C. Jones,[1] Guadalupe Villarreal Jr.,[1]‡ Michael D. Shapiro,[1]§ Shannon D. Brady,[1] Audrey M. Southwick,[2] Devin M. Absher,[3] Jane Grimwood,[3] Jeremy Schmutz,[3] Richard M. Myers,[3] Dmitri Petrov,[4] Bjarni Jónsson,[5] Dolph Schluter,[6] Michael A. Bell,[7] David M. Kingsley[1]‖

The molecular mechanisms underlying major phenotypic changes that have evolved repeatedly in nature are generally unknown. Pelvic loss in different natural populations of threespine stickleback fish has occurred through regulatory mutations deleting a tissue-specific enhancer of the *Pituitary homeobox transcription factor 1* (*Pitx1*) gene. The high prevalence of deletion mutations at *Pitx1* may be influenced by inherent structural features of the locus. Although *Pitx1* null mutations are lethal in laboratory animals, *Pitx1* regulatory mutations show molecular signatures of positive selection in pelvic-reduced populations. These studies illustrate how major expression and morphological changes can arise from single mutational leaps in natural populations, producing new adaptive alleles via recurrent regulatory alterations in a key developmental control gene.

Evolutionary biology has been animated by long-standing debates about the number and type of genetic alterations that underlie evolutionary change. Questions about the roles of genetic changes of infinitesimally small versus large effects, the origin of traits by either natural selection or genetic drift, and the relative importance of coding and regulatory changes in evolution are currently being actively investigated (*1*–*4*). One of the classic examples of major evolutionary change in vertebrates is the extensive modification of paired appendages seen in different species (*5*). Although essential for many forms of locomotion, paired appendages have also been repeatedly lost in some fish, amphibian, reptile, and mammalian lineages, probably via selection for streamlined body forms (*6*).

Threespine stickleback fish (*Gasterosteus aculeatus*) make it possible to analyze the evolution, genetics, and development of major skeletal changes in natural populations (*7*). The pelvic apparatus of marine sticklebacks consists of prominent serrated spines that articulate with an underlying pelvic girdle that extends along the ventral and lateral sides of the fish (inspiring the scientific name *Gasterosteus aculeatus*, or bony stomach with spines). Although most sticklebacks develop a robust pelvic apparatus, over two dozen widely distributed and probably independent freshwater stickleback populations show partial or complete loss of pelvic structures (*8*). Several factors may contribute to repeated evolution of pelvic reduction, including the absence of gape-limited predatory fish, limited calcium availability, and predation by grasping insects (*9*–*12*).

Genome-wide linkage mapping has identified a single chromosome region that explains more than two thirds of the variance in pelvic size in crosses with pelvic-reduced sticklebacks (*13*–*15*). This region contains *Pituitary homeobox 1* (*Pitx1*), a gene expressed in hindlimbs but not forelimbs of many different vertebrates and required for normal hindlimb development (*13*). Although the *Pitx1* gene of pelvic-reduced sticklebacks shows no protein-coding changes as compared with that of ancestral marine fish, its expression in the developing pelvic region is almost completely lost (*13*, *16*). On the basis of the map location, changes in expression, and directional asymmetry shared in both *Pitx1*-null mice and pelvic-reduced sticklebacks, cis-regulatory mutations at the *Pitx1* locus have been proposed as the basis of stickleback pelvic reduction (*13*). However, regulatory mutations are difficult to identify, and the actual sequences controlling pelvic reduction have remained hypothetical (*2*).

cis-regulatory changes at *Pitx1* locus. Although *Pitx1* represents a strong candidate gene for pelvic reduction, other genes in the larger chromosome region could be the real cause of pelvic loss, leading to secondary or trans-acting reduction of *Pitx1* expression (*2*). To test this possibility, we generated F1 hybrids between pelvic-complete [Friant Low (FRIL) and pelvic-reduced (Paxton Lake Benthic (PAXB)] sticklebacks [see table S1 for geographic location of all populations used in this study (*17*)]. F1 hybrid fish develop pelvic structures and contain both *Pitx1* alleles in an identical trans-acting environment. The PAXB allele was expressed at significantly lower levels than the FRIL allele in the restored pelvic tissue of F1 hybrids (n = 19 individuals, two-tailed t test, $P < 0.001$) (Fig. 1). Reduced expression of the PAXB allele was tissue-specific because both *Pitx1* alleles were expressed at similar levels in F1 hybrid head tissue. As a control, we generated F1 hybrids between two pelvic-complete populations [FRIL and Little Campbell River (LITC)] (Fig. 1). In this cross, both *Pitx1* alleles were expressed at comparable levels in both heads and

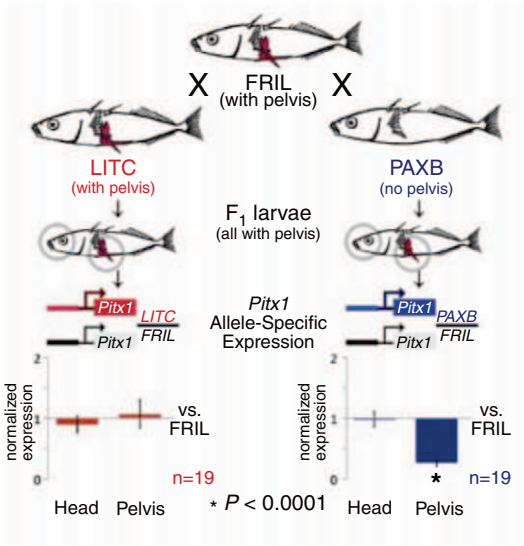

Fig. 1. Alleles of *Pitx1* from pelvic-complete (FRIL and LITC) and pelvic-reduced populations (PAXB) were combined in F1 hybrids, and brain and pelvic tissues were isolated so as to compare the expression of either the LITC or PAXB allele normalized to the level of expression of the FRIL allele in the same trans-acting environment. Expression of the PAXB *Pitx1* allele is greatly reduced in the pelvis but not the head of F1 hybrids (two-tailed t test, $P < 0.0001$), indicating a tissue-specific, cis-regulatory change in the *Pitx1* locus.

[1]Department of Developmental Biology and Howard Hughes Medical Institute, Stanford University, Stanford, CA 94305, USA. [2]Stanford Human Genome Center, Stanford University, Stanford, CA 94305, USA. [3]HudsonAlpha Institute, Huntsville, AL 35806, USA. [4]Department of Biology, Stanford University, Stanford, CA 94305, USA. [5]Institute of Freshwater Fisheries, Sæmundargata 1, 550 Sauðárkrókur, Iceland. [6]Department of Zoology, University of British Columbia, Vancouver, British Columbia V6T 1Z4, Canada. [7]Department of Ecology and Evolution, Stony Brook University, Stony Brook, NY 11794, USA.

*Present address: Max Planck Institute for Evolutionary Biology, 24306 Plön, Germany.
†Present address: University of Chicago, Chicago, IL 60637, USA.
‡Present address: Harvard Medical School, Boston, MA 02115, USA.
§Present address: University of Utah, Salt Lake City, UT 84112, USA.
‖To whom correspondence should be addressed. E-mail: kingsley@stanford.edu

pelves. Allele-specific down-regulation of *Pitx1* in the FRIL × PAXB cross shows that pelvic-specific loss of *Pitx1* expression is due to cis-regulatory change (or changes) at *Pitx1* itself and not to overall failure of pelvic development or changes in unknown trans-acting factors.

Fine mapping of pelvic regulatory region. To further localize the position of the cis-acting changes, we looked for the smallest chromosome region co-segregating with bilateral absence of pelvic structures in a cross between pelvic-complete [Japanese marine (JAMA) and pelvic-reduced (PAXB) fish (*13*)]. High-resolution mapping identified a 124-kb minimal interval, containing only the *Pitx1* and *Histone 2A* (*H2AFY*) genes, which showed perfect concordance between PAXB alleles and absence of the pelvis (fig. S1A).

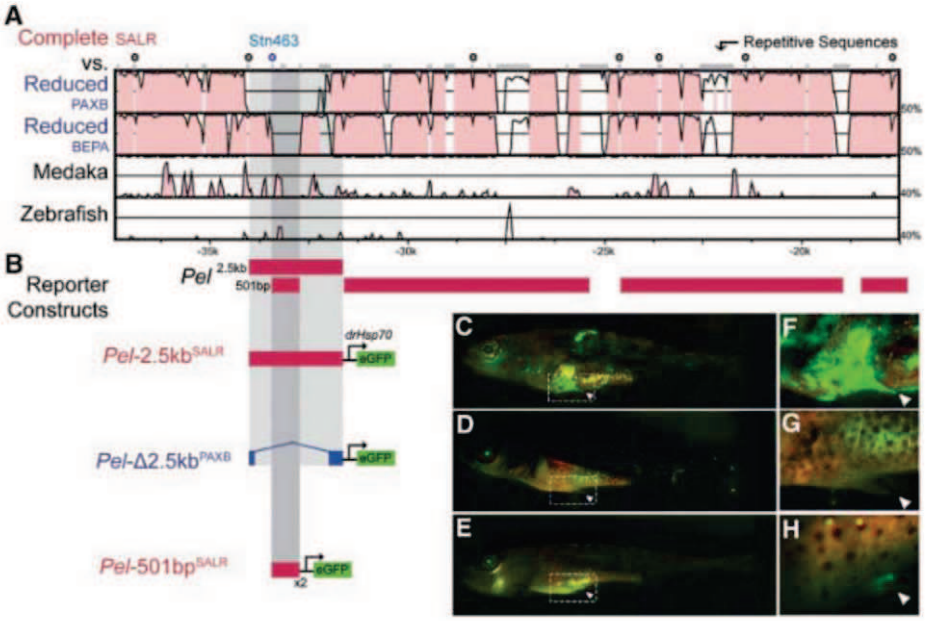

Fig. 2. (**A**) VISTA/mLAGAN (http://genome.lbl.gov/vista/) alignment of *Pitx1* candidate region from pelvic-complete stickleback (SALR), medaka, and zebrafish. Red peaks indicate >40% sequence identity in 20-bp sliding windows; grey bars at top indicate repetitive sequences; and circles indicate microsatellite markers used in association mapping in fig. S1. (**B**) Reporter gene expression in transgenic animals. (**C**) *Pel*-2.5-kb^{SALR} from a marine population drives tissue-specific EGFP (green) expression in the developing pelvic bud of Swarup stage-32 larvae (*36*). (**F**) Detail of (C). (**D** and **G**) Altered *Pel*-Δ2.5-kb^{PAXB} sequence from pelvic-reduced PAXB stickleback fails to drive pelvic EGFP expression. (**E** and **H**) A smaller fragment from marine fish, *Pel*-501-bp^{SALR}, also drives EGFP expression in the developing pelvic bud of multiple stage-30 larvae. This region is completely missing in PAXB.

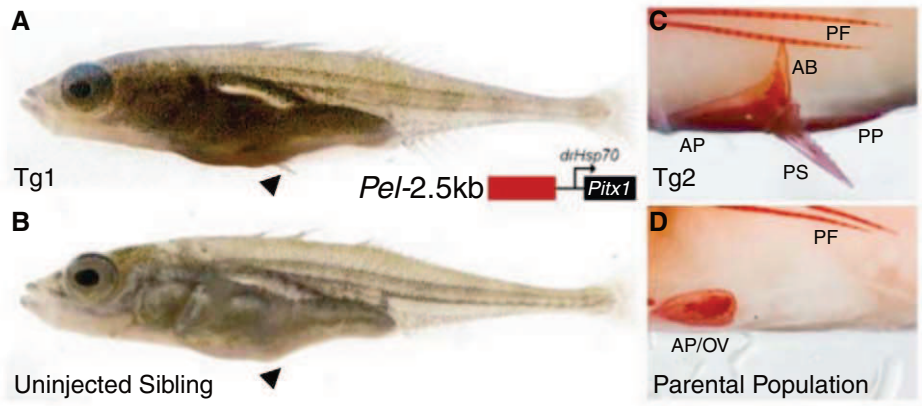

Fig. 3. (**A**) Juvenile pelvic-reduced BEPA stickleback expressing a *Pitx1* transgene driven by the *Pel*-2.5-kb^{SALR} enhancer compared with (**B**) uninjected sibling. External spines form only in transgenic fish (arrowhead). (**C** and **D**) Alizarin red–stained pelvic structures of adult transgenic fish compared with BEPA parental phenotype. BEPA fish normally develop only a small ovoid vestige (OV) of the anterior pelvic process (AP). Transgenic fish show clear development of the AP, ascending branch (AB), and posterior process (PP) of the pelvis, and a prominent serrated pelvic spine. Pectoral fin (PF) rays develop in both fish.

Recombination in natural populations can also be used to narrow the size of regions controlling polymorphic traits in sticklebacks (*18*). We therefore tested whether markers in the *Pitx1* region were associated with the presence or absence of pelvic structures in lakes with dimorphic stickleback forms: benthic and limnetic sticklebacks from Paxton Lake, British Columbia (PAXB/PAXL), and pelvic-complete and pelvic-reduced sticklebacks from Wallace Lake, Alaska (WALR/WALC) (fig. S2) (*13*, *14*). Microsatellite markers located in an intergenic region approximately 30 kb upstream of *Pitx1* showed highly significant allele frequency differences in fish with contrasting pelvic phenotypes ($P < 10^{-35}$) (Fig. S1B and table S2). In contrast, markers around the *Pitx1* and *H2AFY* coding regions showed little or no differentiation above background levels. These results suggest that an approximately 23-kb intergenic region upstream of *Pitx1* controls pelvic development. This region is conserved among zebrafish and other teleosts (Fig. 2A), suggesting that it may contain ancestrally conserved regulatory enhancers.

A small enhancer drives pelvic expression of *Pitx1*. To test for regulatory functions in the *Pitx1* intergenic region, we cloned different subfragments upstream of a basal promoter and enhanced green fluorescent protein (EGFP) reporter gene (Fig. 2B) (*19*). The hsp70 promoter drives modest or no EGFP expression except in the eye (*19*). A construct containing a 2.5-kb fragment from a marine, pelvic-complete fish [Salmon River (SALR)] drove consistent EGFP expression in the developing pelvic region of transgenic sticklebacks (four of five independent transgenics) (Fig. 2, C and F). A smaller 501–base pair (bp) subfragment also drove highly specific pelvic expression (seven of nine transgenics) (Fig. 2, E and H). No consistent expression was seen in pectoral fins or other sites of normal *Pitx1* expression, including the mouth, jaw, and pituitary (*13*, *16*). Thus, the noncoding region upstream of *Pitx1* contains a tissue-specific enhancer for hindfin expression, which we term "*Pel*." *Pel* shows sequence conservation across distantly related teleost fish (Fig. 2A and fig. S3) and contains multiple predicted transcription factor binding sites that might contribute to spatially restricted expression in the developing pelvic region (fig. S4).

Transgenic rescue of pelvic reduction. If regulatory changes in *Pitx1* underlie pelvic reduction in sticklebacks, restoring pelvic expression of *Pitx1* should rescue pelvic structures. We cloned the 2.5-kb *Pel* region from a pelvic-complete population (SALR) upstream of a *Pitx1* minigene that was prepared from coding exons of a pelvic-reduced fish [Bear Paw Lake (BEPA)] (*14*). The rescuing construct was injected into fertilized eggs of BEPA fish, which normally fail to develop any pelvic spine and show no more than a small vestigial remnant of the underlying pelvic girdle (pelvic score ≤ 3) (Fig. 3, B and D, and fig. S5) (*12*). Transgenic fry showed variable but enhanced development of external pelvic spines as com-

pared with those of control uninjected siblings (clutch 1, $n = 16$ injected and 11 uninjected fish, Wilcoxon rank-sum test, $W = 1073.5$, $P < 0.01$; clutch 2, $n = 4$ injected and 18 uninjected fish, $W = 513$, $P < 2.3\times10^{-9}$) (Fig. 3A). Alizarin red skeletal preparations of two adult transgenic fish revealed prominent serrated spines articulating with an enlarged, complex pelvic girdle containing anterior, posterior, and ascending branch structures (Fig. 3C and fig. S5, pelvic score summary). These data provide functional evidence that *Pel-Pitx1* is a major determinant of pelvic formation in sticklebacks.

Nature of mutations in pelvic-reduced fish. Bacterial artificial chromosome sequencing from the PAXB population identified a 1868-bp deletion present in the *Pel*-2.5-kb region (fig. S7). We cloned the PAXB-deleted variant and found that it no longer drove expression in the developing pelvis (zero out of eight transgenic animals) (Fig. 2, D and G), confirming that the molecular deletion in PAXB fish disrupts *Pel* enhancer function.

We also identified a second 757-bp deletion present in the pelvic-reduced BEPA population from Alaska and a third deletion of 973 bp present in the Hump Lake, Alaska, pelvic-reduced population (HUMP). The three different deletions in PAXB, BEPA, and HUMP overlap in a 488-bp region, each partially or completely removing the sequences found in the *Pel*-501-bp enhancer (Fig. 4A and figs. S4, S7, and S8).

To investigate whether a general mechanism and/or shared variants underlie repeated pelvic reduction in sticklebacks, we genotyped PAXB, BEPA, HUMP, and 10 additional pelvic-reduced populations from disparate geographic locations, as well as 21 pelvic-complete populations, using 149 single-nucleotide polymorphisms (SNPs) spanning 321 kb around the *Pitx1* locus (approximately 2-kb spacing) (fig. S8 and tables S1 and S3). Nine of the 13 pelvic-reduced stickleback populations—but zero out of 21 pelvic-complete populations—showed consistent missing genotypes for multiple consecutive SNP markers located in and around the *Pel* enhancer (two-tailed *t* test, $P < 0.001$, df = 12.279) (Fig. 4A, fig. S8, and tables S4 and S5). For the PAXB, BEPA, and HUMP populations, the SNPs corresponding to the missing genotypes fall within the known deletion endpoints from DNA sequencing. The larger genotyping survey identified a total of nine different haplotypes with different staggered deletions, each consistently seen within a pelvic-reduced population, and each overlapping or completely removing the *Pel* enhancer region (Fig. 4 and fig. S8).

Fragile sites. Several features suggest that *Pitx1* may be located within a fragile region of the genome: The gene is located at the telomeric end of linkage group 7; the region contains many repeats and failed to assemble in the stickleback genome; the enhancer region is difficult to amplify and sequence; and close inspection of the deletion boundaries in PAXB and BEPA revealed short 2- or 3-bp sequence identities present on both sides, one of which is retained after deletion (Fig. 4A and fig. S7A). Similar nested deletions and small sequence identities may occur by means of re-ligation of chromosome ends after breakage and repair by nonhomologous end joining (NHEJ) (fig. S7B) (*20*, *21*). In humans, NHEJ is associated with stalled replication forks at fragile chromosomal sites, which also are frequent in subtelomeric regions (*21*). Fragile sites are also enriched in sequences with high DNA flexibility, which is a physical property that can be calculated from known twist angles between different stacked DNA base pairs (*20*). DNA flexibility analysis of *Pitx1* and the entire assembled stickleback genome showed a median flexibility score of 265 with a tail of extreme values. Four of the top 10 flexibility scores in the genome occur in the *Pitx1* region, suggesting that this region is exceptionally flexible and may be prone to deletion (Wilcoxon rank sum = 59,624, $P < 2 \times 10^{-6}$) (Fig. 4C).

Signatures of selection. Recurring deletions could explain how pelvic-reduction alleles arise repeatedly in widespread isolated populations. To test whether pelvic-reduction alleles have also been subject to positive selection, we looked for molecular signatures that commonly accompany selective sweeps, including reduced heterozygosity and an overrepresentation of derived alleles (*22*). Patterns of allelic variation showed an excess of derived alleles near the *Pel* enhancer region of pelvic-reduced populations, as indicated by negative values of Fay and Wu's *H* statistic (Fig. 5A and fig. S9A) (*23*). We also observed a significant reduction in heterozygosity at or near the *Pel* enhancer in pelvic-reduced populations as compared with marine populations (two-tailed *t* test, $P < 0.01$) (Fig. 5, B and C). This reduction cannot be solely explained by population bottlenecks that occurred during freshwater colonization because heterozygosity reduction near *Pel* is specific to pelvic-reduced, but not pelvic-complete, freshwater populations (two-tailed *t* test, $P < 0.002$) (Fig. 5, B and C). In flanking regions of *Pitx1*, and in unlinked control loci, we observed no significant difference in heterozygosity between freshwater fish with a complete or missing pelvis (Fig. 5C). Pelvic-reduced populations were significantly more likely to exhibit minimum heterozygosity close to the *Pel* enhancer region than either marine or freshwater populations with a robust pelvis (two-tailed *t* test, $P < 0.002$) (fig. S9F). The local heterozygosity and *H* statistic minima around the *Pel* enhancer region suggest that changes in this region have been selected in pelvic-reduced stickleback populations.

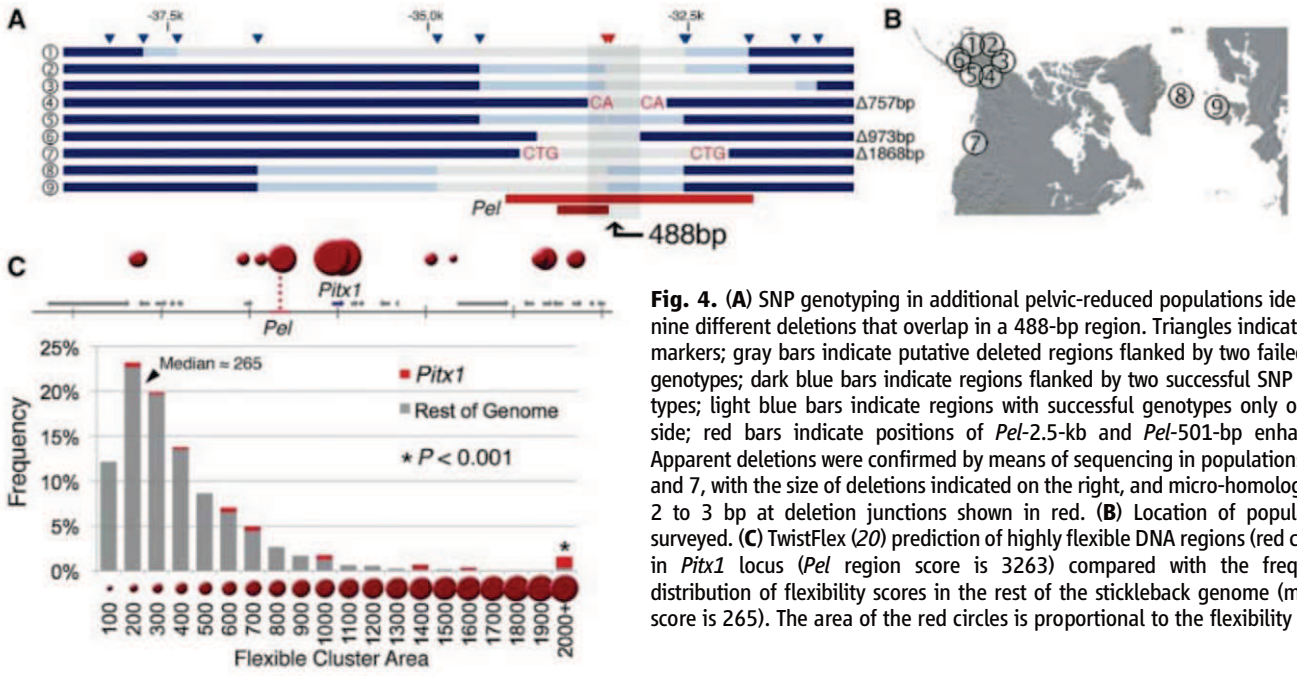

Fig. 4. (**A**) SNP genotyping in additional pelvic-reduced populations identifies nine different deletions that overlap in a 488-bp region. Triangles indicate SNP markers; gray bars indicate putative deleted regions flanked by two failed SNP genotypes; dark blue bars indicate regions flanked by two successful SNP genotypes; light blue bars indicate regions with successful genotypes only on one side; red bars indicate positions of *Pel*-2.5-kb and *Pel*-501-bp enhancers. Apparent deletions were confirmed by means of sequencing in populations 4, 6, and 7, with the size of deletions indicated on the right, and micro-homologies of 2 to 3 bp at deletion junctions shown in red. (**B**) Location of populations surveyed. (**C**) TwistFlex (*20*) prediction of highly flexible DNA regions (red circles) in *Pitx1* locus (*Pel* region score is 3263) compared with the frequency distribution of flexibility scores in the rest of the stickleback genome (median score is 265). The area of the red circles is proportional to the flexibility score.

Discussion. Traditional theories of evolution posit that adaptation occurs through many mutations of infinitesimally small effect. In contrast, recent work suggests that mutation effect sizes follow an exponential distribution, with mutations of large effect contributing to adaptive change in nature (*1*). We narrowed the candidate interval for a pelvic quantitative trait locus with large effects in sticklebacks to the noncoding region upstream of *Pitx1* and identified a tissue-specific enhancer for pelvic expression that has been functionally inactivated in pelvic-reduced fish. Reintroduction of the enhancer and *Pitx1* coding region can restore formation of pelvic structures in derived populations that appear to be monomorphic for pelvic reduction. The combined data from mapping, expression, molecular, transgenic, and population genetic studies illustrate how major morphological evolution can proceed through a regulatory change in a key developmental control gene.

Large evolutionary differences that map to a particular locus can still be caused by many linked small-effect mutations that have accumulated in that gene (*24*, *25*). However, we find that pelvic-reduction in sticklebacks maps to a type of DNA lesion that may produce a large regulatory change in a single mutational leap: deletions that completely remove a regulatory enhancer. Smaller functional lesions might be found in some pelvic-reduced populations, including four populations without obvious deletions. However, three of these populations show unusual morphological features, suggesting that their pelvic loss may have occurred through non–*Pitx1*-mediated mechanisms (*8*, *26*).

The *Pitx1* locus scores as one of the most flexible regions in the stickleback genome, which may reflect a susceptibility to double-stranded DNA breaks and repair through NHEJ (*27*–*29*). We hypothesize that sequence features in the *Pitx1* locus may predispose the locus to structural changes, possibly explaining the high prevalence of independent deletion mutations fixed in different pelvic-reduced stickleback populations. A similar spectrum of independent small-deletion mutations has been seen at the *vernalization 1* locus of plants (*30*), suggesting that recurrent deletions in particular genes may also contribute to parallel evolution of other phenotypes in natural populations.

Mutations in developmental control genes are often deleterious in laboratory animals, leading to long-standing doubts about whether mutations in such genes could ever be advantageous in nature (*31*). Although *Pitx1* coding regions are lethal in mice (*32*), we find clear signatures of positive selection in the *Pitx1* gene of pelvic-reduced sticklebacks. Before this work, the primary evidence that pelvic reduction might be adaptive in sticklebacks came from repeated evolution of similar phenotypes in similar ecological environments and the temporal sequence of pelvic reduction in fossil sticklebacks (*11*, *12*, *33*). The molecular signatures of selection we have identified in the current study are centered on the tissue-specific *Pel* enhancer region rather than the *Pitx1* coding region. Regulatory changes in developmental control genes have often been proposed as a possible basis for morphological evolution (*3*, *34*). However, many proposed examples of regulatory evolution in wild animals have not yet been traced to particular sequences (*2*) or do not show obvious molecular signatures of selection in natural populations (*35*). Identification of the *Pel* enhancer underlying pelvic reduction in sticklebacks connects a major change in vertebrate skeletal structures to specific DNA sequence alterations and provides clear evidence for adaptive evolution surrounding the corresponding region in many different wild populations.

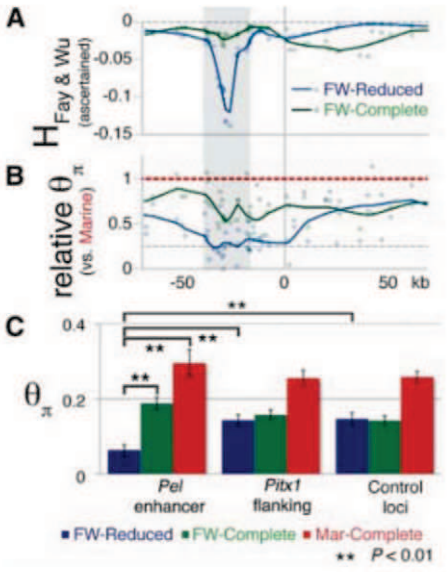

Fig. 5. (**A** and **B**) Fay and Wu's *H* and relative heterozygosity (θ_π) statistics across the *Pitx1* region. Blue (freshwater pelvic-reduced) and green (freshwater pelvic-complete) data points and locally weighted scatterplot–smoothed (α = 0.2) line indicate the behavior in each group. The *Pel*-containing regulatory region of *Pitx1* [gray candidate region (fig. S1B)] shows both negative *H* values, indicating an excess of derived alleles, and reduced heterozygosity in pelvic-reduced fish, which is consistent with positive selection. θ_π values are plotted relative to the grouped marine mean (per SNP) in order to control for variation in ascertainment between SNPs. (**C**) Heterozygosity (θ_π) from different genomic regions, grouped by population type. Freshwater fish show a general decrease in heterozygosity across both *Pitx1* and control loci as compared with that of marine fish (red bars), as is expected from founding of new freshwater populations from marine ancestors. In the *Pel* enhancer region, but not in *Pitx1*-flanking regions or in control loci, pelvic-reduced freshwater populations (blue bars) show even lower heterozygosity than pelvic-complete freshwater populations (green bars) (**$P < 0.01$).

References and Notes

1. H. A. Orr, *Nat. Rev. Genet.* **6**, 119 (2005).
2. H. E. Hoekstra, J. A. Coyne, *Evolution* **61**, 995 (2007).
3. S. B. Carroll, *Cell* **134**, 25 (2008).
4. D. L. Stern, V. Orgogozo, *Evolution* **62**, 2155 (2008).
5. J. R. Hinchliffe, D. R. Johnson, *The Development of the Vertebrate Limb* (Clarendon Press, Oxford, 1980).
6. M. D. Shapiro, M. A. Bell, D. M. Kingsley, *Proc. Natl. Acad. Sci. U.S.A.* **103**, 13753 (2006).
7. D. M. Kingsley, C. L. Peichel, in *Biology of the Three-Spined Stickleback*, S. Ostlund-Nilsson, I. Mayer, F. A. Huntingford, Eds. (CRC Press, London, 2007) pp. 41–81.
8. M. A. Bell, *Biol. J. Linn. Soc. London* **31**, 347 (1987).
9. J. D. Reist, *Can. J. Zool.* **58**, 1253 (1980).
10. T. E. Reimchen, *Can. J. Zool.* **58**, 1232 (1980).
11. N. Giles, *J. Zool.* **199**, 535 (1983).
12. M. A. Bell, G. Ortí, J. A. Walker, J. P. Koenings, *Evolution* **47**, 906 (1993).
13. M. D. Shapiro *et al.*, *Nature* **428**, 717 (2004).
14. W. A. Cresko *et al.*, *Proc. Natl. Acad. Sci. U.S.A.* **101**, 6050 (2004).
15. S. M. Coyle, F. A. Huntingford, C. L. Peichel, *J. Hered.* **98**, 581 (2007).
16. N. J. Cole, M. Tanaka, A. Prescott, C. A. Tickle, *Curr. Biol.* **13**, R951 (2003).
17. Materials and methods are available as supporting material on *Science* Online.
18. P. F. Colosimo *et al.*, *Science* **307**, 1928 (2005).
19. S. Nagayoshi *et al.*, *Development* **135**, 159 (2008).
20. E. Zlotorynski *et al.*, *Mol. Cell. Biol.* **23**, 7143 (2003).
21. S. G. Durkin *et al.*, *Proc. Natl. Acad. Sci. U.S.A.* **105**, 246 (2008).
22. R. Nielsen, *Annu. Rev. Genet.* **39**, 197 (2005).
23. J. C. Fay, C. I. Wu, *Genetics* **155**, 1405 (2000).
24. L. F. Stam, C. C. Laurie, *Genetics* **144**, 1559 (1996).
25. A. P. McGregor *et al.*, *Nature* **448**, 587 (2007).
26. M. A. Bell, V. Khalef, M. P. Travis, *J. Exp. Zool. B Mol. Dev. Evol.* **308**, 189 (2007).
27. D. Mishmar *et al.*, *Proc. Natl. Acad. Sci. U.S.A.* **95**, 8141 (1998).
28. T. W. Glover, M. F. Arlt, A. M. Casper, S. G. Durkin, *Hum. Mol. Genet.* **14** (suppl. 2), R197 (2005).
29. M. Schwartz *et al.*, *Genes Dev.* **19**, 2715 (2005).
30. J. Cockram, I. J. Mackay, D. M. O'Sullivan, *Genetics* **177**, 2535 (2007).
31. E. Mayr, *Populations, Species and Evolution* (Harvard Univ. Press, Cambridge, MA, 1970).
32. C. Lanctôt, A. Moreau, M. Chamberland, M. L. Tremblay, J. Drouin, *Development* **126**, 1805 (1999).
33. G. Hunt, M. A. Bell, M. P. Travis, *Evolution* **62**, 700 (2008).
34. M. C. King, A. C. Wilson, *Science* **188**, 107 (1975).
35. S. Jeong *et al.*, *Cell* **132**, 783 (2008).
36. H. Swarup, *J. Embryol. Exp. Morphol.* **6**, 373 (1958).

37. We thank M. McLaughlin for fish husbandry, M. Nonet for the gift of the pBH-mcs-YFP vector, Broad Institute for the public gasAcu1 genome assembly, and many individuals for valuable fish samples (table S1). This work was supported by a Stanford Affymetrix Bio-X Graduate Fellowship (Y.F.C.); the Howard Hughes Medical Insititute (HHMI) Exceptional Research Opportunities Program (G.V.); the Burroughs Wellcome Fund (M.D.S.); NSF grants DEB0211391 and DEB0322818 (M.A.B.); a Canada Research Chair and grants from the Natural Sciences and Engineering Research Council of Canada and the Guggenheim Foundation (D.S.); NIH grant P50 HG02568 (R.M.M., D.P., and D.M.K.); and an HHMI investigatorship (D.M.K.). Sequences generated for this study are available in GenBank (accession GU130433-7).

Supporting Online Material www.sciencemag.org/cgi/content/full/science.1182213/DC1 Materials and Methods
Figs. S1 to S9
Tables S1 to S5
References

21 September 2009; accepted 6 November 2009
Published online 10 December 2009;
10.1126/science.1182213
Include this information when citing this paper.

Direct Imaging of Bridged Twin Protoplanetary Disks in a Young Multiple Star

Satoshi Mayama,[1]* Motohide Tamura,[1,2] Tomoyuki Hanawa,[4] Tomoaki Matsumoto,[5] Miki Ishii,[3] Tae-Soo Pyo,[3] Hiroshi Suto,[2] Takahiro Naoi,[2] Tomoyuki Kudo,[2] Jun Hashimoto,[1,2] Shogo Nishiyama,[6] Masayuki Kuzuhara,[7] Masahiko Hayashi[1,2]

Studies of the structure and evolution of protoplanetary disks are important for understanding star and planet formation. Here we present the direct image of an interacting binary protoplanetary system. Both circumprimary and circumsecondary disks are resolved in the near-infrared. There is a bridge of infrared emission connecting the two disks and a long spiral arm extending from the circumprimary disk. Numerical simulations show that the bridge corresponds to gas flow and a shock wave caused by the collision of gas rotating around the primary and secondary stars. Fresh material streams along the spiral arm, consistent with the theoretical scenarios in which gas is replenished from a circummultiple reservoir.

Our understanding of star and planet formation has advanced greatly in the past two decades. It has been established that stars form with surrounding protoplanetary disks with radii that reach up to several hundreds of astronomical units (AU) (1 AU is the distance between the Sun and Earth) (*1*). Planets are believed to form from these disks. The structure of protoplanetary disks has been intensively studied at various radiation wavelengths (*2*). Although our understanding of the formation mechanism of a single star has advanced considerably (*2*), that of binaries has many unexplained questions. Studies of protoplanetary disks in multiple systems are essential for describing the general processes of star and planet formation, because most stars form as multiples (*3*, *4*).

The transformation of a circumstellar disk into a planetary system can be inhibited if the local environment is sufficiently hostile to severely disturb or destroy the disk. A common example is dynamical disruption caused by another star in a multiple system. In a binary system, both the primary and secondary stars orbit each other and respectively have circumprimary and circumsecondary disks; the entire system can be surrounded by a circumbinary disk. Numerical simulations demonstrate that the stability of a protoplanetary disk in a multiple system is seriously jeopardized (*5*). In simulations, despite the dynamical interactions between disks and stars, individual circumstellar disks can survive and large gaps are produced in the circumbinary disk. A circumbinary disk can supply mass to the circumstellar disks through a gas stream that penetrates the disk gap without closing it. Therefore, this infalling material through the spiral arm plays an important role in the formation of circumstellar disks.

However, such circummultiple disks and spiral arms in multiple systems have rarely been directly imaged or resolved to date. We investigated the geometry of a young multiple circumstellar disk system, SR24, to understand its nature based on observations and numerical simulations. SR24 is a hierarchical multiple, located 160 pc away in the Ophiuchus star-forming region (*6*–*8*). It is composed of the low-mass T Tauri type stars SR24S (the primary) and SR24N (the secondary). SR24S is a class II source [with a stellar age of 4 million years (*9*)] of spectral type K2 with mass >1.4 times the mass of the Sun ($M_\odot$) (*10*). SR24N is located 810 AU north of SR24S (*10*) and is itself a binary system composed of SR24Nb and SR24Nc, with a projected separation of 30 AU (*10*). The spectral type and mass of SR24Nb are K4-M4 and 0.61 $M_\odot$, respectively (*10*). Those of SR24Nc are K7-M5 and 0.34 $M_\odot$ (*10*). Because the separation between SR24Nb and SR24Nc is comparable to the angular resolution and is much smaller than that between SR24N and SR24S, we consider SR24Nb and SR24Nc together as SR24N with mass 0.95 $M_\odot$. Accordingly, we regard the SR24 system as a binary with a primary-to-secondary mass ratio of 0.68, assuming the mass of SR24S to be 1.4 $M_\odot$.

We obtained an infrared (IR) image of SR24 with the adaptive optics (AO) (*11*) coronagraph CIAO (*12*) mounted on the 8.2-m Subaru Telescope on July 2006. (Fig. 1, left) (*13*). The image reveals faint near-IR nebulosity at a resolution of 0.1 arc sec. The emission arises from dust particles mixed with gas in the circumstellar structures scattering the stellar light. Both the circumprimary and circumsecondary disks are clearly resolved. The primary disk has a radius of 420 AU and is elongated in the northeast-southwest direction. The secondary disk has a radius of 320 AU and is elongated in the east-west direction. Both disks overflow the inner Roche lobes (dotted contours in Fig. 1), which show the regions gravitationally bound to each star, suggesting that the material outside the lobes can fall into either of the inner lobes. A curved bridge of emission is seen (*14*), connecting the primary and secondary disks. This emission begins southeast of the secondary disk, extends to the south while curving to the west, and reaches the north edge of the primary disk. This suggests a physical link, such as a gas flow between the two disks. Another salient feature is a broad arc starting from the southwestern edge of the primary disk, extending to the southeast through the Lagrangian point L3. Its tail is at least 1600 AU from SR24S. This emission is most likely a spiral arm, and that would suggest that the SR24 system rotates counterclockwise. The orbital period of the binary is 15,000 years. The arm would also imply replenishment of the twin-disk gas from the circumbinary disk. The bridge and spiral arm appear to form a connected S-shaped emission.

We performed two-dimensional (2D) numerical simulations of accretion from a circumbinary disk to identify the features seen in the coronagraphic image (*13*) (Fig. 1, right). We assumed that the mass of SR24S is 1.4 $M_\odot$ and, for simplicity, that the orbit is circular. Although the gas flow was not stationary, especially inside the Roche lobes, the stage of the 2D simulations shown in Fig. 1 shared common features with the observed image. A bridge was seen connecting the primary and secondary disks. It ran through the Lagrange point L1. A long spiral arm ran through Lagrange point L3, with a pitch angle consistent with that of the observed spiral arm. These agreements between observation and simulation suggest that the bridge corresponds to gas flow and a shock wave caused by the collision of gas rotating around the primary and secondary stars. The arm corresponds to a spiral wave excited in the circumbinary disk. The bridge and spiral arm seen in the simulations are wave patterns, and their shapes fluctuate with time. The reproduced direction of the bridge in the 2D simulation is not consistent with that of the observed bridge structure.

The effective reflectivity of SR24 (*15*) (Fig. 2, left panel) is defined by

$$\gamma = 4\pi S \left(f_S \Big/ r_S^2 + f_N \Big/ r_N^2 \right)^{-1} \qquad (1)$$

where S denotes the observed surface brightness, f_S and r_S are the brightness of SR24S and the projected distance to SR24S on the sky plane,

[1]The Graduate University for Advanced Studies, Shonan International Village, Hayama-cho, Miura-gun, Kanagawa 240-0193, Japan. [2]National Astronomical Observatory of Japan, 2-21-1, Osawa, Mitaka, Tokyo 181-8588 Japan. [3]Subaru Telescope, National Astronomical Observatory of Japan, 650 North A'ohoku Place, Hilo, HI 96720, USA. [4]Center for Frontier Science, Chiba University, Inage-ku, Chiba 263-8522, Japan. [5]Faculty of Humanity and Environment, Hosei University, Fujimi, Chiyoda-ku, Tokyo 102-8160, Japan. [6]Department of Astronomy, Kyoto University, Kitashirakawa-Oiwake-cho, Sakyo-ku, Kyoto 606-8502, Japan. [7]Department of Earth and Planetary Science, University of Tokyo, Hongo, Tokyo 113-0033, Japan.

*To whom correspondence should be addressed. E-mail: mayama_satoshi@soken.ac.jp

respectively, and f_N and r_N are the brightness and distance to SR24N, respectively. f_S and f_N are 513 and 301 mJy, respectively (*16*). Thus, the denominator of Eq. 1 denotes the local radiation flux at the reflector and is normalized so that the effective reflectivity is nondimensional. The effective reflectivity is expected to be proportional to the product of the reflection efficiency and irradiation angle of the reflector when the reflector surface is nearly tangential to the radiation from the light sources.

We compared the reflection efficiency at the H band relative to that at the optical wavelengths (Fig. 2, right panel). The northeast sides of both disks have higher relative efficiencies, implying that the reflection at the H band is less efficient in the arm and in the southwest side of the primary disk. This inefficiency may be due to a smaller optical depth in the arm.

The effective reflectivity ranges from 0.02 to 0.07 in the disks, suggesting that they are geometrically thin and that their thickness is approximately 5% of the radial distance from the hosting star. The bridge has a similar effective reflectivity and color to those of the disks, indicating that it has almost the same geometrical thickness as the disks. The southeastern end of the spiral arm has a high effective reflectivity of 0.14 despite its blue color. This means that this part has a large-scale height along the line of sight.

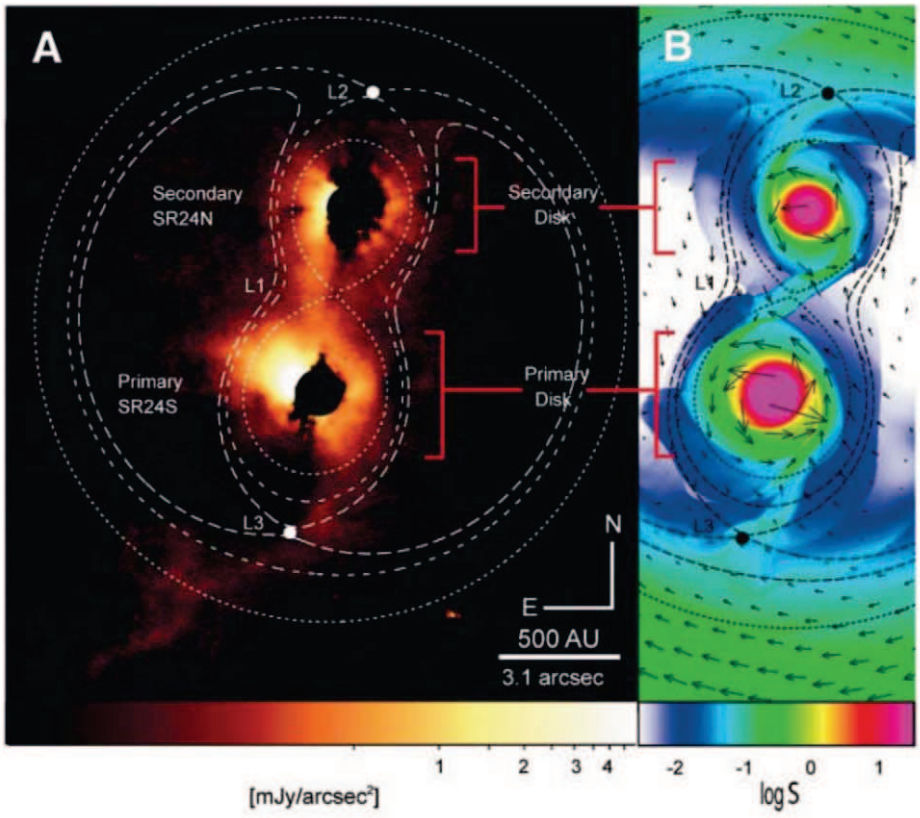

Fig. 1. Observed and simulated images of the young multiple star SR24. (**A**) H-band (1.6-μm) coronagraphic image of SR24 after point spread function (PSF) subtraction of SR24S and SR24N. The total integration time was 1008 s. The length of the bar indicates 500 AU or 3.1 arc sec. The unit of the color bar is mJy/arc sec^2. North is up, and east is toward the left. The edges of the image (east, 2.7 arc sec region; west, 5.1 arc sec region; north, 3.6 arc sec region; and south, 2.3 arc sec region) were trimmed away because no emission was seen on these regions. The PSFs of the final images have sizes of 0.1 arc sec (full width at half maximum) for the H band. The inner and outer Roche lobes are overlaid on the Subaru image as dotted and dashed lines, respectively. L1, L2, and L3 represent the inner Lagrangian point, outer Lagrangian point on the secondary side, and outer Lagrangian point on the primary side, respectively. (**B**) Snapshot of accretion onto the binary system SR24 based on 2D numerical simulations. The color and arrows denote the surface density distribution and velocity distribution, respectively. In the simulations, we treated SR24 as a binary system composed of SR24S and SR24N instead of a triple system composed of SR24S, SR24Nb, and SR24Nc. In the simulation, the SR24 system rotated counterclockwise as suggested by the morphology of the spiral arm.

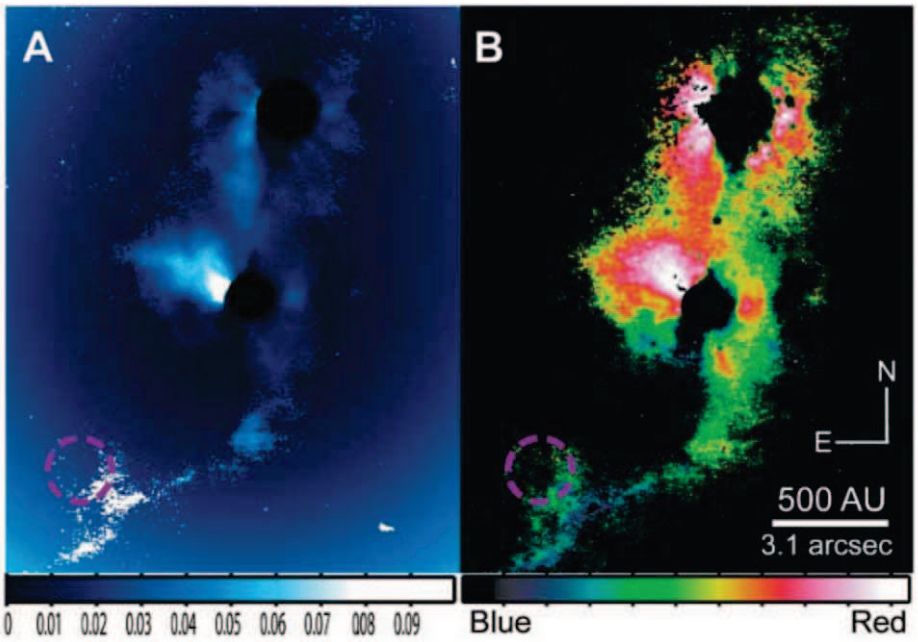

Fig. 2. Effective reflectivity and H-optical images of SR24. The length of the bar indicates 500 AU or 3.1 arc sec. North is up, and east is toward the left. The emission indicated by the purple ring is a ghost. (**A**) Effective reflectivity of SR24 as defined by Eq. 1. (**B**) Ratio of magnitudes at 1.6 μm (H band) and 0.61 μm (optical) of SR24. We retrieved the optical image from the Hubble Space Telescope archive; it was obtained by the Wide Field and Planetary Camera 2 on 28 May 1999, with a total integration time of 500 s. A large ratio of H-band–to–optical magnitude is denoted by red, and a small ratio is denoted by blue.

The eastern part is brighter in both the circumprimary and circumsecondary disks, which suggests that this part is the near side of the disk if we assume that forward scattering dominates, as is the case for Mie scattering of dust grains in the disks.

The primary disk has a larger radial extent than the secondary disk. This is consistent with the fact that only the primary disk was detected in the millimeter-continuum emission (*17*). This may indicate a longer lifetime of the primary disk, as suggested by statistics (*18*). It is also consistent with the accretion rates derived from the hydrogen recombination lines. The mass accretion rate of SR24S is $10^{-6.90}$ $M_{\odot}$/year (*19*) and is significantly higher than that of SR24N, $10^{-7.15}$ $M_{\odot}$/year. Our observations are consistent with expectations from the theory that gas is replenished from the circumbinary disk to the circumstellar disks, which was originally proposed by Artymowicz and Lubow (*20*) but has not been confirmed by direct observations. Moreover, our direct imaging observations show structures associated with a young multiple system that cannot be reproduced by spectroscopic observations or spectral energy distribution model studies.

References and Notes

1. F. H. Shu, F. C. Adams, S. Lizano, *Annu. Rev. Astron. Astrophys.* **25**, 23 (1987).
2. J. S. Greaves, *Science* **307**, 68 (2005).
3. A. M. Ghez, G. Neugebauer, K. Matthews, *Astron. J.* **106**, 2005 (1993).
4. Ch. Leinert *et al.*, *Astron. Astrophys.* **278**, 129 (1993).
5. P. Artymowicz, S. H. Lubow, *Astrophys. J.* **421**, 651 (1994).
6. R. Chini, *Astron. Astrophys.* **99**, 346 (1981).
7. Recent astrometric observations report that the distance to the Ophiuchus star-forming region is 120 ± 5 pc (*8*). However, we adopted a conventional distance of 160 pc in order to compare our data with previous studies.
8. M. Lombardi, C. J. Lada, J. Alves, *Astron. Astrophys.* **480**, 785 (2008).
9. S. M. Andrews, J. P. Williams, *Astrophys. J.* **659**, 705 (2007).
10. S. Correia, H. Zinnecker, Th. Ratzka, M. F. Sterzik, *Astron. Astrophys.* **459**, 909 (2006).
11. H. Takami *et al.*, *Proc. SPIE* **4839**, 21 (2003).
12. M. Tamura *et al.*, *Proc. SPIE* **4008**, 1153 (2000).
13. Materials and methods are available as supporting material on *Science* Online.
14. Although we refer to this emission as a bridge, the word is not used here in the kinematic sense.
15. Because its inclination is difficult to evaluate, we assumed that SR24 is face-on for simplicity.
16. T. P. Greene, B. A. Wilking, P. Andre, E. T. Young, C. J. Lada, *Astrophys. J.* **434**, 614 (1994).
17. S. M. Andrews, J. P. Williams, *Astrophys. J.* **619**, L175 (2005).
18. R. J. White, A. M. Ghez, *Astrophys. J.* **556**, 265 (2001).
19. A. Natta, L. Testi, S. Randich, *Astron. Astrophys.* **452**, 245 (2006).
20. P. Artymowicz, S. H. Lubow, *Astrophys. J.* **467**, L77 (1996).

21. This report is based on data collected at the Subaru Telescope, which is operated by the National Astronomical Observatory of Japan. The Hubble Space Telescope data presented here were obtained from the Multimission Archive at the Space Telescope Science Institute (MAST). The numerical simulations were performed on a Hitachi SR110000 at the Institute of Media and Information Technology, Chiba University, Japan. S.M. acknowledges a fellowship from the Japan Society for the Promotion of Science. This work is supported by grants-in-aid from the Ministry of Education, Culture, Sports, Science and Technology of Japan.

Supporting Online Material www.sciencemag.org/cgi/content/full/science.1179679/DC1 Methods References

27 July 2009; accepted 11 November 2009
Published online 19 November 2009;
10.1126/science.1179679
Include this information when citing this paper.

How the Shape of an H-Bonded Network Controls Proton-Coupled Water Activation in HONO Formation

Rachael A. Relph,[1] Timothy L. Guasco,[1] Ben M. Elliott,[1] Michael Z. Kamrath,[1] Anne B. McCoy,[2] Ryan P. Steele,[1] Daniel P. Schofield,[3] Kenneth D. Jordan,[3] Albert A. Viggiano,[4] Eldon E. Ferguson,[5] Mark A. Johnson[1]*

Many chemical reactions in atmospheric aerosols and bulk aqueous environments are influenced by the surrounding solvation shell, but the precise molecular interactions underlying such effects have rarely been elucidated. We exploited recent advances in isomer-specific cluster vibrational spectroscopy to explore the fundamental relation between the hydrogen (H)–bonding arrangement of a set of ion-solvating water molecules and the chemical activity of this ensemble. We find that the extent to which the nitrosonium ion (NO^+) and water form nitrous acid (HONO) and a hydrated proton cluster in the critical trihydrate depends sensitively on the geometrical arrangement of the water molecules in the network. Theoretical analysis of these data details the role of the water network in promoting charge delocalization.

The strong directionality of the hydrogen bond in water supports a myriad of isomeric architectures in small water clusters (*1*, *2*). This has important implications for the mechanism of hydrolysis reactions in aqueous media, where the cooperativity inherent in the inter-water H-bond is generally thought to induce varying degrees of chemical activation for water molecules occupying distinct sites in an extended network (*3*, *4*). One example of this phenomenon is the often-invoked Grotthuss or relay mechanism for proton transport, thought to be facilitated by the formation of "water wires" (*5*). However, elucidation of the relation between the H-bonding arrangement of a set of water molecules and the chemical activity of this ensemble has proven difficult to establish by direct measurements, illustrating the need for laboratory studies to establish quantitative paradigms for their behavior. This requires determination of the number and character of the isomeric forms generated by sequential condensation. The ion chemistry in the D region of the ionosphere provides another excellent example in which formation of a microscopic wire was envisaged to control the key step in the reaction responsible for the production of nitrous acid (HONO) and the protonated water clusters that dominate the ambient cation distribution (*6*, *7*)

$$NO^+(H_2O)_n + H_2O \rightarrow \{NO^+(H_2O)_{n+1} \rightleftharpoons [(HONO)H^+(H_2O)_n]\} \rightarrow H^+(H_2O)_n + HNO_2 \quad (1)$$

A key property of this intrinsically solvent-mediated reaction system is that, because it is nearly thermoneutral in the tetrahydrate ($n = 4$) clusters (*8*, *9*), controlled addition of water molecules through this critical size range can effectively titrate the extent of conversion to HONO product (*8*, *10*). With the use of advanced gas-phase cluster-ion techniques, we have synthesized and structurally characterized the $NO^+(H_2O)_{1\text{-}4}$ clusters. Furthermore, we have identified multiple isomers for the $n = 3$ and 4 clusters, and theoretical analysis of these results reveals how both the size and shape of the water network facilitate ON–O bond formation between nitrosonium and an activated water molecule, with concomitant proton translocation onto the water network.

The chemical compositions and structures of the associated H-bonded networks in size-selected $NO^+(H_2O)_n$ cluster ions were determined by analysis of the respective vibrational spectra. Although nominally similar to the earlier spectroscopic study of these clusters (*8*), the present effort exploits dramatic improvements in the preparation and spectroscopic characterization of clus

[1]Department of Chemistry, Yale University, Post Office Box 208107, New Haven, CT 06520, USA. [2]Department of Chemistry, The Ohio State University, 100 West 18th Avenue, Columbus, OH 43210, USA. [3]Department of Chemistry, University of Pittsburgh, Pittsburgh, PA 15260, USA. [4]Air Force Research Laboratory, Space Vehicles Directorate, Hanscom Air Force Base, MA 01731, USA. [5]Climate Monitoring and Diagnostics Laboratory, National Oceanic and Atmospheric Administration, Boulder, CO 80305, USA.

*To whom correspondence should be addressed. E-mail: mark.johnson@yale.edu

ter ions. Specifically, whereas the previous study was carried out with the use of infrared multiple photon dissociation (IRMPD) of bare $NO^+(H_2O)_n$ clusters (which undoubtedly retain considerable internal energy), we implement the predissociation messenger technique (*11*) to exclusively monitor vibrationally cold ions in a one-photon (linear) action regime. This allows access to minimum-energy structures that can be characterized over a much broader spectral range. Moreover, we incorporate the capability of sorting isomeric contributions to the ion ensemble with the use of photochemical hole burning (*12*). The resulting spectra of the Ar-tagged $n = 3$ and 4 clusters are qualitatively different than those obtained by IRMPD, including the appearance of strong, broad absorptions in the 2600 to 3000 cm^{-1} range that are telltale signatures of substantial charge delocalization onto intracluster water networks (*13*).

Figure 1 shows the vibrational spectra of the Ar-tagged $NO^+(H_2O)_{1-4}$ clusters in traces A to D, respectively, with the band positions collected in Table 1. Some transitions are common to all of the complexes, such as those highest in energy (3600 to 3800 cm^{-1}) arising from free OH groups and the intramolecular HOH bending mode near 1600 cm^{-1}. The two most important regions, however, are the ranges that explore the extent of charge concentration on the NO^+ solute ion and on the water network. These are highlighted by the color bars at the top of trace A, where the left bar bridges the limiting values for the NO moiety, and the right bar applies to the corresponding situation in water. Note that charge concentration has complementary spectral effects on the two components: As charge is redistributed from the NO^+ onto the water network, the NO stretch evolves from 2344 cm^{-1} in the bare ion (*14*) to 1700 cm^{-1} in the neutral *trans*-HONO product (*15*), whereas the OH stretches vary from ~3700 cm^{-1} in neutral, isolated water (*16*) to 2665 cm^{-1} in the fully hydrated hydronium product (*13*).

The two smallest hydrates (traces A and B) are dominated by transitions associated with essentially neutral water molecules (HOH bend and OH stretches), in addition to a sharp feature close to the limiting value for the isolated NO^+ ion. The calculated structures [coupled-cluster singles and doubles (*17*–*20*)/with the aug-cc-pVDZ basis set (*21*, *22*) (CCSD/aug-cc-pVDZ)] of the $n = 1$ and 2 complexes, displayed as insets, readily explain the observed bands in the context of charge-localized, hydrated NO^+ reactant ions, as inferred from earlier work (*8*). The present spectra also reveal an interesting and important aspect of the NO^+ fundamental transition, which is substantially weakened in the dihydrate and closer to its location in the bare ion (2344 cm^{-1}). Calculations indicate that there is a very strong correlation between red shift in this peak and its intensity. This occurs because the intrinsic intensity in the bare ion is actually quite small (recall that NO^+ is isoelectronic with N_2 and CO), and it gains intensity in the monohydrate through symmetry breaking, along with a small degree of intracluster charge transfer. The blue shift in the NO^+ stretch in the dihydrate is therefore consistent with less perturbation of the NO^+ solute and concomitant diminution in the intensity of its vibrational fundamental. The location and intensity of the NO^+ transition thus provide a convenient, embedded "reporter" for the extent of charge transfer occurring in a particular environment.

Figure 1C presents the spectrum of the trihydrate. Unlike previous work by Choi (*8*), which recovered very similar spectra for $n = 1$, 2, and 3, the Ar-tagged trihydrate displays a much more complex series of bands. The NO stretching region is especially revealing because it features a suite of three peaks, with the weakest (α) lying closest to that of bare NO^+ and the most intense (γ) occurring 257 cm^{-1} below this value, but still well above the characteristic 1700 cm^{-1} N–O

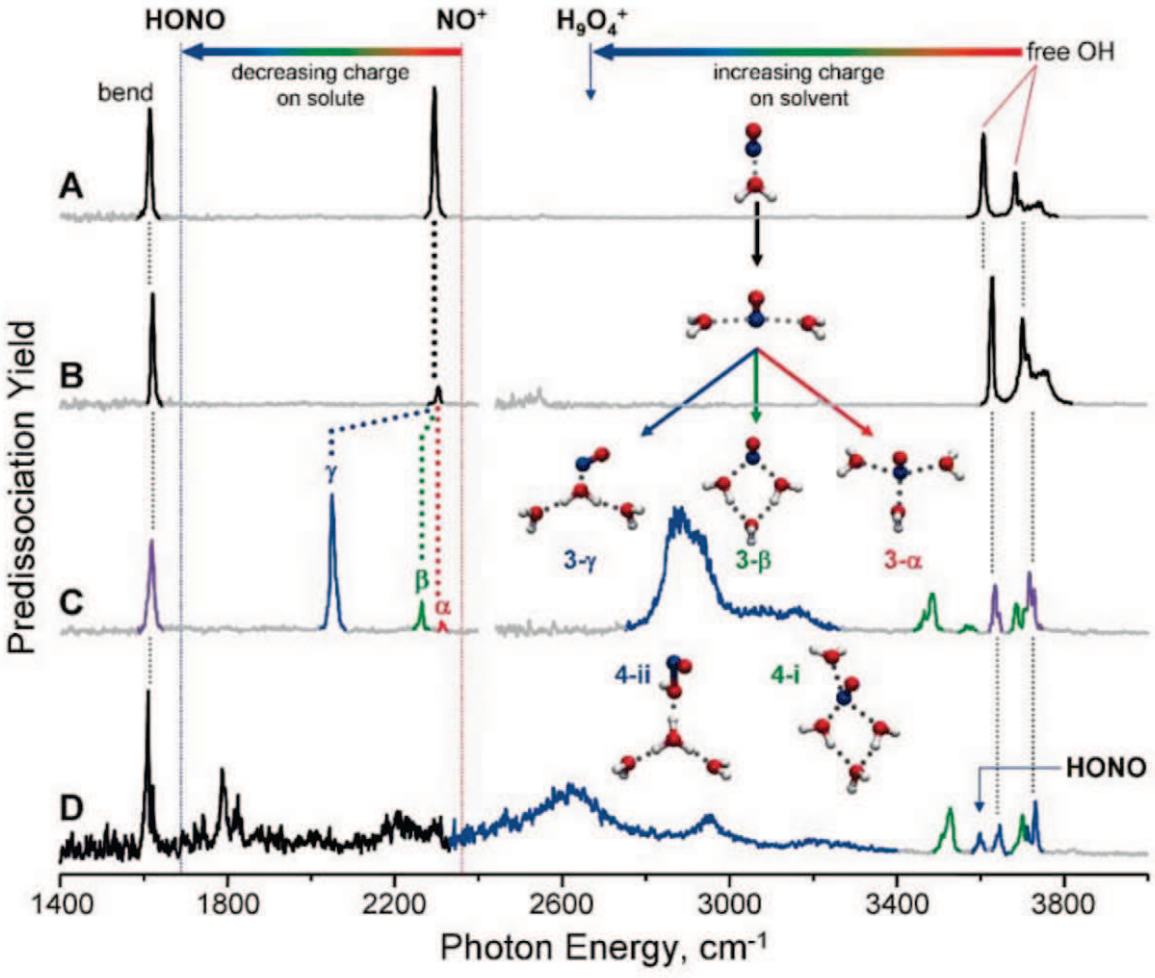

Fig. 1. Vibrational predissociation spectra of $NO^+(H_2O)_n \cdot Ar$, $n = 1$ to 4 [(**A** to **D**), respectively], showing the effect of charge migration in the isomeric structures of the NO^+ hydrates (inset structures calculated at the CCSD/aug-cc-pVDZ level). Features in blue correspond to the isomer labeled 3-γ in (C), whereas those in green and red correspond to the isomers labeled 3-β and 3-α, respectively. The OH stretches in purple are transitions shared with 3-γ and 3-α, whereas the bend near 1600 cm^{-1} is common to all three isomers. The assignments are derived using the photochemical hole-burning method as illustrated in Fig. 2. The effect of decreasing charge localization on the NO moiety is seen in the progression of NO stretch transitions labeled α, β, and γ in (C) and is associated with a concomitant increase in positive charge on the water network, which red shifts and broadens the H-bonded OH stretching transitions. Dotted lines follow evolution of peaks upon increasing solvation.

stretching band in isolated *trans*-HONO (*15*). This suggests that three forms of the trihydrate are present with varying degrees of charge delocalization. The transfer of the positive charge from the NO^+ moiety to the water network should induce perturbations in the OH stretch vibrations. The spectrum in Fig. 1C exhibits a very strong and broad feature near 2900 cm^{-1}, far below the range accessible by the neutral water trimer (*23*) but reminiscent of the low-energy bands found earlier for protonated water clusters (*13*). Finally, the $n = 4$ spectrum is shown in Fig. 1D, where the transitions in the solute region now occur quite close to the limiting value for HONO, and the broad bands in the OH stretching region fall at the same location as the dominant transition in the fully hydrated hydronium ion, $H_9O_4^+$ (*13*).

The complex behavior of the trihydrate spectrum presents the opportunity to explore how distinct solvent arrangements participate in the creation of the ON–OH bond. Such information is encoded in the correlated band patterns displayed by the solute and solvent components of each isomer, leading us to establish the number of isomers present in the ensemble and to isolate each of their spectra. Figure 1 summarizes the results of this effort with a color scheme in which red denotes hydration morphologies that promote localization of the excess charge on the NO^+ reactant, blue designates those associated with extensive intracluster charge transfer, and green presents an intermediate case. Below we describe the experimental and theoretical methodologies used to unravel this picture of solvent-mediated chemistry in a regime where the solvent coordinate is explicitly revealed at the molecular level.

We used IR-IR double resonance (IR^2DR) to obtain isomer-selective spectra. Details of this method are included in the supporting online material (SOM) and also in (*12*). As there are three distinct features in the region nominally associated with NO stretches in Fig. 1C, we first carried out measurements in a single-point mode to verify that these bands are indeed due to different isomers. This was accomplished by tuning a probe laser to each of the three features (α, β, γ) and then saturating other selected transitions throughout the spectrum with a powerful pump laser located before the probe. The results of this procedure are shown in fig. S2 in the SOM and confirm that three isomers are present. Only band γ, the most red-shifted of the NO stretches, is correlated with the broad structure near 2900 cm^{-1}, whereas band β is linked to the sharper band at 3484 cm^{-1}. Band α, the weakest and highest in energy of the three, actually carries most of the intensity of the intramolecular water bend at ~1600 cm^{-1} and is associated with the sharp free OH stretch structure above 3630 cm^{-1}. We denote the three isomers of the trihydrate (3-α, 3-β, and 3-γ) on the basis of the respective NO stretching signature of each.

Because the initial double-resonance survey revealed overlapping bands in the congested region of the free OH stretches (3630 to 3800 cm^{-1}), we carried out the measurements with the pump laser in a scanning mode to capture all the transitions associated with the particular isomer isolated by the probe. This approach was limited to the high-energy (>2500 cm^{-1}) part of the spectrum, where there is sufficient laser power available to saturate the transitions and thus cause large modulations of the probe signal. The resulting spectra are presented in Fig. 2. Figure 2C reproduces the nonselective spectrum (Fig. 1C), whereas the negative-going peaks in the dip spectra (Fig. 2, E and F) result from tuning the probe laser to the frequency indicated by the dagger (†) and asterisk (*), which were linked by fixed point IR^2DR to isomers 3-β and 3-γ, respectively. This procedure establishes that 3-β (Fig. 2E, green) contributes a close doublet in the congested free OH stretching region, whereas 3-γ (Fig. 2F, blue) accounts both for the very broad structure near 2900 cm^{-1} and for two other sharp doublets appearing close to the free OH stretches of bare water. Transitions arising from mixed contributions of the isomers are displayed in purple. Note that the relative intensities of the high-energy OH stretching bands traced to 3-β and 3-γ are similar. Moreover, 3-α also contributes substantially to the free OH stretching bands near 3640 and 3720 cm^{-1} (fig. S1). Because the intrinsic intensities of the spectator OH stretches are not strongly dependent on network shape, we conclude that all three isomers are created in similar abundances. The strongly skewed intensities of the NO-based transitions (α, β, γ) can be mostly traced to the intrinsic diminution in the oscillator strength as the transition energy approaches that of the bare NO^+ fundamental.

Turning to the structural assignments of the isomers, we note that 3-α exhibits the least amount of charge transfer from the NO^+ solute, with its NO stretch (band α at 2264 cm^{-1}) falling closest to that of the bare NO^+ fundamental. This feature falls in line with the NO^+ progression established in the $n = 1$ and 2 spectra and is correlated with only the highest-energy OH stretching bands. This pattern reveals that 3-α is a simple extension of the ion-centered hydration morphology evident at smaller size, with the three noninteracting water molecules independently attached to the N atom of the NO^+ ion. The minimum energy structure with this hydration motif is indicated in Fig. 2A, along with the calculated spectrum (see SOM for details on the anharmonic frequency calculations). This structural assignment is useful because it allows us to gauge the level of theory needed to treat various regions of the vibrational spectrum, given the substantial computational challenges presented by these complexes (SOM text and fig. S3). This structure was the only form identified in the earlier study of the bare ions (*8*).

The structural assignment of 3-β is straightforward based on the marked similarity of its spectrum with that of the related $Cs^+(H_2O)_3$ cluster studied extensively by Miller and Lisy (*24*). That system adopts a cyclic arrangement in which two H-bond acceptor-donor (AD) water molecules attach to the ion and support the third (AA) water molecule located diagonally across the diamond from the ion. The cyclic arrangement has been reported as the global minimum of the $NO^+(H_2O)_3$ cluster (*25*) and is illustrated in Fig. 2B, along with the calculated spectrum for this structure. All important bands in its observed spectrum are recovered as fundamental transitions by this procedure. The resulting assignments of the bands are indicated in Table 1, where the † band is traced to the bonded OH stretches of the AD water molecules.

Table 1. Experimental frequencies (±5 cm^{-1}) for the Ar-tagged $NO^+(H_2O)_n$, $n = 1$ to 4 clusters. Values in parentheses have not yet been assigned by the isomer selective method. Literature values for NO^+, HONO, and H_2O are taken from (*14*–*16*), respectively. ND, not determined; NA, not applicable; sym, symmetric; asym, asymmetric.

Dominant vibrational motion	Literature values	Observed frequencies (cm^{-1})						
		$n = 1$	$n = 2$	$n = 3$ (3-α)	$n = 3$ (3-β)	$n = 3$ (3-γ)	$n = 4$ (4-i)	$n = 4$ (4-ii)
H_2O bend	1595	1620	1627	1621	1621	1621	(1611)	ND
NO^+/NO stretch	2344/1876	2294	2306	2312	2264	2055	(2293)	(1741) (1790)
H_3O^+ motions	NA	NA	NA	NA	NA	NA	NA	(1826) (2180) (2204)
H_2O bend overtone	NA	3203	3218	ND	ND	ND	ND	ND
Shared H^+ stretches	NA	NA	NA	NA	NA	2884 3178	NA	2635 2941 3197
H_2O sym stretch	3657	3607	3628	3637 3644	3466 3484 3577	3637 3644	3526	3645
HNO_2 OH stretch	3590	NA	NA	NA	NA	NA	NA	3597
H_2O asym stretch	3756	3687	3702	3718 3728	3689 3704	3718 3728	3699	3730

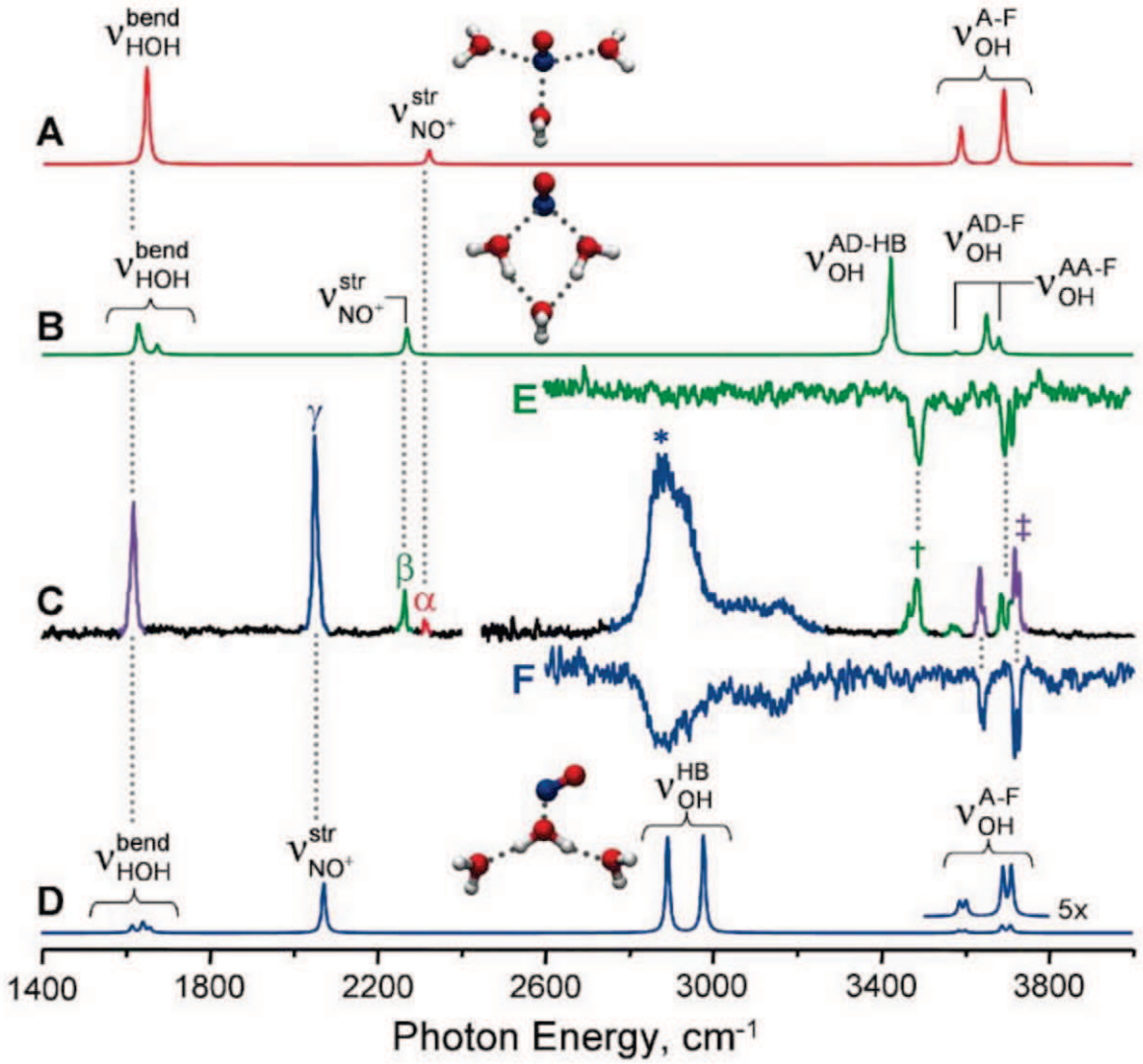

Fig. 2. The vibrational spectrum of $NO^+(H_2O)_3 \cdot Ar$ is reproduced from Fig. 1C in (**C**), flanked by the predissociation dip spectra (**E**) and (**F**) obtained by probing the transitions labeled with the green dagger (†) and blue asterisk (*), respectively. The OH stretches of the third isomer were recovered by probing the transition labeled with the purple double dagger (‡) (see SOM). Calculated (anharmonic, see SOM) spectra for isomers contributing to this spectrum are shown in (**A**), (**B**), and (**D**), with the transitions labeled according to the displacements dominating each mode. In the band assignments (ν), the letters A and D indicate hydrogen-bond (HB) acceptor and donor, respectively; F denotes a free OH group; and str indicates a stretching motion. To account for the energy normalization of the experimental spectra, the calculated transition intensities have been divided by the frequency and have all been normalized to the most intense transition.

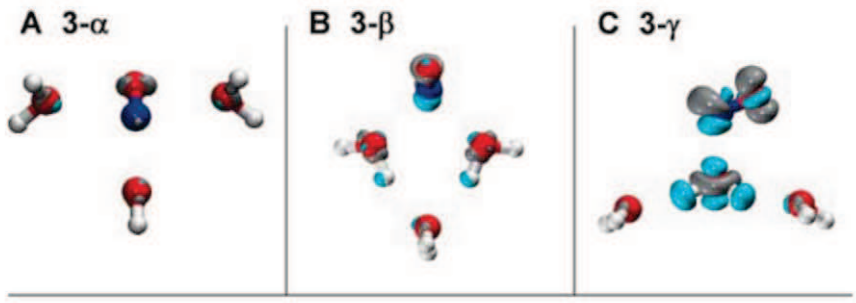

Fig. 3. (**A** to **C**) Electron density difference plots [isovalue = 0.005 atomic units (e/a_0^3, where e is the elementary charge and a_0 is the Bohr radius)] illustrating the differences in charge localization in each of the three $NO^+(H_2O)_3$ clusters relative to its isolated constituents. Gray and teal correspond to increases and decreases in electron density, respectively. The table below (A) to (C) shows the calculated [CCSD(T)/aug-cc-pVDZ, as detailed in the SOM] energies, with zero point energy (ZPE) corrections included in parentheses relative to the lowest-energy isomer, 3-β, for the three structures (optimized at the CCSD/aug-cc-pVDZ level), as well as important bond lengths associated with the NO and the waters in the first solvation shell. r_{NO} denotes the nitrosonium bond, r_{ON-O} is the O-N bond in the process of forming, r_{XO-H} is the O-H bond in the HONO product or bare water, and $r_{XO\ldots H}$ denotes the O-H bond that breaks in the process of proton transfer to the water network.

Calculated Parameters

	3-α	3-β	H_2O	NO^+	HONO	3-γ
ΔE (+ZPE), kcal/mol	2.877 (0.861)	0.0 (0.0)				2.332 (1.695)
r_{NO}, Å	1.075	1.078		1.063	1.173	1.093
r_{ON-O}, Å	2.421	2.334			1.441	1.987
r_{XO-H}, Å	0.965	0.965	0.958		0.947	0.988
$r_{XO\cdots H}$, Å	0.966	0.973	0.958			0.986

The two keys to the structure of the 3-γ isomer are the broad band near 2900 cm^{-1} and the 2055 cm^{-1} (γ) band. Though strongly red-shifted relative to the free OH stretches, the 2900 cm^{-1} feature actually lies far above that of the $H^+(H_2O)_3$ product (1900 cm^{-1}) (*13*), and the sharp 2055 cm^{-1} band falls about midway between those of NO^+ and HONO (see also fig. S4). This frequency distribution suggests a scenario in which only a fraction of the positive charge is delocalized onto a network of water molecules, with concomitant partial reduction of the charge on the NO^+ moiety. Of the previously reported $NO^+(H_2O)_3$ isomers (*8*, *25*), the structure presented in Fig. 2D is most consistent with the trends in the spectra. The water chain in this arrangement is formally analogous to that in the $H^+(H_2O)_3$ cluster, with the caveat that a covalent ON–O linkage is not fully formed, and as a result, much of the excess charge is retained on the NO moiety. To strengthen this empirical assignment, we calculated the spectrum expected for this structure (Fig. 2D, blue) using the same scheme that recovered the spectra of the other isomers. As all features are accurately reproduced, we conclude that 3-β adopts this Y-shaped arrangement with the band assignments in Table 1.

The identification of the structures and vibrational signatures of the three trihydrate isomers allows us to deduce the mechanics driving solvent-induced charge delocalization. A visual way to gauge the extent of charge-transfer at play between the water network and NO^+ is by construction of isosurfaces for electron density differences between that in the minimum energy structure of the cluster ion and those in the isolated NO^+ and $(H_2O)_n$ subunits. These surfaces are presented in Fig. 3, and they provide a quantitative context for the qualitative charge-delocalization discussion motivated by the empirical interpretation of the observed bands. Specifically, the open 3-α isomer (Fig. 3A), with all water molecules in the first hydration shell, optimizes the electrostatic interaction of NO^+ with the three largely unperturbed water molecules. The fact that this arrangement minimizes intracluster charge-transfer can be rationalized in the context that it cannot effectively stabilize excess charge displaced onto the independent water molecules. The cyclic motif adopted by isomer 3-β with one molecule in the second solvation shell does allow partial stabilization of intracluster charge-transfer, as evidenced in the density difference shown in Fig. 3B, but the interaction between NO^+ and the water molecules is still largely electrostatic in nature. In contrast, isomer 3-γ, with two molecules in the second solvent shell, provides a very favorable solvation environment to accommodate charge accumulation on the water in the first shell. The electronic perturbation revealed in the density difference surface (Fig. 3C) is quite large in this case, where the excess charge density is clearly spread over both the NO^+ reactant and the water molecule to which it will eventually form a covalent bond. Key structural parameters indicating the extent of HONO product formation for the three isomers are included at the bottom of Fig. 3. The H-bonding scaffold adopted by 3-γ can be viewed as a hydrated form of protonated nitrous acid, $ONOH_2^+$. In isolation, this species spontaneously breaks up into an $NO^+ \cdot H_2O$ ion-molecule complex, as we see in the mono- and dihydrates of NO^+. The 3-γ structure places a water molecule on each of the two protons that nominally share the excess charge in protonated nitrous acid, thereby stabilizing this incipient form of the product.

The trihydrate behavior is also of interest in the context of the reaction mechanism for nitrous acid formation (Eq. 1). Many reports (*8*, *9*, *25*) have expanded on an early suggestion (*26*) that the intracluster proton transfer at the heart of this process would be mediated by the formation of linear chains of water molecules. Although different in detail from the proposed structure, the most chemically active isomer recovered here, 3-γ, has many features anticipated by the linear "water wire" model. In particular, our calculations recover the relative energies of the three isomers and find 3-γ to be highest in energy, ~1.7 kcal/mol above the global minimum (isomer 3-β). As such, we expect this structure to be sparsely populated at the ambient temperature of the ionosphere (200 K = 0.397 kcal/mol) (*7*). The reaction is observed to occur upon attachment of the fourth water molecule, and the present experiment allows us to explore the reactivity of each isomer as an independent reactant. This is possible because the ion source produces the larger water clusters through sequential condensation reactions onto the clusters with several attached Ar atoms

$$NO^+(H_2O)_n \cdot Ar_m + H_2O \rightarrow$$

$$NO^+(H_2O)_{n+1} \cdot Ar_p + (m - p)Ar \quad (2)$$

As such, the three isomers of the trihydrate are, in fact, the precursors of the $n = 4$ cluster probed spectroscopically.

We therefore carried out a double-resonance survey of the tetrahydrate and found the resulting spectrum (shown in Fig. 1D) to be a superposition of at least two components. Specifically, the $n = 4$ band, close to the † feature in the 3-β spectrum (Fig. 2C), arises from a different species than that responsible for the strong $n = 4$ product bands near 2665 cm^{-1}. This indicates that a large fraction of the tetrahydrate ensemble maintains a pre-reactive, charge-localized form, with the characteristic † band signaling preservation of the cyclic hydration motif. On the other hand, the bands uniquely associated with 3-γ disappear in the $n = 4$ spectrum, suggesting that 3-γ is fundamentally transformed upon addition of another water molecule. Note that the bands arising from the two classes of the tetrahydrate occur with similar relative intensities as those from the different $n = 3$ precursors. This raises the interesting scenario that, under experimentally accessible conditions, the sequential condensation events can be trapped in relatively high-energy, persistent configurations that form preferential reactive pathways. The evidence for such isomer-specific reactivity obtained here warrants further exploration to define the general conditions under which this mechanism can be operative.

References and Notes

1. D. J. Wales, M. A. Miller, T. R. Walsh, *Nature* **394**, 758 (1998).
2. C. J. Tsai, K. D. Jordan, *Chem. Phys. Lett.* **213**, 181 (1993).
3. M. Beyer, E. R. Williams, V. E. Bondybey, *J. Am. Chem. Soc.* **121**, 1565 (1999).
4. G. Niedner-Schatteburg, V. E. Bondybey, *Chem. Rev.* **100**, 4059 (2000).
5. N. Agmon, *Chem. Phys. Lett.* **244**, 456 (1995).
6. F. C. Fehsenfeld, E. E. Ferguson, *J. Geophys. Res. Space Phys.* **74**, 2217 (1969).
7. R. S. Narcisi, A. D. Bailey, *J. Geophys. Res.* **70**, 3687 (1965).
8. J. H. Choi *et al.*, *J. Chem. Phys.* **100**, 7153 (1994).
9. E. Hammam, E. P. F. Lee, J. M. Dyke, *J. Phys. Chem. A* **105**, 5528 (2001).
10. A. J. Stace, J. F. Winkel, R. B. Lopez Martens, J. E. Upham, *J. Phys. Chem.* **98**, 2012 (1994).
11. M. Okumura, L. I. Yeh, J. D. Myers, Y. T. Lee, *J. Chem. Phys.* **85**, 2328 (1986).
12. B. M. Elliott *et al.*, *J. Chem. Phys.* **129**, 094303 (2008).
13. J. M. Headrick *et al.*, *Science* **308**, 1765 (2005).
14. K. P. Huber, G. Herzberg, *Molecular Spectra and Molecular Structure: IV. Constants of Diatomic Molecules* (Van Nostrand Reinhold, New York, 1979).
15. M. E. Jacox, in *NIST Chemistry WebBook, NIST Standard Reference Database Number 69*, P. J. Linstrom, W. G. Mallard, Eds. [National Institute of Standards and Technology, Gaithersburg, MD 20899, http://webbook.nist.gov (retrieved 5 May 2009)].
16. T. Shimanouchi, "Molecular Vibrational Frequencies" in *NIST Chemistry WebBook, NIST Standard Reference Database Number 69*, P. J. Linstrom, W. G. Mallard, Eds. [National Institute of Standards and Technology, Gaithersburg, MD 20899, http://webbook.nist.gov (retrieved 28 December 2009)].
17. J. Čížek, in *Advances in Chemical Physics*, vol. 14, P. C. Hariharan, Ed. (Wiley Interscience, New York, 1969), p. 35.
18. G. D. Purvis, R. J. Bartlett, *J. Chem. Phys.* **76**, 1910 (1982).
19. G. E. Scuseria, C. L. Janssen, H. F. Schaefer, *J. Chem. Phys.* **89**, 7382 (1988).
20. G. E. Scuseria, H. F. Schaefer III, *J. Chem. Phys.* **90**, 3700 (1989).
21. T. H. Dunning Jr., *J. Chem. Phys.* **90**, 1007 (1989).
22. R. A. Kendall, T. H. Dunning Jr., R. J. Harrison, *J. Chem. Phys.* **96**, 6796 (1992).
23. U. Buck, F. Huisken, *Chem. Rev.* **100**, 3863 (2000).
24. D. J. Miller, J. M. Lisy, *J. Am. Chem. Soc.* **130**, 15381 (2008).
25. E. Hammam, E. P. F. Lee, J. M. Dyke, *J. Phys. Chem. A* **104**, 4571 (2000).
26. F. C. Fehsenfeld, M. Mosesman, E. E. Ferguson, *J. Chem. Phys.* **55**, 2120 (1971).

27. M.A.J. thanks the Air Force Office of Scientific Research (grant FA-9550-09-1-0139). We also thank the NSF for support under grants CHE-0616198 and CHE-0911199 (M.A.J.), CHE-0809457 (K.D.J.), CHE-0615882 and OISE-0730114 (R.P.S.), and CHE-0515627/CHE-0848242 (A.B.M.). D.P.S. thanks the New Zealand Foundation for Research, Science and Technology for funding, and A.A.V. thanks the Air Force Office of Scientific Research under project 2303EP.

Supporting Online Material www.sciencemag.org/cgi/content/full/327/5963/308/DC1 SOM Text
Figs. S1 to S4
References

1 June 2009; accepted 10 November 2009
10.1126/science.1177118

Electrocatalytic CO_2 Conversion to Oxalate by a Copper Complex

Raja Angamuthu,[1] Philip Byers,[1] Martin Lutz,[2] Anthony L. Spek,[2] Elisabeth Bouwman[1]*

Global warming concern has dramatically increased interest in using CO_2 as a feedstock for preparation of value-added compounds, thereby helping to reduce its atmospheric concentration. Here, we describe a dinuclear copper(I) complex that is oxidized in air by CO_2 rather than O_2; the product is a tetranuclear copper(II) complex containing two bridging CO_2-derived oxalate groups. Treatment of the copper(II) oxalate complex in acetonitrile with a soluble lithium salt results in quantitative precipitation of lithium oxalate. The copper(II) complex can then be nearly quantitatively electrochemically reduced at a relatively accessible potential, regenerating the initial dinuclear copper(I) compound. Preliminary results demonstrate six turnovers (producing 12 equivalents of oxalate) during 7 hours of catalysis at an applied potential of −0.03 volts versus the normal hydrogen electrode.

Research toward carbon dioxide fixation enjoys much attention at present, as a result of the alarming reports that link global warming and its potentially devastating effects with the steadily increasing concentration of CO_2 in the atmosphere. Chemical activation of carbon dioxide could help to reduce its concentration in the atmosphere while at the same time exploiting it as a carbon feedstock for the production of useful organic compounds (*1*–*5*). Transition-metal complexes, especially of copper and zinc (*6*, *7*), as well as simple salts such as lithium hydroxide monohydrate and soda-lime (mixture of sodium and calcium hydroxides) are well known for their assistance in the stoichiometric transformation of carbon dioxide to carbonate salts (*8*–*17*). Mixtures of glycol and amines (glycol-amine) as well as coordination complexes of polyamines have been reported to bind CO_2 reversibly through the formation of carbamates (*8*, *15*, *17*, *18*). In contrast, reductive conversion of CO_2 into useful products of industrial significance such as formaldehyde, formic acid, methanol, or oxalic acid has proven more challenging to achieve selectively (*19*, *20*).

The one-electron reduction of CO_2 into the $CO_2^{\bullet-}$ radical anion occurs at potentials as high as –1.97 V versus NHE (normal hydrogen electrode) in *N,N*-dimethylformamide, and the $CO_2^{\bullet-}$ may further react to form CO, carbonate, formate, or oxalate (*19*–*21*). Selective production of oxalate would be much preferred because dimethyl oxalate is a useful feedstock, for example, for the production of methyl glycolate. The assistance of transition-metal complexes appears mandatory to direct the reactivity of the $CO_2^{\bullet-}$ radical anion toward a specific product, in addition to optimizing electrochemical parameters such as current density. Moreover, the inner-sphere electron-transfer mechanisms that proceed with most transition metal systems result in less-negative reduction potentials, which may improve overall thermodynamic favorability of the reduction, assuming there is an accessible way to liberate the product after the electron-transfer reaction (*20*). Reductive coupling of CO_2 to form the oxalate dianion has been accomplished by electrochemical methods, including outer-sphere electron transfer using mercury or lead electrodes and inner-sphere electron transfer using transition-metal complexes or anion radicals of aromatic hydrocarbons, esters, and nitriles as electrocatalysts (*20*–*22*). Mechanistic understanding of the metal-catalyzed reduction of CO_2 to C_2 or C_3 fragments is also highly relevant for an improved understanding of the natural photosynthetic transformation of atmospheric CO_2 to functionalized C_3 molecules (3-phosphoglycerate).

We herein report a copper complex, which spontaneously captures and reductively couples CO_2 from the air selectively, yielding an oxalate-bridged copper(II) tetramer in acetonitrile solution. Moreover, we have found that this copper system can be used repeatedly as a catalyst for the reductive coupling of CO_2 to oxalate upon electrochemical reduction. The reduction of the copper(II) complex occurs at a readily accessible potential that is nearly 2 V less negative than that required for outer-sphere reduction of CO_2 to $CO_2^{\bullet-}$.

The ligand HL [*N*-(2-mercaptopropyl)-*N,N*-bis(2-pyridylmethyl)amine] was designed for the synthesis of biomimetic models for nickel-containing superoxide dismutase. In addition to studies with nickel salts, reactions were performed with copper and zinc for comparison. Upon mixing of equimolar amounts of $Cu(acac)_2$ (Hacac is acetylacetone), the ligand HL, and HBF_4 in acetonitrile at room temperature, we obtained a yellow-colored solution, in which as expected the thiolate-containing ligand was oxidized by the copper(II) ion. The solution was analyzed with positive-ion electrospray ionization mass spectroscopy (ESI-MS); a prominent signal at mass/charge (*m/z*) ratio of 335.91 showed an isotopic distribution envelope matching that calculated for the dinuclear copper(I) complex $\mathbf{[1]}^{2+}$ (Fig. 1) (*23*). This complex $\mathbf{[1]}^{2+}$ can also be synthesized by the reaction of the preoxidized disulfide ligand with two equivalents of $[Cu(CH_3CN)_4]BF_4$ in dry acetonitrile. This yellow-colored solution turned greenish-blue upon exposure to air; over the course of 3 days crystals formed, which we isolated in 72% yield and analyzed by x-ray diffraction. We observed a tetranuclear copper(II) structure $[Cu^{II}_2(L\text{-}L)(\mu\text{-oxalato-}\kappa^4O^1,O^2:O^3,O^4)]_2(BF_4)_4$ {$\mathbf{[2]}(BF_4)_4$, Fig. 1}, with bridging oxalate anions that must originate from CO_2 in the air. A positive-ion ESI-MS spectrum acquired from the acetonitrile solution is consistent with this molecular struc-

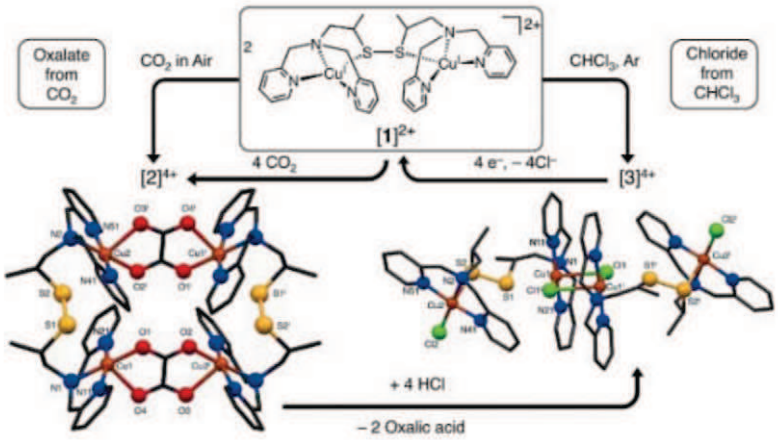

Fig. 1. Schematic overview of the formation and reactivity of the complexes $\mathbf{[1]}^{2+}$, $\mathbf{[2]}^{4+}$, and $\mathbf{[3]}^{4+}$. Cu, brown; N, blue; S, yellow; O, red; Cl, green; C, black. BF_4 anions, solvent molecules, and hydrogen atoms are omitted for clarity. Selected (average) bond lengths (Å) for $\mathbf{[2]}^{4+}$: Cu–O_{eq}, 1.963(2); Cu–O_{ax}, 2.283(2); Cu–N_{py}, 1.991(2); Cu–N_{amine}, 2.026(2); S1–S2, 2.0423(16); Cu1···S1, 2.9837(12); Cu2···S2, 2.9731(12); Cu1···Cu2, 5.3205(6); Cu1···$Cu2^i$, 5.4295(6). Selected (average) bond lengths (Å) for $\mathbf{[3]}^{4+}$: Cu1–$Cl1^i$ 2.2479(6); Cu2–Cl2 2.2440(7); Cu1–Cl1 2.8589(6); Cu–N_{py}, 1.984(1); Cu–N_{amine}, 2.052(2); S1–S2, 2.0388(11); Cu1···S1, 3.0036(9); Cu2–S2, 2.7343(7); Cu1···$Cu1^i$, 3.5677(5); Cu1···Cu2, 6.1248(4). Symmetry operation i; $1-x$, $1-y$, $1-z$. Estimated standard deviations in the last digits are given in parentheses. Further details are provided in (*23*).

[1]Leiden Institute of Chemistry, Gorlaeus Laboratories, Leiden University, Post Office Box 9502, 2300 RA Leiden, Netherlands. [2]Bijvoet Center for Biomolecular Research, Crystal and Structural Chemistry, Utrecht University, Padualaan 8, 3584 CH Utrecht, Netherlands.

*To whom correspondence should be addressed. E-mail: bouwman@chem.leidenuniv.nl

ture, showing a prominent signal at *m/z* of 379.35 (figs. S9 and S10). We thus found that the initial Cu(I) complex is oxidized by CO_2 rather than O_2. Indeed, purging carbon dioxide into a solution of complex $[1]^{2+}$ results in the formation of the tetranuclear oxalate-bridged complex $[2]^{4+}$, which was fully characterized by Fourier transform infrared spectroscopy (FT-IR), ESI-MS, and elemental analysis. That carbon dioxide is the origin of the oxalate dianion was proven with the use of $^{13}CO_2$; the resulting copper(II) complex showed a signal at *m/z* of 381.06 (fig. S11). The reaction of $[1]^{2+}$ in an O_2 atmosphere under strict exclusion of CO_2 resulted in a deep green solution containing a copper(II) compound with a molecular ion peak at *m/z* = 361.16 in positive ion ESI-MS that is consistent with the expected dihydroxo complex of molecular formula $[Cu^{II}(L\text{-}L)Cu^{II}(\mu\text{-}OH)_2(H_2O)]^{2+}$(fig. S12).

In the solid state, $[2]^{4+}$ consists of a cyclic centrosymmetric dimer of two dinuclear moieties bridged by two oxalato dianions (fig. S13). Each dinuclear moiety consists of two crystallographically independent copper(II) ions. The two copper(II) ions within the asymmetric unit bind to the same disulfide ligand and are separated by 5.3205 ± 0.0006 [5.3205(6)] Å. The copper ions are situated in square-pyramidal environments, with the three nitrogen donors of the meridionally coordinated dipicolylamine unit occupying three corners of the basal plane. One of the oxygens from the bridging oxalato dianion is situated at the fourth corner of the basal plane, with another oxygen from the same oxalato dianion occupying the apical position. However, for both copper ions one of the disulfide sulfur atoms can be regarded as a sixth ligand at meaningful axial distances of 2.9837(12) and 2.9731(12) Å. (Further parameters are provided in table S1.)

In an attempt to crystallize the original complex $[1]^{2+}$, chloroform was let to diffuse into the initial reaction mixture containing the copper(I) complex in an argon atmosphere. Interestingly, this yielded the unexpected tetranuclear compound $[ClCu^{II}(L\text{-}L)Cu^{II}(\mu\text{-}Cl)]_2(BF_4)_4$ {$[3](BF_4)_4$, Fig. 1} with bridging and terminal chloride anions that can only originate from chloroform (*24*). The solid-state structure of $[3]^{4+}$ was obtained by x-ray diffraction from a blue crystal of $[3](BF_4)_4$. The molecular structure of $[3]^{4+}$ is confirmed by a positive-ion ESI-MS spectrum of the compound acquired from acetonitrile solution, which shows a prominent signal at *m/z* = 370.71 (figs. S14 and S15). Complex $[3]^{4+}$ is a linear centrosymmetric dimer of two dinuclear moieties bridged by two chloride anions (figs. S16 and S17). The two copper(II) ions within the asymmetric unit are bound to the same disulfide ligand and are separated by 6.1248(4) Å. The copper ions in $[3]^{4+}$ are situated in pentacoordinate environments resembling those in complex $[2]^{4+}$; the thioether sulfur and the chloride donors replace the oxalato oxygen donors in $[2]^{4+}$.

Inspired by this finding, we explored whether complex $[2]^{4+}$ could be converted to this chloride complex $[3]^{4+}$ by treatment with HCl, in the process liberating the CO_2-derived oxalic acid.

Addition of four equivalents of hydrochloric acid to an acetonitrile solution of $[2](BF_4)_4$ indeed leads to elimination of oxalic acid with concurrent formation of $[3](BF_4)_4$ as confirmed by ESI-MS and elemental analysis. The electrochemical reduction of $[3](BF_4)_4$ occurs at the cathodic peak potential (E_{pc}) of +0.06 V versus NHE (fig. S18), producing a copper(I) complex that selectively produces complex $[2]^{4+}$ upon reaction with CO_2. This result stimulated us to explore the possibility of using the copper/disulfide-ligand system as an electrocatalyst for the selective reduction of CO_2.

To that end, we undertook electrochemical reduction of complex $[3]^{4+}$ by using controlled potential coulometry and monitored the process by using electronic absorption spectroscopy. The copper complex $[3](BF_4)_4$ (0.9 g, 0.5 mmol) was dissolved in 100 ml of 0.1 M tetrabutylammonium hexafluoridophosphate in acetonitrile; the solution was then reduced at +0.03 V versus NHE. A current drop was observed after 195 C of charge was passed, the quantity expected for a one-electron reduction of each copper ion. The disappearance of the characteristic *d-d* transition band (~670 nm) of $[3]^{4+}$ during electrolysis confirmed the formation of a copper(I) species (fig. S19). The resulting yellow-colored solution was shown by ESI-MS to contain the dinuclear copper(I) complex $[1]^{2+}$ (fig. S20). The cyclic voltammogram of this solution showed a reversible oxidation process at the anodic peak potential (E_{pa}) of +0.81 V versus NHE (fig. S21).

Bubbling carbon dioxide into this solution turned the color greenish-blue, indicating the formation of complex $[2]^{4+}$ as confirmed by ESI-MS analysis of the solution. The cyclic voltammogram of $[2]^{4+}$ produced in this reaction sequence was identical to that of the independently synthesized and isolated $[2]^{4+}$ and showed an irreversible reduction process at –0.03 V versus NHE (fig. S22). The bulk electrolysis experiment was then repeated under the same conditions but with use of lithium perchlorate as the supporting electrolyte in a CO_2-saturated acetonitrile solution. These conditions resulted in the precipitation of lithium oxalate as the generated copper(I) complex spontaneously reacted with the CO_2 available in the solution to form oxalate (fig. S23). In order to quantify the selectivity of our electrocatalyst, we halted electrolysis after passing 195 C of charge (the charge expected for a one-electron reduction of each copper ion), purged the solution with CO_2, and removed the lithium oxalate precipitate by filtration under an argon atmosphere. The 24-mg (0.24-mmol) yield of lithium oxalate [as confirmed by ESI-MS spectrometry, nuclear magnetic resonance (NMR), and FT-IR spectroscopy, figs. S24 and S25] corresponded to nearly quantitative current efficiency (96%) for formation of the desired product. The remaining blue-colored solution was shown to contain the dinuclear copper(II) complex $[(CH_3CN)Cu^{II}(L\text{-}L)Cu^{II}(CH_3CN)]^{4+}$ $[4]^{4+}$ as characterized by ESI-MS spectrometry (fig. S26). We proceeded to saturate this solution with argon to remove the remaining CO_2 and then subjected it to a second electrolysis run; 185 C of charge was consumed before the current dropped, indicating regeneration of nearly 95% of the copper(I) complex.

Fig. 2. Formation of $[4]^{4+}$ from $[2]^{4+}$ or $[3]^{4+}$.

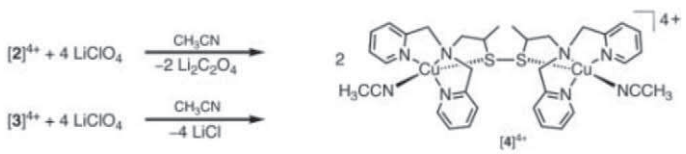

Fig. 3. Proposed electrocatalytic cycle for oxalate formation.

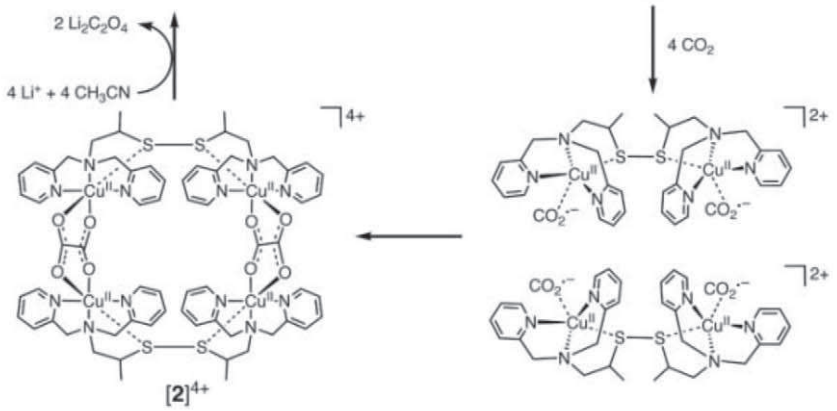

Both complexes $[2]^{4+}$ and $[3]^{4+}$ upon mixing with $LiClO_4$ in acetonitrile yield $[4]^{4+}$ as confirmed by ESI-MS spectrometry (Fig. 2 and figs. S27 and S28). Therefore, in another attempt to use the complex $[2]^{4+}$ as an electrocatalyst in this reaction, the electrochemical cell containing an acetonitrile solution of complex $[2]^{4+}$ and lithium perchlorate (as supporting electrolyte) was stirred to precipitate all the available oxalate. Then the solution was electrolyzed at –0.03 V versus NHE with continuous purging of CO_2. The consumption of current continued linearly for more than 3.3 hours, consuming three equivalents of charge (12 electrons) per four copper ions, with concurrent crystallization of lithium oxalate. Thereafter, the rate of the reaction gradually decreased as the crystallized lithium oxalate started to cover the electrode surface, thereby hampering electron transfer (fig. S29). In total, the electrocatalysis could be extended for more than 7 hours, with consumption of 6 equivalents of charge (24 electrons) and generating 12 equivalents of oxalate per molecule of $[2]^{4+}$.

We have thus devised an electrocatalytic system based on a copper coordination compound that is able to activate and convert CO_2 selectively into oxalate at readily accessible potentials, in the simple but very effective catalytic cycle shown in Fig. 3. The finding that a copper(I) system is oxidized by CO_2 rather than O_2 implies that the selective binding of CO_2 to the copper(I) ions offers a low-energy pathway for the formation of the $CO_2^{\bullet-}$ radical anion. The copper(II) oxalate complex $[2]^{4+}$ is thermodynamically favored; the binding of CO_2 to the Cu(I) centers in $[1]^{2+}$ and the formation of oxalate appears to be highly selective and relatively rapid. Because of the low solubility of lithium oxalate in acetonitrile, the release of the oxalate dianion from $[2]^{4+}$ in the presence of lithium perchlorate is instantaneous, generating the complex $[4]^{4+}$. Therefore, for the current system the electrocatalytic reduction of the copper(II) ion to copper(I) appears to be rate-limiting. The precipitation of the lithium oxalate formed during the reaction onto the electrode surface hampers efficient electron transfer. Tuning the redox potential of the copper complex by altering the ligand structure with a variety of substituents, immobilization of the complex onto the electrode surface, and improved methods for the removal of oxalate may result in improved efficiency of the catalytic system. We believe that our studies will instigate further development of coordination complexes for catalytic CO_2 sequestration, its selective conversion and use as fuels such as methanol or as feedstock in the synthesis of useful organic compounds.

References and Notes

1. T. Reda, C. M. Plugge, N. J. Abram, J. Hirst, *Proc. Natl. Acad. Sci. U.S.A.* **105**, 10654 (2008).
2. M. Aresta, A. Dibenedetto, *Dalton Trans.* **2007**, 2975 (2007).
3. D. P. Schrag, *Science* **315**, 812 (2007).
4. T. Sakakura, J. C. Choi, H. Yasuda, *Chem. Rev.* **107**, 2365 (2007).
5. C. S. Song, *Catal. Today* **115**, 2 (2006).
6. S. Youngme, N. Chaichit, P. Kongsaeree, G. A. van Albada, J. Reedijk, *Inorg. Chim. Acta* **324**, 232 (2001).
7. G. A. van Albada, I. Mutikainen, O. Roubeau, U. Turpeinen, J. Reedijk, *Inorg. Chim. Acta* **331**, 208 (2002).
8. J. Notni, S. Schenk, H. Görls, H. Breitzke, E. Anders, *Inorg. Chem.* **47**, 1382 (2008).
9. B. Sarkar, B. J. Liaw, C. S. Fang, C. W. Liu, *Inorg. Chem.* **47**, 2777 (2008).
10. B. Verdejo *et al.*, *Eur. J. Inorg. Chem.* **2008**, 84 (2008).
11. J. M. Chen, W. Wei, X. L. Feng, T. B. Lu, *Chem. Asian J.* **2**, 710 (2007).
12. A. Company *et al.*, *Inorg. Chem.* **46**, 9098 (2007).
13. R. P. Doyle *et al.*, *Dalton Trans.* **2007**, 5140 (2007).
14. M. Fondo, A. M. García-Deibe, N. Ocampo, J. Sanmartín, M. R. Bermejo, *Dalton Trans.* **2007**, 414 (2007).
15. B. Verdejo *et al.*, *Inorg. Chem.* **45**, 3803 (2006).
16. R. Johansson, M. Jarenmark, A. F. Wendt, *Organometallics* **24**, 4500 (2005).
17. E. García-España, P. Gaviña, J. Latorre, C. Soriano, B. A. Verdejo, *J. Am. Chem. Soc.* **126**, 5082 (2004).
18. H. J. Himmel, *Eur. J. Inorg. Chem.* **2007**, 675 (2007).
19. E. E. Benson, C. P. Kubiak, A. J. Sathrum, J. M. Smieja, *Chem. Soc. Rev.* **38**, 89 (2009).
20. J. M. Savéant, *Chem. Rev.* **108**, 2348 (2008).
21. C. Amatore, J. M. Savéant, *J. Am. Chem. Soc.* **103**, 5021 (1981).
22. Y. Kushi, H. Nagao, T. Nishioka, K. Isobe, K. Tanaka, *J. Chem. Soc. Chem. Commun.* **1995**, 1223 (1995).
23. Synthesis and characterization details are provided as supporting material on *Science* Online.
24. A similar reactivity of coordination complexes with chloroform has been observed and reported before; see, for example, (*25*).
25. I. M. Angulo *et al.*, *Eur. J. Inorg. Chem.* **2001**, 1465 (2001).

26. This work was supported by the Leiden Institute of Chemistry. X-ray crystallographic work was supported (M.L. and A.L.S.) by the Council for the Chemical Sciences of The Netherlands Organization for Scientific Research (CW-NWO). J. Reedijk and M. T. M. Koper are gratefully acknowledged for stimulating discussions. P.B. (Ithaca College, New York) was involved in the project through a summer exchange program. Crystallographic data for $[2](BF_4)_4$ and $[3](BF_4)_4$ have been deposited with the Cambridge Crystallographic Data Center under reference numbers 717726 and 717727.

Supporting Online Material www.sciencemag.org/cgi/content/full/327/5963/313/DC1 Materials and Methods
SOM Text
Figs. S1 to S30
Tables S1 and S2
References

19 June 2009; accepted 25 November 2009
10.1126/science.1177981

Ligand-Enabled Reactivity and Selectivity in a Synthetically Versatile Aryl C–H Olefination

Dong-Hui Wang, Keary M. Engle, Bing-Feng Shi, Jin-Quan Yu*

The Mizoroki-Heck reaction, which couples aryl halides with olefins, has been widely used to stitch together the carbogenic cores of numerous complex organic molecules. Given that the position-selective introduction of a halide onto an arene is not always straightforward, direct olefination of aryl carbon-hydrogen (C–H) bonds would obviate the inefficiencies associated with generating halide precursors or their equivalents. However, methods for carrying out such a reaction have suffered from narrow substrate scope and low positional selectivity. We report an operationally simple, atom-economical, carboxylate-directed Pd(II)-catalyzed C–H olefination reaction with phenylacetic acid and 3-phenylpropionic acid substrates, using oxygen at atmospheric pressure as the oxidant. The positional selectivity can be tuned by introducing amino acid derivatives as ligands. We demonstrate the versatility of the method through direct elaboration of commercial drug scaffolds and efficient syntheses of 2-tetralone and naphthoic acid natural product cores.

Unactivated carbon–hydrogen (C–H) bonds are among the simplest and most common structural motifs in naturally occurring organic molecules, and, as such, they are ideal targets for chemical transformations. Although C–H bonds are generally unreactive, during the past several decades transition metal catalysis has emerged as an effective means of converting unactivated C–H bonds into carbon–heteroatom and carbon–carbon (C–C) bonds (*1*–*5*). This technology has proven to be valuable in natural products synthesis, where several distinct C–H functionalization strategies have been exploited (*6*–*12*).

Traditionally, C–C bonds between aryl and olefinic fragments have been forged through the Pd-catalyzed Mizoroki-Heck reaction, which couples aryl halides or triflates with olefins (Fig. 1A). Considering the prominence of this transformation in organic synthesis (*13*), Pd-catalyzed olefination of aryl C–H bonds has the potential to emerge as a powerful platform for more direct access to carbogenic cores of complex molecules (Fig. 1, A and E), particularly in cases in which the position-selective introduction of a halide is problematic. However, the few pioneering examples of Pd-catalyzed C–H olefination in total synthesis to date are restricted to specific cases, generally including electron-rich heterocycles, such as indoles and pyrroles, and/or

Scripps Research Institute, 10550 North Torrey Pines Road, La Jolla, CA 92037, USA.

*To whom correspondence should be addressed. E-mail: yu200@scripps.edu

stoichiometric palladium (*14*–*17*). The development of Pd-catalyzed arene C–H olefination reactions to provide general routes to commonly occurring carbogenic motifs thus remains an outstanding challenge. This limitation is rooted in two interrelated problems. First, the substrates that are typically effective in palladium-catalyzed C–H activation are synthetically restrictive, either because they are limited to electron-rich arenes or heterocycles, or because they possess impractical chelating functional groups to promote metalation. These directing groups include those that are irremovable and recalcitrant to undergo further synthetic elaboration, such as pyridine, and those that are removable but require several steps for installation and detachment, such as oxazoline (*5*). Second, methods for effecting position-selective C–H activation on multiply substituted arenes (*18*, *19*), particularly via ligand control, remain underdeveloped.

Here, we report a catalytic system that addresses these problems. A practical Pd-catalyzed reaction using molecular oxygen as the terminal oxidant has been developed to perform C–H olefination with synthetically useful phenylacetic acid and 3-phenylpropionic acid substrates. This reaction has remarkably broad substrate scope, which is enabled in part by the use of amino acid ligands to enhance the reactivity of the catalytically active Pd(II) species. Moreover, two distinct methods to control the positional selectivity of C–H activation with multiply substituted arenes have been demonstrated: (i) substrate control, by appending a protecting group (PG) to modulate the intrinsic steric bias; and (ii) catalyst control, by using ligands to alter the steric and electronic properties around the metal center (Fig. 1B). The versatility of this olefination reaction is demonstrated by direct functionalization of commercially available drugs (Fig. 1D) and by atom- and step-economic syntheses of 2-tetralone derivatives (**2**) (key synthetic intermediates for tetraline-based natural products) and two challenging naphthoic acid components in neocarzinostatin (**1**) and kedarcidin (**3**), highly active antibiotics (Fig. 1E).

As part of the overarching goal of developing practically useful C–H functionalization reactions, our laboratory has focused on discovering reactivity with broadly useful substrates, in which all moieties present in the starting material can be used for subsequent synthetic applications in an atom-economical manner. Following this philosophy, we sought to develop a Pd-catalyzed olefination protocol (*20*) for phenylacetic acid substrates, as the resulting carbon skeletons are well-established platforms for the synthesis of 2-tetralones and naphthoic acids. Although carboxy-directed C–H activation involving six atoms in the coordination assembly is rare, we hypothesized that our K^+-promoted Pd insertion procedure for benzoic and phenylacetic acids (*21*, *22*), which promotes C–H activation through the complex-induced proximity effect (*23*), could be exploited for subsequent olefination.

To this end, we began by extensively screening reaction conditions and optimizing with respect to solvent, inorganic base, temperature, and oxidant (see supporting online material). Gratifyingly, we found that 4-methoxyphenylacetic acid could be coupled with ethyl acrylate in the presence of 5 mol% $Pd(OAc)_2$ (Ac, acetyl) to give the desired product in high yield (Fig. 2, **6a$_1$**). As a further practical advantage, 1 atm of O_2 could be used as the terminal oxidant, with 5 mol% benzoquinone (BQ) serving as a ligand to prevent minor formation of the meta- and di-ortho-olefinated products.

A wide range of phenylacetic acid substrates were found to be compatible with this protocol (Fig. 2). Products containing chlorides (**6g**, **6h**, **6j**, **6k**, and **6p**), fluorides (**6f** and **6r**), and ketones (**6l**) could be obtained in high yields. Notably, the tolerance for chlorides on the aromatic ring in this ortho-olefination offers an opportunity for subsequent cross-coupling, facilitating expedient synthesis of highly complex biaryl molecules. Several drug substrates, including ketoprofen (**4l**), ibuprofen (**4n**), and naproxen (**4o**), were found to be compatible with this protocol, affording the respective olefinated products **6l**, **6n**, and **6o**. These results demonstrate the potential for applying C–H olefination to effect direct functionalization of existing bioactive molecular scaffolds in the interest of enabling drug diversification for medicinal chemistry.

A diverse array of substitution patterns at the α position were tolerated, with a higher degree of α substitution corresponding to higher activity resulting from the Thorpe-Ingold effect (**6j** to **6s**). Optically pure compounds with chiral centers at the α position were found to racemize slightly under our reaction conditions; for example, **6o** was formed in 72% enantiomeric excess (ee). In this case, the use of Li_2CO_3 as the base prevented racemization, affording the product in 97% ee, but also lowered the conversion to 24%.

A variety of different olefin coupling partners were found to react well using this catalytic sys-

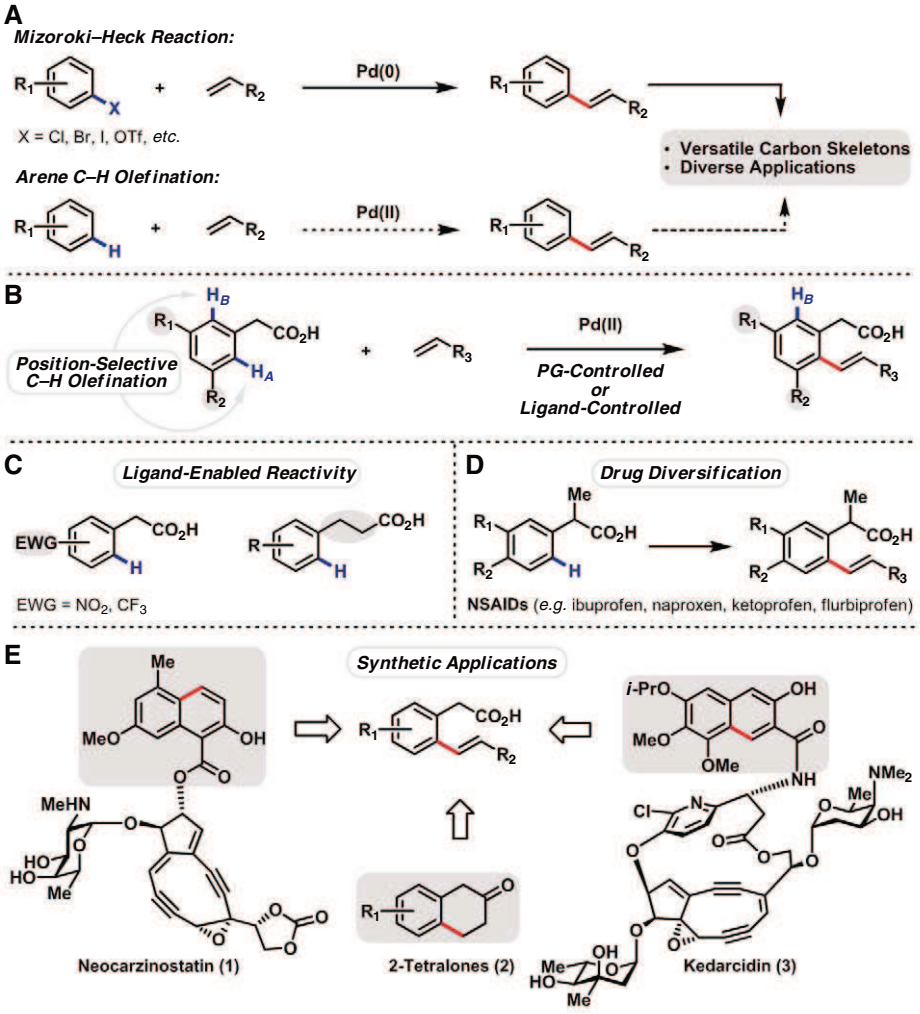

Fig. 1. (**A**) Comparison of the Mizoroki-Heck reaction and arene C–H olefination. (**B**) Schematic depiction of our position-selective C–H activation approach. (**C**) Substrates that were found to be unreactive under our original conditions but could be efficiently olefinated in the presence of amino acid ligands. (**D**) Direct ortho-olefination of commercial nonsteroidal anti-inflammatory drugs (NSAIDs). (**E**) Expedient synthesis of natural product components using position-selective C–H olefination.

tem (Fig. 2, **6a$_2$** to **6a$_5$** and **6b$_2$**). Interestingly, using 1-hexene as the olefin, we found that nonconjugated product **6a$_5$** was formed predominantly (with a 5:1 ratio of *E*:*Z* alkene stereoisomers) over the thermodynamically favorable conjugated system (observed in only trace amounts). Mechanistically, this suggests that after 1,2 migratory insertion of the Pd–aryl moiety into the olefin, the resulting intermediate is conformationally restricted from undergoing subsequent β-hydride elimination with the benzylic hydrogen atoms. A possible explanation is that the carbonyl oxygen atom from the carboxylate group remains coordinated to palladium in an unusual eight-membered ring, which restricts the bond rotation necessary to align the metal for syn elimination. Synthetically, olefinated products such as **6a$_5$** represent a class of substrates beyond the scope of traditional Mizoroki-Heck–type chemistry.

With this highly efficient catalytic C–H olefination protocol in hand, we next sought to control the positional selectivity of this reaction with multiply substituted arenes that yielded isomeric product mixtures under our original conditions (Fig. 1B). For instance, 3-methoxy-5-methylphenylacetic acid (**7**) reacted to form a mixture of positional isomers without substantial bias (1.4:1, **8-A**:**8-B**) (Fig. 3A, entry 1). We hypothesized that tuning the steric properties of the metal center through the coordination of a ligand could provide the site recognition that we sought. Extensive screening of ligands led us to discover that mono-N-protected amino acids were effective in this respect (*24*). During our screening efforts, we observed that the resulting isomeric distribution was substantially dependent on the structure of the amino acid side chain, with Boc-Leu-OH and Boc-Ile-OH giving the best selectivity (7:1 and 8:1, respectively; Boc, *tert*-butoxycarbonyl) (Fig. 3A, entries 5 and 6). We were pleased to find that positional selectivity could be further enhanced by varying the N-protecting group, with Formyl-Ile-OH as the best ligand, giving a 20:1 ratio of positional isomers (Fig. 3A, entry 12). The conversion using this particular ligand was slightly lower than without it, but by increasing the catalyst loading to 7%, the conversion could be improved to 75%. Allowing the reaction to run for 96 hours further improved the conversion to 89%.

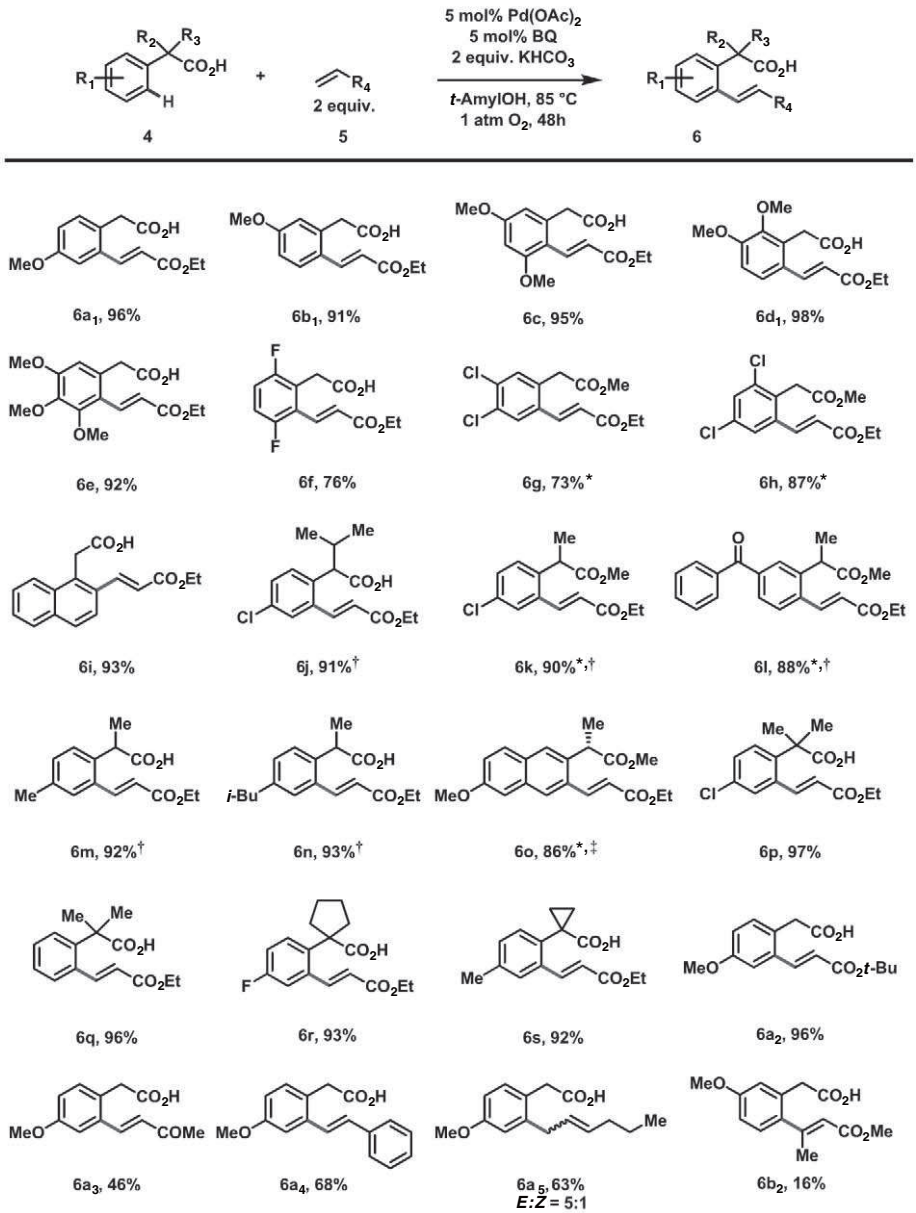

*The corresponding phenylacetic acid substrate was used as starting material; to simplify separation, the product was isolated as the methyl ester following treatment of the crude reaction mixture with CH_2N_2. †Racemic starting material was used. ‡Optically pure naproxen (**4o**, 97% ee) was used as the starting material. The product was obtained in 72% ee. The use of Li_2CO_3 as the base gave 24% conversion (by ^{1}H NMR) and 97% ee. The ee values were determined by chiral HPLC.

Fig. 2. C–H olefination of phenylacetic acid substrates with ethyl acrylate (**6a$_1$**, **6b$_1$**, and **6c** to **6s**) and with other olefin coupling partners (**6a$_2$** to **6a$_5$** and **6b$_2$**).

This ligand-controlled, position-selective C–H olefination protocol could also be applied to other multiply substituted arene substrates, including natural product precursors such as **9** and drug substrates such as flurbiprofen (**11**) (Fig. 3B). With substrate **9**, because the two ortho-C–H bonds are approximately electronically equivalent, the outstanding positional selectivity observed with Boc-Ile-OH is likely a result of the catalyst's recognition of the different steric environments. In contrast, both steric and electronic properties could be contributing to the improvement in positional selectivity with substrates **7**, **11**, **13**, and **15**; the mechanistic details in these cases remain to be fully elucidated. (Unless otherwise noted, the reaction conditions in Fig. 3, B to D, are identical to those described in Fig. 3A.)

To our delight, during this investigation, we also discovered that certain Boc-protected amino acid ligands could markedly improve the yield in this olefination reaction (see supporting online material), with the optimal ligand choice highly dependent on the combination of substrate and coupling partner. For instance, using Boc-Ile-OH, olefinated products **6t** and **17** could be formed quantitatively, even when the catalyst loading was reduced to 1 to 2 mol% of $Pd(OAc)_2$ (Fig. 3C). Moreover, the use of amino acid ligands allowed for efficient di-olefination, fashioning product **17**, for example, in quantitative yield. Thus, our parent C–H olefination protocol and the amino acid–ligated system offer complementary reactivity to access either the mono- or di-olefinated products, depending on which is more useful for a given synthetic application (Fig. 2 and Fig. 3C, respectively).

The strong ligand influence on reactivity in this system encouraged us to examine whether previously unreactive 3-phenylpropionic acid and electron-deficient phenylacetic acid substrates could now be ortho-olefinated in the presence of amino acid ligands. Indeed, we were pleased to find that an array of such substrates

could be olefinated in moderate to good yields (Fig. 3D). Notably, the synthetic flexibility afforded by the extra methylene spacer in **18a** and **18b** greatly expands the range of core structures that can subsequently be accessed.

Finally, we demonstrated the synthetic utility of this highly versatile and scalable olefination reaction by concise syntheses of several natural product core structures, including 2-tetralones and naphthoic acids (Fig. 4). The synthesis of natural products of this type is by no means simple, but impressive efforts by several groups (*25*–*29*) have led to a basic roadmap for how to construct such molecules. In particular, olefinated arenes with structures analogous to **10-A** (Fig. 4C) often serve as key intermediates, and the olefinic moieties are usually introduced via a Wittig reaction with the corresponding aldehyde or via bromination in the early stages to set up a late-stage Mizoroki-Heck reaction. Our C–H olefination reaction offers a departure from these approaches both in the retrosynthetic sense (in that it represents a different synthetic disconnection associated with a distinct pool of starting materials) and in the forward sense (in that the key transformations are highly step- and atom-economical).

Using our original protocol (Fig. 2), commercially available 2,3-dimethoxyphenylacetic acid (**4d**) could be transformed to intermediate $\mathbf{6d_2}$ in high yield. A straightforward sequence of hydrogenation, ester formation, Dieckmann condensation, and decarboxylation yielded 2-tetralone derivative **19** (Fig. 4A) (*29*). Notably, nearly all substrates described in this work could potentially be used to synthesize a diverse range of 2-tetralones.

Next, we demonstrated the utility of both protecting group–controlled and ligand-controlled position-selective olefination by synthesizing the naphthoic acid components of both neocarzinostatin (**1**) and kedarcidin (**3**) (Fig. 4). The use of a triisopropylsilyl (TIPS) group afforded the desired positional selectivity for the preparation of **21-A** (Fig. 4B). This key intermediate could then be cyclized in accordance with literature precedent (*28*) to give the naphthoic acid component **22** of neocarzinostatin (**1**) (*26*). On the other hand, the ligand-controlled position-selective olefination of **9** afforded **10-A** in high yield (Fig. 4C). **10-A** could then be converted into the desired naphthoic acid product (**23**) following a two-step procedure developed by Myers and Hirama: formation of the acid chloride and [6π] electrocyclization (*25*, *27*). In all three of these cases, the reaction sequences are among the highest-yielding and most atom- and step-economical routes achieved to date for accessing these widely studied, commonly occurring core structures.

In this report we have attempted to demonstrate the importance of ligand development (*30*) for enabling unique reactivity and selectivity in C–H activation, as well as to illustrate two conceptual prerequisites for the widespread application of Pd-catalyzed C–H activation in organic synthesis: (i) versatile substrates and coupling partners, and (ii) precise control of positional selectivity in C–H functionalization. We anticipate that this C–H olefination reaction and others grounded in this philosophy will find broad applicability in multifarious synthetic endeavors.

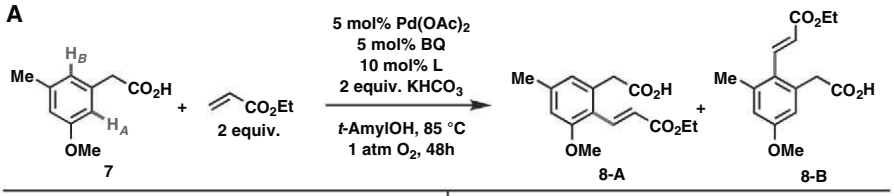

Entry	Ligand	Conv. (%)*	A : B	Entry	Ligand	Conv. (%)*	A : B
1	---	68	1.4 : 1	7	Boc_2-Leu-OH	50	3 : 1
2	Boc-Tyr(Bzl)-OH	17	2.5 : 1	8	H-Leu-OH	16	6 : 1
3	Boc-Abu-OH	17	5 : 1	9	Formyl-Leu-OH	24	13 : 1
4	Boc-Val-OH	23	6 : 1	10	Fmoc-Ile-OH	16	5 : 1
5	Boc-Leu-OH	24	7 : 1	11	Ac-Ile-OH	23	10 : 1
6	Boc-Ile-OH	27†	8 : 1	12	Formyl-Ile-OH	43 (75)‡	20 : 1

*Based on ^{1}H NMR. The di-olefinated product was formed in less than 5% conversion. †24 h. ‡7 mol% $Pd(OAc)_2$, 7 mol% BQ, 14 mol% L.

B

Substrate	Ligand	Conv. (%)*	A : B	Substrate	Ligand	Conv. (%)*	A : B
9	---	65†	1.5 : 1	13	---	63	1.6 : 1
	Boc-Ile-OH	86†	23 : 1		Formyl-Ile-OH	77	3.5 : 1
11	---	82	2.8 : 1	15	---	8	1.2 : 1
	Formyl-Ile-OH	78	5.7 : 1		Formyl-Ile-OH	50‡	4.7 : 1

*Based on ^{1}H NMR. Products derived from substrates **9**, **11**, **13**, and **15** are labeled **10-A/B**, **12-A/B**,**14-A/B**, and **16-A/B** respectively. Only the major products were isolated and characterized. †*t*-Butyl acrylate was used as the coupling partner. ‡15 mol% $Pd(OAc)_2$, 15 mol% BQ, 30 mol% Formyl-Ile-OH.

C

6t

$Pd(OAc)_2$	Ligand	Conv. (%)*,†
2 mol%	---	31
2 mol%	Boc-Ile-OH	>99

17, R = 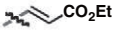

$Pd(OAc)_2$	Ligand	Conv. (%)*,†	Selectivity
2 mol%	---	10	mono
2 mol%	Boc-Ile-OH	>99	di

*Based on ^{1}H NMR. †2 mol% $Pd(OAc)_2$, 2 mol% BQ, 4 mol% Ligand.

D

Product	Ligand	Yield (%)*	Product	Ligand	Yield (%)*
6u	---	12	6w	---	13
	Boc-Val-OH	90		Boc-Ile-OH	85‡
6v	---	0	6x	---	0
	Boc-Val-OH	50†		Boc-Val-OH	57§
18a	---	8	18b	---	22
	Boc-Val-OH	60		PG_1-Leu-OH‖	75¶

*Isolated Yield. †2-Nitrophenylacetic acid was used as substrate; the product was completely decarboxylated under the reaction conditions: 10 mol% $Pd(OAc)_2$, 10 mol% BQ, 20 mol% Boc-Val-OH. ‡Mono:Di = 2:1. §4-Nitrophenylacetic acid was used as substrate; decarboxylated:non-decarboxylated = 2:1. ‖PG_1 = (–)-Menthyl(O_2C). ¶Mono:Di = 3:1.

Fig. 3. (**A**) Selected amino acid ligand screening data for position-selective C–H olefination. (The full ligand screening data are available in table S8.) (**B**) Substrate scope for ligand-controlled position-selective C–H olefination. (**C**) Ligand-enabled C–H olefination with 2 mol% $Pd(OAc)_2$. (**D**) Amino acid ligand–enabled C–H olefination with problematic substrates.

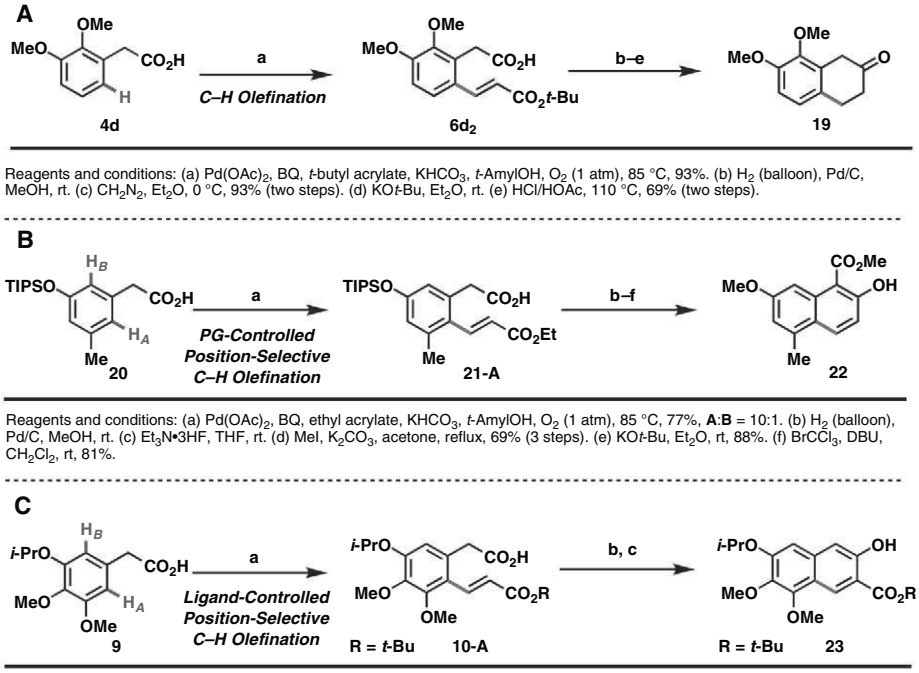

Fig. 4. (**A**) Synthesis of 7,8-dimethoxytetalin-2-one. (**B**) Synthesis of the naphthoic acid component of neocarzinostatin (**1**). (**C**) Synthesis of the naphthoic acid component of kedarcidin (**3**).

References and Notes

1. J. F. Hartwig, *Nature* **455**, 314 (2008).
2. A. R. Dick, M. S. Sanford, *Tetrahedron* **62**, 2439 (2006).
3. O. Daugulis, V. G. Zaitsev, D. Shabashov, Q.-N. Pham, A. Lazareva, *Synlett* **2006**, 3382 (2006).
4. L.-C. Campeau, D. R. Stuart, K. Fagnou, *Aldrichim. Acta* **40**, 35 (2007).
5. J.-Q. Yu, R. Giri, X. Chen, *Org. Biomol. Chem.* **4**, 4041 (2006).
6. B. D. Dangel, K. Godula, S. W. Youn, B. Sezen, D. Sames, *J. Am. Chem. Soc.* **124**, 11856 (2002).
7. A. Hinman, J. Du Bois, *J. Am. Chem. Soc.* **125**, 11510 (2003).
8. A. L. Bowie Jr., C. C. Hughes, D. Trauner, *Org. Lett.* **7**, 5207 (2005).
9. H. M. L. Davies, X. Dai, M. S. Long, *J. Am. Chem. Soc.* **128**, 2485 (2006).
10. A. S. Tsai, R. G. Bergman, J. A. Ellman, *J. Am. Chem. Soc.* **130**, 6316 (2008).
11. K. Chen, P. S. Baran, *Nature* **459**, 824 (2009).
12. E. M. Stang, M. C. White, *Nat. Chem.* **1**, 547 (2009).
13. K. C. Nicolaou, P. G. Bulger, D. Sarlah, *Angew. Chem. Int. Ed.* **44**, 4442 (2005).
14. B. M. Trost, S. A. Godleski, J. P. Genet, *J. Am. Chem. Soc.* **100**, 3930 (1978).
15. P. S. Baran, E. J. Corey, *J. Am. Chem. Soc.* **124**, 7904 (2002).
16. N. K. Garg, D. D. Caspi, B. M. Stoltz, *J. Am. Chem. Soc.* **126**, 9552 (2004).
17. E. M. Beck, R. Hatley, M. J. Gaunt, *Angew. Chem. Int. Ed.* **47**, 3004 (2008).
18. R. J. Phipps, M. J. Gaunt, *Science* **323**, 1593 (2009).
19. Y.-H. Zhang, B.-F. Shi, J.-Q. Yu, *J. Am. Chem. Soc.* **131**, 5072 (2009).
20. For early examples of Pd-catalyzed directed and non-directed arene C–H olefination, see (*31*–*33*). For an early example of Ru-catalyzed directed olefination, see (*34*).
21. T.-S. Mei, R. Giri, N. Maugel, J.-Q. Yu, *Angew. Chem. Int. Ed.* **47**, 5215 (2008).
22. D.-H. Wang, T.-S. Mei, J.-Q. Yu, *J. Am. Chem. Soc.* **130**, 17676 (2008).
23. P. Beak, V. Snieckus, *Acc. Chem. Res.* **15**, 306 (1982).
24. For application of mono-N-protected amino acid ligands for Pd-catalyzed enantioselective C–H activation/C–C cross coupling, see (*35*).
25. A. G. Myers, Y. Horiguchi, *Tetrahedron Lett.* **38**, 4363 (1997).
26. N. Ji, B. M. Rosen, A. G. Myers, *Org. Lett.* **6**, 4551 (2004).
27. S. Kawata, S. Ashizawa, M. Hirama, *J. Am. Chem. Soc.* **119**, 12012 (1997).
28. F. C. Görth, M. Rucker, M. Eckhardt, R. Brückner, *Eur. J. Org. Chem.* **2000**, 2605 (2000).
29. Á. Gorka *et al.*, *Synth. Commun.* **35**, 2371 (2005).
30. For discussion of the importance of ligand development in Pd chemistry, see (*36*).
31. M. Miura, T. Tsuda, T. Satoh, S. Pivsa-Art, M. Nomura, *J. Org. Chem.* **63**, 5211 (1998).
32. C. G. Jia *et al.*, *Science* **287**, 1992 (2000).
33. M. D. K. Boele *et al.*, *J. Am. Chem. Soc.* **124**, 1586 (2002).
34. S. Murai *et al.*, *Nature* **366**, 529 (1993).
35. B.-F. Shi, N. Maugel, Y.-H. Zhang, J.-Q. Yu, *Angew. Chem. Int. Ed.* **47**, 4882 (2008).
36. R. Martin, S. L. Buchwald, *Acc. Chem. Res.* **41**, 1461 (2008).

37. Supported by an A. P. Sloan Foundation fellowship (J.-Q.Y.); predoctoral fellowships from NSF, the U.S. Department of Defense, the Scripps Research Institute, and the Skaggs Oxford Scholarship program (K.M.E.); and the Scripps Research Institute, National Institute of General Medical Sciences grant 1 R01 GM084019-02, NSF grant CHE-0910014, Amgen, and Eli Lilly & Co.

Supporting Online Material www.sciencemag.org/cgi/content/full/science.1182512/DC1 Materials and Methods
Tables S1 to S8
NMR Spectra
References

28 September 2009; accepted 12 November 2009
Published online 26 November 2009;
10.1126/science.1182512
Include this information when citing this paper.

Nanoporous Gold Catalysts for Selective Gas-Phase Oxidative Coupling of Methanol at Low Temperature

A. Wittstock,[1] V. Zielasek,[1] J. Biener,[2]* C. M. Friend,[3]* M. Bäumer[1]*

Gold (Au) is an interesting catalytic material because of its ability to catalyze reactions, such as partial oxidations, with high selectivities at low temperatures; but limitations arise from the low O_2 dissociation probability on Au. This problem can be overcome by using Au nanoparticles supported on suitable oxides which, however, are prone to sintering. Nanoporous Au, prepared by the dealloying of AuAg alloys, is a new catalyst with a stable structure that is active without any support. It catalyzes the selective oxidative coupling of methanol to methyl formate with selectivities above 97% and high turnover frequencies at temperatures below 80°C. Because the overall catalytic characteristics of nanoporous Au are in agreement with studies on Au single crystals, we deduced that the selective surface chemistry of Au is unaltered but that O_2 can be readily activated with this material. Residual silver is shown to regulate the availability of reactive oxygen.

An ever-increasing demand for resources enforces the need of sustainability in all arenas (*1*). This new challenge has triggered a growing interest in a "green chemical industry," especially for the production and processing of commodity chemicals (*2*, *3*), which is based on more efficient processes working under mild conditions (low temperatures and ambient conditions) and relying on cheap and abundant feedstock. In this context, gold (Au)–based catalysts have attracted considerable attention in the past decade because of their nontoxic nature and the ability to promote selective reactions at low temperatures. In particular, the potential of Au for partial oxidation reactions, such as the selective oxidation of alcohols (*4*–*6*) and hydrocarbons (*7*, *8*), was demonstrated in numerous studies. Model studies on single-crystal Au provided molecular-scale insight into the activity of gold, showing that atomic oxygen is the key species that promotes a range of selective oxida-

[1]Institute of Applied and Physical Chemistry, Universität Bremen, Bremen 28359, Germany. [2]Nanoscale Synthesis and Characterization Laboratory, Lawrence Livermore National Laboratory (LLNL), Livermore, CA 94550, USA [3]Department of Chemistry, Harvard University, Cambridge, MA 02138, USA.

*To whom correspondence should be addressed. E-mail: mbaeumer@uni-bremen.de (M.B.), cfriend@seas.harvard.edu (C.M.F.), biener2@llnl.gov (J.B.)

tive transformations (*9*). Its presence activates Au surfaces for reactions with organic species, including methanol (*10*), and also serves as the source of oxygen for other oxidation reactions, such as the transformation of olefins to epoxides. The comparatively weak adsorption of the partial oxidation products on Au allows them to desorb before being further oxidized. This delicate balance between Au's oxidation power and its relatively weak interaction with partial oxidation products distinguishes Au from other catalytic metals, such as Pd and Pt.

Yet, one technological impediment to the use of Au as a catalyst is O_2 dissociation. Studies on single-crystal Au surfaces have shown that the dissociation probability for O_2 is extremely low [$<<10^{-6}$ (*11*)], so that mechanistic studies on such surfaces had to rely on more reactive oxygen sources, such as ozone (*10*, *12*) or oxygen atoms (*13*).

However, it is also well known that Au can be activated as a catalyst by depositing small particles in the range of 2 to 5 nm on suitable oxide supports, such as titania and ceria (*14*–*16*). Mechanistic studies have suggested that undercoordinated atoms (*17*, *18*) play a role in inducing dissociation and that the support (*19*) should be involved in supplying oxygen—for example, at the particle perimeter. However, the structural complexity—including defect sites, the interface to the oxide, hydroxyl groups on the support, and ionic Au species—has limited the understanding of the catalytically important factors. Another barrier to the use of supported Au catalysts is their tendency to sinter (to agglomerate) under reaction conditions. This process often leads to poor long-term stability; thus, there are only a few examples in which Au catalysts are used in industrial heterogeneous catalysis.

In view of these problems, unsupported Au-based material systems have attracted attention (*20*), including nanoporous Au (np-Au), which can be prepared by leaching Ag from an Au-Ag alloy through a route similar to that for the preparation of Raney nickel. This monolithic material consists of a three-dimensional network of ligaments with diameters on the order of 10 to 50 nm, depending on the preparation conditions (Fig. 1 shows an example of np-Au prepared by means of "free corrosion" in nitric acid, which exhibits ligaments in the range of 30 nm), and contains a large fraction of low-coordinated Au on the surface of the material. Although not in contact with an oxide support, np-Au exhibits excellent activity for low-temperature CO oxidation with O_2 as an oxidant at atmospheric pressure (*21*). It is also active for liquid-phase oxidation of glucose (*22*), electrochemical oxidation of methanol (*23*), and O_2 reduction in fuel cell applications (*24*), but it has not been used for more complex reactions in gas-phase catalysis so far. In spite of the reduced structural complexity of the material as compared with that of deposited nanoparticles, the reason for its unexpected catalytic activity is still not clear. We now show that np-Au can catalyze selective oxidative coupling reactions of alcohols in the gas phase, and we present an explanation for its surprising activity.

Oxidation of methanol was chosen as an example because mechanistic studies on Au single crystals recently predicted a highly selective surface chemistry leading to methyl formate as a coupling product of the partial oxidation product formaldehyde and unreacted methoxy. Methyl formate is of great importance as a precursor for formic acid, formamide, and dimethyl formamide. The world market for formic acid alone amounts to several hundred thousand tons per year (*25*). Besides its application as a precursor, methyl formate is also used as a solvent and environmentally friendly blowing agent. The current industrial process for methyl formate production is based on the carbonylation of methanol and generally has undesirable by-products or reagents. The industrial catalyst is sodium methoxide, a caustic base that is generated by the reaction of metallic sodium with methanol (*25*).

Regarding green chemistry, it would be desirable to have a process that requires no solvents or bases and that relies on molecular oxygen as cheap and abundant feedstock. In recent years, processes that used O_2 as an oxidant and transition-metal catalysts were developed for the synthesis of a variety of alcohols in liquid phase (*26*, *27*). Yet in order to achieve satisfactorily high conversion rates, the addition of a base was still necessary, which is in agreement with the presumption that the rate-limiting step is the deprotonation of the alcohol and the formation of the aldehyde. Recently, Jorgensen *et al.* succeeded in the oxidization of ethanol to acetaldehyde without added base in a batch reactor at temperatures of >90°C using a Au catalyst supported on a suitable oxide support (*6*). Here, however, high oxygen partial pressures in the range of 35 bar were necessary. We will show that, by using np-Au as a Au catalyst, the process can be run under continuous-flow conditions and at ambient pressures (1 bar) in temperatures well below 100°C.

Monolithic disks of np-Au (with a diameter of 0.5 cm and thickness of 200 μm) were placed directly into the gas stream within the reactor (fig. S3). The composition of the gas stream at the exit of the reactor was monitored with an infrared gas analyzer (for CO_2 detection) and a gas chromatograph with mass spectrometric detection (fig. S4).

For stoichiometric compositions of methanol and O_2 (1 volume % O_2 + 2 volume % CH_3OH), the coupling product methyl formate is produced almost exclusively. At room temperature (20°C), the selectivity toward methyl formate amounts to ~100% with 10% conversion of methanol. No other partial oxidation products, such as formaldehyde or formic acid, were detected within our detection limit, placing an upper bound of 0.05 volume %. Upon increasing the temperature to 80°C, the selectivity only slightly decreases to 97% (undesired combustion to CO_2 accounts for the remaining 3%), but the conversion increases to 60% (Fig. 2). This reaction rate corresponds to a turnover frequency (TOF, number of converted molecules per surface site and second) of 0.11 s^{-1} if all surface atoms are taken into account (equation S1). When conditions were adjusted to increase the conversion (6 volume % CH_3OH + 10 volume % O_2), TOFs of 0.26 s^{-1} were measured. Because mass-transport limitation (pore diffusion) plays a role, as previously shown for CO oxidation (*28*), and presumably not all surface atoms take part in the reaction, these TOFs are only a lower bound and probably by a factor of

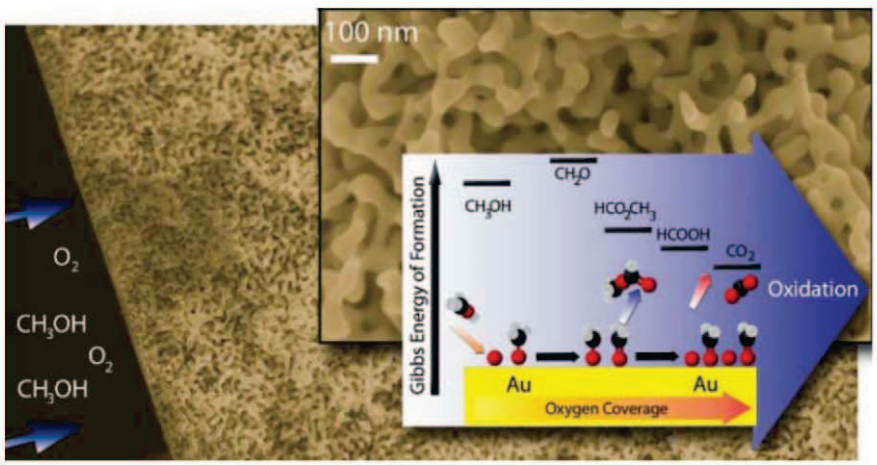

Fig. 1. Scanning electron micrographs showing the structure of monolithic nanoporous Au. The nanoporous structure of the material is homogeneous from the surface into the bulk and is permeable for reactants. (Lower right) Proposed mechanism of selective oxidation of methanol on Au surfaces. Methanol is activated by surface oxygen and bonded at the surface as methoxy. Subsequent deprotonation leads to the aldehyde. Fast reaction of the highly reactive aldehyde with further methoxy leads to the coupling product methyl formate (HCO_2CH_3). In the case of excess oxygen, the aldehyde can be further oxidized, resulting in CO_2 formation. In terms of thermodynamics, the total oxidation product (CO_2) is strongly favored. Gold exhibits a remarkable selectivity toward partial oxidation products, distinguishing it from other transition metals.

two to five higher, as estimated on the basis of the Thiele modulus. In comparison, TOFs reported for the oxidation of alcohols by supported Au catalysts in the liquid phase are usually lower [~0.01 s^{-1} to 1 s^{-1} (*4*)] and strongly depend on the preparation of the catalyst and the support material.

The long-term stability of the catalytic activity was tested at 30°C and 60°C, keeping the sample continuously under reaction conditions (1 volume % O_2 + 1 volume % CH_3OH). Under mild conditions, the activity of the catalyst was constant for more than 7 days. At 60°C, the activity slightly decreased with a rate of ~6% per 24 hours (selectivity unaltered). After 14 days at 60°C, the sample was still active and could even be reactivated. The turnover number (TON) after 14 days at this temperature accounted to 687,000, a notably higher number as compared with typical supported Au catalysts (*4*).

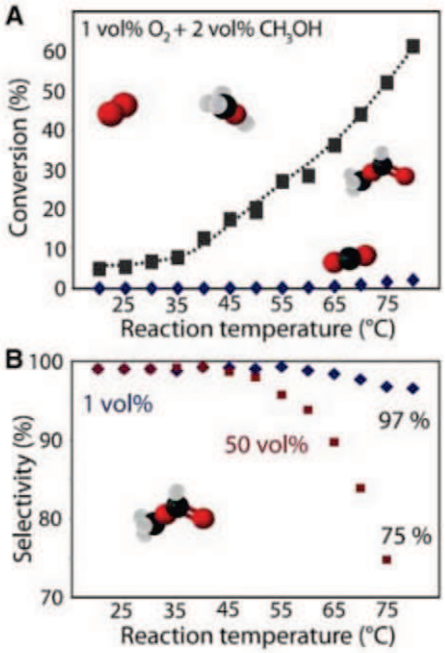

Fig. 2. Catalytic oxidation of methanol on np-Au. (**A**) The activity and selectivity of the oxidation of methanol was investigated under continuous flow conditions at different temperatures [the error bar for each data point is ±0.1% and ±4% for CO_2 and methyl formate, respectively; 20.1 mg np-Au; total gas stream is 50 standard cubic centimeters per minute (sccm); and residual Ag in sample is <1 atomic %]. Already at 20°C, close to 10% of the methanol is converted to methyl formate. Total oxidation (to CO_2; blue rhombuses) as well as partial oxidation (to methyl formate; gray squares) increase with temperature. (**B**) The selectivity (fraction of converted methanol that is converted into methyl formate) depends on the temperature and the partial pressure of oxygen. For low oxygen partial pressures (1 volume %; blue rhombuses), the selectivity remains almost constant, whereas for elevated oxygen partial pressures (50 volume %; red squares), the selectivity decreases with temperature, with the methyl formate still being the main product.

The relative amount of methyl formate production over combustion decreases as the partial pressure of O_2 is increased (Fig. 2), as can be anticipated from mechanistic studies that showed that secondary oxidation is favored for higher adsorbed oxygen (O_{ad})–to-methanol ratios. Nevertheless, even at relatively high O_2 partial pressures the selective oxidative coupling is dominant. Whereas the selectivity is still above 90% at 20°C, it decreased to 78% at 80°C reactor temperature. Thus, for higher oxygen partial pressures, formation of CO_2 is more favored as the temperature is increased.

These findings are understood on the basis of reaction mechanisms derived from model studies carried out under ultrahigh vacuum conditions on single-crystal Au surfaces (*29*): Methanol is activated by surface oxygen, which acts as a Brønsted base so that adsorbed methoxy species can form. Without O_{ad}, no reaction occurs, and molecular bonding is relatively weak. Further deprotonation leads to short-lived formaldehyde that reacts with excess methoxy to methyl formate (Fig. 1). If oxygen is present in excess, a fraction of the aldehyde is further oxidized to formate (HCOO) and subsequently to CO_2. Both methoxy and formate have been identified spectroscopically, providing the basis for this mechanism (*10*). Hence, running an oxygen-rich reactant composition reduces the selectivity and increases the total oxidation yield. The decreasing selectivity with increasing temperature is a result of the higher activation energy for total oxidation pathway [20.8 kcal mol^{-1}, as compared with 14.7 kcal mol^{-1} for partial oxidation (*29*)].

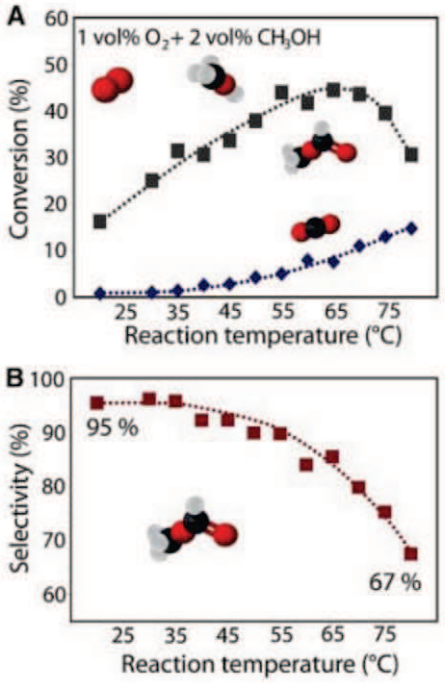

Fig. 3. Catalytic results for np-Au with an increased fraction of residual Ag of 2.5 atomic %. The oxidation of methanol was investigated under continuous flow conditions [error bar for each data point is ±0.1% (CO_2) and ±4% (methyl formate), respectively; 20.6 mg np-Au; total flow of gases is 50 sccm] at different temperatures. (**A**) The partial oxidation toward methyl formate (gray squares) as well as the total oxidation to CO_2 (blue rhombuses) depend on the temperature. (**B**) The selectivity toward methyl formate decreases with rising temperature, reflecting the behavior of samples with a low Ag content in the case of high oxygen partial pressures.

Although the major part of the catalytic steps apparently can be ascribed to the surface chemistry of Au, the efficient dissociation of O_2 is surprising. In previous work, indications were reported that residual Ag in the material participates in the activation of molecular oxygen (*28*). To further elucidate the effect of Ag in view of supplying oxygen, we investigated the methanol oxidation on samples exhibiting the same morphology but different amounts of residual Ag. Fully dealloyed samples contain below 1 atomic % residual Ag, but higher Ag contents can be realized by altering dealloying conditions (fig. S2). For this study, we prepared samples containing 2.5 and 10 atomic % residual Ag content according to energy dispersive x-ray spectroscopic (EDX) quantification. Our experiments show that the selectivity toward partial oxidation decreases with increasing Ag content. Similar conversions were obtained for the 2.5 atomic % Ag np-Au samples and the fully dealloyed ones. The higher Ag content, however, leads to a loss of selectivity as the temperature increases [97% (20°C) → 67% (80°C)], even if stoichiometric mixtures (2 volume % methanol + 1 volume % O_2) (Fig. 3) are applied. This response is similar to that of samples with low Ag content in the case of oxygen-rich mixtures (2 volume % methanol + 50 volume % O_2).

Further increase of the content of Ag to 10 atomic % lowers the selectivity drastically. Methyl formate is no longer formed in the whole temperature range up to 80°C, and the only detectable product observed is CO_2. (In particular, no formaldehyde is detected.) Its production increases to about 10% conversion of methanol when increasing the temperature to 80°C. The activity, however, remains below the overall activity level (conversion to methyl formate + CO_2) detected for the samples with <1 and 2.5 atomic % residual Ag, respectively.

The data indicate that Ag regulates the availability of reactive oxygen on the surface and thus controls the selectivity in the case of methanol oxidation. An increased Ag content results in a loss of selectivity toward methyl formate, favoring total oxidation. Thus, the oxidation power of the material can be tuned by adjusting the Ag concentration. Two possible explanations are conceivable. Either a dilute alloy of Au and Ag results in a local change of the d-band structure, making the Au locally "less noble," or oxygen is dissociated on Ag patches, which deliver the oxygen to the Au through spillover or at the perimeter.

A direct involvement of silver in the coupling activity, on the other hand, is unlikely. Although Ag can also catalyze the partial oxidation of

methanol (*29*), there are strong arguments against such a contribution. First, the major product on Ag is formaldehyde (*30*). Second, high temperatures are needed for the reaction [>250°C (*31*)]; the industrial process that uses Ag as a catalyst works at over 600°C in order to achieve sufficiently high yields (*25*). Third, the overall catalytic activity of np-Au does not increase but decreases as the residual Ag content increases.

The conclusion that the observed coupling reactivity and selectivity is due to Au surface sites as reactive sites is also confirmed by experiments in which an aldehyde was co-dosed to the methanol stream. According to our reaction model, the coupling product methyl formate is formed by the reaction of formaldehyde with methoxy groups. Thus, the formation of mixed coupling products can be expected when a different aldehyde is added to the reactant mixture—a result that was recently obtained in model studies on O/Au(111) (*32*). Thus, selective cross-coupling of different alcohols and aldehydes should also be feasible on np-Au. In fact, the mechanistic model predicts that the methyl esters will selectively form because co-feeding the aldehyde circumvents the rate-determining β-C-H activation step in the reaction. As an example, we chose the reaction of methanol and acetaldehyde, which is expected to produce methyl acetate. When adding acetaldehyde to the gas stream (1 volume % H_3C_2HO + 2 volume % CH_3OH + 10 volume % O_2), methyl acetate—the coupling product between methoxy and the co-fed acetaldehyde—is the only product (except for small amounts of CO_2). No methyl formate is detected, as is anticipated from the molecular-scale mechanism. Thus, the reactivity of the aldehyde causes the selectivity to change toward the new coupling product and opens the door to a rich coupling chemistry on np-Au.

Application of np-Au as a large-scale catalyst will depend on the economical viability, which is strongly connected to an economic use of the precious metal. One approach is to crush the material; another one is to coat the alloy on templates working as a backbone for catalyst pellets before dealloying. In this way, mass transport limitation because of pore diffusion can also be largely avoided. The feasibility of the latter approach was already proven, resulting in np-Au material with a relative density in the range of only 1.5% (*33*), which lies in the range of metal loadings of supported commercial catalysts. Future investigations will focus on an expansion of the scope of reactions to larger primary and secondary alcohols, such as ethanol or *tert*-butanol.

References and Notes

1. United Nations World Commission on Environment and Development (WCED), "Our Common Future (The Brundtland Report)" (Annex to General Assembly document A/42/427, Oxford Univ. Press, Oxford, 1987).
2. M. Poliakoff, P. Licence, *Nature* **450**, 810 (2007).
3. V. Gewin, *Nature* **440**, 378 (2006).
4. A. Abad, P. Concepcion, A. Corma, H. Garcia, *Angew. Chem. Int. Ed.* **44**, 4066 (2005).
5. T. Ishida, M. Haruta, *Angew. Chem. Int. Ed.* **46**, 7154 (2007).
6. B. Jorgensen, S. E. Christiansen, M. L. D. Thomsen, C. H. Christensen, *J. Catal.* **251**, 332 (2007).
7. A. K. Sinha, S. Seelan, S. Tsubota, M. Haruta, *Top. Catal.* **29**, 95 (2004).
8. M. D. Hughes *et al.*, *Nature* **437**, 1132 (2005).
9. R. J. Madix, *Science* **233**, 1159 (1986).
10. B. J. Xu, X. Y. Liu, J. Haubrich, R. J. Madix, C. M. Friend, *Angew. Chem. Int. Ed.* **48**, 4206 (2009).
11. X. Y. Deng, B. K. Min, A. Guloy, C. M. Friend, *J. Am. Chem. Soc.* **127**, 9267 (2005).
12. X. Y. Liu, B. J. Xu, J. Haubrich, R. J. Madix, C. M. Friend, *J. Am. Chem. Soc.* **131**, 5757 (2009).
13. J. Gong, D. W. Flaherty, R. A. Ojifinni, J. M. White, C. B. Mullins, *J. Phys. Chem. C* **112**, 5501 (2008).
14. M. Haruta, T. Kobayashi, H. Sano, N. Yamada, *Chem. Lett.* **16**, 405 (1987).
15. G. J. Hutchings, *Catal. Today* **100**, 55 (2005).
16. J. Schwank, S. Galvagno, G. Parravano, *J. Catal.* **63**, 415 (1980).
17. H. Falsig *et al.*, *Angew. Chem. Int. Ed.* **47**, 4835 (2008).
18. B. Hvolbaek *et al.*, *Nano Today* **2**, 14 (2007).
19. G. C. Bond, D. T. Thompson, *Gold Bull.* **33**, 41 (2000).
20. M. Haruta, *ChemPhysChem* **8**, 1911 (2007).
21. V. Zielasek *et al.*, *Angew. Chem. Int. Ed.* **45**, 8241 (2006).
22. H. M. Yin *et al.*, *J. Phys. Chem. C* **112**, 9673 (2008).
23. J. T. Zhang, P. P. Liu, H. Y. Ma, Y. Ding, *J. Phys. Chem. C* **111**, 10382 (2007).
24. R. Zeis, T. Lei, K. Sieradzki, J. Snyder, J. Erlebacher, *J. Catal.* **253**, 132 (2008).
25. *Ullmann's Encyclopedia of Industrial Chemistry* (Wiley, New York, ed. 7, 2009); www.wiley-vch.de/vch/software/ullmann/index.php?page=home.
26. I. E. Marko, P. R. Giles, M. Tsukazaki, S. M. Brown, C. J. Urch, *Science* **274**, 2044 (1996).
27. T. Mallat, A. Baiker, *Chem. Rev.* **104**, 3037 (2004).
28. A. Wittstock *et al.*, *J. Phys. Chem. C* **113**, 5593 (2009).
29. X. Y. Liu, R. J. Madix, C. M. Friend, *Chem. Soc. Rev.* **37**, 2243 (2008).
30. W. S. Sim, P. Gardner, D. A. King, *J. Phys. Chem.* **99**, 16002 (1995).
31. C. B. Wang, G. Deo, I. E. Wachs, *J. Phys. Chem. B* **103**, 5645 (1999).
32. B. J. Xu, X. Y. Liu, J. Haubrich, C. M. Friend, *Nat. Chem.*, published online 29 November 2009 (doi:10.1038/nchem.467).
33. G. W. Nyce, J. R. Hayes, A. V. Hamza, J. H. Satcher, *Chem. Mater.* **19**, 344 (2007).

34. We are grateful to R. Schlögl (Fritz-Haber-Institute, Berlin) for critically reading the manuscript. Work at LLNL was performed under the auspices of the U.S. Department of Energy (DOE) by LLNL under contract DE-AC52-07NA27344. C.M.F. acknowledges a Senior Research Award from the Alexander von Humboldt Foundation and a fellowship from the Hanse-Wissenschaftskolleg in Germany as well as research support from the U.S. DOE under contract DE-FG02-84-ER13289. M.B. acknowledges financial support from the University of Bremen.

Supporting Online Material

www.sciencemag.org/cgi/content/full/327/5963/319/DC1
Materials and Methods
Figs. S1 to S4

20 October 2009; accepted 17 November 2009
10.1126/science.1183591

Large-Scale Controls of Methanogenesis Inferred from Methane and Gravity Spaceborne Data

A. Anthony Bloom,[1] Paul I. Palmer,[1]* Annemarie Fraser,[1] David S. Reay,[1] Christian Frankenberg[2]

Wetlands are the largest individual source of methane (CH_4), but the magnitude and distribution of this source are poorly understood on continental scales. We isolated the wetland and rice paddy contributions to spaceborne CH_4 measurements over 2003–2005 using satellite observations of gravity anomalies, a proxy for water-table depth Γ, and surface temperature analyses T_S. We find that tropical and higher-latitude CH_4 variations are largely described by Γ and T_S variations, respectively. Our work suggests that tropical wetlands contribute 52 to 58% of global emissions, with the remainder coming from the extra-tropics, 2% of which is from Arctic latitudes. We estimate a 7% rise in wetland CH_4 emissions over 2003–2007, due to warming of mid-latitude and Arctic wetland regions, which we find is consistent with recent changes in atmospheric CH_4.

The atmospheric concentration of methane (CH_4), an important greenhouse gas, is determined by a balance between natural and anthropogenic sources and sinks (*1*), leading to an atmospheric lifetime of approximately 9 years (*2*). Renewed interest in global budget calculations of CH_4 levels is due to (i) the largely unexplained stability of CH_4 concentrations during 1999–2006 and the renewed growth since early 2007 (*3*); (ii) laboratory and field measurements that support a small, previously unidentified, aerobic source of CH_4 from terrestrial vegetation (*4*); and (iii) new satellite observations that provide additional constraints on current understanding (*5*). Concentration measurements of CH_4 provide global constraints for emission estimates, but without additional, independent information it is difficult to attribute observed variability to individual sources and sinks.

Emissions from wetlands are the largest single source of CH_4, representing 20 to 40% of the total CH_4 emissions budget (*1*), of which 70% is estimated to originate from southern and tropical latitudes (*6*). Rice cultivation accounts for 6 to 20% of global CH_4 emissions (*1*), the majority of which originates from south and southeast Asia (*7*). Methanogenesis, the biogenic

[1]School of GeoSciences, University of Edinburgh, Edinburgh, UK. [2]SRON Netherlands Institute for Space Research, Utrecht, Netherlands.

*To whom correspondence should be addressed. E-mail: pip@ed.ac.uk

production of CH_4, occurs in natural wetlands and rice paddies by the anaerobic degradation of organic matter by methanogenic archaea. Production rates are controlled by the availability of suitable substrates; alternative electron acceptors for competing redox reactions, such as sulfate reduction (*8*); temperature; and soil salinity (*9*). Aerobic oxidation of CH_4 by methanotrophs is a key factor in controlling CH_4 emissions (*10*), with net fluxes to the atmosphere being primarily determined by the balance between CH_4 production and consumption in the wetland soils. Emergent wetland vegetation can also increase the transport of CH_4 between the soil and atmosphere (*11*). Although the controls on methanogenesis from wetlands and rice paddies are similar, the two sources are typically spatially distinct (*12*). Nevertheless, there is substantial uncertainty and regional variation associated with all these controlling factors. Wetland emissions dominated the interannual variability of CH_4 sources over 1984–2003 (*13*). A decrease in wetland emissions over the past decade has reportedly masked a coincident increase in anthropogenic emissions (*13*), leading to stable global mean CH_4 concentrations (*14*). Changes in the OH sink during 2006–2007 were not large enough to explain observed changes in CH_4 concentration (*3*).

We present an approach to understanding the role of wetlands and rice cultivation in producing observed CH_4 concentrations, using spaceborne measurements of gravity and CH_4 over the 3-year period from 2003 to 2005. We used three data sets. First, we used satellite column observations of CH_4 from the Scanning Imaging Absorption Spectrometer for Atmospheric Chartography (SCIAMACHY) instrument (*15*) aboard the Envisat satellite, which have been retrieved from solar-backscattered radiation at wavelengths from 1630 to 1679 nm (*5*), accounting for new water spectroscopic parameters (*16*). Retrieved columns, which are most sensitive to CH_4 in the lower troposphere (*5*), range from 1630 to 1810 parts per billion, with the largest values generally over mid-latitude and tropical continents (*16*).

Second, we used gravity anomaly measurements from the Gravity Recovery and Climate Experiment (GRACE) satellite (*17*). These measurements, used in previous studies to investigate changes in groundwater, have been corrected for geophysical mass variations such as tides, atmo-

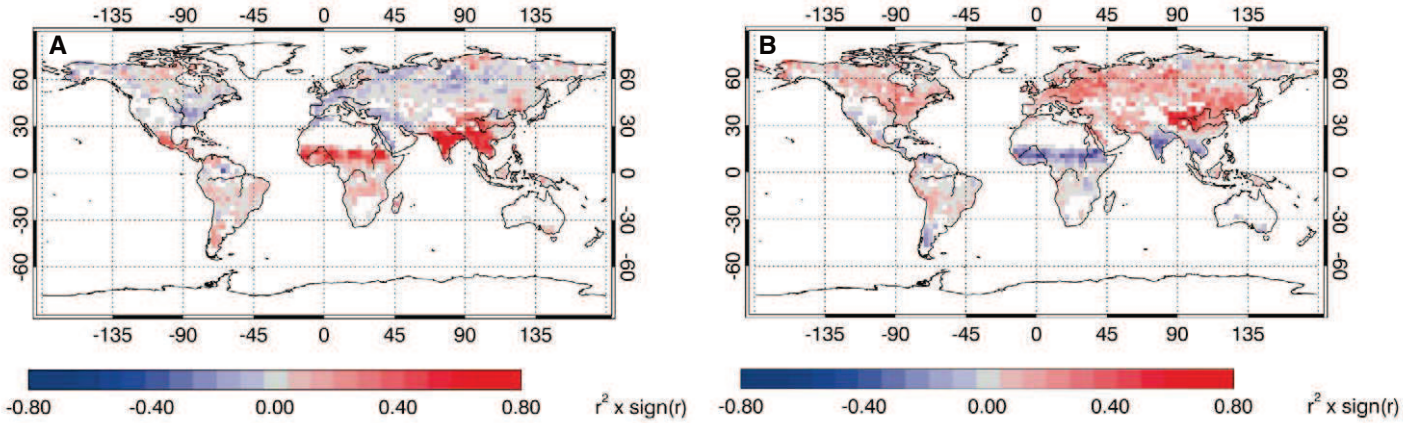

Fig. 1. Correlations (r^2) between cloud-free SCIAMACHY CH_4 column volume mixing ratios (VMRs) (in parts per million) and (**A**) equivalent groundwater depth (in meters), determined from gravity anomaly measurements from the GRACE satellites (*18*) and (**B**) NCEP/NCAR surface skin temperatures (in kelvin), calculated on a 3° × 3° horizontal grid over 2003–2005. The correlation at a given point is determined by at least 15 and typically 60 CH_4, groundwater, and temperature measurements. See SOM for a description of individual data sets.

Fig. 2. Time series of SCIAMACHY CH_4 column VMR and groundwater depth over the (**A**) Ganges, (**B**) Niger, (**C**) South Amazon, and (**D**) South Congo river basins. The correlation (r^2) between the variables is given for each panel. River basins are geographicaly defined with total runoff-integrating pathways (*26*). Vertical lines denote the start and end of each calendar year. A spatial representation of river basin correlations between CH_4 and groundwater is included in the SOM.

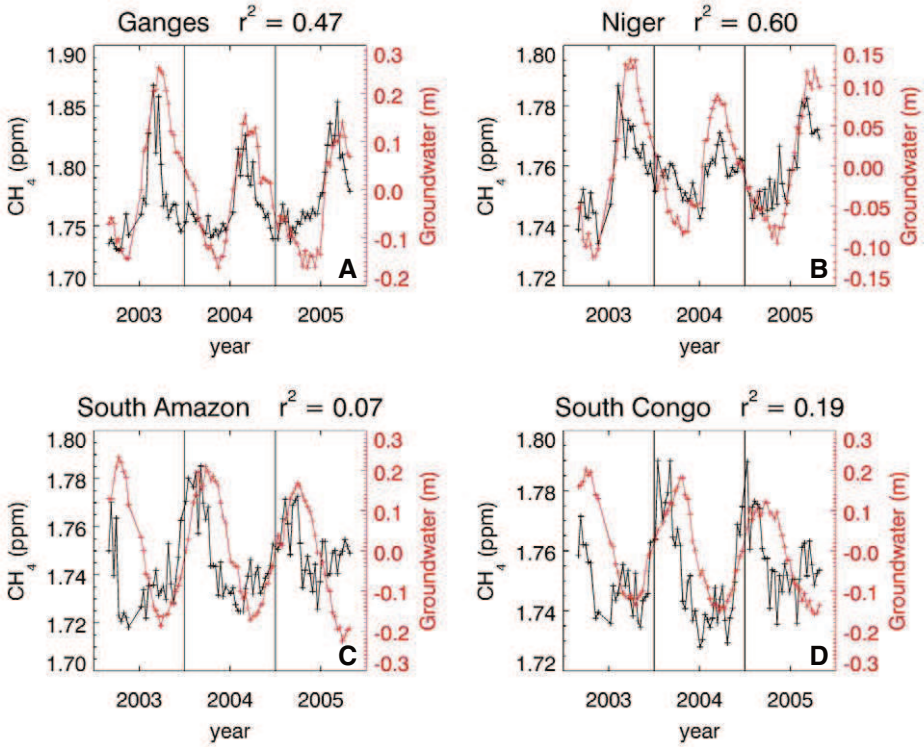

spheric pressure, and wind (*18*). Relative equivalent water height Γ (in meters), inferred from gravity [see supporting online material (SOM)], shows seasonal variability ranging from 5 to 20 cm over major river basins (*19*). We used a Γ data set with a 10-day time step (*18*), which we regridded to 3° × 3°. Finally, we used surface skin temperature fields T_S (in kelvin) from the National Centre for Environmental Prediction/National Centre for Atmospheric Research (NCEP/NCAR) weather analyses (*20*) as a proxy for soil temperature (SOM). We resolved all three data sets at the temporal and spatial resolutions of the Γ data set (SOM).

We find that that changes in wetlands and rice emissions dominate the observed variability of CH_4 columns over wetland regions [square of the correlation coefficient (r^2) = 0.7, SOM], and hence we interpret changes in these columns as changes in surface sources. We find that seasonal variations in the OH sink (*21*) and the CH_4 source from fires (*22*) typically explain <10 and 3% of the observed CH_4 column variability, respectively. CH_4 column data are available only over cloud-free daytime scenes; changes in controls on wetland CH_4 emissions on time scales shorter than 1 or 2 days due to processes such as rainfall, associated with cloudy conditions, are not well described by GRACE or Envisat. We excluded analysis over oceans, deserts, and regions with permanent ice cover.

To quantify the role of wetlands and rice cultivation in determining the observed variability of column CH_4, we correlated these data with concurrent changes in Γ and T_S over 2003–2005 (Fig. 1). We find that changes in Γ explain between 40 and 80% of the observed variability in CH_4 measurements over the tropics. We find high correlations over many major river basins (SOM), with the exception of the Amazon basin, which is described below. We generally find a negative correlation between Γ and CH_4 at high latitudes, which can be explained by high Γ in winter due to snow accumulation and associated low CH_4 emission, and low Γ in spring and summer due to displacement of snow melt and higher CH_4 emission as the exposed wetland is progressively warmed. At higher latitudes, we find that observed variations in CH_4 are mostly explained by changes in T_S (used here as a proxy for soil temperature). Changes in T_S over the tropics explain little of the observed variation in CH_4. Analysis of the deseasonalized time series shows similar but reduced correlations between CH_4 and Γ and T_S (SOM). This analysis provides global observations of the latitude dependence of the controlling factors—water table depth and soil temperature—that determine large-scale variations in wetland and rice paddy CH_4 emissions (*6*). This work supports our model calculations (SOM) that show that wetland and rice paddy emissions are largely responsible for observed CH_4 column variations.

Although variations in methanogenesis are predominantly attributed to variations in either groundwater or temperature, we account for the more complex dependence of methanogenesis with respect to both quantities (*23*). Within tropical latitudes, Γ is expected to be the dominant term in

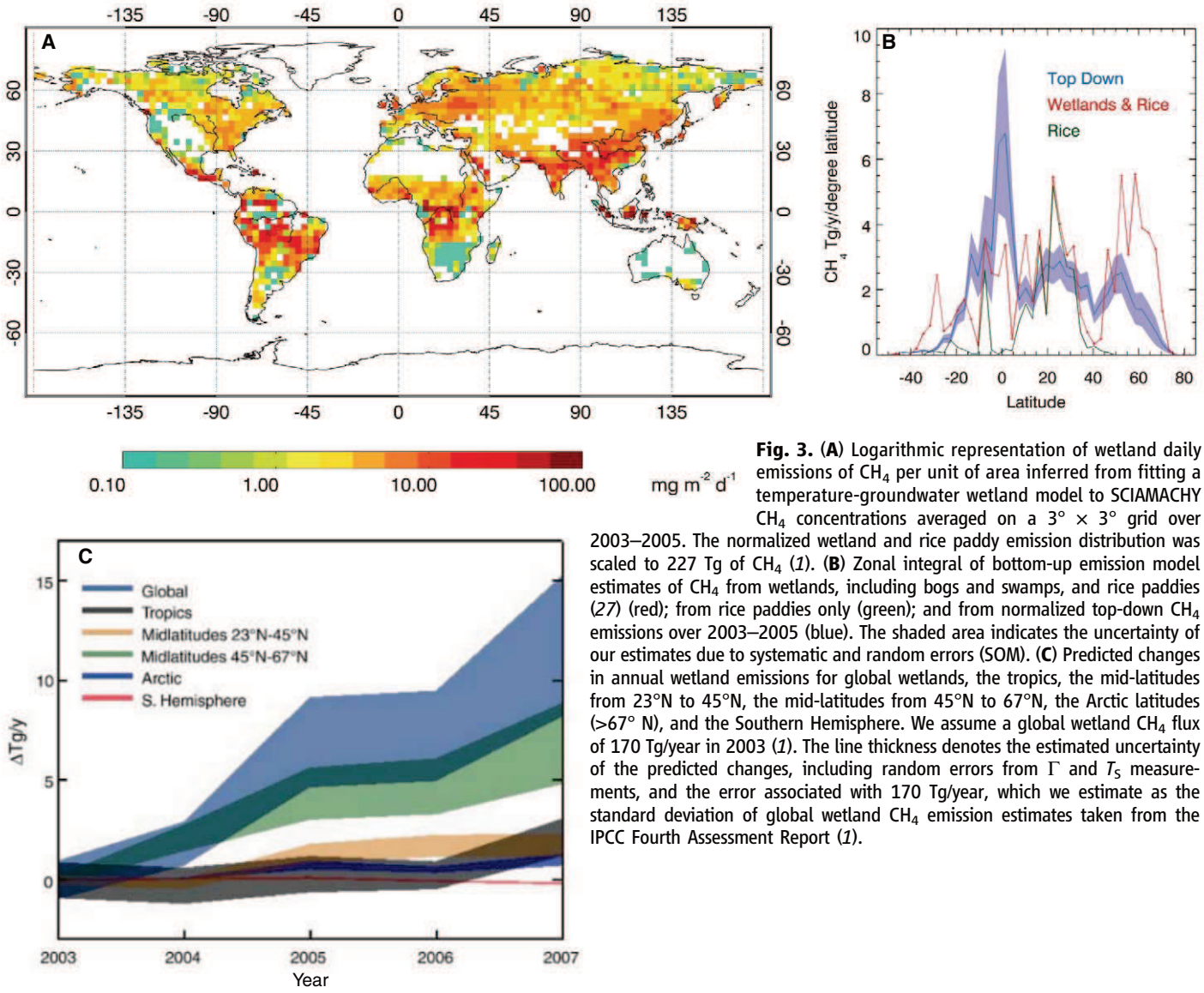

Fig. 3. (**A**) Logarithmic representation of wetland daily emissions of CH_4 per unit of area inferred from fitting a temperature-groundwater wetland model to SCIAMACHY CH_4 concentrations averaged on a 3° × 3° grid over 2003–2005. The normalized wetland and rice paddy emission distribution was scaled to 227 Tg of CH_4 (*1*). (**B**) Zonal integral of bottom-up emission model estimates of CH_4 from wetlands, including bogs and swamps, and rice paddies (*27*) (red); from rice paddies only (green); and from normalized top-down CH_4 emissions over 2003–2005 (blue). The shaded area indicates the uncertainty of our estimates due to systematic and random errors (SOM). (**C**) Predicted changes in annual wetland emissions for global wetlands, the tropics, the mid-latitudes from 23°N to 45°N, the mid-latitudes from 45°N to 67°N, the Arctic latitudes (>67° N), and the Southern Hemisphere. We assume a global wetland CH_4 flux of 170 Tg/year in 2003 (*1*). The line thickness denotes the estimated uncertainty of the predicted changes, including random errors from Γ and T_S measurements, and the error associated with 170 Tg/year, which we estimate as the standard deviation of global wetland CH_4 emission estimates taken from the IPCC Fourth Assessment Report (*1*).

areas with distinct dry and wet seasons. In areas where the preexisting groundwater volume is large with respect to Γ variations, a combined Γ-T_S relationship is expected. Figure 2 shows time series over four regions that exemplify the relationship between changes in Γ and column CH_4. For the Niger and the Ganges basins, changes in Γ coincide closely with the CH_4 variability, as is expected if the CH_4 signal is due to methanogenesis. Over the Amazon basin, the overall correlation between Γ and CH_4 is negligible ($r^2_{Amazon} = 0.01$). Changes in Γ over the Amazon basin are much larger than values observed over other river basins (Fig. 2) and lag behind CH_4 changes by 1 to 3 months in the north of the basin, possibly due to the seasonal migration of the intertropical convergence zone (SOM), but we find a statistically significant correlation over the southern half of the basin (south of 4°S, $r^2 = 0.07$). Although the CH_4 seasonal cycles over the north and south Amazon are synchronous, the seasonal cycle of wetland groundwater over the north Amazon precedes the south Amazon cycle by approximately 2 months; considering the east-west divide of the Amazon basin does not improve the correlation. Wetland emissions over the Amazon basin coincide with the Amazon River system and its varzeas (*24*). We acknowledge that even large temporal changes in wetland groundwater, Γ(t), over this basin will not necessarily represent large changes in surface soil moisture because of the depth of the wetland groundwater, $D + \Gamma(t)$, where D represents the initial volume of the water column.

To determine the distribution of wetland emissions of CH_4 ($F^{w,\Gamma}_{CH_4}$, in mg/m^2/day), we developed a simple model (SOM) that describes the time-dependent relation between these emissions and T_S, and $D + \Gamma(t)$

$$F^{w,\Gamma}_{CH_4}(t) = k[D + \alpha\Gamma(t)]Q_{10}(T_S)^{\frac{T_s(t) - T_0}{10}} \quad (1)$$

where α is the fractional influence of Γ(t) on the total wetland groundwater volume $D + \Gamma(t)$ (where $0 < \alpha < 1$); $Q_{10}(T_S)$ describes the change in methanogenesis rate with a 10 K increase in temperature, where T_0 is a constant ($T_0 = 273.16$ K) (*23*); and k (mg/m^3/day) incorporates other controlling factors (such as soil pH). The temperature dependence of $Q_{10}(T_S)$ can be approximated by $Q_{10}(T_0)^{[(T_0)/(T_S)]}$ (*23*). We acknowledge that the derived values of $Q_{10}(T_S)$ represent the relation between methanogenesis and T_S as opposed to soil temperature (SOM). We maximized the local linear correlation between $F^{w,\Gamma}_{CH_4}$ and SCIAMACHY CH_4 columns by varying (D/α) on a per grid basis and globally fitting $Q_{10}(T_0)$, where the gradient is proportional to changes in wetland emissions and the intercept is the sum of the remaining sources and sinks (SOM). We expect wetland and rice paddy emissions to follow a similar seasonal cycle, reflecting necessary hydrological and temperature conditions, but acknowledge that rice paddy emissions occur at specific intervals during the rice cultivation process. The global value of $Q_{10}(T_0)$ that best fits the data is 1.65 ± 0.15, although we find that wetland and rice paddy emission distributions remain similar within the range $1 < Q_{10}(T_0) < 2$.

The resulting normalized $F^{w,\Gamma}_{CH_4}$ distribution was then scaled to a total global wetland and rice paddy source of 227 Tg of CH_4/year, using the median value from the Intergovernmental Panel on Climate Change (IPCC) Fourth Assessment Report (*1*) to derive global emission rates shown in Fig. 3A. We find the largest CH_4 fluxes over South America, equatorial Africa, and southeast Asia. Emissions over the extratropical Northern Hemisphere are generally lower, but have elevated values over northern Europe and central Siberia and local peaks over North America. We find that uncertainties associated with extratropical CH_4 fluxes are an order of magnitude smaller than those associated with tropical fluxes (SOM).

We used prior information about rice paddy distributions (*12*) to isolate wetland regions from our emission estimates. The resulting latitudinal distribution of wetland emissions is similar to those produced by independent bottom-up emission estimates (Fig. 3B) and is within the range of the large intermodel differences (*25*). We find that the tropics account for 55.5 ± 2.5% of global wetland emissions, with the Amazon and Congo river basins accounting for 20.0 ± 2.6 Tg of CH_4/year and 25.7 ± 1.7 Tg of CH_4/year, respectively. We find that rice paddy areas account for 29.1 ± 0.6% (66.0 ± 1.4 Tg of CH_4/year) of the total rice plus wetland CH_4 source, acknowledging that a small proportion of this may be attributed to the spatial coincidence of rice paddies and wetlands. We find that rice paddy emissions centered over China and south and southeast Asia account for 32.5 ± 3.7 Tg of CH_4/year of the global rice paddy source, which is in agreement with bottom-up emission estimates (*12*).

We used our $F^{w,\Gamma}_{CH_4}$ model to determine the evolution of wetland CH_4 emissions over 2003–2007 relative to 2003 emissions. The change in annual emissions over that 5-year period was evaluated using the product of the fractional emission change and the wetland CH_4 map in Fig. 3A. We omitted areas of rice cultivation (*12*), where year-to-year changes in CH_4 emissions are determined by irrigation and other management regimes. We find a progressive global increase in CH_4 from wetlands over 2003–2007, due mainly to temperature increases at extratropical latitudes (45° to 67°N). We also find that Arctic wetland emissions (>67°N) increased by 30.6 ± 0.9% over 2003–2007 to approximately 4.2 ± 1.0 Tg of CH_4/year (SOM). We find that emissions from tropical wetlands remained constant over 2003–2006, with the exception of a 2.1 ± 0.7 Tg/year increase during 2007, most of which is accounted for by increased fluxes over the Congo (0.7 ± 0.2 Tg of CH_4/year) and Sahel (0.9 ± 0.2 Tg of CH_4/year) regions, as a result of increasing groundwater volume. The declining groundwater volume over tropical river basins over 2003–2006 did not significantly affect year-to-year changes in global wetland emissions. Our emissions calculations lead to better agreement with observed surface CH_4 anomalies over 2003–2008 than those obtained using bottom-up wetland emissions (SOM), reproducing the observed post-2006 positive anomaly in both the Northern and Southern Hemispheres. This supports the idea that changes in wetland emissions have significantly contributed to recent changes in atmospheric CH_4 concentrations.

There is substantial potential for wetland emissions to feed back positively to changes in climate (*23*), and therefore it is critical that we understand the extent of overlap between wetlands and regions that are most sensitive to projected future warming. We anticipate that the new constraints developed here will ultimately improve model predictions of this feedback.

References and Notes

1. K. Denman *et al.*, in *Climate Change 2007: The Physical Science Basis. Contribution of Working Group I to the Fourth Assessment Report of the Intergovernmental Panel on Climate Change*, S. Solomon *et al.*, Eds. (Cambridge Univ. Press, Cambridge, 2007), pp. 499–588.
2. E. J. Dlugokencky *et al.*, *Geophys. Res. Lett.* **30**, 1992 (2003).
3. M. Rigby *et al.*, *Geophys. Res. Lett.* **35**, L22805 (2008).
4. A. R. McLeod *et al.*, *New Phytol.* **180**, 124 (2008).
5. C. Frankenberg *et al.*, *Atmos. Chem. Phys.* **8**, 5061 (2008).
6. B. P. Walter, M. Heimann, E. Matthews, *J. Geophys. Res.* **106**, 34189 (2001).
7. E. Matthews, I. Fung, J. Lerner, *Global Biogeochem. Cycles* **5**, 3 (1991).
8. D. M. Ward, M. R. Winfrey, *Adv. Aquat. Microbiol.* **3**, 141 (1985).
9. R. Segers, *Biogeochemistry* **41**, 23 (1998).
10. J. Le Mer, P. Roger, *Eur. J. Soil Biol.* **37**, 25 (2001).
11. A. Joabsson, T. R. Christensen, B. Wallén, *Trends Ecol. Evol.* **14**, 385 (1999).
12. I. Fung *et al.*, *J. Geophys. Res.* **96**, (D7), 13033 (1991).
13. P. Bousquet *et al.*, *Nature* **443**, 439 (2006).
14. J. R. Evans, *New Phytol.* **175**, 1 (2007).
15. H. Bovensmann *et al.*, *J. Atmos. Sci.* **56**, 127 (1999).
16. C. Frankenberg *et al.*, *Geophys. Res. Lett.* **35**, L15811 (2008).
17. B. D. Tapley, S. Bettadpur, J. C. Ries, P. F. Thompson, M. M. Watkins, *Science* **305**, 503 (2004).
18. J.-M. Lemoine *et al.*, *Adv. Space Res.* **39**, 1620 (2007).
19. J. L. Chen, C. R. Wilson, J. S. Famiglietti, M. Rodell, *J. Geod.* **81**, 237 (2007).
20. E. Kalnay *et al.*, *Bull. Am. Meteorol. Soc.* **77**, 437 (1996).
21. A. Fiore *et al.*, *J. Geophys. Res. (Atmos.)* **108**, 4787 (2003).
22. G. R. van der Werf *et al.*, *Atmos. Chem. Phys.* **6**, 3423 (2006).
23. N. Gedney, P. M. Cox, C. Huntingford, *Geophys. Res. Lett.* **31**, L20503 (2004).
24. J. M. Melack *et al.*, *Glob. Change Biol.* **10**, 530 (2004).
25. M. Cao, S. Marshall, K. Gregson, *J. Geophys. Res.* **101**, (D9), 14399 (1996).
26. T. Oki, Y. C. Sud, *Earth Interact.* **2**, 1 (1998).
27. E. Matthews, I. Fung, *Global Biogeochem. Cycles* **1**, 61 (1987).

28. We thank J. Melack for providing feedback on the manuscript and R. Hipkin and F. Simons for assistance with GRACE gravity data. This work is funded by United Kingdom Natural Environmental Research Council studentship NE/F007973/1 and the National Centre for Earth Observation.

Supporting Online Material www.sciencemag.org/cgi/content/full/327/5963/322/DC1 SOM Text
Figs. S1 to S6
Table S1
References

20 April 2009; accepted 11 November 2009
10.1126/science.1175176

Lower Predation Risk for Migratory Birds at High Latitudes

L. McKinnon,[1]* P. A. Smith,[2] E. Nol,[3] J. L. Martin,[4] F. I. Doyle,[5] K. F. Abraham,[6] H. G. Gilchrist,[7] R. I. G. Morrison,[2] J. Bêty[1]

Quantifying the costs and benefits of migration distance is critical to understanding the evolution of long-distance migration. In migratory birds, life history theory predicts that the potential survival costs of migrating longer distances should be balanced by benefits to lifetime reproductive success, yet quantification of these reproductive benefits in a controlled manner along a large geographical gradient is challenging. We measured a controlled effect of predation risk along a 3350-kilometer south-north gradient in the Arctic and found that nest predation risk declined more than twofold along the latitudinal gradient. These results provide evidence that birds migrating farther north may acquire reproductive benefits in the form of lower nest predation risk.

Life history theory predicts that the costs of migration must be compensated for by benefits to lifetime reproductive success (*1*, *2*). Costs of migration include the metabolic and energetic requirements of flight (*3*), high mortality risk (*4*, *5*), and exposure to extreme weather events (*6*, *7*). Such negative effects are expected to be important for migrant birds that breed in the Arctic, where severe weather events during migration or upon arrival at the breeding grounds can lead to poor body condition, breeding failure, complete reverse migration, and even death (*8*). Bird migration patterns have been thought to be determined mainly by food availability (*9*), habitat-related parasite pressures (*10*), and predation risk during migration (*4*).

Arctic-nesting birds exhibit some of the most impressive migratory strategies, such as flying from wintering areas at the southern tip of South America, southern Africa, and Oceania to their breeding grounds in the Arctic (*11*, *12*). The physiological costs of migrating to and breeding at these arctic sites have been well documented for species such as shorebirds (*7*, *13*, *14*). Birds could reduce these costs by breeding at more southerly latitudes, thereby decreasing both migration costs and the metabolic costs of breeding in the extreme arctic environment. However, if competition for food resources, risk of parasite infection, and predation at southern sites are high, then increasing migration distance could have reproductive and/or survival benefits. Potential fitness benefits of breeding at higher latitudes have been quantified in terms of reduced parasite loads (*15*) and greater food availability due to longer daylight hours (*16*).

Reduced predation at higher-latitude sites has yet to be quantified. Predation risk has emerged as a dominant force in the evolution of avian life history, influencing the selection of nest sites and underlying latitudinal clines in the clutch size of passerines (*17*). We thus predicted that the risk of nest predation could also play a key role in balancing the costs of long-distance migration. If so, we would expect a negative relationship between nest predation risk and latitude in arctic ground-nesting shorebirds. To test for this relationship, we systematically measured predation risk by monitoring the survival of 1555 artificial nests for a minimum of two summers at seven shorebird breeding sites (table S1) (*18*) over a latitudinal gradient of 29° (~3350 km) from sub-Arctic to High-Arctic regions of Canada (Fig. 1). By monitoring artificial nests, we controlled for the heterogeneity in survival associated with real nests [temporal, spatial, interspecific, and intraspecific behavioral differences (*19*)] to yield a controlled effect of predation risk. We monitored artificial nests during early and late shorebird incubation periods. We then tested for the effect of latitude on predation risk, using Cox proportional hazards regression (*18*, *20*).

As predicted, nest predation risk was negatively correlated with latitude. For an increase in 1° of latitude, the relative risk of predation declined by 3.6% (coefficient –0.0360, SE 0.0045, χ^2_1 = 63.77, $P < 0.0001$; Figs. 1 to 3). This equates to a decrease in predation risk of 65% over the studied latitudinal transect of 29°. Previous studies investigating latitudinal trends in predation risk on the nests of temperate-breeding neotropical migrants failed to detect any clear south-north gradient (*21*). These differences in results could be attributed to differences in real patterns of predation risk between temperate versus arctic environments, or they could be due to differences in methodological approaches. In our study, artificial nests enabled us to measure a standardized predation risk, as opposed to the nest success of

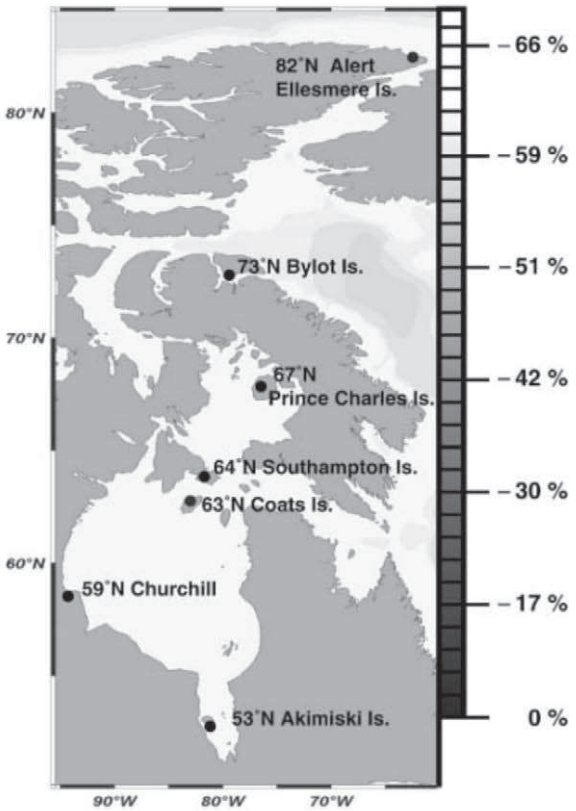

Fig. 1. Average latitudinal decrease in nest predation risk and map of the shorebird breeding sites where artificial nests were monitored. The decrease in predation risk (3.6% per degree relative to the southernmost site, Akimiski Island) is indicated at 5° intervals on the latitudinal scale at right.

[1]Département de Biologie, Université du Québec à Rimouski and Centre d'Etudes Nordiques, Rimouski, Québec, G5L3A1, Canada. [2]Environment Canada, National Wildlife Research Centre, Ottawa, Ontario, K1A0H3, Canada. [3]Ecology and Conservation Group, Environment and Life Sciences Graduate Program and Biology Department, Trent University, Peterborough, Ontario, K9J7B8, Canada. [4]Département Dynamique des Systèmes Ecologiques, Centre d'Ecologie Fonctionnelle et Evolutive, Centre National de la Recherche Scientifique, Montpellier, France. [5]Wildlife Dynamics Consulting, Telkwa, British Colombia, V0J2X0, Canada. [6]Wildlife Research & Development Section, Ontario Ministry of Natural Resources, Peterborough, Ontario, K9J7B8, Canada. [7]Environment Canada, National Wildlife Research Centre and Department of Biology, Carleton University, Ottawa, Ontario, K1S5B6, Canada.

*To whom correspondence should be addressed. E-mail: laura.mckinnon3@gmail.com

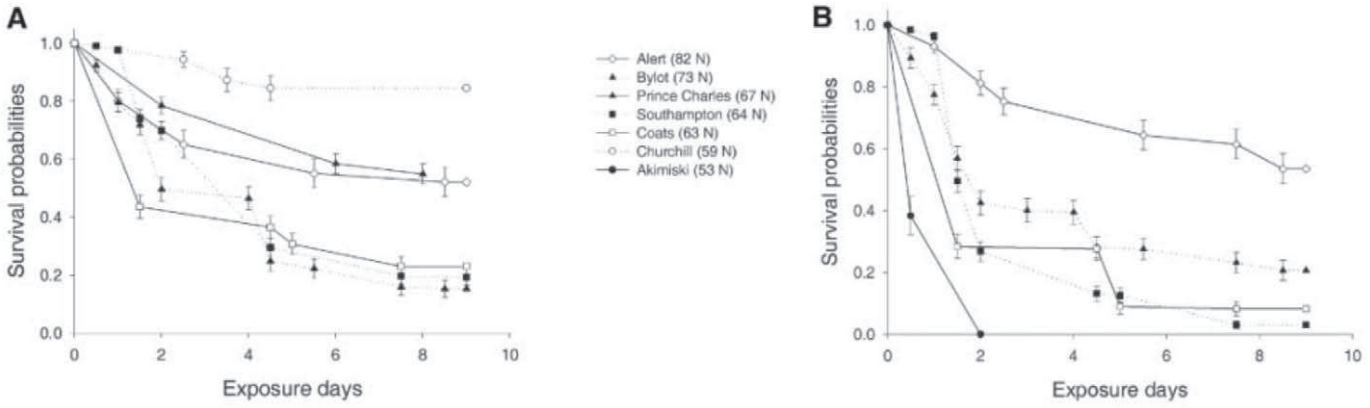

Fig. 2. Kaplan-Meier survival probabilities over 9 exposure days for artificial nests by site for all years during early (**A**) and late (**B**) shorebird incubation periods. Each data point on the curve represents the Kaplan-Meier survival estimate at time *t* (±SEM), which provides the probability that a nest will survive past time *t*. Survival probabilities are based on 2 to 4 years of data per site [see table S1 for details (*18*)]

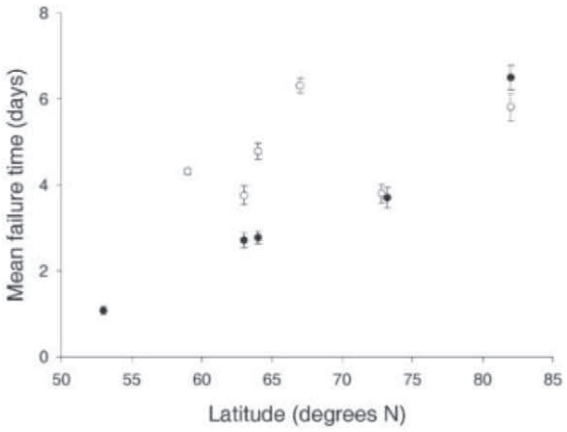

Fig. 3. Mean failure time in days (±SEM) for depredated artificial nests by latitude for all years during early (open circles) and late (solid circles) shorebird incubation periods. Low mean failure times indicate rapid nest loss (high predation risk). Each data point is based on 2 to 4 years of data per site [see table S1 for details (*18*)]. Overlapping data points for Bylot Island (73° N) have been offset by ±0.2°.

real nests, which is affected by several factors other than predation pressure [for example, parent birds can compensate for an increased risk of predation by increasing the defense of their nest (*22*)].

These results provide evidence that the costs of migrating farther north could be compensated for by decreases in predation risk at higher latitudes. However, can lower predation risk at higher latitudes really compensate for the increased migration distances and increased metabolic harshness experienced by High-Arctic–nesting species? Though we may have good estimates of the energetic costs of flying (*23*) and how standard metabolic rates change with latitude (they increase by 1% per degree of latitude) (*24*), we still lack the basic understanding of how these variables affect adult survival. The apparent cost associated with migrating to Arctic breeding areas is indicated by the reduced survival of adults that fail to achieve adequate condition before leaving the last spring staging area (*7*, *13*); however, it is not known whether the increased mortality is associated with migration, breeding, or both. To explore these trade-offs, we require better estimates of demographic parameters for birds breeding at various latitudes, so that we can model the contrasting effects of adult survival versus reproductive components. By combining studies on marked individuals with systematic sampling of ecological conditions experienced on the breeding grounds, we will better be able to link individual itineraries with life history events, thus improving our theoretical understanding of the ecology and evolution of long-distance migration.

References and Notes

1. S. C. Stearns, *Q. Rev. Biol.* **51**, 3 (1976).
2. T. Alerstam, A. Hedenstrom, S. Akesson, *Oikos* **103**, 247 (2003).
3. M. Wikelski *et al.*, *Nature* **423**, 704 (2003).
4. R. C. Ydenberg, R. W. Butler, D. B. Lank, B. D. Smith, J. Ireland, *Proc. Biol. Sci.* **271**, 1263 (2004).
5. A. J. Baker *et al.*, *Proc. Biol. Sci.* **271**, 875 (2004).
6. R. W. Butler, *Auk* **117**, 518 (2000).
7. R. I. G. Morrison, N. C. Davidson, J. R. Wilson, *J. Avian Biol.* **38**, 479 (2007).
8. B. Ganter, H. Boyd, *Arctic* **53**, 289 (2000).
9. D. J. Levey, F. G. Stiles, *Am. Nat.* **140**, 447 (1992).
10. T. Piersma, *Oikos* **80**, 623 (1997).
11. J. M. Boland, *Condor* **92**, 284 (1990).
12. J. van de Kam, P. J. de Goeij, T. Piersma, L. I. Zwarts, *Shorebirds: An Illustrated Behavioural Ecology* (KNNV Publishers, Utrecht, Netherlands, 2004).
13. R. I. G. Morrison, *Ardea* **94**, 607 (2006).
14. T. Piersma *et al.*, *Funct. Ecol.* **17**, 356 (2003).
15. M. Laird, *Can. J. Zool*. **39**, 209 (1961).
16. H. Schekkerman, I. Tulp, T. Piersma, G. H. Visser, *Oecologia* **134**, 332 (2003).
17. T. E. Martin, P. R. Martin, C. R. Olson, B. J. Heidinger, J. J. Fontaine, *Science* **287**, 1482 (2000).
18. See supporting material on *Science* Online.
19. T. E. Martin, J. Scott, C. Menge, *Proc. Biol. Sci.* **267**, 2287 (2000).
20. D. R. Cox, *J. R. Stat. Soc. Ser. B Methodol.* **34**, 187 (1972).
21. T. E. Martin, *Ecol. Monogr.* **65**, 101 (1995).
22. J. Kis, A. Liker, T. Székely, *Ardea* **88**, 155 (2000).
23. A. Kvist, A. Lindström, M. Green, T. Piersma, G. H. Visser, *Nature* **413**, 730 (2001).
24. W. W. Weathers, *Oecologia* **42**, 81 (1979).
25. Funded by ArcticNet, Environment Canada, Fonds Québécois de Recherche sur la Nature et les Technologies, a Garfield Weston Foundation Award for Northern Research, Institut Paul Emile Victor (formerly Institut Français de Recherches et Technologies Polaires), International Polar Year (IPY) Project ArcticWOLVES, Natural Sciences and Engineering Research Council of Canada (Northern Internship Program and Discovery Grant), Northern Ecosystem Initiatives, Northern Scientific Training Program, and the Ontario Ministry of Natural Resources. Logistical support was provided by the Ontario Ministry of Natural Resources, the Polar Continental Shelf Project, Parks Canada, and D. Leclerc. We also thank the Department of National Defense and staff of the Environment Canada weather station for logistic support at Alert; Vicky Johnston and crew for support on Prince Charles Island; the many field assistants who monitored artificial nests: A. Blachford, A. Béchet, J. Carrier, M. Cloutier, A.-M. d'Aoust-Messier, E. d'Astous, T. Daufresne, S. Gan, D. Hogan, L. Jolicoeur, C. Juillet, J.-R. Julien, B. Laliberté, P. Y. l'Hérault, R. Lopez, P. Meister, M. Nelligan, D. Ootoova, L. Qangug, D. C. Rabouam, G. Reid, N. Ward, and S. Williams; G. Gauthier and D. Berteaux, leaders of the IPY ArcticWOLVES project, for fostering collaboration between the authors; and O. Gilg, C. Juillet, L. P. Nguyen, T. Piersma, D. Reid, and two anonymous reviewers for helpful discussions or comments on early versions of the manuscript.

Supporting Online Material

www.sciencemag.org/cgi/content/full/327/5963/326/DC1
Materials and Methods
SOM Text
Table S1
References

7 October 2009; accepted 1 December 2009
10.1126/science.1183010

The Genetic Map of *Artemisia annua* L. Identifies Loci Affecting Yield of the Antimalarial Drug Artemisinin

Ian A. Graham,[1]* Katrin Besser,[1] Susan Blumer,[1] Caroline A. Branigan,[1] Tomasz Czechowski,[1] Luisa Elias,[1] Inna Guterman,[1] David Harvey,[1] Peter G. Isaac,[2] Awais M. Khan,[1] Tony R. Larson,[1] Yi Li,[1] Tanya Pawson,[1] Teresa Penfield,[1] Anne M. Rae,[1] Deborah A. Rathbone,[1] Sonja Reid,[1] Joe Ross,[1] Margaret F. Smallwood,[1] Vincent Segura,[1] Theresa Townsend,[1] Darshna Vyas,[1] Thilo Winzer,[1] Dianna Bowles[1]*

Artemisinin is a plant natural product produced by *Artemisia annua* and the active ingredient in the most effective treatment for malaria. Efforts to eradicate malaria are increasing demand for an affordable, high-quality, robust supply of artemisinin. We performed deep sequencing on the transcriptome of *A. annua* to identify genes and markers for fast-track breeding. Extensive genetic variation enabled us to build a detailed genetic map with nine linkage groups. Replicated field trials resulted in a quantitative trait loci (QTL) map that accounts for a significant amount of the variation in key traits controlling artemisinin yield. Enrichment for positive QTLs in parents of new high-yielding hybrids confirms that the knowledge and tools to convert *A. annua* into a robust crop are now available.

Malaria is a global health problem with more than 1 billion people living in areas with a high risk of the disease. Artemisinin combination therapies (ACTs) are the recommended treatment for uncomplicated malaria caused by the *Plasmodium falciparum* parasite (*1*). Parasite resistance to artemisinin has recently been confirmed in western Cambodia (*2*). It has long been recognized that the problem of artemisinin resistance is best addressed by increasing access to ACTs and discouraging the use of artemisinin monotherapies (*3*). This approach has strong support from the global health community with both funding and demand for ACTs expected to increase massively in the short- to midterm (*3*). However, there is growing concern that the supply chain will be unable to consistently produce high-quality artemisinin in the quantities that will be required (*3*). Artemisinin is a sesquiterpenoid synthesized in the glandular trichomes of the Chinese medicinal plant *Artemisia annua* L. (*4*–*10*). For a pharmaceutical with annual sales exceeding 100 million treatments, ACT supply remains reliant on the agricultural production of artemisinin. Plant-based production of artemisinin is challenging because *A. annua* remains relatively undeveloped as a crop. An alternative microbial-based system that synthesizes an artemisinin precursor for chemical conversion is in development (*11*, *12*). This would supplement but not replace agricultural production, which will continue to be an essential source of supply (*3*). Improved varieties of *A. annua* for developing-world farmers would bring immediate benefits to the existing artemisinin supply chain by reducing production costs, stabilizing supplies, and improving grower confidence in the crop (*3*).

[1]Centre for Novel Agricultural Products, Department of Biology, University of York, York YO10 5YW, UK. [2]IDna Genetics Ltd., Norwich Research Park, Norwich NR4 7UH, UK.

*To whom correspondence should be addressed. E-mail: iag1@york.ac.uk (I.A.G.); djb32@york.ac.uk (D.B.)

A. annua is a member of the *Asteraceae* family that favors outcrossing over selfing (*13*). The artemisinin content of plants from different origins varies considerably and is highly heritable (*14*). The market leader for artemisinin production, at present, is Artemis, an F_1 hybrid (population) variety developed by Mediplant (Conthey, Switzerland) (*14*). Artemis seed is produced from a cross between two heterozygous and genetically different parental genotypes, called C4 and C1, that are themselves maintained vegetatively. In this study, we have used the Artemis pedigree to establish genetic linkage and QTL maps for this species and independently validated positive QTL for artemisinin yield.

We used the Roche 454 pyrosequencing platform to produce expressed sequence tag (EST) databases from cDNA libraries derived from enriched glandular trichome preparations of young leaves, mature leaves, and flower buds from the Artemis hybrid (*15*). cDNA libraries and EST databases were also prepared from meristem tissue (including very young leaf tissue) and cotyledons. A selection of key genes associated with metabolic pathways and phenotypic traits such as trichome development and plant architecture that could affect artemisinin yield are illustrated in fig. S1, together with their relative abundance in the different libraries (SOM Text and table S1). The EST sequences were also used for in silico identification of single-nucleotide polymorphisms (SNPs), short sequence repeats (SSRs), and insertions/deletions (InDels), which can be used as molecular markers for mapping and breeding (*15*). We identified 34,419 SNPs from DNA sequences contained in the five EST databases derived from the Artemis F_1 hybrid material, representing a mean SNP frequency of 1 in 104 base pairs

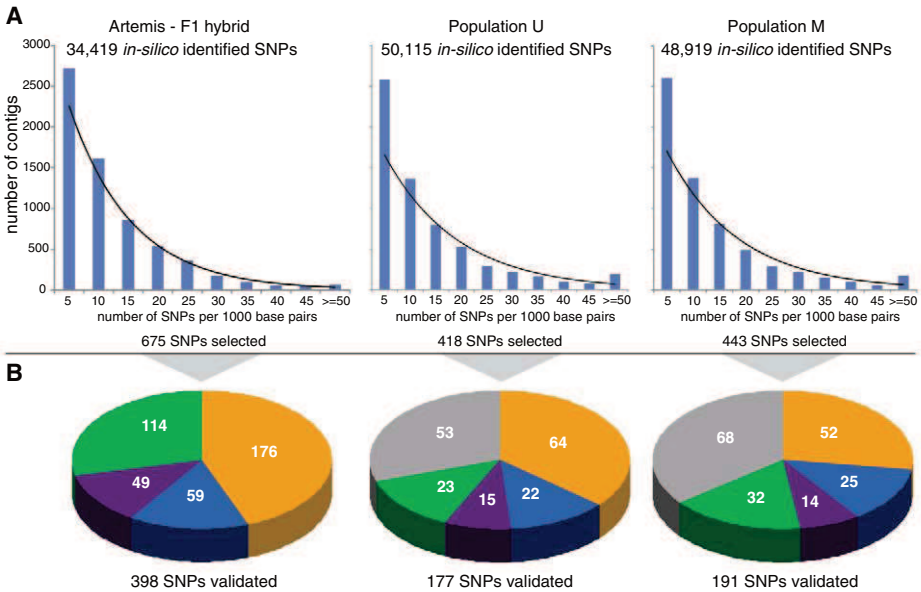

Fig. 1. High-throughput identification and validation of SNP markers in three *A. annua* populations. (**A**) Frequency distribution of potential SNPs identified in silico from EST databases produced by pyrosequencing cDNA libraries from the Artemis F_1 hybrid, Population U (commercially grown in Uganda) and Population M (commercially grown in Madagascar). The observed distribution of SNP frequency correlates closely with an exponential distribution for each data set as indicated by the curved black lines, which trace the expected distribution and R^2 values that are greater than 0.85 in all cases. Stringent selection criteria resulted in approximately only 10% of contigs being used for SNP identification (*15*). (**B**) Genotyping the Artemis pedigree. Subsets of in silico–identified SNPs from each population were selected for hybridization-based detection on the Illumina Goldengate Genotyping platform. The three pie charts show the genotyping of the Artemis pedigree with SNPs from Artemis, and Populations U and M. Color coding illustrates the proportion of SNPs that were polymorphic in the C4 parent (orange), polymorphic in the C1 parent (blue), polymorphic in both parents (purple), monomorphic in both parents for opposite alleles (green), and monomorphic in both parents for the same alleles (gray). This latter class is due to alleles being polymorphic in Population M or Population U but not in Artemis.

(Fig. 1A). This polymorphism was confirmed experimentally with 19 amplified fragment length polymorphism (AFLP) primer combinations that revealed 322 polymorphic markers (table S2). The in silico approach also identified 49 SSR markers that segregated in the Artemis F_1 population (table S3). We extended the in silico approach to two other *A. annua* populations, commercially grown in Uganda (Population U) and Madagascar (Population M), and found that the mean SNP frequencies of 1 in 88 and 1 in 91 base pairs, respectively, are only slightly higher than that of the Artemis F_1 hybrid (Fig. 1A).

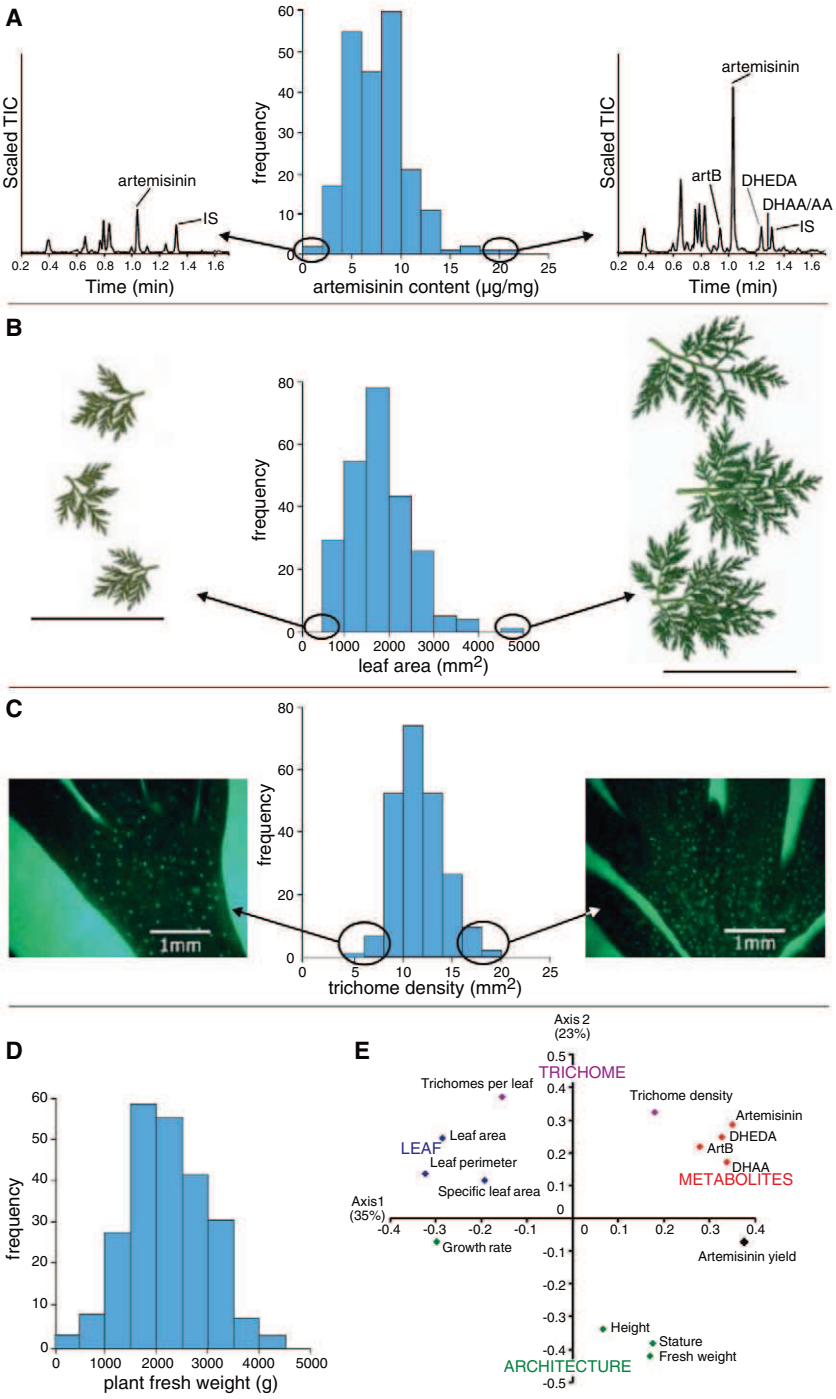

Fig. 2. Phenotypic variation in the Artemis F_1 grown in UK field trials in 2007. The distribution of four traits related to artemisinin yield is illustrated. (**A**) Artemisinin concentration at harvest (7 months after sowing). Metabolite profiles showing artemisinin and related metabolites from the lowest- and highest-yielding plants relative to an internal standard (IS) are presented. artB, arteannuin B; DHEDA, dihydro-epi-deoxyarteannuin B; DHAA, dihydroartemisinic acid; AA, artemisinic acid. (**B**) Leaf area 5 months after sowing. Images show leaves from positions 20, 21, and 22 from the apical meristem. (**C**) Trichome density 5 months after sowing. The abaxial surface of leaves 15, 16, and 17 from the apical meristem was visualized by fluorescent microscopy. Glandular trichomes appear as bright green spots. (**D**) Fresh weight of aboveground plant material at harvest (7 months after sowing). (**E**) Principal component analysis of traits related to artemisinin yield. Architecture, leaf, and metabolite traits additional to those detailed in (A) to (D) are also included in the analysis as shown.

Fig. 1B). Of SNPs derived from Populations U and M, 70% and 64%, respectively, were also found to segregate in the Artemis pedigree. The heterozygosity in C4 is roughly double that of C1, reflecting differences in the history of these genotypes. A number of markers are monomorphic in both parents for opposite alleles. These fixed differences between parents will segregate in generations beyond the F_1, thereby offering additional segregation of alleles not revealed in Artemis.

Phenotypic variation can be seen in the Artemis pedigree, consistent with the high level of genetic variation. This is shown in Fig. 2 for our mapping population of the Artemis F_1, grown in UK field trials during 2007 (UK07). Metabolite profiling revealed concentrations of artemisinin that ranged from 0.93 to 20.65 μg/mg dry weight, with associated metabolites also showing variation (Fig. 2A). Leaf area ranged between 508.76 and 4696.08 mm^2 (Fig. 2B), glandular trichome density between 4.89 and 19.11 mm^{-2} (Fig. 2C), and plant fresh weight between 160 and 4440 g (Fig. 2D). These traits are targets for increasing artemisinin yield, which is a product of both artemisinin concentration and plant fresh weight.

The fact that the Artemis parents are heterozygous enabled us to produce genetic linkage maps for each parent based on data derived from an F_1 mapping population of 242 individuals (fig. S2) (*15*). Using a minimum LOD (logarithm of the odds ratio for linkage) score of 4.0, we defined nine linkage groups for the C4 parent and seven linkage groups for C1 (fig. S2). We hypothesized that the C1 map is missing two linkage groups, designated LG8 and LG9, because two chromosomes in the C1 parent are either homozygous or have a very low level of heterozygosity and therefore do not segregate for markers from this parent in the F_1, so cannot be mapped in this generation. To test this hypothesis, an individual F_1 plant showing high heterozygosity in molecular analysis was self-pollinated to produce an F_2 generation. Markers seen to be homozygous for opposite alleles in the parents, and therefore heterozygous in all F_1 progeny, were genotyped in the F_2 generation

together with markers known to map to LG8 and LG9 in the C4 parent. In support of our hypothesis, a number of these markers were found to segregate in the F_2 generation. These data allowed F_2 linkage groups for LG8 and LG9 to be defined and anchored to the corresponding C4 linkage groups (fig. S2). The identification of nine LGs is consistent with cytological studies reporting the diploid number of chromosomes to be 18 in *A. annua* (*16*). The marker positions shown on the map were validated by three independent approaches: coalignment on the C4 and C1 maps, common location of multiple markers from single candidate genes, and robustness of marker order after reconstruction of the map with a subset of markers (SOM Text).

We used vegetative propagation to replicate individuals from the mapping population, which enabled us to perform three independent field trials using the same genotypes. A single replicate of each genotype was tested in 2007 in the UK (UK07) and three replicates of each genotype were tested both in the UK (UK08) and Switzerland (SW08) in 2008. Fourteen traits were scored that could affect artemisinin yield (Fig. 2E). All these traits exhibited a moderate to high heritability ranging from 0.41 to 0.62, resulting in the discovery of multiple QTLs. Stable QTLs for artemisinin concentration were identified on C4 LG1, LG4, and LG9 (Fig. 3 and table S4), which describe 20% of the variation in UK07 and between 30 and 38% in

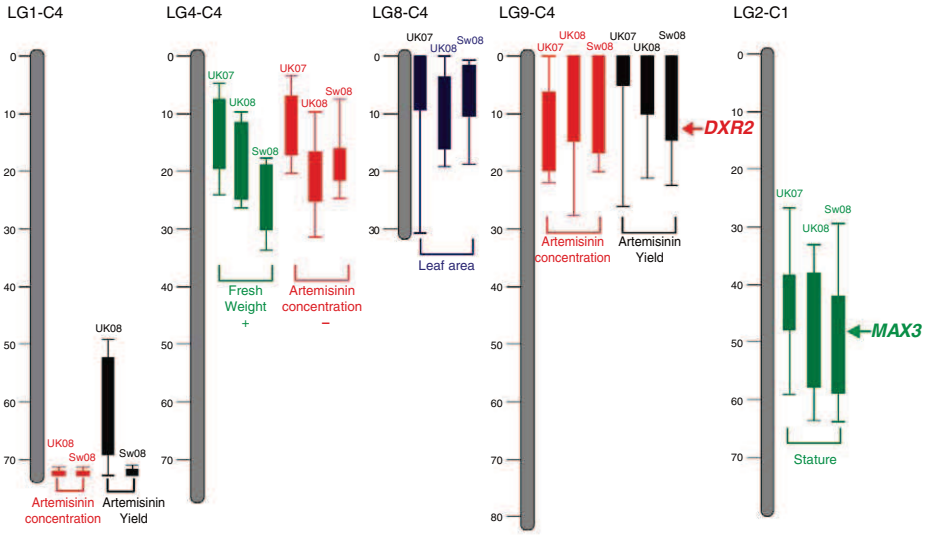

Fig. 3. A selection of QTLs for key traits identified across three field trials. QTLs are shown to the right and distances in centimorgans to the left of each linkage group. Thick and thin lines indicate the confidence intervals of the QTLs corresponding to 1 and 2 LOD units below the maximum LOD score, respectively. QTLs are shown for artemisinin concentration (in red), artemisinin yield (artemisinin concentration × fresh weight) (in black), architecture (fresh weight and stature) (in green), and leaf area (in blue). Trials in which QTLs were detected are denoted as UK07, UK08 and SW08. Candidate genes associated with QTL are *DXR2* (*1-Deoxy-D-Xylulose 5-phosphate Reductoisomerase 2*) and *MAX3* (*More Axillary Branching 3*).

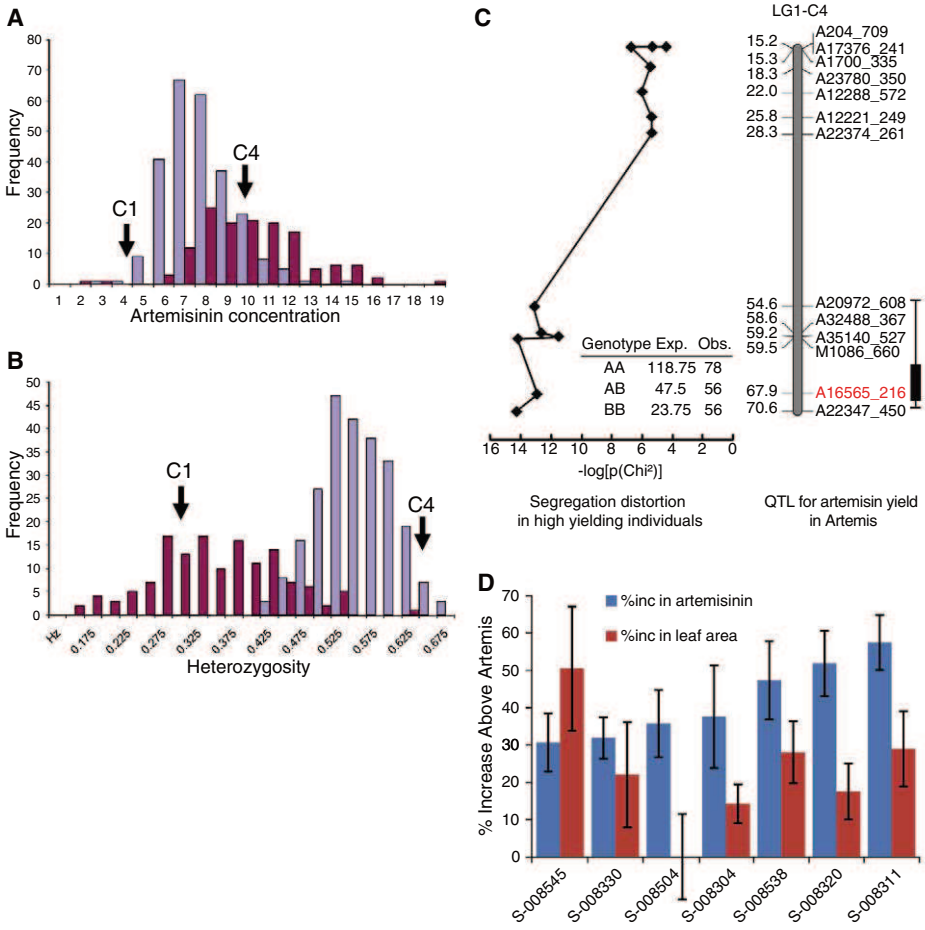

Fig. 4. Genetic analysis of high-yielding plants. (**A**) Distribution of artemisinin concentration (μg/mg dry weight) in the F_1 mapping population of 242 individuals is shown in blue and that in 130 selected high-yielding F_2 individuals grown in the same trial (UK08), is shown in red. The artemisinin concentrations of C4 and C1 grown in the same trial are indicated. (**B**) Distribution of heterozygosity scores for the same individuals as in (A). (**C**) The position of a major QTL for artemisinin yield on LG1 and markers in this region show high segregation distortion in favor of the increasing alleles in 190 F_2 high-yielding individuals. For the marker highlighted in red, the B allele has a positive effect on yield ($P = 4.4 \times 10^{-7}$) and is overrepresented in the high-yielding individuals summarized in the table inset. The plotted values for segregation distortion represent the –log [Chi-squared] based on the observed and expected values for genotype classes at a number of markers on linkage group 1. (**D**) The percentage increase in artemisinin concentration (in red) and leaf area (in blue), over Artemis F_1 for seven hybrids produced from crosses of selected high-yielding individuals. Values are the mean ± SE for a minimum of five individual replicates.

UK08 and SW08. Artemisinin yield is a product of both artemisinin concentration and fresh weight. QTLs for yield colocate to those for artemisinin concentration on LG1 and LG9, thus representing targets for a breeding program. The artemisinin concentration QTL on LG4 colocates with a QTL for fresh weight but with opposing effects on artemisinin yield (Fig. 3). Markers in candidate genes colocate with a number of the QTLs. For example, the precursor supply gene candidate *DXR2* colocates with the QTL for artemisinin yield on C4 LG9 and the architectural trait candidate gene *MAX3* colocates with the QTL for stature on C1 LG2.

In parallel with the development of the marker-assisted breeding program, we performed a high-throughput screen for artemisinin content in 23,000 12-week-old glasshouse-grown F_2 and F_3 plants derived from F_1 Artemis seed that had been mutagenized with ethylmethane sulfonate (*15*). The mutation frequency in this material was determined with the TILLING method and found to be approximately one EMS-induced mutation per 5.4 Mb (*15*). This is less than the SNP frequency determined for Artemis at one polymorphism per 104 base pairs. This screen should therefore identify individuals carrying beneficial mutations derived from the EMS treatment and also individuals carrying improved genetic backgrounds as a result of segregation of favorable alleles derived from natural variation. We found that the distribution of artemisinin content among selected high-yielding F_2 individuals is higher than in the UK08 Artemis F_1 mapping population (Fig. 4A) even though overall heterozygosity is lower (Fig. 4B). Next, we determined whether any of the QTLs we had identified for artemisinin yield on the basis of field trials are overrepresented in the high-yielding individuals that had been selected under glasshouse conditions. We found strong segregation distortion in favor of the advantageous alleles for an artemisinin yield QTL on C4 LG1 (Fig. 4C). These data validate this QTL and confirm that for artemisinin yield, the genotype has a strong influence on both glasshouse-grown and field-grown material.

An ongoing empirical hybridization program of high-yielding plants identified in the high-throughput phenotypic screen produced hybrid progeny that outperformed Artemis for artemisinin concentration and leaf area after 12 weeks' growth under glass (Fig. 4D). The choice of parents for this program preceded the availability of QTL data and was based on phenotypic characteristics (*15*). In terms of utility in a molecular breeding program, we found a significant association of positive artemisinin yield QTL in those parents that produced hybrids with increased artemisinin yield ($P < 0.001$).

Our study has established the molecular basis for marker-assisted breeding of this medicinal plant species and highlights the reduced timelines that are now feasible for developing this platform of knowledge and tools. The artemisinin from *A. annua* is the key component in the ACT treatment of malaria, and demand for ACTs is expected to increase in the immediate future. Development of new high-yielding varieties optimized for production in different geographic regions is now a realistic target.

References and Notes

1. World Malaria Report 2008, World Health Organisation; http://apps.who.int/malaria/wmr2008/malaria2008.pdf.
2. A. M. Dondorp *et al*., *N. Engl. J. Med.* **361**, 455 (2009).
3. "*Saving Lives, Buying Time: Economics of Malaria Drugs in an Age of Resistance*," National Academy of Sciences 2004, www.nap.edu/catalog/11017.html. Global Malaria Action Plan, Report of the 2008 Artemisinin Conference, 8 to 10 October, York, UK (www.york.ac.uk/org/cnap/artemisiaproject/pdfs/AEconference-report-web.pdf).
4. M. V. Duke, R. N. Paul, H. N. Elsohly, G. Sturtz, S. O. Duke, *Int. J. Plant Sci.* **155**, 365 (1994).
5. C. M. Bertea *et al*., *Planta Med.* **71**, 40 (2005).
6. C. M. Bertea *et al*., *Arch. Biochem. Biophys.* **448**, 3 (2006).
7. K. H. Teoh, D. R. Polichuk, D. W. Reed, G. Nowak, P. S. Covello, *FEBS Lett.* **580**, 1411 (2006).
8. Y. Zhang *et al*., *J. Biol. Chem.* **283**, 21501 (2008).
9. K. H. Teoh, D. R. Polichuk, D. W. Reed, P. S. Corvello, *Can. J. Bot.* **87**, 635 (2009).
10. P. S. Covello, *Phytochemistry* **69**, 2881 (2008).
11. M. C. Chang, R. A. Eachus, W. Trieu, D. K. Ro, J. D. Keasling, *Nat. Chem. Biol.* **3**, 274 (2007).
12. D. K. Ro *et al*., *Nature* **440**, 940 (2006).
13. J. F. S. Ferreira, J. Janick, *Int. J. Plant Sci.* **156**, 807 (1995).
14. N. Delabays, X. Simonnet, M. Gaudin, *Curr. Med. Chem.* **8**, 1795 (2001).
15. Information on materials and methods is available on *Science* Online.
16. M. Torrell, J. Vallés, *Genome* **44**, 231 (2001).

17. We thank L. Doucet, H. Martin, N. Nattriss, M. Segura, and A. Czechowska for horticulture assistance; G. Chigeza for horticulture management; S. Graham, S. Heywood, B. Kowalik, S. Pandey, R. Simister, and C. Whitehead for laboratory assistance; C. Calvert, P. Dickes, W. Lawley, and D. Rotherham for project management; E. Bartlet for communications advice; and P. Roberts for graphic design. We thank T. Brewer, H. Klee, and K. Stuart for insightful advice on this project. We thank X. Simonnet and Médiplant for access to the Artemis pedigree. We acknowledge financial support for this project from The Bill and Melinda Gates Foundation and Medicines for Malaria Venture, as well as from The Garfield Weston Foundation for the Centre for Novel Agricultural Products.

Supporting Online Material www.sciencemag.org/cgi/content/full/327/5963/328/DC1 Materials and Methods
SOM Text
Figs. S1 to S6
Tables S1 to S4
References

29 September 2009; accepted 20 November 2009
10.1126/science.1182612

Tetrathiomolybdate Inhibits Copper Trafficking Proteins Through Metal Cluster Formation

Hamsell M. Alvarez,[1]* Yi Xue,[1]* Chandler D. Robinson,[1] Mónica A. Canalizo-Hernández,[1] Rebecca G. Marvin,[1] Rebekah A. Kelly,[3] Alfonso Mondragón,[2] James E. Penner-Hahn,[3] Thomas V. O'Halloran[1,2]†

Tetrathiomolybdate (TM) is an orally active agent for treatment of disorders of copper metabolism. Here we describe how TM inhibits proteins that regulate copper physiology. Crystallographic results reveal that the surprising stability of the drug complex with the metallochaperone Atx1 arises from formation of a sulfur-bridged copper-molybdenum cluster reminiscent of those found in molybdenum and iron sulfur proteins. Spectroscopic studies indicate that this cluster is stable in solution and corresponds to physiological clusters isolated from TM-treated Wilson's disease animal models. Finally, mechanistic studies show that the drug-metallochaperone inhibits metal transfer functions between copper-trafficking proteins. The results are consistent with a model wherein TM can directly and reversibly down-regulate copper delivery to secreted metalloenzymes and suggest that proteins involved in metal regulation might be fruitful drug targets.

Excess dietary molybdate (MoO_4^{2-}) uptake was first linked to a fatal disorder in cattle known as "teart" pastures syndrome (*1*) and later to a neurological disorder in sheep known as "swayback" (*2*). Both disorders arise from Mo-induced copper deficiency, and the symptoms are readily reversed with copper supplementation. Although molybdate itself has little or no affinity for copper ions, the active copper-depleting agent, TM (MoS_4^{2-}), is formed in the ruminants' digestive track and readily reacts with Cu^{I} or Cu^{II} to form insoluble compounds. These zoogenic studies inspired the development of molybdenum compounds to treat copper-dependent diseases in humans (*3*). The potent chelating and antiangiogenic activities of orally active formulations of TM, such as the ammonium salt [$(NH_4)_2(MoS_4)$] (*4*–*6*) and the choline salt (ATN-224) (*7*, *8*), have been used in treatment of Wilson's disease, where copper accumulation leads to hepatic and neurological disorders, as well as in the inhibition of metastatic cancer progression in a number of clinical trials (*9*–*11*). TM inhibits several copper enzymes, including ceruloplasmin (Cp), ascorbate oxidase, cytochrome oxidase, superoxide dismutase (SOD1), tyrosinase, and the *Enterococcus*

[1]The Chemistry of Life Processes Institute, Northwestern University, Evanston, IL 60208, USA. [2]Department of Biochemistry, Molecular Biology and Cell Biology, Northwestern University, Evanston, IL 60208, USA. [3]Department of Chemistry, The University of Michigan, Ann Arbor, MI 48109, USA.

*These authors contributed equally to this work.
†To whom correspondence should be addressed. E-mail: t-ohalloran@northwestern.edu

hirae adenosine triphosphatase (ATPase) (CopB) (*12*, *13*), and also down-regulates the expression of cytokines, such as the vascular endothelial growth factor, as well as transcription factors, such as nuclear factor κB, involved in angiogenesis signaling pathways (*14*, *15*). Although TM can bind to Cu-Cp (*12*), copper–bovine serum albumin (Cu-BSA) (*16*), and Cu-containing metallothioneins (Cu-MT) (*17*) and has been proposed to inhibit SOD1 by partially removing copper from the enzyme (*8*, *18*), the reaction chemistry and structures of these complexes have not been resolved.

Metallochaperones constitute a particular kind of protein that delivers metal ions to specific cytoplasmatic targets in the cell (*19*). The prototypical metallochaperone, yeast Atx1, transfers Cu^{I} along a trafficking pathway via electrostatic interactions with structurally homologous N-terminal domains of the ATPase, Ccc2 (*20*, *21*). Likewise, the closely related human copper metallochaperone, antioxidant 1 (Atox1), can transfer copper to N-terminal domains of the copper-transporting ATPases 7a and 7b, also known as the Menkes and Wilson disease proteins. All three of these proteins are important in mammalian copper homeostasis and provide copper to secreted enzymes that are important in vascular integrity such as Cp and extracellular SOD (ecSOD). We anticipated that TM would readily remove Cu^{I} from its binding site in Atx1 with subsequent formation of a typical polymeric CuMo sulfide precipitate. We found instead a robust TM-metallochaperone complex with metal sulfur ratios reminiscent of the FeMo cofactor complex in nitrogenase (*22*) and elucidated how this anti-angiogenic drug affects the structure and function of a canonical metal-trafficking domain.

Direct reaction of TM with Cu-Atx1 leads to rapid formation of an air-stable purple complex that can be readily isolated by size-exclusion chromatography (*23*). Crystals of this complex diffract to 2.3 Å (fig. S1), and the x-ray structure reveals the presence of 12 Cu-Atx1 molecules in the asymmetric unit arranged as four TM-Cu-Atx1 noncrystallographic trimers (fig. S2). The overall structure of each Atx1 monomer is similar to previously determined structures, retaining the "ferredoxin-like" βαββαβ fold (*24*), with two cysteines involved in copper binding (Cys^{15} and Cys^{18}) located at the protein surface. Superposition of the coordinates of Hg-Atx1 (PDB code

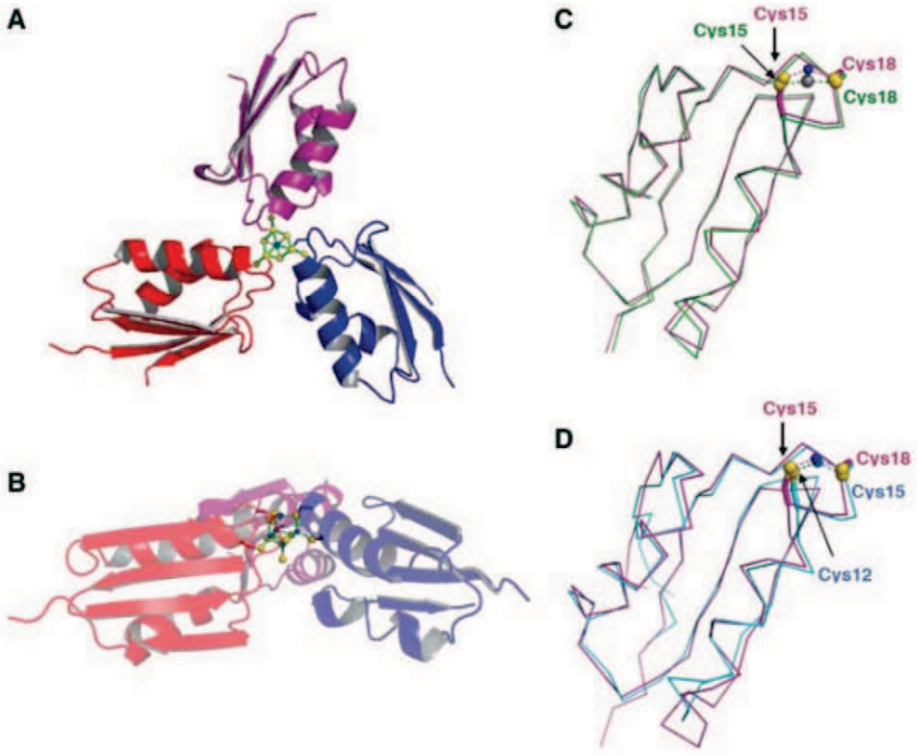

Fig. 1. Structure of the [TM][(Cu)(Cu-Atx1)$_3$] drug-protein adduct and comparison of Hg-Atx1 and Cu-Atox1 with Cu-Atx1 (monomer B) from the [TM][(Cu)(Cu-Atx1)$_3$] complex (see movie S1). (**A**) Top view of the trimer cluster. (**B**) Side view of the trimer cluster. Atx1 monomers are shown as blue, purple, and red cartoon ribbon diagrams, and copper atoms are shown as blue spheres. The TM- and metal-binding cysteines are represented with a ball-and-stick model, where a molybdenum atom is shown as a cyan sphere, and sulfur atoms are shown as yellow spheres. The coordination bonds are denoted with green dashed lines. Superposition of Cu-Atx1 (monomer B) (purple chain) from the TM-Cu-Atx1 complex with (**C**) Hg-Atx1 (green chain, PDB code 1CC8), and (**D**) with Cu-Atox1 (cyan chain, PDB code 1FEE). Sulfur atoms from Cys^{15} (Atx1) and Cys^{18} (Atx1) are shown as yellow spheres, copper atoms from Cu-Atx1 (monomer B) are shown as blue spheres, mercury atom from Hg-Atx1 is shown as a gray sphere, and copper atom from Cu-Atox1 is shown as a light blue sphere. (Note: TM is not shown.) The similarities of the peptide fold around the metal–binding loop regions in these three structures suggest that binding of Cu by Atx1 in the TM-Cu-Atx1 complex is not disturbed by TM. The Cu coordination environment in Cu-Atx1 from TM-Cu-Atx1 is very similar to the one found in Cu-Atox1 (dimer) (*25*), but differs with the nearly linear coordination of Hg in Hg-Atx1 (*24*).

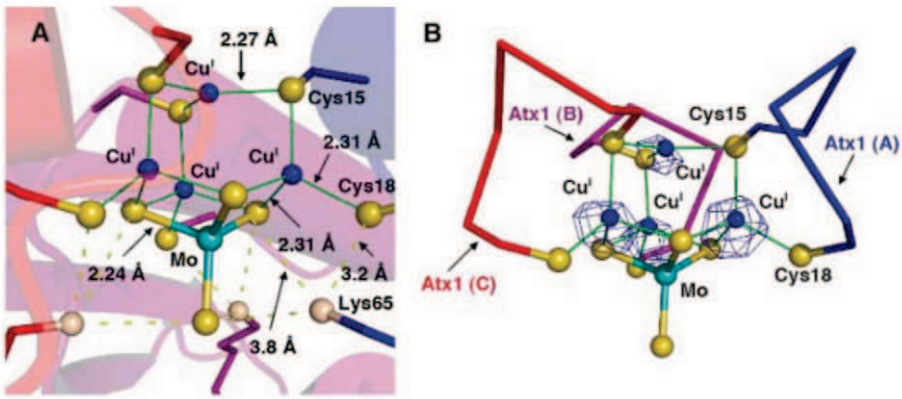

Fig. 2. Structure of the nest-shaped [$S_6Cu_4MoS_4$] cluster in the [TM][(Cu)(Cu-Atx1)$_3$] trimer complex (see movie S1). (**A**) Structure of the [$S_6Cu_4MoS_4$] cluster with average interatomic distances. The cluster is represented with a ball-and-stick model. Atx1 monomers are as in Fig. 1. Copper atoms are shown as blue spheres; sulfur atoms from Cys^{15} (Atx1), Cys^{18} (Atx1), and TM are shown as yellow spheres; a molybdenum atom is shown as a cyan sphere; and nitrogen atoms from Lys^{65} (Atx1) are shown as tan spheres. The hydrogen bonds are denoted with yellow dashed lines. (**B**) Cu anomalous peaks in the final model of the [$S_6Cu_4MoS_4$] cluster (blue mesh of the anomalous difference Fourier map are contoured at 10.0 σ level). Sulfur atoms from Cys^{15} and Cys^{18} of each of the three Atx1 are connected by blue, purple, and red lines. The molybdenum atom is tetrahedrally coordinated by four sulfur atoms. The top copper atom displays a trigonal-planar geometry and is coordinated by thiolates from Cys^{15} (Atx1), whereas each of the other three neighboring copper atoms adopts a distorted tetrahedral coordination with ligands from both TM and Atx1.

1CC8) (*24*) and Cu-Atox1 (human analog of Atx1, PDB code 1FEE) (*25*) on the monomers in the complex (Fig. 1, C and D) reveals that the peptide fold around the metal-binding loop is unperturbed by TM binding, with an average root mean square deviation for the C_α atoms of ~0.67 Å (Hg-Atx1) and ~1.3 Å (Cu-Atox1). In the structure, each Atx1 trimer coordinates four copper atoms and one TM molecule, with the stoichiometry [TM][(Cu)(Cu-Atx1)$_3$], which is corroborated by independent elemental analysis of the complex (*23*). The Cu x-ray absorption near-edge structure of the complex indicates that the copper remains in the Cu^I oxidation state, whereas the Mo K near-edge spectrum strongly resembles that of tetrathiomolybdate (Mo^{VI}) (fig. S3). Aside from a few H-bonding interactions between monomers, the dominant forces stabilizing the trimer are the coordinate covalent bonds between the protein CysS atoms and the metal cluster.

A "nest-shaped" copper-molybdenum cluster, unprecedented in metalloproteins, is located at the center of the Atx1 trimer (Fig. 1, A and B) on the threefold axis. The cluster consists of four Cu^I ions, $[MoS_4]^{2-}$, and three pairs of Atx1 CysS atoms to give a $[S_6Cu_4MoS_4]$ cluster (Fig. 2). The Mo atom remains tetrahedrally coordinated by four sulfide ions with Mo–S distances in the range 2.18 to 2.26 Å (mean: 2.22 Å), as expected for Cu–S–Mo cluster interactions and commensurate with the ones observed in the parent drug (2.17 to 2.20 Å, mean: 2.19 Å) (*7*). Three of the copper atoms bind to the sulfur atoms of cysteines 15 and 18, and each of these atoms also binds two sulfides from $[MoS_4]^{2-}$, which results in a distorted tetrahedral coordination environment for the coppers with similar distances for the Cu-S bonds to protein side chains (2.21 to 2.44 Å, mean: 2.30 Å) or the sulfides of TM (2.24 to 2.40 Å, mean: 2.29 Å). The Mo-Cu distances are in the range of 2.74 to 2.82 Å (mean: 2.77 Å). The fourth sulfide of TM does not coordinate copper or interact with protein. On the other side of the complex, the fourth copper atom is bound by three $(Cys^{15})S_\gamma$ atoms (2.22 to 2.30 Å, mean: 2.26 Å) and exhibits a trigonal planar coordination. Thus, three of the four sulfide ions in TM form a μ_3-S bridge between the Mo atom and two tetrahedral Cu atoms, whereas each of the $(Cys^{15})S_\gamma$ atoms of three Atx1 behave as a bridging ligand between one tetrahedral and one trigonal planar copper center. In the tetrahedrally coordinated coppers, the $(Cys^{15})S_\gamma$–Cu–$S_\gamma(Cys^{18})$ bond angles are larger (118° to 125°, mean: 122°) than the (TM)S–Cu–S(TM) bond angles (99° to 103°, mean: 101°), consistent with a distorted tetrahedral site. The geometry at the Mo atom is only slightly distorted from tetrahedral, with (TM)(μ_3-S)–Mo–(μ_3-S)(TM) and (TM)(μ_3-S)–Mo–S(TM) bond angles of 103° to 110° (mean: 106°) and 109° to 116° (mean: 112°), respectively. Protein-TM interactions partially neutralize the

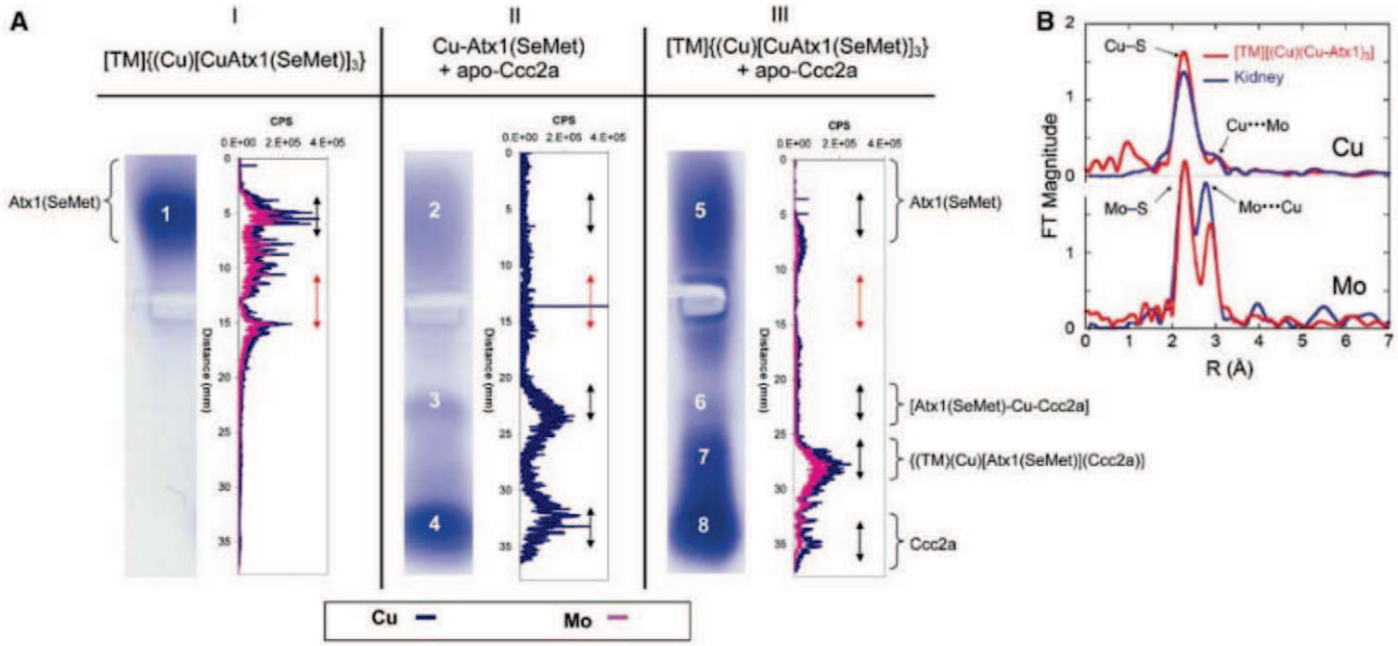

Fig. 3. TM inhibition of Atx1 copper chaperone activity, and physiological relevance of the [TM][(Cu)(Cu-Atx1)$_3$] complex. (**A**) TM interferes with copper transfer from the Atx1(SeMet) copper chaperone to its target Ccc2a. Inhibition of the copper transfer function was assayed by native gel electrophoresis and qualitative LA-ICP-MS. Gel lanes (I, II, and III) were cut from gel (fig. S6). The [TM]{(Cu)[Cu-Atx1(SeMet)]$_3$} (lane I) is represented by band 1, the Cu-Atx1(SeMet) + *apo*-Ccc2a (1:1) mixture (lane II) yields bands 2, 3, and 4, and the [TM]{(Cu)[Cu-Atx1(SeMet)]$_3$} + *apo*-Ccc2a (1:1) mixture (lane III) yields bands 5, 6, 7, and 8. LA-ICP-MS scans are represented by the intensities (CPS, counts per second) of ^{65}Cu (blue) and ^{95}Mo (pink) (*x* axis), and the length of the gel (mm) (*y* axis). The protein band lengths are shown as black double-headed arrows (↔); the protein loading wells are shown as red double-headed arrows. Excision and gel digestion ICP-MS analysis of band 1 shows a Cu/Mo ratio of 3.6 ± 0.09 (table S1), whereas LA-ICP-MS scans reveal a significant concentration of both metals, leading us to assign band 1 as [TM]{(Cu)[Cu-Atx1(SeMet)]$_3$}. Bands 3 (lane II) and 6 (lane III) are identified as the [Atx1(SeMet)-Cu-Ccc2a] heterodimer complex on the basis of metal and protein analysis of each band. Band 7 contains a mixture of apo-Atx1(SeMet) and apo-Ccc2a with an approximate Cu/Mo ratio of 3.1 ± 0.08 (ICP-MS) (table S1), which is confirmed by a qualitative LA-ICP-MS identification of both metals, indicating the formation of a {(TM)(Cu)[Atx1(SeMet)](Ccc2a)} complex. Elemental analysis by ICP-MS of band 8 reveals copper is at or below the detection limit, indicating that less than 10% of Cu in the TM-Cu-Atx1 complex is transferred to Ccc2a (table S1). Quantitative analysis of the gel slice is consistent with LA-ICP-MS scans showing that most of the Cu of lane III is contained in band 7. These experiments indicate that the formation of the [TM]{(Cu)[Cu-Atx1(SeMet)]$_3$} complex disrupts copper translocation from Cu-Atx1(SeMet) to the domain A of the P-type ATPase Ccc2. (**B**) Cu and Mo K-edge extended x-ray absorption fine structure (EXAFS) Fourier transforms phase-shift overlay (experimental data) for [TM][(Cu)(Cu-Atx1)$_3$], and a kidney sample extracted from LPP rats treated with TM [from (*29*)]. The slightly higher amplitude of the Mo•••Cu peak for the kidney sample compared with the [TM][(Cu)(Cu-Atx1)$_3$] reflects the slight difference in the Mo EXAFS best fits, 3 and 2–3 Mo•••Cu, respectively. The Cu•••Mo peak is slightly more intense for the [TM][(Cu)(Cu-Atx1)$_3$] complex than for the kidney sample, modeled by 1 Cu•••Mo instead of 0.5, respectively. Cu and Mo K-edge EXAFS spectra and EXAFS Fourier transform including experimental data and best fits are included in figure S13. The fit results are summarized in table S2.

negative charge delocalized over the $[Cu_4MoS_4]^{4-}$ cluster (fig. S4 and Fig. 2A). Three positively charged lysines (Lys^{65}), one from each Atx1 monomer, form hydrogen bonds with the sulfides from TM and the thiolates of Cys^{18}. Strong interactions are observed for the only terminal S thiolate ligand in the cluster (Cys^{18}–S–Lys^{65}–Nζ = 3.3 Å) relative to μ_3-S bridging sulfide ligands (TM–μ_3-S–Lys^{65}–Nζ = 3.8 Å). In addition, H bonds from backbone amides (Thr^{14} and Gly^{17}) at the amino terminus of α helix 2 to metal-bound thiolates further neutralize the negative charge of the buried cluster.

Although this type of cluster has not been previously reported in metalloproteins, analogous nest-shaped $[Cu_3MoS_3O]$ inorganic units (with P- and N-donor ligands) are components of larger clusters (*26*). The closest fragment analog of the protein-drug adduct is a component of the $[Bu^n_4N]_4[Cu_{12}Mo_8S_{32}]$ complex. Here, a $[S_6Cu_3MoS_4]$ unit exhibits similar cluster framework with Mo–Cu distances from 2.69 to 2.75 Å, Mo–S distances from 2.06 to 2.25 Å and Cu–S distances from 2.29 to 2.36 Å (*27*) (fig. S5). Another structurally distinct CuSMo center is observed in the Cu-Mo-pterin enzyme carbon monoxide dehydrogenase from *Oligotropha carboxidovorans*, where a single diagonally coordinated Cu atom is bound via a bridging sulfide to a Mo active site forming a [CuSMo(=O)OH] cluster (*28*).

To determine whether TM interaction with Atx1 inhibits its copper chaperone activity, we developed a native gel–based copper transfer assay that monitors metal occupancy in a mixture of TM-Cu-Atx1 trimer and Ccc2a, the physiological partner of Atx1 (fig. S6). The assay takes advantage of the fact that apo- and Cu-Atx1 are clearly distinguishable from Ccc2a and TM-Cu-Atx1 in a native agarose gel system (*23*), where the protein and metal content of the bands are characterized by a variety of analytical techniques to establish the metallation state of each protein (fig. S7 to S12 and table S1). The assay was validated by a combination of electrospray ionization protein mass spectrometry (ESI-MS) and quantitative elemental analysis via inductively coupled plasma MS (ICP-MS) of samples extracted from gel slices, as well as by qualitative laser scanning elemental analysis, that is, laser ablation with ICP-MS (LA-ICP-MS) of the electrophoresis gel itself. Three key lanes are shown in Fig. 3A. The TM-Cu-Atx1(SeMet) migrates as a positive species containing copper and molybdenum (lane I). Mixing of apo-Ccc2a and Cu-Atx1 (SeMet) results in the transfer of copper from Cu-Atx1(SeMet) to Ccc2a (lane II). The transfer of copper from Atx1(SeMet) to Ccc2a is almost completely abolished by the presence of TM (lane III). Both native Atx1 and the SeMet analog give similar results. It is intriguing that protein analysis indicates formation of a new Cu-TM protein complex that contains the Ccc2 domain, as well as TM and Cu-Atx1. The formation of this heteromeric protein complex suggests that other proteins with a surface-exposed MxCxxC copper-binding motif will be able to form similar complexes with TM.

These results suggest a new model for how a drug can disrupt a key protein-protein interaction for metal-trafficking pathways. Support for the physiological occurrence of this type of metal-protein cluster is shown in Fig. 3B by the highly similar Cu and Mo K-edge extended x-ray absorption fine structure analysis of the $[TM][(Cu)(Cu\text{-}Atx1)_3]$ complex, and a kidney sample extracted from TM-treated LPP rats (animal model of Wilson's disease), where a similar $[(CuSR)_3S_4Mo]^{2-}$-type interaction is proposed (*29*). The stoichiometry of three chaperone molecules and four copper atoms per drug molecule has several physiological implications. By sequestering multiple copper chaperones and the metal cargo destined for trafficking to the trans-Golgi, TM may suppress Cu incorporation into secreted copper enzymes, including those involved in modification of the vasculature such as ecSOD, copper amine oxidases, lysyl oxidase, and Cp. The TM-mediated sequestration of copper-loaded metallochaperones may perturb other proposed roles of Atox1 in regulation of copper-related tumor angiogenic factors (*30*).

The structure and biochemistry of the TM-Cu-Atx1 complex also provides chemical insights into the puzzling stoichiometry of the dietary Cu-Mo antagonism (*31*) and suggests why ternary complex formation between TM and specific Cu proteins can have pronounced physiological consequences (*32*). A relatively small amount of dietary molybdenum clearly perturbs the timely dissemination of a larger pool of copper in deficiency disorders such as swayback and teart pasture syndrome. Our results raise the possibility that the active agent, TM, functionally suppresses copper trafficking domains that control the secretion of the active forms of copper-dependent enzymes. Finally, our results suggest that proteins involved in such metallation pathways may be targets for the development of new classes of pharmaceutical agents.

References and Notes

1. W. S. Ferguson, A. H. Lewis, S. J. Watson, *Nature* **141**, 553 (1938).
2. C. F. Mills, B. F. Fell, *Nature* **185**, 20 (1960).
3. G. J. Brewer, *Exp. Biol. Med. (Maywood)* **226**, 665 (2001).
4. J. M. Walshe, in *Orphan Diseases and Orphan Drugs*, I. H. Scheinberg, J. M. Walshe, Eds. (Manchester Univ. Press, Manchester, UK, 1986), pp. 76–85.
5. G. J. Brewer *et al*., *Arch. Neurol.* **48**, 42 (1991).
6. P. J. Sadler, C. Muncie, M. A. Shipman, in *Biological Inorganic Chemistry: Structure and Reactivity*, I. Bertini, H. B. Gray, E. I. Stiefel, J. S. Valentine, Eds. (University Science Books, Sausalito, CA, 2007), pp. 95–135.
7. V. E. Lee, J. M. Schulman, E. I. Stiefel, C. C. Lee, *J. Inorg. Biochem.* **101**, 1707 (2007).
8. J. C. Juarez *et al*., *Clin. Cancer Res.* **12**, 4974 (2006).
9. G. J. Brewer *et al*., *Clin. Cancer Res.* **6**, 1 (2000).
10. B. G. Redman *et al*., *Clin. Cancer Res.* **9**, 1666 (2003).
11. Active trials: TM (2001), ATN-224 (2006) at ClinicalTrials.gov.
12. M. V. Chidambaram, G. Barnes, E. Frieden, *J. Inorg. Biochem.* **22**, 231 (1984).
13. K. D. Bissig, T. C. Voegelin, M. Solioz, *FEBS Lett.* **507**, 367 (2001).
14. L. Mandinov *et al*., *Proc. Natl. Acad. Sci. U.S.A.* **100**, 6700 (2003).
15. Q. Pan *et al*., *Cancer Res.* **62**, 4854 (2002).
16. E. K. Quagraine, R. S. Reid, *J. Inorg. Biochem.* **85**, 53 (2001).
17. K. T. Suzuki, Y. Ogra, *Res. Commun. Mol. Pathol. Pharmacol.* **88**, 187 (1995).
18. J. C. Juarez *et al*., *Proc. Natl. Acad. Sci. U.S.A.* **105**, 7147 (2008).
19. L. A. Finney, T. V. O'Halloran, *Science* **300**, 931 (2003).
20. R. A. Pufahl *et al*., *Science* **278**, 853 (1997).
21. D. L. Huffman, T. V. O'Halloran, *J. Biol. Chem.* **275**, 18611 (2000).
22. J. B. Howard, D. C. Rees, *Proc. Natl. Acad. Sci. U.S.A.* **103**, 17088 (2006).
23. Material and methods are available as supporting material on *Science* Online.
24. A. C. Rosenzweig *et al*., *Structure* **7**, 605 (1999).
25. A. K. Wernimont, D. L. Huffman, A. L. Lamb, T. V. O'Halloran, A. C. Rosenzweig, *Nat. Struct. Biol.* **7**, 766 (2000).
26. C. Zhang *et al*., *Eur. J. Inorg. Chem.* **2002**, 55 (2002).
27. L. Jiguo, X. Xinquan, Z. Zhongyuan, Y. Kaibei, *J. Chem. Soc. Chem. Commun.* **1991**, 249 (1991).
28. H. Dobbek, L. Gremer, R. Kiefersauer, R. Huber, O. Meyer, *Proc. Natl. Acad. Sci. U.S.A.* **99**, 15971 (2002).
29. L. Zhang *et al*., *Biochemistry* **48**, 891 (2009).
30. S. Itoh *et al*., *J. Biol. Chem.* **283**, 9157 (2008).
31. H. R. Marston, *Physiol. Rev.* **32**, 66 (1952).
32. C. F. Mills, *Philos. Trans. R. Soc. London B Biol. Sci.* **288**, 51 (1979).

33. This manuscript is dedicated to the memory of E. Stiefel and his contributions to the field of molybdenum sulfide chemistry. This work was supported by grant GM54222 and GM38784 (T.V.O.) and GM38047 (J.E.P.-H.) from the NIH. The Robert H. Lurie Comprehensive Cancer Center provided a Malkin Fellowship (H.M.A.) and support for Structural Biology Facility. Use of the Advanced Photon Source [Structural Biology Center-Collaborative Access Team (CAT) and Industrial Macromolecular Crystallography Association CAT] and the Stanford Synchrotron Radiation Laboratory (SSRL) was supported by the U.S. Department of Energy, Office of Basic Energy Sciences, with additional support (at SSRL) from the National Center for Research Resources, NIH. Use of the Chicago Biomedical Consortium (CBC)–University of Illinois at Chicago Proteomics Facility was supported by The Searle Funds at the CBC, and use of LA-ICP-MS was supported by a National Aeronautics and Space Administration grant to the Quantitative Bioelement Imaging Center in the Chemistry of Life Processes Institute at Northwestern University. We thank P. Focia for assistance with x-ray diffraction collection, M. Clausén for assistance in the early stages of XAS measurements, Y. Wang for assistance with the protein MS, A. Davis for providing *apo*-Ccc2a, and A. Mazar for helpful discussions. The atomic coordinates have been deposited at the Protein Data Bank with code 3K7R.

Supporting Online Material www.sciencemag.org/cgi/content/full/science.1179907/DC1 Materials and Methods
Fig. S1 to S16
Table S1 to S4
References
Movie S1

30 July 2009; accepted 4 November 2009
Published online 26 November 2009;
10.1126/science.1179907
Include this information when citing this paper.

Global Analysis of Short RNAs Reveals Widespread Promoter-Proximal Stalling and Arrest of Pol II in *Drosophila*

Sergei Nechaev,[1] David C. Fargo,[2] Gilberto dos Santos,[1] Liwen Liu,[3] Yuan Gao,[4] Karen Adelman[1]*

Emerging evidence indicates that gene expression in higher organisms is regulated by RNA polymerase II stalling during early transcription elongation. To probe the mechanisms responsible for this regulation, we developed methods to isolate and characterize short RNAs derived from stalled RNA polymerase II in *Drosophila* cells. Significant levels of these short RNAs were generated from more than one-third of all genes, indicating that promoter-proximal stalling is a general feature of early polymerase elongation. Nucleotide composition of the initially transcribed sequence played an important role in promoting transcriptional stalling by rendering polymerase elongation complexes highly susceptible to backtracking and arrest. These results indicate that the intrinsic efficiency of early elongation can greatly affect gene expression.

Recent genome-wide studies of RNA polymerase II (Pol II) distribution have demonstrated that Pol II accumulates at promoters of many developmentally regulated and stimulus-responsive genes in their uninduced states (*1*–*3*). These findings challenge a common paradigm for gene regulation, which holds that recruiting the polymerase to a promoter is sufficient for gene activation, and indicate that regulation of many genes occurs after transcription initiates. An appealing model for such regulation involves promoter-proximal stalling, wherein an actively engaged polymerase pauses 25 to 50 nucleotides (nt) downstream of the transcription start site (TSS) (*4*–*6*). Release of stalled Pol II into productive elongation is rate-limiting for the expression of several *Drosophila* and mammalian genes (*4*, *5*, *7*), and mounting evidence suggests that promoter-proximal stalling is a widespread strategy for governing transcription output (*8*). However, efforts to define the prevalence and mechanisms of Pol II stalling have been hampered by the lack of a high-resolution, high-throughput method to detect transcriptionally engaged polymerase.

[1]Laboratory of Molecular Carcinogenesis, National Institute of Environmental Health Sciences, National Institutes of Health, Research Triangle Park, NC 27709, USA. [2]Library and Information Services, National Institute of Environmental Health Sciences, National Institutes of Health, Research Triangle Park, NC 27709, USA. [3]Biostatistics Branch, National Institute of Environmental Health Sciences, National Institutes of Health, Research Triangle Park, NC 27709, USA. [4]Department of Computer Science, Virginia Commonwealth University, Richmond, VA 23284, USA.

*To whom correspondence should be addressed. E-mail: adelmank@niehs.nih.gov

To overcome this obstacle, we developed a strategy to map promoter-proximal Pol II in *Drosophila* on a genome-wide scale and with single-nucleotide resolution. We isolated RNAs derived from stalled polymerase, making use of their characteristic properties as previously delineated for heat shock (*hsp*) genes: short size (<100 nt), nuclear localization, and presence of the 7-methylguanosine cap that is added to the 5′ end of nascent mRNA shortly after initiation (fig. S1) (*6*, *9*–*11*). Short RNA libraries were prepared from two independent biological replicates of *Drosophila* embryo–derived S2 cells and sequenced on an Illumina Genome Analyzer, yielding a combined total of 16.5 million uniquely mappable reads (table S1) (*12*).

Our approach efficiently selected for Pol II transcripts: ~75% of the reads mapped within 200 base pairs (bp) of the annotated TSSs of mRNA genes (fig. S2). About 98% of short RNAs that mapped near promoters aligned with the sense DNA strand (fig. S2), presenting no evidence for divergent transcription in *Drosophila*. Statistically significant levels of short RNAs were observed from more than 7400 TSSs ($P < 0.005$) (fig. S3), including >93% of genes that were previously defined as possessing stalled polymerase in chromatin immunoprecipitation coupled to genomic DNA microarray (ChIP-chip) studies (Fig. 1, A and C) (*1*). Genes with stalled Pol II generated considerably more short RNAs than genes with Pol II that did not appear stalled [Fig. 1C ($P < 0.0001$) and fig. S4] (*1*). However, >85% of genes that were not considered stalled in previous work also produced short RNAs, presumably as transient intermediates on the pathway to productive transcription (Fig. 1, B and C, and fig. S4). Although the number of short RNAs was a

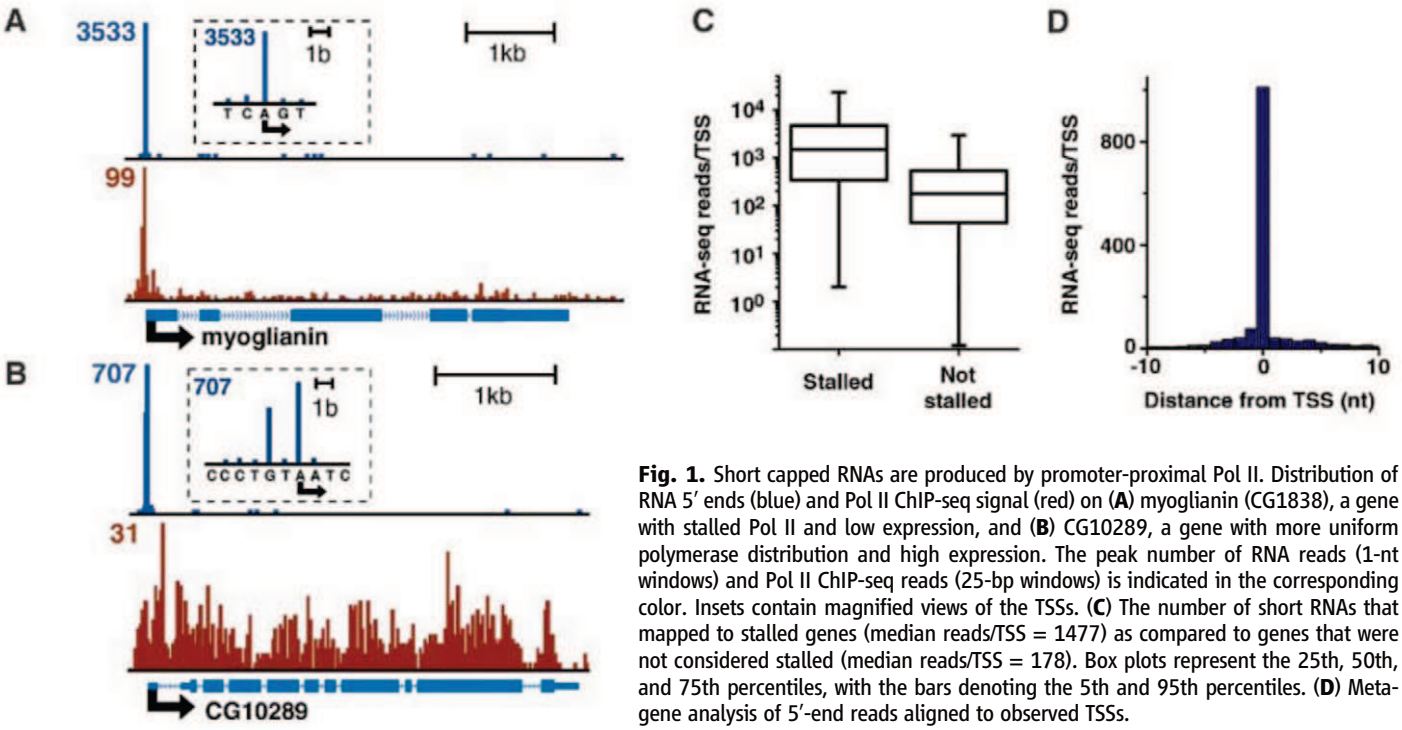

Fig. 1. Short capped RNAs are produced by promoter-proximal Pol II. Distribution of RNA 5′ ends (blue) and Pol II ChIP-seq signal (red) on (**A**) myoglianin (CG1838), a gene with stalled Pol II and low expression, and (**B**) CG10289, a gene with more uniform polymerase distribution and high expression. The peak number of RNA reads (1-nt windows) and Pol II ChIP-seq reads (25-bp windows) is indicated in the corresponding color. Insets contain magnified views of the TSSs. (**C**) The number of short RNAs that mapped to stalled genes (median reads/TSS = 1477) as compared to genes that were not considered stalled (median reads/TSS = 178). Box plots represent the 25th, 50th, and 75th percentiles, with the bars denoting the 5th and 95th percentiles. (**D**) Metagene analysis of 5′-end reads aligned to observed TSSs.

poor predictor of gene expression level (fig. S5), it was highly correlated with Pol II signal near the TSS in ChIP coupled to high-throughput sequencing (ChIP-seq) experiments (fig. S4). This finding agrees well with recent work indicating that much of the polymerase detected promoter-proximally is indeed engaged in early elongation (*8*).

The 5′-end reads around many TSSs mapped to a single nucleotide position (Fig. 1D), consistent with the idea that initiation in *Drosophila* is highly focused at most promoters (*13*). The observed 5′-end positions frequently differed from annotated TSSs, as suggested in earlier examinations of capped mRNA (fig. S6 and table S2) (*14*). Analysis of the sequences surrounding short RNA 5′ ends revealed a much better match to the consensus initiator element (*13*) than sequences around the annotated TSSs (fig. S6), indicating that we have accurately identified TSSs. The TSSs observed from short RNAs were in good agreement with those observed from capped RNAs isolated without size restriction (fig. S7) (*15*), indicating that polymerases generating short RNAs initiated from the same TSSs as those that synthesized full-length mRNA.

Although our approach readily detected short RNAs derived from stalled polymerase, pinpointing Pol II location precisely required mapping the RNA 3′ ends. Because currently available high-throughput procedures allow sequencing of RNAs only from 5′ ends, we designed new RNA adapters to sequence RNAs directly from their 3′ ends. The resultant RNA libraries, prepared from the same RNA samples as above, remained fully compatible with commercial sequencing primers and chemistry (figs. S2 and S3 and table S1).

We confirmed that the 3′ ends of short RNAs accurately defined locations of Pol II stalling by comparing their distribution to positions of engaged Pol II independently determined by permanganate probing. Permanganate reacts with single-stranded thymines on DNA, such as those in an open transcription bubble, and is currently the most authoritative means to detect stalled polymerase in vivo (*16*, *17*). We found a remarkable correspondence between locations of short RNA 3′ ends and regions of permanganate reactivity at newly identified genes (Fig. 2) and in published studies (fig. S8) (*1*, *2*, *17*, *18*). Metagene analysis showed that the 3′ ends were distributed primarily between +25 and +60 relative to the TSS (Fig. 3A) (~6500 genes), which agreed well with previous analysis of permanganate reactivity on ~60 genes (*17*).

Because Pol II stalls within the same promoter-proximal interval globally, we wondered whether the initially transcribed sequence might contribute to stalling. Given that the stability of the 9-bp RNA-DNA hybrid in the elongation complex greatly influences the efficiency of elongation (*19*, *20*), we calculated the melting temperature (T_m) of each 9-bp sequence across the initially transcribed region for genes shown in Fig. 3A and for control genes that did not generate significant short RNAs (Fig. 3B). There were clear

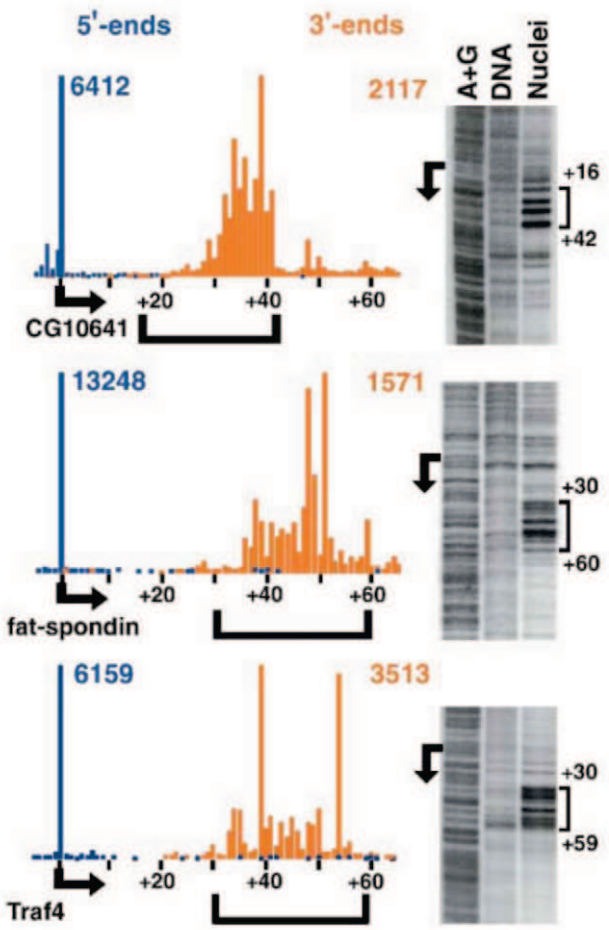

Fig. 2. The 3′ ends of short RNAs identify sites of polymerase stalling. The 5′-end (blue) and 3′-end (orange) RNA reads are shown for example genes, designated by Flybase gene names, with observed TSSs indicated by arrows. The number of 5′- and 3′-end reads at the peak locations is given in the corresponding colors. Permanganate footprints from nuclei are shown for each gene, alongside purified DNA and the adenine + guanine (A+G) DNA ladder. Numbers in black indicate positions relative to the TSS, and brackets show areas of permanganate reactivity.

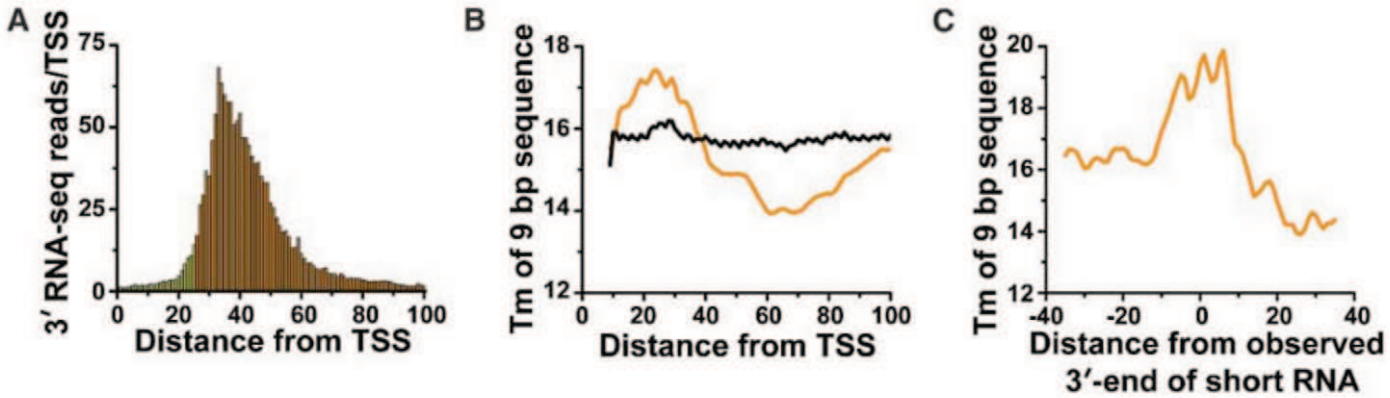

Fig. 3. Promoter-proximal sequences affect Pol II stalling. (**A**) The 3′-end reads were aligned relative to observed TSSs. RNAs shorter than 26 nt are not efficiently mapped to the genome (colored in yellow). (**B**) Metagene analysis of melting temperatures (°C) for 9-bp sequences across the initially transcribed regions for genes that generate significant numbers of short RNAs (orange) and all other genes (black). (**C**) T_m analysis of 9-bp sequences surrounding the primary 3′-end location for a subset of genes with focused 3′-end positions (N = 434).

differences between these profiles: Whereas the profile of the control group was essentially flat, genes that produced short RNAs exhibited a peak of T_m between positions +20 and +35 that corresponded to the primary sites of Pol II stalling. This peak was followed by a decline in T_m, which would serve to progressively destabilize the elongation complex (Fig. 3B) (*19*, *20*). These observations support a two-step model of stalling wherein the elongating polymerase first pauses transiently within the downstream region of weak RNA-DNA hybrid stability and then slides backward along DNA to a site with high thermodynamic stability (*21*–*23*). To verify that the position of stalling coincides with the peak in hybrid stability, we repeated T_m analysis on a subset of genes that displayed one predominant 3′-end position and found that it aligned with the region of highest T_m (Fig. 3C and fig. S9).

Although there were clear differences in the T_m profiles between genes that produced short RNAs and those that did not, some genes that lacked short RNAs in S2 cells nonetheless displayed an elevated T_m within the region from +20 and +35 (Fig. 3B). To investigate whether these genes might be stalled in another cell type, we isolated short RNAs from 0- to 16-hour-old *Drosophila* embryos and found >1500 genes that did not generate short RNAs in S2 cells but did so during embryo development. The T_m within the promoter-proximal region (+20 to +35) of these new genes was significantly higher than for genes without short RNAs (fig. S10) ($P < 0.0001$), and calculation of a T_m profile around the embryo-derived 3′ ends confirmed that they mapped within a peak in melting temperature. These results indicated that sequence composition of the initially transcribed region predisposes the polymerase to stall, and could be used to predict genes that are most likely to possess stalled Pol II under different conditions.

Our data suggested that stalled elongation complexes have undergone backtracking after transient pausing. The transcript cleavage factor TFIIS (IIS) has been shown to reactivate Pol II in backtracked and arrested elongation complexes (Fig. 4A), including stalled Pol II at the *Drosophila hsp70* gene (*24*) (fig. S11). If backtracking is a general feature of early polymerase elongation, then we should be able to detect evidence for IIS-mediated cleavage and shortening of promoter-proximal RNAs by comparing RNA profiles in mock-treated and IIS-depleted cells. Indeed, RNA interference-mediated depletion of IIS caused a global increase in RNA lengths (Fig. 4B) ($P < 10^{-15}$). Moreover, RNAs between 35 and 60 nt long were specifically enriched in IIS-depleted cells, indicating that they are the primary targets of IIS-induced cleavage (Fig. 4B). A concomitant reduction in 20- to 35-nt RNAs in IIS-deficient cells suggested that these RNAs are produced in part by IIS. Genes with stalled Pol II were significantly more likely to exhibit RNA lengthening upon IIS depletion than genes lacking stalled polymerase (fig. S12) ($P < 10^{-4}$), indicating that polymerase stalling generally involves backtracking. Comparison of short RNA and permanganate reactivity profiles on individual genes showed that, unlike the RNA 3′ ends, which were clearly shifted downstream in IIS-depleted cells, the location of the transcription bubble did not change (Fig. 4C). These results indicated that the primary location of the stalled elongation complex at steady state reflected the position to which the polymerase has backtracked.

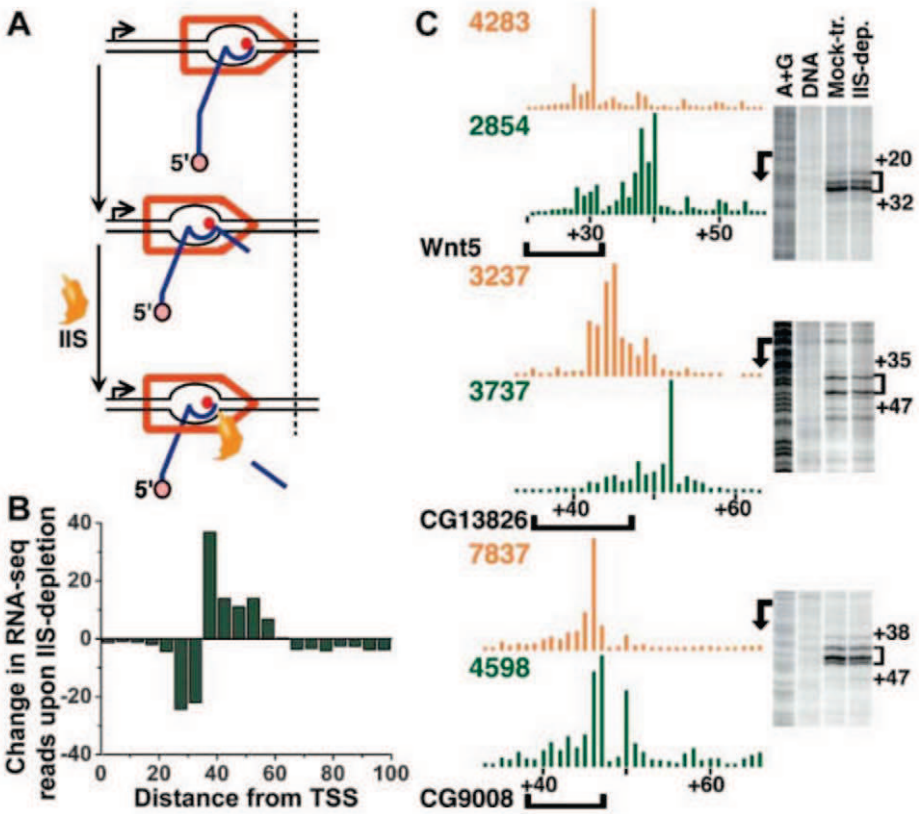

Fig. 4. Stalled polymerase complexes are predominantly backtracked. (**A**) The role of transcription cleavage factor IIS in rescuing arrested Pol II elongation complexes. After transcriptional pausing (top) the polymerase can backtrack along DNA (middle panel), which dislodges the RNA 3′ end from the polymerase active site (shown as a red dot) and blocks further transcription. IIS induces internal cleavage of nascent RNA (bottom), realigning the 3′ end with the active site, such that Pol II can resume transcription. (**B**) Depletion of IIS leads to an increase in RNA length within the promoter-proximal region. Shown is the difference between the normalized number of reads in IIS-depleted and mock-treated samples, binned in 5-nt windows. (**C**) IIS depletion affects RNA 3′-end positions but not permanganate reactivity profiles. RNA 3′ ends from mock-treated samples are shown in orange and IIS-depleted cells in green. Brackets denote regions of permanganate reactivity.

Recent work has underscored the importance of early transcription elongation and its regulation in vivo (*1*–*3*, *25*, *26*). Our data reveal that fluctuations in RNA-DNA hybrid stability in the initially transcribed sequence make the polymerase susceptible to pausing and backtracking. This tendency is likely amplified by the presence of downstream nucleosomes and the reported absence of secondary structures within these short RNAs that would inhibit backtracking (*17*, *27*). Furthermore, elongation factors specifically target promoter-proximal Pol II to regulate the duration of stalling. For example, the negative transcription elongation factor NELF has been shown biochemically to both enhance the duration of intrinsic pauses and to inhibit IIS activity (*28*, *29*).

Our data indicate that stalled polymerase complexes do not efficiently escape into productive elongation even after rescue by IIS-induced cleavage. In fact, many rounds of pausing, backtracking and cleavage, or perhaps even termination, may ensue before a positive signal such as the activity of the positive transcription elongation factor b (PTEF-b) kinase releases the stalled Pol II from the promoter-proximal region (*28*, *29*). In addition, our data suggest that transient stalling of polymerase is a general feature of early elongation, even at highly active genes, because we observe short RNAs with similar distributions arising from nearly all active genes (fig. S13). Thus, understanding how the duration of stalling is regulated under various conditions is of considerable interest, and our RNA-based approach opens a possibility for detailed dissection of this process on a genome-wide scale.

References and Notes

1. G. W. Muse *et al.*, *Nat. Genet.* **39**, 1507 (2007).
2. J. Zeitlinger *et al.*, *Nat. Genet.* **39**, 1512 (2007).

3. M. G. Guenther, S. S. Levine, L. A. Boyer, R. Jaenisch, R. A. Young, *Cell* **130**, 77 (2007).
4. A. Krumm, L. B. Hickey, M. Groudine, *Genes Dev.* **9**, 559 (1995).
5. A. E. Rougvie, J. T. Lis, *Mol. Cell. Biol.* **10**, 6041 (1990).
6. E. B. Rasmussen, J. T. Lis, *J. Mol. Biol.* **252**, 522 (1995).
7. M. Aida *et al.*, *Mol. Cell. Biol.* **26**, 6094 (2006).
8. L. J. Core, J. J. Waterfall, J. T. Lis, *Science* **322**, 1845 (2008).
9. E. B. Rasmussen, J. T. Lis, *Proc. Natl. Acad. Sci. U.S.A.* **90**, 7923 (1993).
10. J. A. Coppola, A. S. Field, D. S. Luse, *Proc. Natl. Acad. Sci. U.S.A.* **80**, 1251 (1983).
11. R. Jove, J. L. Manley, *J. Biol. Chem.* **259**, 8513 (1984).
12. Materials and methods are available as supporting material on *Science* Online.
13. T. Juven-Gershon, J. Y. Hsu, J. W. Theisen, J. T. Kadonaga, *Curr. Opin. Cell Biol.* **20**, 253 (2008).
14. B. Ahsan *et al.*, *Nucleic Acids Res.* **37**, D49 (2009).
15. K. Fejes-Toth *et al.*; Affymetrix ENCODE Transcriptome Project; Cold Spring Harbor Laboratory ENCODE Transcriptome Project, *Nature* **457**, 1028 (2009).
16. M. Kainz, J. Roberts, *Science* **255**, 838 (1992).
17. C. Lee *et al.*, *Mol. Cell. Biol.* **28**, 3290 (2008).
18. D. A. Gilchrist *et al.*, *Genes Dev.* **22**, 1921 (2008).
19. V. R. Tadigotla *et al.*, *Proc. Natl. Acad. Sci. U.S.A.* **103**, 4439 (2006).
20. M. Palangat, R. Landick, *J. Mol. Biol.* **311**, 265 (2001).
21. N. Komissarova, M. Kashlev, *J. Biol. Chem.* **272**, 15329 (1997).
22. T. C. Reeder, D. K. Hawley, *Cell* **87**, 767 (1996).
23. R. N. Fish, C. M. Kane, *Biochim. Biophys. Acta* **1577**, 287 (2002).
24. K. Adelman *et al.*, *Mol. Cell* **17**, 103 (2005).
25. D. D. Kephart, N. F. Marshall, D. H. Price, *Mol. Cell. Biol.* **12**, 2067 (1992).
26. M. Pal, D. McKean, D. S. Luse, *Mol. Cell. Biol.* **21**, 5815 (2001).
27. M. L. Kireeva *et al.*, *Mol. Cell* **18**, 97 (2005).
28. D. B. Renner, Y. Yamaguchi, T. Wada, H. Handa, D. H. Price, *J. Biol. Chem.* **276**, 42601 (2001).
29. M. Palangat, D. B. Renner, D. H. Price, R. Landick, *Proc. Natl. Acad. Sci. U.S.A.* **102**, 15036 (2005).

30. We thank P. Wade, T. Kunkel, and members of the Adelman laboratory for insightful discussions. We acknowledge S. Dai and J. Grovenstein for computational support. Sequence data are in the Gene Expression Omnibus (GEO) database under accession number GSE18643. This research was supported by the Intramural Research Program of the NIH, National Institute of Environmental Health Sciences (Z01 ES101987).

Supporting Online Material www.sciencemag.org/cgi/content/full/science.1181421/DC1 Materials and Methods
Figs. S1 to S13
Tables S1 and S2
References

2 September 2009; accepted 23 November 2009
Published online 10 December 2009;
10.1126/science.1181421
Include this information when citing this paper.

Unidirectional Airflow in the Lungs of Alligators

C. G. Farmer[1]* and Kent Sanders[2]

The lungs of birds move air in only one direction during both inspiration and expiration through most of the tubular gas-exchanging bronchi (parabronchi), whereas in the lungs of mammals and presumably other vertebrates, air moves tidally into and out of terminal gas-exchange structures, which are cul-de-sacs. Unidirectional flow purportedly depends on bellowslike ventilation by air sacs and may have evolved to meet the high aerobic demands of sustained flight. Here, we show that air flows unidirectionally through parabronchi in the lungs of the American alligator, an amphibious ectotherm without air sacs, which suggests that this pattern dates back to the basal archosaurs of the Triassic and may have been present in their nondinosaur descendants (phytosaurs, aetosaurs, rauisuchians, crocodylomorphs, and pterosaurs) as well as in dinosaurs.

Airflow in the avian lung is believed to be unique because gases move in the same direction during inhalation and exhalation through small tubes, the parabronchi. Although airflow is caused by volumetric changes in air sacs, the unidirectional pattern is achieved without mechanical valves. Soot-laden air was used to demonstrate unidirectional flow, and this pattern of airflow was attributed to the configuration of the bronchi giving rise to jetting and Venturi effects (in which increases in fluid velocity decrease lateral pressure) (*1*, *2*).

Crocodilian lungs are distinct from bird lungs and are thought to have a large alveolar-arterial blood gas difference, large ventilation-perfusion inhomogeneity, and parenchyma consisting of cubicles (ediculae) (*3*–*5*). However, the topography of the intrapulmonary bronchus and of the first generation of bronchi is similar in birds and crocodilians (*3*, *6*, *7*).

[1]Department of Biology, University of Utah, 257 South 1400 East, Salt Lake City, UT 84112, USA. [2]Department of Radiology, Musculoskeletal Division, 50 North Medical Drive, Room 1A71, University of Utah Health Sciences Center, Salt Lake City, UT 84132, USA.

*To whom correspondence should be addressed. E-mail: cg.frmr@gmail.com

Key features of the avian aerodynamic valve appear to be present in the alligator lung. The green bronchus shown in Fig. 1, the cervical ventral bronchus (CVB), is strikingly similar to the avian ventral bronchus that connects with the cervical air sacs. The small ostium to the CVB opens into a funnel-shaped vestibule acutely angled with the intrapulmonary bronchus, so that the bronchus makes a hairpin turn ventrocranially before coursing cranially to the apex of the lung (Fig. 1A, B). Distal to the CVB ostium, the intrapulmonary bronchus widens and becomes partially enclosed as it curves caudally and laterally and gives rise to a pair of small medial paracardiac bronchi (Fig. 1, red bronchi), a large individual dorsolateral bronchus (Fig. 1, chartreuse bronchus), and three caudal bronchi originating from a common terminal intrabronchial chamber (Fig. 1, blue bronchi). Their orifices are larger than the CVB orifice and better aligned with the intrapulmonary bronchus. Most of these latter bronchial passages spiral dorsolaterally toward the apex of the lung in a manner similar to the avian dorsal bronchi. We have discovered that the dorsal bronchi connect to each other and to the CVB through numerous anastomosing parabronchi, approximately 1 to 1.5 mm in diameter at the orifice to the bronchi (arrowheads, Fig. 1C) [supporting online material (SOM)]. As in birds, small ostia to caudoventral bronchi (arrows, Fig. 1C) occur opposite the ostia of the dorsal bronchi.

The anatomical similarity with the avian lung led us to hypothesize that airflow might also be unidirectional in crocodilians. Previously, measurements of airflow in alligator lungs did not identify unidirectional flow (*8*). Perry discussed the possibility that crocodilians have unidirectional airflow, but concluded that airflow is tidal in crocodilians and that unidirectional flow evolved in coelurosaurian-grade dinosaurs (*9*–*12*). Furthermore, for avian-style respiration to occur in birds and nonavian dinosaurs, abdominal air sacs have been presumed to be critical (*13*), and the hepatic piston mechanism of ventilation of crocodilians has been presumed incompatible (*14*).

To test the hypothesis that airflow in alligator lungs is unidirectional, we implanted dual thermistor flowmeters in the CVB (green bronchus of Fig. 1) and a dorsal bronchus (a blue bronchus of Fig. 1) of four alligators, artificially ventilated the lungs with both negative and positive pressure inspiration, and observed that air in the CVB moved in a cranial-to-caudal direction and air in the dorsal bronchus moved in a ventrolateral to dorsomedial direction during expiration and during both types of inspiration (Fig. 2).

To determine whether similar patterns of flow occur in vivo, we monitored airflow in the CVB during normal breathing in five alligators with single-bead thermistors and in one alligator with a dual thermistor flow meter. In the former experiments, the flow continued during the transition from inspiration to expiration rather than dropping to zero, as would be the case if the direction of the flow had reversed. In vivo recordings with the dual thermistor flow meter showed that the air moved in a cranial-to-caudal direction during both inspiration and expiration; which is the same pattern of flow observed in excised lungs (Fig. 3). The amplitude of the expiratory flow was greater than the amplitude of the inspiratory flow, as in the excised lungs.

We also visualized flow by filling an excised lung with saline containing fluorescent microspheres. In the CVB, the microspheres flowed in a cranial-to-caudal direction as the fluid was pushed into and pulled out of the lung (movies S1 and S2). In the parabronchi, the spheres also flowed unidirectionally (movie S3). All three methods—in vivo recordings of airflow, recordings of airflow in artificially ventilated excised lungs, and visualization of water flow in artificially ventilated lungs—indicate that fluid flows unidirectionally through the lungs of alligators in a strikingly birdlike pattern.

Our data suggest that airflow in the alligator is extremely birdlike, but it is unknown how it is possible to have unidirectional flow without air sacs and with diaphragmatic breathing. A mechanism for unidirectional flow in bird lungs as a consequence of the topography of the intrapulmonary bronchi (*1*) that does not depend on air sacs or the mechanics of breathing is shown in Fig. 1, H and I. During exhalation, the configuration of the laterobronchial ostia may cause air to move dorsally to enter the ostia of the dorsobronchi, rather than leaving the lung directly by way of the mesobronchus (*1*). During inspiration, rapid flow of air along the intrapulmonary bronchus past the ostia to the ventrobronchi may reduce lateral pressure at this location because of the Venturi effect, and the low pressure may act

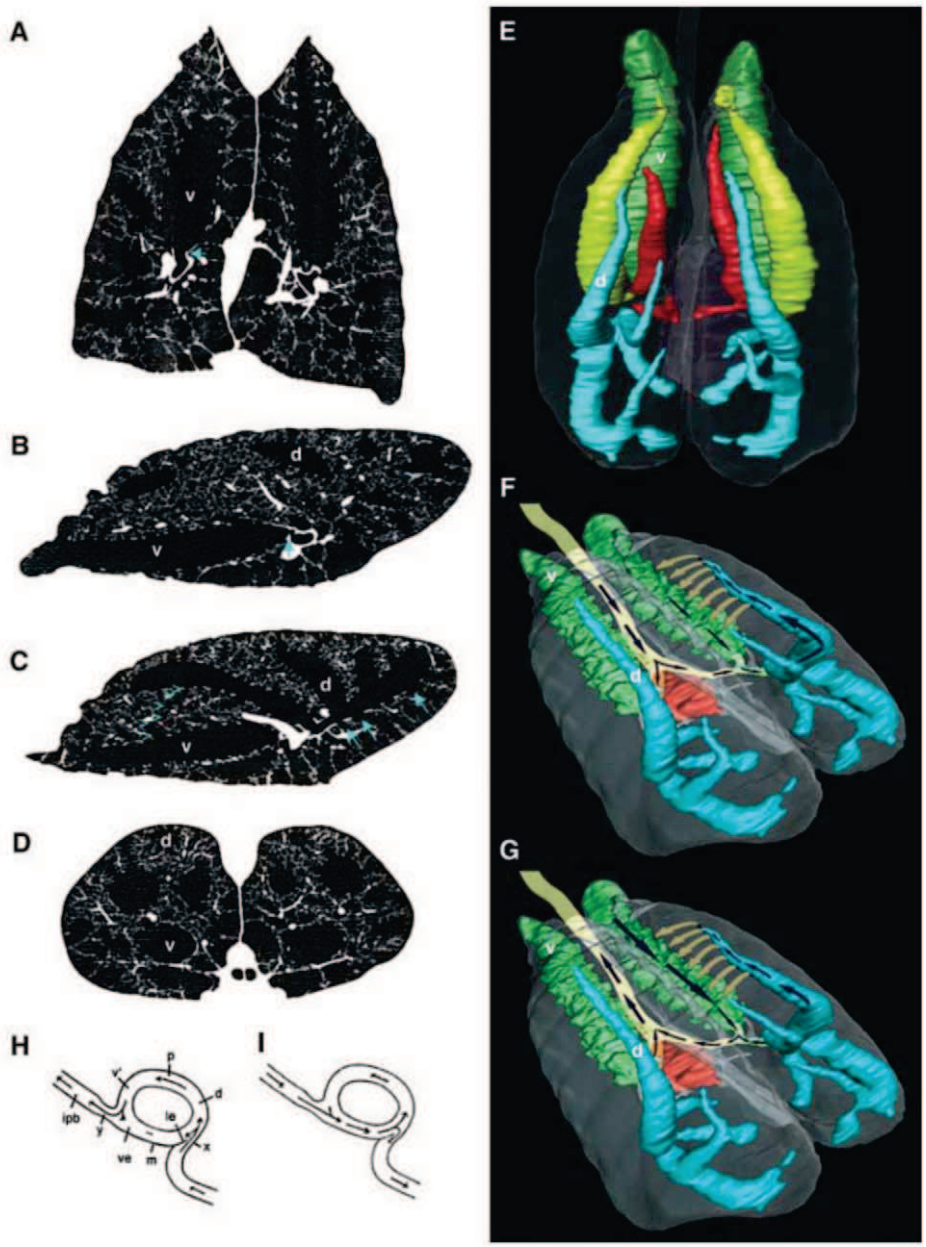

Fig. 1. Airflow in alligator lungs. Computed tomography images (left) show the hairpin turn (blue arrow) into the CVB (v) in the coronal (**A**) and medial sagittal (**B**) views. The lateral sagittal view shows the larger ostia to the dorsal bronchi (**C**), some of the ostia of ventral and lateral bronchi (blue arrows), a parabronchus (blue arrowheads), and the dorsal bronchus in which flow was recorded (d). The axial view (**D**) shows the bifurcation of the primary bronchi. An oblique dorsal view of the major bronchi is shown in (**E**). A simplified view shows airflow during inspiration (**F**) and exhalation (**G**) in the trachea, CVB, dorsal bronchus, and parabronchi. Hazelhoff's model of exhalation (**H**) and inspiration (**I**). ipb, intrapulmonary bronchus; le, guiding dam; ve, vestibulum; v, ventrobronchus; m, mesobronchus; p, parabronchus; d, dorsobronchus; x,y, sites of constriction.

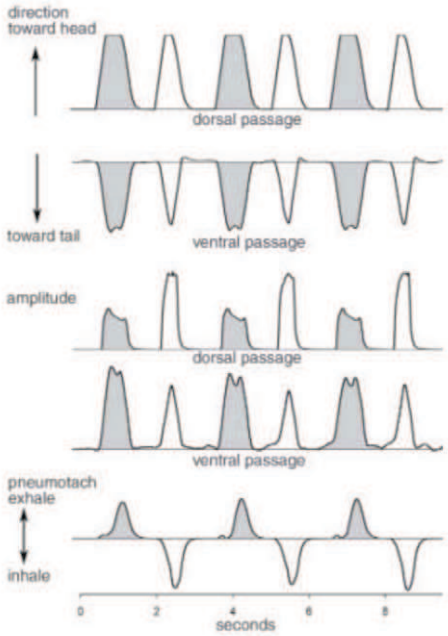

Fig. 2. Airflow in excised lungs. The top two traces show the direction of intrapulmonary airflow recorded from the dorsal bronchus (d in Fig. 1) and CVB (v in Fig. 1) with dual thermistor flow meters. The middle two traces show the relative amplitude of these flows. The bottom trace shows flow into and out of the trachea, recorded with a pneumotach.

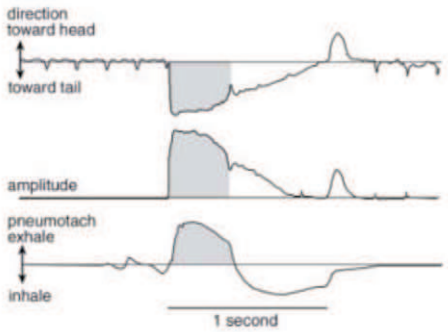

Fig. 3. Airflow observed in vivo. The top trace shows the direction of intrapulmonary airflow recorded in the CVB (v of Fig. 1) with a dual thermistor flow meter. The small pulse of air moving toward the head after airflow in the trachea has ceased occurs when the glottis is closed and the muscles of the trunk relax (*21*). The middle trace shows the amplitude of the flow. The bottom trace shows flow into and out of the trachea, recorded with a pneumotach.

as a suction pump to draw air past the mouths of the ventrobronchi into the mesobronchus (*1*). A glass model demonstrated how this geometry gives rise to unidirectional airflow (*1*).

The mechanism of unidirectional flow in alligator lungs is yet to be determined, but our data support Hazelhoff's model (*1*), in which key features of the bronchial tree give rise to unidirectional flow. During inspiration, air may jet past the obliquely oriented vestibule of the CVB to enter the larger dorsal bronchial openings and reduce lateral pressure at the CVB orifice to draw air from the CVB into the intrapulmonary bronchus. During exhalation, air in the caudoventral bronchi may jet dorsally (blue arrows in Fig. 1C) to enter the ostia of the dorsobronchi. In this way, a simple arrangement of the bronchi by themselves might give rise to unidirectional airflow. Also, the mechanism of gas exchange in crocodilians is not known; a crosscurrent mechanism has been hypothesized (*11*), but a countercurrent mechanism cannot be ruled out. Furthermore, the importance of unidirectional airflow for gas exchange efficiency in the alligator lung is not known and cannot be determined from our data, which consist of measurements of airflow.

Previous scenarios for the evolution of unidirectional airflow are that it arose in dinosaurs of coelurosaurian grade (*12*), convergently in theropods and pterosaurs (*13*, *15*), or not at all in dinosaurs because of a hepatic piston mechanism of breathing (*14*). Our findings contrast with these previous views in several ways. They demonstrate that the hepatic piston mechanism of breathing, which crocodilians have but birds lack, does not preclude the evolution of unidirectional flow and that pneumaticity, which crocodilians lack, cannot be used to diagnose unidirectional airflow in fossil taxa, as previously suggested (*13*, *15*). Crocodilians and birds are crown-group Archosauria. Therefore, in contrast to previous views, we suggest that unidirectional flow evolved before the divergence of crurotarsan and dinosaurian archosaurs and was present in the basal archosaurs and their descendants, including phytosaurs, aetosaurs, "rauisuchians," and crocodylomorphs. The crurotarsans and, somewhat later, the dinosaurs supplanted the synapsids as the dominant members of the Triassic terrestrial vertebrate assemblage, with Triassic mammals existing as diminutive mouselike forms (*16*, *17*). The roles of contingency and competition in the faunal turnover that occurred in the aftermath of the End Permian mass extinction are controversial. The basal archosaurs and archosauromorphs, animals such as *Euparkaria*, appear to have expanded their capacity for vigorous exercise (*18*) during a period of relative environmental hypoxia (*19*). In bird lungs, unidirectional airflow coupled with a crosscurrent mechanism of gas exchange facilitates the extraction of oxygen under conditions of hypoxia (*20*). If such a lung was present at the base of the archosaur radiation, this clade may have been better able than the synapsids to compete for niches that required a capacity for vigorous exercise.

References and Notes

1. E. H. Hazelhoff, *Poult. Sci.* **30**, 3 (1951).
2. H. Dotterweich, *Z. Vgl. Physiol.* **23**, 744 (1936).
3. S. F. Perry, in *Biology of the Reptilia*, C. Gans, A. S. Gaunt, Eds. (Society for the Study of Amphibians and Reptiles, Ithaca, NY, 1998), vol. 19, pp. 1–92.
4. J. W. Hicks, F. N. White, *Respir. Physiol.* **88**, 23 (1992).
5. F. L. Powell, A. T. Gray, *Respir. Physiol.* **78**, 83 (1989).
6. F. Moser, *Arch. Mikrosk. Anat. Entwicklungsmech.* **60**, 587 (1902).
7. S. Wolf, *Zool. Jahrb. Abt. Anat. Ontol.* **57**, 139 (1933).
8. P. E. Bickler, R. G. Spragg, M. T. Hartman, F. N. White, *Am. J. Physiol.* **249**, R477 (1985).
9. S. F. Perry, *J. Exp. Biol.* **134**, 99 (1988).
10. S. F. Perry, in *Comparative Pulmonary Physiology. Current Concepts,* S. C. Wood, Ed. (Marcel Dekker, NY, 1989), pp. 193–236.
11. S. F. Perry, *J. Comp. Physiol. B* **159**, 761 (1990).
12. S. F. Perry, in *Physiological Adaptations in Vertebrates; Respiration, Circulation, and Metabolism*, S. Wood, R. Weber, A. Hargens, R. Millard, Eds. (Marcel Dekker, NY, 1992), pp. 149–167.
13. P. M. O. O'Connor, L. P. A. M. Claessens, *Nature* **436**, 253 (2005).
14. J. A. Ruben, N. R. Geist, W. J. Hillenius, T. D. Jones, M. Signore, C. Dal Sasso, *Science* **283**, 514 (1999).
15. L. P. A. M. Claessens, P. M. O. O'Connor, D. M. Unwin, P. Sereno, *PLoS ONE* **4**, e4497 (2009).
16. S. L. Brusatte, M. J. Benton, M. Ruta, G. T. Lloyd, *Science* **321**, 1485 (2008).
17. A. W. Crompton, F. A. Jenkins, in *Mesozoic Mammals,* J. A. Lillegraven, Z. Kielan-Jaworowska, W. A. Clemens, Eds. (Univ. of California Press, Berkeley, CA, 1979), pp. 59–73.
18. D. R. Carrier, C. G. Farmer, *Paleobiology* **26**, 271 (2000).
19. R. A. Berner, J. M. Vandenbrooks, P. D. Ward, *Science* **316**, 557 (2007).
20. P. Scheid, J. Piiper, in *Bird Respiration,* T. J. Seller, Ed. (CRC Press, Boca Raton, FL, 1987), vol. I, pp. 97–129.
21. C. G. Farmer, D. R. Carrier, *J. Exp. Biol.* **203**, 1679 (2000).

22. This work was supported by NSF (grant IOS-0818973 to C.G.F.).

Supporting Online Material www.sciencemag.org/cgi/content/full/327/5963/338/DC1 Materials and Methods
Fig. S1
References
Movies S1 to S3

5 August 2009; accepted 12 November 2009
10.1126/science.1180219

G Protein Subunit $G\alpha_{13}$ Binds to Integrin $\alpha_{IIb}\beta_3$ and Mediates Integrin "Outside-In" Signaling

Haixia Gong, Bo Shen, Panagiotis Flevaris, Christina Chow, Stephen C.-T. Lam, Tatyana A. Voyno-Yasenetskaya, Tohru Kozasa, Xiaoping Du*

Integrins mediate cell adhesion to the extracellular matrix and transmit signals within the cell that stimulate cell spreading, retraction, migration, and proliferation. The mechanism of integrin outside-in signaling has been unclear. We found that the heterotrimeric guanine nucleotide–binding protein (G protein) $G\alpha_{13}$ directly bound to the integrin β_3 cytoplasmic domain and that $G\alpha_{13}$-integrin interaction was promoted by ligand binding to the integrin $\alpha_{IIb}\beta_3$ and by guanosine triphosphate (GTP) loading of $G\alpha_{13}$. Interference of $G\alpha_{13}$ expression or a myristoylated fragment of $G\alpha_{13}$ that inhibited interaction of $\alpha_{IIb}\beta_3$ with $G\alpha_{13}$ diminished activation of protein kinase c-Src and stimulated the small guanosine triphosphatase RhoA, consequently inhibiting cell spreading and accelerating cell retraction. We conclude that integrins are noncanonical $G\alpha_{13}$-coupled receptors that provide a mechanism for dynamic regulation of RhoA.

Integrins mediate cell adhesion and transmit signals within the cell that lead to cell spreading, retraction, migration, and proliferation (*1*). Thus, integrins have pivotal roles in biological processes such as development, immunity, cancer, wound healing, hemostasis, and thrombosis. The platelet integrin $\alpha_{IIb}\beta_3$ typically displays bidirectional signaling function (*2*, *3*). Signals from within the cell activate binding of $\alpha_{IIb}\beta_3$ to extracellular ligands, which in turn triggers signaling within the cell initiated by the occupied receptor (so-called "outside-in" signaling). A major early consequence of integrin "outside-in" signaling is cell spreading, which requires activation of the protein kinase c-Src and c-Src–mediated inhibition of the small guanosine triphosphatase (GTPase) RhoA (*4*–*7*). Subsequent cleavage of the c-Src binding site in β_3 by calpain allows activation of RhoA, which stimulates cell retraction (*7*, *8*). The molecular mechanism coupling ligand-bound $\alpha_{IIb}\beta_3$ to these signaling events has been unclear.

Heterotrimeric guanine nucleotide–binding proteins (G proteins) consist of Gα, Gβ, and Gγ subunits (*9*). G proteins bind to the intracellular side of G protein–coupled receptors (GPCRs) and transmit signals that are important in many intracellular events (*9*–*11*). $G\alpha_{13}$, when activated by GPCRs, interacts with Rho guanine-nucleotide exchange

Department of Pharmacology, University of Illinois at Chicago, 835 South Wolcott Avenue, Room E403, Chicago, IL 60612, USA.

*To whom correspondence should be addressed. E-mail: xdu@uic.edu

factors (RhoGEF) and thus activates RhoA (*11*–*14*), facilitating contractility and rounding of discoid platelets (shape change). To determine whether $G\alpha_{13}$ functions in signaling from ligand-occupied integrin, we investigated whether inhibition of $G\alpha_{13}$ expression with small interfering RNA (siRNA) affected $\alpha_{IIb}\beta_3$-dependent spreading of platelets on fibrinogen, which is an integrin ligand. We isolated mouse bone marrow stem cells and transfected them with lentivirus encoding $G\alpha_{13}$ siRNA. The transfected stem cells were transplanted into irradiated C57/BL6 mice (*15*). Four to six weeks after transplantation, nearly all platelets isolated from recipient mice were derived from transplanted stem cells, as indicated by the enhanced green fluorescent protein (EGFP) encoded in lentivirus vector (Fig. 1A and fig. S1). Platelets from $G\alpha_{13}$ siRNA-transfected stem cell recipient mice showed >80% decrease in $G\alpha_{13}$ expression (Fig. 1B). When platelets were allowed to adhere to immobilized fibrinogen [$\alpha_{IIb}\beta_3$ binding to immobilized fibrinogen does not require prior "inside-out" signaling activation (*16*)], platelets depleted of $G\alpha_{13}$ spread poorly as compared with control platelets (Fig. 1A and fig. S2). The inhibitory effect of $G\alpha_{13}$ deficiency is unlikely to be caused by its effect on GPCR-stimulated $G\alpha_{13}$ signaling because (i) washed resting platelets were used and no GPCR agonists were added, and (ii) prior treatment with 1 mM aspirin [which abolishes thromboxane A_2 (TXA_2) generation (*17*)] did not affect platelet spreading on fibrinogen (fig. S2), making unlikely the endogenous TXA_2-mediated stimulation of $G\alpha_{13}$. Furthermore, $G\alpha_{13}$ siRNA inhibited spreading of Chinese hamster ovary (CHO) cells expressing human $\alpha_{IIb}\beta_3$ (123 cells) (*18*), which was rescued by an siRNA-resistant $G\alpha_{13}$ (fig. S3). Thus, $G\alpha_{13}$ appears to be important in integrin "outside-in" signaling leading to cell spreading.

To determine whether $G\alpha_{13}$ serves as an early signaling mechanism that mediates integrin-induced

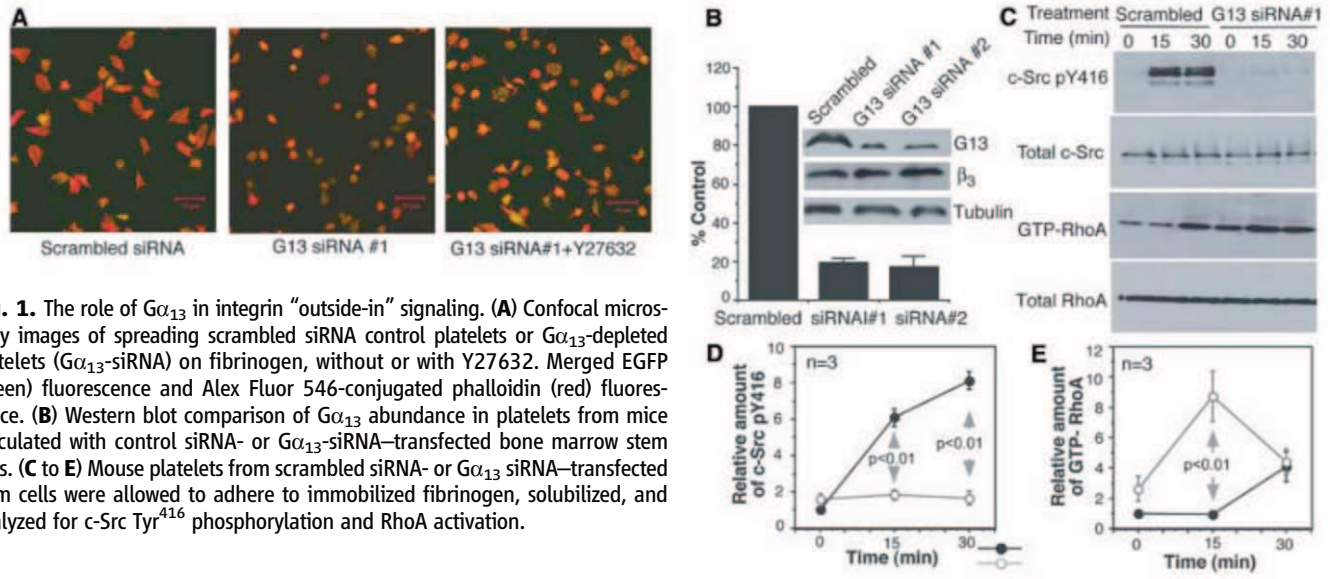

Fig. 1. The role of $G\alpha_{13}$ in integrin "outside-in" signaling. (**A**) Confocal microscopy images of spreading scrambled siRNA control platelets or $G\alpha_{13}$-depleted platelets ($G\alpha_{13}$-siRNA) on fibrinogen, without or with Y27632. Merged EGFP (green) fluorescence and Alex Fluor 546-conjugated phalloidin (red) fluorescence. (**B**) Western blot comparison of $G\alpha_{13}$ abundance in platelets from mice inoculated with control siRNA- or $G\alpha_{13}$-siRNA–transfected bone marrow stem cells. (**C** to **E**) Mouse platelets from scrambled siRNA- or $G\alpha_{13}$ siRNA–transfected stem cells were allowed to adhere to immobilized fibrinogen, solubilized, and analyzed for c-Src Tyr^{416} phosphorylation and RhoA activation.

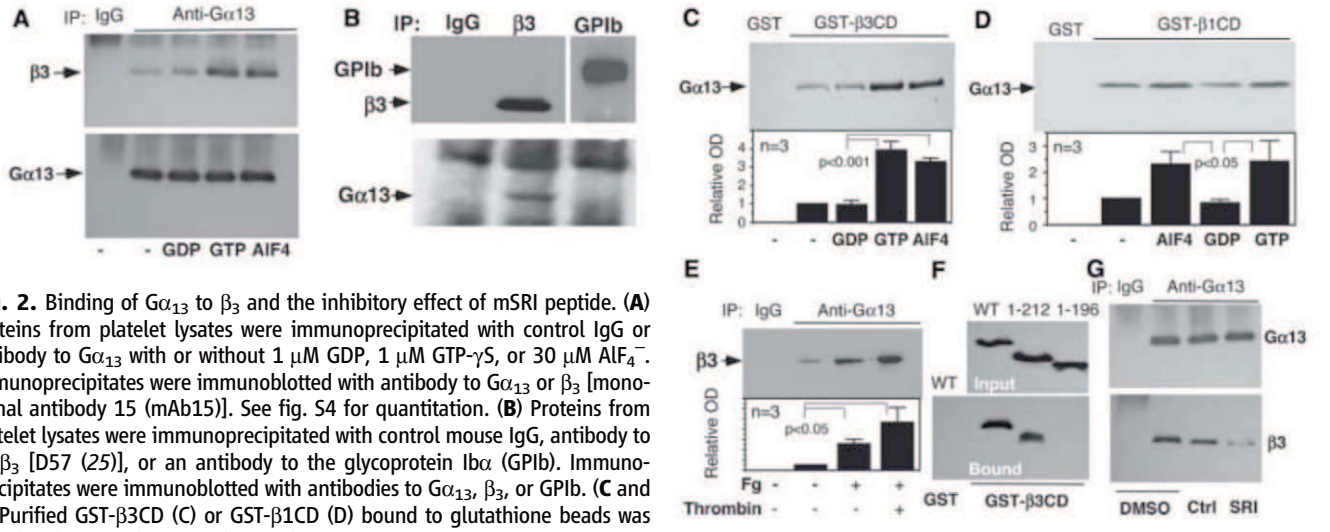

Fig. 2. Binding of $G\alpha_{13}$ to β_3 and the inhibitory effect of mSRI peptide. (**A**) Proteins from platelet lysates were immunoprecipitated with control IgG or antibody to $G\alpha_{13}$ with or without 1 μM GDP, 1 μM GTP-γS, or 30 μM AlF_4^-. Immunoprecipitates were immunoblotted with antibody to $G\alpha_{13}$ or β_3 [monoclonal antibody 15 (mAb15)]. See fig. S4 for quantitation. (**B**) Proteins from platelet lysates were immunoprecipitated with control mouse IgG, antibody to $\alpha_{IIb}\beta_3$ [D57 (*25*)], or an antibody to the glycoprotein Ibα (GPIb). Immunoprecipitates were immunoblotted with antibodies to $G\alpha_{13}$, β_3, or GPIb. (**C** and **D**) Purified GST-β3CD (C) or GST-β1CD (D) bound to glutathione beads was mixed with purified $G\alpha_{13}$ with or without 1 μM GDP, 1 μM GTP-γS, or 30 μM AlF_4^-. Bound proteins were immunoblotted with antibody to $G\alpha_{13}$. Quantitative data are shown as mean ± SD and *P* value (*t* test). (**E**) Lysates of control platelets or platelets adherent to fibrinogen in the absence or presence of 0.025 U/ml thrombin were immunoprecipitated with antibody to $G\alpha_{13}$ and then immunoblotted with mAb15. Quantitative data are shown as mean ± SD and *P* value (*t* test). (**F**) Lysates from 293FT cells transfected with Flag-tagged wild-type $G\alpha_{13}$ or indicated truncation mutants (see fig. S5) were precipitated with GST-β_3CD- or GST-bound glutathione beads. Bead-bound proteins were immunoblotted with antibody to Flag (Bound). Flag-tagged protein amounts in lysates are shown by anti-Flag immunoblot (Input). (**G**) Protein from platelet lysates treated with 0.1% dimethyl sulfoxide (DMSO), 250 μM scrambled control peptide (Ctrl), or mSRI were immunoprecipitated with antibody to $G\alpha_{13}$. Immunoprecipitates were immunoblotted with antibody to $G\alpha_{13}$ or β_3. See fig. S4 for quantitation.

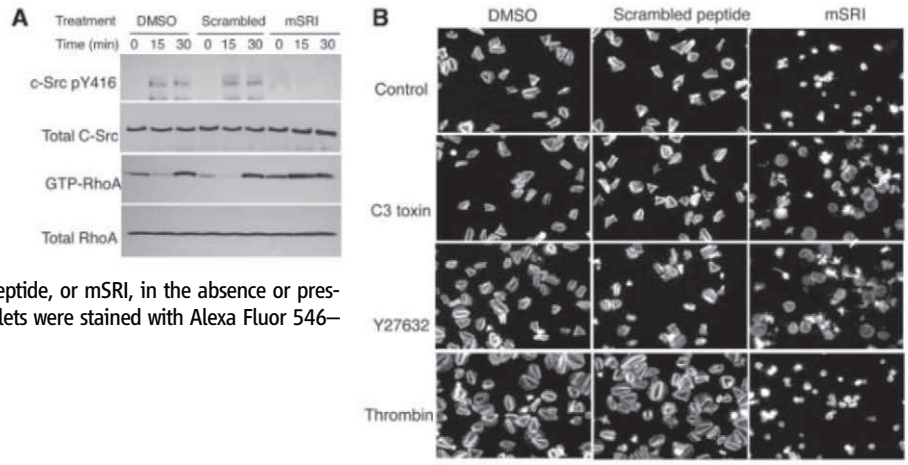

Fig. 3. Effects of mSRI on integrin-induced c-Src phosphorylation, RhoA activity, and platelet spreading. (**A**) Washed human platelets pretreated with DMSO, mSRI, or scrambled control peptide were allowed to adhere to fibrinogen and then solubilized at indicated time points. Proteins from lysates were immunoblotted with antibodies to c-Src phosphorylated at Tyr^{416}, c-Src, or RhoA. GTP-bound RhoA was measured by association with GST–Rhotekin rho-binding domain (GST-RBD) beads (*26*). See fig. S4 for quantitative data. (**B**) Spreading of platelets treated with 0.1% DMSO, scrambled control peptide, or mSRI, in the absence or presence of C3 toxin, Y27632, or 0.01 U/ml thrombin. Platelets were stained with Alexa Fluor 546–conjugated phalloidin.

activation of c-Src, we measured phosphorylation of c-Src at Tyr^{416} (which indicates activation of c-Src) in control and fibrinogen-bound cells. Depletion of $G\alpha_{13}$ in mouse platelets or 123 cells abolished phosphorylation of c-Src Tyr^{416} (Fig. 1C and fig. S3), indicating that $G\alpha_{13}$ may link integrin $\alpha_{IIb}\beta_3$ and c-Src activation. Because c-Src inhibits RhoA (*7*, *19*), we also tested the role of $G\alpha_{13}$ in regulating activation of RhoA. RhoA activity was suppressed to baseline 15 min after platelet adhesion and became activated at 30 min (Fig. 1C), which is consistent with transient inhibition of RhoA by c-Src (*7*). The integrin-dependent delayed activation of RhoA was not inhibited by depletion of $G\alpha_{13}$, indicating its independence of the GPCR-$G\alpha_{13}$-RhoGEF pathway (Fig. 1C). In contrast, depletion of $G\alpha_{13}$ accelerated RhoA activation (Fig. 1C). Thus, $G\alpha_{13}$ appears to mediate inhibition of RhoA. The inhibitory effect of $G\alpha_{13}$ depletion on platelet spreading was reversed by Rho-kinase inhibitor Y27632 (Fig. 1A), which suggests that $G\alpha_{13}$-mediated inhibition of RhoA is important in stimulating platelet spreading. These data are consistent with $G\alpha_{13}$ mediating integrin "outside-in" signaling inducing c-Src activation, RhoA inhibition, and cell spreading.

The integrin $\alpha_{IIb}\beta_3$ was coimmunoprecipitated by antibody to $G\alpha_{13}$, but not control immunoglobulin G (IgG), from platelet lysates (Fig. 2A). Conversely, an antibody to β_3 immunoprecipitated $G\alpha_{13}$ with β_3 (Fig. 2B). Coimmunoprecipitation of β_3 with $G\alpha_{13}$ was enhanced by guanosine triphosphate γS (GTP-γS) or AlF_4^- (Fig. 2A and fig. S4). Thus, β_3 is present in a complex with $G\alpha_{13}$, preferably the active GTP-bound $G\alpha_{13}$. To determine whether $G\alpha_{13}$ directly binds to the integrin cytoplasmic domain, we incubated purified recombinant $G\alpha_{13}$ (*20*) with agarose beads conjugated with glutathione S-transferase (GST) or a GST-β_3 cytoplasmic domain fusion protein (GST-β_3CD). Purified $G\alpha_{13}$ bound to GST-β_3CD, but not to GST (Fig. 2C). Purified $G\alpha_{13}$ also bound to the β_1 integrin cytoplasmic domain fused with GST (GST-β_1CD) (Fig. 2D). The binding of $G\alpha_{13}$ to GST-β_3CD and GST-β_1CD was detected with GDP-loaded $G\alpha_{13}$,

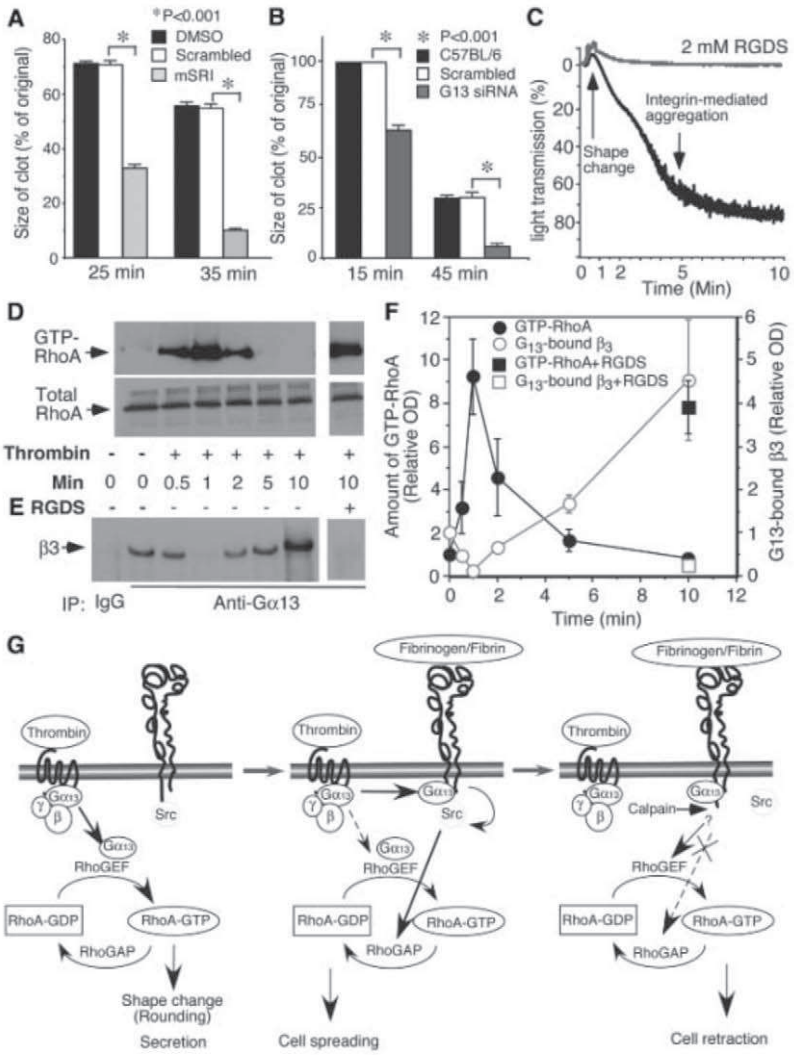

Fig. 4. The role of $G\alpha_{13}$ in clot retraction and dynamic RhoA regulation. (**A**) Effect of 250 μM mSRI peptide on clot retraction of human platelet-rich plasma compared with DMSO and scrambled peptide. Clot sizes were quantified using Image J (mean ± SD, $n = 3$, t test). (**B**) Comparison of clot retraction (mean ± SD, $n = 3$, t test) mediated by control siRNA platelets and $G\alpha_{13}$-depleted platelets. (**C** to **F**) Platelets were stimulated with thrombin with or without 2 mM RGDS and monitored for turbidity changes of platelet suspension caused by shape change and aggregation (C). The platelets were then solubilized at indicated time points and analyzed for amount of β_3 coimmunoprecipitated with $G\alpha_{13}$ (D) and amount of GTP-RhoA bound to GST-RBD beads (E) by immunoblot. (F) Quantitative data (mean ± SD) from three experiments. (**G**) A schematic illustrating $G\alpha_{13}$-dependent dynamic regulation of RhoA and crosstalk between GPCR and integrin signaling.

but enhanced by GTP-γS and AlF_4^- (Fig. 2, C and D), indicating that the cytoplasmic domains of β_3 and β_1 can directly interact with $G\alpha_{13}$ and that GTP enhances the interaction. The $G\alpha_{13}$-β_3 interaction was enhanced in platelets adherent to fibrinogen, and by thrombin, which stimulates GTP binding to $G\alpha_{13}$ via GPCR (Fig. 2E). Hence, the interaction is regulated by both integrin occupancy and GPCR signaling.

To map the β_3 binding site in $G\alpha_{13}$, we incubated cell lysates containing Flag-tagged wild type or truncation mutants of $G\alpha_{13}$ (fig. S5) with GST-β_3CD beads. GST-β_3CD associated with wild-type $G\alpha_{13}$ and the $G\alpha_{13}$ 1 to 212 fragment containing α-helical region and switch region I (SRI), but not with the $G\alpha_{13}$ fragment containing residues 1 to 196 lacking SRI (Fig. 2F). Thus, SRI appears to be critical for β_3 binding. To further determine the importance of SRI, $G\alpha_{13}$-β_3 binding was assessed in the presence of a myristoylated synthetic peptide, Myr-LLARRPTKGIHEY (mSRI), corresponding to the SRI sequence of $G\alpha_{13}$ (197 to 209) (*21*, *22*). The mSRI peptide, but not a myristoylated scrambled peptide, inhibited $G\alpha_{13}$ binding to β_3 (Fig. 2G), indicating that mSRI is an effective inhibitor of β_3-$G\alpha_{13}$ interaction. Therefore, we further examined whether mSRI might inhibit integrin signaling. Treatment of platelets with mSRI inhibited integrin-dependent phosphorylation of c-Src Tyr^{416} and accelerated RhoA activation (Fig. 3A). The effect of mSRI is unlikely to result from its inhibitory effect on the binding of RhoGEFs to $G\alpha_{13}$ SRI because $G\alpha_{13}$ binding to RhoGEFs stimulates RhoA activation, which should be inhibited rather than promoted by mSRI (*22*). Thus, these data suggest that β_3-$G\alpha_{13}$ interaction mediates activation of c-Src and inhibition of RhoA. Furthermore, mSRI inhibited integrin-mediated platelet spreading (Fig. 3B), and this inhibitory effect was reversed by C3 toxin (which catalyzes the ADP ribosylation of RhoA) or Y27632, confirming the importance of $G\alpha_{13}$-dependent inhibition of RhoA in platelet spreading. Thrombin promotes platelet spreading, which requires cdc42/Rac pathways (*23*). However, thrombin-promoted platelet spreading was also abolished by mSRI (Fig. 3B), indicating the importance of $G\alpha_{13}$-β_3 interaction. Thus, $G\alpha_{13}$-integrin interaction appears to be a mechanism that mediates integrin signaling to c-Src and RhoA, thus regulating cell spreading.

To further determine whether $G\alpha_{13}$ mediates inhibition of integrin-induced RhoA-dependent contractile signaling, we investigated the effects of mSRI and depletion of $G\alpha_{13}$ on platelet-dependent clot retraction (shrinking and consolidation of a blood clot requires integrin-dependent retraction of platelets from within) (*7*, *8*). Clot retraction was accelerated by mSRI and depletion of $G\alpha_{13}$ (Fig. 4, A and B, and fig. S6), indicating that $G\alpha_{13}$ negatively regulates RhoA-dependent platelet retraction and coordinates cell spreading and retraction. The coordinated cell spreading-retraction process is also important in wound healing, cell migration, and proliferation (*24*).

The function of $G\alpha_{13}$ in mediating the integrin-dependent inhibition of RhoA contrasts with the traditional role of $G\alpha_{13}$, which is to mediate GPCR-induced activation of RhoA. However, GPCR-mediated activation of RhoA is transient, peaking at 1 min after exposure of platelets to thrombin, indicating the presence of a negative regulatory signal (Fig. 4, D and F). Furthermore, thrombin-stimulated activation of RhoA occurs during platelet shape change before substantial ligand binding to integrins (Fig. 4, C, D, and F). In contrast, after thrombin stimulation, β_3 binding to $G\alpha_{13}$ was diminished at 1 min when $G\alpha_{13}$-dependent activation of RhoA occurs, but increased after the occurrence of integrin-dependent platelet aggregation (Fig. 4, E and F). Thrombin-stimulated binding of $G\alpha_{13}$ to $\alpha_{IIb}\beta_3$ and simultaneous RhoA inhibition both require ligand occupancy of $\alpha_{IIb}\beta_3$ and are inhibited by the integrin inhibitor Arg-Gly-Asp-Ser (RGDS) (Fig. 4, D to F). Thus, our study demonstrates not only a function of integrin $\alpha_{IIb}\beta_3$ as a noncanonical $G\alpha_{13}$-coupled receptor but also a new concept of $G\alpha_{13}$-dependent dynamic regulation of RhoA, in which $G\alpha_{13}$ mediates initial GPCR-induced RhoA activation and subsequent integrin-dependent RhoA inhibition (Fig. 4G). These findings are important for our understanding of how cells spread, retract, migrate, and proliferate, which is fundamental to development, cancer, immunity, wound healing, hemostasis, and thrombosis.

References and Notes

1. R. O. Hynes, *Cell* **110**, 673 (2002).
2. M. H. Ginsberg, A. Partridge, S. J. Shattil, *Curr. Opin. Cell Biol.* **17**, 509 (2005).
3. Y. Q. Ma, J. Qin, E. F. Plow, *J. Thromb. Haemost.* **5**, 1345 (2007).
4. S. J. Shattil, *Trends Cell Biol.* **15**, 399 (2005).
5. A. Obergfell *et al.*, *J. Cell Biol.* **157**, 265 (2002).
6. E. G. Arias-Salgado *et al.*, *Proc. Natl. Acad. Sci. U.S.A.* **100**, 13298 (2003).
7. P. Flevaris *et al.*, *J. Cell Biol.* **179**, 553 (2007).
8. P. Flevaris *et al.*, *Blood* **113**, 893 (2009).
9. N. A. Riobo, D. R. Manning, *Trends Pharmacol. Sci.* **26**, 146 (2005).
10. L. F. Brass, D. R. Manning, S. J. Shattil, *Prog. Hemost. Thromb.* **10**, 127 (1991).
11. A. Moers *et al.*, *Nat. Med.* **9**, 1418 (2003).
12. T. Kozasa *et al.*, *Science* **280**, 2109 (1998).
13. M. J. Hart *et al.*, *Science* **280**, 2112 (1998).
14. B. Klages, U. Brandt, M. I. Simon, G. Schultz, S. Offermanns, *J. Cell Biol.* **144**, 745 (1999).
15. V. Senyuk *et al.*, *Cancer Res.* **69**, 262 (2009).
16. B. S. Coller, *Blood* **55**, 169 (1980).
17. Z. Li, G. Zhang, R. Feil, J. Han, X. Du, *Blood* **107**, 965 (2006).
18. M. Gu, X. Xi, G. D. Englund, M. C. Berndt, X. Du, *J. Cell Biol.* **147**, 1085 (1999).
19. W. T. Arthur, L. A. Petch, K. Burridge, *Curr. Biol.* **10**, 719 (2000).
20. S. Tanabe, B. Kreutz, N. Suzuki, T. Kozasa, *Methods Enzymol.* **390**, 285 (2004).
21. Single-letter abbreviations for amino acid residues are as follows: A, Ala; C, Cys; D, Asp; E, Glu; F, Phe; G, Gly; H, His; I, Ile; K, Lys; L, Leu; M, Met; N, Asn; P, Pro; Q, Gln; R, Arg; S, Ser; T, Thr; V, Val; W, Trp; and Y, Tyr.
22. J. S. Huang, L. Dong, T. Kozasa, G. C. Le Breton, *J. Biol. Chem.* **282**, 10210 (2007).
23. C. Vidal, B. Geny, J. Melle, M. Jandrot-Perrus, M. Fontenay-Roupie, *Blood* **100**, 4462 (2002).
24. K. Moissoglu, M. A. Schwartz, *Biol. Cell* **98**, 547 (2006).
25. X. P. Du *et al.*, *Cell* **65**, 409 (1991).
26. X. D. Ren, M. A. Schwartz, *Methods Enzymol.* **325**, 264 (2000).

27. This work was supported by grants HL080264, HL062350, and HL068819 from the National Heart, Lung, and Blood Institute (X.D.) and GM061454 and GM074001 from the National Institute of General Medical Sciences (T.K.). We thank G. Nucifora for help with bone marrow transplantation and K. O'Brien and M. K. Delaney for proofreading.

Supporting Online Material www.sciencemag.org/cgi/content/full/327/5963/340/DC1 Materials and Methods
Figs. S1 to S6
References

9 April 2009; accepted 4 December 2009
10.1126/science.1174779

Functional and Evolutionary Insights from the Genomes of Three Parasitoid *Nasonia* Species

The *Nasonia* Genome Working Group*†

We report here genome sequences and comparative analyses of three closely related parasitoid wasps: *Nasonia vitripennis*, *N. giraulti*, and *N. longicornis*. Parasitoids are important regulators of arthropod populations, including major agricultural pests and disease vectors, and *Nasonia* is an emerging genetic model, particularly for evolutionary and developmental genetics. Key findings include the identification of a functional DNA methylation tool kit; hymenopteran-specific genes including diverse venoms; lateral gene transfers among Pox viruses, *Wolbachia*, and *Nasonia*; and the rapid evolution of genes involved in nuclear-mitochondrial interactions that are implicated in speciation. Newly developed genome resources advance *Nasonia* for genetic research, accelerate mapping and cloning of quantitative trait loci, and will ultimately provide tools and knowledge for further increasing the utility of parasitoids as pest insect-control agents.

Parasitoid wasps are insects whose larvae parasitize various life stages of other arthropods (for example, insects, ticks, and mites). Female wasps sting, inject venom, and lay eggs on or in the host, where the developing offspring consume and eventually kill it. Parasitoids

are widely used in the biological control of insect pests, and they are very diverse, with estimates of over 600,000 species (*1*, *2*). *Nasonia* is the second genus of Hymenoptera to have whole-genome sequencing, after *Apis mellifera* (Fig. 1), and *Nasonia* comprises four closely related parasitoid species: *N. vitripennis*, *N. giraulti*, *N. longicornis*, and *N. oneida* (*3*, *4*). *Nasonia* are genetically tractable organisms with short generation time (~2 weeks), large family size, ease of laboratory rearing, and cross-fertile species. Like other hymenopterans, haploid males develop from unfertilized eggs, and diploid females develop from fertilized eggs. Cross-fertile species facilitate the mapping and cloning of genes that are involved in species differences. Haploid genetics assist efficient genotyping, mutational screening (*5*), and evaluation of gene interactions (epistasis) without the added complexity of genetic dominance. As a result, *Nasonia* are now emerging as genetic model organisms, particularly for complex trait analysis, developmental genetics, and evolutionary genetics (*4*).

We sequenced, assembled, annotated, and analyzed the genome of *N. vitripennis* from sixfold Sanger sequence genome coverage by using a highly inbred line of *N. vitripennis* (*6*). The draft genome assembly comprises 26,605 contigs [total length of 239.8 Mb, with half of the bases residing in contigs larger than 18.5 kb (N_{50}), 40.6% guanine plus cytosine content (GC)]. Contigs were placed with mate-pair information into 6,181 scaffolds (total size 295 Mb, N_{50} =709 kb). We assessed the *N. vitripennis* assembly for completeness and accuracy by comparing it with 19 finished bacterial artificial chromosome (BAC) sequences and 18,000 expressed sequence tags (ESTs). The genome assembly contained 98% of the BAC and 97% of the EST sequences, with an error rate of 5.9×10^{-4}. Thus the assembly is a high-quality representation of both genomic and transcribed *N. vitripennis* sequences.

Highly inbred lines of the two sibling species *N. giraulti* and *N. longicornis* (Fig. 1B) were sequenced with onefold Sanger and 12-fold, 45–base pair (bp) Illumina genome coverage. Assembled by alignment to the *N. vitripennis* reference using stringent criteria (*6*), these reads cover 62% and 62.6% of the *N. vitripennis* assembly, and 84.7% and 86.3% of protein coding regions, respectively. These were used for genome comparisons and provided resources [for example, single nucleotide polymorphisms (SNPs) and microsatellites] for scaffold, gene, and quantitative trait loci (QTL) mapping. Sequence error rates for the *N. giraulti* alignment are estimated to be 3.8×10^{-3} for the entire alignment and 1.47×10^{-4} for coding sequences on the basis of comparison to three finished *N. giraulti* BACs (*6*). Sequences of 25 coding genes in both species perfectly matched their respective aligned sequences.

Normally, the intracellular bacteria *Wolbachia* prevent the formation of interspecies hybrids; however, antibiotically cured strains are cross-fertile (*7*). Hybrid crosses (Fig. 1C) (*6*) were used to map scaffolds and visible mutations onto the five chromosomes of *Nasonia* (Fig. 2). Several interspecies QTL have already been mapped using genetic/genomic resources, including wing size (*8*, *9*), host preference (*10*), female mate preference (*11*), and in this study, sex-ratio control and male courtship (*6*). Linkage analysis has revealed that the genome-wide recombination rate in *Nasonia* is 1.4 to 1.5 centimorgans (cM)/Mb, which is lower than that of honeybees (*12*, *13*), and shows a 100-fold difference in rate between high- and low-recombination regions of the genome (Fig. 2) (*6*).

An official gene set (OGS v1.1) was generated from comparisons to *A. mellifera*, *Tribolium castaneum*, *Drosophila melanogaster*, *Pediculus humanus*, *Daphnia pulex*, and *Homo sapiens* [details are given in (*6*)]. Overall, *Nasonia* encodes a typical insect gene repertoire (Fig. 3) (*6*), of which 60% of genes have a human ortholog, 18% are arthropod-specific, and 2.4% appear to be hymenoptera-specific, showing high conservation between *Nasonia* and *Apis* and low conservation or absence in other taxa. An additional 12% are either *Nasonia*-specific or without clear orthology. Many (63%) single-copy orthologs shared between *Nasonia* and *Apis* occur in microsynteny blocks, which is similar to the amount of microsynteny blocks in *Aedes aegypti*/*Anopheles gambiae* and *H. sapiens*/*Gallus gallus* (*14*). Four hundred and forty-five orthologs between *Nasonia* and humans lack a candidate homolog in *D. melanogaster* (table S1), including the human transcription factors E2F7 and E2F8, which are involved in cell-cycle regulation. Further refinement of the gene set resulted in OGS v1.2 (*15*), which totals 17,279 genes, of which 74% have tiling microarray or EST support (*6*).

Nasonia is abundant in transposable elements (TEs) and other repetitive DNA (table S2 and fig. S1). This contrasts with a paucity of TEs in *A. mellifera* (*16*). TE diversity in *Nasonia* is 30% higher (2.9 TE types/Mb) than the next most diverse insect (*Bombyx mori*, 2.1 TE types/Mb), and is 10-fold higher than the average dipteran (*6*, *17*). *Nasonia* also contains an unusual abundance of nuclear-mitochondrial insertions and a higher density of microsatellites (10.9 kb/Mb) than most other arthropod species (*18*, *19*), suggesting that the accumulation of repetitive DNA is a feature of these insects.

The *Nasonia* genome encodes a full DNA methylation tool kit, including all three DNA cytosine-5-methyltransferase (Dnmt) types (Fig. 1A).

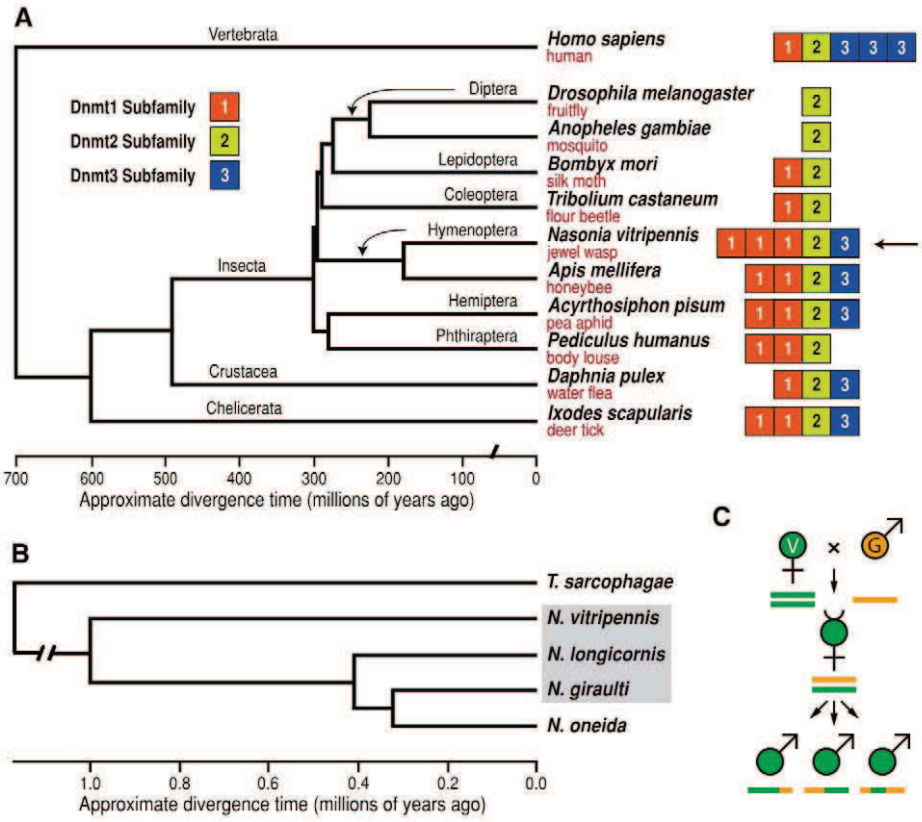

Fig. 1. Phylogenetic relationships of *Nasonia* and the DNA methylation tool kit. (**A**) *Nasonia* relationships to other sequenced genomes (*6*). Right: DNA methyltransferase subfamilies (Dnmt1, Dnmt2, Dnmt3) in these taxa. (**B**) Relationships among the three sequenced *Nasonia* genomes. (**C**) Crossing scheme used for mapping scaffolds on the *Nasonia* chromosomes and for studies of nuclear-cytoplasmic incompatibility.

*All authors with their affiliations appear at the end of this paper.
†To whom correspondence should be addressed. E-mail: werr@mail.rochester.edu (J.H.W.); stephenr@bcm.tmc.edu (S.R.)

In vertebrates, Dnmt3 establishes DNA methylation patterns, Dnmt1 maintains these patterns, and Dnmt2 is involved in tRNA methylation (*20*). The *Nasonia* genome encodes three Dnmt1 genes, one Dnmt2, and one Dnmt3, in contrast with *D. melanogaster*, which has only Dnmt2. The presence of all three subfamilies in both *Nasonia* and *Apis* (Fig. 1) raises the question of whether methylation has similar regulatory functions in Hymenoptera as it does in vertebrates. DNA methylation is important in *Apis* caste development (*21*) and is suggested for *Nasonia* sex determination (*22*). Coding exons of both *Nasonia* and *Apis* show bimodal distributions in observed/expected CpG (fig. S2) (*6*, *23*), which is consistent with mutational biases due to DNA methylation of hyper- and hypomethylated genes. We confirmed methylated CpG dinucleotides in five examined *N. vitripennis* genes by bisulfite sequencing (fig. S3). These results suggest that epigenetic modifications by DNA methylation may be important in Hymenoptera. *Nasonia* also has the largest number of ankyrin (ANK) repeat–containing proteins (over 200) so far found in any insect (table S3) (*6*), suggesting a regulatory importance through protein-protein interactions (*24*).

Systemic RNA interference (RNAi) in *Nasonia* allows for gene expression knockdowns (*4*, *25*). The *Nasonia* genome encodes homologs for the majority of genes implicated in small RNA processes (table S4). However, as in *Tribolium* and *Apis*, *Nasonia* lacks an RNA-dependent RNA polymerase (RdRp) ortholog, indicating a different systemic RNAi mechanism than in *Caenorhabditis*. Using various computational approaches (*6*), we identified 52 putative micro RNAs (miRNAs) with homologies to known miRNAs (*26*), nine that were previously unknown, and 11 additional Hymenoptera-specific miRNAs (table S5). Small-RNA library sequencing confirmed 39 predicted and identified 59 additional miRNAs (table S6).

Nasonia shares a long germ-band mode of embryonic development with *Drosophila*, but exhibits significant differences in the genetic mechanisms involved (*5*, *27*, *28*) (see fig. S4). All major components of the dorso-ventral patterning system are present, with many *Nasonia*-specific gene duplications in the Toll pathway. Orthologs of vertebrate genes absent from *Drosophila* include the transforming growth factor–β (TGFβ) ligands *ADMP* and *myostatin*, and the bone morphogenesis protein (BMP) inhibitors *BAMBI* and *DAN*, but their functions in *Nasonia* are not yet known. *A. mellifera* shows an expansion of the *yellow/major royal jelly* (*yellow/MRJP*) genes that are linked to caste formation and sociality (*29*). *Nasonia* has the largest number of *yellow/MRJP* genes so far found in any insect, including an independent amplification of MRJP-like proteins (fig. S5) (*6*, *29*). Although their function in *Nasonia* is unknown, these genes are expressed broadly in different tissues and life stages (table S7). The insect sex peptide/receptor system, which causes female re-mating refractoriness (*30*), is highly conserved in insects but is absent in *Nasonia* and *Apis* (table S8) (*6*). Instead, *Nasonia* males inhibit female re-mating behaviorally with a special "post-copulatory display" (*31*). Additional features analyzed (*6*) include those related to sex determination (fig. S6), pathogens and immunity (fig. S7), neuropeptides (tables S9 and S10), cuticular proteins (table S11), xenobiotics (fig. S8), and diapause (table S12).

We investigated genome microevolution, including rapidly evolving genes that are potentially involved in species differences and speciation, by using the genomes of the three closely related *Nasonia* species. Synonymous divergence between *N. vitripennis* and its sibling species *N. giraulti* and *N. longicornis* is 0.031 ± 0.0002 SE and 0.030 ± 0.0002 SE, respectively, and between *N. giraulti* and *N. longicornis* is 0.014 ± 0.0001 SE (*6*), which is comparable to those among *Drosophila* sibling species (*32*). We compared the ratio of synonymous-to-nonsynonymous substitutions (*dN*/*dS*) between *Nasonia* species pairs with respect to gene ontology (GO) term categories, using genes with high-quality alignments and 1:1 orthologs between *Nasonia* and *Drosophila*. Nuclear genes that interact with mitochondria revealed significantly elevated *dN*/*dS* [by comparison of *dN*/*dS* distributions for each GO term to resampled distributions, see (*6*) and table S13], specifically those encoding mitochondrial ribosomes ($P < 0.003$ for all species pairs) and oxidative phosphorylation complex I ($P < 0.03$ for *N. vitripennis*/*N. giraulti* and *N. vitripennis*/*N. longicornis*) and complex V ($P < 0.04$ for all species pairs). This finding is consistent with the rapid evolutionary rate of *Nasonia* mitochondria (*33*) and studies implicating nuclear-mitochondrial incompatibilities in F2 hybrid breakdown (*7*, *31*). For example, reciprocal crosses between *N. giraulti* × *N. vitripennis* have identical F1 nuclear genotypes, but their mitochondrial haplotypes differ. Yet, microarray hybridization (Fig. 2) (*6*) of DNA from pooled surviving adult F2 haploid males shows distortion in the recovery of particular regions of the genome, which is dependent upon their mitochondrial haplotype (*giraulti* versus *vitripennis*). Because hybrid mortality is post-embryonic (*7*) and embryo ratios are Mendelian (*33*), these distortions reflect larval to adult mortality. In particular, F2 males with *N. vitripennis* alleles on the left arm of chro-

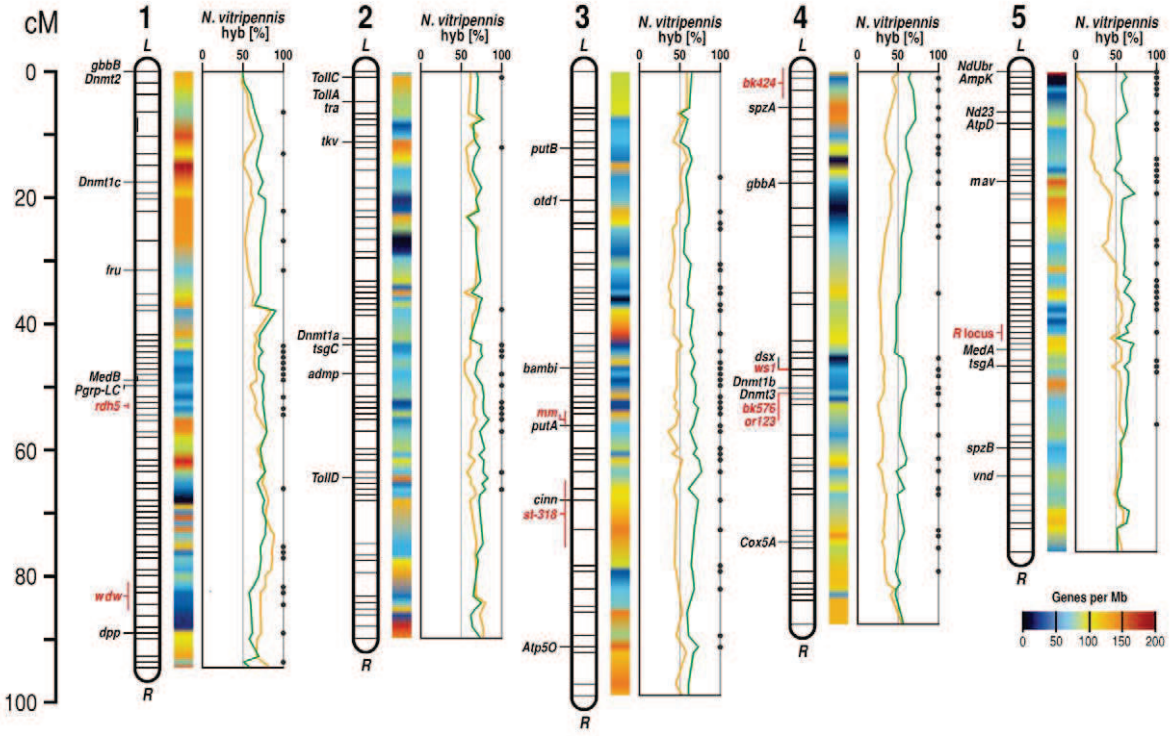

Fig. 2. A high-resolution recombination map of the five *Nasonia* chromosomes is shown (*6*), with estimated gene density and locations of visible markers, landmark genes, and QTL. The hybridization percentage to *N. vitripennis* alleles is shown among surviving adult *N. vitripennis* × *N. giraulti* F2 hybrid males with either *N. vitripennis* (green curve) or *N. giraulti* (orange curve) mitochondria. Dots specify genome regions with significant differences in the hybridization ratio between the reciprocal crosses ($P < 0.01$).

mosome 5 and *N. girault*i mitochondria suffer nearly 100% mortality (Fig. 2). This region contains three genes encoding mitochondrial interacting proteins, *atpD*, *ampK*, and *nadh-ubiquinone oxireductase* (Fig. 2). Coevolution of nuclear and mitochondrial genomes can accelerate evolution (*34*, *35*), and these findings indicate that such interactions contribute to reproductive incompatibility and speciation in *Nasonia*.

Sequences of 25 gene regions from multiple strains for the three *Nasonia* species (*6*) show low levels of intraspecific variation (table S14) with synonymous site variation ranging from 0.0005 in *N. girault*i to 0.0026 in *N. vitripennis*, which are much lower than in *Drosophila* species and more akin to levels observed in humans (*36*). This low nuclear variation could be explained by founder events, purging of deleterious mutations in haploid males, or inbreeding.

Recent lateral gene transfers from the bacterial endosymbiont *Wolbachia* into the genomes of *Nasonia* and other arthropods have been identified (*37*). Detecting ancient lateral transfers is more problematic. By examining protein domain arrangements in *Nasonia* relative to other organisms, we uncovered an ancient lateral gene transfer involving Pox viruses, *Wolbachia*, and *Nasonia*. Thirteen ANK repeat–bearing proteins encoded in the *N. vitripennis* genome also contain C-terminal PRANC (Pox proteins repeats of ankyrin–C terminal) domains. This domain was previously only described in Pox viruses, where it is associated with ANK repeats and inhibits the nuclear factor κB (NF-κB) pathway in mammalian hosts (*38*). A computational screen revealed ANK-PRANC–bearing genes in some *Wolbachia* and a related Rickettsiales (Fig. 4). Screening additional *Wolbachia* confirmed the presence of ANK-PRANC genes in diverse *Wolbachia*. The *Nasonia* PRANC genes are clearly integrated in the genome (*6*) and are expressed in different life stages (table S15). Phylogenetic analysis of the PRANC-domain sequences suggests that the *Nasonia* lineage acquired one or more of these proteins from *Wolbachia*, with subsequent amplification and divergence (Fig. 4). Such lateral gene transfers between bacteria and animals could be an important source of evolutionary innovation (*37*).

Nasonia is a carnivore, feeding on an amino acid–rich diet both as larva and adult (*4*). Mapping of *Nasonia* genes onto metabolic pathways (*39*) revealed loss or rearrangement in some amino acid metabolic pathways, including tryptophan and aminosugar metabolism (fig. S9) (*6*). The changes may reflect its specialized carnivorous diet and can inform efforts to produce artificial diets for more economical parasitoid rearing.

The venom of parasitoids, injected into a host before oviposition, serves to condition the host for successful development of wasp progeny (*1*, *2*). Unlike the defensive *Apis* venom that inflicts pain and damage, parasitoid venoms have diverse physiological effects on hosts, including developmental arrest; alteration in growth and physiology; suppression of immune responses; induction of paralysis, oncosis, or apoptosis; and alteration of host behavior (*40*). The identification of *Nasonia*

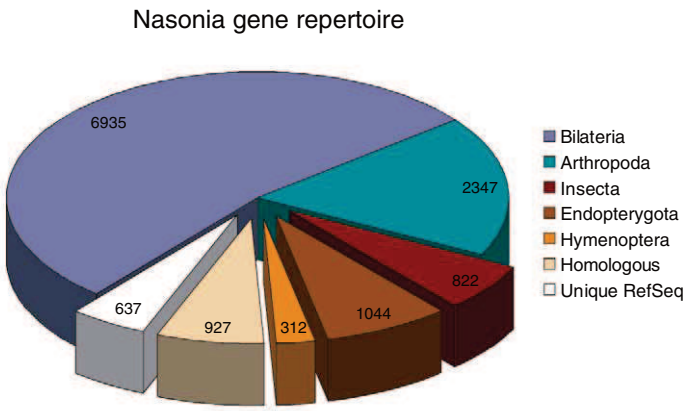

Fig. 3. Distribution of recognizable *Nasonia* orthologs and *Nasonia*-specific genes among gene models with expression sequencing support (*6*).

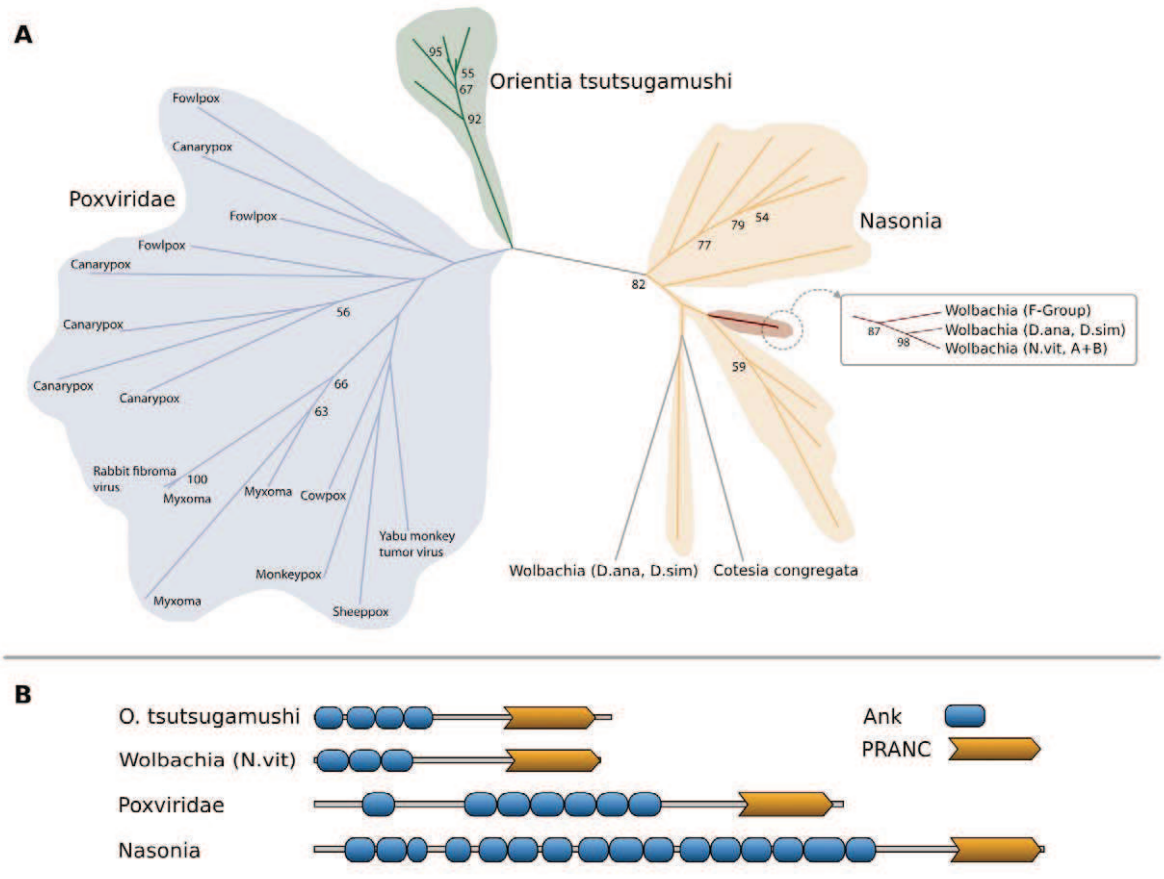

Fig. 4. PRANC domain proteins in *Nasonia*, Pox viruses, and *Wolbachia*. (**A**) Maximum-likelihood tree of PRANC-domain sequences found in Pox viruses, rickettsia (*Wolbachia* and *Orientia*), and parasitoids (*N. vitripennis* and *Cotesia congregata*). The tree was estimated using RaxML with 1000 bootstrap replicates and model settings estimated by ProtTest [see (*6*); alignment deposited in Treebase with ID SN4709]. Bootstrap values above 50% are shown by the corresponding nodes. The phylogenetic relationships suggest lateral transfer from *Wolbachia* to the *Nasonia* lineage. (**B**) Representative domain arrangements for ANK-PRANC proteins.

genes with venom features and proteomic analyses of venom reservoir tissues have uncovered a rich assemblage of 79 candidate venom proteins (table S16) (*41*). Some *Nasonia* venom reservoir proteins belong to previously known insect venom families such as serine proteases; however, nearly half were not related to any known insect venoms. As expected, many of these venom candidates show highly elevated expression in the female reproductive tract, which includes the venom glands and reservoirs. Venom genes also showed significantly higher *dN*/*dS* ratios between *N. vitripennis* and *N. giraulti* than nonvenom genes did (Mann-Whitney U test, $P < 2 \times 10^{-6}$), suggesting that changes in host use between the species may be accompanied by rapid evolution of venom proteins. The large venom protein set found in *Nasonia* with diverse physiological effects (*40*) and abundance of parasitoid species (*1*, *2*) suggests that parasitoids may contain a rich venom pharmacopeia of potential new drugs.

N. vitripennis is a generalist parasitoid with a wide host utilization of many fly species, whereas the other *Nasonia* species are specialists (*4*, *10*). Using genomic tools, a major host preference locus has been mapped to a region of ~2 cM (*10*). Other genes in the *Nasonia* genome that are potentially involved in host finding include odorant binding proteins (table S17) and chemoreceptors (*42*), which show expansions, contractions, and pseudogenization, indicative of rapid turnover.

A suite of genetic tools and resources is available or under development for the *Nasonia* system (*4*, *6*, *11*, *28*), and the genome resources presented here can be used for fine-scale mapping (*6*, *9*-*11*) and positional cloning (*8*) of QTLs. By combining haploid genetics, ease of rearing, short generation time, systemic RNAi, interfertile species, and new genome resources for three species, *Nasonia* shows promise as a genetic model system for evolutionary and developmental genetics. Genome resources described here and our resulting enhanced understanding of parasitoid biology will also open avenues for improving parasitoid utility in biological control of pests of agricultural and medical importance.

References and Notes

1. D. L. J. Quicke, *Parasitic Wasps* (Chapman & Hall, London, 1997).
2. J. Heraty, in *Insect Biodiversity: Science and Society*, R. Tootti and P. Alder, Eds. (Wiley-Blackwell, Hoboken, NJ, 2009), pp. 445–462.
3. R. Raychoudhury *et al., Heredity* 10.1038/hdy.2009.147 (2010).
4. J. H. Werren, D. Loehlin, *Cold Spring Harb. Protocols* 10.1101/pdb.emo134 (2009).
5. M. A. Pultz *et al*., *Genetics* **154**, 1213 (2000).
6. Materials and methods and supplementary text are available as supporting material on *Science* Online.
7. J. A. J. Breeuwer, J. H. Werren, *Evolution* **49**, 705 (1995).
8. D. W. Loehlin *et al*., *PLoS Genet.* 10.1371/journal.pgen.1000821 (2010).
9. D. W. Loehlin, L. S. Enders, J. H. Werren, *Heredity* 10.1038/hdy.2009.146 (2010).
10. C. A. Desjardins, F. Perfecti, J. D. Bartos, L. S. Enders, J. H. Werren, *Heredity* 10.1038/hdy.2009.145 (2010).
11. B. J. Velthuis, W. Yang, T. van Opijnen, J. H. Werren, *Anim. Behav.* **69**, 1107 (2005).
12. O. Niehuis *et al*., *PLoS ONE* 10.1371/journal.pone.0008597 (2010).
13. L. Wilfert, J. Gadau, P. Schmid-Hempel, *Heredity* **98**, 189 (2007).
14. E. M. Zdobnov, P. Bork, *Trends Genet.* **23**, 16 (2007).
15. The official gene set OGS v1.2 is available at http://nasoniabase.org/nasonia_genome_consortium/datasets.html.
16. Honeybee Genome Sequencing Consortium, *Nature* **443**, 931 (2006).
17. C. D. Smith *et al*., *Gene* **389**, 1 (2007).
18. L. Viljakainen, D. C. S. G. Oliveira, J. H. Werren, S. K. Behura, *Insect Mol. Biol.* **19**, 27 (2010).
19. B. A. Pannebakker, O. Niehuis, A. Hedley, J. Gadau, D. M. Shuker, *Insect Mol. Biol.* **19**, 91 (2010).
20. T. P. Jurkowski *et al*., *RNA* **14**, 1663 (2008).
21. R. Kucharski, J. Maleszka, S. Foret, R. Maleszka, *Science* **319**, 1827 (2008).
22. L. W. Beukeboom, A. Kamping, L. van de Zande, *Semin. Cell Dev. Biol.* **18**, 371 (2007).
23. N. Elango, B. G. Hunt, M. A. D. Goodisman, S. V. Yi, *Proc. Natl. Acad. Sci. U.S.A.* **106**, 11206 (2009).
24. L. K. Mosavi, T. J. Cammett, D. C. Desrosiers, Z. Y. Peng, *Protein Sci.* **13**, 1435 (2004).
25. J. A. Lynch, C. Desplan, *Nat. Protoc.* **1**, 486 (2006).
26. D. Gerlach, E. V. Kriventseva, N. Rahman, C. E. Vejnar, E. M. Zdobnov, *Nucleic Acids Res.* **37**, D111 (2009).
27. J. A. Lynch, A. E. Brent, D. S. Leaf, M. A. Pultz, C. Desplan, *Nature* **439**, 728 (2006).
28. A. E. Brent, G. Yucel, S. Small, C. Desplan, *Science* **315**, 1841 (2007).
29. M. D. Drapeau, S. Albert, R. Kucharski, C. Prusko, R. Maleszka, *Genome Res.* **16**, 1385 (2006).
30. N. Yapici, Y. J. Kim, C. Ribeiro, B. J. Dickson, *Nature* **451**, 33 (2008).
31. O. Niehuis, A. K. Judson, J. Gadau, *Genetics* **178**, 413 (2008).
32. J. M. Flowers *et al*., *Mol. Biol. Evol.* **24**, 1347 (2007).
33. J. van den Assem, J. Visser, *Biol. Comport.* **1**, 37 (1976).
34. D. C. S. G. Oliveira, R. Raychoudhury, D. V. Lavrov, J. H. Werren, *Mol. Biol. Evol.* **25**, 2167 (2008).
35. D. M. Rand, R. A. Haney, A. J. Fry, *Trends Ecol. Evol.* **19**, 645 (2004).
36. C. F. Aquadro, V. B. Dumont, F. A. Reed, *Curr. Opin. Genet. Dev.* **11**, 627 (2001).
37. J. C. Dunning-Hotopp *et al*., *Science* **317**, 1753 (2007).
38. S. J. Chang *et al*., *J. Virol.* **83**, 4140 (2009).
39. M. Kanehisa *et al*., *Nucleic Acids Res.* **36**, D480 (2008).
40. D. B. Rivers, Y. A. Yoder, L. Ruggiero, *Trends Entomol.* **2**, 1 (1999).
41. D. C. de Graaf *et al*., *Insect Mol. Biol.* **19**, 11 (2010).
42. H. M. Robertson, J. Gadau, K. W. Wanner, *Insect Mol. Biol.* **19**, 121 (2010).

43. Genome sequencing, assembly and annotation were funded by the National Human Genome Research Institute (NHGRI U54 HG003273). The whole-genome shotgun project has been deposited at the DNA Databank of Japan (DDBJ)/European Molecular Biology Laboratory (EMBL)/GenBank under accession numbers AAZX00000000 (*N. vitripennis*), ADAO00000000 (*N. giraulti*), and ADAP00000000 (*N. longicornis*). Additional support, acknowledgments, and accession numbers are provided in the supporting online material.

Author List: The *Nasonia* Genome Working Group

John H. Werren,[1]*† Stephen Richards,[2]*† Christopher A. Desjardins,[1] Oliver Niehuis,[3]‡ Jürgen Gadau,[3] John K. Colbourne,[4] Leo W. Beukeboom,[5] Claude Desplan,[6] Christine G. Elsik,[7] Cornelis J. P. Grimmelikhuijzen,[8] Paul Kitts,[9] Jeremy A. Lynch,[10] Terence Murphy,[9] Deodoro C. S. G. Oliveira,[1]§ Christopher D. Smith,[11,12] Louis van de Zande,[5] Kim C. Worley,[2] Evgeny M. Zdobnov,[13,14,15] Maarten Aerts,[16] Stefan Albert,[17] Victor H. Anaya,[18] Juan M. Anzola,[19] Angel R. Barchuk,[20] Susanta K. Behura,[21] Agata N. Bera,[22] May R. Berenbaum,[23] Rinaldo C. Bertossa,[24] Márcia M. G. Bitondi,[25] Seth R. Bordenstein,[26,27] Peer Bork,[28] Erich Bornberg-Bauer,[29] Marleen Brunain,[30] Giuseppe Cazzamali,[8] Lesley Chaboub,[2] Joseph Chacko,[2] Dean Chavez,[2] Christopher P. Childers,[7] Jeong-Hyeon Choi,[4] Michael E. Clark,[1] Charles Claudianos,[31] Rochelle A. Clinton,[32] Andrew G. Cree,[2] Alexandre S. Cristino,[31,33] Phat M. Dang,[34] Alistair C. Darby,[35] Dirk C. de Graaf,[30] Bart Devreese,[16] Huyen H. Dinh,[2] Rachel Edwards,[1] Navin Elango,[36] Eran Elhaik,[37] Olga Ermolaeva,[9] Jay D. Evans,[38] Sylvain Foret,[39] Gerald R. Fowler,[2] Daniel Gerlach,[13,14] Joshua D. Gibson,[3] Donald G. Gilbert,[40] Dan Graur,[37] Stefan Gründer,[41] Darren E. Hagen,[7] Yi Han,[2] Frank Hauser,[8] Da Hultmark,[42] Henry C. Hunter IV,[11] Gregory D. D. Hurst,[35] Shalini N. Jhangian,[2] Huaiyang Jiang,[2] Reed M. Johnson,[43] Andrew K. Jones,[22] Thomas Junier,[13] Tatsuhiko Kadowaki,[44] Albert Kamping,[5] Yuri Kapustin,[9] Bobak Kechavarzi,[45] Jaebum Kim,[46] Jay Kim,[11] Boris Kiryutin,[9] Tosca Koevoets,[5] Christie L. Kovar,[2] Evgenia V. Kriventseva,[47] Robert Kucharski,[48] Heewook Lee,[45] Sandra L. Lee,[2] Kristin Lees,[22] Lora R. Lewis,[2] David W. Loehlin,[1] John M. Logsdon Jr.,[49] Jacqueline A. Lopez,[4] Ryan J. Lozado,[2] Donna Maglott,[9] Ryszard Maleszka,[48] Anoop Mayampurath,[45] Danielle J. Mazur,[49] Marcella A. McClure,[32] Andrew D. Moore,[29] Margaret B. Morgan,[2] Jean Muller,[28] Monica C. Munoz-Torres,[7,50] Donna M. Muzny,[2] Lynne V. Nazareth,[2] Susanne Neupert,[51] Ngoc B. Nguyen,[2] Francis M. F. Nunes,[25,52] John G. Oakeshott,[53] Geoffrey O. Okwuonu,[2] Bart A. Pannebakker,[5,54] Vikas R. Pejaver,[45] Zuogang Peng,[36] Stephen C. Pratt,[3] Reinhard Predel,[51] Ling-Ling Pu,[2] Hilary Ranson,[55] Rhitoban Raychoudhury,[1] Andreas Rechtsteiner,[4,56] Justin T. Reese,[7,57] Jeffrey G. Reid,[2] Megan Riddle,[58]‖ Hugh M. Robertson,[23] Jeanne Romero-Severson,[59] Miriam Rosenberg,[6] Timothy B. Sackton,[60] David B. Sattelle,[22] Helge Schlüns,[61] Thomas Schmitt,[62] Martina Schneider,[8] Andreas Schüler,[29] Andrew M. Schurko,[49] David M. Shuker,[63] Zilá L. P. Simões,[25] Saurabh Sinha,[46] Zachary Smith,[4] Victor Solovyev,[64] Alexandre Souvorov,[9] Andreas Springauf,[41] Elisabeth Stafflinger,[8] Deborah E. Stage,[1] Mario Stanke,[65] Yoshiaki Tanaka,[66] Arndt Telschow,[29] Carol Trent,[58] Selina Vattathil,[2]¶ Eveline C. Verhulst,[5] Lumi Viljakainen,[67] Kevin W. Wanner,[68] Robert M. Waterhouse,[15] James B. Whitfield,[23] Timothy E. Wilkes,[35] Michael Williamson,[8] Judith H. Willis,[69] Florian Wolschin,[70,3] Stefan Wyder,[13] Takuji Yamada,[28] Soojin V. Yi,[36] Courtney N. Zecher,[27] Lan Zhang,[2] Richard A. Gibbs[2]

[1]Department of Biology, University of Rochester, Rochester, NY 14627, USA. [2]Human Genome Sequencing Center, Baylor College of Medicine, Houston, TX 77030, USA. [3]School of Life Sciences, Arizona State University, Tempe, AZ 85287, USA. [4]The Center for Genomics and Bioinformatics, Indiana University, Bloomington, IN 47405, USA. [5]Evolutionary Genetics–Centre for Ecological and Evolutionary Studies, University of Groningen, 9750 AA Haren, Netherlands. [6]Department of Biology, New York University, New York, NY 10003, USA. [7]Department of Biology, Georgetown University, Washington, DC 20057, USA. [8]Center for Comparative and Functional Insect Genomics, Department of Biology, University of Copenhagen, DK-2100 Copenhagen, Denmark. [9]National Center for Biotechnology Information, National Library of Medicine, National Institutes of Health, Bethesda, MD 20894, USA. [10]Institut für Entwicklungsbiologie, Universität zu Köln, 50923 Köln, Germany. [11]Department of Biology, San Francisco State University, San Francisco, CA 94132, USA. [12]Drosophila Heterochromatin Genome Project, Lawrence Berkeley National Laboratory, Berkeley, CA 94720, USA. [13]Department of Genetic Medicine and Development, University of Geneva Medical School, CH-1211 Geneva, Switzerland. [14]Swiss Institute of Bioinformatics, CH-1211 Geneva, Switzerland. [15]Imperial College London, London, SW7 2AZ, UK. [16]Laboratory of Protein Biochemistry and Biomolecular Engineering, Ghent University, B-9000 Ghent, Belgium. [17]BEEgroup and Institute of Pharmaceutical Biology, University of Würzburg, 97082 Würzburg, Germany. [18]Institute for Theoretical Biology, Humboldt University Berlin, 10115 Berlin, Germany. [19]Animal Science and Biology, Texas A&M University, College Station, TX 77843, USA. [20]Departamento de Ciências Biomédicas, Universidade Federal de Alfenas, Alfenas, Minas Gerais, 37130-000, Brazil. [21]Eck Institute for Global Health, Department of Biological Sciences, University of Notre Dame, Notre Dame, IN 46556, USA. [22]Medical Research Council Functional Genomics Unit, Department of Physiology Anatomy and Genetics, University of Oxford, Oxford OX1 3QX, UK. [23]Department of Entomology, University of Illinois at Urbana-Champaign, Urbana, IL 61801, USA. [24]Chronobiology–Centre for Behavior and Neurosciences, University of Groningen, 9750 AA Haren, Netherlands. [25]Faculdade de Filosofia,

Ciências e Letras de Ribeirão Preto, Departamento de Biologia, Universidade de São Paulo, Ribeirão Preto, São Paolo 14040-901, Brazil. [26]Department of Biological Sciences, Vanderbilt University, Nashville, TN 37235, USA. [27]Josephine Bay Paul Center for Comparative Molecular Biology and Evolution, Marine Biological Laboratory, Woods Hole, MA 02536, USA. [28]European Molecular Biology Laboratory, 69117 Heidelberg, Germany. [29]Institute for Evolution and Biodiversity, University of Münster, 48143 Münster, Germany. [30]Laboratory of Zoophysiology, Ghent University, B-9000 Ghent, Belgium. [31]The Queensland Brain Institute, The University of Queensland, Brisbane, Queensland 4072, Australia. [32]Department of Microbiology and the Center for Computational Biology, Montana State University, Bozeman, MT 59715, USA. [33]Instituto de Física de São Carlos, Departamento de Física e Informática, Universidade de São Paulo, São Carlos, São Paolo 13560-970, Brazil. [34]Subtropical Insects Research Unit, United States Department of Agriculture–Agricultural Research Service (USDA-ARS), U.S. Horticultural Research Lab, Fort Pierce, FL 34945, USA. [35]School of Biological Sciences, University of Liverpool, Liverpool L69 7ZB, UK. [36]School of Biology, Georgia Institute of Technology, Atlanta, GA 30332, USA. [37]Department of Biology and Biochemistry, University of Houston, Houston, TX 77204, USA. [38]Bee Research Lab, USDA-ARS, Beltsville, MD, 20705, USA. [39]Australian Research Council Centre of Excellence for Coral Reef Studies, James Cook University, Townsville, Queensland 4811, Australia. [40]Department of Biology, Indiana University, Bloomington, IN 47405, USA. [41]Institute of Physiology, Rheinisch-Westfaelische Technische Hochschule (RWTH) Aachen University, D-52074 Aachen, Germany. [42]Department of Molecular Biology, Umeå University, S-901 87 Umeå, Sweden. [43]Department of Entomology, University of Nebraska, Lincoln, NE 68583, USA. [44]Graduate School of Bioagricultural Sciences, Nagoya University, Nagoya 464-8601, Japan. [45]School of Informatics, Indiana University, Bloomington, IN 47405, USA. [46]Department of Computer Science, University of Illinois at Urbana-Champaign, Urbana, IL 61801, USA. [47]Department of Structural Biology and Bioinformatics, University of Geneva Medical School, CH-1211 Geneva, Switzerland. [48]Research School of Biology, Australian National University, Canberra, Australian Capital Territory 2601, Australia. [49]Roy J. Carver Center for Comparative Genomics and Department of Biology, University of Iowa, Iowa City, IA 52242, USA. [50]Department of Genetics and Biochemistry, Clemson University, Clemson, SC 29634, USA. [51]Institute of General Zoology, University of Jena, D-7743 Jena, Germany. [52]Faculdade de Medicina de Ribeirão Preto, Departamento de Genética, Universidade de São Paulo, Ribeirão Preto, São Paolo 14049-900, Brazil. [53]Department of Entomology, Commonwealth Scientific and Industrial Research Organisation, Canberra, Australian Capital Territory 2601, Australia. [54]Institute of Evolutionary Biology–School of Biological Sciences, University of Edinburgh, Edinburgh EH9 3JT, UK. [55]Vector Group, Liverpool School of Tropical Medicine, Liverpool L3 5QA, UK. [56]Department of Molecular, Cell, and Developmental Biology, University of California, Santa Cruz, Santa Cruz, CA 95064, USA. [57]Reese Consulting, 157/10 Tambon Ban Deau, Amphur Muang, Nong Khai, 43000, Thailand. [58]Department of Biology, Western Washington University, Bellingham, WA 98225, USA. [59]Department of Biological Sciences, University of Notre Dame, Notre Dame, IN 46556, USA. [60]Department of Organismic and Evolutionary Biology, Harvard University, Cambridge, MA 02138, USA. [61]School of Marine and Tropical Biology and Centre for Comparative Genomics, James Cook University, Townsville, Queensland 4811, Australia. [62]Department of Evolutionary Biology and Animal Ecology, University of Freiburg, 79104 Freiburg, Germany. [63]School of Biology, University of St Andrews, St Andrews KY16 9TH, UK. [64]Department of Computer Science, Royal Holloway, University of London, Egham, Surrey TW20 0EX, UK. [65]Institut für Mikrobiologie und Genetik, Universität Göttingen, 37077 Göttingen, Germany. [66]Division of Insect Sciences, National Institute of Agrobiological Science, Tsukuba, Ibaraki 305-8634, Japan. [67]Department of Biology and Biocenter Oulu, University of Oulu, 90014 Oulu, Finland. [68]Department of Plant Sciences and Plant Pathology, Montana State University, Bozeman, MT 59717, USA. [69]Department of Cellular Biology, University of Georgia, Athens, GA 30602, USA. [70]Department of Biotechnology, Chemistry, and Food Science, Norwegian University of Life Sciences, N-1432 Ås, Norway.

*These authors contributed equally to this work.
†To whom correspondence should be addressed. E-mail: werr@mail.rochester.edu (J.H.W.); stephenr@bcm.tmc.edu (S.R.)
‡Current address: Verhaltensbiologie, Universität Osnabrück, 49076 Osnabrück, Germany.
§Current address: Departament de Genètica i de Microbiologia, Universitat Autònoma de Barcelona, 8193 Bellaterra, Spain. ||Current address: Weill Cornell Medical College, New York, NY 10065, USA.
¶Current address: Department of Epidemiology, University of Texas, M.D. Anderson Cancer Center, Houston, TX 77030, USA.

Supporting Online Material www.sciencemag.org/cgi/content/full/327/5963/343/DC1 Materials and Methods
SOM Text
Figs. S1 to S25
Tables S1 to S57
References

22 June 2009; accepted 24 November 2009
10.1126/science.1178028

Zebrafish Behavioral Profiling Links Drugs to Biological Targets and Rest/Wake Regulation

Jason Rihel,[1]*† David A. Prober,[1]*‡ Anthony Arvanites,[2] Kelvin Lam,[2] Steven Zimmerman,[1] Sumin Jang,[1] Stephen J. Haggarty,[3,4,5] David Kokel,[6] Lee L. Rubin,[2] Randall T. Peterson,[3,6,7] Alexander F. Schier[1,2,3,8,9]†

A major obstacle for the discovery of psychoactive drugs is the inability to predict how small molecules will alter complex behaviors. We report the development and application of a high-throughput, quantitative screen for drugs that alter the behavior of larval zebrafish. We found that the multidimensional nature of observed phenotypes enabled the hierarchical clustering of molecules according to shared behaviors. Behavioral profiling revealed conserved functions of psychotropic molecules and predicted the mechanisms of action of poorly characterized compounds. In addition, behavioral profiling implicated new factors such as ether-a-go-go–related gene (ERG) potassium channels and immunomodulators in the control of rest and locomotor activity. These results demonstrate the power of high-throughput behavioral profiling in zebrafish to discover and characterize psychotropic drugs and to dissect the pharmacology of complex behaviors.

Most current drug discovery efforts focus on simple in vitro screening assays. Although such screens can be successful, they cannot recreate the complex network interactions of whole organisms. These limitations are particularly acute for psychotropic drugs because brain activity cannot be modeled in vitro (*1*–*3*). Motivated by recent small-molecule screens that probed zebrafish developmental processes (*4*–*7*), we developed a whole organism, high-throughput screen for small molecules that alter larval zebrafish locomotor behavior. We used an automated rest/wake behavioral assay (*3*, *8*) to monitor the activity of larvae exposed to small molecules at 10 to 30 μM for 3 days (Fig. 1A) (*3*). Multiple behavioral parameters were measured, including the number and duration of rest bouts, rest latency, and waking activity (i.e., activity not including time spent at rest) (Fig. 1B) (*3*). We screened 5648 compounds representing 3968 unique structures and 1680 duplicates and recorded more than 60,000 behavioral profiles. Of these, 547 compounds representing 463 unique structures significantly altered behavior relative to controls, according to a stringent statistical cutoff (*3*).

Because the alterations in behavior were multidimensional and quantitative, we assigned a behavioral fingerprint to each compound and applied clustering algorithms to organize molecules according to their fingerprints (Fig. 2A and figs. S1 to S3). This analysis organized the data set broadly into arousing and sedating compounds and identified multiple clusters corresponding to specific phenotypes (Fig. 2, B to F; Fig. 3, A to C; Fig. 4, B and C; and figs. S1 to S4). Clustering allowed us to address three questions: (i) Do structural, functional, and behavioral profiles overlap? (ii) Does the data set predict links between known and unknown small molecules and their mechanisms of action? (iii) Does the data set identify unexpected

[1]Department of Molecular and Cellular Biology, Harvard University, Cambridge, MA 02138, USA. [2]Harvard Stem Cell Institute, Harvard University, Cambridge, MA 02138, USA. [3]Broad Institute of MIT and Harvard, Cambridge, MA 02142, USA. [4]Stanley Center for Psychiatric Research, Broad Institute of MIT and Harvard, Cambridge, MA 02142, USA. [5]Center for Human Genetic Research, Massachusetts General Hospital, Boston, MA 02114, USA. [6]Developmental Biology Laboratory, Cardiovascular Research Center, Massachusetts General Hospital, Charlestown, MA 02129, USA. [7]Department of Medicine, Harvard Medical School, Boston, MA 02115, USA. [8]Division of Sleep Medicine, Harvard Medical School, Boston, MA 02215, USA. [9]Center for Brain Science, Harvard University, Cambridge, MA 02138, USA.

*These authors contributed equally to this work.
†To whom correspondence should be addressed. E-mail: schier@fas.harvard.edu (A.F.S.); rihel@fas.harvard.edu (J.R.)
‡Present address: Division of Biology, California Institute of Technology, Pasadena, CA 91125, USA.

candidate pathways that regulate rest/wake states?

Cluster analysis revealed several lines of evidence that molecules with correlated behavioral phenotypes often shared annotated targets or therapeutic indications (Fig. 2, B to F, and figs. S1 to S4). First, drug pairs were more likely to be correlated if the compounds shared at least one annotated target (median correlation when sharing one target, 0.561 versus 0.297 when sharing zero targets; fig. S5, A and B). Second, analysis of 50 different structural and therapeutic classes revealed that drugs belonging to the same class produced highly correlated behaviors in nearly all cases (fig. S5C and fig. S6) (*3*). For example, several structurally diverse selective serotonin reuptake inhibitors (SSRIs) similarly reduced waking, and sodium channel agonist insecticides induced large increases in waking activity (fig. S5C and fig. S6). Third, behavioral profiling uncovered the polypharmacology of drugs with multiple targets. For example, the profile of the dopamine reuptake inhibitor and muscarinic acetylcholine receptor antagonist 3α-bis-(4-fluorophenyl) methoxytropane correlated only with drugs that also shared both properties, such as the anti-Parkinson's drug trihexyphenidyl (fig. S7) (*3*). Fourth, modulators of the major neurotransmitter pathways often induced locomotor and rest/wake effects in zebrafish larvae similar to those seen in mammals (figs. S8 to S15) (*3*). For example, α_2-adrenergic receptor agonists (e.g., clonidine) were sedating, whereas β-adrenergic agonists (e.g., clenbuterol) were arousing, as in mammals (fig. S8). These analyses indicate that compounds with shared biological targets yield similar and conserved phenotypes in our high-throughput behavioral profiling.

Detailed analyses revealed that the clustering of well-known and poorly characterized drugs could predict targets for compounds whose mode of action has been unclear (Fig. 3). For example, the pesticide amitraz coclustered with α_2-adrenergic agonists (Fig. 3A), consistent with reports that amitraz causes clonidine-like side effects in mammals and binds to α_2-adrenergic receptors (*9*). Similarly, sinapic acid methyl ether coclustered with *N*-methyl-D-aspartate (NMDA) receptor antagonists (Fig. 3B), which suggests that the mild anxiolytic effect of sinapic acid in mice is due to NMDA receptor antagonism rather than γ-aminobutyric acid (GABA) receptor activation, as proposed (*10*). Indeed, several sinapic acid analogs are known to block NMDA-induced excitotoxicity in vitro (*11*, *12*). Finally, MRS-1220, an adenosine A3 receptor antagonist (*13*), clustered with monoamine oxidase (MAO) inhibitor antidepressants (Fig. 3C). To directly test whether MRS-1220 inhibits MAO, we performed an in vitro activity assay and found a median inhibitory concentration (IC_{50}) of ~1 μM (Fig. 3D). Thus, behavioral profiling in zebrafish larvae can predict and identify targets of poorly characterized compounds.

In addition to revealing a conserved neuropharmacology between zebrafish and mammalian rest/wake states (figs. S8 to S15) (*3*), behavioral profiling identified additional pathways involved in rest/wake behaviors:

1) L-type calcium channel inhibitors of the verapamil class increased rest with minimal effects on waking activity (fig. S16). This is likely a direct effect on rest regulation, because average waking activity and associated muscle activity were unaffected.

2) Cluster analysis identified two structurally related podocarpatrien-3-ones that specifically increased rest latency (Fig. 4A). These and other compounds also revealed that total rest, rest latency, and waking activity can be disassociated, indicating that these processes can be regulated by distinct mechanisms (*3*).

3) Although inflammatory cytokine signaling has long been known to promote sleep during infection, a role for the immune system in normal vertebrate sleep/wake behavior has not been described (*14*). Behavioral profiling revealed that a diverse set of anti-inflammatory compounds increased waking activity during the day with much less effect at night (Fig. 4B and fig. S17). These anti-inflammatory compounds included the steroidal glucocorticoids, the nonsteroidal anti-inflammatory drugs (NSAIDs), phosphodiesterase (PDE) inhibitors, and other compounds with anti-inflammatory properties, including the immunosuppressant cyclosporine and the mood stabilizer valproic acid. Taken together, these data suggest that inflammatory signaling pathways not only induce sleep during infection (*14*) but also play a role in setting normal daytime activity levels.

4) Ether-a-go-go–related gene (ERG) potassium channel blockers selectively increased waking activity at night without affecting total rest (Fig. 4C and fig. S18). This phenotype was induced by compounds with divergent therapeutic indications (e.g., the antimalarial halofantrine, the antipsychotic haloperidol, the antihistamine terfenadine); however, these drugs also inhibit the ERG channel and can cause the heart rhythm disorder long QT syndrome (*15*, *16*). Rank-sorting all the screened compounds by their fingerprints' mean correlation to the ERG-blocking cluster resulted in a significant enrichment of known ERG blockers in the top ranks (Fig. 4D). Moreover, the specific ERG inhibitor dofetilide increased nighttime activity, whereas structurally related non-ERG blocking compounds, including the antihistamines fexofenadine and cetirizine, did not (fig. S18B). Finally, this phenotype was not caused by general misregulation of potassium channels, because psora-4, a drug that blocks the related shaker potassium channel Kv1.3, induced a distinct phenotype (fig. S18A). These results suggest that ERG potassium channels play a role in regulating wakefulness at night that is distinct

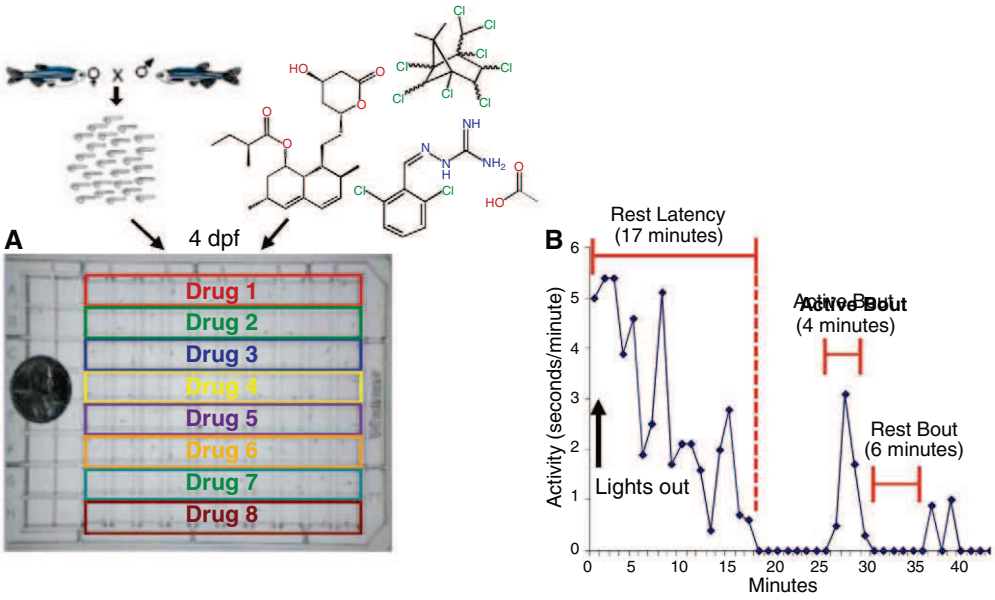

Fig. 1. Larval zebrafish locomotor activity assay. (**A**) At 4 days post-fertilization (dpf), an individual zebrafish larva is pipetted into each well of a 96-well plate with small molecules. Automated analysis software tracks the movement of each larva for 3 days. Each compound is tested on 10 larvae. (**B**) Locomotor activity of a representative larva. The rest and wake dynamics were recorded, including the number and duration of rest bouts [i.e., a continuous minute of inactivity (*8*)], the timing of the first rest bout after a light transition (rest latency), the average waking activity (average activity excluding rest bouts), and the average total activity. Together, these measurements generate a behavioral fingerprint for each compound.

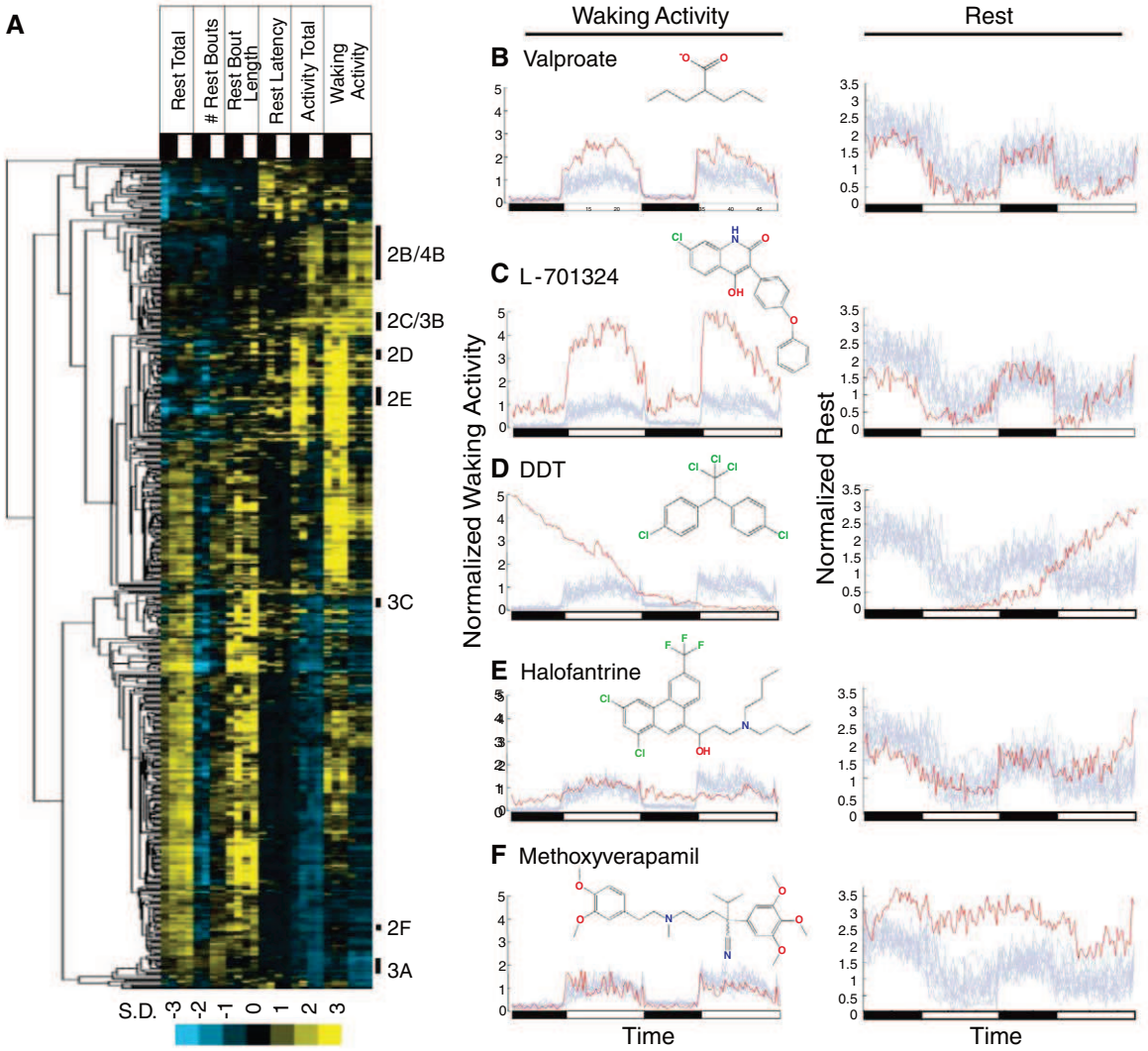

Fig. 2. Hierarchical clustering reveals the diversity of drug-induced behaviors. (**A**) Behavioral profiles are hierarchically clustered to link compounds to behaviors. Each square of the clustergram represents the average relative value in standard deviations (yellow, higher than controls; blue, lower than controls) for a single behavioral measurement. Dark bars indicate specific clusters analyzed in subsequent figures. (**B** to **F**) Normalized waking activity and rest graphs are plotted for behavior-altering compounds (red trace; average of 10 larvae) and representative controls (10 blue traces; average of 10 larvae each). Compounds that altered behavior include the mood stabilizer and antiepileptic drug sodium valproate (B), the psychotomimetic NMDA antagonist L-701324 (C), the sodium channel agonist pesticide DDT (D), the antimalarial halofantrine (E), and the calcium channel blocker methoxyverapamil (F).

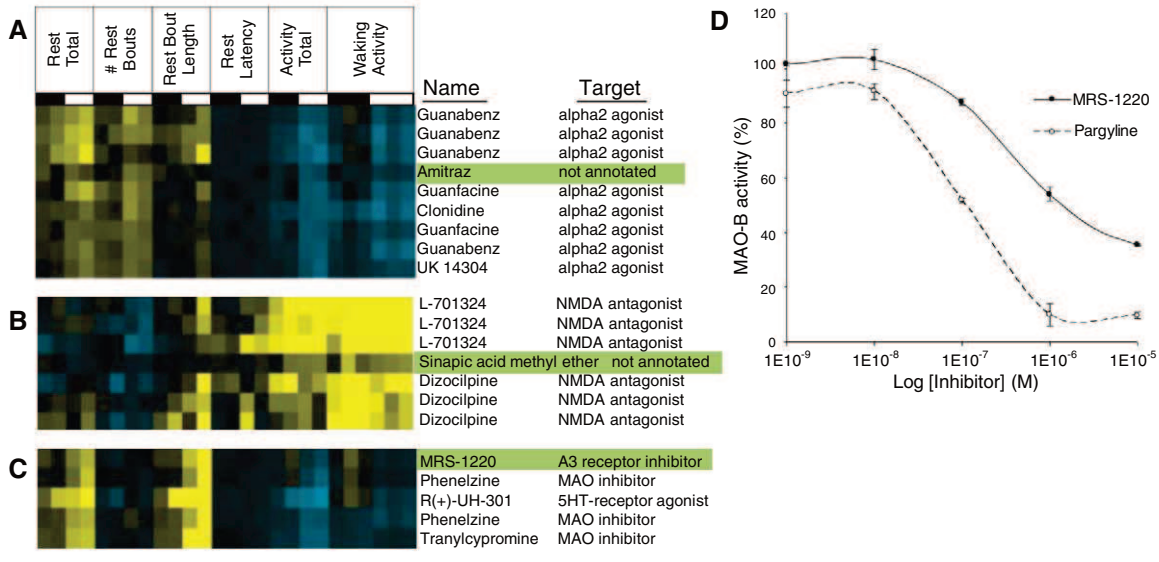

Fig. 3. Predicting primary and secondary biological targets for poorly characterized compounds. (**A**) The pesticide amitraz coclusters with α_2-adrenergic agonists. (**B**) Sinapic acid methyl ether coclusters with NMDA antagonists. (**C**) MRS-1220 coclusters with MAO inhibitors. (**D**) MRS-1220 inhibits MAO-B activity in an enzymatic assay with an IC_{50} of ~1 μM. Pargyline is a known MAO-B inhibitor (*19*). The clusters include repeats from different chemical libraries.

from the role of shaker channels in regulating sleep in flies and mice (*17*, *18*).

As applied here, behavioral profiling reveals relationships between drugs and their targets, demonstrates a conserved vertebrate neuropharmacology, and identifies regulators of rest/wake states. Our findings have two major implications for the fields of neurobiology, pharmacology, and systems biology. First, behavioral profiling has the potential to complement traditional drug discovery methodologies by combining the physiological relevance of in vivo

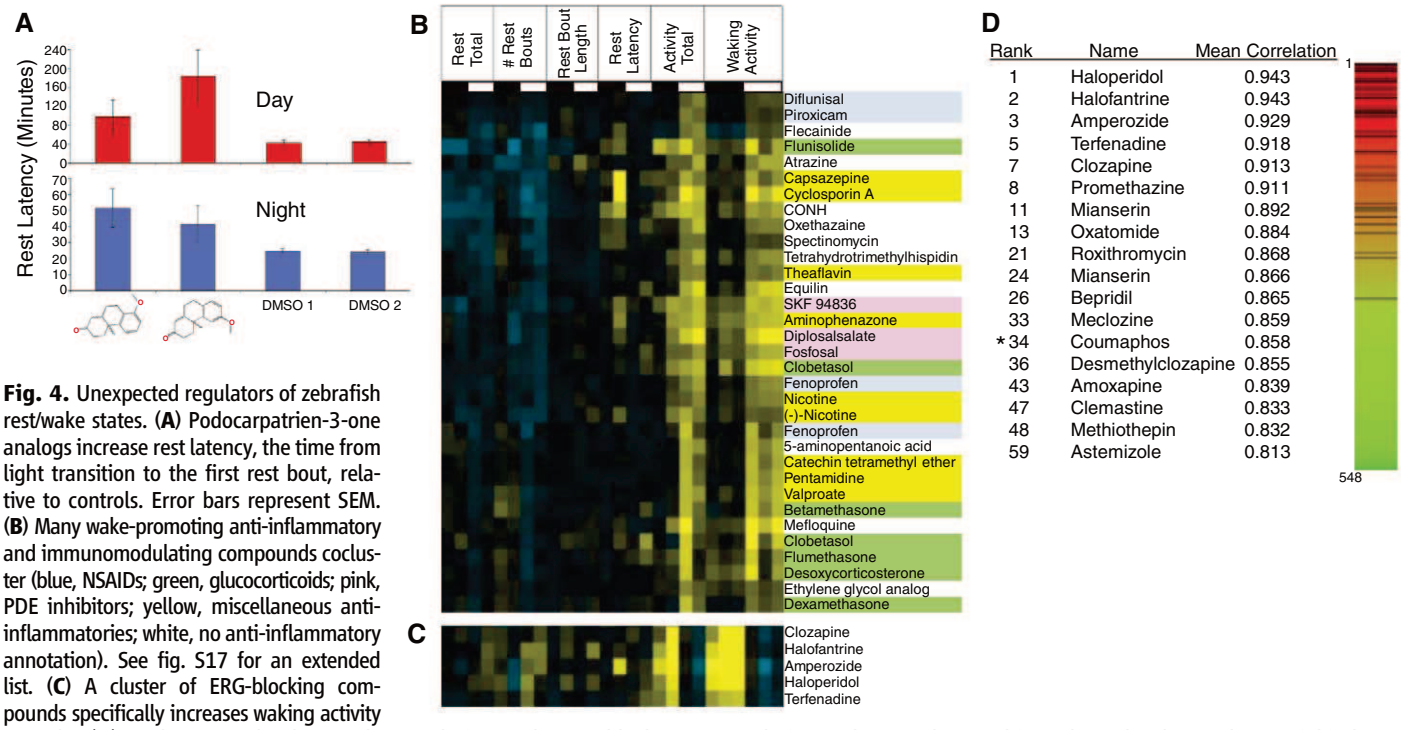

Fig. 4. Unexpected regulators of zebrafish rest/wake states. (**A**) Podocarpatrien-3-one analogs increase rest latency, the time from light transition to the first rest bout, relative to controls. Error bars represent SEM. (**B**) Many wake-promoting anti-inflammatory and immunomodulating compounds cocluster (blue, NSAIDs; green, glucocorticoids; pink, PDE inhibitors; yellow, miscellaneous anti-inflammatories; white, no anti-inflammatory annotation). See fig. S17 for an extended list. (**C**) A cluster of ERG-blocking compounds specifically increases waking activity at night. (**D**) Rank-sorting the data set by correlation to the ERG blocking cluster results in a significant enrichment of ERG blockers in the top ranks [$P < 10^{-13}$ by the Kolmogorov-Smirnov statistic (*3*)]. Black lines indicate known ERG blockers; red indicates high correlation, green indicates low correlation to the ERG cluster. This analysis also detected potential indirect regulators of ERG function, such as the organophosphate coumaphos (marked with an asterisk), which causes long QT through an unknown mechanism (*20*).

assays with high-throughput, low-cost screening (*3*). Future screens can be expanded to include many more uncharacterized compounds and to assay additional phenotypes, including those associated with human psychiatric disorders. In this way, behavioral profiling can characterize large classes of compounds and reveal differences in effectiveness, potential side effects, and combinatorial properties that might not be detected in vitro. Second, behavioral profiling allows for the systematic dissection of the pharmacology of complex behaviors. Our screen profiled the effects of dozens of neurotransmitter pathways and identified small molecules that regulate discrete aspects of rest/wake states. Future experiments can test drug combinations to identify synergistic or antagonistic effects among psychotropic compounds and to build interaction maps. High-throughput behavioral profiling thus may enable application of the logic and approaches of systems biology to neuropharmacology and behavior.

References and Notes

1. Y. Agid *et al.*, *Nat. Rev. Drug Discov.* **6**, 189 (2007).
2. M. N. Pangalos, L. E. Schechter, O. Hurko, *Nat. Rev. Drug Discov.* **6**, 521 (2007).
3. See supporting material on *Science* Online.
4. R. T. Peterson, M. C. Fishman, *Methods Cell Biol.* **76**, 569 (2004).
5. R. D. Murphey, H. M. Stern, C. T. Straub, L. I. Zon, *Chem. Biol. Drug Des.* **68**, 213 (2006).
6. T. E. North *et al.*, *Nature* **447**, 1007 (2007).
7. T. E. North *et al.*, *Cell* **137**, 736 (2009).
8. D. A. Prober, J. Rihel, A. A. Onah, R. J. Sung, A. F. Schier, *J. Neurosci.* **26**, 13400 (2006).
9. P. G. Jorens, E. Zandijk, L. Belmans, P. J. Schepens, L. L. Bossaert, *Hum. Exp. Toxicol.* **16**, 600 (1997).
10. B. H. Yoon *et al.*, *Life Sci.* **81**, 234 (2007).
11. A. Matteucci *et al.*, *Exp. Brain Res.* **167**, 641 (2005).
12. M. B. Wie *et al.*, *Neurosci. Lett.* **225**, 93 (1997).
13. K. A. Jacobson *et al.*, *Neuropharmacology* **36**, 1157 (1997).
14. L. Imeri, M. R. Opp, *Nat. Rev. Neurosci.* **10**, 199 (2009).
15. U. Langheinrich, G. Vacun, T. Wagner, *Toxicol. Appl. Pharmacol.* **193**, 370 (2003).
16. E. Raschi, V. Vasina, E. Poluzzi, F. De Ponti, *Pharmacol. Res.* **57**, 181 (2008).
17. C. L. Douglas *et al.*, *BMC Biol.* **5**, 42 (2007).
18. C. Cirelli *et al.*, *Nature* **434**, 1087 (2005).
19. C. J. Fowler, T. J. Mantle, K. F. Tipton, *Biochem. Pharmacol.* **31**, 3555 (1982).
20. E. Bar-Meir *et al.*, *Crit. Rev. Toxicol.* **37**, 279 (2007).

21. We thank J. Dowling, D. Milan, and G. Vanderlaan for suggestions and reagents and D. Schoppik, G. Uhl, and I. Woods for critical reading of the manuscript. Supported by a Bristol-Myers Squibb postdoctoral fellowship of the Life Sciences Research Foundation (J.R.), a Helen Hay Whitney Foundation postdoctoral fellowship (D.A.P.), a NIH Pathway to Independence grant (D.A.P.), the Stanley Medical Research Institute (S.J.H.), the Harvard Stem Cell Institute (L.L.R.), NIH grants MH086867 and MH085205 (R.T.P.), and grants from NIH and the McKnight Endowment Fund for Neuroscience (A.F.S.). L.L.R. is a founder of iPierian Inc., a biotechnology company, and is a member of its scientific advisory board.

Supporting Online Material www.sciencemag.org/cgi/content/full/327/5963/348/DC1 Materials and Methods
SOM Text
Figs. S1 to S18
Table S1
References

8 October 2009; accepted 11 December 2009
10.1126/science.1183090

Science

This abbreviated version of *Science*'s Information for Authors is printed in one issue of each year. The current, complete Information for Authors is available at www.sciencemag.org/about/authors.

Science is a weekly peer-reviewed journal that publishes significant, original scientific research, plus reviews and analyses of current research and science policy. We welcome submissions from all fields of science and from any source. Competition for space in *Science* is keen, and many papers are returned without in-depth review. Priority is given to papers that reveal novel concepts of broad interest.

PEER-REVIEWED MANUSCRIPTS

Research Articles (up to ~4500 words or ~5 pages in print) are expected to present a major advance. Research Articles include an abstract, an introduction, up to six figures or tables, sections with brief subheadings, and a maximum of about 40 references. Materials and methods, along with other information needed to support the conclusions, are usually included in the supporting online material.

Reports (up to ~2500 words or ~3 pages in print) present important new research results of broad significance. Reports should include an abstract, an introductory paragraph, up to four figures or tables, and a maximum of about 30 references. Materials and methods, and other information needed to support the conclusions, are usually included in the supporting online material.

Brevia (one page; about 800 words and one figure or table, and a maximum of about 10 references) are short peer-reviewed papers presenting novel results of broad general interest.

Technical Comments (up to 1000 words) discuss papers published in *Science* within the previous 6 months. Comments should include a 60-word abstract, up to 2 figures or tables, and a maximum of about 15 references. The authors of the original paper are given an opportunity to reply. Comments and replies are reviewed and edited as needed. Abstracts of the discussions appear in print; the full text appears online.

Reviews (4 print pages, on average) describe new developments of interdisciplinary significance and highlight unresolved questions and future directions. They include an abstract, an introduction that outlines the main point, sections with brief subheadings, and a maximum of about 40 references. Most Reviews are solicited by the editors, but unsolicited submissions may also be considered.

Science's Commentary section presents analysis by scientists and other experts on issues of interest to *Science* readers.

Policy Forums (1000 or up to 2000 words) present issues at the intersection between science and society that relate to science policy. **Education Forums** (1000 or up to 2000 words) present essays on science education and its practice, from preschool through postgraduate education. (Research results related to education should be submitted to the Reports section.) **Books *et al.*** (up to 1000 words) present reviews of current books, multimedia, exhibitions, and films of interest to *Science* readers. **Perspectives** (up to 1000 words) analyze recent research developments but do not primarily discuss the author's own work. Book reviews, Education and Policy Forums, and Perspectives are frequently solicited by the editors, but unsolicited contributions will be considered.

Letters (~300 words) discuss topical issues of general interest or material published in *Science* in the past 3 months. Humorous pieces will also be considered. Letters should be submitted through our Web submission site (www.submit2science.org). Letters are not acknowledged upon receipt, nor are authors generally consulted before publication. Letters may be edited for clarity and space. E-letters are online-only contributions (up to 400 words) that promote rapid, timely discussions.

Science Contact Information

Phone: (1)-202-326-6550 (USA)
(44)-1223-326500 (UK)

Fax: (1)-202-289-7562 (USA)
(44)-1223-326501 (UK)

E-mail: science_editors@aaas.org
science@science-int.co.uk (Europe)

MANUSCRIPT SELECTION

We are committed to the prompt evaluation and publication of submitted papers through our fully electronic submission and review process. Papers are assigned to a staff editor who has knowledge of the field discussed in the manuscript. Most submitted papers are rated for suitability by members of the Board of Reviewing Editors (see the masthead). The editors at *Science* consider this advice in selecting papers for in-depth review. Authors of papers that are not highly rated are notified promptly, by e-mail only, within about 1 to 2 weeks. Membership in AAAS is not a factor in selection.

Papers are reviewed in depth by at least two anonymous referees. Reviewers are contacted before being sent a paper and are asked to return comments within 1 to 2 weeks. We are able to expedite the review process for papers that require rapid assessment. Papers are edited to improve accuracy and clarity and to shorten, if necessary. Authors and reviewers are expected to notify editors if a manuscript could be considered to report dual use research of concern (DURC). Papers identified as possible DURC will be brought to the attention of the Editor-in-Chief for further evaluation. If necessary, outside reviewers with expertise in the area will be consulted. Papers cannot be resubmitted over a disagreement on interest or relative merit. If a paper was rejected on the basis of serious reviewer error, resubmission may be considered. Papers submitted to *Science* but not accepted for publication may, in some cases, be eligible for publication in *Science Signaling* or *Science Translational Medicine*. Most papers are published 4 to 8 weeks after acceptance; selected papers are published rapidly online in *Science* Express (www.sciencexpress.org).

Submitting a Manuscript or Letter

Science accepts submissions of manuscripts and letters only through our Web site: www.submit2science.org. We are not able to accept submissions by e-mail. Your submission should include a cover letter containing a statement of the paper's main point, any information needed to ensure a fair review process, and names of colleagues who have reviewed the paper for you.

Our online submission site cannot accept copies of related papers (see submission requirements). They should be sent as a PDF by e-mail to science_editors@aaas.org along with your Web submission number. Very big figure files or movies may be too large for the Web submission site. These should be sent on a CD or DVD to *Science*, 1200 New York Avenue, NW, Washington, DC 20005, USA, or to *Science* International, Bateman House, 82-88 Hills Road, Cambridge CB2 1LQ, UK.

SUBMISSION REQUIREMENTS

Authorship. All authors must agree to be so listed and must have seen and approved the manuscript, its content, and its submission to *Science*. Any changes in authorship must be approved in writing by all the original authors. Submission of a paper that has not been approved by all authors will result in immediate rejection without appeal.

Prior publication. *Science* will not consider any paper or component of a paper that has been published or is under consideration elsewhere. Distribution on the Internet may be considered prior publication and may compromise the originality of the paper. Reporting the main findings of a paper in the mass media may compromise the novelty of the work and thus its appropriateness for *Science*. Please contact the editors with questions regarding these policies.

Human studies. Informed consent must have been obtained for studies on humans after the nature and possible consequences of the studies were explained. All research on humans must have approval from the author's Institutional Review Board (IRB) or equivalent body.

Animal care. Care of experimental animals must be in accordance with the author's institutional guidelines.

Related papers. Copies of papers submitted to other journals by any of the authors that relate to the paper submitted to *Science* must be included with the submission.

Unpublished data and personal communications. Citations to unpublished data and personal communications cannot be used to support claims in the paper.

CONDITIONS OF ACCEPTANCE

Authorship, funding, and conflict of interest. All authors must disclose all affiliations, funding sources, and financial or management relationships related to a paper, including those that could be perceived as potential sources of bias, before acceptance. *Science* now requires all authors of accepted papers to affirm their contribution to a paper and agree to our policies on data and materials availability. The senior author from each group is required to have examined the raw data their group has produced. See our conflict-of-interest policy, detailed at www.sciencemag.org/about/authors.

Data deposition. Before publication, large data sets, including microarray data, protein or DNA sequences, and atomic coordinates and structure factors for macromolecular or chemical structures must be deposited in an approved database, an accession number must be included in the published paper, and the deposited information must be released at the time of publication. Electron micrograph maps must also be deposited. Approved databases are listed at www.sciencemag.org/about/authors. Large data sets with no appropriate approved repository must be housed as supporting online material at *Science*, or when this is not possible, on the author's Web site, provided a copy of the data is held in escrow at *Science* to ensure availability to readers.

Data availability and materials sharing. After publication, all data necessary to understand, assess, and extend the conclusions of the manuscript must be available to any reader of *Science*, and all reasonable requests for materials must be fulfilled. Before acceptance, *Science* must be informed of any restrictions on sharing of materials [Material Transfer Agreements (MTAs), for example]. Unreasonable restrictions may preclude publication.

License and access policies. Authors retain copyright but must agree to grant to *Science* an exclusive license to publish the paper in print and online. Any author whose university or institution has policies or other restrictions limiting their ability to assign exclusive publication rights (e.g., Harvard, MIT, Open University) must apply for a waiver or other exclusion from that policy or those restrictions. After publication, authors may post the accepted version of the paper on their personal Web site and are provided one referrer link that can be posted on a personal or institutional Web page, through which users can freely access the published paper on *Science*'s online site. *Science* allows deposition of accepted papers into the NIH PubMed Central or other PMC International repository 6 months after publication, in accord with the requirements of the funders NIH and Wellcome Trust, provided that a link to the final version published in *Science* is included. Original research papers are freely accessible with registration on *Science*'s Web site 12 months after publication.

Press coverage. The paper should remain a privileged document and should not be released to the press or the public before publication. Questions should be referred to the AAAS Office of Public Programs (202-326-6440).

Manuscript Preparation

See Information for Authors at www.sciencemag.org/about/authors for more detailed information.

Titles should be no more than 96 characters (including spaces) for Reports, Research Articles, and Reviews, and 64 characters plus spaces for Brevia.

One-sentence summaries capturing the most important point should be submitted for all papers.

Abstracts explain to the general reader why the research was done and why the results are important. The abstract should present background information to convey the context of the research, describe the results, and draw general conclusions.

Text starts with a brief introduction describing the paper's significance, which should be intelligible to readers in other disciplines. Technical terms should be defined. Symbols, abbreviations, and acronyms should be defined the first time they are used. All tables and figures should be cited in numerical order.

References and notes are numbered in the order in which they are cited, first through the text, then through the text of the references, and then through the figure and table legends. Each reference should have a unique number; do not combine references or embed references in notes. Do not use op. cit. or ibid. We now accept titles in references and will include these in our online version.

Acknowledgments, including complete funding information, accession numbers, and any information related to authorship conflict of interest, should be gathered into the last numbered reference.

Tables should be included at the end of the references and should supplement, not duplicate, the text. The first sentence of the table legend should be a brief descriptive title. Every vertical column should have a heading, consisting of a title with the unit of measure in parentheses. Units should not change within a column.

Figure legends should be double-spaced in numerical order. The figure title should be given as the first line of the legend. No single legend should be longer than ~200 words. Nomenclature, abbreviations, symbols, and units used in a figure should match those used in the text. Units should be metric and follow SI conventions.

Supporting online material (SOM) is posted permanently on *Science* Online, is linked to the manuscript, and is freely available. SOM includes materials and methods plus extra text, figures, tables, references, and video or audio clips that are important for the integrity of the paper. Detailed instructions on preparing SOM can be found at www.sciencemag.org/about/authors/prep/prep_online.dtl.

Figures should be submitted as part of the online submission or, if necessary for large files only, on a CD. No part of a figure may be selectively manipulated. When figures are assembled from multiple gels or micrographs, a line or space should indicate the border between two original images. See our online Information for Authors for information on preparing art. We can include high-resolution images as SOM.

NEW PRODUCTS FOCUS: AUTOMATION

IFC SYSTEM

The Fluidigm BioMark IFC Controller MX is designed to automatically prime and load 48.48 Dynamic Array and Digital Array integrated fluidic circuits (IFCs). The MX is a compact, fully integrated system with an internal computer, touch-screen control, and internal air source capable of setting up 2,304 reactions within minutes. It is suitable for labs undertaking gene expression, genotyping, and real-time and digital polymerase chain reaction (PCR) experiments that have lower throughput requirements, tight budgets, and limited bench space. It automates the setup of dynamic array or digital array chips. After samples and assays have been pipetted into the inlets of the input frame, the chip is placed onto the controller and with a few taps of the touch screen, samples and assays are loaded into the IFCs. After setup, the IFCs are placed on the BioMark Real-Time PCR system for thermal cycling and data collection.

Fluidigm Europe

For info: +33-44-259-3861 | www.fluidigm.com

MULTIPURPOSE CENTRIFUGE

The multipurpose Centrifuge 5430 R spins tubes from 0.2 ml to 50 ml, as well as microplates. It has a maximum speed of 30,130 x g (17,500 rpm) and requires only 15 inches of bench space, so users can spin 15 ml and 50 ml conical tubes as well as plates for polymerase chain reaction and enzyme-linked immunosorbent assays directly on the lab bench. A refrigerated model with superior temperature management options is available.

Eppendorf North American

For info: 800-645-3050 | www.eppendorf.com

MICROPLATE HEAT SEALER

The TriSeal Pro is a budget-priced continuous-roll microplate heat sealer for medium to high throughput plate-sealing applications. Designed to produce a tight seal on any standard microplate from a thin polymerase chain reaction plate to deep-well plates, the TriSeal Pro includes a 610-meter sealing-film roll, which can seal up to 5,000 plates without intervention. A unique turntable design allows simultaneous loading, unloading, and sealing for a plate-sealing rate of three per minute. It provides precisely adjustable temperature control from 50°C to 185°C, enabling it to operate with more foil and film seals. Pneumatically operated, it requires only compressed air and mains voltage for routine operation.

Porvair Sciences

For info: +44-1932-240255 | www.porvair-sciences.com

HEATER AND SHAKER PACKAGE

The Microlab Nimbus Heater/Shaker Package incorporates high-speed automated pipetting with orbital plate shaking and heating. This preconfigured, turnkey package provides streamlined functionality for a variety of applications that require heat for solute mixing or shaking, such as in colorimetric, fluorescent, or luminescent bioassays; cell viability assays; and magnetic separations. The package includes device-mounting hardware, optimized test methods, and a choice of either the new Hamilton Heater Shaker module or one of several Variomag Teleshake models. Pipetting can be done directly to microplates on the heater/shaker and plates can be transported to and from the device with an optional labware gripper. The devices are compatible with standard microplate formats and provide accurate Peltier-based temperature control and orbital shaking with variable speed control.

Hamilton

For info: 775-858-3000 | www.hamiltonrobotics.com

HIGH THROUGHPUT PIPETTING

The enhanced Liquidator 96 is a powerful personal research tool that adds speed and flexibility to high throughput manual pipetting. It is suitable for applications involved in proteomics and genomics, such as kinetics, gene expression, protein-protein interaction, and enzyme-linked immunosorbent assays. It can be used in cell-based assays and many other studies. Its uses include adding sample, filling plates, mother-daughter plate replication, reformatting from 96-well to 384-well plates, and adding sample to chemotaxis plates. Liquidator 96's precision and accuracy ensure reproducible results well-to-well and plate-to-plate, without the need for complicated programming or dedicated technician time.

Rainin Instrument

For info: 510-564-1600 | www.rainin.com

MICROCENTRIFUGE

More powerful than the personal SCF1 Spinner, the SCF2 Microcentrifuge is a compact, variable speed unit that accommodates a fixed angle rotor holding 12 tubes or a strip tube rotor. Versatility and ease of use are key features of the new unit. The fixed angle rotor holds up to 12 x 1.5-ml or 2.2-ml microfuge tubes and, using the supplied adapters, 0.5-ml and 0.2-ml tubes can also be centrifuged. The strip tube rotor holds four strips of 8 x 02.-ml tubes. No tools are required to install the rotors and spin speed is variable, up to 13,500 rpm for the fixed angle rotor and 6,000 rpm for the strip tube rotor. Centrifugation speed can be displayed in rpm or rcf, and the timer can be set for run times from 1 to 30 minutes. A pulse button enables rapid spindown.

Bibby Scientific

For info: +44-(0)-1785-812121 | www.bibby-scientific.com

Electronically submit your new product description or product literature information! Go to www.sciencemag.org/products/newproducts.dtl for more information.

Newly offered instrumentation, apparatus, and laboratory materials of interest to researchers in all disciplines in academic, industrial, and governmental organizations are featured in this space. Emphasis is given to purpose, chief characteristics, and availabilty of products and materials. Endorsement by *Science* or AAAS of any products or materials mentioned is not implied. Additional information may be obtained from the manufacturer or supplier.

POSITIONS OPEN

LIBER ERO CHAIR IN COASTAL STUDIES
Simon Fraser University

The Faculty of Science and the Faculty of Environment at Simon Fraser University invite applications for the first Liber Ero Chair in Coastal Studies. We are seeking an outstanding scientist with an established international reputation, or an exceptionally promising junior scientist, in an area of environmental research complementary to those of an already outstanding group of researchers (Tom Buell British Columbia Leadership Chair in Salmon Conservation, Centre for Coastal Studies, Centre for Natural Hazards Research, Centre for Wildlife Ecology, School of Resource and Environmental Management). Potential research areas include, but are not limited to, coastal ecosystem dynamics, land-ocean interactions, integrated coastal management, ecosystem-based management, and marine biodiversity conservation. It is anticipated that the Chair will be appointed in one of the science departments or in the newly created Faculty of the Environment. The rank of the appointment will depend on the experience of the successful candidate. Income from the substantial Liber Ero Endowment will provide a significant annual research budget for the Chair. The Chair will be expected to mount a strong and highly visible research program, to contribute to our undergraduate and graduate teaching programs, and to collaborate with the Centre for Coastal Studies on outreach activities.

Research on environmental issues is a very high priority for Simon Fraser University and the Province of British Columbia, which recently created the Pacific Institute for Climate Solutions that engages the four primary research universities in the province. Given the high degree of public interest in the environment, the ability of the Liber Ero Chair to engage the public, relevant stakeholders, and government agencies in constructive dialogue will be considered an asset.

Applicants should send curriculum vitae, a concise research proposal, and a list of at least three individuals willing to act as references to:

Dr. Michael Plischke
Dean of Science
Simon Fraser University
8888 University Drive
Burnaby, BC, Canada V5A 1S6
E-mail: scdean@sfu.ca

This competition will remain open until the position is filled. Screening of applications will commence on March 1, 2010.

All qualified candidates are encouraged to apply; however, Canadians and permanent residents of Canada will be given priority. Simon Fraser University is committed to an equity employment program that includes special measures to achieve diversity among its faculty and staff. We therefore particularly encourage applications from qualified women, aboriginal Canadians, persons with disabilities, and members of visible minorities.

POSTDOCTORAL POSITION, BOSTON
in Tuberous Sclerosis and LAM

The Henske laboratory at Harvard Medical School and the Brigham and Women's Hospital (BWH) is seeking a highly motivated Postdoctoral Fellow with training in genetics, biochemistry, or cell biology to study tuberous sclerosis complex (TSC) and/or lymphangioleiomyomatosis (LAM). Please send curriculum vitae, cover letter, and names of three references to: **Dr. Elizabeth Petri Henske, Brigham and Women's Hospital, One Blackfan Circle, Sixth Floor, Boston, MA 02115. E-mail: henskelab@gmail.com.** *BWH is an Affirmative Action/Equal Opportunity Employer.*

CAREER OPPORTUNITY. Doctor of Optometry (O.D.) degree in 27 months for Ph.D.s in science and M.D.s. Excellent career opportunities for O.D.-Ph.D.s and O.D.-M.D.s in research, education, industry, and clinical practice. This unique program starts in March of each year, features small classes, and has 12 months devoted to clinical care.

Contact the **Admissions Office, telephone: 800-824-5526** at **The New England College of Optometry, 424 Beacon Street, Boston, MA 02115.** Additional information at **website: http://www.neco.edu. Email: admissions@neco.edu.**

POSITIONS OPEN

UNIVERSITY OF SOUTH CAROLINA
SCHOOL OF MEDICINE

ENDOWED CHAIR IN INFLAMMATION AND VISION RESEARCH

The University of South Carolina invites inquiries, nominations, and applications for an outstanding scientist to help establish a statewide Vision Science Center of Economic Excellence (COEE) and serve as the USC director. This is a tenured Endowed Chair that provides a unique opportunity to use the basic and clinical resources at USC to develop an area of advanced research in any of the inflammatory or autoimmune diseases that affect the eye. Applicants should have a Ph.D., M.D., D.V.M., or equivalent degree with experience in immunology and/or cellular/molecular biology and use genetic or pharmacological tools to address the role of inflammation or autoimmunity in the broad area of ocular biology and disease. A history of significant grant funding and experience leading a research team is required. In addition to running a successful research team, the selected candidate will take the lead in the hiring and mentoring of junior faculty in inflammation research involving ocular biology. Also, opportunities exist to collaborate with researchers from NIH Center for Inflammatory and Autoimmune Diseases (**website: http://camcenter.med.sc.edu/**) located at the University of South Carolina School of Medicine (**website: http://www.med.sc.edu/**). Inquiries and nominations should be sent electronically to **Prakash Nagarkatti, Ph.D, Associate Dean for Basic Science, e-mail: pnagark@uscmed.sc.edu**. Applications with curriculum vitae, brief statement of research interests, and names of four references should be sent electronically to **e-mail: vision@uscmed.sc.edu**. *The University of South Carolina is an Affirmative Action/Equal Opportunity Employer. Minorities and women are especially encouraged to apply. The University of South Carolina does not discriminate in educational or employment opportunities or decisions for qualified persons on the basis of race, color, religion, sex, national origin, age, disability, sexual orientation, or veteran status.*

ASSISTANT/ASSOCIATE PROFESSOR
in Pharmaceutical Sciences
Northeastern University

Applications are invited for two tenure-track or tenured faculty positions in medicinal chemistry and drug discovery, and in pharmaceutics and drug delivery. Successful candidates are expected to establish extramurally funded research programs, participate in Pharm.D. and graduate (M.S. and Ph.D.) teaching, and engage in service. Applicants with current transferable funding will be given priority. The medicinal chemistry position will be associated with the Center for Drug Discovery (CDD), one of several research centers in the Department. Northeastern University is located in the heart of Boston within close proximity to major biotechnology/pharmaceutical companies, academic institutions, and medical centers.

Interdisciplinary appointments and highly competitive startup packages are available to qualified applicants. The start date for these positions is September 2010. Evaluation of candidates will begin immediately and applications will be accepted until the positions are filled.

Applications must be submitted online at **website: http://www.northeastern.edu/provost/faculty/positions.html** by clicking on Access Faculty Positions. More information about the Department and the CDD may be found at **websites: http://www.northeastern.edu/pharmsci/** and **http://www.cdd.neu.edu/**. Applicants may also contact search chairs **Alex Makriyannis** (medicinal chemistry and drug discovery) at **e-mail: a.makriyannis@neu.edu**, or **John Gatley** (pharmaceutics and drug delivery) at **e-mail: s.gatley@neu.edu**.

The successful candidates must have experience in, or commitment to, working with diverse student populations and/or in a culturally diverse work and educational environment. Northeastern University is an Equal Opportunity/Affirmative Action, Title IX, and ADVANCE Institution. Minorities, women, and persons with disabilities are strongly encouraged to apply.

DENMARK

BETTER. FASTER. STRONGER.

LEADING THE WAY
IN TRANSLATIONAL MEDICINE

WEBINAR

Translational medicine is a field that continues to grow rapidly. Encouraging, supporting, and developing basic translational research and its therapeutic application is essential to building a strong foundation in science. This webinar will focus on what Denmark is doing to advance research, strengthen ties between academia and industry, and provide a fertile environment for innovation. Discussion will cover government initiatives (Danish and EU) to support translational medicine, as well as the infrastructure put in place within Denmark to support and nurture domestic and foreign investment in this research.

February 10, 2010

5 pm CET, 4 pm GMT, 11 am EST, 8 am PST

During this webinar our panelists will:

- Discuss the importance of translational research and its impact on scientific discovery and drug development within Denmark.
- Outline government and other programs that encourage partnerships between academic institutions and industry.
- Talk about the potential advantages for companies of relocation to Denmark to carry out translational research–related work.
- Answer your questions live.

If you are looking to move your business operations to Denmark or to invest in Denmark, then make sure you participate in this live webinar!

Register Now!

Sign Up At :

www.sciencemag.org/webinar

Participating Experts:

Prof. Lars Arendt-Nielsen
Aalborg University
Aalborg, Denmark

Dr. Neils Porksen
Eli Lilly & Company
Indianapolis, IN

Prof. Liselotte Højgaard
Rigshospitalet
Copenhagen, Denmark

Science
AAAS

Brought to you by the
AAAS/*Science* Business Office

Webinar sponsored by Invest in Denmark

DENMARK:
MAKING GLOBAL CONNECTIONS

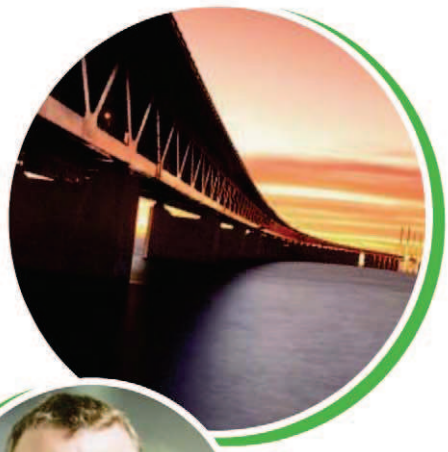

Denmark's Øresund bridge—connecting Copenhagen to southern Sweden—symbolizes the country's strengths in connecting basic and applied research, and academic and corporate interests. "Denmark has a well-educated population, a number of leading life science companies, and an international research environment," says Prime Minister **Lars Løkke Rasmussen.** Minister of Economic and Business Affairs, **Lene Espersen,** adds that Denmark encourages scientific entrepreneurship with "a skilled and flexible labor force, and government policy that nurtures new and emerging technologies and innovative companies." Both ministers say green technology is especially encouraged. According to the prime minister, "We have pursued an ambitious environmental and climate policy. This gives us an advantage now that these issues are getting global attention."

By Chris Tachibana

Lars Løkke Rasmussen

Connecting Bench and Bedside, Academics and Industry

Denmark has a long history of bringing basic research results to the marketplace. "We have a more than century-old tradition of generating successful pharmaceutical companies and conducting clinical trials, and a decade of experience in creating biotechnology companies," says **Ole Frijs-Madsen,** Director of Invest in Denmark (IDK). In the 1920s, in an early example of translational research, scientists and physicians partnered with the companies that became Novo Nordisk and LEO Pharma to develop insulin for clinical use. **Mads Krogsgaard Thomsen,** chief science officer of Novo Nordisk, says, "Denmark has traditionally been very strong in biomedical research. Some of the most cited clinical research in diabetes and metabolic disease comes from this part of the world." **Liselotte Højgaard,** professor in medicine and technology, University of Copenhagen agrees. "We have done translational research for a long time, we've just called it something else." Clinical studies are facilitated by "a strong emphasis on taking basic research results into patient studies," says Højgaard. "The population in Denmark knows that medical research improves patient treatment."

Based on these strengths, the Danish government launched a globalization strategy in 2006, outlined in the *Science* feature, "Denmark—Building on Tradition" (dx.doi.org/10.1126/science.opms.r0600008). That strategy aimed to increase funding for research and development to 3 percent of gross domestic product, with 1 percent from public sources. Prime Minister Løkke Rasmussen says the public expenditure goal will be met. "It is important to maintain focus, despite the global recession." According to IDK Director Frijs-Madsen, of the $1.8 billion allocated for the 2010-2012 globalization funds, $1.4 billion is for advancing science and innovation. The strategy also planned to double the number of Ph.D. scholarships, and this appears to be on target. At Aarhus University, in Denmark's second largest city, **Erik Meineche Schmidt,** dean of natural sciences, says, "We have seen a major increase over the last three or four years in the number of Ph.D. students. We used to accept maybe 80 a year. Last year we admitted 130." About one-third are foreign students, many recruited from Eastern Europe. continued »

> "The number of foreigners coming to work here has almost tripled since 2001, and the number of international students has doubled. This is a very positive development."

UPCOMING FEATURES

Diversity 1: Women in Science—February 12

Postdoc 1: Life Beyond the Bench—March 5

Faculty 1: Lab Management—March 12

CREDIT: (TOP) ISTOCKPHOTO.COM/RAMBERG

Denmark encourages scientific entrepreneurship with "a skilled and flexible labor force, and government policy that nurtures new and emerging technologies and innovative companies."

— Lene Espersen

Corporate-Clinical-Academic Partnerships

For students and scientists seeking training in both academia and industry, Denmark offers excellent opportunities. The Danish Technical University, whose main campus is in Lyngby, north of Copenhagen, specializes in applied research and industry collaboration, covering areas from robotics to food science. A prime example of academic-corporate collaborations is the industrial Ph.D. scholarship, each of which is co-funded by the government and a company, and includes a mandatory business course. Students are trained in the "commercial aspects of research and development," and create personal networks between companies and universities. In 2008, 119 industrial Ph.D. scholarships were granted, up from 50 in 2002, the first year of the program. Most are in biomedicine, engineering, and technology, but fields like agriculture and fisheries are also funded.

The biotechnology company Exiqon has hosted several industrial Ph.D. students, and all now have industry careers. According to CEO **Lars Kongsbak,** the students "learn the importance of delivering a product of value to customers, which you need to know to start a business." They also gain communication experience. "An industry Ph.D. student sees the value of communicating, not only in academic papers and posters at scientific meetings, but also in sales brochures and public presentations."

Another program that encourages academic-corporate collaborations is the Innovation Consortia program, started by the Danish government in 2007. A successful example is CureND, a consortium focused on finding drugs and diagnostics for Parkinson's disease. It includes academic labs at Aarhus and Aalborg universities, and several companies, including Wyeth (now part of Pfizer). IDK's Frijs-Madsen calls CureND "a targeted and innovative discovery research program, and an excellent public-private collaboration model." **Daniel Otzen** is CureND's director, and says the program works because "companies don't want to just bankroll academic research but want genuine partnerships." At CureND, "each partner has well-defined tasks. My lab was able to take the time to find the best conditions for a high throughput screen that was subsequently turned into a genuine screening assay by Wyeth."

Otzen exemplifies the easy flow between industry and academia. Between his Ph.D. and his postdoc in Lund, Sweden, he worked as a staff scientist at Novozymes, and says his work there became a major focus of his basic research at Aarhus University. "A stint in industry is great—I would strongly encourage it for everybody. It opens your mind for other working environments, and makes it easier to subsequently engage in transparent and mutually beneficial private-public collaborations." This attitude has spurred biotechnology in Medicon Valley, as the network of biomedical research interests in Denmark and southern Sweden is known. In 2008, Ernst and Young ranked Denmark first out of 15 European countries in pipeline growth, with a 23 percent increase from 2006 to 2007 in the number of drug candidates in development.

Industry partnerships thrive at the Center for Sensory-Motor Interaction at Aalborg University in northern Denmark, a global leader in pain research. With a Center of Excellence grant from the Danish Research Foundation 15 years ago, Director **Lars Arendt-Nielsen** implemented a philosophy of "keeping key senior scientists as free as possible from administrative duties, so they can spend their energy on research projects." Funding has increasingly focused on industrial partnerships, he says, so "over the last five years we have entered into more and more collaborations with industry," and they now work with approximately 15 pharmaceutical companies.

Despite his success with industry partnerships, Arendt-Nielsen advises balance in research funding. "Without funding for basic science, we do not have new fundamental knowledge to move into applied research projects. Basic science and applied science must go hand in hand." Aarhus University's Otzen also warns about "a tendency of universities to bend over backwards to show they can apply their research."

Thomas Mandrup-Poulsen, professor in medical research methodology, University of Copenhagen, conducts both basic and clinical diabetes research at the Hagedorn Research Institute and Steno Diabetes Center. He finds "growing interest in industry to engage with universities to address basic research problems, to enhance basic knowledge of disease mechanisms." He suggests "a way to promote basic and translational research at the same time, is to have Ph.D. or postdoctoral fellowships that require collaboration between a basic research institute, a clinical institute, and industry."

Support from the Private Sector

Basic and applied research receive strong support from private science foundations in Denmark. In late 2009, the Lundbeck Foundation announced a grant of $6 million to establish the Lundbeck Foundation Nanomedicine Centre for Individualised Management of Tissue Damage and Regeneration, at Aarhus University. The goals are to apply expertise in biomedicine and nanotechnology to develop new methods in continued »

INVEST IN DENMARK
MINISTRY OF FOREIGN AFFAIRS OF DENMARK

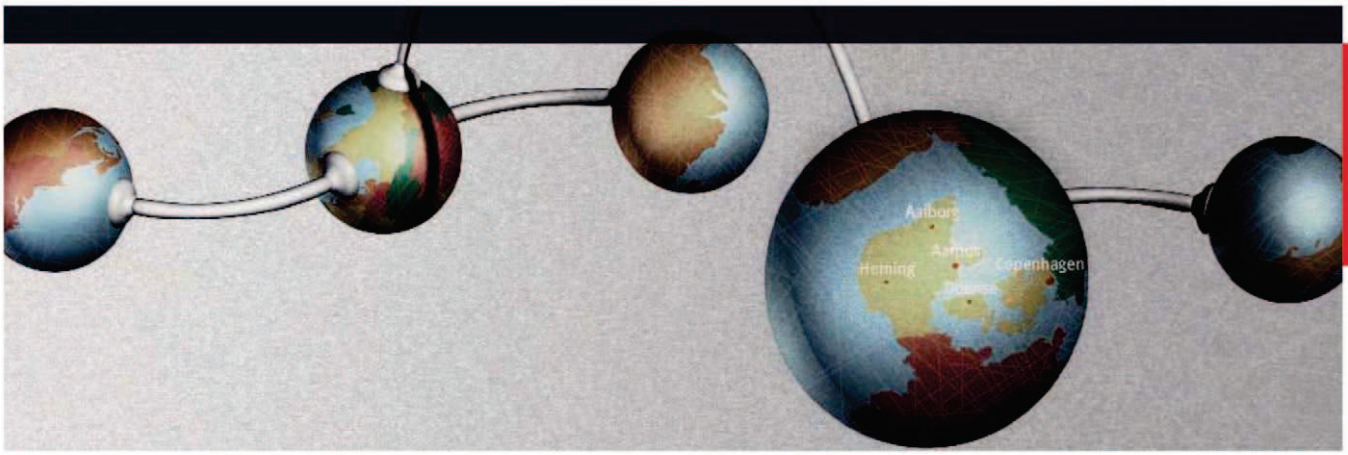

WE OPEN THE DOOR TO DENMARK

THE BEST PLACE IN THE WORLD TO DO BUSINESS*

* ECONOMIST INTELLIGENCE UNIT & FORBES, 2009

Invest in Denmark's global team provides you with professional advice, services and connects you to the right people.

Whether your company considers to relocate, consolidate, set up new production facilities, is on the lookout for new R&D partners or other strategic business solutions in Europe, Invest in Denmark is a good place to begin.

www.investindk.com

HEADQUARTER	EUROPE	NORTH AMERICA	ASIA	CHINA AND INDIA
Invest in Denmark Ministry of Foreign Affairs of Denmark 2, Asiatisk Plads 1448 Copenhagen K Denmark	Invest in Denmark Ambassade Royale de Danemark 77, avenue Marceau 75116 Paris France	Invest in Denmark Royal Danish Consulate General 885, Second Avenue, 18th Floor New York, N.Y. 10017, USA	Invest in Denmark Royal Danish Embassy 29-6 Sarugaku-cho Shibuya-ku Tokyo 150-0033 Japan	Invest in Denmark Royal Danish Innovation Center Denmark, 100 Qin Zhou Road, Room 711 Shanghai 200235 ,China
Tel.: +45 33 92 11 16	Tel.: +33 1 4431 2193	Tel.: +1 212 223 4545	Tel.: +81 3 3496 3001	Tel.: +86 21 6209 0500
info@investindk.com	info@investindk.com	info@investindk.com	info@investindk.com	info@investindk.com

diagnostic imaging, and tissue-specific protective and regenerative therapies. The Novo Nordisk Foundation (NNF) has been supporting research since 1926, and is a major force in Danish science. According to Director **Birgitte Nauntofte,** the NNF wants Denmark "to be recognized internationally as a hot spot for health science and biotech research, and to be associated with quality, seriousness, innovation, openness, and creativity." Nauntofte says the NNF has had an "extremely positive experience" funding large-scale initiatives, and "is likely to continue this strategy over the next couple of years."

The NNF recently gave protein science a boost, with $113 million for the NNF Center for Protein Research (CPR), which opened in June 2009. **Ulla Wewer,** dean of the Faculty of Health Sciences at the University of Copenhagen, where the CPR is housed, says they are "recruiting a strong team of international scientists to do basic research, knowing this will eventually strengthen industry." The CPR will be building up its staff to 150, and will use systems biology, high throughput protein production, and proteomics to study therapeutically relevant proteins.

Another new initiative, co-funded by the NNF and the Danish Ministry of Science, Technology and Innovation, is the Danish Biobank at the Statens Serum Institute in Copenhagen. **Mads Melbye,** executive vice president of the institute, says they are cataloging approximately 15 million existing blood, tissue, and DNA samples from various pathology banks, and expect 200,000 new specimens annually. Physical samples will be coordinated with the wealth of data in Danish health registries, which include "birth characteristics of all newborns, hospital and outpatient diagnoses, a registry of prescribed medications, and a registry of all childhood vaccinations since 1990, which is unique worldwide," says Melbye. Information can be tracked through generations, for inherited diseases, or by address, for infectious disease research. Citizens can opt out, but Melbye hopes that in two and a half years, aggregated population data, without personal information, will be available electronically to researchers around the world.

Bridges Across Borders

Julio Celis, director of the Institute of Cancer Biology for the Danish Cancer Society, is also distributing research information on an international scale. He is developing a network to link cancer experts in European Union countries, explaining: "Different countries have niches of expertise, so instead of duplicating them in all countries, it's easier to connect them, so that we are faster in getting discoveries to the patient." The realization that "cancer is complicated, and no single institute, country, or even continent would be able to deal with it," led to the Stockholm Declaration, a commitment to join forces signed by the directors of 18 European cancer centers. Celis says the network will encourage mobility of expertise, students, and data, and create a "single-stop shop for industry discovery programs." The network structure, and pilot projects on disease prevention and early detection, are in the planning stages.

Other globalization efforts are less virtual, aiming to bring scientists from other countries to Denmark. Nauntofte of the NNF says, "Denmark is a small country, so we have a limited pool of research talent. We must recruit highly competent foreign researchers, and our research groups must continued »

FEATURED PARTICIPANTS

Aalborg University
en.aau.dk

Aarhus University
www.au.dk/en

Center for Sensory-Motor Interaction
www.smi.auc.dk

CureND
www.neurocampus.au.dk/menu55-en

Danish Cancer Society
www.cancer.dk

Danish National Research Foundation
www.dg.dk

Danish Technical University
www.dtu.dk/English.aspx

Exiqon
www.exiqon.com

Hagedorn Research Institute
www.hagedorn.dk

Industrial Ph.D program
en.fi.dk/research/industrial-phdprogramme

Invest in Denmark
www.investindk.com

LEO Pharmaceuticals
www.leo-pharma.com

Lundbeck Foundation
www.lundbeckfonden.dk/en

Medicon Valley
www.mediconvalley.com

Ministry of Science, Technology and Innovation
en.vtu.dk

Novo Nordisk Foundation Center for Protein Research
www.cpr.ku.dk

Novo Nordisk Foundation
www.novonordiskfonden.dk/en/

Novo Nordisk
www.novonordisk.com

Novozymes
www.novozymes.com

Statens Serum Institut
www.ssi.dk/sw379.asp

Steno Diabetes Center
www.stenodiabetescenter.com

University of Copenhagen
www.ku.dk/english

Wyeth (Pfizer)
www.pfizer.com

CREDIT: ISTOCKPHOTO.COM/ENDLESSADVENTURE

The Novo Nordisk Foundation

Center for Protein Research

The Novo Nordisk Foundation Center for Protein Research, located in central Copenhagen, has recently been established at the Faculty of Health Sciences, University of Copenhagen, to promote basic and applied discovery research on human proteins of medical relevance. The establishment of the Center, opened in June 2009, has been made possible by a donation of 116 million USD from the Novo Nordisk Foundation, **www.novonordiskfonden.dk/en**, and other significant contributions from the University. The Center which operates as an integral part of the Faculty of Health Sciences, has already secured world-class capabilities in a number of protein focused research areas and disciplines.

The Center – covering 4,500 m^2 newly renovated facilities – comprises a wide range of expertise and resources, from ***in silico*** target identification, high throughput protein production and characterisation to chemical biology as well as disease systems biology, mass spectrometry based proteomics and specific research programs on ubiquitin modified signaling and molecular endocrinology. The Center will contribute to the progress of translational research within medicine and provide fundamental insights which can be used to promote drug discovery and development. We want to establish the Center as an internationally competitive organisation focused on medically relevant proteins.

For additional information and details, see **www.cpr.ku.dk**

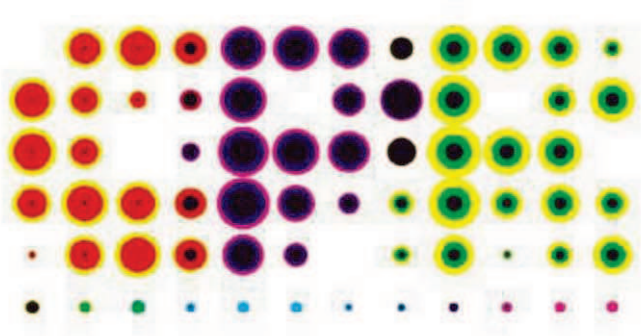

Research Directors and Group Leaders

We are now seeking excellent scientists to further strengthen our research capabilities – internationally renowned and established as well as promising younger scientists particularly in the area of protein focused disease biology. Successful candidates will establish research groups carrying out independent research of highest scientific impact and standard as well as work with us on integrated collaborative projects. Currently, the Center management team consists of Dr. Michael Sundström (Managing Director), Professor Matthias Mann (Research Director, Proteomics) and Professor Søren Brunak (Research Director, Disease Systems Biology).

The successful candidates should have an excellent track record, international reputation and documented abilities. We will prioritise applicants with protein focused experience in relation to human health and disease – such as signaling pathways, metabolism, protein degradation and aggregation as well as analysis of post-translational modifications. Our goal is to establish a highly integrated research environment; thus collaborative interest is essential. In addition, your vision on how the unique environment and resources at the Center will benefit your research projects will be of particular interest to us. Successful candidates will be offered generous start-up packages and competitive salaries.

Are you interested in becoming a Group Leader or Research Director at the Center?
Please send a letter of interest, including a brief CV/biography as well as a summary of planned future research to **contact@cpr.ku.dk** preferably before April 1st 2010.

For additional information regarding the Center please contact **michael.sundstrom@cpr.ku.dk**.

FACULTY OF HEALTH SCIENCES
UNIVERSITY OF COPENHAGEN

Full Professorships

at the Faculties of Engineering, Science and Medicine, Aalborg University, Denmark

The Faculties of Engineering, Science and Medicine have decided to invest in strengthening their research programs in basic research within selected disciplines, where new ground breaking results could have potentials for being of vital importance for new, smarter and sustainable solutions to globally important problems.

The Aalborg University research environment of today builds on a combination of innovative disciplinary insight and cross disciplinary research interactions. It is enriched and inspired by close networking relations to modern knowledge intensive enterprises and nurse entrepreneurship among the graduate students and the junior research staff.

The purpose of the new professorships is to strengthen the "new type" of university research environment, where basic research interacts closely with solution focused research. The aim is to create breeding ground for shorter time from conceptual breakthroughs to societal and business impact; and at the same time to grow the faculty with even more international level role models for the young researchers. Mutual inspiration comes as an added benefit for the scientists involved as well as the students and the partners.

The positions (position no. 60030) are a part of the Danish Globalisation Programme and are open for appointment beginning June 1st 2010 or soon thereafter for a period of 3-5 years and will be filled in one or more of the following research areas:

ICT Energy Solutions
Physics of Nanomaterials
Energy Storage Technologies
Translational Pain Research
Neurobiology and Motor Learning.

In order to apply for this position, all applicants must read the complete job notice at: http://stillinger.aau.dk/.

Enquiries may be addressed to: Dean, Professor Frede Blaabjerg, by e-mail: fbl@adm.aau.dk or mobile: +45 2129 2454.

Deadline for applications is: April 1st 2010.

The mission of Aalborg University (AAU) is to ensure high quality in research and higher education within the fields of Engineering, Natural Sciences, Medicine and Social and Human Sciences. Leading the way in pedagogical teaching, Aalborg University uses Problem Based Learning (PBL): a unique teaching model close to optimal for the learning process. With an annual budget around DKK 2 billion, more than 15,000 students, 600 Ph.D. students, more than 2,000 employees and strong ties to industry and business life, Aalborg University has established its position as a considerable force within higher research and education both nationally and internationally.

POSITIONS WITHIN BIOINFORMATICS AND SYSTEMS BIOLOGY

Center for Biological Sequence Analysis

Applications are invited for the following positions:

- 4 PhD/postdocs within metagenomics
- 4 PhD/postdocs within disease systems biology and functional human variation
- 1 PhD position within immunological bioinformatics
- 1 research assistant/postdoc within gene expression bioinformatics
- 1 PhD/postdoc within non-coding RNA systems biology
- 1 postdoc within molecular epidemiology
- 1 scientific programmer within molecular epidemiology

The full description of the positions can be found at www.dtu.dk/vacancy. Contact information for each position can also be found here. Other questions can be directed to center administrator Dorthe Kjærsgaard, tel.: +45 45 25 24 80, email: dorthek@cbs.dtu.dk, website: www.cbs.dtu.dk

Application deadline: **1 March 2010**

The Center for Biological Sequence Analysis at DTU was formed in 1993, and conducts basic research in the fields of bioinformatics and systems biology. The center is divided into ten specialist research groups, has a highly multi-disciplinary profile (biologists, biochemists, MDs, physicists, statisticians, and computer scientists) with a ratio of 2:1 of bio-to-nonbio backgrounds. CBS represents one of the large bioinformatics groups in academia in Europe.

DTU is a leading technical university in Europe. Our total staff of 4,500 is dedicated to create value and to promote welfare for the benefit of society through science and technology; and our 6,000 students are being trained to address the technological challenges of the future. While safeguarding academic freedom and scientific independence we collaborate with business, industry, government, public agencies as well as other universities around the world.

Further details: dtu.dk/vacancy

develop international collaborations." Krogsgaard Thomsen of Novo Nordisk agrees, adding, "to be a little bit multicultural, a little bit diverse in your way of thinking, can only help creativity." Aalborg University's Arendt-Nielsen has always recruited from a global pool. "I founded my group 25 years ago with the policy from day one: interdisciplinarity and internationalization." Half of his 80 researchers and 75 Ph.D. students are from outside the country.

According to Prime Minister Løkke Rasmussen, "It is important to attract scientists and specialists from other countries. We have made it easier in recent years to come to Denmark to work or study. The number of foreigners coming to work here has almost tripled since 2001, and the number of international students has doubled. This is a very positive development and a clear indication that Denmark is an attractive place to pursue a career."

"We have a more than century-old tradition of generating successful pharmaceutical companies and conducting clinical trials."
— Ole Frijs-Madsen

Danish Strengths and Challenges

As Denmark looks to the future, several challenges must be met. Knowledge of English is widespread, and English is the official language of the Center for Sensory-Motor Interaction, and the corporate language of Novo Nordisk. However, the default language for many classes and meetings is Danish. Højgaard of the University of Copenhagen says, "When we train people to be bioengineers or doctors in Danish, it's because, well, we're Danish. But that's an obstacle to having a truly international system. We have to acknowledge that English is the language of science, and develop a more bilingual system."

Making improvements in postdoctoral training is another challenge. Danish students complete Master's and Ph.D. projects in different laboratories, and their Ph.D. training includes a period abroad, but professorships do not require postdoctoral experience. Aarhus University's Otzen says, "The idea here is that when you have a Ph.D, you are a fully fledged scientist. But it doesn't matter if you're going into academics or industry, you need to have a postdoc period," which he compares to adolescence, "where you mature and find your feet." Aalborg's Arendt-Nielsen adds, "Over the last 10 years, a lot of money has gone into collaborative Ph.D. projects between universities and industry. It is time for Denmark to also focus on postdoctoral education." Mandrup-Poulsen of the University of Copenhagen advocates mandatory postdoctoral training to qualify for an assistant professorship. He also expresses "concerns about the mismatch between the number of postdoctoral positions relative to the pressure to educate ever more Ph.D.s," and suggests transferring funds from Ph.D. programs to postdoctoral grants.

Inge Mærkedahl, director of the government's Agency for Science, Technology and Innovation, recognizes that "increasing the enrollment of Ph.D. students also increases the need to fund more postdoctoral fellowships." She said that in addition to annual postdoctoral funds from the Danish Council for Independent Research (DFF), a new source of support is the Sapere Aude program. "This comprehensive career program is being launched in 2010 by the DFF, with total funding of approximately $72 million," explains **Linn Hoff Jensen,** head of section at DFF. "In the first year, it expects to fund 45 postdocs and a minimum of 27 associate professors." The program hopes "to enhance the international opportunities for excellent and experienced researchers, both male and female, creating role models to inspire younger researchers."

One of Denmark's strengths is its attractive work environment. **Meineche Schmidt** of Aarhus University says, "The Danish labor market is known for high employment security and flexibility," with good government support during job transitions. "People are reasonably well paid, although the cost of living is also high." The small size of Denmark, with 5.5 million people, is an advantage for networking. Krogsgaard Thomsen of Novo Nordisk says, "People may find it awkward to move here from a big country like the United States, but once they settle down they tend to like it."

Denmark continues to be a leader in "epidemiology, clinical research, and basic research directed at understanding disease mechanisms," according to Mandrup-Poulsen. Celis of the Danish Cancer Society adds, "The environment is especially good for translational research because of the high standards in clinics. And patients like to participate in clinical trials." Another advantage to working in Denmark is 5-6 weeks of paid vacation, although Celis says, "Most of our scientists don't take all the holidays!"

Danish institutions have a flat power structure, stemming from the Jante Law, a social principle that says no one is better than anyone else. The University of Copenhagen's Højgaard says, "There is a straightforward, old Viking attitude that knowledge and competence count more than rank and title." Aalborg University's Arendt-Nielsen agrees, saying, "The only thing that counts is your scientific merits." Combining the Jante Law with a natural pride in Denmark's strengths, Højgaard states, "It's difficult to brag about your own country, but we are doing well in research in Denmark."

Chris Tachibana is a science writer based in Seattle, USA, and Copenhagen, Denmark.
DOI: 10.1126/science.opms.r1000083

WWW.NIH.GOV
Positions @ NIH
THE NATIONAL INSTITUTES OF HEALTH

Scientific Director
National Human Genome Research Institute

The National Human Genome Research Institute (NHGRI), a major research component of the National Institutes of Health (NIH) and the Department of Health and Human Services (DHHS), seeks to identify an outstanding Scientific Director to lead its Division of Intramural Research (DIR; see genome.gov/DIR), located in Bethesda, Maryland. The NHGRI Scientific Director leads a basic and clinical research program that has consistently been at the forefront of scientific innovation, developing a variety of research approaches that have accelerated the understanding of the molecular basis of human disease. The Scientific Director is responsible for an annual budget exceeding $100 million and a staff of ~550. In addition to providing scientific and administrative leadership of this premier research enterprise, the Scientific Director is expected to be an internationally recognized and highly accomplished researcher in genetics and/or genomics.

This position offers a unique and exciting opportunity to develop and implement an overall vision for the NHGRI/DIR that is consistent with the mission and strategic objectives of the Institute. The Scientific Director is responsible for the recruitment and professional development of the NHGRI research faculty. S/he plays a key role in creating and maintaining a nurturing research environment that encourages creativity, collaboration among scientists from different disciplines, effective training of students and postdoctoral fellows, and efficient utilization of common resources. The ability to develop productive interactions among NHGRI investigators, other NIH Institutes, and the research community at large is critical, as is the ability to serve as a spokesperson for NHGRI/DIR research.

Applicants must have an M.D. and/or Ph.D or equivalent degree in the biomedical sciences, as well as a broad knowledge of the field of human genetics and genomics and a compelling vision for the future of the field, including clinical applications. S/he must have proven experience in directing and managing a scientific research program, with well-honed administrative and interpersonal skills to meet the demands of both research and program direction.

Salary is competitive and will be commensurate with the candidate's experience. A full Federal benefit package is available, including retirement, health and life insurance, long-term care insurance, annual and sick leave, and the Thrift Savings Plan (401K equivalent). Appropriate support for an ongoing independent research program will be provided.

Interested applicants should submit a cover letter that includes a brief description of research and administrative experience, a current curriculum vitae and bibliography, names and contact information of five references, and a brief written vision for leading the NHGRI/DIR. Questions about the position and applications themselves should be sent to Ms. Ellen Rolfes via email at ellenr@exchange.nih.gov. All information provided by the candidates will remain confidential and will not be released outside the NHGRI search process without a signed release from the candidate.

Applications will be reviewed starting March 1st, 2010, and will be accepted until the position is filled.

DHHS and NIH are Equal Opportunity Employers and encourage applications from women and minorities.

NATIONAL HUMAN GENOME RESEARCH INSTITUTE Division of Intramural Research
U.S. DEPARTMENT OF HEALTH AND HUMAN SERVICES | NATIONAL INSTITUTES OF HEALTH | genome.gov/DIR

Department of Health and Human Services
National Institutes of Health
Deputy Director of NIH
Division of Program Coordination, Planning, and Strategic Initiatives

The Office of the Director (OD), National Institutes of Health (NIH) in Bethesda, Maryland, is seeking a Director of the newly created Division of Program Coordination, Planning, and Strategic Initiatives (DPCPSI). Exceptional candidates with the scientific vision to identify innovative, high impact science and the ability to integrate research across traditional disciplines are encouraged to apply.

The DPCPSI Director will serve as a Deputy Director of the NIH and report to the NIH Director. The primary responsibilities of the Division are to (1) develop innovative, high-risk high-reward initiatives that will have national and international impact, supported by the NIH Common Fund; (2) advise the NIH Director on issues involving trans-NIH planning, analysis, implementation, performance assessment, and evaluation activities; (3) develop and conduct scientific analyses relevant to NIH research portfolio analysis; and (4) coordinate the activities of the DPCPSI Program Offices (Office of AIDS Research; Office of Research on Women's Health; Office of Behavioral and Social Sciences Research; Office of Disease Prevention; and Office of Strategic Coordination) to maximize their collective impact and to ensure that their efforts are aligned with the mission of NIH.

The DPCPSI Director will exercise leadership, initiative, and creativity in establishing and maintaining relationships with key Federal and non-Federal officials, nationally and internationally recognized scientific leaders and officials of academic, research, and other institutes and organizations, and professional and advocacy groups.

Salary is commensurate with experience; a full package of benefits (including retirement, health, life, long term care insurance, Thrift Savings Plan participation, etc.) is available.

A Search Committee chaired by Drs. Katherine Hudson and Lawrence Tabak will review applications for this position. A detailed vacancy announcement that includes mandatory qualifications requirements, and application procedures may be obtained at NIH's Executive Jobs site: **http://www.jobs.nih.gov/vacancies/executive.htm, or by calling Regina Reiter at (301) 402-1130**. Interested applicants must send a Curriculum Vitae, Bibliography, a Vision Statement, and responses to the qualifications requirements, electronically, to **Ms. Regina Reiter, at SeniorRe@OD.NIH.GOV, 301-402-1130.** If you need additional information, please contact **Ms. Reiter at 301-402-1130**.

Applications must be received by close of business March 8, 2010.

DHHS and NIH are Equal Opportunity Employers

UMASS AMHERST

2 Tenure-Track Assistant Professor Positions in Biophysics:

Biology Department - Cellular Biophysics
Physics Department - Biological Physics

The University of Massachusetts Amherst invites applications for two tenure-track Assistant Professor positions to be hired as a cluster in Biophysics to start as soon as September 1, 2010. One position will be in the Biology Department, in Cellular Biophysics; the other will be in the Physics Department, in Biological Physics. We seek individuals with outstanding research, a strong commitment to teaching, and the potential to develop and maintain an extramurally funded research program. A Ph.D. and postdoctoral experience are required. Evaluation of applications for both positions will begin on February 15, 2010 and continue until the positions are filled. Positions will be filled contingent upon University funding.

Assistant Professor of Biology. The Biology Department (www.bio.umass.edu) seeks a well-trained biologist who employs biophysical techniques to study cellular or tissue function. Research areas might include, but are not limited to, the investigation of biophysical properties of excitable cells, including membrane biophysics. Electrophysiological approaches that are combined with imaging and/or genetic techniques are of particular interest. The successful candidate would have a primary appointment in the Biology Department and would interact with a growing number of biophysics research groups across campus. The UMass Amherst Biology Department provides a broad and interactive research environment, with faculty research spanning all levels of biological organization. Especially strong research clusters focus on Neural Development, Cell Biology, Plant Biology, Functional Morphology, and Evolution. **Application materials should include a curriculum vita, research plan, teaching statement and 3 letters of recommendation. Paper applications can be sent to: Biology Biophysics Search #R38398, Biology Department, Attn: Karen Nelson, 611 North Pleasant Street, University of Massachusetts, Amherst, MA 01003. Alternatively, application materials may be sent via email to Bio-BiophysicsSearch@bio.umass.edu**

Assistant Professor of Physics. The Physics Department (www.physics.umass.edu) is committed to expanding its Biological Physics group, which currently includes three faculty members and substantial newly renovated laboratory space and facilities. The Department also has a strong condensed matter group, with emphasis on both hard and soft matter. We seek a physicist who will employ the methods and ideas of physics to investigate biological systems and processes. The research area should complement ongoing work in the department and have synergy with biophysics research groups in the Biology, Biochemistry and Molecular Biology, and/or Chemistry Departments. The Physics Department currently has programs in single molecule imaging and manipulation, the dynamics of molecular motors and the cytoskeleton, membrane biophysics, and investigation of forces between biomolecules. **Applicants should submit a letter of application, a CV, and a statement of research and teaching, as well as arranging to have three letters of reference sent to: Biological Physics Search, #R36982, Physics Department, 710 North Pleasant St., University of Massachusetts, Amherst, MA 01003. Alternatively, application materials may be sent to search@physics.umass.edu**

The University is part of the Five-College Consortium (www.fivecolleges.edu) in the Pioneer Valley in western Massachusetts, two hours from Boston and three hours from New York City. The University provides an intellectual environment committed to providing academic excellence and diversity including mentoring programs for faculty. The College of Natural Sciences and the Physics and Biology Departments are committed to increasing the diversity of the faculty, student body and the curriculum. We strongly encourage women and members of minority groups to apply. The University of Massachusetts is an Affirmative Action/Equal Opportunity Employer.

THE UNIVERSITY OF HONG KONG
香 港 大 學

Founded in 1911, The University of Hong Kong is committed to the highest international standards of excellence in teaching and research, and has been at the international forefront of academic scholarship for many years. Ranked 24th among the top 200 universities in the world by the UK's *Times Higher Education*, the University has a comprehensive range of study programmes and research disciplines spread across 10 faculties and about 100 sub-divisions of studies and learning. There are over 23,400 undergraduate and postgraduate students coming from 50 countries, and more than 1,200 members of academic and academic-related staff, many of whom are internationally renowned.

Assistant Professor in the Department of Pharmacology and Pharmacy (Ref.: RF-2009/2010-328)

Applications are invited for appointment as Assistant Professor in the Department of Pharmacology and Pharmacy, from November 2010 or as soon as possible thereafter, on a three-year fixed-term basis, with the possibility of renewal. The appointee who has demonstrated sustained strong performance will be considered for tenure after satisfactory completion of a second fixed-term contract.

Applicants should possess a Ph.D., Pharm.D. or an equivalent qualification; and have teaching experience in Pharmacology and pharmacy practice at the undergraduate and/or postgraduate levels. Those with working experience in curriculum planning in tertiary education and a good track record in research and scholarly activities would have an advantage. The appointee will contribute to teaching and the curriculum development of the pharmacy programme. He/She is expected to establish a research programme in an area complementary to the major research interest in Vascular Biology of the Department. Further information about the Department can be obtained at http://www3.hku.hk/pharma/current/.

Annual salary for Assistant Professorship will be in the range of HK$504,480 – 779,640 (approximately US$1 = HK$7.8) (subject to review from time to time at the entire discretion of the University). At current rates, salaries tax does not exceed 15% of gross income. The appointment will attract a contract-end gratuity and University contribution to a retirement benefits scheme, totalling up to 15% of basic salary, as well as leave, and medical/dental benefits. Housing benefits will be provided as applicable.

Further particulars and application forms (152/708) can be obtained at http://www.hku.hk/apptunit/; or from the Appointments Unit (Senior), Human Resource Section, Registry, The University of Hong Kong, Hong Kong (**fax** (852) 2540 6735 or 2559 2058; **e-mail**: senrappt@hku.hk). **Closes March 15, 2010**. Candidates who are not contacted within 3 months of the closing date may consider their applications unsuccessful.

The University is an equal opportunity employer and is committed to a No-Smoking Policy

---

Albert-Ludwigs-Universität Freiburg

UNI FREIBURG

The University of Freiburg invites applications for the

Research Group Programme – Call for Proposals 2010

The University of Freiburg **(www.unifreiburg.de)** has been awarded for its institutional research strategy by the German Excellence Initiative. As part of this strategy, the Research Group Programme provides funding for frontier research in emerging research areas. With this programme the University of Freiburg intends to establish two new research groups in autumn 2010 and invites applications of highly qualified young investigators at postdoctoral level. Project proposals in all fields of research are eligible. Disciplines or research areas that are not yet represented at the Freiburg Institute for Advanced Studies (www.frias.uni-freiburg.de) will receive special attention. Future research should broaden and further strengthen existing research portfolios at the University of Freiburg and enhance the linkages to national and international research institutions and facilities. We are looking for young external candidates who have completed their doctoral studies with distinction and who have already demonstrated exceptional ability in research with an outstanding track record. The successful applicant is expected to build a strong junior research group and be experienced in acquiring external funding. Applications of highly qualified female researchers are particularly welcome. The group leader shall be appointed assistant professor ("W1 Juniorprofessur") with tenure track option. A successful female candidate can be offered the Bertha-Ottenstein-Professorship, in recognition of the first woman who earned professorial lecturing qualification in Freiburg. Funding of the research group will be provided by means of the German Excellence Initiative. The initial appointment will be for four years and can be extended to six years following successful evaluation. Applications including a cover letter, research proposal with envisaged local collaborators and institutions (15 pages maximum including an executive summary), a curriculum vitae with publication record, a description of prior research and research interests, as well as details of experience and interest in outreach should be sent directly to **RG2010.ResearchGroupProgramme@pr.uni-freiburg.de.** Applicants should also arrange for two or three references sent to the same address. Informal enquiries relating to this post may be directed to Dr. Frank Krüger, Science Support Centre **(info.ResearchGroupProgramme@pr.unifreiburg.de).**

Closing date for applications and references is 28 February 2010. Interviews will be held over 1 and 2 June 2010. Further information will be available at

http://www.uni-freiburg.de/universitaet-en/exzellenz/exzellenzinitiative-en.

ETH

Eidgenössische Technische Hochschule Zürich
Swiss Federal Institute of Technology Zurich

Professor or Assistant Professor (Tenure Track) of Observational / Experimental Astrophysics

The Institute for Astronomy at ETH Zurich (www.phys.ethz.ch) invites applications for a professorship in Observational/Experimental Astrophysics. The new professor is expected to develop an outstanding research program in observational or experimental astrophysics, which may include the leadership of observational programs on major facilities, the development of advanced instrumentation, or the phenomenological modeling of data. The primary criterion is either demonstrated or potential excellence in research and teaching, rather than a particular scientific field. The Chair comes with sufficient resources to establish a significant research group. Teaching responsibilities include courses in introductory physics and more advanced courses in astrophysics. The new professor will be expected to teach undergraduate level courses (German or English) and graduate level courses (English).The appointment will be at a level commensurate with experience.

Assistant professorships have been established to promote the careers of younger scientists. The initial appointment is for four years with the possibility of renewal for an additional two-year period and promotion to a permanent position.

Please submit your application together with a curriculum vitae and a list of publications and a brief statement of present and future research interests **to the President of ETH Zurich, Prof. Dr. Ralph Eichler, ETH Zurich, Raemistrasse 101, 8092 Zurich, Switzerland (or via e-mail to faculty-recruiting@sl.ethz.ch), no later than April 30, 2010**. With a view toward increasing the number of female professors, ETH Zurich specifically encourages qualified female candidates to apply.

Grant opportunities for Russian scientists living abroad

The Federal Agency of Science and Innovation of Russia is inviting members of the Russian scientific diaspora to participate in Federal Program "Human capital for science and education in innovative Russia". Russian scientists living abroad and willing to direct research projects of resident Russian scientific groups are invited to take part in a grant competition for the 2010-2011 round of the Program.

For more information, please consult the Agency site **http://fcpk.ru.**

Questions regarding the Program can be directed to **Dr. Dmitry Bugreev at: dbugreev@inkk.ru, +7-495-951-79-10.**

UNIVERSITY OF OXFORD

www.ox.ac.uk/jobs

Post Doctoral Research Assistant in Tropical Carbon Dynamics,

Junior Research Fellowship in Tropical Forest Science, Oriel College

£28,839 - £30,594 p.a.

School of Geography and the Environment, Environmental Change Institute

Applications are invited for a post-doctoral research associate to work on implementing studies of carbon allocation and cycling at forest sites across the Amazon and Andes region. This is a 30 month contract commencing March 2010 or soon thereafter, based at ECI, School of Geography and the Environment, University of Oxford.

The post involves close collaboration with partners in the University of Umea (Sweden), University of Leeds, and across South America, including fieldwork to conduct long-term studies of above and below ground productivity, autotrophic respiration and microclimate at six sites across the Amazon Basin (in Peru, Bolivia and Brazil).

A PhD in a quantitative environmental science, experience of tropical forest fieldwork, proficiency in Spanish or Portuguese, or ability to become proficient, excellent field leadership, high level of organisation, self-discipline, communication and mentoring skills are essential.

For further information see **http://www.geog.ox.ac.uk/news/jobs/** or contact the HR Office on tel: 01865 285082. For informal enquiries, contact Prof Yadvinder Malhi (yadvinder.malhi@ouce.ox.ac.uk).

Closing date: 12 February 2010. Interviews in late February 2010.

Committed to equality and valuing diversity

UNIVERSITY OF OXFORD

www.ox.ac.uk/jobs

University Lecturer in Conservation Biology

Mathematical, Physical and Life Sciences Division

Department of Zoology in association with Somerville College

The Department of Zoology proposes to appoint a University Lecturer in Conservation Biology with effect from 1 September 2010 or as soon as possible thereafter. The successful candidate will be offered a Tutorial Fellowship by Somerville College, under arrangements described in the further particulars. The combined University and College salary will be on a scale up to £56,917 per annum. The College will provide an additional housing allowance of £7,100 per annum.

The successful candidate will have a strong background in conservation biology, including a doctorate (PhD or equivalent) in a cognate area. Duties of the post are to lead a research programme and research group in conservation biology; to give undergraduate lectures and tutorials; and to carry out examining and administrative duties in the Department and the College.

Informal enquiries can be sent to paul.harvey@zoo.ox.ac.uk

Further particulars can be downloaded from **http://www.zoo.ox.ac.uk/jobs** or are available from the Personnel Office,Department of Zoology, South Parks Road, Oxford OX1 3PS, telephone: 01865 271190, e-mail: recruit@zoo.ox.ac.ukApplications, together with a CV and contact details of three referees, should be sent to the above address quoting reference number AT09043. The closing date for receipt of applications is 15 February 2010.

Committed to equality and valuing diversity

PRINCETON Neuroscience INSTITUTE

C V Starr Foundation Fellowships in Neuroscience

The Princeton Neuroscience Institute (PNI) at Princeton University is looking to fill one or two CV Starr Fellowships in Neuroscience. PNI is a newly formed unit at Princeton that focuses on interdisciplinary research in neuroscience, spanning from molecular, cellular and genetic approaches to systems and human cognitive neuroscience. PNI houses state of the art facilities for experimental research in all of these areas, as well as advanced computational resources that support its emphasis on theoretical and quantitative approaches to neuroscience.

PNI aims to recruit and support one or two exceptional individuals who are expecting or have recently obtained a PhD degree in neuroscience or areas relevant to neuroscience (molecular biology, psychology, computer science, engineering, physics, or mathematics).

The program provides a generous salary and an annual research budget. Fellows are not expected to apply for outside funding. Independent research is typically carried out under the mentorship of one or more core faculty members in the Institute, although those who wish to pursue a specific independent research program will also be considered.

For more information about the Institute, see **http://www.princeton.edu/neuroscience/**.

Applications should be submitted online at **http://jobs.princeton.edu** under Req **#0900612**. Candidates must submit a CV, a list of publications, a statement of research interests and goals, and the contact information for three references. References will be contacted directly. Finalists will be invited to Princeton to present a talk concerning their current research.

Princeton University is an Equal Opportunity Employer and complies with applicable EEO and Affirmative Action regulations. For general application information and how to self identify, see http://www.princeton.edu/dof/ApplicantsInfo.htm.

Director, Climate and Environmental Sciences Division, Office of Biological and Environmental Research, Office of Science, U.S. Department of Energy

The U.S. Department of Energy, Office of Science, Office of Biological and Environmental Research (BER), is seeking a Director of the Climate and Environmental Sciences Division. BER advances world-class biological, climatic, and environmental research programs and scientific facilities for DOE mission needs in energy, environment, and basic research. The Climate and Environmental Sciences Division supports a broad research portfolio in multidisciplinary and interdisciplinary science including atmospheric systems research, environmental system science, and climate and Earth system modeling. The Division Director also supports two state-of-the-art scientific user facilities: the Atmospheric Radiation Measurement Climate Research Facility and the Environmental Molecular Sciences Laboratory. The Director leads a group of 15 program managers and support staff with a budget of over $250 million. The Director is involved in strategic planning, multi-year program planning and implementation, and budgeting. The position is within the Senior Executive Service, with a salary range of $117,787 to $177,000.

The job announcement, which closes **February 23, 2010**, is advertised as either a biologist or a physical scientist. For further information about this position and the instructions on how to apply and submit an application, please go to the following urls:

Physical Scientists and Engineers should apply at the following url:
http://jobview.usajobs.gov/GetJob.aspx?JobID=85147660&JobTitle=Director%2c+Climate+and+Environmental+Sciences+Division&q=09-SES-SC-HQ-001+(cg)&sort=rv%2c-dtex&cn=&rad_units=miles&brd=3876&pp=50&jbf565=1&vw=d&re=134&FedEmp=N&FedPub=Y&caller=ses.aspx&AVSDM=2009-12-16+00%3a03%3a00

Biologists and Ecologists should apply at the following url:
http://jobview.usajobs.gov/GetJob.aspx?JobID=85147678&JobTitle=Director%2c+Climate+and+Environmental+Sciences+Division&q=09-SES-SC-HQ-002+(cg)&sort=rv%2c-dtex&cn=&rad_units=miles&brd=3876&pp=50&jbf565=1&vw=d&re=134&FedEmp=N&FedPub=Y&caller=ses.aspx&AVSDM=2009-12-16+00%3a03%3a00

It is imperative that you follow the instructions as stated on the announcement (**09-DE-SC-HQ-065 (cg)**). To be considered for this position, you must apply online.

Washington University in St. Louis

Multiple Tenure-track/Tenured Faculty Positions

The Department of Computer Science and Engineering (CSE) and the School of Medicine (WUSM) are jointly searching for multiple tenure-track faculty members with outstanding records of computing research and a serious interest in collaborative research on problems related to biology and/or medicine. Appointments may be made wholly within CSE or jointly with the Departments of Medicine, Genetics, or Pathology and Immunology.

CSE and WUSM have a long-term strategic commitment to integrating computing and science. As part of that commitment, we expect to make synergistic hires with a combined research portfolio spanning the range from fundamental computer science/engineering to applied research focused on science or medicine. Specific areas of interest include, but are not limited to:

- Analysis of complex genetic, genomic, proteomic, and metabolomic datasets;
- Algorithms for statistical genetics including genome-wide association studies;
- Molecular systems biology and pathway/network modeling;
- Databases or data mining applied to medical records;
- Natural language processing with the potential for biomedical applications;
- Computer engineering with applications to medicine or the natural sciences;
- Wireless sensor networks with medical applications;
- Visualization with the potential for biomedical applications;
- Theory/Algorithms with the potential for biomedical applications;
- All areas of medical informatics, clinical or public-health informatics;
- All areas of computational biology and biomedical informatics

These positions will continue a successful, ongoing strategy of collaborative research between CSE and the School of Medicine, which is consistently ranked among the top 3 medical schools in the United States. CSE seeks to build on and complement its strengths in biological sequence analysis, biomedical image analysis, and biomedical applications of novel computing architectures.

Washington University is a private university with roughly 6,000 full-time undergraduates and 6,000 graduate students. It has one of the most attractive university campuses anywhere and is adjacent to one of the nation's largest urban parks, in the heart of a vibrant metropolitan area. St. Louis is a wonderful place to live, providing access to a wealth of cultural and entertainment opportunities without the everyday hassles of the largest cities.

We anticipate appointments at the rank of Assistant Professor; however, in the case of exceptionally qualified candidates appointments at any rank may be considered. Applicants must have a Ph.D. in computer science, computer engineering, electrical engineering, biomedical engineering, computational biology, biomedical informatics, statistical genetics, or a closely related quantitative field and a record of excellence in teaching and research appropriate to the appointment level. The selected candidate is expected to build an externally-supported research program, teach and mentor students at the graduate and undergraduate levels, and foster interdisciplinary interactions with colleagues throughout the university. Candidates who would contribute to enhancing diversity at the departmental and university levels are strongly encouraged to apply. Applications from academic couples are welcomed and encouraged.

Qualified applicants should submit a complete application (cover letter, curriculum vitae, research statement, teaching statement, and names of at least three references) electronically by following the directions provided at **http://cse-wusm-faculty-search.wustl.edu**. Other communications may be directed to **Prof. Michael Brent, Department of Computer Science and Engineering, Campus Box 1045, Washington University, One Brookings Drive, St. Louis, MO 63130-4899**.

Applications submitted before **January 31, 2010** will receive full consideration.

Washington University is an Equal Opportunity/Affirmative Action Employer.

EVMS
Eastern Virginia Medical School

Scientific Director—Glennan Center for Geriatrics and Palliative Care

EVMS seeks applications for the position of Scientific Director of the Glennan Center for Geriatrics and Palliative Care with a faculty appointment in the Department of Internal Medicine at the level of associate professor or professor. Candidates should have an MD or PhD degree, must have demonstrated excellence in research and possess exceptional leadership qualities. The Director will have the opportunity to lead a prominent center, emphasizing excellence in research and teaching related to aspects of aging and palliative care. EVMS is undergoing a significant expansion in the areas of basic and translational research. There are significant resources available, including excellent laboratory space, an endowed professorship, and other support for the program.

The Glennan Center for Geriatrics and Palliative Care has gained national and international recognition for excellence in immunology, driving and cognition in the context of aging research. The program is ranked in the top 50 in the latest US News and World Report ranking. The Center is also a leader in clinical care, providing innovative services to meet the special health care needs of older adults across a full range of practice settings from independent living to assisted living, long-term care, palliative care, and hospital care. The Center offers a comprehensive program for clinicians and scientists that provide training in geriatrics, palliative care and gerontology for medical students, residents, fellows, other health care professionals and junior faculty members. Excellent collaboration is available with the basic science departments and affiliated Universities in the region.

Eastern Virginia Medical School is located in coastal southeastern Virginia in the nation's 27th largest metropolitan statistical area. The region offers premier waterfront communities, large beaches, excellent golf, tennis, sailing and other recreational opportunities, and top ranked schools.

Please send a letter of interest including current curriculum vitae to the Executive Search Committee by e-mail at **execcomm@evms.edu**.

AA-EOE.

SYNTHETIC BIOLOGY POSTDOCTORAL FELLOWSHIP (SBPF)

Nanyang Technological University

University of California, Berkeley

NANYANG TECHNOLOGICAL UNIVERSITY

Nanyang Technological University and University of California, Berkeley are jointly offering Synthetic Biology Postdoctoral Fellowship (SBPF) to outstanding graduate research scientists at postdoctoral level to support their full-time research efforts. SBPF provides a unique educational and research opportunity for highly qualified, doctoral scientists to advance their scholarship in synthetic biology at Nanyang Technological University, and in Professor Jay Keasling's laboratory at University of California, Berkeley (**http://cheme.berkeley.edu/faculty/keasling**). Upon successful completion of the program, outstanding fellows may be considered for a tenure-track faculty position at the School of Chemical and Biomedical Engineering, Nanyang Technological University.

Synthetic biology is the engineering and manipulation of microorganisms to contain multiple genes so as to enable them to work together for the production of a desired product. Compared to synthetic chemistry, synthetic biology can potentially produce a chemical, such as a drug, much more quickly, in few steps, economically and with less toxic waste products. Synthetic biology is envisioned to be able to produce myriad compounds applicable such as drugs, biofuels, smart biomaterials, implantable continuous biosensors, and therapeutic vectors. In particular, SBPF's research projects will focus on, but not limited to, engineering microbes to produce valuable fuels and developing foundational tools for synthetic biology.

The fellowships are tenable for up to 3 years. Successful applicants will be offered attractive remuneration packages. Airfare and additional subsistence allowance will be provided during the research attachment at University of California, Berkeley. The fellowships are awarded based on previous academic and research accomplishments.

Interested, qualified applicants are invited to fill out the application form obtainable from **http://www.ntu.edu.sg/ohr/Career/CurrentOpenings/ResearchOpenings/Documents/Researchform.doc**. The completed application form with detailed curriculum vitae, sample research publications, supporting documents (e.g. degree certificates and transcripts), and three references may be submitted by email to:

Professor Chi Bun Ching
Nanyang Technological University
School of Chemical and Biomedical Engineering
Block N1.2-1-10, 62 Nanyang Drive, Singapore 637459
Email: CBChing@ntu.edu.sg
Phone: +65-6790-6731
Fax: +65-6794-9220

www.ntu.edu.sg

The University of Massachusetts Amherst

The Department of Microbiology invites applications from Ph.D.-level scientists for **a tenure-track position at the level of ASSISTANT PROFESSOR**. We seek candidates taking innovative approaches related to basic and applied microbiology. We are particularly interested in candidates that complement ongoing programs within The Institute of Massachusetts Biofuels Research (TIMBR) and the Institute of Cellular Engineering (ICE), an interdisciplinary group of biologists, chemists and engineers focused on renewable energy. The successful candidate will have access to students from several interdepartmental graduate programs, training grants and will participate in teaching at both undergraduate and graduate levels.

Applicants should send a curriculum vitae, a statement of research and teaching interests, reprints of recent publications, and at least three letters of recommendation to:

Chair of Microbiology Search Committee
Department of Microbiology
University of Massachusetts
N203 Morrill IV North
Amherst, MA 01003
microbio-dept@microbio.umass.edu

The search committee will begin reviewing applications on **March 1, 2010** and will continue until the position is filled. Hiring is contingent upon the availability of funds. The Five College Consortium, comprised of Smith College, Amherst College, Mount Holyoke College, Hampshire College, and the University of Massachusetts Amherst, provides an intellectual environment committed to providing academic excellence and diversity including mentoring programs for faculty. The College and the Department are committed to increasing the diversity of the faculty, student body and the curriculum.

The University of Massachusetts is an Affirmative Action/ Equal Opportunity Employer. Women and members of minority groups are encouraged to apply.

NIMS ICYS

Research Position at ICYS, NIMS, Japan

The International Center for Young Scientists (ICYS) of the National Institute for Materials Science (NIMS) is now seeking a few researchers. Successful applicants are expected to pursue innovative research on broad aspects of materials science using most advanced facilities in NIMS **(http://www.nims.go.jp/eng/index.html).**

In the ICYS, we offer a special environment that enables young scientists to work independently based on their own idea and initiatives. All management and scientific discussions will be conducted in English. An annual salary between 5.03 and 5.35 million yen (level of 2009) will be offered depending on qualification and experience. The basic contract term is two years and may be renewed to one additional year depending on the person's performance. A research grant of 2 million yen per year will be supplied to the ICYS researcher.

All applicants must have obtained a PhD degree within the last ten years. Applicants should submit an application form, which can be downloaded from our web site, together with a resume (CV) and a list of publications. A research proposal on an interdisciplinary or integrated area related to the materials science should also be submitted. The application letter should reach the following address via e-mail or air mail by March 31, 2010. Visit our website for more details **(http://www.nims.go.jp/icys/newicys/).**

ICYS Administrative Office,
National Institute for Materials Science
Sengen 1-2-1, Tsukuba, Ibaraki 305-0047, Japan
E-mail: **icys-recruit@nims.go.jp**

Postdoctoral Fellowships Available

The Lombardi Comprehensive Cancer Center at Georgetown University, a multidisciplinary NCI-designated cancer research center, is currently recruiting postdoctoral fellows into positions funded by an NCI training grant. The goal is to develop strong basic and translational scientists with an interest in cancer research. Successful applicants will choose a mentor from an interdisciplinary group of investigators who are committed to cancer research. Research programs include:

- The role of growth factor signal pathways
- The development of hormone and drug insensitivity
- The genetic and molecular mechanisms of malignant progression
- Invasion metastasis angiogenesis
- Stem cells in cancer
- Development of novel immunological and anticancer therapies
- The etiology of cancer, biomarkers, and molecular epidemiology
- Bioinformatics and cancer

Go to **http://lombardi.georgetown.edu/education/TBio/postdoc.html** for further information.

Salary is competitive and commensurate with qualifications and experience. Applicants should send curriculum vitae, a short statement of research interests and career goals, and the names and addresses of three references to **Karen Shepherd** at **bivinsk@georgetown.edu**.

Minorities and women are strongly encouraged to apply. US citizenship or permanent residency is required.

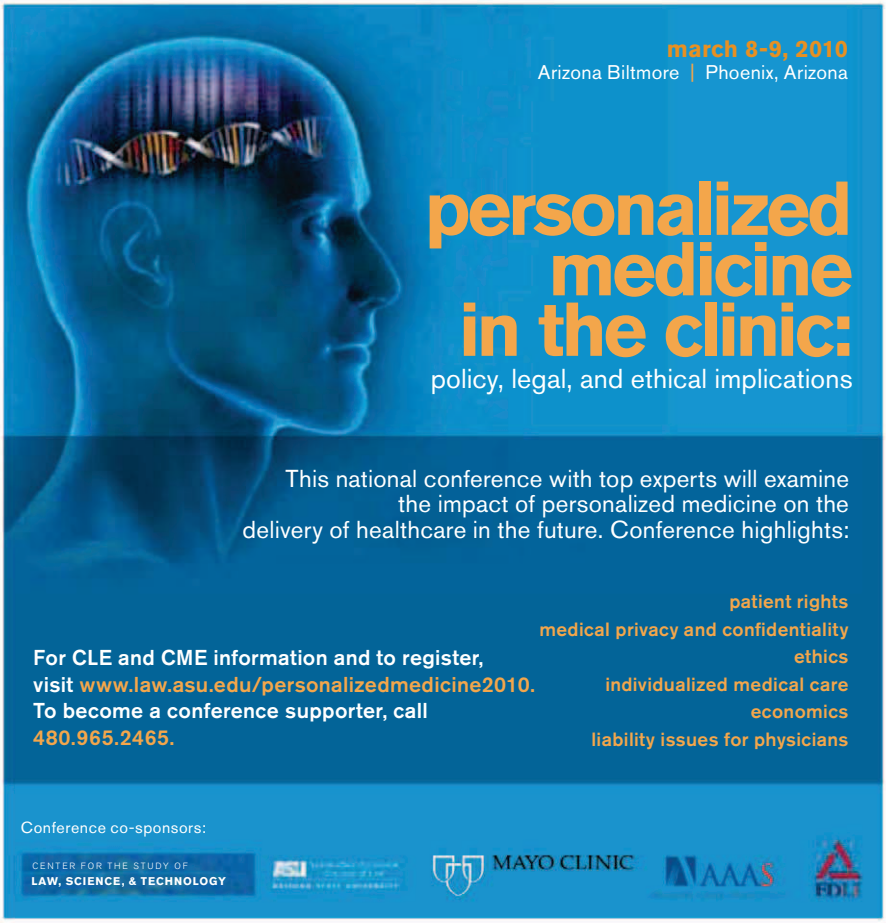

LONDON SCHOOL OF HYGIENE & TROPICAL MEDICINE

Director of the School

The London School of Hygiene & Tropical Medicine is seeking to appoint a Director, the head of the institution, in succession to Professor Sir Andrew Haines.

The mission of the School, an independent UK Higher Education Institution, is to contribute to the improvement of health worldwide through the pursuit of excellence in research, postgraduate teaching, and advanced training in national and international public health and tropical medicine, and through informing policy and practice in these areas.

The Director is the Chief Executive Officer of the School and is responsible to the Council for its academic, financial and administrative affairs. The School is enjoying a period of particular success with its research and teaching programmes attracting international accolade for their breadth, depth and quality. The Council is seeking to identify an outstanding candidate with the ability to develop strategy and gain support for its implementation, and with the capacity and vision to provide energetic leadership in a global institution in a challenging health-related higher education environment. They will have experience of successful management at a senior level and an internationally recognised academic record.

Detailed information about this position, the School and application requirements may be obtained from the Secretary & Registrar, London School of Hygiene & Tropical Medicine, Keppel Street London WC1E 7HT; telephone +44 (0)20 7927 2277; fax: +44 (0)20 7636 7679; e-mail: ruth.kipling@lshtm.ac.uk to whom applications should be submitted by Friday **12 February 2010**. The reference for this post is **TL-1**.

The London School of Hygiene & Tropical Medicine is committed to being an equal opportunities employer.

LMU LUDWIG-MAXIMILIANS-UNIVERSITÄT MÜNCHEN — GENE CENTER MUNICH

The Gene Center and the Department of Biochemistry at the University of Munich (LMU) invite applications for the position of a

W2-Professorship for Biochemistry (tenure-track, initially for 6 years)

Candidates must have an outstanding record of internationally recognized research accomplishments in Cellular Biochemistry, ideally with a research emphasis on the molecular mechanism of genome expression and maintenance in S. cerevisiae. The research group is expected to contribute to the establishment of molecular systems biology at the LMU and to participate in the national cluster of excellence „Center for Integrated Protein Science Munich" (CIPSM).

Candidates are expected to conduct an independent research program that complements existing research efforts, to obtain extramural funding, and to participate in the innovative teaching program of the Center (lectures may be given in English). Primary selection criteria are research excellence, teaching ability and potential for scientific interactions. The Gene Center offers a stimulating and interdisciplinary research environment, and is committed to expand the research focus in the above area.

The tenure-track position is initially for six years and can be converted to tenure pending a positive evaluation after a minimum of three years. In exceptional cases, a tenured position can be offered directly.

The University of Munich seeks to increase the participation of women in research and teaching and invites qualified women to apply. The LMU offers a Dual Career Service. Handicapped candidates with identical qualifications will be given preference.

Applicants should submit a curriculum vitae including a list of publications, a research summary with up to five relevant publications, and a summary of teaching activities in printed form before February 15, 2010 to:
Dekan der Fakultät für Chemie und Pharmazie, Prof. Dr. Martin Biel, Ludwig-Maximilians-Universität, Butenandtstr. 5-13, 81377 Munich, Germany

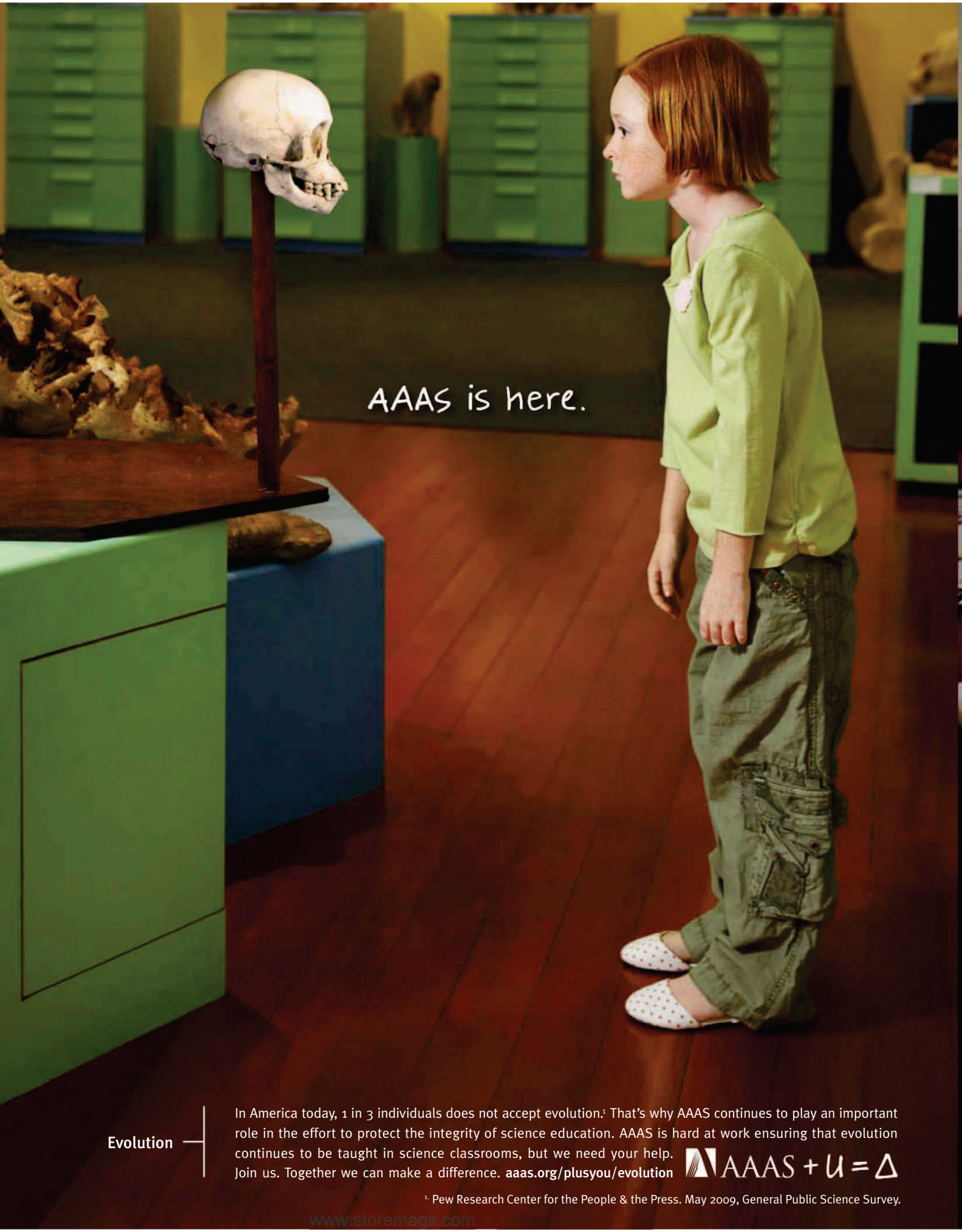

Evolution

In America today, 1 in 3 individuals does not accept evolution.[1] That's why AAAS continues to play an important role in the effort to protect the integrity of science education. AAAS is hard at work ensuring that evolution continues to be taught in science classrooms, but we need your help. Join us. Together we can make a difference. **aaas.org/plusyou/evolution**

AAAS + U = Δ

[1] Pew Research Center for the People & the Press. May 2009, General Public Science Survey.

HBCU-UP National Research Conference

Historically Black Colleges and Universities (HBCUs) increase the number of underrepresented ethnic minorities qualified for education and research in science, technology, engineering, and mathematics (STEM). AAAS partners with NSF to host a national gathering that highlights undergraduate student research to enhance the quality of STEM education. And this is just one of the ways that AAAS is committed to advancing science to support a healthy and prosperous world. Join us. Together we can make a difference. **aaas.org/plusyou/hbcuup**

AAAS + U = Δ

AWARDS

HUMAN FRONTIER SCIENCE PROGRAM (HFSP)

CALL FOR NOMINATIONS FOR THE 2010 HFSP NAKASONE AWARD

In keeping with its mission to stimulate innovative international research, HFSP invites nominations for a new annual award highlighting frontier contributions in the life sciences. This award recognizes the vision of former Prime Minister Nakasone of Japan in the creation of HFSP. Typically these will be conceptual breakthroughs for investigating the complex mechanisms of living organisms which have important consequences for scientists throughout the world. Both theoretical and methodological contributions are eligible.

This is an open competition, not limited to HFSP awardees and there is no age limit for candidates. However the jury will pay particular attention to recent breakthroughs by younger scientists. Two or more investigators may be nominated jointly if the breakthrough resulted from their close collaboration. Nominations should be made before March 1st 2010 via the HFSP website using the standard one-page nomination form (download from http://bit.ly/4Oxjgz). After an initial selection by the HFSP Council of Scientists, the final decision will be made by a prestigious Award Committee (membership to be announced later on the website).

The winner of the award will receive an unrestricted research grant of 10.000 USD, a commemorative medal and will be expected to deliver a plenary lecture at the HFSP annual awardees meeting (in Kerala, India from November 1st to 3rd, 2010).

Please see our web site www.hfsp.org for further information

HFSPO, 12 quai Saint-Jean, 67080 STRASBOURG Cedex, FRANCE

STaR SEARCH

Congratulations to the Awardees

Professor H. Phillip Koeffler
Department of Medicine,
Yong Loo Lin School of Medicine,
National University of Singapore

Professor H. Phillip Koeffler's cancer research endeavours to identify unique genomic abnormalities of selected Asian cancers, and to explore the biologic and clinical significance of PAX5 deletions, mutations and fusion products in acute leukaemia.

Professor David Bruce Matchar
Duke-NUS Graduate Medical School Singapore

Professor Matchar's research relates to clinical practice improvement - from the development of clinical policies to their implementation in real world clinical settings. His work covers a broad range of clinical issues including cardiovascular disease, disabling neurological disorders such as stroke and dementia, and oncology.

Professor Teh Bin Tean
National Cancer Centre Singapore

A leading kidney cancer research scientist, Professor Teh Bin Tean is working on setting up a hereditary cancer clinic and a molecular diagnostics laboratory in National Cancer Centre Singapore. He is also helping to establish key regional and international collaborations that will enhance the status of Singapore as the regional hub for translational cancer research.

Professor Daniel G. Tenen
Cancer Science Institute of Singapore,
National University of Singapore

A world-renowned cancer research scientist, Professor Daniel Tenen is researching to devise an effective and safe in vivo gene delivery system targeting hematopoitetic stem/progenitor cells that have wide applicability in treating leukaemias and lymphomas. If successful, it will be a breakthrough in stem cell cancer research.

Professor Michael Chee Wei-Liang
Duke-NUS Graduate Medical School Singapore

Professor Michael Chee investigates the functional imaging correlates of cognitive changes in acutely sleep-deprived adults. He seeks to identify cognitive vulnerabilities as well as to why some persons are susceptible to sleep deprivation. He also contributes to efforts to characterise cognitive aging in Asians and supports a flagship project on persons at high-risk of conversion to schizophrenia.

Professor David M. Virshup
Duke-NUS Graduate Medical School
Singapore

A leading researcher in cell signaling, Professor David Virshup studies regulatory proteins that control cell growth and development. These pathways control cancer and stem cell proliferation. Through his work in Singapore, he aims to find means to selectively kill cancer cells.

Professor Wong Tien Yin
Singapore Eye Research Institute,
Singapore National Eye Centre

Research on retinal vascular imaging by Professor Wong Tien Yin and his team found that by studying the blood vessels in the retina, it can predict diabetes, stroke, heart disease, hypertension and other vascular diseases, independent of conventional risk factors and diagnostic modalities. Now the team is looking into designing a software to measure retinal vascular changes which can non-invasively predict cardio vascular disease.

SINGAPORE TRANSLATIONAL RESEARCH (STAR) INVESTIGATOR AWARD

The STaR Investigator Award is a prestigious award, jointly offered by the Singapore Ministry of Health's National Medical Research Council (NMRC) and the Agency for Science, Technology and Research (A*STAR), to recognise and support investigators with outstanding qualifications in translational and clinical research.

Tenable in Singapore, STaR Investigators can start a new research programme which can potentially advance Singapore's priorities in biomedical research and healthcare, and spend up to 20% of their time engaging in direct patient care. Recipients of the award will receive 3- to 5-year salary remuneration, research support and a one-time start-up grant.

The award is funded by the Singapore National Research Foundation.

If you have the star quality that we are looking for, why not send us your research proposal.
For more information, please visit us at https://www.nmrc.gov.sg.

MINISTRY OF HEALTH
SINGAPORE

Singapore Translational Research (STaR) Investigator Award
National Medical Research Council (NMRC)
11 Biopolis Way, #09-10/11 Helios, Singapore 138667
For further enquiries, you may email to: MOH_STAR_NMRC@moh.gov.sg

Agency for Science, Technology and Research
SINGAPORE

Entry Point!
Students with Disabilities

To meet the challenge of the competitive economy in the new millennium, private industry and government research agencies must expand the pool of technical talent. AAAS started Entry Point!, a program that offers students with disabilities competitive internship opportunities in science, engineering, mathematics, computer science, and some fields of business. And this is just one of the ways that AAAS is committed to advancing science to support a healthy and prosperous world. Join us. Together we can make a difference. **aaas.org/plusyou/entrypoint**

AAAS + U = Δ

Geospatial Technologies
Human Rights

Remote, isolated, catastrophic events occur across the globe that affect civilians, the environment, indigenous rights, and more. The AAAS Science and Human Rights Program uses geospatial technologies to broaden the ability of non-governmental organizations to rapidly gather, analyze, and disseminate information in these times of crisis. And this is just one of the ways that AAAS is committed to advancing science to support a healthy and prosperous world. Join us. Together we can make a difference. **aaas.org/plusyou/humanrights**

AAAS + U = Δ

POSITIONS OPEN

UF UNIVERSITY of FLORIDA
The Foundation for The Gator Nation

CHAIR, DEPARTMENT OF PHYSIOLOGICAL SCIENCES
University of Florida

The University of Florida, College of Veterinary Medicine, is seeking nominations and applications for Chair of the Department of Physiological Sciences. The Chair is the administrative officer of the Department with overall responsibilities for faculty recruitment, mentoring, and promotion; budget management; and instructional activities. The Chair is expected to provide strong leadership in research, veterinary student education, graduate student education, and service. The Chair will work with the hospital board to provide high quality diagnostic clinical pathology service for the Veterinary Medical Center. The Chair is also expected to provide close liaison with the scientific community of the Health Science Center, Institute of Food and Agricultural Sciences, and the University and state of Florida at large.

The Department is responsible for teaching anatomy, physiology, pharmacology, toxicology, and clinical pathology in the veterinary curriculum. Department faculty members also provide graduate student training in areas of research expertise. Current areas of Department research expertise include neuroscience, cardiopulmonary physiology, aquatic and nano toxicology, bone biology, and rickettsial diseases of blood.

The successful candidate will have an earned Doctorate and be qualified for appointment to the rank of **FULL PROFESSOR.** A strong record of research and university instruction, substantial leadership, and organizational skills and a commitment to equality of opportunity are required.

Letters of application should include curriculum vitae, names of three persons who can provide letters of reference, and a statement of career goals. Applications should be received by April 1, 2010. All correspondence should be directed to:

Dr. Charles Courtney, Search Committee Chair
College of Veterinary Medicine
University of Florida
P.O. Box 100125
Gainesville, FL 32610-0125
Telephone: 352-294-4211
E-mail: courtneych@vetmed.ufl.edu

The University of Florida is an Equal Opportunity Access/Affirmative Action Employer. Women and minority candidates are especially encouraged to apply.

NYU School of Medicine

The Department of Environmental Medicine at New York University (NYU) Langone Medical Center is seeking individuals using contemporary cellular and molecular approaches with research interests in epigenetics and toxicology or environmental disease etiology such as cancer or cardiovascular disease for a full-time, tenure-track position at the **ASSISTANT** or **ASSOCIATE PROFESSOR** level. The laboratories (100,000 square foot facility) are located 45 minutes northwest of Manhattan near Tuxedo, New York. Please electronically send letter of application, curriculum vitae, description of research interests and goals, and a list of three references to **Dr. Max Costa, Professor and Chair, e-mail: max.costa@nyumc.org.**

POSITIONS OPEN

THE UNIVERSITY OF MISSISSIPPI MEDICAL CENTER

FACULTY POSITIONS
in Pharmacology and Toxicology
University of Mississippi Medical Center

The Department of Pharmacology and Toxicology invites applications from outstanding scientists for several tenure-track positions at all academic levels, persons with research interests in cardiovascular pharmacology, diabetes and metabolic diseases, anticancer agents, and pharmacogenomics/genetics. Outstanding applicants with interests in other areas of pharmacology will also be considered. Candidates must hold a Ph.D. and/or M.D. degree and have postdoctoral experience. Applicants will maintain a strong, extramurally funded research program and participate in the Department's teaching programs. We can offer an excellent startup package, modern laboratory facilities, hard money salary support, and access to institutional core facilities. The Jackson area is a rapidly expanding metropolitan area with a moderate climate, low housing costs, and excellent schools. Review of applications will begin in January 2010. Please send curriculum vitae, a description of research interests, and a list of three references to: **Richard J. Roman, Professor and Chair, Department of Pharmacology and Toxicology, University of Mississippi Medical Center, 2500 North State Street, Jackson, MS 39216-4505. E-mail: rroman@pharmacology.umsmed.edu.** *Equal Opportunity Employer, Minorities/Females/Persons with Disabilities/Veterans.*

MERCER UNIVERSITY

BASIC SCIENCE FACULTY
Mercer University School of Medicine
Savannah, Georgia, Campus

Mercer University School of Medicine invites applications for two full-time, tenure-track (rank open) Faculty appointments in the Department of Biomedical Sciences at the new expansion campus on the site of Memorial Health University Medical Center in Savannah, Georgia.

Successful applicants are expected to participate in an interdisciplinary, clinically relevant, problem-based learning curriculum for medical students. A demonstrated ability to develop an independent research program capable of attracting extramural funding is strongly desired.

Candidates must hold a doctoral degree (Ph.D., M.D., or equivalent) from an accredited university/college and have appropriate postdoctoral experience. Preference will be given to applicants with educational or teaching expertise in one or more of the following disciplines: medical histology/embryology, microbiology, and physiology.

Review of applications will begin immediately and continue until positions are filled. Priority will be given to applications received by March 1, 2010. For full description and qualifications of the position, please refer to **website: http://www.mercerjobs.com.** *Affirmative Action/Equal Opportunity Employer/ADA.*

FACULTY POSITION
Medical School

Saint James School of Medicine invites applications from candidates with teaching, research, and/or administrative experience in any of the basic medical sciences for its campuses in the Caribbean and its corporate office in Chicago. Immediate needs in anatomy, physiology, pathology, and pharmacology. Applicants should hold an M.D., D.O., and/or Ph.D. with a minimum of five years of experience.

U.S. teaching experience desirable. Retired persons with experience in medical education are encouraged to apply. Attractive salary and benefits. Submit curriculum vitae electronically to **e-mail: career@sjsm.org** or mail to: **HRDS, Inc., 1480 Renaissance Drive, Suite 300, Park Ridge, IL 60068.**

POSITIONS OPEN

Two **POSTDOCTORAL POSITIONS** are immediately available at The University of Utah School of Medicine in Salt Lake City to study the role of stem and progenitor cell maintenance and differentiation on the mechanisms of myofibrillar diseases linked to redox dysfunction and protein misfolding disorders (**Rajasekaran, N.S. et al.,** *Cell* **130(3):**427-39, 2007; **Rajasekaran, N.S. et al.,** *Physiol. Genomics* **35(2):**165-72, 2008). Outstanding Ph.D. candidates will be selected from major disciplines in biochemistry, cell biology, metabolomics, and genetics. Our location in Salt Lake City, Utah, combines fabulous outdoors in both winter and summer sports with an international atmosphere in our laboratory. Successful candidates will join an integrated team using systems biology of cell-based therapies to unravel the underlying mechanisms between redox biology and human protein misfolding diseases. Competitive salaries between $39,000 and $46,000 (U.S.) are based on experience, skills, and levels of independence. Applications are due before March 5, 2010. Please send curriculum vitae and two letters of recommendation and/or references to: **Professor Ivor J. Benjamin, c/o Jennifer Schroff, 30 N. 1900 E., Salt Lake City, UT 84132. Or e-mail: jennifer.schroff@hsc.utah.edu.**

The University of Utah is an Affirmative Action/Equal Opportunity Employer and does not discriminate based upon race, national origin, color, religion, sex, age, sexual orientation, gender identity/expression, disability, or status as a protected veteran. Upon request, reasonable accommodations in the application process will be provided to individuals with disabilities. To inquire about the University's nondiscrimination policy or to request disability accommodation, please contact: ***Director, Office of Equal Opportunity and Affirmative Action, 201 S. Presidents Circle, Room 135, telephone: 801-581-8365.***

The University of Utah values candidates who have experience working in settings with students from diverse backgrounds, and possess a demonstrated commitment to improving access to higher education for historically underrepresented students.

ASSISTANT PROFESSOR
Integrative Physiologist
McMaster University, Department of Biology

McMaster University, a research-intensive institution and leading centre for biological and biomedical research, invites applications for a tenure-track position in the Department of Biology, effective July 1, 2010. We are in search of an applicant with a productive research program, who studies the physiological response to stress at multiple levels (molecular, cellular, genetic, organismal, population, or ecosystem). We seek applications from candidates at the Assistant Professor level; however, exceptional candidates at the Associate Professor rank will also be considered. The successful applicant will be expected to establish and maintain an independent and externally funded research program and contribute to the education of undergraduate and graduate students. Exceptional candidates will be considered for a Canada Research Chair Career award (**website: http://www.chairs.gc.ca/**). More information on research strengths in the Department can be obtained at **website: http://www.biology.mcmaster.ca/index.html**.

Applicants should submit curriculum vitae, a statement of their research goals, a statement of their teaching interests and experience, names of three references, and three of their most important publications to be sent to: **Dr. Patricia Chow-Fraser, Professor and Chair, Department of Biology, McMaster University, 1280 Main Street West, Hamilton, Ontario L8S 4K1, Canada. E-mail: biolappl@mcmaster.ca**. Electronic submission is preferred. The closing date for applications is March 15, 2010, or until the position is filled.

All qualified candidates are encouraged to apply; however, Canadians and permanent residents will be given priority. McMaster University is strongly committed to employment equity within its community, and to recruiting a diverse faculty and staff. The University encourages applications from all qualified candidates, including women, members of visible minorities, Aboriginal persons, members of sexual minorities, and persons with disabilities.

Moving Stem Cell Research Forward

The Need for Standardization

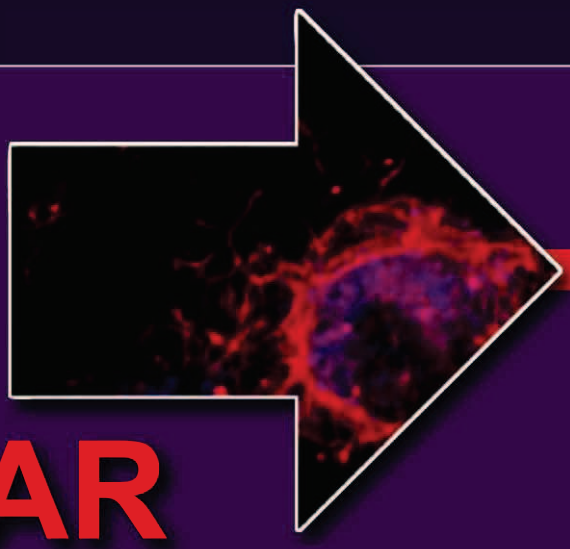

WEBINAR

January 28, 2010

11 am EST, 8 am PST, 4 pm GMT

Stem cell research has the potential to significantly impact a broad range of life science endeavors, ranging from improved drug discovery processes to revolutionary new therapeutics. The ability to control differentiation of stem cells into specialized cell types with high yield and precision is a key success factor that will determine the ultimate utility of such research. However, researchers are facing significant challenges in these efforts because stem cells are difficult to handle and there are very few automated or standardized tools available in this relatively new field. In this hour, we will hear from three panelists on the need for, and progress toward, a new level of standardization and automation in the management and handling of stem cell cultures and their differentiated progeny.

Webinar viewers will:

- learn about common hurdles to be overcome when culturing stem cells
- obtain guidance on best practices for handling and manipulating stem cells
- hear about the latest technologies for standardizing and automating stem cell culture
- have the chance to put their questions to the panelists live!

Participating Experts:

Ron McKay, Ph.D.
National Institutes of Health
Bethesda, MD

Mark D. Noble, Ph.D.
University of Rochester Medical Center
Rochester, NY

Amy Wagers, Ph.D.
Harvard University
Boston, MA

Register Now!

Sign Up At :

www.sciencemag.org/webinar

Science
AAAS

Brought to you by the AAAS/*Science* Business Office

Webinar sponsored by Cyntellect